SYSTEM PERFORMANCE AND PERFORMANCE ENHANCEMENT RELATIVE TO ELEMENT POSITION LOCATION ERRORS FOR DISTRIBUTED LINEAR ANTENNA ARRAYS

By

Andrew Adrian

A DISSERTATION

Submitted to
Michigan State University
in partial fulfillment of the requirements
for the degree of

Electrical Engineering - Doctor of Philosophy

2014

ABSTRACT

SYSTEM PERFORMANCE AND PERFORMANCE ENHANCEMENT RELATIVE TO ELEMENT POSITION LOCATION ERRORS FOR DISTRIBUTED LINEAR ANTENNA ARRAYS

By

Andrew Adrian

For the most part, antenna phased arrays have traditionally been comprised of antenna elements that are very carefully and precisely placed in very periodic grid structures. Additionally, the relative positions of the elements to each other are typically mechanically fixed as best as possible. There is never an assumption the relative positions of the elements are a function of time or some random behavior. In fact, every array design is typically analyzed for necessary element position tolerances in order to meet necessary performance requirements such as directivity, beamwidth, sidelobe level, and beam scanning capability.

Consider an antenna array that is composed of several radiating elements, but the position of each of the elements is not rigidly, mechanically fixed like a traditional array. This is not to say that the element placement structure is ignored or irrelevant, but each element is not always in its relative, desired location. Relative element positioning would be analogous to a flock of birds in flight or a swarm of insects. They tend to maintain a near fixed position with the group, but not always. In the antenna array analog, it would be desirable to maintain a fixed formation, but due to other random processes, it is not always possible to maintain perfect formation.

This type of antenna array is referred to as a distributed antenna array.

A distributed antenna array's inability to maintain perfect formation causes degradations in the antenna factor pattern of the array. Directivity, beamwidth, sidelobe level and beam pointing error are all adversely affected by element relative position error. This impact is studied as a function of element relative position error for linear antenna arrays. The study is performed over several nominal array element spacings, from $1/4\,\lambda$ to $7/8\,\lambda$, several sidelobe levels (20 to 50 dB) and across multiple array illumination tapers.

Knowing the variation in performance, work is also performed to utilize a minimum variance array processing method to minimize the effects of the distributed array element mis-positioning. The extent of array factor performance enhancement is demonstrated for several linear distributed array designs where the input to the enhancement algorithm is only the element position information.

This work is dedicated to those who supported and sometimes tolerated my effort to complete this, especially my wife Margaret. Additional dedication goes out to my sons Alexander and David for their positive support.

ACKNOWLEDGMENTS

Leo Kempel, my dissertation advisor, is acknowledged here for the support he has given me in pursuit of my degree.

Tim Holzheimer is credited for introducing Leo and I to each other.

The rest of my committee, Ed Rothwell, Shanker Balasubramaniam, and Andrew Christlieb are acknowledged for their support of this research as well.

My employer, Texas Instruments, Inc., is acknowledged for their financial support of my tuition through their Educational Assistance Benefit.

TABLE OF CONTENTS

LIST OF TABLES

LIST OF FIGURES

KEY TO SYMBOLS

a	A Taylor amplitude taper.
$\mathbf{a}_i$	Antenna element acceleration.
A_i	The current amplitude of an antenna element.
A_n	An antenna element excitation coefficient.
A_{si}	The current amplitude of a stationary antenna element.
$\mathbf{A}_T$	The transverse magnetic vector potential.
AF	Array factor.
AF_S	The array factor of stationary antenna elements.
ARG	Exponential argument.
B	Bandwidth in Hz.
B_i	The vibration mode amplitude of a specific vibrating mode of an antenna element.
c	The speed of light.
d	The distance between elements in a uniformly spaced linear array.
D	Directivity.
$d\mathbf{S}'_i$	Differential surface of integration.
$\mathbf{e}$	The antenna element voltages vector due to plane waves emenating from a desired array response direction(s).
$\mathbf{E}$	The time harmonic electric intensity field vector in phasor form.
$\vec{\mathscr{E}}$	Electric field intensity vector in time domain form.
EF	Element factor.

$\mathbf{F}_T$ The transverse electric vector potential.

h Normalized pedestal height for a powers of cosine on a pedestal excitation.

$\mathbf{H}$ The time harmonic magnetic intensity field vector in phasor form.

$\mathbf{i}$ Normalized electric current distribution.

$\mathbf{i}_m$ Normalized magnetic current distribution.

I Complex current amplitude of an array element.

$\mathbf{I}$ The identity matrix.

j $\sqrt{-1}$.

J_o The zero-order Bessel function of the first kind.

k The wave number, either $\frac{2\pi}{\lambda}$ or $\frac{\omega}{c}$ or $\omega\sqrt{\mu_0\varepsilon_0}$.

$\mathbf{K}$ Electric surface current.

$\mathbf{K}_m$ Magnetic surface current.

L Aperture length.

n The number of elements in a population set.

$\overline{n}$ The number of "equal" amplitude sidelobes adjacent to the main beam on one side for a Taylor aperture illumination.

$\hat{\mathbf{n}}$ The normal to a surface.

N The antenna element count of an array – each array consists of N+1 antenna elements.

$\mathbf{P}$ A random position vector representing a random position that is delineated by the random spherical coordinate (R,Θ,Φ).

PF Propagaiton factor.

r Radial distance.

r_ε Randomization radius.

$\mathbf{r}$ A position vector.

$\hat{\mathbf{r}}$ The unit vector in the radial direction away from the coordinate system origin.

$\mathbf{r}_a$ The position trajectory of a moving array.

$\mathbf{r}_{ei}$ The time dependent element position error vector.

$\mathbf{r}_i$ The time dependent antenna element position vector.

$\mathbf{r}_{ir}$ A randomized position vector relative to nominal element position.

$\mathbf{r}_{mi}$ The position of a moving antenna element.

$\mathbf{r}_{si}$ The stationary antenna element position vector.

R The design sidelobe voltage ratio (main beam over sidelobe level) or a random variable representing a random value of r.

$\mathbf{R}$ Array correlation matrix.

S The surface of Integration.

T_m The Chebyshev polynomial of order m.

u The array factor variable for a linear array.

$\hat{\mathbf{u}}$ The unit vector in an arbitrary direction.

$\mathbf{v}_i$ Antenna element velocity.

$\mathbf{w}_0$ The array weight excitation vector.

x The first corrdinate of a position vector $\mathbf{r} = x\hat{\mathbf{x}} + y\hat{\mathbf{y}} + z\hat{\mathbf{z}}$ in a Cartesian coordinate system.

x_{ei} The x component of $\mathbf{r}_{ei}$.

x_i The x component of $\mathbf{r}_i$.

x_p A zero of a Chebyshev polynomial.

x_{si} The x component of $\mathbf{r}_{si}$.

$\hat{\mathbf{x}}$ The unit vector in x-direction of a Cartesian coordinate system.

X A random variable representing a random value of x that is a transformation from $\mathbf{P}$.

y The second corrdinate of a position vector $\mathbf{r} = x\hat{\mathbf{x}} + y\hat{\mathbf{y}} + z\hat{\mathbf{z}}$ in a Cartesian coordinate system.

y_{ei} The y component of $\mathbf{r}_{ei}$.

y_i The y component of $\mathbf{r}_i$.

y_{si} The y component of $\mathbf{r}_{si}$.

$\hat{\mathbf{y}}$ The unit vector in y-direction of a Cartesian coordinate system.

Y A random variable representing a random value of y that is a transformation from $\mathbf{P}$.

$\mathbf{Y}$ The antenna element voltages vector due to plane waves emenating from undesired array response direction(s).

z The third corrdinate of a position vector $\mathbf{r} = x\hat{\mathbf{x}} + y\hat{\mathbf{y}} + z\hat{\mathbf{z}}$ in a Cartesian coordinate system.

z_{ei} The z component of $\mathbf{r}_{ei}$.

z_i The z component of $\mathbf{r}_i$.

z_p A zero of a uniformly spaced Dolph-Chebyshev excited linear array.

z_{si} The z component of $\mathbf{r}_{si}$.

$\hat{\mathbf{z}}$ The unit vector in z-direction of a Cartesian coordinate system.

Z A random variable representing a random value of z that is a transformation from $\mathbf{P}$.

α Element phase delay.

α_{si} The element phase delay of a stationary antenna element.

β The excitation parameter for a uniformly spaced linear array with a modified Taylor excitation.

η_o Impedance of free space, either $\frac{|E_T|}{|H_T|}$ where E_T and H_T are the respective transverse components of **E** and **H**, or $\sqrt{\frac{\mu_0}{\varepsilon_0}}$.

θ The spherical angular coordinate, theta, measured from the z-axis.

Θ A random variable representing a random value of θ.

λ Wavelength.

μ_0 The permeability of free space.

μ_p The mean of pooled populations.

υ_i The vibration mode phase of a specific vibrating mode of an antenna element.

σ Standard deviation.

σ^2 Noise variance of white Gaussian noise.

σ_p^2 The variance of pooled populations.

ϕ The spherical angular coordinate, phi, measured from the x-axis.

Φ A random variable representing a random value of ϕ.

ψ The array factor variable for a uniformly spaced Dolph-Chebyshev excited linear array.

ω Radial frequency.

Ω_A Beam solid angle.

1.0 Introduction

1.1 Antenna Arrays

In today's modern world, we are surrounded by items that generate and utilize electromagnetic radiation. Society has become dependent upon them: cell phones and cell sites, wireless networking, communications transceivers, broadcast transmitters and receivers, Radio Detection and Ranging (RADAR), MRI scanners, Bluetooth [1], microwave communications links, satellite communications, GPS, security scanners, and many others. In each of these systems, the transformation of electric signals on wires and circuits into an electromagnetic wave and back is accomplished through an antenna system – the antenna system being the structure that radiates or receives radio waves [2].

Often a single element comprises the antenna system. In other systems, several physically separated elements work in concert to further enhance the electrical transformation characteristics of the antenna system beyond what is possible utilizing a single structure. When several elements form the antenna system, they are collectively referred to as an antenna array [3], [4], [5]. Antenna arrays are evident in many well know items. Wireless routers that operate under the *IEEE 802.11n* [6], and soon *IEEE 802.11ac* [7] specifications, automobiles with diversity FM antennas, RADAR's, and radio telescopes are just a few well known types of systems that have antenna arrays designed into them.

1.2 Element Position and Mechanical Fixing

The elements of an antenna array are designed to coherently operate in concert. In some antenna arrays, *apriori* knowledge of the exact antenna transformation characteristics are not required due to the specific signal processing and use cases involved. In these cases, performance is verified at a much higher system level. For example, automotive FM diversity antenna systems consist of two or more antennas. The performance of the individual antennas is known, but the performance of the array is very dynamic and depends upon specific electromagnetic reception conditions. In this case constant modulus processing is often used to enhance the performance of the receiver by uniquely and constantly modifying the complex weighting of each antenna signal over time prior to summation and demodulation [8]. As a result of this processing, the array performance of the system is in constant flux, but the system performance is verified through radio reception field trials in long delay multipath conditions, not antenna array performance measurements. 802.11n and 802.11ac router antenna systems are also arrays where the specific electromagnetic transformation characteristics are often unknown. Phased array RADAR and radio telescopes such as the Very Large Array (VLA) [9] are examples of systems with antenna arrays where the specific electromagnetic transformation properties are important aspects of their respective systems. In order to *apriori* determine and design the transformation characteristics of an array, the relative position of each element to the other elements must be known. With this information, the time/phase relationship of the signals among the elements is adjusted to obtain optimum antenna array system performance for the particular use case. Relative element position information is vital to design the array so that it can achieve specific, desired antenna array system pattern performance and operation.

Limiting subsequent discussion to antenna arrays whose electromagnetic transformation characteristics are designed to meet specific criteria, in most cases, relative element position is known because each element is mechanically fixed to a structure that permanently defines its position. As a result, the only uncertainty in element position information is due to the manufacturing tolerances of the array. Position tolerances are kept small enough so that their effect is minimized, and the antenna array meets its performance objectives. In this scenario, the relative position of the array elements is not considered to be a function of time. Alternatively speaking, the relative positions of the array elements are constant. The research that follows shows that performance can be measurably degraded with element position perturbations less than $\lambda/100$ for 20 dB sidelobe linear arrays.

Many studies have been performed of how errors in arrays affect their performance. Early studies examined excitation tolerances in element current amplitude and phase. Excitation tolerance studies of antennas were presented for continuous and discrete arrays by J. Ruze where he considered physical limitations on antennas [10] and antenna current tolerance issues [11] [12]. In his initial work, pattern errors due to imperfect current magnitude and phase of aperture distributions were considered. Zarghamee further elaborated on Ruze's developments [13]. These types of tolerance issues do not directly address position errors of array elements, although a relationship can be seen between the two, especially in the case of current on the reflector of a reflector antenna.

Shaw examined position errors in space deployed antenna systems [14]. His analysis approximated a small spaced large array as a large continuous aperture with correlated modal variation in one dimension of the radiating structure. His results indicated significant gain, beam pointing and sidelobe degradation. He also performed an analysis based upon random errors that showed significant gain and sidelobe issues. However, his position variation was only in one dimension.

Choi and Sarkar studied the implications of position errors for a two dimensional array with Tseng window weights [15] [16]. Expectation and variance of the array pattern was derived as a function of element spacing statistics along each axis. Hence, this analysis is broken down into random variables that represent position errors that lay in the plane of the array – not above or below it. Their presented example analysis was performed for a 128x128 element planar array with undisclosed grid spacing.

Trastoy *et. al.* did analyze the antenna pattern variation due to position, amplitude, and phase errors in a 19 element linear array with *cosθ* element patterns that was pattern reconfigurable [17]. The probability of the array achieving it specifications with varying degrees of element position error was examined for the specific pattern beam shape and sidelobe level requirements of this particular array.

Mechanical errors in phased arrays have also been analyzed by Wang [18]. He reformulated Ruze's analysis to include position errors. His formulation was based upon a planar array with a rectangular or triangular grid. It was organized about an array that was intentionally designed to have small errors in nominal positioning and excitation. His research was motivated about an electrically large planar structure whose only significant variation from a plane was modal bending. The position error analysis was also organized about a Cartesian coordinate system for the array, having position errors assigned a random variable in each axis of the measurement system. In the end Wang demonstrated his theory utilizing a 28,798 element planar array with a 2-dimensional Gaussian taper [19].

Several additional topics related to element position and its effects on array performance along with methods to compensate for inexact element position have been studied. Yonezawa *et. al.* examined methods of determining phase errors in phased arrays due to element position inaccuracies as a result of incomplete deployment of space based arrays [20]. Element position adjustment to steer nulls in arrays was discussed by Ismail and Dawoud [21] [22]; Abu-Al-Nadi, Ismail and Mismar [23]; Guney, Babayigit and Akdagli [24]; and Guney and Onay [25]. Array element position adjustment for performance enhancement [26], and direction finding [27] has been researched in addition to random element placement within arrays and its impact to performance [28] [29].

1.3 Independent Element Position Control, and Distributed Arrays

In all but one case of the research in Sec. 1.2, analysis was performed upon arrays that were assumed to be part of a continuous structure. What happens when the elements in an array are no longer part of the same mechanical structure? What if each element can move independently of the others in the array? That is not to say that the all of the elements move completely randomly relative to each other, but while attempting to maintain a constant position, relative to each other, their absolute position always has some uncertainty in it. In other words, each element’s position vector cannot maintain constant position offsets to all of the other elements' position vectors as time progresses. Effectively, the motion of each element is independent of the motion of the other elements, even if they are trying to maintain a formation. An antenna array of this type has been described as a *distributed array*.

Steinberg described an array that was distributed over an entire airframe and how its performance could exceed that of a conventional rotating aircraft antenna [30]. In this implementation the elements were assumed to not have a constant position offset from each other; however, the amount of relative movement was due to vibration and flexing of the airframe. He also described how to cohere the array by using a target for calibration to determine the necessary phase adjustments in order to focus the array on the target [31]. This method does not directly "locate" the antennas on the airframe to facilitate direct determination of the array pattern. Taheri and Steinberg demonstrated the amount of tolerance relaxation in element position location that could be achieved in a distributed array while still maintaining accurate beam scanning and gain performance [32]. Their technique involved phase locking all of the receive mode antenna signals.

In a distributed array, the aperture is comprised of several mechanically disjointed antenna elements or sub-arrays that work cooperatively as a single antenna array. TechSat 21, a system of this general architecture was proposed for space deployment [33] [34] [35]. In this system, several small/micro-satellites with X band RADAR were to be deployed. They would work in concert to form an array with satellite spacing varying from 100m to 5km [36]. The end result is a sparse array.

Considering micro-satellites flying in formation with baselines of 3000 to 17,000 wavelengths, it becomes abundantly clear that the array factor grating lobes will be extraordinarily significant. While developing signal processing techniques to address the grating lobes, Schindler et al. [37], Steyskal *et al.* [38], and Heimiller et al. [39] all commented on the impact of position errors for each element or sub-array. However, much of the effort associated with distributed space based arrays was focused upon developing necessary signal processing. Signal processing concepts for satellite distributed arrays that utilize spread spectrum or orthogonal wave forms have been developed by J.P. Aguttes [40] [41] and R. Advea *et al.* [42]. These methodologies, however, do not focus directly on the impacts to the array performance due to relative position ambiguities.

Another distributed array structure that is gaining significant attention consists of Aerial Drone Vehicles (ADVs). Position ambiguity impact to ADV array performance has been studied by Namin *et. al.* [43], and Petko and Werner [44]. Their examples contained 49 to 319 elements. Issues of beam pointing error and increases in sidelobe level were demonstrated. They also developed phase corrections to the excitations to attempt to resolve the beam pointing and sidelobe level issues. However, no method was demonstrated to obtain the phase correction parameters.

1.4 Element Position Errors

Whether an array is distributed or not, a little studied question in array theory is what happens to the electromagnetic performance of an array when the elements are not mechanically fixed relative to each other. Alternatively, what if the uncertainty of the relative element positions grows? How large can the uncertainty become before significantly affecting the radiation performance of the antenna array? As these questions are moved to distributed arrays, how well can relative position be determined so that it may be compensated with phase adjustments to the elements' excitations? The research described herein examines array performance of linear arrays as the uncertainty of their position increases. Element position uncertainty is allowed to increase in a sphere about the desired element position. This is repeated for several array designs using several illumination tapers at several scan angles.

1.5 Pattern Impact

Certainly, there will be array radiation pattern impact. Ideal patterns are developed and scanned in one dimension to establish baselines. Element positions are allowed to randomly vary in a confined volume about their nominal location, and the patterns are recomputed (including scan angels) to establish statistics about pattern performance metrics as a function of element position variation. Pointing error, 3 and 10 dB beamwidths, distance between first nulls, and sidelobe level statistics are some of the metrics that are evaluated as functions of element position error.

1.6 Taper Dependency of Pattern Impact

An additional part of study of the impact to array pattern performance as the element position error increases is illumination taper of the array. Is there a taper dependency found in the statistical results? Dolph-Chebyshev [45], modified Taylor

[46], powers of cosine on a pedestal [47], and Taylor [48] illumination distributions are considered.

1.7 Motion

After analysis of the position error impact, expressions will be developed for the array factor as a function of motion of the individual elements. An example of the array pattern expression will be examined as a function of time. This will show the dependence of the pattern upon the relative motion of the elements.

1.8 Mitigation of Errors

With the array elements randomly mis-positioned, methods of compensating for the position error will be discussed. Along with potential enhancement methods, system performance expectations will be developed.

2.0 Array Theory

2.1 General Formulation

The work herein is developed assuming time harmonic electromagnetic waves propagating through free space. Representations of field quantities are actually phasors where the time dependence is assumed to be $e^{j\omega t}$ and is generally suppressed. Consequently, time derivatives reduce to a $j\omega$ multiplicative operator. Considering antenna far field electric, **E**, and magnetic, **H**, (vector) fields, in a spherical geometry, due to electric and magnetic current sources, the radiation in the far field can be mathematically described by the following equations:

$$\mathbf{E} = -j\omega\mathbf{A}_T + jk\left(\hat{\mathbf{r}} \times \mathbf{F}_T\right) \tag{2.1a}$$

$$\mathbf{H} = \frac{1}{\eta_o}\hat{\mathbf{r}} \times \mathbf{E} \tag{2.1b}$$

where

ω = the radial frequency of the time harmonic wave

$\hat{\mathbf{r}}$ = the unit vector in the radial direction away from the coordinate system origin.

k = the wave number, either $\dfrac{2\pi}{\lambda}$ or $\dfrac{\omega}{c}$ or $\omega\sqrt{\mu_0\varepsilon_0}$.

η_o = the impedance of free space, either $\dfrac{|E_T|}{|H_T|}$ where E_T and H_T are the respective transverse components of **E** and **H**, or $\sqrt{\dfrac{\mu_0}{\varepsilon_0}}$.

$\mathbf{A}_T$ = the transverse magnetic vector potential.

$\mathbf{F}_T$ = the transverse electric vector potential.

$\mathbf{A}_T$ and $\mathbf{F}_T$ are respectively derived from the directional weighting function of the electric and magnetic source currents and the outgoing spherical wave factor.

$$\mathbf{A}_T = \mu_0 \frac{e^{-jkr}}{4\pi r} \oiint_{S'} \mathbf{K}(\mathbf{r}') e^{jk\hat{\mathbf{r}}\cdot\mathbf{r}'} d\mathbf{S}' \tag{2.2a}$$

$$\mathbf{F}_T = \frac{e^{-jkr}}{4\pi r} \oiint_{S'} \mathbf{K}_m(\mathbf{r}') e^{jk\hat{\mathbf{r}}\cdot\mathbf{r}'} d\mathbf{S}' \tag{2.2b}$$

where $\mathbf{K}$ is the electric surface current on the antenna, and $\mathbf{K}_m$ is the magnetic surface current on the antenna. Aperture fields can be related to these surface currents as

$$\mathbf{K} = \hat{\mathbf{n}} \times \mathbf{H}\big|_{S'} \tag{2.3a}$$

$$\mathbf{K}_m = -\hat{\mathbf{n}} \times \mathbf{E}\big|_{S'} \tag{2.3b}$$

The integrals are evaluated over the surface, S', of the antenna [49]. (2.3a) represents the relationship of the electric surface current density in amps per square meter on the surface of the antenna to its tangential magnetic field. Similarly, (2.3b) represents the relationship of the magnetic surface current density in volts per square meter on the surface of the antenna to the tangential electric field.

Consider (2.1). $\mathbf{E}$ and $\mathbf{H}$ radiation fields for a given source are the result of current sources $\mathbf{K}$ and $\mathbf{K}_m$ described in (2.2). If an ensemble of $(N+1)$ antennas with known source currents is arbitrarily arranged in space, the total $\mathbf{E}$ and $\mathbf{H}$ far fields are due to a summation of the surface integral of all the currents on all of the antennas.

$$\mathbf{E} = \sum_{i=0}^{N} \left[-j\omega \mathbf{A}_{Ti} + jk\left(\hat{\mathbf{r}} \times \mathbf{F}_{Ti}\right) \right] \tag{2.4a}$$

$$\mathbf{A}_{Ti} = \mu_0 \frac{e^{-jkr}}{4\pi r} \oiint_{S'_i} \mathbf{K}_i(\mathbf{r}') e^{jk\hat{\mathbf{r}}\cdot\mathbf{r}'} d\mathbf{S}' \tag{2.4b}$$

$$\mathbf{F}_{Ti} = \frac{e^{-jkr}}{4\pi r} \oiint_{S'_i} \mathbf{K}_{mi}(\mathbf{r}') e^{jk\hat{\mathbf{r}}\cdot\mathbf{r}'} d\mathbf{S}' \tag{2.4c}$$

In this scenario, each antenna element in the ensemble is denoted by the subscript *i*. Each antenna element, *i*, is assumed to contain electric, $\mathbf{K}_i$, and magnetic, $\mathbf{K}_{mi}$, current on its surface. S_i denotes the surface of the i^{th} antenna. Combining (2.4) in to one equation

$$\mathbf{E} = jk \frac{e^{-jkr}}{4\pi r} \left[-\omega\eta \left(\sum_{i=0}^{N} \oiint_{S'_i} \mathbf{K}_i(\mathbf{r}') e^{jk\hat{\mathbf{r}}\cdot\mathbf{r}'} d\mathbf{S}' \right) + \left(\sum_{i=0}^{N} \hat{\mathbf{r}} \times \oiint_{S'_i} \mathbf{K}_{mi}(\mathbf{r}') e^{jk\hat{\mathbf{r}}\cdot\mathbf{r}'} d\mathbf{S}' \right) \right] \tag{2.5}$$

results in a definition of the electric radiation far field, $\mathbf{E}$, in terms of all the source currents on all of the antennas. Note that the element currents need not be identical.

Up until now, there have been no assumptions about the antennas other than there are $(N+1)$ of them. No constraints have been placed upon their design, placement or orientation. As a first constraint, consider that each antenna in the ensemble is identical such that the current distribution functions, $\mathbf{K}_i$ and $\mathbf{K}_{mi}$, are the same as $\mathbf{K}_{i+1}$, and $\mathbf{K}_{m(i+1)}$, for all *i* from $i = 0$ to $i = N$ except for a translation, orientation, and multiplicative constant.

If orientation is constrained such that each antenna is rotationally oriented in the same direction from a spherical theta (θ) and phi (ϕ) perspective, when calculating

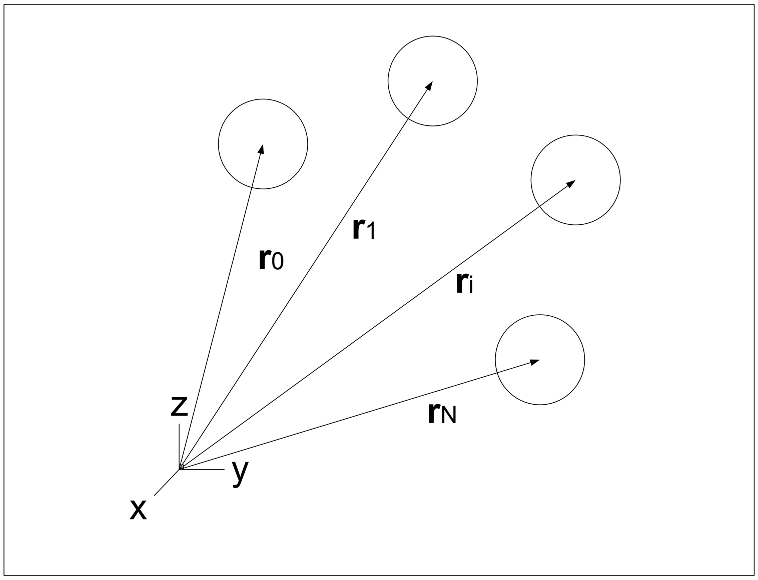

Figure 2.1. *Schematic representation of an N+1 element array.* Elements are located at N+1 position vectors, $\mathbf{r}_i$.

(2.5), instead of performing the integration over a single coordinate system, a change of variable can be applied such that the integration is only performed once for the electric currents and once for the magnetic currents. If each antenna is displaced by vector $\mathbf{r}_i$ from the origin, when considering the integrals in (2.5),

$$\mathbf{r}' = \mathbf{r}_i + \mathbf{r}'_i \,. \tag{2.6}$$

$\mathbf{r}'_i$, in this case, is relative to a local coordinate system of integration on each antenna in the ensemble, and $\mathbf{r}_i$ is a fixed offset of each antenna from the ensemble origin. Applying (2.6) to (2.5), causes a modification in the exponential within the integrand terms.

$$e^{jk\hat{\mathbf{r}}\cdot\mathbf{r}'} = e^{jk\hat{\mathbf{r}}\cdot\mathbf{r}_i} e^{jk\hat{\mathbf{r}}\cdot\mathbf{r}'_i} \tag{2.7}$$

The first term on (2.7) can be removed from the surface integral of (2.5). Since that

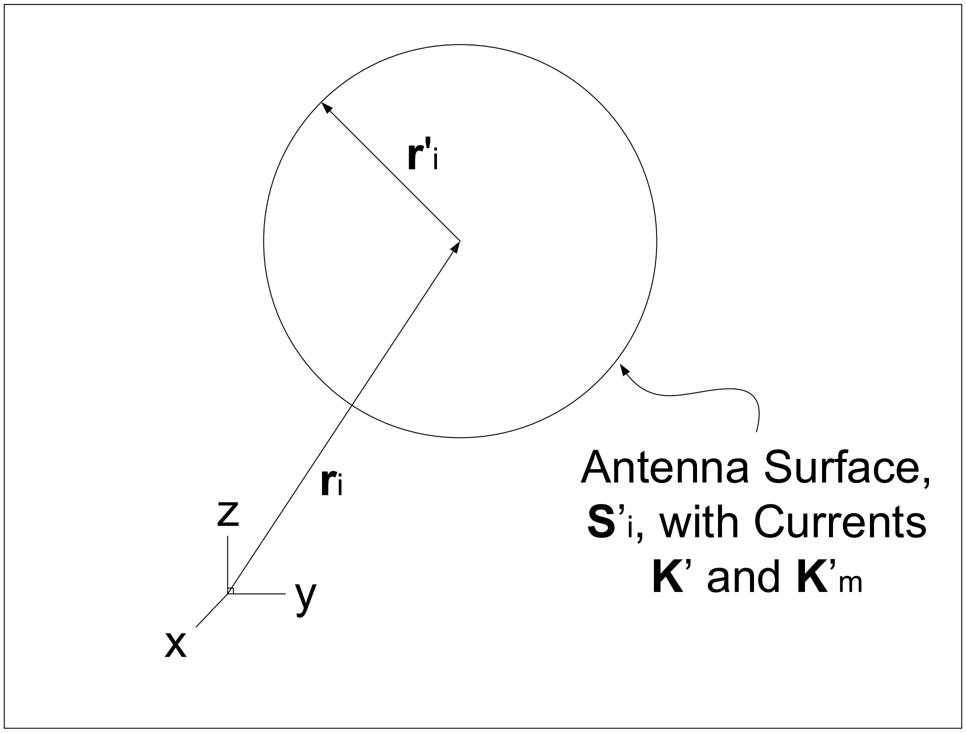

Figure 2.2. *Expanded view of the array's* i^{th} *antenna element surface.*

same term from (2.7) is a scalar, it can also be placed in front of the cross product, resulting in

$$\mathbf{E} = jk\,\frac{e^{-jkr}}{4\pi r}\left[-\omega\eta\left(\sum_{i=0}^{N} e^{jk\hat{\mathbf{r}}\cdot\mathbf{r}_i}\oiint_{S'_i}\mathbf{K}_i(\mathbf{r}')e^{jk\hat{\mathbf{r}}\cdot\mathbf{r}'_i}\,d\mathbf{S}'_i\right)+\sum_{i=0}^{N} e^{jk\hat{\mathbf{r}}\cdot\mathbf{r}_i}\,\hat{\mathbf{r}}\times\left(\oiint_{S'_i}\mathbf{K}_{mi}(\mathbf{r}')e^{jk\hat{\mathbf{r}}\cdot\mathbf{r}'_i}\,d\mathbf{S}'_i\right)\right] \quad (2.8).$$

With the current distributions among the antennas in the ensemble related to each other by a multiplicative, potentially complex, constant, the currents can be described as follows:

$$\mathbf{K}_i = I_i\mathbf{i} \quad (2.9a)$$

$$\mathbf{K}_{mi} = I_i\mathbf{i}_m\,. \quad (2.9b)$$

In (2.9), I_i is a multiplicative constant. $\mathbf{i}$ and $\mathbf{i}_m$ are normalized current distribution functions that are identical from antenna to antenna. Additionally, since the current distribution functions among the antennas are identical and identically oriented, the surface of integration, S'_i, and its differential, $d\mathbf{S}'_i$, no longer depend upon the specific antenna surface of integration. Hence, the summation index can be dropped from the tracking of the surface and its differential. A similar argument applies to the $\mathbf{r}'_i$ term within the integrals. This allows the integrals in (2.8) to be placed in front of the summations and the result is reduced to contain only a single summation.

$$\mathbf{E} = \frac{e^{-jkr}}{4\pi r}\left\{jk\left[-\omega\eta\left(\oiint_{S'} \mathbf{i}(\mathbf{r}')e^{jk\hat{\mathbf{r}}\cdot\mathbf{r}'}d\mathbf{S}'\right)+\hat{\mathbf{r}}\times\left(\oiint_{S'} \mathbf{i}_m(\mathbf{r}')e^{jk\hat{\mathbf{r}}\cdot\mathbf{r}'}d\mathbf{S}'\right)\right]\right\}\left(\sum_{i=0}^{N} I_i e^{jk\hat{\mathbf{r}}\cdot\mathbf{r}_i}\right) \tag{2.10}$$

The first term in (2.10) is called the propagation factor, and it represents the spherical wave. The second term in (2.10) within the "{ }" is an antenna element term or element factor. The third term contains the current amplitudes and the location information of each antenna in the ensemble, the array term or array factor. When all the antennas in the array have the same normalized current distribution, are oriented the same, and exhibit no mutual coupling, (2.10) is applicable. It states that the result is a multiplication of the propagation factor with the antenna element factor and the array factor.

$$\mathbf{E} = PF\cdot\mathbf{EF}\cdot AF \tag{2.11a}$$

$$PF = \frac{e^{-jkr}}{4\pi r} \tag{2.11b}$$

$$\mathbf{EF} = -\frac{j}{\varepsilon}\left(\frac{2\pi}{\lambda}\right)^2\left(\oiint_{S'} \mathbf{i}(\mathbf{r}')e^{jk\hat{\mathbf{r}}\cdot\mathbf{r}'}d\mathbf{S}'\right)+jk\hat{\mathbf{r}}\times\left(\oiint_{S'} \mathbf{i}_m(\mathbf{r}')e^{jk\hat{\mathbf{r}}\cdot\mathbf{r}'}d\mathbf{S}'\right) \tag{2.11c}$$

$$AF = \sum_{i=0}^{N} I_i e^{jk\hat{\mathbf{r}}\cdot\mathbf{r}_i} \tag{2.11d}$$

The normalized product of the element factor with the array factor gives the pattern of the array. In this research, the antennas in the array are considered to be isotropic radiators with uniform patterns. This simply equates (2.11c) to unity, focusing the research to be presented on the impacts to the array term or array factor and its impacts to system pattern performance.

The reason for limiting the research herein to the array factor relates to system design of a distributed array. If the system is not viable from an array factor perspective, the addition of mutual coupling generally adds additional constraints that further limit the performance of an array. Additionally, the focus on the array factor allows for clear identification of system limits and what element factor performance would be required to achieve desired specification objectives, hence the array factor calculation places a bound upon a system design prior to element design and mutual coupling impact.

The current term in (2.11d), I_i , is a complex quantity that can be expressed as the product of a real scalar and an exponential with a phase delay.

$$I_i = A_i e^{-j\alpha_i} \tag{2.12}$$

Consequently, the array factor, AF, can be rewritten as

$$AF = \sum_{i=0}^{N} A_i e^{j\left(k\hat{\mathbf{r}}\cdot\mathbf{r}_i - \alpha_i\right)} . \tag{2.13}$$

α_i's are referred to as the phase taper while the A_i's compose the amplitude taper of the array [50]. By properly adjusting the phase of each of the array's elements, the pointing direction of the main beam can be manipulated.

Often it is easier to denote the antenna element positions in Cartesian coordinates. It is desirable to obtain the antenna factor function in terms of spherical coordinate directions, θ and ϕ. Converting $\hat{\mathbf{r}}$ into its Cartesian equivalent and taking the dot product with $\mathbf{r}_i$ results in a function that has independent variables, θ, ϕ, and the array element location in Cartesian coordinates. A very useful form of the array factor then emerges.

$$\hat{\mathbf{r}} \cdot \mathbf{r}_i = x_i \sin\theta \cos\phi + y_i \sin\theta \sin\phi + z_i \cos\theta \tag{2.14a}$$

$$AF = \sum_{i=0}^{N} A_i e^{j\left[k\left(x_i \sin\theta\cos\phi + y_i \sin\theta\sin\phi + z_i \cos\theta\right) - \alpha_i\right]} \tag{2.14b}$$

Expression (2.14b) is maximized at the AF's main beam peak. At the AF's peak of beam, all the exponential arguments in the summation are in phase. The only way to guarantee that they are in phase for a given direction, (θ_o, ϕ_o), is to force the exponential arguments to zero when $(\theta, \phi) = (\theta_o, \phi_o)$. This of course, assumes that the phases of A_i for the entire summation are also phase aligned. Without a loss of generality, the A_i's can be assumed to be real because the imaginary part is included in the α_i terms as indicated by (2.12). As a result, choosing

$$\alpha_i = k\left(x_i \sin\theta_o \cos\phi_o + y_i \sin\theta_o \sin\phi_o + z_i \cos\theta_o\right) \tag{2.15}$$

results in the main beam of the AF peak occurring in the direction of (θ_o, ϕ_o). Consequently, the phase taper determines the scan angle of the AF, and it depends upon the specific element locations and the desired peak of beam direction.

2.2 Linear Arrays

Element locations within an array can take on several geometries from random to linear to planar and 3-dimmensional with several density and population schemes [51] [52] [53]. In a linear array, as the name indicates, the elements are placed in a line.

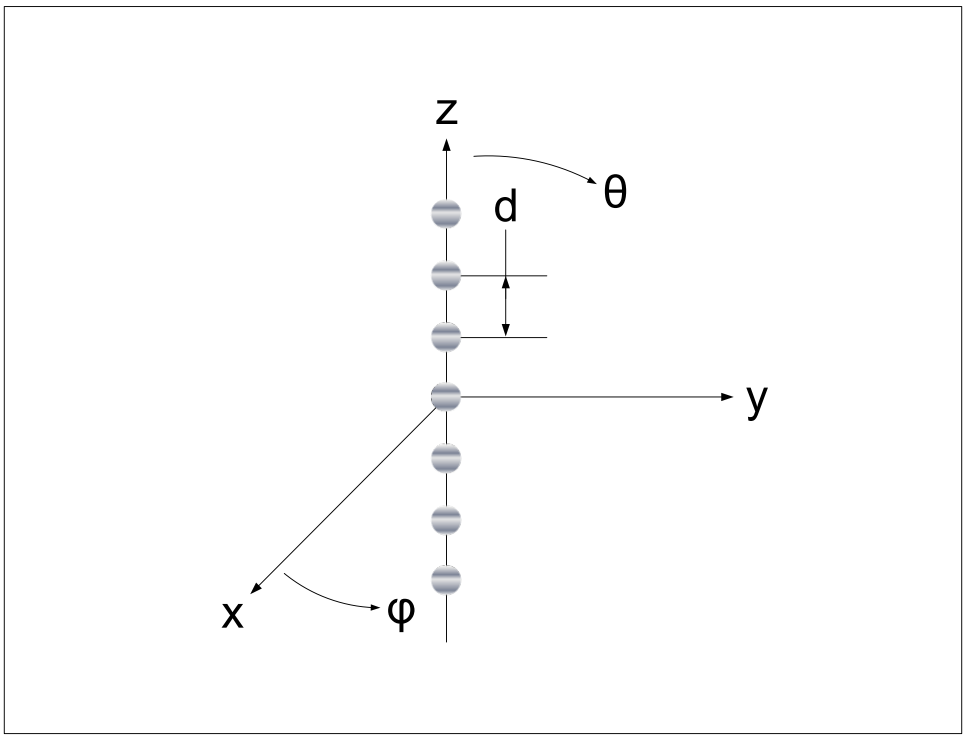

Figure 2.3. *Linear array geometry with uniformly spaced elements.*

Consider several antenna elements placed along a line on the z-axis. Each of the elements are uniformly spaced a distance “d” apart. The array is centered about the coordinate origin. In this scenario, the array factor becomes circularly symmetric about the z-axis. $\mathbf{r}_i$ has no x or y dependence and z_i is only a function of N and d .

$$z_i = \left(i - \frac{N}{2} \right) d \tag{2.16}$$

$\hat{\mathbf{r}} \cdot \mathbf{r}_i$ is greatly simplified, and the antenna factor becomes

$$AF = \sum_{i=0}^{N} A_i e^{j\left[k\left(i - \frac{N}{2} \right) d \cos\theta - \alpha_i \right]} . \tag{2.17}$$

In (2.17) the $\left(i - \frac{N}{2} \right)$ term varies between $-\frac{N}{2}$ and $\frac{N}{2}$ in integer increments for a total of $N+1$ unique values. In order to steer the linear array beam to an angle θ_o by adjusting the steering phases, the α_i's must take the form

$$\alpha_i = k\left(i - \frac{N}{2} \right) d \cos\theta_o \text{ [54].} \tag{2.18}$$

The array factor then becomes

$$AF = \sum_{i=0}^{N} A_i e^{j\left[k\left(i - \frac{N}{2} \right) d \left(\cos\theta - \cos\theta_o \right) \right]} . \tag{2.19}$$

Its peak of beam is located at θ_o.

3.0 Array Amplitude Tapers

3.1 Introduction

As mentioned previously the A_i's of the antenna factor, beginning with (2.13), form the amplitude taper of the array. By adjusting current amplitudes of the taper, the sidelobe and beamwidth performance of the array factor can be adjusted for a given number of elements, element spacing and geometry. In the case of this research, the arrays were designed to be linear arrays with uniform spacing. As a result, the tapers that are utilized are designed for linear arrays. What immediately follow are taper descriptions for various linear arrays. All taper descriptions assume geometry similar to Figure 2.3.

3.2 Uniform

The very simplest of tapers is a uniform taper or no taper at all. Excitations of all the elements in a uniformly excited array have identical amplitudes. For large arrays, the peak sidelobe level is 13.26 dB below the main beam [55]. This result is calculated by setting all the amplitude coefficients, A_i, to 1 and calculating the far field as a sum of the individual fields from each of the elements. Simplifying and normalizing the far field expression results in the following:

$$AF(\theta) = \frac{1}{N} \frac{sin\left(\frac{(N+1)\pi u}{2}\right)}{sin\left(\frac{\pi u}{2}\right)} \tag{3.1a}$$

$$u = 2\frac{d}{\lambda}(cos\,\theta - cos\,\theta_o) \tag{3.1b}$$

where

$N+1$= the number of elements in the array

d = the spacing between elements

λ= the wavelength

θ= the angle from the z-axis

θ_o=the beam peak angle of the array from the z-axis.

(3.1a) also has phase terms dropped from it. Taking the derivative of 3.1a with respect to u, setting the expression equal to zero and solving for the argument that satisfies the equality, results in

$$(N+1)\pi\frac{u}{2} = tan\left[(N+1)\pi\frac{u}{2}\right] \tag{3.2}$$

for large N. The first solution (first sidelobe peak) is $(N+1)\frac{u}{2} = 1.4303$ [56]. Inserting this expression back into (3.1a) for large values of N yields an asymptote of 13.26 dB below the main beam. Consequently all uniformly excited linear arrays have a sidelobe level of about 13 dB and approach 13.26 as N+1 becomes large.

3.3 Dolph-Chebyshev

In a Dolph-Chebyshev array, the Chebyshev polynomial is mapped to the array factor pattern [57] [58] [59] [60]. The Dolph-Chebyshev array has the feature of being the most efficient aperture for a given sidelobe level. This is because beyond the main beam, the peaks of the sidelobes are constant across the remaining angular sector. An example can be seen in Figure 3.1. It is the array factor for an N+1=10 element array with $1/2\lambda$ spacing that is scanned to $\theta_o = 90^o$.

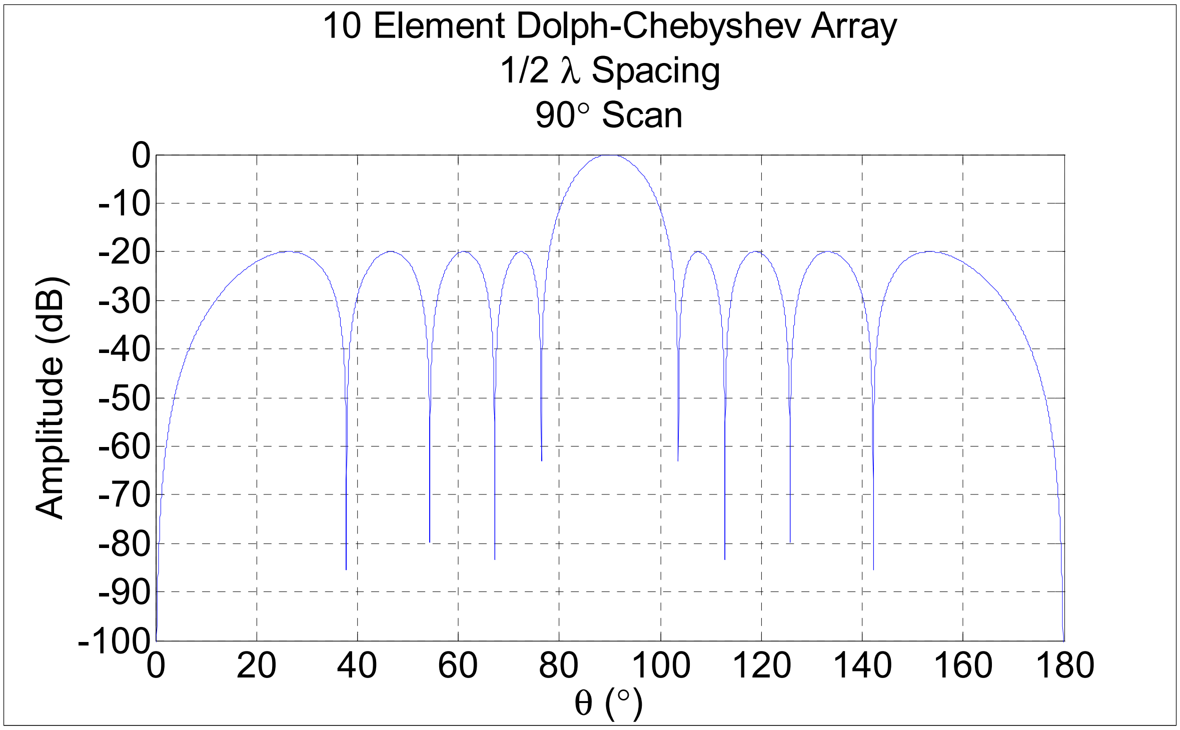

Figure 3.1. *Dolph-Chebyshev array factor for a 10 element,* $1/2\lambda$ *element spaced, broadside scanned (*$\theta_o = 90^o$*), 20 dB sidelobe linear array.*

This type of array factor is developed by mapping the zeros, between $\pm$ 1, of the Chebyshev polynomial argument to the zeros of the array factor, while the curve above 1 is mapped to the main beam. The Chebyshev polynomial definition is

$$T_m(x) = \begin{cases} (-1)^m \cos(m \cdot a\cosh|x|) & x < -1 \\ \cos[m \cdot a\cos(x)] & |x| \le 1 \\ \cos(m \cdot a\cosh|x|) & x > 1 \end{cases}. \tag{3.3}$$

In the case of array element spacing that is greater than or equal to $1/2\lambda$, the Chebyshev polynomial variable, x, is mapped to the array factor by the transformation

$$x = x_0 \cos\left(\frac{\psi}{2}\right) \tag{3.4}$$

where ψ is the array factor variable

$$\psi = k\hat{\mathbf{r}} \cdot \mathbf{r}_i = k\left(i - \frac{N}{2}\right)d\left(\cos\theta - \cos\theta_o\right) \tag{3.5a}$$

$$AF = \sum_{i=0}^{N} I_i e^{j\psi} \ . \tag{3.5b}$$

Utilizing the desired sidelobe level, x_0, is determined by

$$x_0 = \cosh\left[\frac{a\cosh(R)}{N}\right] \tag{3.6}$$

where R is the voltage sidelobe ratio (main beam/sidelobe level), for an N+1 element array. x_0 solves

$$R = T_N\left(x_0\right). \tag{3.7}$$

Once x_0 is determined, the $x_p{}'s$ that are the zeros of the Chebyshev polynomial of order m=N are calculated

$$x_p = \cos\left[\frac{\left(p - \frac{1}{2}\right)\pi}{N}\right], \quad p = 1,2,3 \ldots N\,. \tag{3.8}$$

The zeros of the Chebyshev polynomial are then mapped to the zeros of the array factor, z_p ,using (3.4).

$$z_p = e^{j\psi p} \tag{3.9a}$$

$$\psi_p = a\cos\left(\frac{x_p}{x_0}\right) \tag{3.9b}$$

The z_p's (roots) are used to determine the array amplitude coefficients. Array factor current coefficients, A_n , are the coefficients of a characteristic, polynomial equation whose roots are the z_p terms. The coefficients in decreasing polynomial order form the amplitude taper for the array from one end to the other. As a result, the larger coefficients are at the center of the array with generally decreasing amplitudes towards the ends. The amplitude taper from the above example is illustrated below.

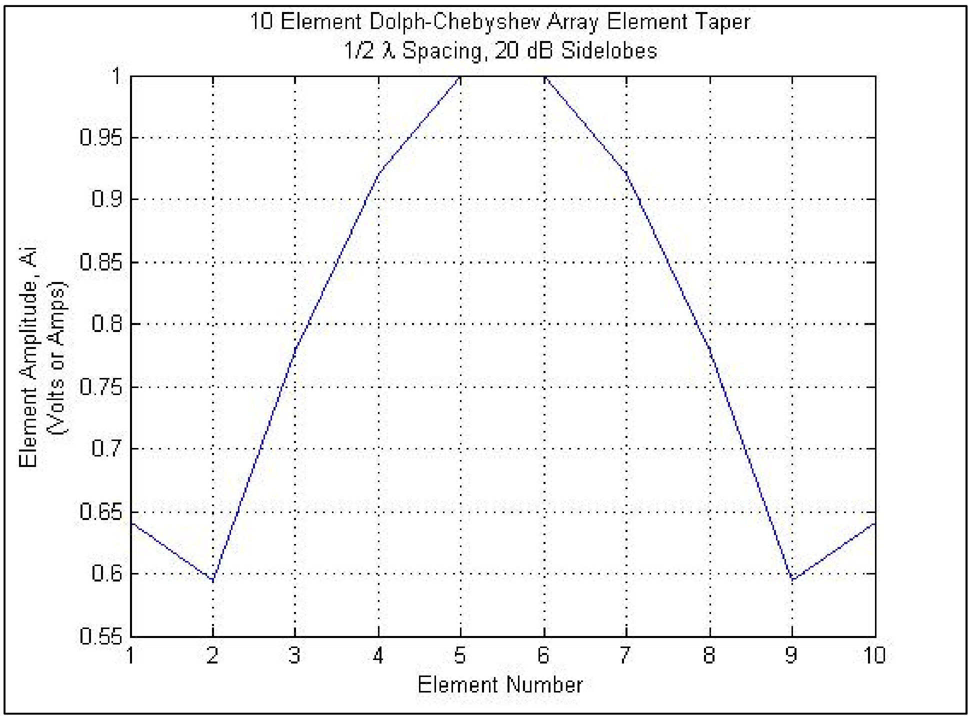

Figure 3.2. *Dolph-Chebyshev amplitude illumination taper for a 10 element,* $1/2\lambda$ *element spaced, 20 dB sidelobe linear array.*

3.4 Taylor

The Taylor distribution attempts to keep the peaks of the first $\bar{n}$ sidelobes of the antenna factor on either side of the main beam at an equal level. The sidelobe amplitude of the array factor then decays as the inverse of the argument of the array factor function. Expressions (3.10) govern the behavior of a Taylor taper over a linear array.

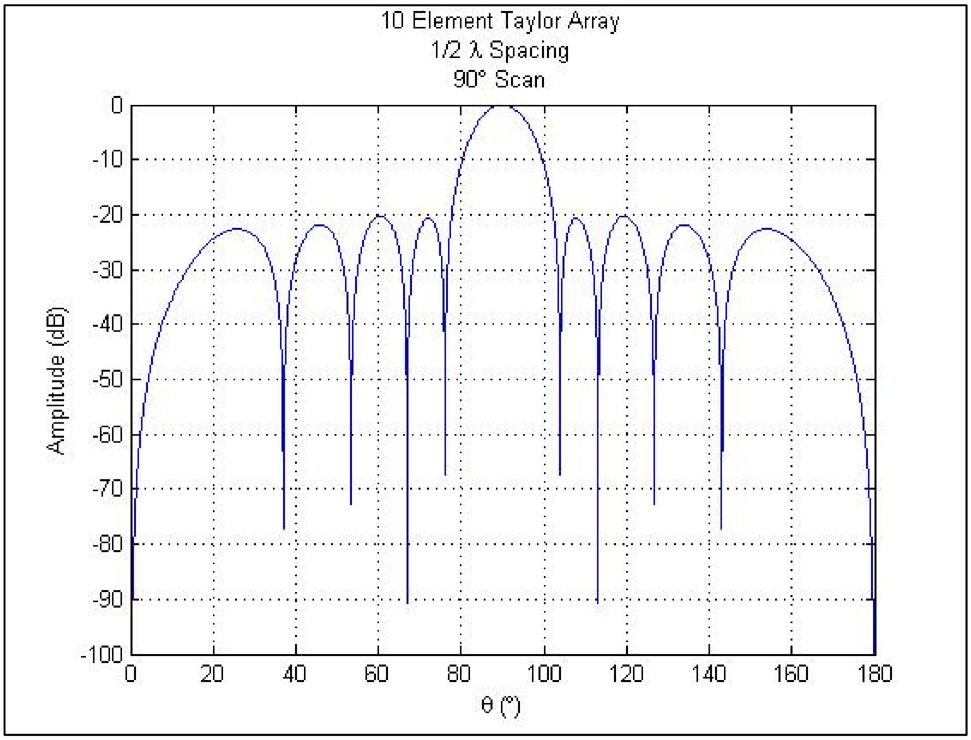

Figure 3.3. *Taylor array factor for a 10 element,* $1/2\lambda$ *element spaced, broadside scanned (*$\theta_o = 90^o$*), 20 dB sidelobe linear array.*

$$a\,(x, A, \bar{n}\,) = \frac{1}{2\pi}\left\{F(0, a, \bar{n}) + 2\sum_{n=1}^{\bar{n}-1} F(n, A, \bar{n})\, cos\left(\frac{n\pi x}{L}\right)\right\} \tag{3.10a}$$

$$F(n, A, \bar{n}) = \frac{[(\bar{n}-1)!]^2 \prod_{m=1}^{\bar{n}-1}\left(1 - \dfrac{n^2}{\sigma^2\left[A^2 + \left(m - \frac{1}{2}\right)^2\right]}\right)}{(\bar{n}-1+n)!\,(\bar{n}-1-n!)} \tag{3.10b}$$

$$A = \frac{1}{\pi}\, a\, cosh(R) \tag{3.10c}$$

$$\sigma = \frac{\bar{n}}{\sqrt{A^2 + \left(\bar{n} - \frac{1}{2}\right)^2}} \tag{3.10d}$$

where

a = the amplitude taper as a function of distance and $\bar{n}$

x = the distance from the center of the aperture

L = the half length of the aperture

$\bar{n}$ = the number of “equal” amplitude sidelobes adjacent to the main beam on one side, and

R = the design sidelobe voltage ratio (main beam over sidelobe level) [61] [62] [63].

Figure 3.3 illustrates the array factor for a 10 element, $1/2\lambda$ spacing, 20 dB sidelobe array with a Taylor taper. That same array factor is generated with the taper that is illustrated in Figure 3.4.

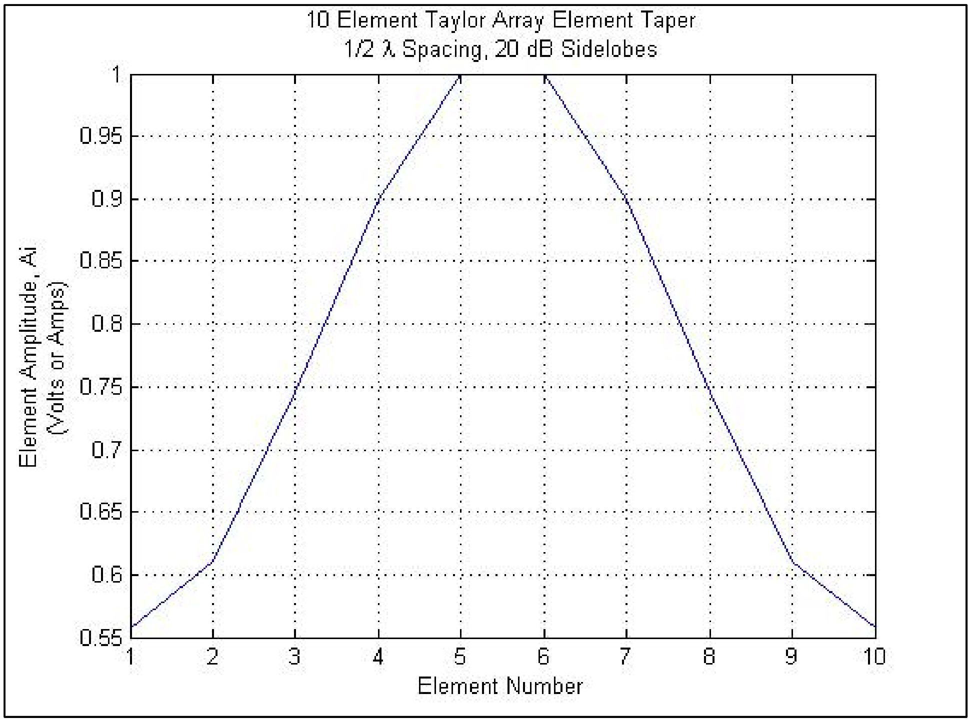

Figure 3.4. *Taylor amplitude illumination taper for a 10 element,* $1/2\lambda$ *element spaced, 20 dB sidelobe linear array.*

3.5 Modified Taylor

In a modified Taylor illumination, a single parameter, β , determined by the sidelobe level, governs the taper [64] [65] [66]

$$a(x) = J_o\left[j\pi\beta\sqrt{1-\left(\frac{2x}{L}\right)^2}\right] \qquad (3.11a)$$

where

a = the amplitude taper as a function of distance

x = the distance from the center of the aperture

L = the total length of the aperture

J_o = the zero-order Bessel function of the first kind

β solves the equation

$$R = 4.60333\,\frac{sin(\pi\beta)}{\pi\beta}, \tag{3.11b}$$

and R is the voltage ratio of the main beam amplitude to the amplitude of the first sidelobe. If we consider a 10 element array with $1/2\lambda$ spacing and 20 dB

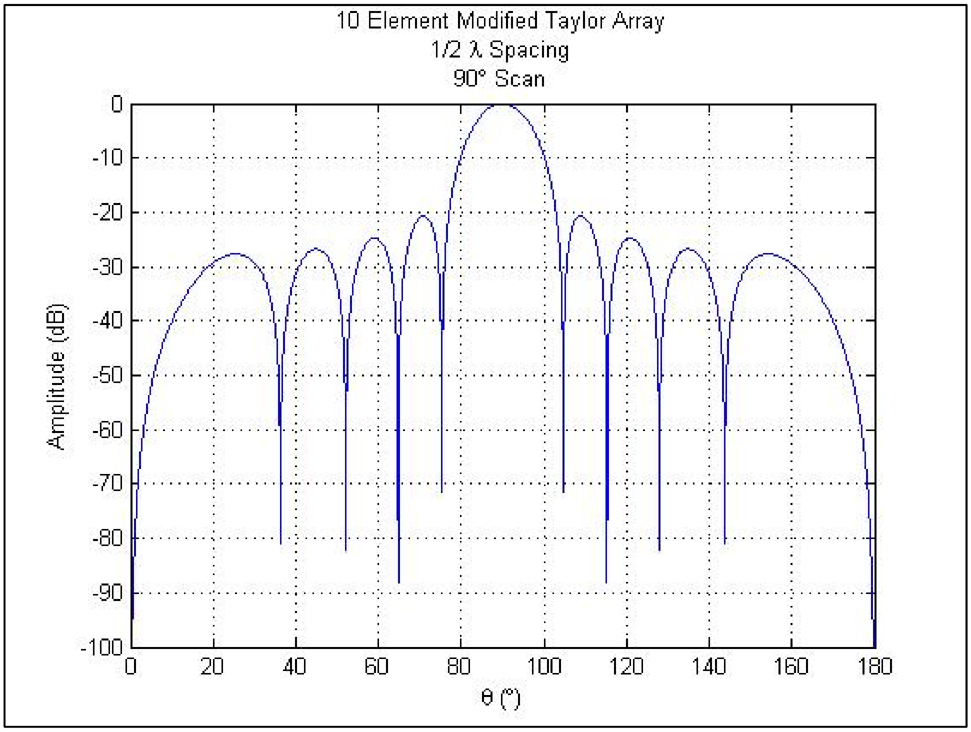

Figure 3.5. *Modified Taylor array factor for a 10 element, $1/2\lambda$ element spaced, broadside scanned ($\theta_o = 90^o$), 20 dB sidelobe linear array.*

sidelobes, a modified Taylor taper results in the array factor illustrated in Figure 3.5 utilizing the taper plotted in Figure 3.6 that was developed utilizing the above mathematics and an R value of 8.9125.

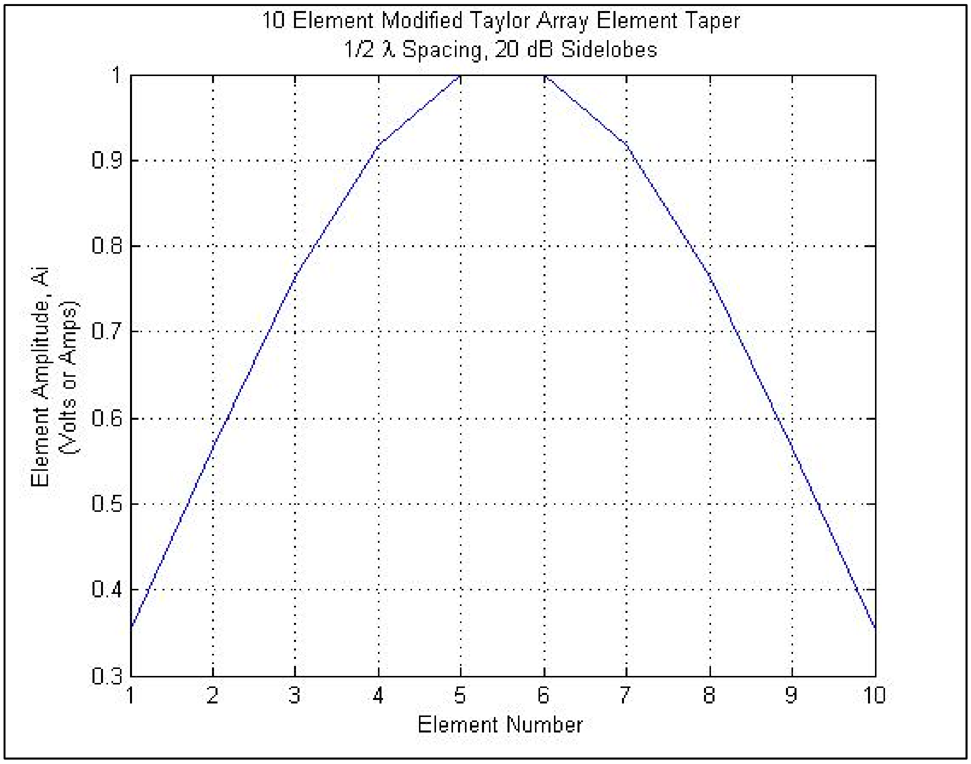

Figure 3.6. *Modified Taylor amplitude illumination taper for a 10 element,* $1/2\lambda$ *element spaced, 20 dB sidelobe linear array.*

3.6 Powers of Cosine on a Pedestal

The power of cosine on a pedestal taper is simply a cosine function raised to a known power that is set on a pedestal. The taper, a(x), is governed by 3.12. [67].

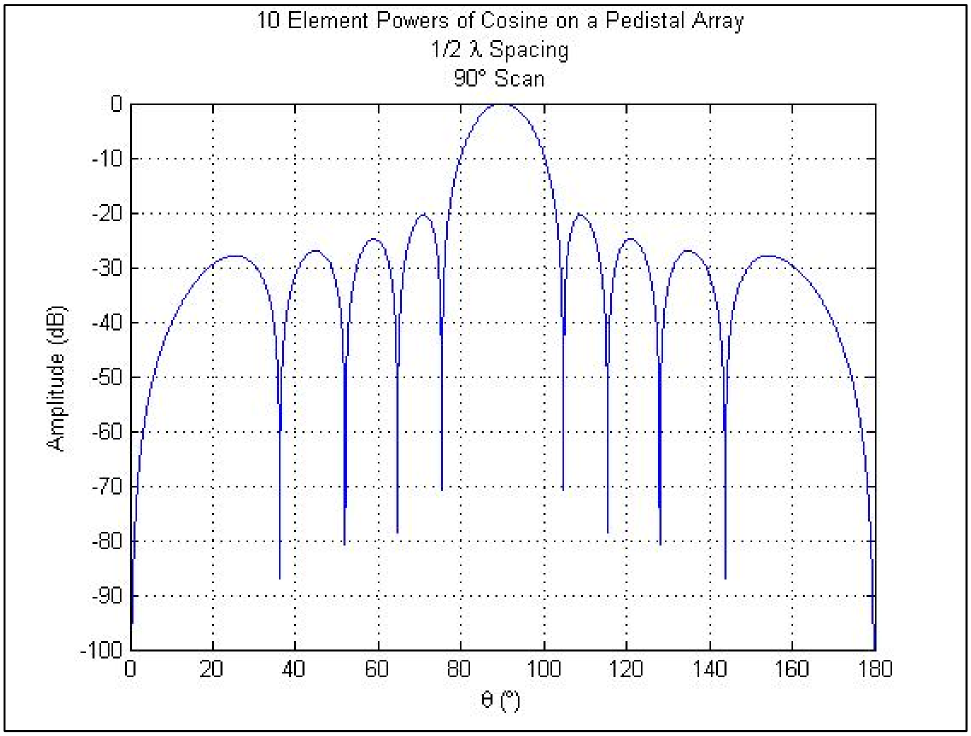

Figure 3.7. *Powers of cosine on a pedestal array factor for a 10 element,* $1/2\lambda$ *element spaced, broadside scanned (*$\theta_o = 90^o$*), 20 dB sidelobe linear array.*

$$a(x) = h + (1-h)\cos^m\left(\frac{\pi x}{L}\right) \tag{3.12}$$

where

x = the distance from the center of the aperture

L = the total length of the aperture

h = the normalized pedestal height, $0 \le h \le 1$

m = the cosine power.

For this taper, creating an array with $1/2\lambda$ spacing and 20 dB sidelobes requires 10 elements, an h value of 0.4, and an m value of 1. The array factor is illustrated in Figure 3.7 and the taper, in Figure 3.8.

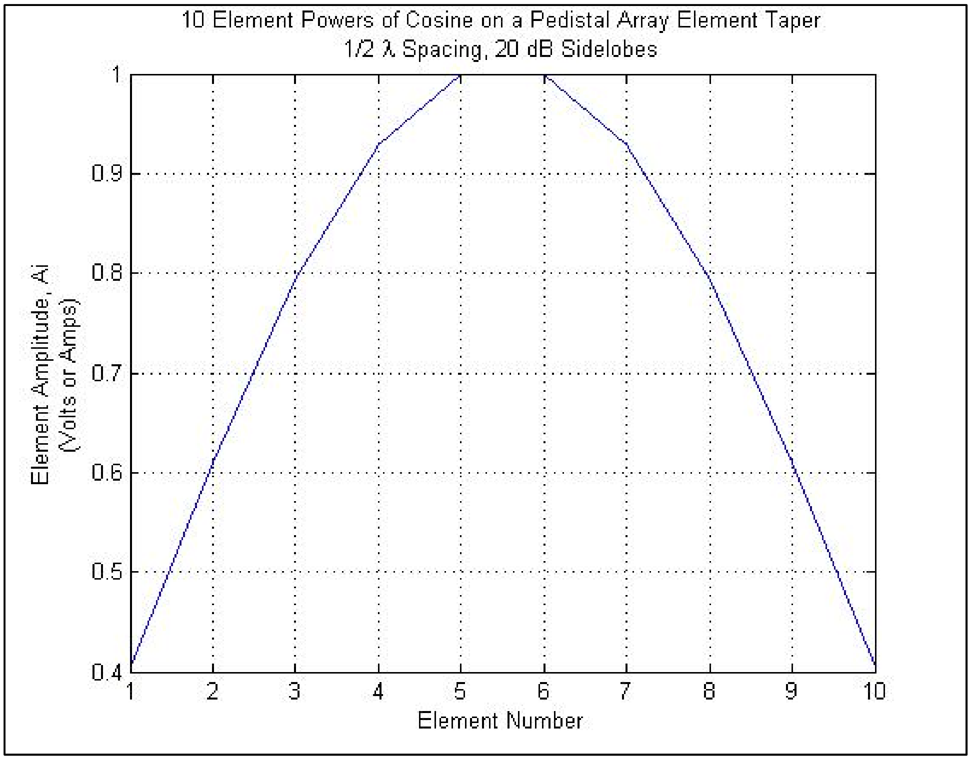

Figure 3.8. *Powers of cosine on a pedestal amplitude illumination taper for a 10 element, $1/2\lambda$ element spaced, 20 dB sidelobe linear array.*

4.0 Element Position Errors

4.1 Baseline Setup

This analysis considers antenna factors for linear arrays with uniform element spacing that are designed utilizing Dolph-Chebyshev, modified Taylor, powers of cosine on a pedestal, and Taylor tapers. Spacing is varied from $1/4\,\lambda$ to $7/8\,\lambda$ in $1/8\,\lambda$ increments. For each element spacing, arrays with modified Taylor, powers of cosine on a pedestal, and Taylor tapers are developed with sidelobe levels of 20, 30, 40, and 50 dB. For spacing of $1/2\,\lambda$ and greater, arrays with Dolph-Chebyshev tapers in addition to all of the above mentioned tapers are also developed for 20, 30, 40, and 50 dB sidelobes. Dolph-Chebyshev tapers on linear arrays with spacing of less than $1/2\,\lambda$ are scan dependent [68] and therefore not considered in this research for that reason. All of the array factor patterns are circularly symmetric. Since these are circularly symmetric structures about the z-axis, the patterns for the initial designs as described here will also be circularly symmetric about the z-axis, that is have no variation in ϕ. However, the array factors will have variation that is a function of θ. Due to the circular symmetry, scanning is only performed in θ cuts.

For each spacing/sidelobe level/taper combination, baseline array designs were developed. The array factors for each illumination type, were initially designed using the minimum number of elements possible to achieve the desired sidelobe level for scan angles within $\pm 50^{o}$ of broad side, in the visible region of the array for element spacings less than or equal to $1/2\,\lambda$. In cases where the spacing was $5/8\,\lambda$ or $3/4\,\lambda$, array designs were developed for scans up to $\pm 20^{o}$ and $\pm 10^{o}$, of broad side, respectively. The $7/8\lambda$ spacing array designs were developed for fixed broadside operation. This initial design set became the “Minimum Number of Elements” (MNE) designs for each spacing/sidelobe level combination.

A second set of arrays were subsequently designed where the same number of elements were utilized for each array illumination of a given desired spacing/sidelobe level. For each spacing/sidelobe level group, the largest number of elements for any array taper from the MNE design group was used for the second array design set for all tapers. The second set of illumination tapers are also designed to achieve the desired sidelobe levels, in the visible region of each array, for each taper type, and for the same scan angles as the MNE designs. This second group is referred to as the “Equal Number of Elements” (ENE) designs.

The result is two major comparisons: one among tapers with a minimal number of elements for a given spacing/sidelobe level and another among tapers with an equal number of elements for the same spacing/sidelobe level. Table 4.1 delineates the number of elements for each design. Table 4.2 illustrates similar information as Table 4.1, except in this case, the electrical length for each array case is documented in wavelengths (λ).

Spacing (λ)	Taper Type	Number of Array Elements							
		20 dB SLL		30 dB SLL		40 dB SLL		50 dB SLL	
		MNE	ENE	MNE	ENE	MNE	ENE	MNE	ENE
1/4	Modified Taylor	20	20	27	27	35	35	42	55
	Powers of Cosine on a Pedistal	19	20	25	27	32	35	55	55
	Taylor	19	20	25	27	32	35	39	55
3/8	Modified Taylor	14	14	18	18	24	24	28	37
	Powers of Cosine on a Pedistal	14	14	17	18	22	24	37	37
	Taylor	13	14	17	18	23	24	27	37
1/2	Dolph-Chebyshev	9	10	13	17	16	23	19	28
	Modified Taylor	10	10	15	17	18	23	22	28
	Powers of Cosine on a Pedistal	10	10	17	17	23	23	28	28
	Taylor	10	10	14	17	18	23	21	28
5/8	Dolph-Chebyshev	7	8	9	12	12	17	14	21
	Modified Taylor	8	8	11	12	14	17	16	21
	Powers of Cosine on a Pedistal	8	8	12	12	17	17	21	21
	Taylor	8	8	12	12	17	17	19	21
3/4	Dolph-Chebyshev	9	10	12	14	15	22	18	28
	Modified Taylor	10	10	14	14	18	22	21	28
	Powers of Cosine on a Pedistal	10	10	13	14	22	22	28	28
	Taylor	10	10	14	14	18	22	21	28
7/8	Dolph-Chebyshev	9	10	12	14	15	21	17	27
	Modified Taylor	10	10	14	14	17	21	20	27
	Powers of Cosine on a Pedistal	10	10	12	14	21	21	27	27
	Taylor	9	10	13	14	17	21	20	27

Table 4.1. *Number of array elements for each initial MNE and ENE design.* Element spacing, taper type, and sidelobe level are listed.

The development of the array taper parameters for the arrays listed in Tables 4.1 and 4.2, were created while examining the performance at the maximum scan angle from broadside (or $\theta = 90^o$). Scanning was investigated in 10^o increments. The scan angle that was the greatest multiple of 10^o away from broadside without introducing grading lobes in the visible region was established as the maximum scan angle for a particular element spacing. As mentioned earlier, for spacing less than or equal to $1/2\,\lambda$, $\pm 50^o$ of broad side, were the maximum scan angles considered. Limiting the array scan for the less than or equal to $1/2\,\lambda$ element spacing cases was more of an issue of main beam containment than grating lobe prevention. This way the entire main beam was contained within the visible spectrum between $\theta = 0^o$ or $\theta = 180^o$, and the pattern was at least as far down as the sidelobel level from the peak of beam at its endpoints. For array designs with $5/8\lambda$ or $3/4\lambda$ element spacing, $\pm 20^{o}$ and $\pm 10^{o}$, of broad side, respectively, were established as scan limits. In the case of $7/8\lambda$ element spacing, array designs were developed for fixed broadside operation only. Scan angle limits or the lack there of, for these last 3 spacing cases were primarily an issue of grating lobe prevention.

		Electrical Length (λ)							
Spacing	Taper Type	20 dB SLL		30 dB SLL		40 dB SLL		50 dB SLL	
(λ)		MNE	ENE	MNE	ENE	MNE	ENE	MNE	ENE
1/4	Modified Taylor	4.750	4.750	6.500	6.500	8.500	8.500	10.250	13.500
	Powers of Cosine on a Pedistal	4.500	4.750	6.000	6.500	7.750	8.500	13.500	13.500
	Taylor	4.500	4.750	6.000	6.500	7.750	8.500	9.500	13.500
3/8	Modified Taylor	4.875	4.875	6.375	6.375	8.625	8.625	10.125	13.500
	Powers of Cosine on a Pedistal	4.875	4.875	6.000	6.375	7.875	8.625	13.500	13.500
	Taylor	4.500	4.875	6.000	6.375	8.250	8.625	9.750	13.500
1/2	Dolph-Chebyshev	4.000	4.500	6.000	8.000	7.500	11.000	9.000	13.500
	Modified Taylor	4.500	4.500	7.000	8.000	8.500	11.000	10.500	13.500
	Powers of Cosine on a Pedistal	4.500	4.500	8.000	8.000	11.000	11.000	13.500	13.500
	Taylor	4.500	4.500	6.500	8.000	8.500	11.000	10.000	13.500
5/8	Dolph-Chebyshev	3.750	4.375	5.000	6.875	6.875	10.000	8.125	12.500
	Modified Taylor	4.375	4.375	6.250	6.875	8.125	10.000	9.375	12.500
	Powers of Cosine on a Pedistal	4.375	4.375	6.875	6.875	10.000	10.000	12.500	12.500
	Taylor	4.375	4.375	6.875	6.875	10.000	10.000	11.250	12.500
3/4	Dolph-Chebyshev	6.000	6.750	8.250	9.750	10.500	15.750	12.750	20.250
	Modified Taylor	6.750	6.750	9.750	9.750	12.750	15.750	15.000	20.250
	Powers of Cosine on a Pedistal	6.750	6.750	9.000	9.750	15.750	15.750	20.250	20.250
	Taylor	6.750	6.750	9.750	9.750	12.750	15.750	15.000	20.250
7/8	Dolph-Chebyshev	7.000	7.875	9.625	11.375	12.250	17.500	14.000	22.750
	Modified Taylor	7.875	7.875	11.375	11.375	14.000	17.500	16.625	22.750
	Powers of Cosine on a Pedistal	7.875	7.875	9.625	11.375	17.500	17.500	22.750	22.750
	Taylor	7.000	7.875	10.500	11.375	14.000	17.500	16.625	22.750

Table 4.2. *Electrical length of arrays (λ) for each initial MNE and ENE design.* Element spacing, taper type, and sidelobe level are listed.

While developing the array parameters for a given spacing/sidelobe level/taper, the furthest scan from broadside was considered. The number of elements and the individual taper parameters were adjusted to not only obtain the proper sidelobe level, but to also have a resultant array factor pattern that included the entire mainlobe as subsequently described. Achieving this requires that at either $\theta = 0^o$ or $\theta = 180^o$, whichever side the main beam is closest, the array factor amplitude would need to be at least as low as the sidelobe level. For example, when the array spacing is $1/4\,\lambda$ with the design sidelobe level of 50 dB and the parameters are optimized for a powers of cosine on a pedestal taper, a 55 element array when scanned to $\theta = 40^o$ produces an acceptable result at $\theta = 0^o$ with the amplitude being 51.9 dB below the peak of beam (Figure 4.1). Decreasing the number of elements by 1 while holding all the other parameters constant, results in an array factor amplitude of only 46.5 dB below the peak of beam at $\theta = 0^o$ (Figure 4.2). Hence a 55 element array was used as the baseline

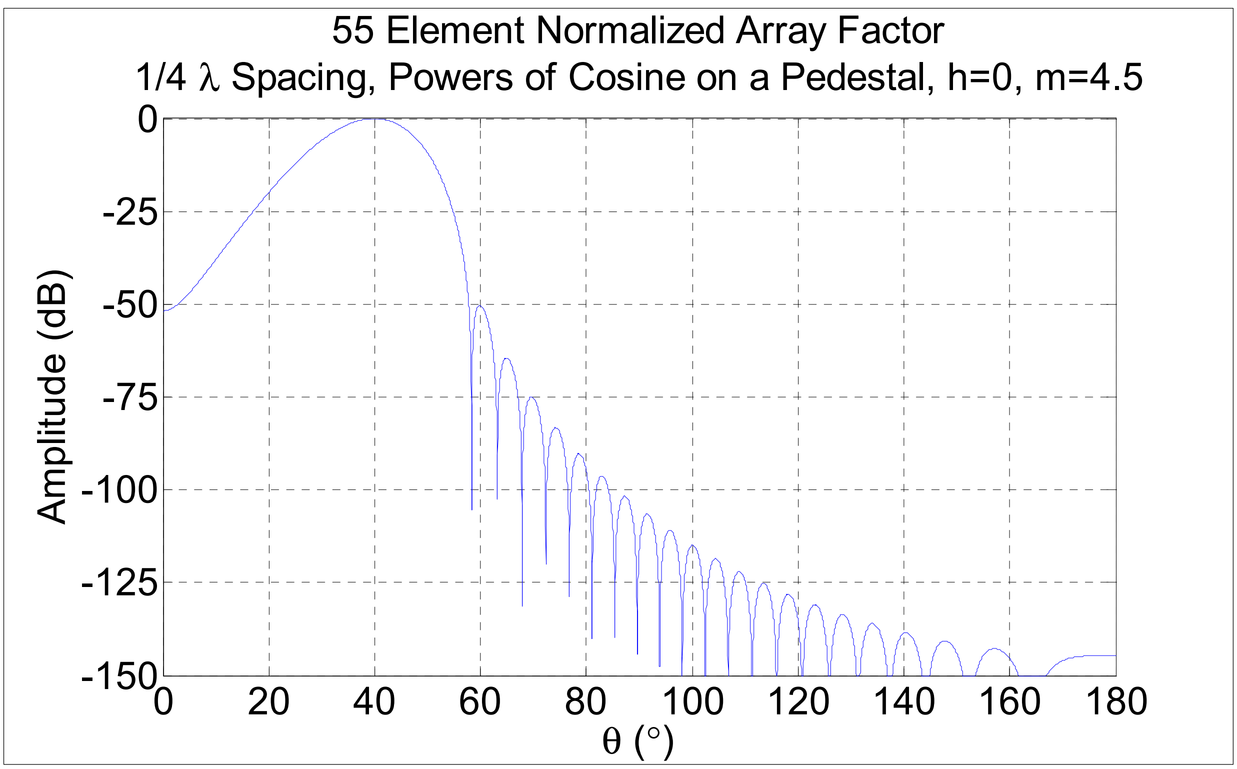

Figure 4.1. *Array factor for a $1/4\,\lambda$ spaced, 55 element powers of cosine on a pedestal taper.* The array factor amplitude at 0^o is -51.9 dB.

design for this spacing/sidelobe level/taper combination. This basic process of design was executed for every antenna array design listed in Tables 4.1 and 4.2.

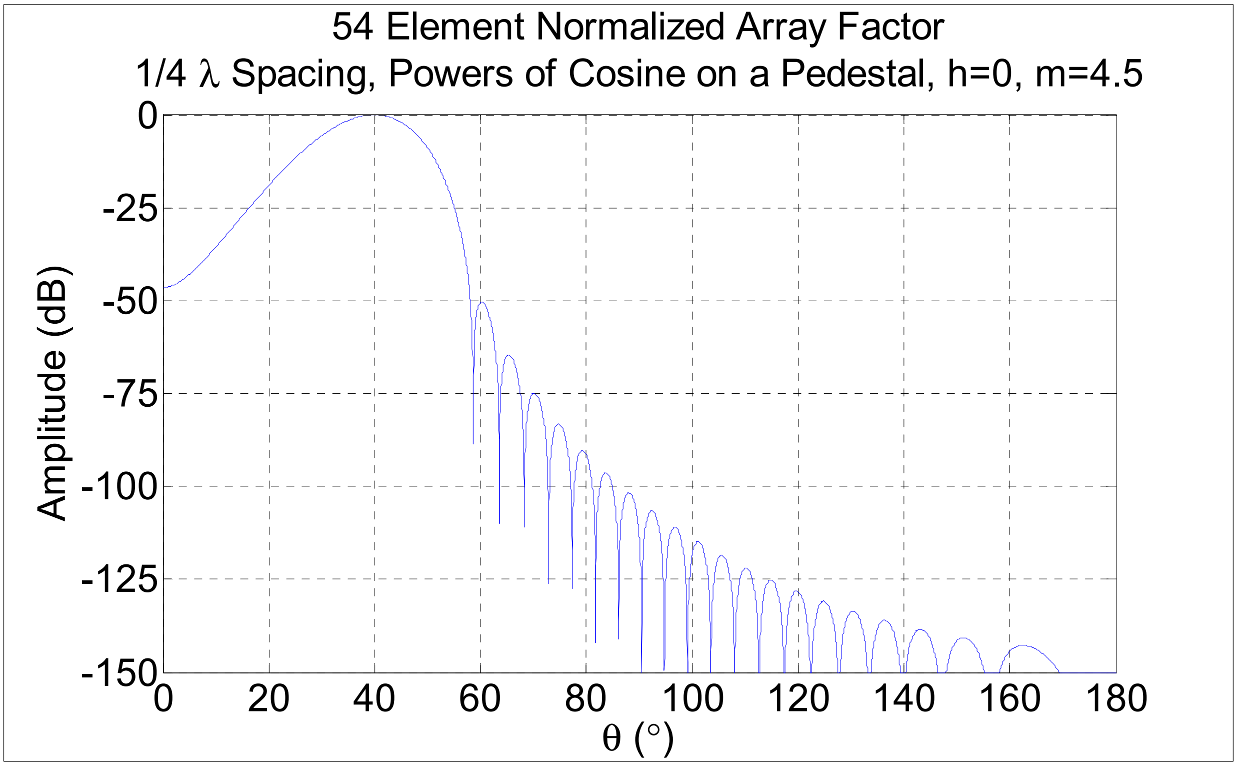

Figure 4.2. *Array factor for a* $1/4\,\lambda$ *spaced, 54 element powers of cosine on a pedestal taper.* The array factor amplitude at 0^{o} is -46.5 dB.

Taper parameters of each design are identified in Table 4.3. For illumination tapers that explicitly utilized a desired sidelobe level as an input (Dolph-Chebyshev, modified Taylor and Taylor), the sidelobe level was adjusted in 1 dB increments when trying to establish the minimum number of elements design. In all cases of the Taylor illumination taper, in (3.10), $\bar{n}$ was adjusted in increments of 1 along with the 1 dB resolution of the design sidelobe level ($20\,log_{10}\,R$), to establish the minimum number of elements required to meet the sidelobe level requirement. It was also an objective to minimize $\bar{n}$ in the process as well. For arrays utilizing the powers of cosine on a pedestal, h and m from (3.12) were adjusted in increments of 0.1 when optimizing the array designs.

			Taper Parameters							
Spacing	Taper		20 dB SLL		30 dB SLL		40 dB SLL		50 dB SLL	
(λ)	Type	Parameter	MNE	ENE	MNE	ENE	MNE	ENE	MNE	ENE
1/4	Modified Taylor	SLL	20	20	29	29	40	40	51	51
	Powers of Cosine on a Pedestal	h	0.4	0.4	0.2	0.2	0.1	0.1	0.0	0.0
		m	1.1	1.1	1.5	1.5	0.8	1.8	4.5	4.5
	Taylor	SLL	19	19	30	30	40	40	50	50
		$\bar{n}$	2	2	4	4	6	6	9	8
3/8	Modified Taylor	SLL	20	20	28	28	40	40	51	51
	Powers of Cosine on a Pedestal	h	0.4	0.4	0.2	0.2	0.1	0.1	0.0	0.0
		m	1.1	1.1	1.5	1.5	1.8	1.8	4.5	4.5
	Taylor	SLL	20	19	30	30	41	41	52	51
		$\bar{n}$	2	2	4	4	6	6	9	8
1/2	Dolph-Chebyshev	SLL	20	20	30	30	40	40	50	50
	Modified Taylor	SLL	19	19	28	28	40	39	51	51
	Powers of Cosine on a Pedestal	h	0.4	0.4	0.0	0.0	0.0	0.0	0.0	0.0
		m	1.0	1.0	1.9	1.9	3.2	3.2	4.5	4.5
	Taylor	SLL	19	19	31	30	42	41	56	52
		$\bar{n}$	2	2	5	4	7	6	7	9
5/8	Dolph-Chebyshev	SLL	20	20	30	30	40	40	50	50
	Modified Taylor	SLL	19	19	27	27	39	39	51	51
	Powers of Cosine on a Pedestal	h	0.4	0.4	0.1	0.1	0.0	0.0	0.0	0.0
		m	0.9	0.9	1.9	1.9	3.1	3.1	4.5	4.5
	Taylor	SLL	21	21	32	32	44	44	55	54
		$\bar{n}$	2	2	4	4	5	5	10	9
3/4	Dolph-Chebyshev	SLL	20	20	30	30	40	40	50	50
	Modified Taylor	SLL	19	19	28	28	39	39	51	51
	Powers of Cosine on a Pedestal	h	0.3	0.3	0.2	0.2	0.0	0.0	0.0	0.0
		m	0.8	0.8	1.4	1.4	3.1	3.1	4.5	4.5
	Taylor	SLL	19	19	31	31	44	42	55	52
		$\bar{n}$	2	2	4	4	5	5	8	8
7/8	Dolph-Chebyshev	SLL	20	20	30	30	40	40	50	50
	Modified Taylor	SLL	19	19	28	28	39	39	51	51
	Powers of Cosine on a Pedestal	h	0.3	0.3	0.2	0.2	0	0	0	0
		m	0.8	0.8	1.4	1.4	3.1	3.1	4.5	4.5
	Taylor	SLL	20	19	32	31	43	42	56	53
		$\bar{n}$	2	2	4	4	6	6	8	8

Table 4.3. *Taper parameters for each array design identified in Tables 4.1 and 4.2.*

Once all the array factors were established, parametrics of each design were determined. Directivity, sidelobe level, 3 dB beamwidth, 10 dB beamwidth, and first null beamwidth (FNB) were measured for each scan angle of each pattern. These initial performance metrics are displayed in Appendix A, tables A.1 through A.24.

Calculating these antenna factors and their metrics, involved some numerical considerations and methodologies beyond the electromagnetic array factor theory such as sampling interval and available computer RAM (4 GB or less). Due to the previously mentioned circular symmetry about the z-axis, the array factors will only have variation that is a function of θ. This brings up the question of the sampling interval for θ when calculating array factors. In order to not miss any "high frequency" θ variation in the array factor pattern, the θ increment for calculating the 3-dimensional array factor was highly oversampled at 0.03125^{o} (1/32nd of a degree). Since no variation in ϕ is present in these initial patterns, ϕ was incremented in 10^{o} steps. The 10^{o} steps were utilized to facilitate creating a 3-dimensional plot of the pattern if this became necessary. As a result, the array factor was calculated on 207,396 points over spherical (θ,ϕ) space for each array design delineated in Tables 4.1 through 4.3. This calculation was containable with the available 4 GB RAM, but adding too many intervals in ϕ without reducing the number of points in θ would result in an "insufficient memory" issue.

With the available pattern data, the performance parameters listed in Tables A.1 through A.24 were calculated. The most numerically consuming calculation is the directivity integral (4.1) [69].

$$D = \frac{4\pi}{\Omega_A} \tag{4.1a}$$

$$\Omega_A = \int_0^{2\pi}\int_0^{\pi} \left|AF(\theta,\phi)\right|^2 \sin\theta d\theta d\phi \tag{4.1b}$$

(4.1) is numerically approximated as a 2 dimensional integral over 2 polar coordinate systems that utilized triangular approximations of the array factor pattern function variation between the 207,396 spherical points that it was calculated over.

Initial peak of beam directions were simply verified to match the designed scan angle. For the $\phi = 0^o$ cut of each array design, the sidelobe level, 3 dB, 10 dB and First Null Beamwidths (FNB's) were determined for each scan angle. These last four parameters were the results of controlled criteria searches over the $\phi = 0^o$ cut of the array factor pattern.

4.2 Array Element Position Randomization

With the baseline array designs developed, the question of degradation resulting from random element position movement about their nominal locations was investigated. The motivation comes from the very definition of a distributed array (see Chapter 1, Section 3).

This portion of the analysis was performed for each array design at each θ scan angle. Each array was analyzed as though each element were randomly located within a constrained volume of its desired design position. In Figure 4.3(a), a linear array is illustrated with its elements located randomly within a spherical volume centered about their optimum positions. This is illustrated in expanded fashion in Figure 4.3(b) about a single element of an array. Its position can be anywhere within or on a sphere of radius r_ε centered at the optimum element position. Although the elements are illustrated as having a finite volume for visual purposes, they are in fact point sources without volume.

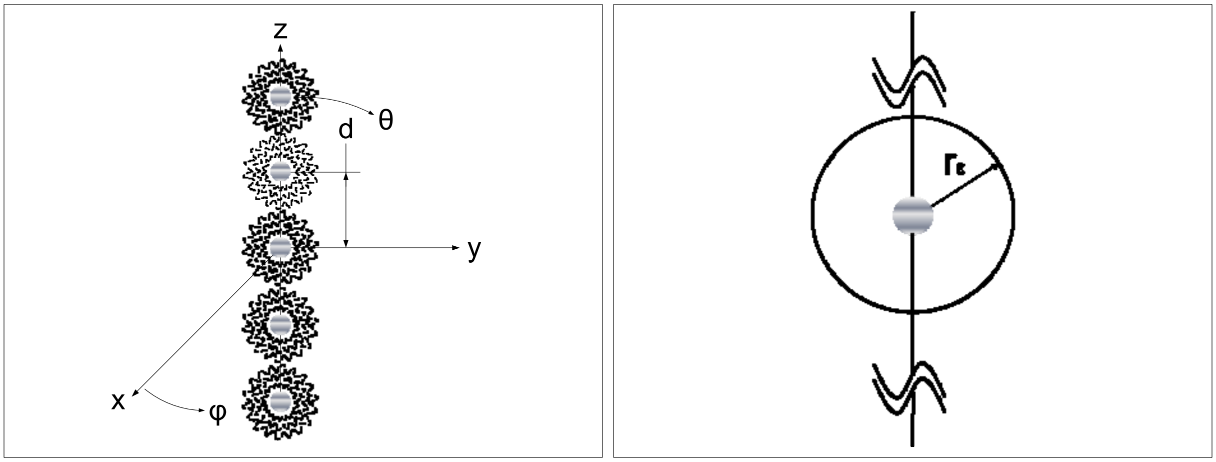

(a) (b)

Figure 4.3. *A linear array shown with its elements randomly located.* The elements are located within a constrained volume of their nominal position. All elements of the full array are shown (a), with one element illustrated in expanded fashion indicating the maximum extent of position uncertainty, r_ε ,(b).

To further clarify, several linear arrays have been designed assuming perfect placement of the elements. These designs have been reanalyzed while allowing the elements to be randomly located at positions within a volume of a known radius of their optimum location for each scan angle.

With random locations of the elements, random processes need to be considered. Constraints need to be established on the random process for the calculations. Alternatively expressed, a method of randomly locating any array element within a sphere of radius r_ε of its nominal, original position must be established including identification and definition of random variables. The approach taken to vary each element location was driven from an element specific view point. Consider Figure 4.3(b). If an element centric coordinate system is considered, a random vector defined by $\mathbf{P}(R,\Theta,\Phi)$ added to the optimum element location $\mathbf{r}_i$ can define a random position for a given element.

$$\mathbf{r}_{ir} = \mathbf{r}_i + \mathbf{P}\ ;\ |\mathbf{P}| \le r_\varepsilon \tag{4.2}$$

(R,Θ,Φ) is a spherical coordinate relative to an array element origin. R, Θ, and Φ are each chosen to be uniform random variables. R spans $[-r_\varepsilon, r_\varepsilon]$. Θ spans $[0{,}90]$ degrees. And Φ spans $[0{,}360)$ degrees. The negative values of R work in conjunction with the fact that Θ is limited to $[0{,}90]$ instead of $[0{,}180]$ degrees. A negative value of R simply means that Θ is treated as $180-\Theta$. Applying a transformation to convert $\mathbf{P}(R,\Theta,\Phi)$ into Cartesian coordinates given (R,Θ,Φ) is done in the usual method even though R can take on negative values.

$$\mathbf{P}(X,Y,Z) = X(R,\Theta,\Phi)\hat{x} + Y(R,\Theta,\Phi)\hat{y} + Z(R,\Theta) \tag{4.3a}$$

$$X(R,\Theta,\Phi) = R\, sin\,\Theta\, cos\,\Phi \tag{4.3b}$$

$$Y(R,\Theta,\Phi) = R\, sin\,\Theta\, sin\,\Phi \tag{4.3c}$$

$$Z(R,\Theta) = R\, cos\,\Theta \tag{4.3d}$$

Due to the transformation in 4.3, X, Y, and Z are not uniform random variables.

In this research, the calculations were performed using MATLAB, Version 7.12.0.635 (R2011a), 32 bit [70]. Three random variables were calculated using the rand(m,n) function with m set to 1 and n set to the number of elements in the array that were being position randomized. Each output was separately rescaled for the valid intervals of R, Θ, and Φ resulting in 3 random vectors representing R, Θ, and Φ. Each element of the R, Θ, or Φ vector corresponded to an element in the array. Having established each $\mathbf{P}(R,\Theta,\Phi)$, it was then transformed into $\mathbf{P}(X,Y,Z)$ using

(4.3). Each $\mathbf{r}_{ir}$ was calculated using (4.2), and each AF was calculated for each array randomization using (2.14) and (2.18) with each $\mathbf{r}_{ir}$ utilized in place of each $\mathbf{r}_i$. The AF's were recalculated utilizing 100 sets of randomizations for each array design. They were recalculated for every scan angle with the same 100 randomizations of position for each element. However, every array design did not use the same set of element position randomizations. The same values of A_i and α_i were utilized in every randomized array as were originally used in the baseline array designs.

In this process, the only real independent variable is r_ε. r_ε was varied as fractions of a wavelength in a quasi-logarithmic fashion. The values of r_ε were 0.00010 λ, 0.00025 λ, 0.00050 λ, 0.00075 λ, 0.00100 λ, 0.00250 λ, 0.00500 λ, 0.00750 λ, 0.01000 λ, 0.02500 λ, 0.05000 λ, 0.07500 λ, and 0.10000 λ. For every array scan angle, there are an additional 13 sets of AF data containing 100 repetitions of randomization as described above.

4.3 Performance Degradation Metrics

Once $AF's$ were calculated for arrays with randomized elements, several metrics were calculated from the pattern data. Recall that baseline performance data of all the studied arrays is laid out in Appendix A. Performance characteristics were calculated as deviations or deltas from the baseline results. Mean and standard deviations of the metric deltas from the baseline arrays were calculated for several parameters. The parameters of interest include all of the documented parameters in Appendix A. plus some additional items also listed in Table 4.4. Table 4.5 lists the explicit formulas used to calculate the parameters in Table 4.4. All of these parameters were calculated from the $(0 \leq \theta \leq 180, \phi = 0)$ plane of the associated array factor patterns.

Parameter	Definition
DdBDeltasM	Mean of the directivity differences in dB from the baseline result.
DdBDeltasS	The square root of the unbiased estimator of the variance (standard deviation) of the directivity differences in dB from the baseline result.
SLLdBDeltasM	Mean of the SideLobe Level differences in dB from the baseline result.
SLLdBDeltasS	The square root of the unbiased estimator of the variance (standard deviation) of the SideLobe Level differences in dB from the baseline result.
LSLLdBOrigFrsM	Large SideLobe Level dB Original Fraction Mean - Angular span of sidelobes that are larger than the baseline SideLobe Level divided by the angular span of the original baseline sidelobes (180 -FNB). Mean of this ratio over the randomized population.
LSLLdBOrigFrsS	Large SideLobe Level dB Original Fraction Standard Deviation - Angular span of sidelobes that are larger than the baseline SideLobe Level divided by the angular span of the original baseline sidelobes (180 -FNB). The square root of the unbiased estimator of the variance (standard deviation) of this ratio over the randomized population.
LSLLdBErrFrsM	Large SideLobe Level dB position Error Fraction Mean - Angular span of sidelobes that are larger than the baseline SideLobe Level divided by the angular span of the randomized array sidelobes (180 -FNB). Mean of this ratio over the randomized population.
LSLLdBErrFrsS	Large SideLobe Level dB position Error Fraction Standard Deviation - Angular span of sidelobes that are larger than the baseline SideLobe Level divided by the angular span of the randomized array sidelobes (180 -FNB). The square root of the unbiased estimator of the variance (standard deviation) of this ratio over the randomized population.
ThPkAngDeltasM	Mean of the peak of beam differences in degrees from the baseline result.

Table 4.4. Statistical parameters of the randomization analysis.

Table 4.4. (cont'd)

Parameter	Definition
ThPkAngDeltasS	The square root of the unbiased estimator of the variance (standard deviation) of the peak of beam differences in degrees from the baseline result.
Bwidth3DeltasM	Mean of the 3 dB beamwidth differences in degrees from the baseline result.
Bwidth3DeltasS	The square root of the unbiased estimator of the variance (standard deviation) of the 3 dB beamwidth differences in degrees from the baseline result.
Bwidth10DeltasM	Mean of the 10 dB beamwidth differences in degrees from the baseline result.
Bwidth10DeltasS	The square root of the unbiased estimator of the variance (standard deviation) of the 10 dB beamwidth differences in degrees from the baseline result.
FNBDeltasM	Mean of the First Null Beamwidth differences in degrees from the baseline result.
FNBDeltasS	The square root of the unbiased estimator of the variance (standard deviation) of the First Null Beamwidth differences in degrees from the baseline result.

Of the parameters listed in Tables 4.4 and 4.5, the majority should be very recognizable to those skilled in the art. However, LSLLdBOrigFrsM, LSLLdBOrigFrsS, LSLLdBErrFrsM, and LSLLdBErrFrsS may not be so obvious. These parameters speak to the issue that when there are many small variations in the current distribution of an antenna system, the result manifests itself as few variations over narrow angular sectors of the pattern. This comes from the Fourier Transform nature of the relationship between the current distribution of an antenna and its radiation pattern. This is evidenced in (2.11d). Rewritten below as (4.4), it is evident that the AF is a Fourier Transform except for a scale factor. Equation (4.4) has been simplified into a discrete form since the current distribution only exists over a finite number points.

$$AF = \sum_{i=0}^{N} I_i e^{jk\hat{\mathbf{r}} \cdot \mathbf{r}_i} \tag{4.4}$$

Parameter	Formula
DdBDeltasM	$DdBErr\,(n)$ = Directivity of the n[th] randomization run in dB, using (4.1). DdB = Directivity of baseline result in dB, using (4.1). $DdBDelta(n) = DdBErr(n) - DdB$. $DdBDeltasM = \left(\frac{1}{n}\right)\sum_{i=1}^{n} DdBDelta\,(n);\ n = 100$
DdBDeltasS	$DdBDeltasS = \left\{\left(\frac{1}{n-1}\right)\sum_{i=1}^{n}[DdBDelta(n) - DdBDeltasM]^2\right\}^{\frac{1}{2}};$ $n = 100$
SLLdBDeltasM	$SLLdBErr\,(n)$ = SideLobe Level of the n[th] randomization run in dB. $SLLdB$ = SideLobe Level of baseline result in dB. $SLLdBDelta(n) = SLLdBErr(n) - SLLdB$. $SLLdBDeltasM = \left(\frac{1}{n}\right)\sum_{i=1}^{n} SLLdBDelta\,(n);\ n = 100$
SLLdBDeltasS	$SLLdBDeltasS = \left\{\left(\frac{1}{n-1}\right)\sum_{i=1}^{n}[SLLdBDelta(n) - SLLdBDeltasM]^2\right\}^{\frac{1}{2}};$ $n = 100$
LSLLdBOrigFrsM	$LSLLdBOrigFrs(n)$ = LSLLdBOrigFrs of the n[th] randomization run. $LSLLdBOrigFrsM = \left(\frac{1}{n}\right)\sum_{i=1}^{n} LSLLdBOrigFrs(n);\ n = 100$
LSLLdBOrigFrsS	$LSLLdBOrigFrsS =$ $\left\{\left(\frac{1}{n-1}\right)\sum_{i=1}^{n}[LSLLdBOrigFrs(n) - LSLLdBOrigFrsM]^2\right\}^{\frac{1}{2}};$ $n = 100$

Table 4.5. *Mathematical formulas for the statistical parameters of the randomization analysis.*

Table 4.5. (cont'd)

Parameter	Formulas
LSLLdBErrFrsM	$LSLLdBErrFrs(n)$ = LSLLdBErrFrs of the n^{th} randomization run. $LSLLdBErrFrsM = \left(\frac{1}{n}\right)\sum_{i=1}^{n} LSLLdBErrFrs(n);\ n = 100$
LSLLdBErrFrsS	$LSLLdBErrFrsS =$ $\left\{\left(\frac{1}{n-1}\right)\sum_{i=1}^{n}[LSLLdBErrFrs(n) - LSLLdBErrFrsM]^2\right\}^{\frac{1}{2}};$ $n = 100$
ThPkAngDeltasM	$ThPkAngErr(n)$ = Theta Peak Angle of the n^{th} randomization run in degrees. $ThPkAng$ = Theta Peak Angle of baseline array in degrees. $ThPkAngDelta(n) = ThPkAngErr(n) - ThPkAng.$ $ThPkAngDeltasM = \left(\frac{1}{n}\right)\sum_{i=1}^{n} ThPkAngDelta(n);\ n = 100$
ThPkAngDeltasS	$ThPkAngDeltasS =$ $\left\{\left(\frac{1}{n-1}\right)\sum_{i=1}^{n}[ThPkAngDelta(n) - ThPkAngDeltasM]^2\right\}^{\frac{1}{2}};$ $n = 100$
Bwidth3DeltasM	$Bwidth3Err(n)$ = 3 dB Beamwidth of the n^{th} randomization run in degrees. $Bwidth3$ = 3 dB Beamwidth of the baseline array in degrees. $Bwidth3Delta(n) = Bwidth3Err(n) - Bwidth3.$ $Bwidth3DeltasM = \left(\frac{1}{n}\right)\sum_{i=1}^{n} Bwidth3Delta(n);\ n = 100$
Bwidth3DeltasS	$Bwidth3DeltasS =$ $\left\{\left(\frac{1}{n-1}\right)\sum_{i=1}^{n}[Bwidth3Delta(n) - Bwidth3DeltasM]^2\right\}^{\frac{1}{2}};$ $n = 100$

Table 4.5. (cont'd)

Parameter	Formulas
Bwidth10DeltasM	$Bwidth10Err(n)$ = 10 dB Beamwidth of the nth randomization run in degrees. $Bwidth10$ = 10 dB Beamwidth of the baseline array in degrees. $Bwidth10Delta(n) = Bwidth10Err(n) - Bwidth10.$ $Bwidth10DeltasM = \left(\frac{1}{n}\right)\sum_{i=1}^{n} Bwidth10Delta(n);\ n = 100$
Bwidth10DeltasS	$Bwidth10DeltasS =$ $\left\{\left(\frac{1}{n-1}\right)\sum_{i=1}^{n}[Bwidth10Delta(n) - Bwidth10DeltasM]^2\right\}^{\frac{1}{2}};$ $n = 100$
FNBDeltasM	$FNBErr(n)$ = First Null Beamwidth of the nth randomization run in degrees. FNB = First Null Beamwidth of the baseline array in degrees. $FNBDelta(n) = FNBErr(n) - FNB.$ $FNBDeltasM = \left(\frac{1}{n}\right)\sum_{i=1}^{n} FNBDelta(n);\ n = 100$
FNBDeltasS	$FNBDeltasS =$ $\left\{\left(\frac{1}{n-1}\right)\sum_{i=1}^{n}[FNBDelta(n) - FNBDeltasM]^2\right\}^{\frac{1}{2}};$ $n = 100$

In the linear arrays studied, variations in position constitute variations in the current distribution. When the randomization of spatial variation of element positions occurs at a fairly constant rate, the AF deviations from the baseline pattern will be narrow in angular span. When the randomization of position variations occur at varying rates, the impact to the pattern will be over a wider angular span of the AF, as compared to the baseline result. LSLLdBOrigFrsM, LSLLdBOrigFrsS, LSLLdBErrFrsM, and LSLLdBErrFrsS attempt to measure the impact of this phenomenon as it affects the angular span of the sidelobes that are adversely affected by array element position randomization. Potentially, this could be one of the key results that system designers would use in order to determine how much performance degradation can be tolerated before the system performance is inadequate.

The concept is illustrated in Figures 4.4 and 4.5. Figure 4.4(a) illustrates the normalized AF of a 9 element, $1/2\,\lambda$ spacing, array with a 20 dB Dolph-Chebyshev taper without any randomization. Note that the pattern is rotationally symmetrical in ϕ. The sidelobe level for this array is exactly 20 dB. The sidelobe level can be verified in the zoomed in plot about the -20 dB amplitude line in Figure 4.4(b). Figure 4.5(a) illustrates the AF of the same array with randomization allowed. In all of the research herein, when element positions are randomized, only the AF patterns over θ for $\phi = 0$ are examined. In this particular case r_{ε} is limited to 0.00100 λ. As can be seen from the zoomed in plot about the -20 dB amplitude line in Figure 4.5(b), parts of the element randomized AF do not meet the 20 dB sidelobe level of the original AF. In Figure 4.5(b), the FNB (First Null Beamwidth) is labeled between two arrows. Also in Figure 4.5(b), the angular extent where one of the sidelobes fails to meet the sidelobe level of the original AF (-20 dB amplitude in this case) is also labeled as LSLL (Large SideLobe Level). When determining LSLLdBOrigFrsM, LSLLdBOrigFrsS, LSLLdBErrFrsM, or LSLLdBErrFrsS, the LSLL beamwidths of all large sidelobes are summed for each individually element randomized AF. This value is referred to as $LSLLdBErr(n)$ for the nth randomization run. Dividing $LSLLdBErr(n)$ by the quantity $(180 - FNB)$ from the original baseline AF results in the quantity $LSLLdBOrigFrs(n)$

(Frs refers to Fraction). Division of $LSLLdBErr(n)$ by $[180 - FNBErr(n)]$ from the AF of the n^th randomization (or position error) run results in the quantity $LSLLdBErrFrs(n)$. Expression (4.5) summarize the above. Means and standard deviations are calculated as outlined in Table 4.5.

In (4.5), when referring to element position randomization $AF's$, the AF is considered only for θ over $\phi = 0$. Any quantity noted with (n) at the end refers to a result from a single array element position randomization AF.

$LSLLdBErr(n)$ = The summed angular extent of all sidelobes that do not meet the SideLobe Level of the baseline AF (4.5a)

FNB = The First Null Beamwidth of the baseline array AF (4.5b)

$FNB(n)$ = The First Null Beamwidth of the element position randomized AF (4.5c)

$$LSLLdBOrigFrs(n) = \frac{LSLLdBErr(n)}{180 - FNB} \quad (4.5d)$$

$$LSLLdBErrFrs(n) = \frac{LSLLdBErr(n)}{180 - FNB(n)} \quad (4.5e)$$

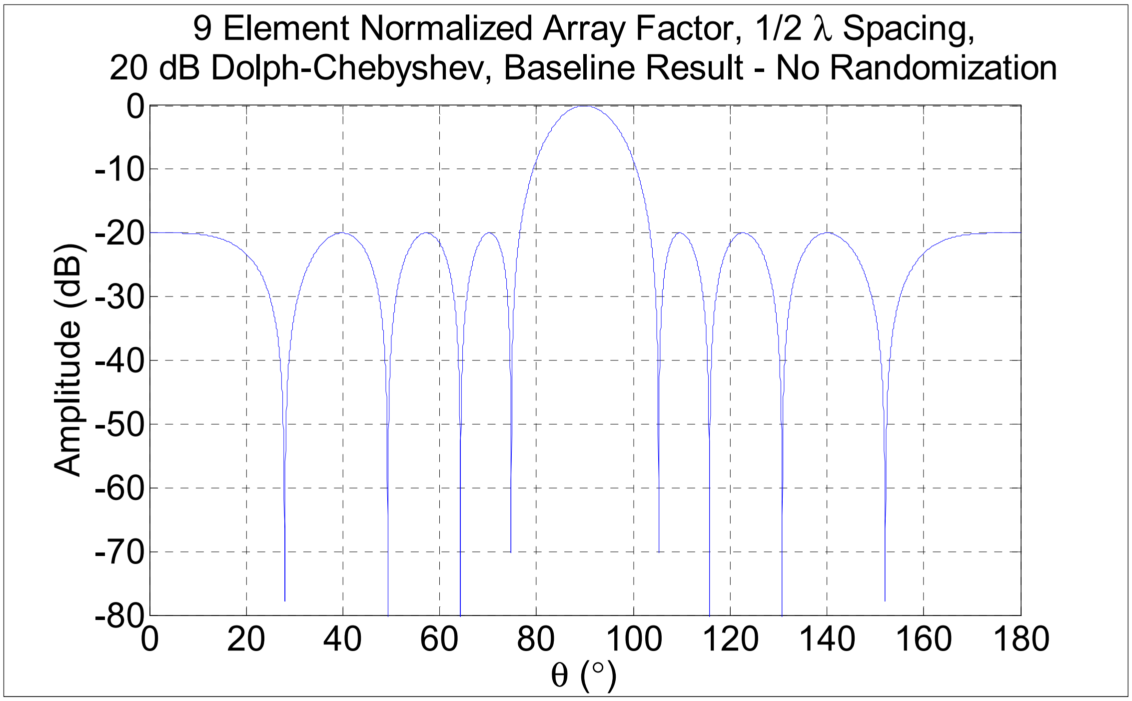

(a)

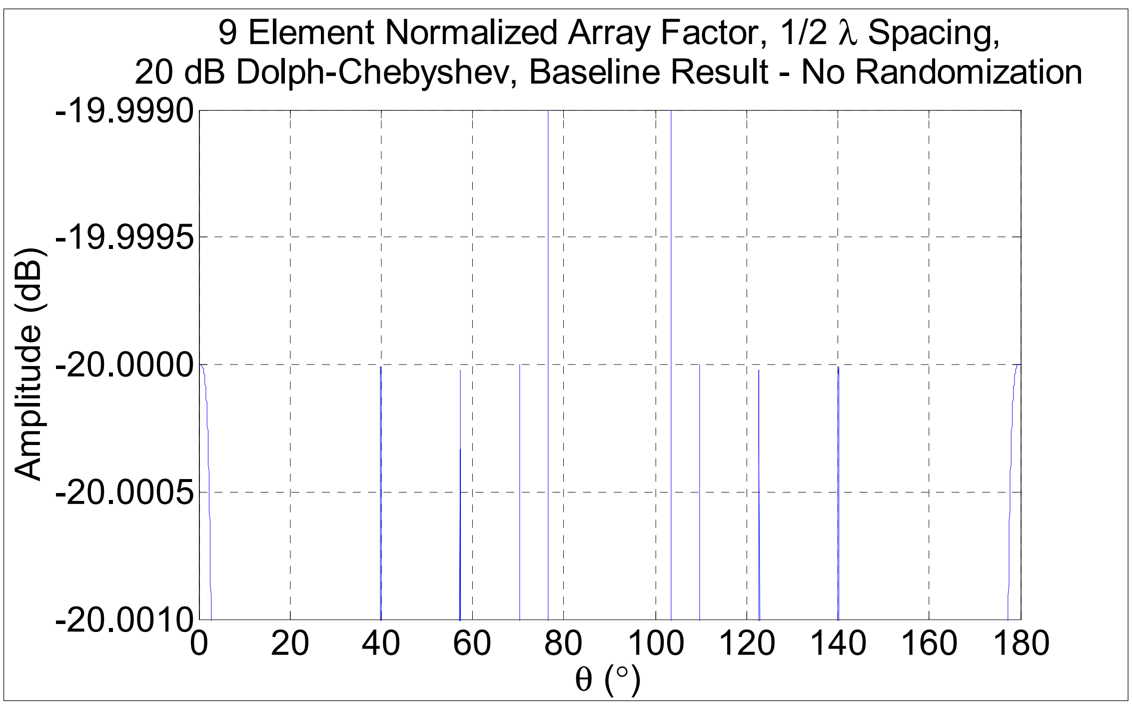

(b)

Figure 4.4. *Dolph-Chebyshev array factor for a 9 element,* $1/2\lambda$ *element spaced, broadside scanned (*$\theta_o = 90^o$*), 20 dB sidelobe linear array, no randomization.* Shown with full dynamic range (a) and expanded about -20 dB (b).

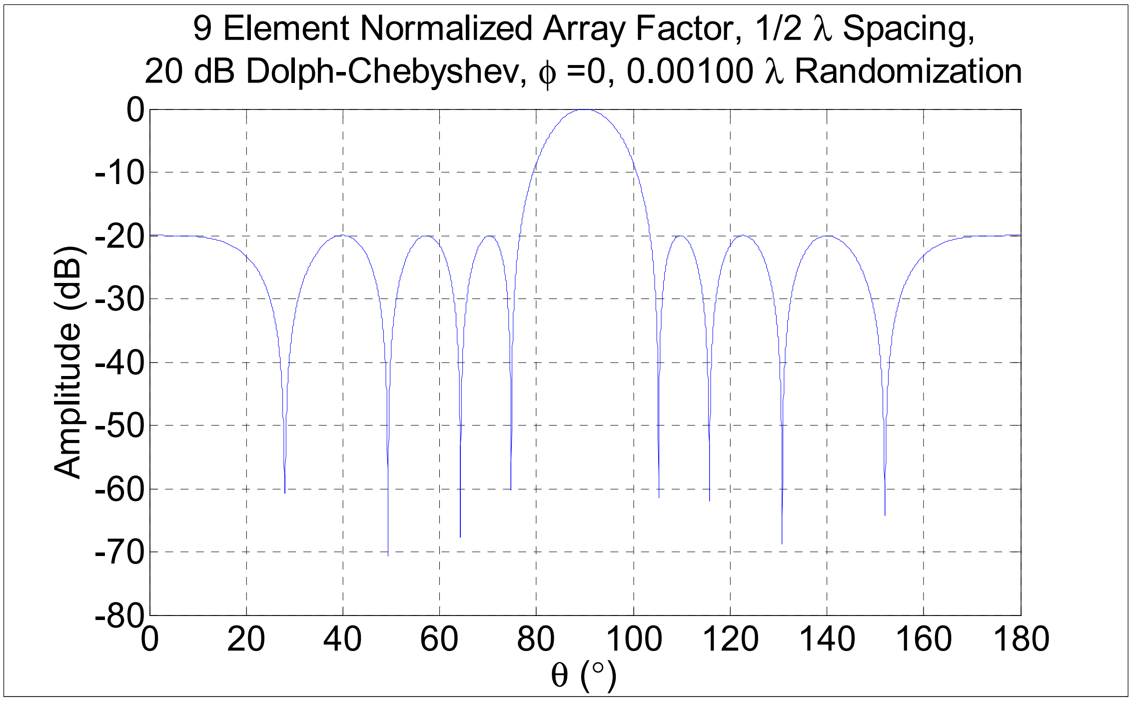

(a)

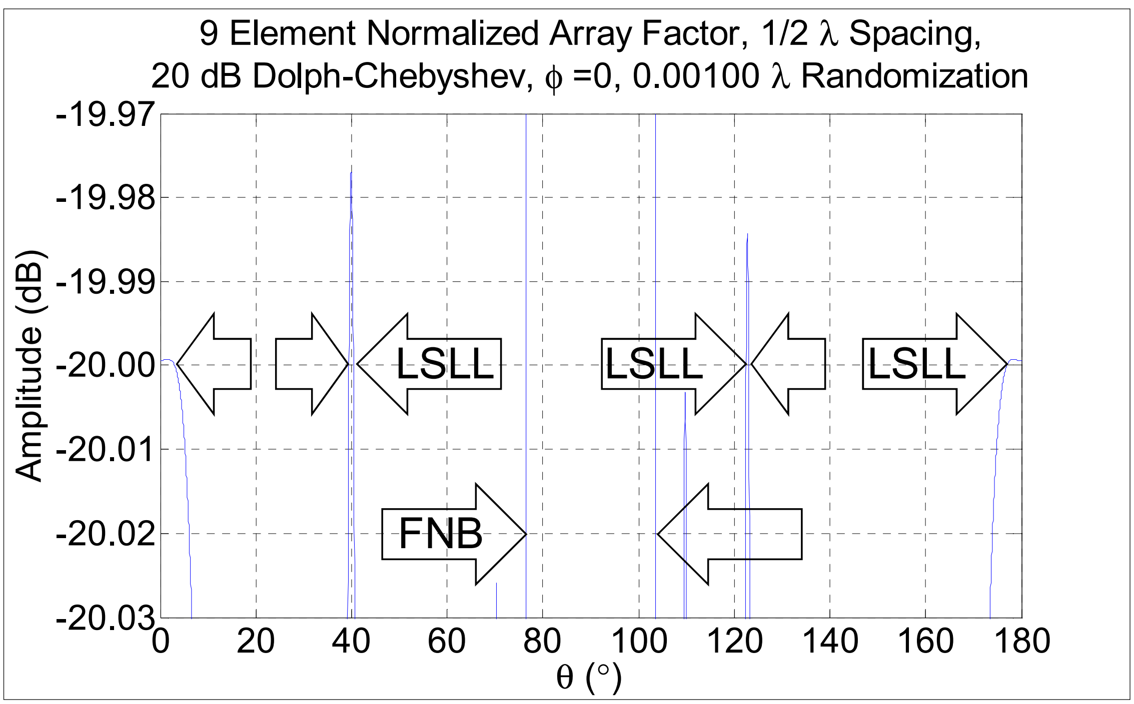

(b)

Figure 4.5. *Dolph-Chebyshev array factor for a 9 element, $1/2\lambda$ element spaced, broadside scanned ($\theta_o = 90^o$), 20 dB sidelobe linear array, 0.00100 λ randomization.* Shown with full dynamic range (a) and expanded about -20 dB (b).

4.4 Element Randomization Results

Some comments regarding the analysis over scan angles are appropriate here. When the array design is regular and periodic, the AF can be calculated as a periodic function of an array variable such as illustrated in (4.6a) for a linear array with uniform element spacing oriented on the z-axis and centered at the origin. This results in a periodic function for the AF (4.6b). (4.6b) is simply a variable transformation of (2.19) with (4.6a) substituted into it.

$$u = 2\frac{d}{\lambda}\left(\cos\theta - \cos\theta_o\right) \tag{4.6a}$$

$$AF = \sum_{i=0}^{N} A_i e^{j\left[\left(i-\frac{N}{2}\right)\pi u\right]} \tag{4.6b}$$

When considering the randomization process, the system is no longer regular. The array variable would become (4.7a), and unique to each element in the summation. The AF would be expressed as (4.7b). The array variable would no longer be periodic. The expressions in (4.7) are developed from combining (2.14), (2.18), and (4.2).

$$u_i = \frac{2}{\lambda}\left[x_{ir}\sin\theta\cos\phi + y_{ir}\sin\theta\sin\phi + z_{ir}\cos\theta - \left(i-\frac{N}{2}\right)d\cos\theta_o\right] \tag{4.7a}$$

$$AF = \sum_{i=0}^{N} A_i e^{j\pi u_i} \tag{4.7b}$$

The magnitude of x_{ir} and y_{ir} are less than r_ε making the dominating term of the position vector in (4.7a) z_{ir}. Consequently, (4.7b) will asymptotically tend towards (4.6b) as r_ε tends toward zero. However, the randomness being applied to $\mathbf{r}_{ir}$ will cause randomly located grating lobes that may or may not be included in the visible portion of the AF as a function of the particular scan angle. This will lead to varying sidelobe levels over scan angle. As a result, analysis taken all the way down to the visible portion of specific scan angles is necessary. Variations in sidelobe levels versus scan angle for given randomization runs demonstrate this need. Figures 4.6(a) and (b) illustrate this for $1/2\lambda$ element spacing Dolph-Chebyshev arrays – a 10 element 20 dB, and a 28 element 50 dB sidelobe level designs. Both levels of randomization are 0.10000 λ and n=1 for both cases.

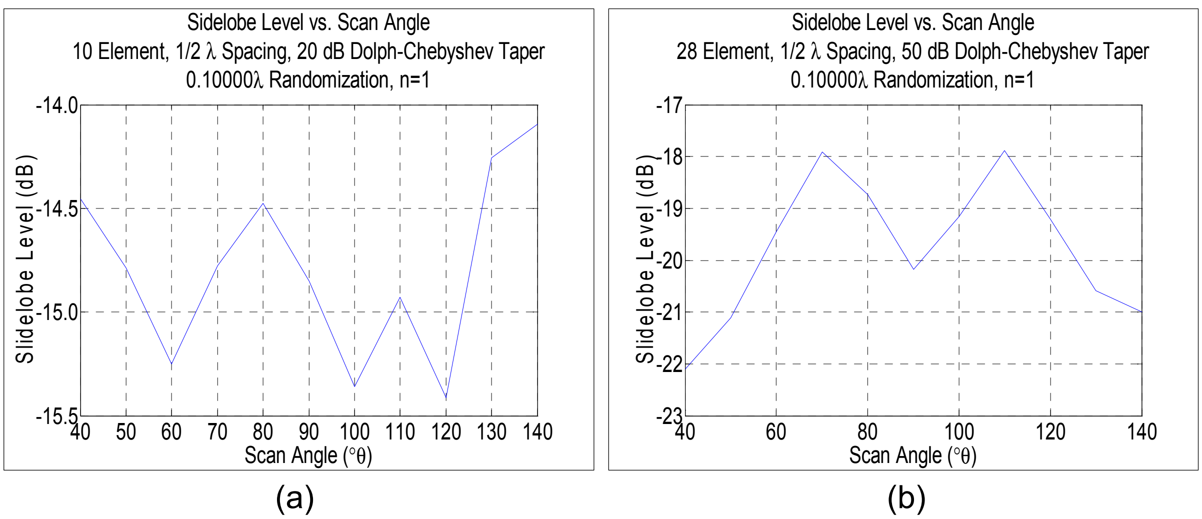

Figure 4.6. *Sidelobe level vs. scan for 0.10000 λ randomization, n=1, $1/2\lambda$ element spacing arrays.* Illustrated are sidelobe levels after randomization of a 10 element, 20 dB Dolph-Chebyshev (a), and a 28 element, 50 dB Dolph-Chebyshev (b) arrays.

As can be seen in the two examples in Figure 4.6, the sidelobe levels vary with scan; in one of these cases up to almost 3 dB.

The following sections are divided up by array element spacing. Each section is then subdivided into groups by initial sidelobe level design. The initial sidelobe level design groups are split into taper groups by the minimum number of elements and equal number of elements as previously described in Section 4.1. The output of the randomization analysis runs will be presented in this manner.

This study is based upon linear arrays. Initially, this analysis was performed and tracked by θ angle of scan. These arrays prior to randomization are symmetric about the x-y plane. Hence angles of scan, equally above and below $\theta = 90^o$ or broadside, are just reflections through the x-y plane of each other. Therefore, statistical randomization results for elevation angles of scan that are angularly equal above and below broadside, should yield the same parameter statistics if the data is properly reflected through the x-y plane. After running randomization data by θ scan angle, it was later converted to data by elevation scan angle – degrees above and below $\theta = 90^o$. Statistical data from negative elevation angles of scan was reflected through the x-y plane, and the means and standard deviations from the positive and negative elevation angles of scan were pooled for each parameter as the union of two sample sets. With (4.8), the individual means and variances of the parameters by angle of scan, positive and negative (reflected through the x-y plane), were used to calculate the mean and variance of the pooled set [71] [72] [73].

$$\mu_p = \frac{1}{n_1 + n_2}(n_1\mu_1 + n_2\mu_2) \tag{4.8a}$$

$$\sigma_p^2 = \frac{1}{n_1 + n_2 - 1}\left[(n_1 - 1)\sigma_1^2 + (n_2 - 1)\sigma_2^2 + \frac{n_1 n_2^2 + n_2 n_1^2}{(n_1 + n_2)^2}(\mu_2 - \mu_1)^2\right] \tag{4.8b}$$

where

μ_1 is the mean of population set 1

μ_2 is the mean of population set 2

μ_p is the mean of the pooled population of the union of sets 1 and 2

σ_1^2 is the variance of population set 1

σ_2^2 is the variance of population set 2

σ_p^2 is the variance of the pooled population of the union of sets 1 and 2

n_1 is the number of elements of population set 1

n_2 is the number of elements of population set 2.

Final statistics are represented over scan by positive, symmetric, elevation angles of scan.

Randomization results from each elevation scan angle will not be presented. Only the worst case graph for each parameter is represented in Appendix B. Additional data in the form of figures and tables that is associated with randomization results is is also illustrated in Appendix B.

$1/4$ λ Element Spacing

The first array group evaluated is arrays with $1/4$ λ element spacing. This group is broken down into 4 subgroups by initial design sidelobe level – 20, 30, 40, and 50 dB. The array designs of each of these subgroups can be found summarized in Tables 4.1, 4.2 and 4.3.

20 dB Initial Design Sidelobe Level

As indicated in Table 4.1, the $1/4$ λ element spacing, 20 dB sidelobe group consisted of three types of tapers that were analyzed for their performance under element position randomization conditions – modified Taylor, powers of cosine on a pedestal, and Taylor. The MNE arrays were a 20 element modified Taylor array, a 19 element powers of cosine on a pedestal array, and a 19 element Taylor array. Figures B.1 to B.3, respectively, illustrate the array parameter metrics relative to randomization for the MNE arrays.

From Table A.1, the initial performance metrics of the arrays prior to randomization can be examined. 3 dB beamwidths increase very slightly. The 3σ degradation is less than 0.8^o for all 3 MNE arrays as compared to initial 3 dB beamwidths that range from 11.9^o to 19.8^o. This is insignificant. The degradation of the 10 dB beamwidths is also very insignificant. 3σ degradation is less than 1.7^o for beamwidths that range from 20.3^o to 36.1^o. FNB shows a bit more degradation; 3σ variation is as high as 9.5^o for initial FNB's that ranged from 29.2^o to 59.8^o. Although the relative variation of FNB is relatively large, this is not where the performance impact to the system really lies. For the beamwidths that are significant to system operation, 3 and 10 dB, the impacts are negligible. Note, the beamwidth performance degradation that has been identified occurs at or near 0.10000 λ radial randomization levels. Less randomization produces less degradation.

Examining the pointing error illustrates that the 3σ beam pointing error is less than 1.9^o. Relative to the 3 dB beamwidths, this is quite small. Again, this is maximum degradation at radial randomization of 0.10000 λ. Directivity shows similar insignificant degradation. Its 3σ is less than 0.24 dB for initial AF directivities greater than 9.49 dB for this MNE group.

Sidelobe levels are where the real issues arise. Worst case among the 3 MNE arrays at the worst case randomization produces 3σ sidelobe degradation of 8.3 dB. That means the sidelobe level went from -20.4 dB to -12.1 dB. This occurred with the 19 element powers of cosine on a pedestal array. The other two arrays experienced 7.30 dB and 7.53 dB of sidelobe level degradation. This resulted in sidelobe levels of -13.6 dB for the 20 element modified Taylor array and -12.9 dB for the 19 element Taylor array. For this set of MNE arrays, the modified Taylor array seemed to provide the least degradation under randomization. Examining the fraction of high sidelobes at the 3σ performance level, again at the 0.10000 λ randomization, it is evident that 48% to 54% of the sidelobes are degraded compared to their pre-randomization performance. The power of cosine on a pedestal array is the worst while the Taylor array is the best. The modified Taylor array falls in the middle with 3σ of its degraded sidelobes equaling 50%. The rest of the sidelobes would still meet the initial performance metric.

Since the longest array in the MNE set of arrays was 20 elements (modified Taylor), the powers of cosine on a pedestal and Taylor arrays were redesigned for 20 elements also. These three, 20 element, arrays together make up the ENE group. Figures B.4 and B.5, illustrate the array parameter metrics for the 2 additional 20 element arrays relative to randomization.

Comparing the ENE group beamwidths shown in Figures B.1(d), B.4(d), and B.5(d), the 3σ degradation in 3 dB beamwidth increases slightly to 1^{o}. The 10 dB, 3σ beamwidth degradation, however, increased to 2.5^{o}. FNB also experienced additional degradation with a 3σ beamwidth increase of up to 12.2^{o} due to randomization as compared to the 9.5^{o} for the MNE group. Again, these are worst case numbers for the worst case randomization of 0.10000 λ. With all of the initial design beamwidths for the ENE group being similar to the NME group, the relative impact is similar, although slightly worse.

Examining the pointing error illustrates that the 3σ beam pointing error is less than 1.7^{o}. Relative to the 3 dB beamwidths, this is quite small but slightly larger than the MNE group. Pointing error is significantly less than the array resolution. Again, this is maximum degradation at radial randomization of 0.10000 λ. Directivity shows similar insignificant degradation. Its 3σ is less than 0.23 dB for initial AF directivities greater than 9.65 dB for this ENE group.

Worst case among the 3 ENE arrays produces 3σ sidelobe degradation of 7.7 dB with the sidelobe level going from -20.3 dB to -12.6 dB. This occurs at the 0.10000 λ randomization radius with the 20 element powers of cosine on a pedestal array. The other two arrays experienced 7.3 dB and 7.1 dB of sidelobe level degradation at the same level of randomization. This resulted in sidelobe levels of -13.6 dB for the 20 element modified Taylor array and -13.2 dB for the 20 element Taylor array. Examining the fraction of high sidelobes at the 3σ performance level and 0.10000 λ randomization radiuses, it is evident that 45% to 57% of the sidelobes are degraded compared to their pre-randomization performance. The Taylor array is the worst while the power of cosine on a pedestal array is the best. The modified Taylor array falls in the middle with 3σ of its degraded sidelobes, again, equaling 50%. The rest of the sidelobes would still meet the initial performance metric.

30 dB Initial Design Sidelobe Level

As indicated in Table 4.1, the $1/4$ λ element spacing, 30 dB sidelobe group consisted of the three same types of tapers that were analyzed for their performance under element position randomization conditions as the 20 dB group – modified Taylor, powers of cosine on a pedestal, and Taylor. The MNE arrays were a 27 element modified Taylor array, a 25 element powers of cosine on a pedestal array, and a 25 element Taylor array. Figures B.6 to B.8, respectively, illustrate the array parameter metrics relative to randomization for these MNE arrays.

From Table A.2, the initial performance metrics of the arrays prior to randomization can be examined. 3 dB beamwidths increase very slightly. The 3σ degradation is less than 0.5^o for all 3 MNE arrays as compared to initial 3 dB beamwidths that range from 10.4^o to 16.7^o. This, as in the 20 dB group, is insignificant. The degradation of the 10 dB beamwidths is also very insignificant. 3σ degradation is less than 1.1^o for beamwidths that range from 18.0^o to 30.4^o. FNB shows a bit more degradation; 3σ variation is as high as 21.1^o for initial FNB's that ranged from 28.3^o to 59.1^o. Although the relative variation of FNB is relatively large, this is not where the performance impact to the system really lies. For the beamwidths that are significant to system operation, 3 and 10 dB, the impacts are negligible. Note, the beamwidth performance degradation that has been identified occurs at or near 0.10000 λ radial randomization levels. Less randomization produces less degradation.

Examining the pointing error illustrates that the 3σ beam pointing error is less than 1.3^o. Relative to the 3 dB beamwidths, this is quite small. Again, this is maximum degradation at radial randomization of 0.10000 λ. Directivity shows similar insignificant degradation. Its 3σ is less than 0.21 dB for initial AF directivities greater than 10.19 dB for this MNE group.

Here as well, sidelobe levels are where the real issues arise. Worst case among the 3 MNE arrays at the worst case randomization produces 3σ sidelobe degradation of 15.6 dB. That means the sidelobe level went from -30.8 dB to -15.2 dB. This occurred with the 25 element Taylor array. The other two arrays experienced 14.6 dB and 14.9 dB of sidelobe level degradation. This resulted in sidelobe levels of -15.9 dB for the 27 element modified Taylor array and -15.6 dB for the 25 element powers of cosine on a pedestal array. For this set of MNE arrays, the Modified Taylor array seemed to provide the least degradation under randomization. Examining the fraction of high sidelobes at the 3σ performance level for 0.10000 λ randomization, indicates that more than 100% of the population of arrays have sidelobes above their original design level. If Figures B.6(b), B.7(b) and B.8(b) are closely examined, the standard deviation curves rise to a peak and begin to tail off back towards zero. The exact shape of this curve certainly varies with taper.

Since the longest array in the MNE set of arrays was 27 elements (modified Taylor), the powers of cosine on a pedestal and Taylor arrays were redesigned for 27 elements also. These three, 27 element, arrays together make up the ENE group. Figures B.9 and B.10, illustrate the array parameter metrics for the two additional 27 element arrays relative to randomization.

Comparing the ENE group beamwidths, Figures B.6(d), B.9(d), and B.10(d), the 3σ increase in 3 dB beamwidth is less than 0.6^{o}. The 10 dB, 3σ beamwidth degradation, however, increased to 1.7^{o} from 1.1^{o}. FNB degradation, however, underwent a decrease compared to the MNE group. The 3σ beamwidth was 17.2°, down from the MNE group result of 21.1°. Again, these are worst case numbers for the worst case randomization of 0.10000 λ. With all of the initial design beamwidths for the ENE group being similar to the NME group, the relative impact is similar.

Examining the pointing error illustrates that the 3σ beam pointing error is less than 1.2°. Relative to the 3 dB beamwidths, this is quite small but slightly larger than the MNE group. Again, this is maximum degradation at radial randomization of 0.10000 λ. Directivity shows similar insignificant degradation. At 0.10000 λ randomization, its 3σ degradation is less than 0.20 dB for initial *AF* directivities greater than 10.29 dB for this ENE group.

Worst case among the 3 ENE arrays produces 3σ sidelobe degradation of 15.1 dB for the sidelobe level going from -30.8 dB to -15.7 dB. This occurs at the 0.10000 λ randomization radius with the 27 element Taylor array. The other 2 arrays experienced 14.6 dB and 14.4 dB of sidelobe level degradation at the same level of randomization. This resulted in sidelobe levels of -15.9 dB for the 27 element modified Taylor and powers of cosine on a pedestal arrays. For this set of ENE arrays, the Taylor array seemed to provide the least degradation under randomization, but the best system sidelobe level performance was from the other 2 arrays – 0.2 dB better. Examining the fraction of high sidelobes at the 3σ performance level for 0.10000 λ randomization, indicates that more than 100% of the population of arrays have sidelobes above their original design level. If Figures B.6(b), B.9(b) and B.10(b) are closely examined, the standard deviation curves rise to a peak and begin to tail off back towards zero. The exact shape of this curve varies with taper.

40 dB Initial Design Sidelobe Level

As indicated in Table 4.1, the $1/4\ \lambda$ element spacing, 40 dB sidelobe group consisted of the three same types of tapers that were analyzed for their performance under element position randomization conditions as the 20 and 30 dB groups – modified Taylor, powers of cosine on a pedestal, and Taylor. The MNE arrays were a 35 element modified Taylor array, a 32 element powers of cosine on a pedestal array, and a 32 element Taylor array. Figures B.11 to B.13, respectively, illustrate the array parameter metrics relative to randomization for the MNE arrays.

From Table A.3, the initial performance metrics of the arrays prior to randomization can be examined. 3 dB beamwidths increase very slightly. The 3σ degradation is less than 0.3^o for all 3 MNE arrays as compared to initial 3 dB beamwidths that range from 9.1^o to 14.4^o. This, as in the 20 and 30 dB groups, is insignificant. The degradation of the 10 dB beamwidths is also very insignificant. 3σ degradation is less than 0.9^o for beamwidths that range from 16.0^o to 26.2^o. FNB shows a bit more degradation; 3σ variation is as high as 32.4^o for initial FNB's that ranged from 27.5^o to 58.7^o. Although the relative variation of FNB is relatively large, this is not where the performance impact to the system really lies. Additionally, the worst case FNB degradations occur at 40^o elevation scan, where the FNB is in excess of 39^o (Taylor array). For the beamwidths that are significant to system operation, 3 and 10 dB, the impacts are negligible. Note, the beamwidth performance degradation that has been identified here occurs at or near 0.10000 λ radial randomization levels. Less randomization produces less degradation.

Examining the pointing error illustrates that the 3σ beam pointing error is less than 1.1^{o}. Relative to the 3 dB beamwidths, this is quite small, significantly less than the array resolution. Again, this is maximum degradation at radial randomization of 0.10000 λ. Directivity shows similar insignificant degradation. Its 3σ degradation is less than 0.22 dB for initial AF directivities greater than 10.79 dB for this MNE group.

Here as well, sidelobe levels are where the real issues arise. Worst case among the 3 MNE arrays at the worst case randomization produces 3σ sidelobe degradation of 25.1 dB. That means the sidelobe level went from -40.7 dB to -15.6 dB. This occurred with the 35 element modified Taylor array. The other two arrays experienced 24.6 dB of sidelobe level degradation. This resulted in sidelobe levels of -16.2 dB for the 32 element powers of cosine on a pedestal array and -15.8 dB for the 32 element Taylor array. For this set of MNE arrays, the powers of cosine on a pedestal array seemed to provide the least degradation under randomization. Examining the fraction of high sidelobes at the 3σ performance level for 0.10000 λ randomization, indicates that more than 100% of the population of arrays have sidelobes above their original design level. If Figures B.11(b), B.12(b) and B.13(b) are closely examined, the standard deviation curves rise to a peak and begin to tail off back towards zero. The exact shape of this curve certainly varies with taper.

The longest array in the MNE set of arrays was 35 elements (modified Taylor). Since the powers of cosine on a pedestal and Taylor arrays were shorter, they were redesigned for 35 elements to create an ENE group. Figures B.9 and B.10, graphically illustrate the array parameter metrics for the two additional 35 element arrays relative to randomization.

Comparing the ENE group beamwidths, Figures B.11(d), B.14(d), and B.15(d), the 3σ increase in 3 dB beamwidth is less than 0.3^{o}. The 10 dB, 3σ beamwidth degradation, remained at 0.9^{o}. FNB degradation, however, underwent a slight decrease compared to the MNE group. The 3σ beamwidth was 29.8^{o}, down from the MNE group result of 32.4^{o}. Again, these are worst case numbers for the worst case randomization less than or equal to 0.10000 λ. With all of the initial design beamwidths for the ENE group being similar to the NME group, the relative impact is similar.

Examining the pointing error illustrates that the 3σ beam pointing error is less than 1.0^{o}. Relative to the 3 dB beamwidths, this is quite small and slightly smaller that the MNE group. Again, this is maximum degradation at radial randomization of 0.10000 λ or less. Directivity shows similar insignificant degradation. Its 3σ again is 0.22 dB for initial AF directivities greater than 10.82 dB for this ENE group.

Worst case among the three ENE arrays produces 3σ sidelobe degradation of 25.1 dB for the sidelobe level going from -40.7 dB to -15.6 dB. This occurs at the 0.10000 λ randomization radius with the 35 element modified Taylor array. The other two arrays experienced 23.4 dB and 23.7 dB of sidelobe level degradation at the same level of randomization. This resulted in sidelobe levels of -17.4 dB for the 35 element powers of cosine on a pedestal array and -16.8 dB for the Taylor array. For this set of ENE arrays, the powers of cosine on a pedestal array provided the least degradation under randomization and the best system sidelobe level performance. Examining the fraction of high sidelobes at the 3σ performance level for 0.10000 λ randomization, indicates that 100% of the population of arrays have sidelobes above their original design level. If Figures B.11(b), B.14(b) and B.15(b) are closely examined, the standard deviation curves rise to a peak and begin to tail off back towards zero. The exact shape of this curve also varies with taper.

50 dB Initial Design Sidelobe Level

As indicated in Table 4.1, the $1/4\ \lambda$ element spacing, 50 dB sidelobe group consisted of the three same types of tapers that were analyzed for their performance under element position randomization conditions as the 20, 30 and 40 dB groups – modified Taylor, powers of cosine on a pedestal, and Taylor. The MNE arrays were a 42 element modified Taylor array, a 55 element powers of cosine on a pedestal array, and a 39 element Taylor array. Figures B.16 to B.18, respectively, illustrate the array parameter metrics relative to randomization for the MNE arrays.

From Table B.4, the initial performance metrics of the arrays prior to randomization can be examined. The 3 dB beamwidths increase very slightly. The 3σ degradation is less than 0.3° for all 3 MNE arrays as compared to initial 3 dB beamwidths that range from 6.3° to 13.1°. This, as in the 20, 30 and 40 dB groups, is insignificant. The degradation of the 10 dB beamwidths is also very insignificant. 3σ degradation is less than 0.8° for beamwidths that range from 11.2° to 23.9°. FNB shows a bit more degradation; 3σ degradation is as high as 35.2° for initial FNB's that ranged from 20.8° to 58.1°. Although the relative variation of FNB is relatively large, this is not a significant impact to the system because they indicate first null locations. The worst case FNB degradations occur at 40° elevation scan, where the FNB is in excess of 27.9° (powers of cosine on a pedestal). For the beamwidths that are significant to system operation, 3 and 10 dB, the impacts are negligible. Note, the beamwidth performance degradation that has been identified here occurs at or near 0.10000 λ radial randomization levels. Less randomization produces less degradation.

Examining the pointing error illustrates that the 3σ beam pointing error is less than 0.9°. Relative to the 3 dB beamwidths, this is quite small, significantly less than the array resolution. Again, this is maximum degradation at radial randomization of 0.10000 λ. Directivity shows similar insignificant degradation. Its 3σ is less than 0.19 dB for initial AF directivities greater than 11.17 dB for this MNE group.

Here as well, sidelobe levels are where the real issues arise. Worst case among the 3 MNE arrays at the worst case randomization produces 3σ sidelobe degradation of 34.0 dB for the 42 element modified Taylor and the 39 element Taylor array. That means the sidelobe levels went from -50.6 dB to -16.6 dB for both arrays. The 55 element powers of cosine on a pedestal array experienced 33.9 dB of sidelobe level degradation. This resulted in sidelobe levels of -16.8 dB. For this set of MNE arrays, the powers of cosine on a pedestal array seemed to provide the least degradation under randomization. Examining the fraction of high sidelobes at the 3σ performance level for 0.10000 λ randomization, indicates that 100% of the population of arrays have sidelobes above their original design level. If Figures B.16(b), B.17(b) and B.18(b) are closely examined, the standard deviation curves rise to a peak and begin to tail off back towards zero. The exact shape of this curve certainly varies with taper.

The longest array in the MNE set of arrays was 55 elements (powers of cosine on a pedestal). Since the modified Taylor and Taylor arrays were shorter, they were redesigned for 55 elements to create an ENE group. Figures B.19 and B.20, graphically illustrate the array parameter metrics for the two additional 55 element arrays relative to randomization.

Comparing the ENE group beamwidths, Figures B.17(d), B.19(d), and B.20(d), the 3σ increase in 3 dB beamwidth remains less than 0.3^{o}. The 10 dB, 3σ beamwidth degradation, remained at 0.8^{o}. FNB degradation, however, underwent a slight decrease compared to the MNE group. The 3σ beamwidth was 32.0^{o}, down from the MNE group result of 35.2^{o}. Again, these are worst case numbers for the worst case randomization less than or equal to 0.10000 λ. With all of the initial design beamwidths for the ENE group being similar to the NME group, the relative impact is similar.

Examining the pointing error illustrates that the 3σ beam pointing error is also less than 0.9^{o}. Relative to the 3 dB beamwidths, this is quite small. Again, this is maximum degradation at radial randomization of 0.10000 λ or less. Directivity shows similar insignificant degradation. Its 3σ again is 0.19 dB for initial AF directivities greater than 12.36 dB for this ENE group.

Worst case among the 3 ENE arrays produces 3σ sidelobe degradation of 33.9 dB for the sidelobe level going from -50.7 dB to -16.8 dB. This occurs at the 0.10000 λ randomization radius with the 55 element powers of cosine on a pedestal array. The other two arrays experienced 33.1 dB and 32.6 dB of sidelobe level degradation at the same level of randomization. This resulted in sidelobe levels of -17.8 dB for the 55 element modified Taylor and Taylor arrays. For this set of ENE arrays, the modified Taylor array provided the least degradation under randomization and the best system sidelobe level performance. Examining the fraction of high sidelobes at the 3σ performance level for 0.10000 λ randomization, indicates that 100% of the population of arrays have sidelobes above their original design level. If Figures B.17(b), B.19(b) and B.20(b) are closely examined, the standard deviation curves rise to a peak and begin to tail off back towards zero. The exact shape of this curve also varies with taper.

Commentary

When considering all of the arrays in the $1/4\ \lambda$ element spacing group, all showed similar trends and comparable delta magnitudes for the 0.10000 λ, worst case studied, randomization cases. However, the upward directed knee in each of the graphs begins to occur at smaller and smaller randomization levels as the number of elements is increased. As the data indicates, sidelobe levels are the biggest issue. Table B.1 summarizes the 3σ sidelobe performance of this group for 0.10000 λ radial randomization. As the number of elements and the initial designed sidelobe level is increased, the sidelobe level due to randomization does improve slightly. This is also exemplified in Figure B.21, where the 3σ sidelobe level compared to initial designed sidelobe level is plotted for the MNE and NME array groups by taper, also for 0.10000 λ randomization. Consequently, depending on the application needs, better sidelobes are achievable with less randomization. Therefore, initial designed sidelobe level requirements should be considered very carefully.

Even though the 3σ sidelobe levels are quite high, it should be noted that not all of the sidelobes are at that level. As different random states of element position occur, the sidelobes do change dramatically. Figure B.22 shows the sidelobes of the first 35 randomized states for the $1/4\ \lambda$ element spacing, 20 dB, 20 element modified Taylor array with 0.10000 λ radial variation scanned to broadside. As can be seen, the main beam characteristics are pretty stable. The sidelobes show considerable movement. As it turns out, the sidelobes are sometimes even better than the initial design. This is demonstrated in Figure B.23 which shows array factor plots of the worst (-14.4 dB), nominal (-17.6 dB), and best (-22.8 dB) sidelobe levels from the same array. These correlate with the histogram of SLLdBDeltas for the broadside scan (Figure B.24).

With the statistics following similar trends for the 30, 40, and 50 dB arrays from the $1/4\,\lambda$ spacing group, this entire analysis will not be repeated. Instead, analogous plots of the SLLdBDeltas histogram and range of array factors (worst, nominal and best) from only the 50 dB modified Taylor array in the MNE group for broadside scan with 0.10000 λ randomization will be reviewed. The histogram of SLLdBDeltas (Figure B.25) illustrates the statistically nominal degradation in the sidelobe level performance is approximately 28.25 dB, which equates to a sidelobe level of about -22.4 dB. Of these 100 runs, the best sidelobe level is -26.8 dB and the worst is -18.5 dB. The worst, nominal, and best sidelobe array factors for this scan angle and array are illustrated Figure B.26.

Examining the randomized $1/4\,\lambda$ spacing, 50 dB Modified Taylor MNE array at broadside, does indicate that an almost 20 dB sidelobe array with the directivity of a 50 dB sidelobe array can be design executed and not need to very critically maintain position. The cost is extra elements. Another way of looking at this array; it is mostly a 19+ dB sidelobe array with some out of specification sectors near the end of the patterns while maintaining the directivity of a 50 dB sidelobe array. All 100 runs are plotted in Figure B.27.

$3/8\lambda$ Element Spacing

The $3/8\lambda$ element spacing array group consisted of arrays with $3/8\lambda$ element spacing. This group too is also broken down into four subgroups by initial design sidelobe level – 20, 30, 40, and 50 dB. The array designs of each of these subgroups can be found summarized in Tables 4.1, 4.2 and 4.3. Again, each subgroup consisted of arrays with MNE and ENE designs.

20 dB Initial Design Sidelobe Level

As indicated in Table 4.1, the $3/8\lambda$ element spacing, 20 dB sidelobe group consisted of three types of tapers that were analyzed for their performance under element position randomization conditions – modified Taylor, powers of cosine on a pedestal, and Taylor. The MNE arrays were 14 element modified Taylor and powers of cosine on a pedestal arrays, and a 13 element Taylor array. Figures B.28 to B.30, respectively, illustrate the array parameter metrics relative to randomization for the MNE arrays. The ENE array set consisted of the two previously listed 14 element arrays and a 14 element Taylor array. The statistical metrics for these arrays are plotted in Figures B.28, B.29, and B.31. The metrics indicate very similar behavior to the $1/4\lambda$ element spaces arrays, again showing that sidelobe level is the primary attribute that is affected. The big difference between the 20 dB initial design $1/4\lambda$ element spaces arrays and these arrays is the SLLdBDeltasM parameter (the difference between the mean sidelobe level of the randomized array and the sidelobe level of the initial designed array). SLLdBDeltasM for each array design of the $3/8\lambda$ spaced set increased by about 1 dB at the 0.10000 λ randomization.

30 dB Initial Design Sidelobe Level

As indicated in Table 4.1, the $3/8\,\lambda$ element spacing, 30 dB sidelobe group consisted of the same three types of tapers that were analyzed for their performance under element position randomization conditions as the $3/8\,\lambda$ element spacing, 20 dB sidelobe group. The MNE arrays consisted of an 18 element modified Taylor array, and 17 element powers of cosine on a pedestal and Taylor arrays. Figures B.32 to B.34, respectively, illustrate the array parameter metrics relative to randomization for the MNE arrays. The ENE array set consisted of the previously listed 18 element modified Taylor array and additional 18 element powers of cosine on a pedestal and Taylor arrays. The statistical randomization metrics for these arrays are plotted in Figures B.32, B.35, and B.36. The metrics indicate very similar behavior to the $1/4\,\lambda$ element spaces arrays, again showing that sidelobe level is the primary attribute that is affected. The big difference between the 30 dB initial design $1/4\,\lambda$ element spaced arrays and these arrays is the SLLdBDeltasM and SLLdBDeltasS parameters (the mean difference between the sidelobe level of the randomized arrays and the sidelobe level of the initial array design and its associated standard deviation). Mean plus 3σ performance and absolute sidelobe level performance is illustrated in Table B.2 for the 0.10000 λ randomization cases comparing the $1/4$ and $3/8\,\lambda$ element spacing. Sidelobe levels increase from the analogous $1/4\,\lambda$ element spacing, 0.10000 λ randomization arrays from 0.5 to 3.6 dB. The Taylor and powers of cosine on a pedestal arrays maintain the best sidelobe performance of the three taper types for the least number of elements, although the MNE Taylor array experienced the least element degradation.

40 dB Initial Design Sidelobe Level

As indicated in Table 4.1, the $3/8\lambda$ element spacing, 40 dB initial sidelobe group MNE arrays consisted of a 24 element modified Taylor array, a 22 element powers of cosine on a pedestal array, and a 23 element Taylor array. Figures B.37 to B.39, respectively, illustrate the array parameter metrics relative to randomization for the $3/8\lambda$ element spacing, 40 dB initial sidelobe group MNE arrays. The ENE array set consisted of the previously listed 24 element Modified Taylor array and additional 24 element powers of cosine on a pedestal and Taylor arrays. The statistical randomization metrics for these arrays are plotted in Figures B.37, B.40, and B.41. The metrics indicate very similar behavior to the $1/4\lambda$ element spaces arrays, again showing that sidelobe level is the primary attribute that is affected. The big difference between the 40 dB initial design $1/4\lambda$ element spaced arrays and these arrays is the SLLdBDeltasM and SLLdBDeltasS. At 0.10000 λ randomization, SLLdBDeltasM for all of the analogous $1/4\lambda$ element spaced arrays was approximately 18 dB whereas for the $3/8\lambda$ element spaced arrays it was approximately 2 dB greater. The matching SLLdBDeltasS parameters for this group are about 0.5 dB greater than the analogous $1/4\lambda$ spacing group. Directivity, pointing error and beamwidths are virtually unaffected.

50 dB Initial Design Sidelobe Level

As indicated in Table 4.1, the $3/8\lambda$ element spacing, 50 dB initial sidelobe group MNE arrays consisted of a 28 element modified Taylor array, a 37 element powers of cosine on a pedestal array, and a 27 element Taylor array. Figures B.42 to B.44, respectively, illustrate the array parameter metrics relative to randomization for the $3/8\,\lambda$ element spacing, 50 dB initial sidelobe group MNE arrays. The ENE array set consisted of additional 37 element modified Taylor and Taylor arrays and the mentioned 37 element powers of cosine on a pedestal array. The statistical randomization metrics for these arrays are plotted in Figures B.45, B.43, and B.46. The metrics indicate very similar behavior to the $1/4\,\lambda$ element spaces arrays, again showing that sidelobe level is the primary attribute that is affected. Directivity, pointing error and beamwidths are virtually unaffected. Sidelobe level metrics are only slightly worse than the equivalent $1/4\,\lambda$ element spaces arrays. SLLdBDeltasM only degrades by approximately 1 dB at 0.10000 λ randomization, whereas SLLdBDeltasS is virtually equivalent.

$1/2\,\lambda$ Element Spacing

The $1/2\,\lambda$ element spacing array group consisted of arrays with $1/2\,\lambda$ element spacing that was subdivided into four subgroups by initial design sidelobe level – 20, 30, 40, and 50 dB. Array designs of each of these subgroups can be found summarized in Tables 4.1, 4.2 and 4.3. Again, each subgroup consisted of arrays with MNE and ENE designs. In addition to modified Taylor, powers of cosine on a pedestal and Taylor tapers, Dolph-Chebyshev tapers are also included in this overall group.

20 dB Initial Design Sidelobe Level

As indicated in Table 4.1, the $1/2\,\lambda$ element spacing, 20 dB sidelobe group MNE arrays were 9 element Dolph-Chebyshev, and 10 element modified Taylor, powers of cosine on a pedestal and Taylor arrays. Figures B.47 to B.50, respectively, illustrate the array parameter metrics relative to randomization for the MNE arrays. The ENE array set consisted of the three previously listed 10 element arrays and a 10 element Dolph-Chebyshev array. The statistical metrics for this array are plotted in Figure B.51. The metrics indicate very similar behavior to the $1/4$ and $3/8\,\lambda$ element spaced arrays, again showing that sidelobe level is the primary attribute that is affected. Here SLLdBDeltasM shows another 1 dB nominal increase from the $3/8\,\lambda$ spaced 20 dB arrays at the 0.10000 λ randomization level.

30 dB Initial Design Sidelobe Level

As indicated in Table 4.1, the $1/2\,\lambda$ element spacing, 30 dB sidelobe group MNE arrays were 13 element Dolph-Chebyshev, 15 element modified Taylor, 17 element powers of cosine on a pedestal and 14 element Taylor arrays. Figures B.52 to B.55, respectively, illustrate the array parameter metrics relative to randomization for the MNE arrays. The ENE array set consisted of 17 element arrays of the same four types; the previously listed powers of cosine on a pedestal and the additional three whose statistical metrics are additionally illustrated in Figures B.56 to B.58. The metrics indicate very similar behavior to the analogous $1/4$ and $3/8\,\lambda$ element spaced arrays, again showing that sidelobe level is the primary attribute that is affected. Here, for 0.10000 λ randomization, SLLdBDeltasM comes in between 11 and 12 dB with SLLdBDeltasS remaining at about 2 dB.

40 dB Initial Design Sidelobe Level

As indicated in Table 4.1, the $1/2\,\lambda$ element spacing, 40 dB sidelobe group MNE arrays were 16 element Dolph-Chebyshev, 18 element modified Taylor, 23 element powers of cosine on a pedestal and 18 element Taylor arrays. Figures B.59 to B.62, respectively, illustrate the array parameter metrics relative to randomization for the MNE arrays. The ENE array set consisted of 23 element arrays of the same four types; the previously listed powers of cosine on a pedestal and the additional three whose statistical metrics are additionally illustrated in Figures B.63 to B.65. The metrics indicate very similar behavior to the analogous $1/4$ and $3/8\,\lambda$ element spaced arrays, again showing that sidelobe level is the primary attribute that is affected. Here, for 0.10000 λ randomization, SLLdBDeltasM comes in between 20 and 22 dB with SLLdBDeltasS remaining at about 2 dB. Additional degradation with increase in spacing appears to not have occurred in a general sense with these two groups.

50 dB Initial Design Sidelobe Level

As indicated in Table 4.1, the $1/2\,\lambda$ element spacing, 50 dB sidelobe group MNE arrays were 19 element Dolph-Chebyshev, 22 element modified Taylor, 28 element powers of cosine on a pedestal and 21 element Taylor arrays. Figures B.66 to B.69, respectively, illustrate the array parameter metrics relative to randomization for the MNE arrays. The ENE array set consisted of 28 element arrays of the same four types; the previously listed powers of cosine on a pedestal and the additional three whose statistical metrics are additionally illustrated in Figures B.70 to B.72. The metrics indicate very similar behavior to the analogous $1/4$ and $3/8\,\lambda$ element spaced arrays, again showing that sidelobe level is the primary attribute that is affected. Here, for 0.10000 λ randomization, SLLdBDeltasM comes in between 30 and 32 dB with SLLdBDeltasS remaining just about 2 dB. Additional degradation with increase in spacing appears to not have occurred in a general sense with these two groups as well.

$5/8\lambda$ Element Spacing

20 dB initial sidelobe level MNE arrays in the $5/8\lambda$ element spacing group consist of a 7 element Dolph-Chebyshev array and 8 element modified Taylor, powers of cosine on a pedestal, and Taylor arrays (see Tables 4.1 to 4.3). Statistical metrics for these arrays are illustrated in Figures B.73 to B.76. The addition of Figure B.77 adds statistical metrics for an 8 element Dolph-Chebyshev array to complete the ENE data set of 8 element arrays.

In the 30 dB initial sidelobe level $5/8\lambda$ element spacing group, there is a 9 element Dolph-Chebyshev, an 11 element modified Taylor, and 12 element powers of cosine on a pedestal and Taylor arrays that comprise the MNE set (Tables 4.1 to 4.3). Their statistics are plotted in Figures B.78 to B.81. 12 element Dolph-Chebyshev and modified Taylor arrays are additionally statistically analyzed to complete the ENE group (Figures B.82 and B.83).

A 12 element Dolph-Chebyshev array, a 14 element modified Taylor array, and 17 element powers of cosine on a pedestal and Taylor arrays make up the 40 dB initial sidelobe level $5/8\lambda$ element spacing MNE group (Tables 4.1 to 4.3). The associated ENE group is made up of the two aforementioned 17 element arrays and 17 element Dolph-Chebyshev and modified Taylor arrays (Tables 4.1 to 4.3). Randomization metrics are graphically illustrated in Figures B.84 to B.87 (MNE set) and B.88 and B.89 (additional ENE arrays not in the MNE set).

The 50 dB initial sidelobe level $5/8\lambda$ element spacing MNE arrays are a 14 element Dolph-Chebyshev array, a 16 element modified Taylor array, a 21 element powers of cosine on a pedestal array, and a 19 element Taylor array (Tables 4.1 to 4.3). Randomization metrics for these arrays can be examined in Figures B.90 to B.93. The ENE arrays for the same sidelobe level and element spacing all have 21 elements of the same four tapers (Tables 4.1 to 4.3). Their randomization metrics are plotted in Figures B.94, B.95, B.92, and B.96, respectively, for the Dolph-Chebyshev, modified Taylor, powers of cosine on a pedestal, and Taylor tapered array factors.

Examination of the entire $5/8\lambda$ element spacing array factor randomization metrics leads to similar conclusions as were previously developed for the narrower element spaced randomized array factors. The primary performance criterion of concern is the sidelobe level. The other metrics tend to not vary much. Additionally, SLLdBDeltasM and SLLdBDeltasS appear to remain at a unique plateau for each initial sidelobe level – independent of element spacing.

$3/4\lambda$ Element Spacing

In the 20 dB initial sidelobe level $3/4\lambda$ element spacing group, there is a 9 element Dolph-Chebyshev array, and 10 element modified Taylor, powers of cosine on a pedestal and Taylor arrays that comprise the MNE set (Tables 4.1 to 4.3). Their statistics are plotted in Figures B.97 to B.100. A 10 element Dolph-Chebyshev array is additionally statistically analyzed to complete the ENE group (Figure B.101).

The 30 dB initial sidelobe level MNE arrays in the $3/4\lambda$ element spacing group consist of a 12 element Dolph-Chebyshev array, a 14 element modified Taylor array, a 13 element powers of cosine on a pedestal array, and a 14 element Taylor array (see Tables 4.1 to 4.3). Statistical metrics for these arrays are illustrated in Figures B.102 to B.105. The addition of Figures B.106 and B.107 add statistical metrics for 14 element Dolph-Chebyshev and powers of cosine on a pedestal arrays to complete the ENE data set of 14 element arrays (Tables 4.1 to 4.3).

A 15 element Dolph-Chebyshev array, an 18 element modified Taylor array, a 22 element powers of cosine on a pedestal array and an 18 element Taylor array make up the 40 dB initial sidelobe level $3/4\lambda$ element spacing MNE group (Tables 4.1 to 4.3). The associated ENE group is made up of the aforementioned 22 element array and 22 element Dolph-Chebyshev, modified Taylor, and Taylor arrays (Tables 4.1 to 4.3). Randomization metrics are graphically illustrated in Figures B.108 to B.111 (MNE set) and B.112 to B.114 (additional ENE arrays not in the MNE set).

The 50 dB initial sidelobe level $3/4\lambda$ element spacing MNE arrays are an 18 element Dolph-Chebyshev array, a 21 element modified Taylor array, a 28 element powers of cosine on a pedestal array, and a 21 element Taylor array (Tables 4.1 to 4.3). Randomization metrics for these arrays can be examined in Figures B.115 to B.118. The ENE arrays for the same sidelobe level and element spacing all have 28 elements of the same four tapers (Tables 4.1 to 4.3). Their randomization metrics are plotted in Figures B.119, B.120, B.117, and B.121, respectively, for the Dolph-Chebyshev, modified Taylor, powers of cosine on a pedestal, and Taylor tapered array factors.

Examination of the entire $3/4\lambda$ element spacing array factor randomization metrics leads to similar conclusions as were previously developed for the narrower element spaced randomized array factors. The primary performance criterion of concern is the sidelobe level. The other metrics tend to not vary much. Additionally, SLLdBDeltasM and SLLdBDeltasS appear to remain at a unique plateau for each initial sidelobe level – independent of element spacing.

$7/8\lambda$ Element Spacing

The 9 element Dolph-Chebyshev and Taylor arrays, and 10 element modified Taylor and powers of cosine on a pedestal arrays comprise the 20 dB initial sidelobe level, $7/8\lambda$ element spacing MNE group (Tables 4.1 to 4.3). The associated ENE group is made up of the aforementioned 10 element arrays and 10 element Dolph-Chebyshev and Taylor arrays (Tables 4.1 to 4.3). Randomization metrics are graphically illustrated in Figures B.122 to B.125 (MNE set) and B.126, and B.127 (additional ENE arrays not in the MNE set).

In the 30 dB initial sidelobe level $7/8\lambda$ element spacing group, there is a 12 element Dolph-Chebyshev array, a 14 element modified Taylor array, a 12 element powers of cosine on a pedestal array, and a 13 element Taylor array that comprise the MNE set (Tables 4.1 to 4.3). Their statistics are plotted in Figures B.128 to B.131. 14 element Dolph-Chebyshev, powers of cosine on a pedestal, and Taylor arrays are additionally statistically analyzed to complete the ENE group (Figures B.132 to B.134).

40 dB initial sidelobe level MNE arrays in the $7/8\lambda$ element spacing group consist of a 15 element Dolph-Chebyshev array, a 17 element modified Taylor array, a

21 element powers of cosine on a pedestal array, and a 17 element Taylor array (see Tables 4.1 to 4.3). Statistical metrics for these arrays are illustrated in Figures B.135 to B.138. The addition of Figures B.139 to B.141 add statistical metrics for 21 element Dolph-Chebyshev, powers of cosine on a pedestal and Taylor arrays to complete the ENE data set of 21 element arrays (Tables 4.1 and 4.3).

A 17 element Dolph-Chebyshev array, a 20 element modified Taylor array, a 27 element powers of cosine on a pedestal array and a 20 element Taylor array make up the 50 dB initial sidelobe level $7/8\lambda$ element spacing MNE group (Tables 4.1 to 4.3). The associated ENE group is made up of the aforementioned 27 element array and 27 element Dolph-Chebyshev, modified Taylor, and Taylor arrays (Tables 4.1 to 4.3). Randomization metrics are graphically illustrated in Figures B.142 to B.145 (MNE set) and B.146 to B.148 (additional ENE arrays not in the MNE set – see Tables 4.1 to 4.3).

Examination of the $7/8\lambda$ element spacing array factor randomization metrics leads to similar conclusions as were previously developed for the narrower element spaced randomized array factors. Again, the primary performance criterion of concern is the sidelobe level. The other metrics tend to not vary much. Additionally, SLLdBDeltasM and SLLdBDeltasS appear to remain at a unique plateau for each initial sidelobe level – independent of element spacing.

4.5 Element Randomization Results – Additional Discussion

In the previous section, the worst case randomization results were presented for each array design by element spacing and taper over scan. Randomization data from every scan output was not presented, just the worst case for each array design.

Results were presented from 0.00010 to 0.10000 λ randomization. Now the task is to draw some conclusions versus taper type, element spacing, and initial design sidelobe level.

When trying to determine if one thing works better than another, both are often subjected to equivalent testing that takes them past their limits. That is how the data from the previous section can be further analyzed. In this particular case, the testing is comparison of performance at 0.10000 λ randomization. Since it was previously analyzed that sidelobe level is the only performance metric that gets significantly impacted by the randomization process, it is focused upon in this section.

Baseline sidelobe level, SLLdBDeltasM, and SLLdBDeltasS, data was aggregated for the 0.10000 λ randomization cases. It was sorted by element spacing, initial design sidelobe level, taper type and whether the array came from an MNE or ENE set. After significant analysis, it turns out regardless of if the array was in an MNE or ENE group, there was not a significant difference in sidelobe level performance due to MNE or ENE grouping. This is evident in Figures 4.7 to 4.10. In these figures, the minimum and maximum baseline sidelobe level, SLLdBDeltasM, and SLLdBDeltasS are plotted by element separation for 20 (Figure 4.7), 30 (Figure 4.8), 40 (Figure 4.9), and 50 dB (Figure 4.10) initial design sidelobe levels. Recall, the SLLdBDeltasM and SLLdBDeltasS data came from the worst case array performers for from the randomization analysis of each initial design sidelobe level. Hence, the maximum SLLdBDeltasM and SLLdBDeltasS are the worst of the worst for a given initial design sidelobe level and element separation. The minimum SLLdBDeltasM and SLLdBDeltasS are the “best” of the worst. Maximum and minimum baseline sidelobe levels are just that – the best and worst initial sidelobe level broken down by initial design sidelobe level group and array element separation.

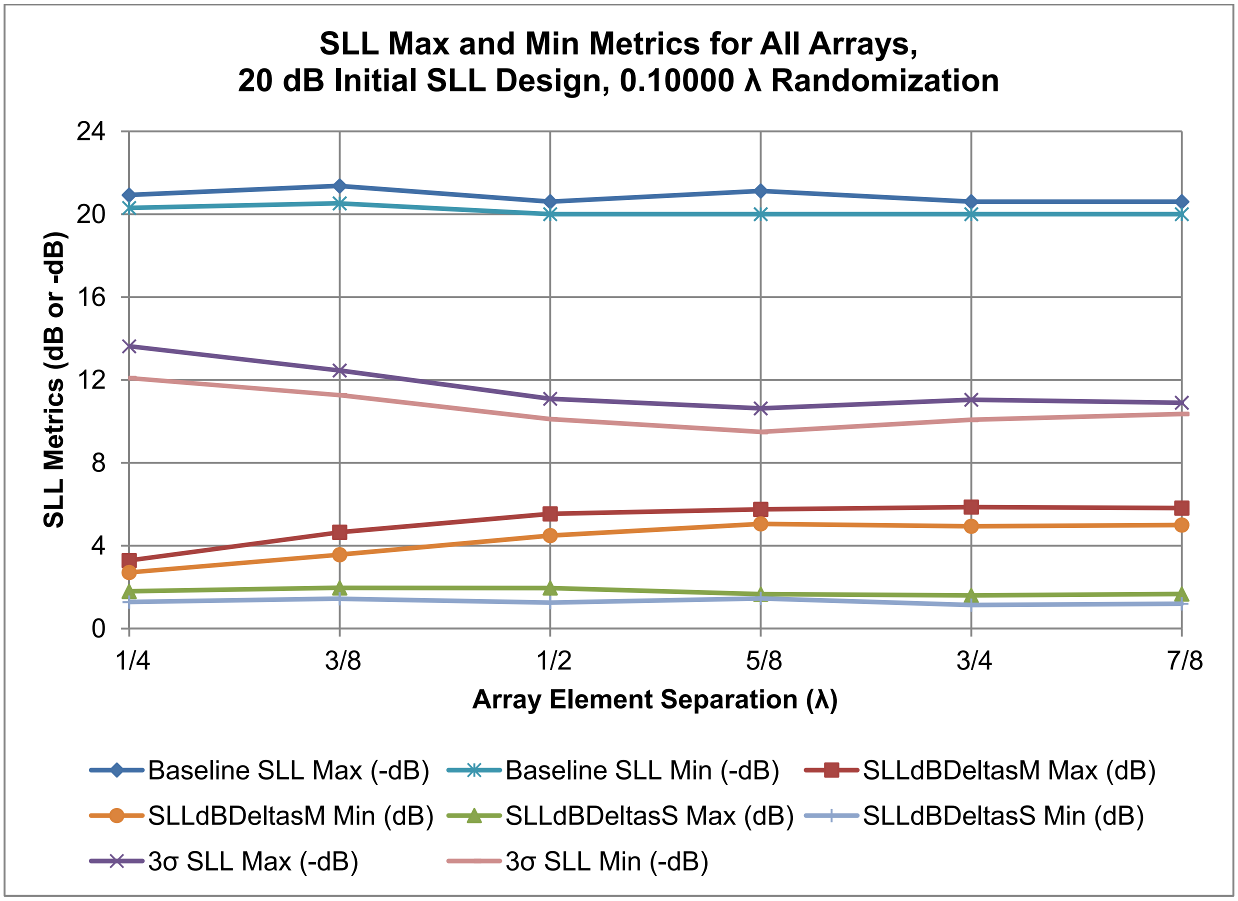

Figure 4.7. *Sidelobe level maximum and minimum metrics by array element nominal spacing for initial 20 dB sidelobe arrays.*

Also presented in Figures 4.7 to 4.10 is a calculated 3σ worst case performance limit.

$$3\sigma SLL = baselineSLL - (SLLdBDeltasM + 3 * SLLdBDeltasS) \qquad (4.9)$$

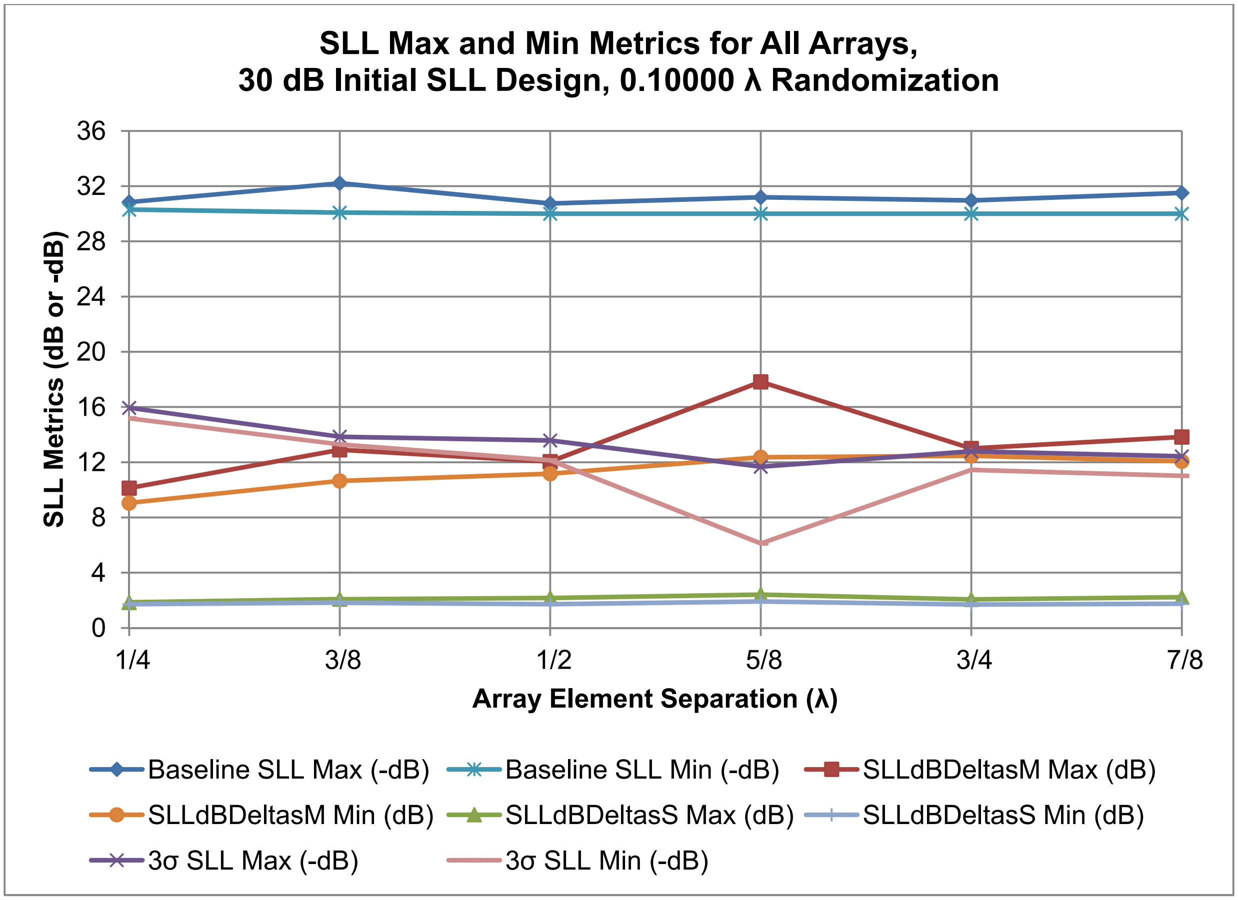

Figure 4.8. *Sidelobe level maximum and minimum metrics by array element nominal spacing for initial 30 dB sidelobe arrays.*

This type of calculation presumes a Gaussian distribution for the sidelobe level performance, which is generally true. Quick examination of histograms supports this. However, for cases with low levels of randomization, this histograms and statistics indicate an exponential distribution of the population relative to sidelobe level. For these particular plots (Figures 4.7 to 4.10), a Gaussian assumption appears quite valid (see Figure B.24). Even if the Gaussian approximation is not strictly valid, $3\sigma SLL$ provides a scaled means of aggregating overall sidelobe level performance data into one metric. The $3\sigma SLL$ was calculated for every array at the 0.10000 λ randomization level. For each initial design sidelobe level group (20, 30, 40, and 50 dB), the maximum and minimum values were plotted over array element separation.

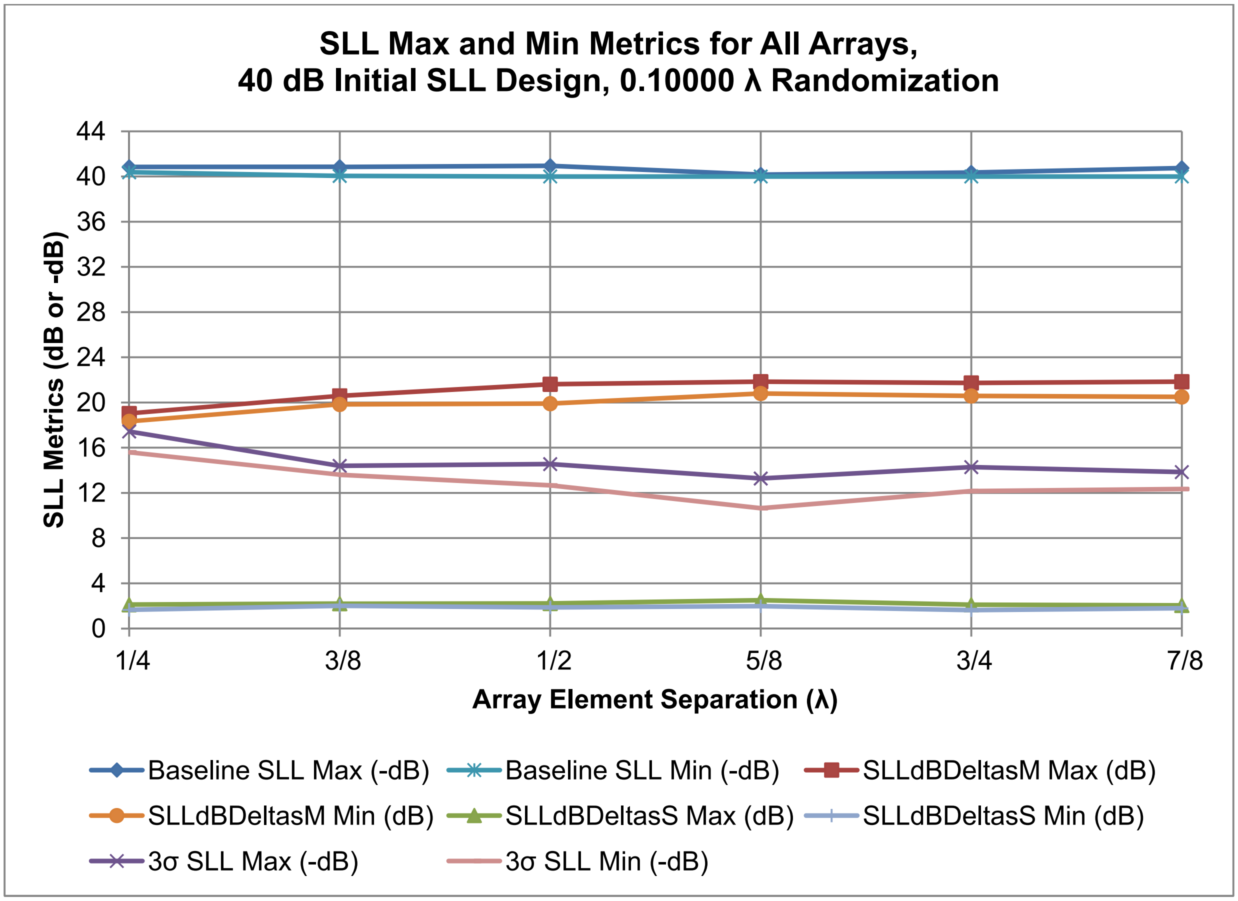

Figure 4.9. *Sidelobe level maximum and minimum metrics by array element nominal spacing for initial 40 dB sidelobe arrays.*

As was mentioned in the previous section, array sidelobe level performance appeared to approach an asymptotic level for each initial sidelobe level design as element spacing was increased. This is evident in Figures 4.7 to 4.10. The $3\sigma SLL$ maximum and minimums appear to level out as the spacing is increased. Each initial sidelobe level plot reaches a slightly higher value as the initial design sidelobe level is increased. SLLdBDeltasM also appears to illustrate a unique asymptotic behavior by initial design sidelobe level. SLLdBDeltasS on the other hand, appears to remain near constant over the entire range of data.

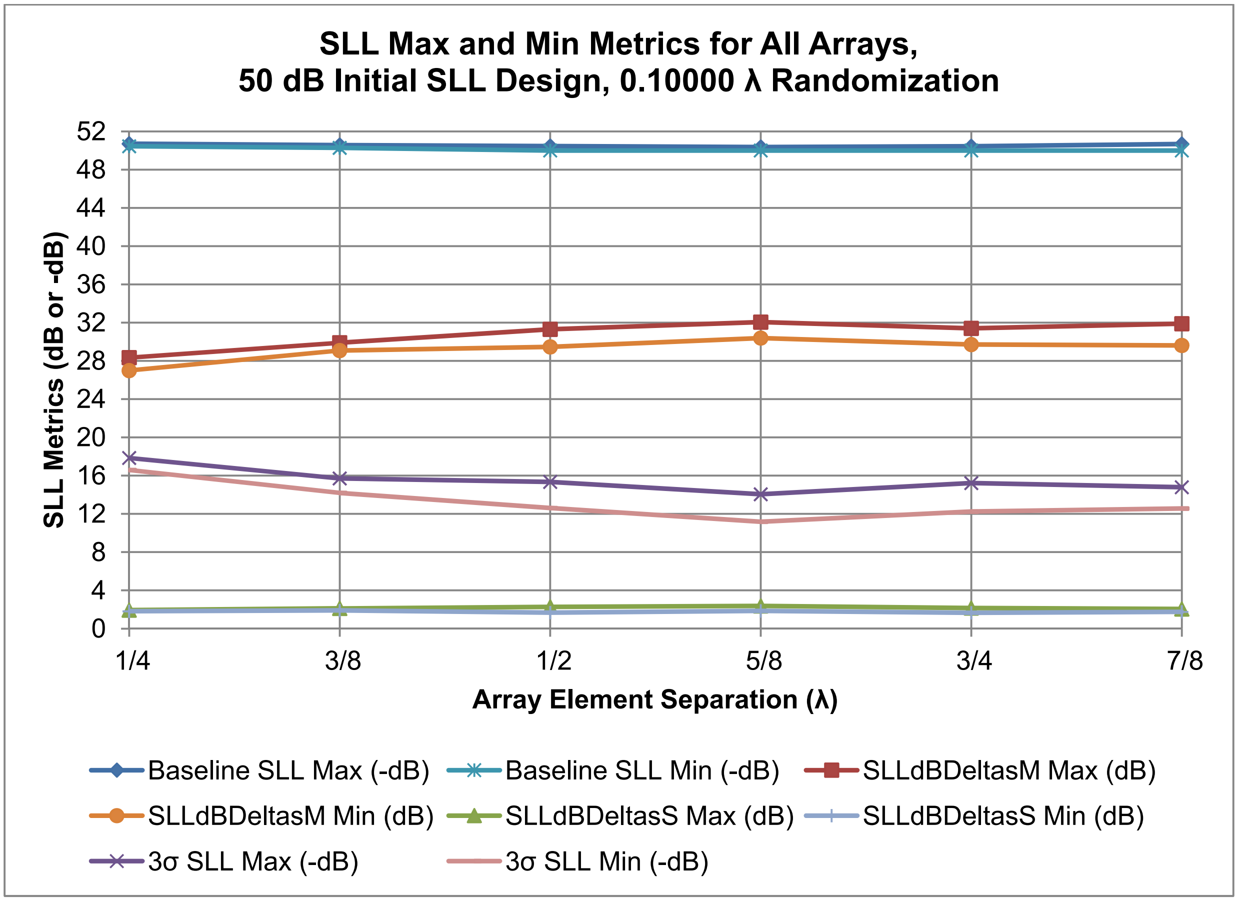

Figure 4.10. *Sidelobe level maximum and minimum metrics by array element nominal spacing for initial 50 dB sidelobe arrays.*

In each of the plots, the range between an individual metric maximum and minimum is generally quite small – typically about 2 dB. This supports the claim that the choice of taper, whether a minimum number of elements or near minimum number, only has a secondary affect upon the final sidelobe level. The same can be said for element spacing. However, element spacing will still affect scanning ability of the array design as usual.

5.0 Independent Element Motion

In the previous chapter, linear array performance degradation was examined in detail as a function of random element position errors. All of this analysis was performed from a stationary point of view. The intent of this chapter is to examine the problem from a dynamic point view. What happens to the far field AF when each element of an array exhibits time varying movement that is independent of the other elements? How can any errors be rectified?

The assumptions for this portion of the study are the same as the rest of the study. Element patterns are considered isotropic, hence antenna orientation is not important or considered. Second is an assumption of no mutual coupling between the elements. Only linear arrays will be evaluated, and polarization is ignored. As mentioned previously, in this scenario, the results obtained would represent the best performance that can be expected for a given linear array configuration; assuming mutual coupling and attitude errors affecting polarization and element patterns will degrade performance further. Hence the research is intended to place a bound on expected performance.

A conceptual, operation use case is schematically illustrated in Figure 5.1. In this case there are five antenna elements illuminating the same target. The five elements could be independent satellites illuminating a ground target, airborne platforms interacting with a surface or other airborne object, surface RADAR, or any other distributed array. In order to focus the array beam on the target, the position of the elements relative to each other will need to be known.

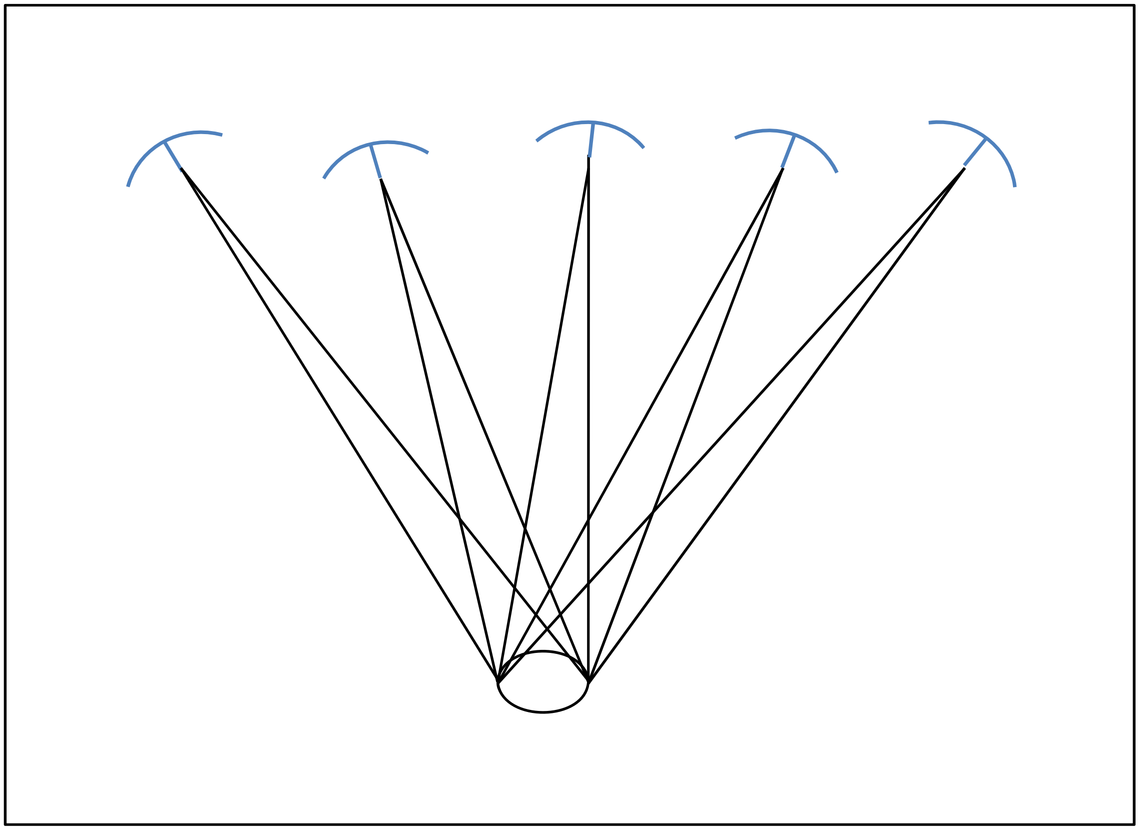

Figure 5.1. *Distributed array concept of operation.* A five element distributed array illuminating a target. The five elements are mechanically independent of each other.

5.1 Formulation – Time Dependent Array Factor

In the often usual case of an array, all of the radiating elements do not exhibit any intentional movement or motion relative to each other. Their electromagnetic array pattern design can be developed as though the system of elements is fixed in space. In this case the array factor can be computed from (2.13). It is restated here with some modified subscripts.

$$AF_s(\theta,\phi)=\sum_{i=0}^{N} A_{si}e^{j\left(k\hat{\mathbf{r}}\cdot\mathbf{r}_{si}-\alpha_{si}\right)}. \tag{5.1}$$

AF_S is the stationary array factor. The result is generated as a sum over all of the "i " elements that are each located at $\mathbf{r}_{si}$ and each having phase delay of α_{Si}, sometimes also called the steering phase. $\hat{\mathbf{r}}$ denotes the unit radial vector in spherical coordinates in the direction of observation. "k" is the scalar wave number, and A_{Si} is the amplitude coefficient of the "i^{th}" radiating element. Careful examination of (5.1) shows it to be a function of angle due to the θ and ϕ dependence of $\hat{\mathbf{r}}$. The "s" subscript throughout (5.1) is intended to denote that all of the array elements are stationary.

When adding time dependent movement to the individual array elements, $\mathbf{r}_{si}$ becomes an independent function of time for each of the "i^{th}" radiating elements. The array factor transforms into

$$AF(\theta,\phi,t)=\sum_{i=0}^{N} A_{si}e^{j\left[k\hat{\mathbf{r}}\cdot\mathbf{r}_i(t)-\alpha_{Si}\right]} \tag{5.2}$$

where $AF(\theta,\phi,t)$ is the time dependent version of AF_S. $\mathbf{r}_i(t)$ is simply a time dependent position vector that defines the instantaneous position of the "i^{th}" radiating element in space at time "t".

Recall that the unit vector, $\hat{\mathbf{r}}$, is defined as

$$\hat{\mathbf{r}}=\hat{\mathbf{x}}\,sin\,\theta\,cos\,\phi+\hat{\mathbf{y}}\,sin\,\theta\,sin\,\phi+\hat{z}\,cos\,\theta\,. \tag{5.3}$$

The position vector of the "i^{th}" radiating element, $\mathbf{r}_i(t)$, expressed in Cartesian coordinates is

$$\mathbf{r}_i(t)=\hat{\mathbf{x}}x_i(t)+\hat{\mathbf{y}}y_i(t)+\hat{\mathbf{z}}z_i(t). \tag{5.4}$$

Expressing $\hat{\mathbf{r}}$ and $\mathbf{r}_i(t)$ in terms of (5.3) and (5.4) and substituting back into (5.2) produces and alternative expression for the exponential argument in (5.2).

$$ARG = j\langle k\{x_i(t) \sin\theta \cos\phi + y_i(t) \sin\theta \sin\phi + z_i(t) \cos\theta\} - \alpha_{si}\rangle \tag{5.5}$$

(5.5) can be rewritten in terms of a matrix equation that greatly facilitates the calculation of the array factor as a function of time.

$$ARG = j\left\langle k\begin{bmatrix} x_i(t) & y_i(t) & z_i(t) \end{bmatrix}\begin{bmatrix} \sin\theta & 0 & 0 \\ 0 & \sin\theta & 0 \\ 0 & 0 & \cos\theta \end{bmatrix}\begin{bmatrix} \cos\phi \\ \sin\phi \\ 1 \end{bmatrix} - \alpha_{si}\right\rangle \tag{5.6}$$

Combining the matrix form of the argument (5.6) with the time dependent array factor expression (5.2) results in a numerically efficient calculation for $AF(\theta, \varphi, t)$.

$$AF(\theta, \phi, t) = \sum_{i=0}^{N} A_{si} e^{j\left\{k\begin{bmatrix} x_i(t) & y_i(t) & z_i(t) \end{bmatrix}\begin{bmatrix} \sin\theta & 0 & 0 \\ 0 & \sin\theta & 0 \\ 0 & 0 & \cos\theta \end{bmatrix}\begin{bmatrix} \cos\phi \\ \sin\phi \\ 1 \end{bmatrix} - \alpha_{si}\right\}} \tag{5.7}$$

Equation (5. 7) is valid for a single instant in time. The convenience of this representation comes from the fact that the angular dependency of $\hat{\mathbf{r}} \cdot \mathbf{r}_{si}$ is first calculated for a (θ, ϕ) pair and the effects of the time dependence upon position can be sequentially calculated for all desired points in time for one of the (θ, ϕ) pairs.

The next step is to define $\mathbf{r}_i(t)$. To that end, the derivation can take two directions. In the first, the array can be considered to be a group of elements that can be described as though they are vibrating in place (Figure 5.2).

The second approach assumes that all the elements in the entire array are attempting to move in unison along a specific trajectory. In the latter case, each element is independently attempting to match the movement of all the other array elements in position, velocity, and acceleration (Figure. 5.3). They are trying to maintain constant relative positioning while attempting to follow parallel trajectories. These two avenues of additional analysis only affect the description of the position matrix $([x_i(t) \quad y_i(t) \quad z_i(t)])$ in (5.7).

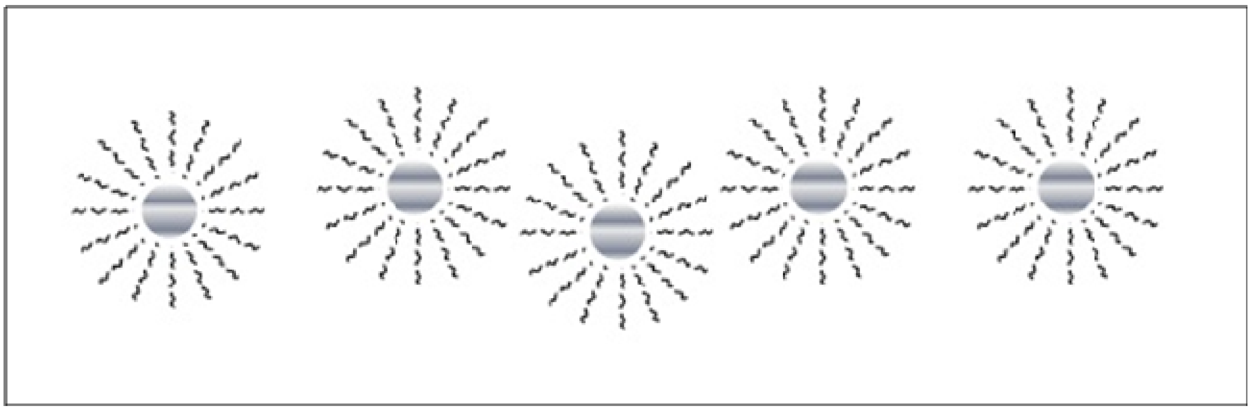

Figure 5.2. *A linear antenna array with vibrating elements at an instant in time.* All elements are intended to be aligned on the same line, but due to vibration they have momentarily moved out of their desired position.

5.2 Vibrating in Place

In the case where the motion of the elements is considered to be vibrating in place, $\mathbf{r}_i(t)$ can be broken into two pieces. One piece is $\mathbf{r}_{si}$ from (5.1), that is a constant position vector. It can be considered to be the nominal element position vector for optimum array performance. The other piece is an error vector, $\mathbf{r}_{ei}(t)$, that begins at the position denoted by $\mathbf{r}_{si}$ and ends at the instantaneous position of the "i^{th}" element (Figure 5.4).

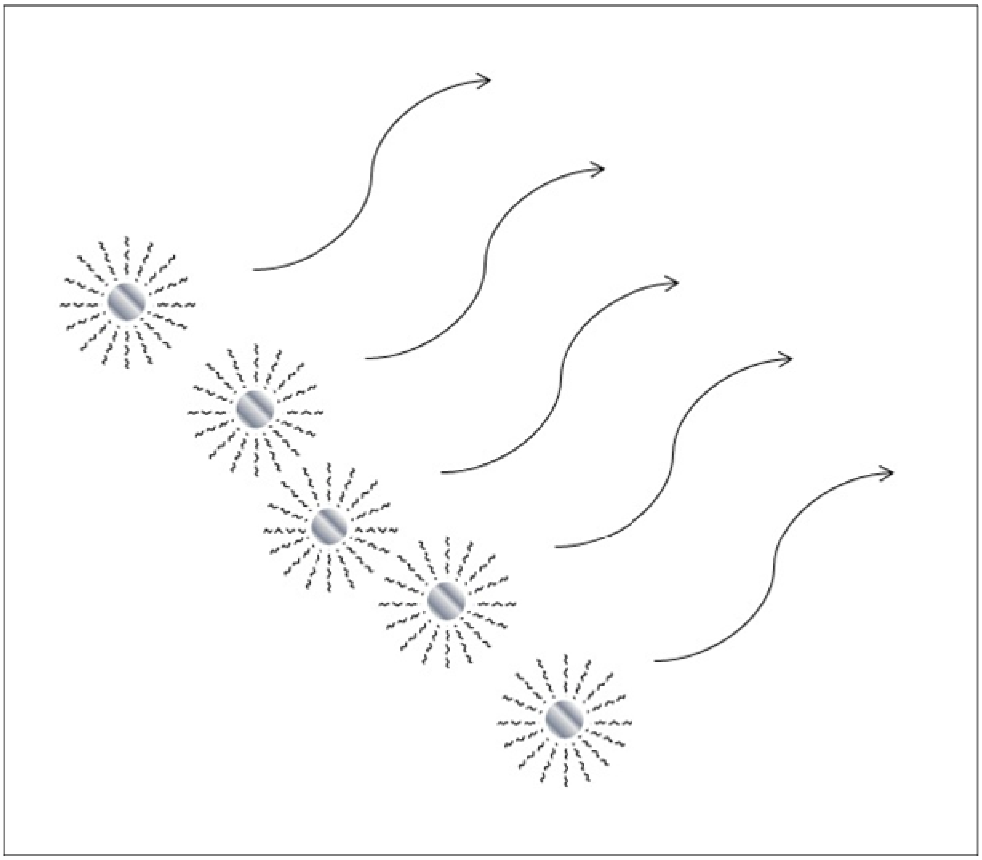

Figure 5.3. *Linear antenna array elements attempting to move along parallel trajectories at an instant in time.* All elements are attempting to follow parallel paths, but due to vibration their placement at any instant in time is not constant relative to each other.

Consequently, the resulting relationship among $\mathbf{r}_i(t)$, $\mathbf{r}_{si}$, and $\mathbf{r}_{ei}(t)$ becomes

$$\mathbf{r}_i(t) = \mathbf{r}_{si} + \mathbf{r}_{ei}(t) \tag{5.8}$$

By substitution of (5.8) back into (5.2), the time dependent array factor ($AF(\theta,\phi,t)$) becomes

$$AF(\theta,\phi,t) = \sum_{i=0}^{N} A_{si} e^{j\left[k\hat{\mathbf{r}}\cdot\mathbf{r}_{si} - \alpha_{si} + k\hat{\mathbf{r}}\cdot\mathbf{r}_{ei}(t)\right]}. \tag{5.9}$$

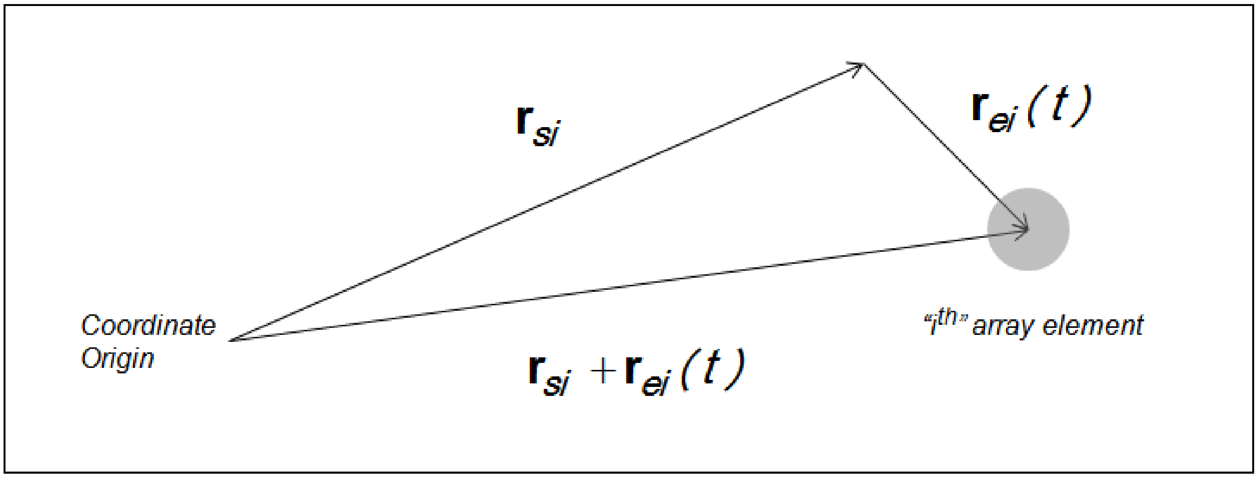

Figure 5.4. *The "i^{th}" array element as it vibrates in place. Its position as a function of time is the sum of a stationary, nominal position vector and an error vector.*

Note the similarity of (5.9) to (5.1). They only differ by a phase factor due to the error vectors. The vector $\mathbf{r}_{si}$ is defined as

$$\mathbf{r}_{si} = \hat{\mathbf{x}}x_{si} + \hat{\mathbf{y}}y_{si} + \hat{\mathbf{z}}z_{si} \tag{5.10}$$

where x_{si}, y_{si}, and z_{si} are the (x, y, z) coordinates of the vector. Similarly, $\mathbf{r}_{ei}$ is defined to be

$$\mathbf{r}_{ei} = \hat{\mathbf{x}}x_{ei} + \hat{\mathbf{y}}y_{ei} + \hat{\mathbf{z}}z_{ei} \tag{5.11}$$

where the components of $\mathbf{r}_{ei}$ are determined from the vector difference between $\mathbf{r}_i(t)$ and $\mathbf{r}_{si}$. As a result, (5.9) can be rewritten in the same form as (5.7), again resulting in a numerically efficient form for calculation (5.12).

$$AF(\theta,\phi,t) = \sum_{i=0}^{N} A_{si} e^{j\left\langle k\left[\{x_{si}+x_{ei}(t)\}\ \{y_{si}+y_{ei}(t)\}\ \{z_{si}+z_{ei}(t)\}\right]\times \begin{bmatrix} \sin\theta & 0 & 0 \\ 0 & \sin\theta & 0 \\ 0 & 0 & \cos\theta \end{bmatrix}\begin{bmatrix} \cos\phi \\ \sin\phi \\ 1 \end{bmatrix} - \alpha_{si} \right\rangle} \tag{5.12}$$

Without any loss of generalization, $\mathbf{r}_{ei}(t)$ can be represented as the sum of three orthogonal vectors where each vector is the sum of several sinusoidal vibrations with unique amplitudes, frequencies and initial phase (5.13). In others words, it can be represented as a Fourier series or transform.

$$\begin{aligned} \mathbf{r}_{ei}(t) &= \hat{\mathbf{u}}_a \sum_{d=1}^{m} B_{iad}\, sin(\omega_{iad} t + \upsilon_{iad}) \\ &+ \hat{\mathbf{u}}_b \sum_{f=1}^{n} B_{ibf}\, sin(\omega_{ibf} t + \upsilon_{ibf}) \\ &+ \hat{\mathbf{u}}_c \sum_{g=1}^{p} B_{icg}\, sin(\omega_{icg} t + \upsilon_{icg}) \end{aligned} \tag{5.13}$$

$\hat{\mathbf{u}}_a$, $\hat{\mathbf{u}}_b$, and $\hat{\mathbf{u}}_c$ are orthogonal unit vectors. The "i" subscript throughout (5.13) indicates that each array element can have several vibration modes associated with it. The upper limits of the summations indicate the number of vibration modes for a particular element in the direction of the associated unit vector. The "B" coefficients are the amplitudes of the individual modes, while the "ω" coefficients correspond to the radial frequencies, and the "υ" coefficients denote the phase of each vibration mode at time $t = 0$. The subscripts track the element number, unit vector, and summation index.

Setting $\hat{\mathbf{u}}_a$, $\hat{\mathbf{u}}_b$, and $\hat{\mathbf{u}}_c$ equal to $\hat{\mathbf{x}}$, $\hat{\mathbf{y}}$, and $\hat{\mathbf{z}}$, and incorporating (5.13), the position argument of (5.12), $[\{x_{si} + x_{ei}(t)\} \;\; \{y_{si} + y_{ei}(t)\} \;\; \{z_{si} + z_{ei}(t)\}]$, can be rewritten as

$$\left[\{x_{si} + x_{ei}(t)\} \quad \{y_{si} + y_{ei}(t)\} \quad \{z_{si} + z_{ei}(t)\}\right] =$$

$$\left[\left\{x_{si} + \sum_{d=1}^{m} B_{ixd} \, sin(\omega_{ixd} t + \upsilon_{ixd})\right\} \quad \left\{y_{si} + \sum_{f=1}^{n} B_{iyf} \, sin(\omega_{iyf} t + \upsilon_{iyf})\right\} \right. \tag{5.14}$$

$$\left. \left\{z_{si} + \sum_{g=1}^{p} B_{iyg} \, sin(\omega_{iyg} t + \upsilon_{iyg})\right\}\right].$$

(5.14) is strictly a time domain driven equation. It is one of the three matrices in the exponential argument of (5.12). Each of the other matrices in (5.12) correspond to the θ and ϕ directions of the array factor calculation. Using this matrix representation, the calculation is easily broken down into independent time, θ and ϕ components of the time dependent array factor ($AF(\theta,\phi,t)$).

5.3 Moving in Unison

When the elements in the entire array are attempting to move in unison along a specific trajectory, the element level calculations of $x_i(t)$, $y_i(t)$ and $z_i(t)$ in (5.7) can be determined from an accelerometer output approach. In this approach, it is assumed that initial conditions for velocity and position are known or can be easily determined through some accurate means at time $t = 0$, for each element, i. Utilizing an accelerometer, at each element, acceleration, $\mathbf{a}_i(t)$, is known as a function of time. For any instant in time, velocity, $\mathbf{v}_i(t = \alpha)$, is simply the initial velocity plus the integral of the acceleration up to time $t = \alpha$ (5.15).

$$\mathbf{v}_i(t = \alpha) = \mathbf{v}_i(t = 0) + \int_0^{\alpha} \mathbf{a}(\tau) d\tau \tag{5.15}$$

Similarly, instantaneous position, $\mathbf{r}_i(t=o)$, is the initial position plus the integral of the velocity function (5.16).

$$\mathbf{r}_i(t=o)=\mathbf{r}_i(t=0)+\int_0^o \mathbf{v}_i(\psi)d\psi \tag{5.16}$$

Again in the moving case, the motion of any element can be broken into two parts. The first part represents the desired position of the moving element, $\mathbf{r}_{mi}(t)$, and the other is the error vector, $\mathbf{r}_{ei}(t)$, that begins at $\mathbf{r}_{mi}(t)$ and ends at the instantaneous position of the "i^{th}" element, $\bar{r}_i(t)$. $\mathbf{r}_{mi}(t)$ is the apriori desired position of the "i^{th}" element in order for the array to perform at its optimum design. Similar to (5.8), the resulting relationship among $\mathbf{r}_i(t)$, $\mathbf{r}_{mi}$, and $\mathbf{r}_{ei}(t)$ becomes

$$\mathbf{r}_i(t)=\mathbf{r}_{mi}(t)+\mathbf{r}_{ei}(t). \tag{5.17}$$

$\mathbf{r}_{mi}(t)$ can be know *a priori*, provided on an incremental, virtually instantaneous basis, or calculated from other incrementally provided data. Considering the entire array's trajectory, without any roll included, an array origin position vector can also be defined that is a function of time that defines the array's desired trajectory. This trajectory is assumed to be the same for all of the elements except for a fixed vector offset. Let this vector be referred to as $\mathbf{r}_a(t)$. If there is no position error,

$$\mathbf{r}_i(t)-\mathbf{r}_a(t)=\mathbf{r}_{mi}(t)-\mathbf{r}_a(t)=\mathbf{r}_{si} \tag{5.18}$$

Recall, $\mathbf{r}_{si}$ is the "i^{th}" radiating element position vector from the stationary array as indicated in 5.1. With position error included,

$$\mathbf{r}_i(t)-\mathbf{r}_a(t)=\mathbf{r}_{mi}-\mathbf{r}_a+\mathbf{r}_{ei}=\mathbf{r}_{si}+\mathbf{r}_{ei}(t). \tag{5.19}$$

This illustrates that the difference between the time dependent position vector, $\mathbf{r}_i(t)$, and the time dependent array origin position vector, $\mathbf{r}_a(t)$, can be used to calculate the array performance in the same numerical fashion that is illustrated in (5.12) by substituting the (x,y,z) components of the quantity $\{\mathbf{r}_i(t)-\mathbf{r}_a(t)\}$ in pace of the (x,y,z) components of $\{\mathbf{r}_{si}+\mathbf{r}_{ei}(t)\}$.

Further considering the accelerometer measurements, the components of the vector differences between the element position vector and the array origin position vector can be calculated (5.20).

$$x_i(t=o)-x_a(t=o)=x_i(t=0)-x_a(t=0)+ \int_{\psi=0}^{o}\left\{v_{xi}(\alpha=0)-v_{xa}(\alpha=0)+\int_{\tau=0}^{\alpha}[a_{xi}(\tau)-a_{xa}(\tau)]d\tau\right\}d\psi \tag{5.20a}$$

$$y_i(t=o)-y_a(t=o)=y_i(t=0)-y_a(t=0)+ \int_{\psi=0}^{o}\left\{v_{yi}(\alpha=0)-v_{ya}(\alpha=0)+\int_{\tau=0}^{\alpha}[a_{yi}(\tau)-a_{ya}(\tau)]d\tau\right\}d\psi \tag{5.20b}$$

$$z_i(t=o)-z_a(t=o)=z_i(t=0)-z_a(t=0)+ \int_{\psi=0}^{o}\left\{v_{zi}(\alpha=0)-v_{za}(\alpha=0)+\int_{\tau=0}^{\alpha}[a_{zi}(\tau)-a_{za}(\tau)]d\tau\right\}d\psi \tag{5.20c}$$

In (5.20), non-subscript a's represent acceleration, where v's represent velocity. Subscript x's, y's, and z's denote their respective coordinate values of a vector quantity. Subscript a's indicate vector components that are associated with the array origin position vector. ψ and τ are dummy time variables associated with the velocity and acceleration function integrations, respectively. In similar fashion to (5.12) as mentioned above, the array factor is then calculated according to (5.21).

$$AF(\theta,\phi,t)=\sum_{i=0}^{N}A_{si}e^{j\left\langle k\left[\{x_i(t)-x_a(t)\}\quad\{y_i(t)-y_a(t)\}\quad\{z_i(t)-z_a(t)\}\right]\times\begin{bmatrix}\sin\theta & 0 & 0\\ 0 & \sin\theta & 0\\ 0 & 0 & \cos\theta\end{bmatrix}\begin{bmatrix}\cos\phi\\ \sin\phi\\ 1\end{bmatrix}-\alpha_{si}\right\rangle} \tag{5.21}$$

The vector, $\mathbf{r}_a(t)$, deserves some additional discussion. As previously mentioned, $\mathbf{r}_a(t)$, essentially describes a moving array origin. It can be known *a priori*, as the desired path that the array is intending to pursue. Alternatively, it can be established as the actual position vector of one of the elements in the array. In this case, $\{\mathbf{r}_i(t)-\mathbf{r}_a(t)\}$ is always zero for that particular element, and all phase calculations are centered about it.

In reality, the best solution is to consider each element individually without tracking an array moving origin and using an equation similar to (5.12) with $\mathbf{r}_{si}$ replaced with $\mathbf{r}_{mi}(t)$.

$$AF(\theta,\phi,t)=\sum_{i=0}^{N}A_{si}e^{j\left\langle k\left[\{x_{mi}+x_{ei}(t)\}\quad\{y_{mi}+y_{ei}(t)\}\quad\{z_{mi}+z_{ei}(t)\}\right]\times\begin{bmatrix}\sin\theta & 0 & 0\\ 0 & \sin\theta & 0\\ 0 & 0 & \cos\theta\end{bmatrix}\begin{bmatrix}\cos\phi\\ \sin\phi\\ 1\end{bmatrix}-\alpha_{si}\right\rangle} \tag{5.21}$$

Recording acceleration of each element and performing the integration to calculate $\mathbf{r}_i(t)$, then subtracting off $\mathbf{r}_{mi}(t)$ (known *a priori*) produces the error vector $\mathbf{r}_{ei}(t)$. This can then be used to determine $AF(\theta,\phi,t)$ and subsequent corrections to enhance array performance.

5.4 Phasors and Time Domain Notation

In the previous sections of this chapter, some time domain notation has been combined with the phasor notation of the array factor ($AF(\theta,\phi,t)$). This is a bit unusual, but justifiable. The entire representation of the of the field from the array is

$$\vec{\mathscr{E}}(t,r,\theta,\phi) = e^{j\omega t}\frac{e^{-jkr}}{4\pi r}\mathbf{EF}\sum_{i=0}^{N} A_{si} e^{j\{k\hat{\mathbf{r}}\cdot[\mathbf{r}_{si}+\mathbf{r}_{ei}(t)]-\alpha_{si}\}}. \tag{5.22}$$

This notation is in complex time harmonic form. In a strict sense, it is only absolutely accurate for frequency use. However, it is often utilized as the approximation when the system is assumed to be narrow band. A narrow band assumption would assume that the bandwidth of the signal (B) in hertz is significantly less than the center or carrier frequency of the array.

$$B << \frac{\omega}{2\pi} \tag{5.23}$$

In this particular case, to meet the requirements of (5.23), the time dependent quantities in the array factor exponential argument would need to be very small. 10 KHz frequency content in $\mathbf{r}_{ei}(t)$ would satisfy this requirement, even in the case of HF carrier frequencies.

Another way to look at this is in terms of narrow band phase modulation on each antenna element. Rearranging the terms in 5.22, results in an array system that appears to have a unique phase modulation for every element.

$$\vec{\mathscr{E}}(t,r,\theta,\phi) = e^{j\omega t}\frac{e^{-jkr}}{4\pi r}\mathbf{EF}\sum_{i=0}^{N} A_{si} e^{jk\hat{\mathbf{r}}\cdot\mathbf{r}_{ei}(t)} e^{j[k\hat{\mathbf{r}}\cdot\mathbf{r}_{si}-\alpha_{si}]} \tag{5.24}$$

Finally, examining the exponential in $AF(\theta,\phi,t)$ in terms of a Taylor series leads to the understanding that a time harmonic representation is still valid. Previously, $\mathbf{r}_i(t)$, was defined as a time dependent sum that included an error position.

$$\mathbf{r}_i(t) = \mathbf{r}_{si} + \mathbf{r}_{ei}(t) \tag{5.25a}$$

$$\mathbf{r}_i(t) = \hat{\mathbf{x}}x_i(t) + \hat{\mathbf{y}}y_i(t) + \hat{\mathbf{z}}z_i(t) \tag{5.25b}$$

$$x_i(t) = x_{si} + x_{ei}(t) \tag{5.25c}$$

$$y_i(t) = y_{si} + y_{ei}(t) \tag{5.25d}$$

$$z_i(t) = z_{si} + z_{ei}(t) \tag{5.25e}$$

Utilizing the defined terms in (5.25), and taking a Taylor sum of $x_i(t)$ about x_{si}, results in the series representation

$$x_i(t) = x_{si} + x_{ei}\frac{dx_{ei}(t)}{dt} + \frac{x_{ei}^2}{2!}\frac{d^2x_{ei}(t)}{dt^2} + \frac{x_{ei}^3}{3!}\frac{d^3x_{ei}(t)}{dt^3} + \cdots \tag{5.26}$$

(5.26) can be used to bound the value of $x_i(t)$. For all of the analysis in this study, the magnitude of x_{ei}, y_{ei}, and z_{ei} are bounded (5.27).

$$0.00010\lambda \le |x_{ei}|,|y_{ei}|,|z_{ei}| \le 0.10000\lambda \tag{5.27}$$

Continuing with only x-components, each $x_{ei}(t)$ can be approximated as a sum of sinusoids. Any of its derivatives will be no larger than the amplitude of the sinusoid. The maximum amplitude of any sinusoid is 0.1λ, and the maximum derivative of any order cannot be larger than 0.1λ. Consequently,

$$|x_i(t)| \le |x_{si}| + 1.0\cdot10^{-2}\lambda^2 + 5\cdot10^{-4}\lambda^3 + 1.\overline{6}\cdot10^{-5}\lambda^4 + \cdots \tag{5.28}$$

The desired x_{ei} relative to other elements is zero in this analysis. Consequently, $x_i(t)$ is being modulated by no more than 0.01 of a square wavelength at the highest frequency of vibration. As part of the time function, this caries a scalar multiplier of $\frac{\omega}{c}$ as compared to the scalar multiplier of ω for the main time dependence. This is approximately 11 orders of magnitude smaller than the coefficient on the carrier time t. An identical argument can be made for $y_i(t)$ and $z_i(t)$.

When examining the entire representation of the field as indicated in (5.22), the time term with an ω coefficient present in the exponential argument is 11 orders of magnitude greater than the $\frac{\omega}{c}$ coefficient of $\mathbf{r}_{ei}(t)$ not including the bounding analysis. The positions errors are zero mean processes. This is evident from the pointing error means in Chapter 4. Hence, the phase contribution of $\mathbf{r}_{ei}(t)$ relative to the carrier frequency is orders of magnitude less. Even if the frequency content of the error process is on the order of 10 KHz, its contribution to the carrier phase accumulation is at least 6 orders of magnitude less when limited to 0.10000 λ variation.

All of these arguments emanate from a central notion; the velocity of movement of the elements is significantly less than the speed of light. From three view points, the use of $\mathbf{r}_{ei}(t)$ in the antenna factor phasor exponential in (5.22) is an acceptable approach.

5.5 System Performance Enhancement

While utilizing a distributed array, it would be desirable to be able to correct for the phase errors that come up in real time and maintain as much of the sidelobe performance as possible. To do this the, the error term, $\mathbf{r}_{ei}(t)$, in the exponent of each term of (5.22) ideally needs to be driven to zero by adjusting the array element weights during real time processing. At first glance, one considers the possibility of compensating for the phase error by adjusting the error phase of each term in the desired look direction to zero. If the phase deviation is small compared to the carrier phase, it would seem that zeroing out this phase term might eliminate the perturbation and recover the sidelobe performance. This type phase alignment is known as Maximum Ration Combining (MRC). MRC processing solves the beam pointing error, but off axis of the main beam, the desired cancelation in the sidelobe region does not occur. In fact it is so unremarkable, that it looks like the uncorrected patterns without the beam pointing errors. Consequently, an example is not even presented here.

This eliminates the possibility of each element being able to correct of its own mis-positioning independently of the other elements. It now places a requirement upon the system for high speed sharing of relative position information in order to determine enhancements to the array element coefficients on a global basis and communicating the enhancements to each element for popper element weighting.

An alternative method becomes necessary for weight determination. Since this is a real time system, multiple data snapshots are not a desirable requirement. In other words, it is desired to be able to update the array weights with every set of position data updates. Adaptive array algorithms that operated on single data snapshots were researched; multiple RF samples are undesirable if position information is available. Three algorithms that met this requirement were investigated – direct data transformation by Kim, Sarkar, and Salazar–Palma [74] [75], minimum variance processing by J. Capon [76], and array pattern synthesis techniques by Ng [77] and Ng, Hwa, and Kot [78].

Of the three adaptive algorithms, the direct data and Ng's array pattern synthesis techniques did not enhance the antenna patterns. Capon's minimum variance method, however, did produce some improvements over the unprocessed array results outlined in the previous chapter. In this method, the desired peak of beam direction is identified. In addition, the angular locations where pattern nulls are required to enhance the performance of the sidelobes are also established. This set of information along with the position of the array elements at a given moment in time are utilized to calculate a correlation matrix and calculate a set of array element weights to enhance the performance of the array factor.

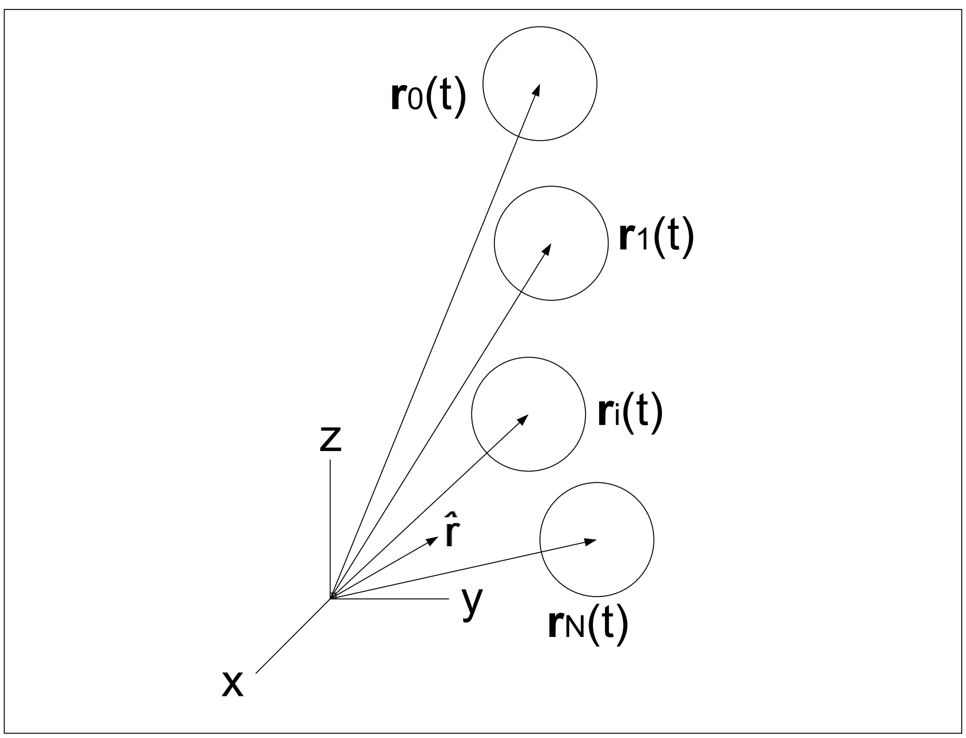

Figure 5.5. *Distributed array geometry at time "t" with "*$\hat{\mathbf{r}}$*" and element position vectors indicated.* $\hat{\mathbf{r}}$ denotes the direction from which an incoming plane wave is approaching the array.

The geometry is illustrated in Figure 5.5. Each array element is illustrated at its position at time "t." At that moment in time, the relative voltages that would be received at each element, for a unit amplitude plane wave coming from a desired "look" direction $\hat{\mathbf{r}}$, phase referenced to the origin, are calculated. $\hat{\mathbf{r}}$ is in the desired direction of the array main beam or scan angle. These relative voltages are placed into a vector.

$$\mathbf{e} = \begin{bmatrix} e^{-jk\hat{\mathbf{r}}\cdot\mathbf{r}_0(t)} \\ e^{-jk\hat{\mathbf{r}}\cdot\mathbf{r}_1(t)} \\ e^{-jk\hat{\mathbf{r}}\cdot\mathbf{r}_2(t)} \\ \cdot \\ \cdot \\ \cdot \\ e^{-jk\hat{\mathbf{r}}\cdot\mathbf{r}_N(t)} \end{bmatrix}. \tag{5.29}$$

Often, multiple incoming desired plane waves are utilized in the calculation of $\mathbf{e}$. In this case, each element of $\mathbf{e}$ is a sum of voltages due to plane waves arriving from multiple directions, all of which are phase referenced to the origin. $\mathbf{e}$ then becomes

$$\mathbf{e} = \begin{bmatrix} \sum_{\xi=1}^{g} e^{-jk\hat{\mathbf{r}}_\xi\cdot\mathbf{r}_0(t)} \\ \sum_{\xi=1}^{g} e^{-jk\hat{\mathbf{r}}_\xi\cdot\mathbf{r}_1(t)} \\ \sum_{\xi=1}^{g} e^{-jk\hat{\mathbf{r}}_\xi\cdot\mathbf{r}_2(t)} \\ \cdot \\ \cdot \\ \cdot \\ \sum_{\xi=1}^{g} e^{-jk\hat{\mathbf{r}}_\xi\cdot\mathbf{r}_N(t)} \end{bmatrix} \tag{5.30}$$

where "g" is the number of desired incoming plane wave directions.

For the same moment in time the $\mathbf{e}$ vector was calculated, a similar vector is calculated for the angular locations where nulls are required in the pattern to enhance the sidelobe performance. In this case, an amplitude term is included with each wave to allow for non-unit waves.

$$\mathbf{Y} = \begin{bmatrix} \sum_{h=1}^{q} A_h e^{-jk\hat{\mathbf{r}}_h \cdot \mathbf{r}_0(t)} \\ \sum_{h=1}^{q} A_h e^{-jk\hat{\mathbf{r}}_h \cdot \mathbf{r}_1(t)} \\ \sum_{h=1}^{q} A_h e^{-jk\hat{\mathbf{r}}_h \cdot \mathbf{r}_2(t)} \\ \cdot \\ \cdot \\ \cdot \\ \sum_{h=1}^{q} A_h e^{-jk\hat{\mathbf{r}}_h \cdot \mathbf{r}_N(t)} \end{bmatrix}. \tag{5.31}$$

From $\mathbf{Y}$, a correlation matrix is calculated.

$$\mathbf{R} = \sigma^2 \mathbf{I} + \mathbf{Y}\mathbf{Y}^H . \tag{5.32}$$

In (5.32), the super script H refers to the Hermitian transpose. $\mathbf{I}$ is the N+1xN+1 identity matrix, and σ^2 represents the variance of uncorrelated white noise that is added to the calculation.

Finally, new array weights are calculated [79]

$$\mathbf{w}_0 = \frac{\mathbf{R}^{-1}\mathbf{e}}{\mathbf{e}^H \mathbf{R}^{-1}\mathbf{e}} . \tag{5.33}$$

A new array factor for time "t" is recalculated with the new weights

$$AF(\theta,\phi,t) = \sum_{i=0}^{N} w_{0i} e^{j[k\hat{\mathbf{r}} \cdot \mathbf{r}_i(t)]}. \tag{5.34}$$

5.6 System Performance Enhancement Examples

Enhancements were examined for several array configurations with element uncertainty variation of 0.10000 λ. Generally, two configurations were examined for each nominal element spacing. Table 5.1 lists all the configurations where enhancement was investigated.

Element Spacing (λ)	Initial Design SLL (dB)	Number of Elements	Taper Type	Scan Angles (°θ)
1/4	20	19	Power of Cosine on a Pedestal	40, 50, 60, 70, 80, 90, 100, 110, 120, 130, 140
	50	55	Modified Taylor	90
3/8	20	13	Taylor	40, 50, 60, 70, 80, 90, 100, 110, 120, 130, 140
	50	37	Modified Taylor	90
1/2	20	9	Dolph-Chebyshev	40, 50, 60, 70, 80, 90, 100, 110, 120, 130, 140
	50	28	Dolph-Chebyshev	90
5/8	20	7	Dolph-Chebyshev	70, 80, 90, 100, 110
	50	21	Dolph-Chebyshev	90
3/4	20	9	Dolph-Chebyshev	80, 90, 100
	50	28	Dolph-Chebyshev	90
7/8	20	9	Dolph-Chebyshev	90
	50	27	Modified Taylor	90

Table 5.1. *Array configurations with 0.10000 λ randomization where pattern enhancement was investigated.*

The process of developing the parameters for the **e** and **Y** vectors starts with examining an array that has it elements located in the ideal position. The minimum variance algorithm is first applied to the ideal array. On the **e** vector side of the analysis, the algorithm is run without any undesired plane waves. Desired plane waves are added until the beamwidth is no longer increasing. At that point, the first few sidelobe peaks away from the main beam are identified. Undesired plane waves are added at the same angles as the near main beam sidelobe peaks to optimize for the lowest sidelobe level. These desired and undesired plane wave parameters are then used with the randomly positioned elements to help enhance the sidelobe levels from the results outlined in Chapter 4. In all cases, ϕ was set to 0^{o} for both the **e** and **Y** vector calculations, as was the case for the randomization analysis.

For example, consider the $1/4\,\lambda$ spacing, 20 dB, 19 element, powers of cosine on a pedestal linear array. If we begin generating the array factor for a $1/4\,\lambda$ spacing, 19 element array with a single desired look angle of 90^{o} and no interferers, the resultant array factor pattern is illustrated in Figure 5.6(a). If the single look angle is modified to two look angles at 85^{o} and 95^{o}, 84^{o} and 96^{o}, or 83^{o} and 97^{o} (Figure 5.6(b) to 5.6(d)), the beamwidth and sidelobe level change with the settings. The look angles of 84^{o} and 96^{o} illustrate the best sidelobe level performance; consequently, they are used to generate the **e** vector. Once the desired look angles are established, work begins to establish the undesired plane wave angles.

To further enhance the sidelobe performance, undesired signals of unit amplitude are added to the **Y** vector. The angular locations of the first sidelobes are determined.

These angles are used to generate the **Y** vector. In the example illustrated in Figure 5.6(c), the first sidelobes have their maximums at 67° and 113° θ. Applying this to

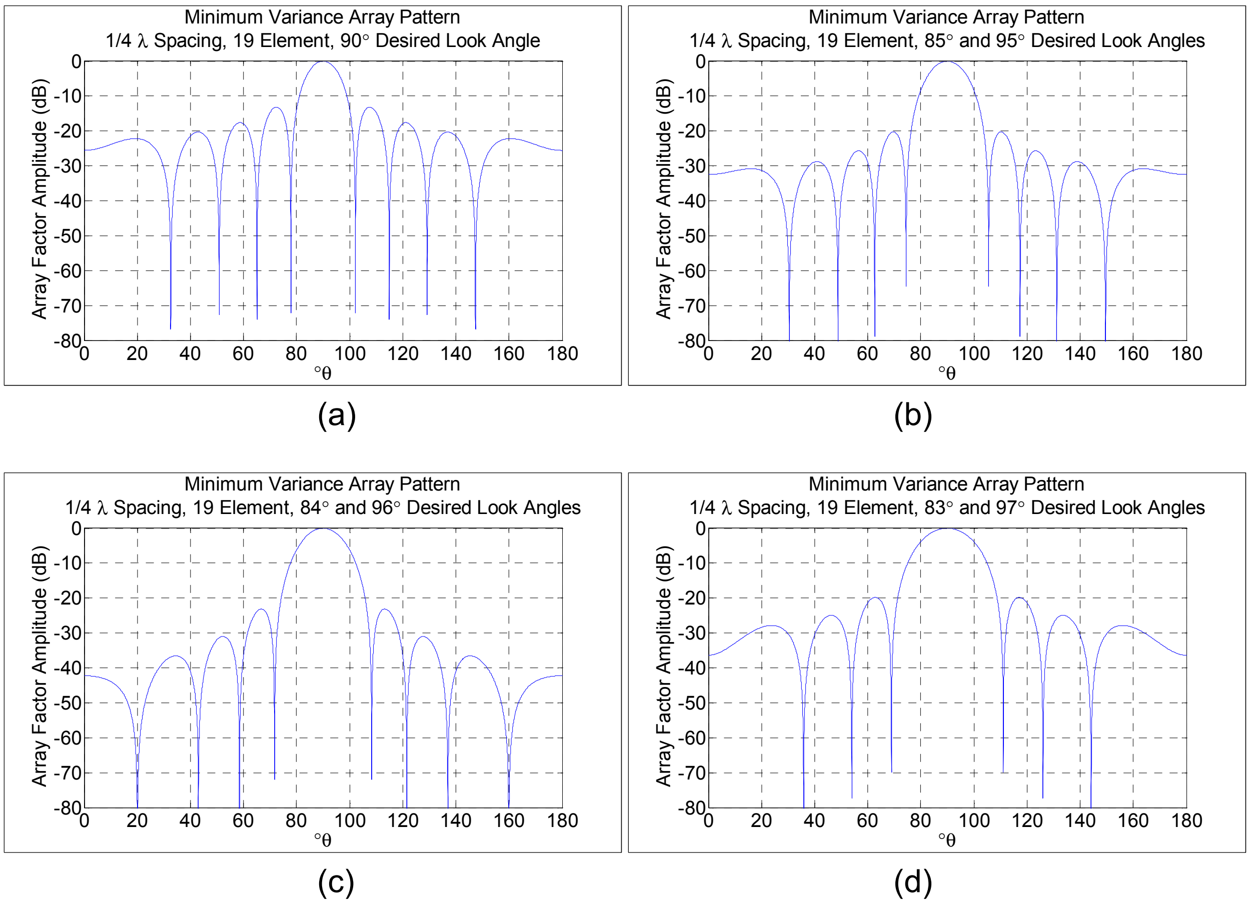

Figure 5.6. *Minimum variance patterns for a $1/4\,\lambda$ spacing, 19 element linear array with ideally positioned elements.* 90° (a), 85° and 95° (b), 84° and 96° (c), and 83° and 97° (d) desired wave look angles and no undesired interferers are utilized for generating the array factor patterns.

same ideal array with the two look angles produces a further optimized sidelobe result (Figure 5.7(a)). At this point one would think that adding additional interferers would further enhance the result. The next sidelobe peaks for the ideal array with 84° and 96° desired wave look angles are located at 52.28125° and 127.71875°. Applying the two desired look angles with the four undesired wave directions (52.28125°, 67°, 113°, and

127.71875°) results in the array factor pattern plotted in Figure 5.7(b). As can be seen, this does not help the sidelobe situation. Consequently, using the two optimum desired look angles (84° and 96°) with the undesired look angles that correspond to the first sidelobe peaks (67°, 113°), results in the best initial characteristic set for enhancement under mis-positioned element conditions for the distributed array of 19 almost linear elements with desired $1/4\,\lambda$ spacing.

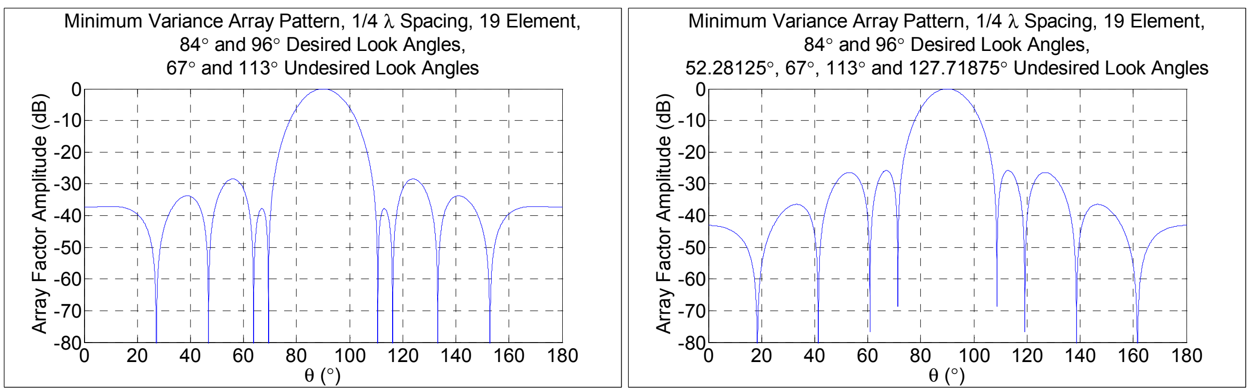

(a) (b)

Figure 5.7. *Minimum variance patterns for a $1/4\,\lambda$ spacing, 19 element linear array with ideally positioned elements and desired look angles of 84° and 96°.* Additional undesired interferers placed at 67° and 113° (a) or 52.28125°, 67°, 113°, and 127.71875° are also utilized to generate the array factor patterns.

In (5.32), the addition of uncorrelated white noise with variance σ^2 was included in the calculation of the correlation matrix $\mathbf{R}$. All of the examples plotted in Figures 5.6 and 5.7 utilized a noise variance of eight. The value of eight was determined empirically by calculating array factor patterns using various levels of noise. Eight worked out to be an optimum value for minimizing sidelobes and was used for all enhancement calculations. Without noise in the calculation, the minimum variance calculation does not work for cases without undesired interferers.

With the parameters for the $\mathbf{e}$ and $\mathbf{Y}$ vectors identified, all that is left is to run the algorithm for the mis-positioned locations of the array elements and examine its performance. For the specific cases listed in Table 5.1, corrections to element randomization of 0.10000λ with exact knowledge of the element positions was executed as well as adding a 0.01000λ uncertainty to the 0.10000λ case and utilizing the 0.10000λ position for the enhancement calculations. The latter condition is intended to simulate a small uncertainty in the element position knowledge.

Continuing with the 19 almost linear elements with desired $1/4\,\lambda$ spacing, The 100, 0.10000λ radial position randomization previous runs without correction were rerun with the enhancement algorithm assuming perfect knowledge of their position. These 100 patterns per scan angle are plotted as a group for each scan angle (Figure 5.8). Close examination of these patterns shows an angular space near the main beam that has reduced sidelobes. This phenomenon shows significant occurrence on all the scan angles except for the 40^o and 140^o beam scan cases. For comparison purposes, the initial 100, 0.10000λ radial position randomization runs per scan angle without correction for the same 19 element array are plotted in Figure 5.9. The initial runs show degraded sidelobes over the entire scan, including the angular space near the main beam. However, maximum sidelobe levels between the two sets of runs are essentially the same.

As previously noted in the initial analysis of the degradations due to mis-positioning of the array elements, the primary performance impact is in the sidelobe

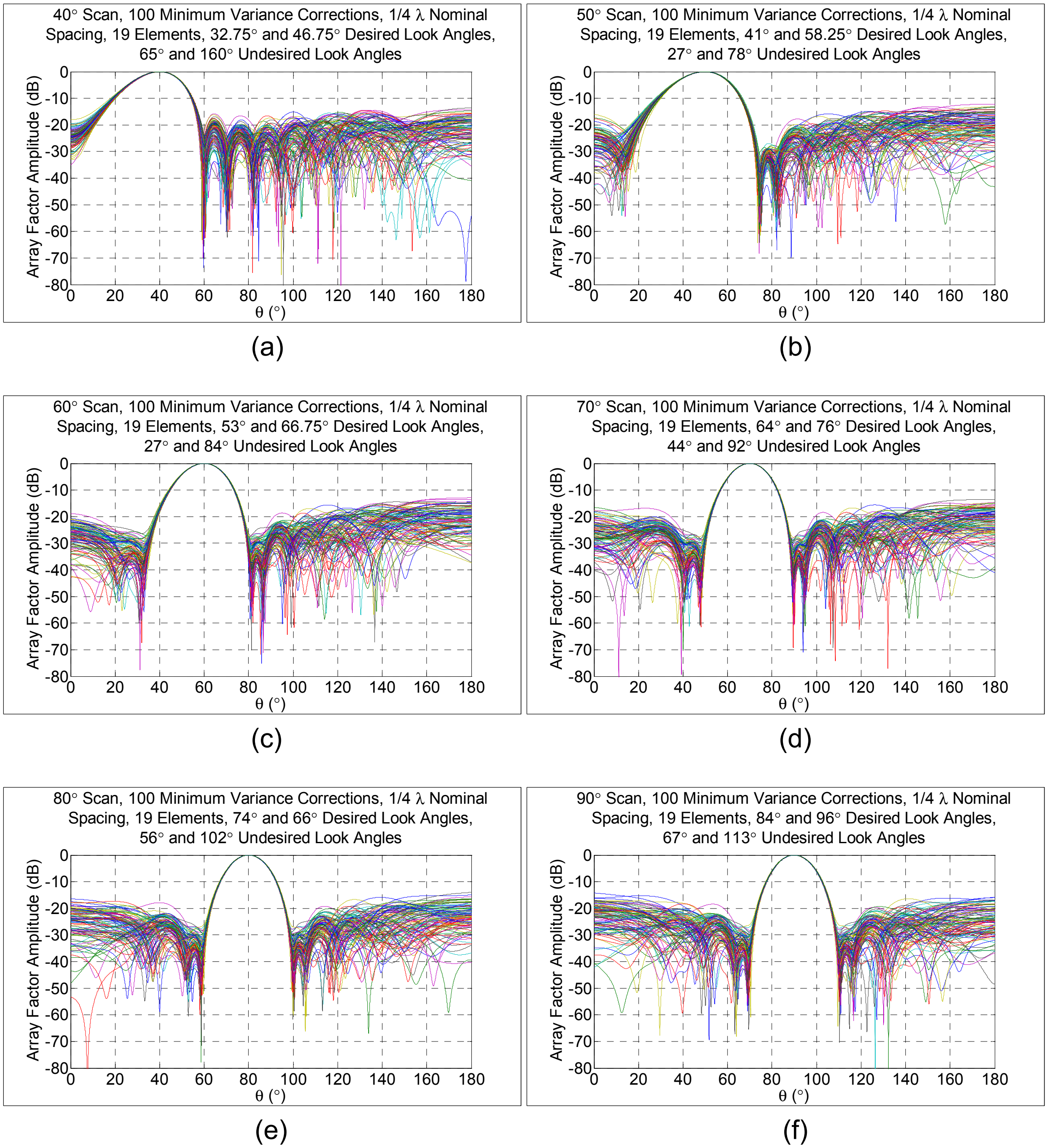

Figure 5.8. *19 almost linear elements with nominal* $1/4\,\lambda$ *spacing and minimum variance enhancement.* Rerun of 100, 0.10000λ radial element position randomization runs per scan angle (a-k) with application of the minimum variance enhancement algorithm as described previously. Perfect knowledge of each element position is assumed for this enhancement.

Figure 5.8. (cont'd)

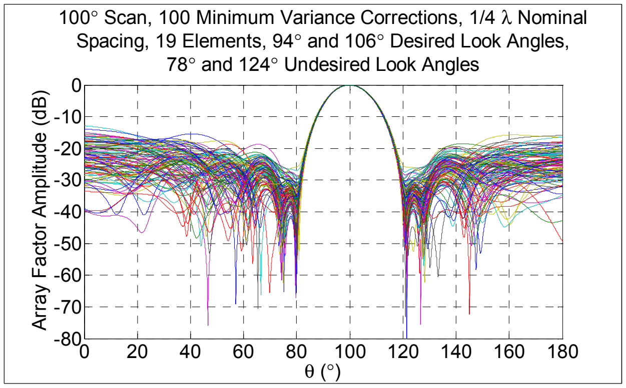

(g)

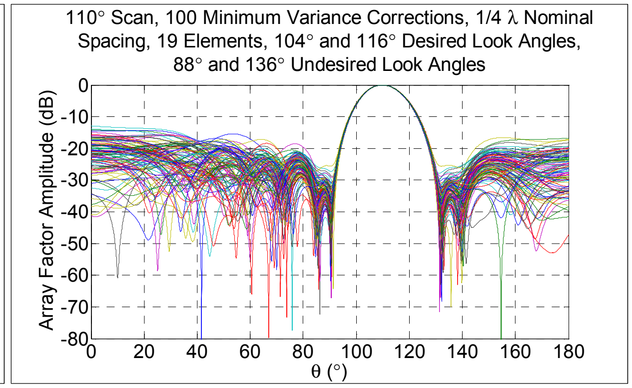

(h)

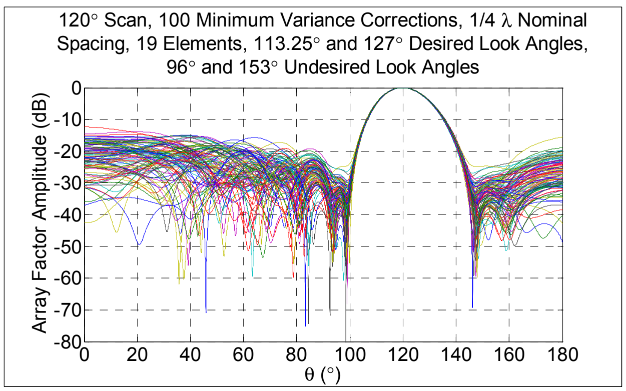

(i)

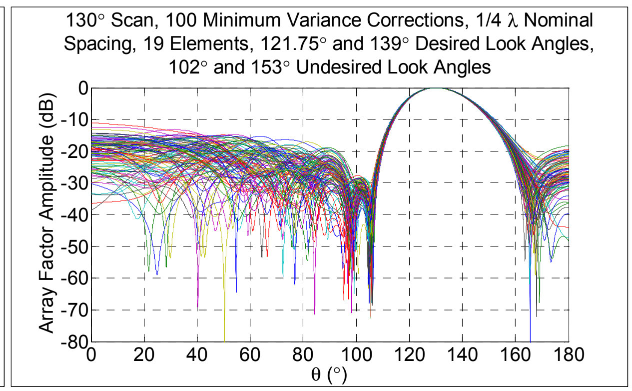

(j)

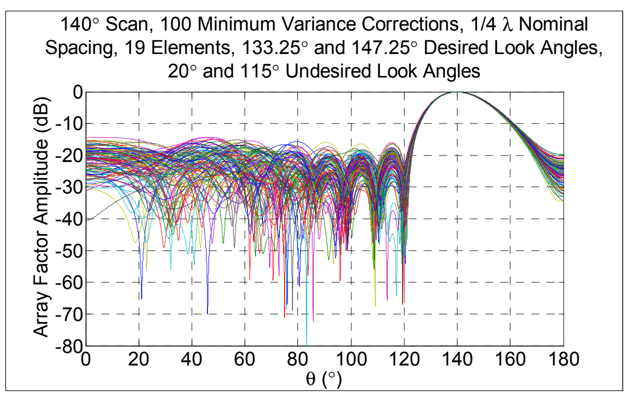

(k)

level of the arrays. Graphically comparing the sidelobe level statistics between the non-enhanced and enhanced array factors for the $1/4\,\lambda$ nominal spacing, 19 element arrays

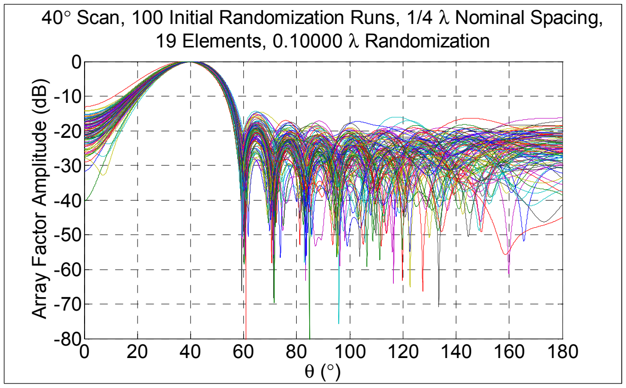

(a)

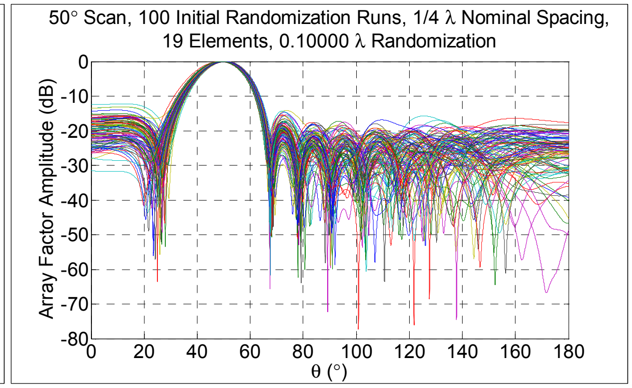

(b)

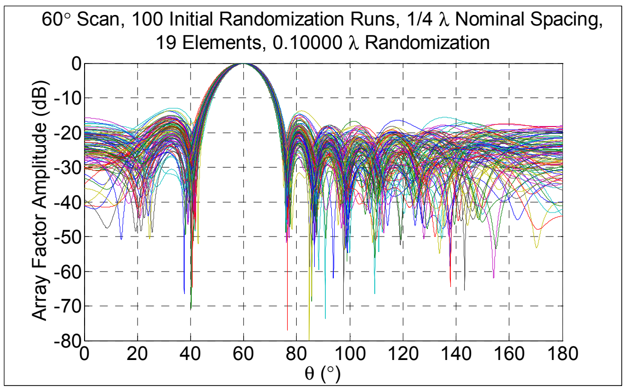

(c)

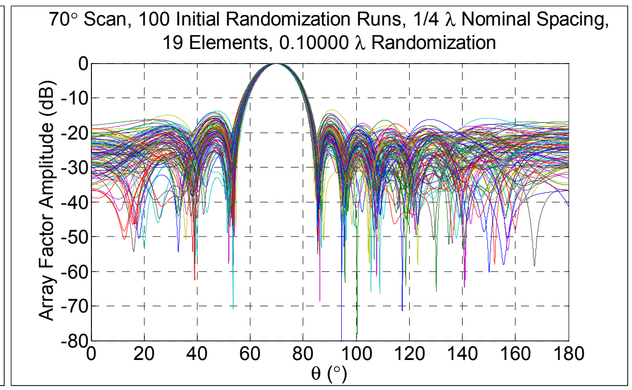

(d)

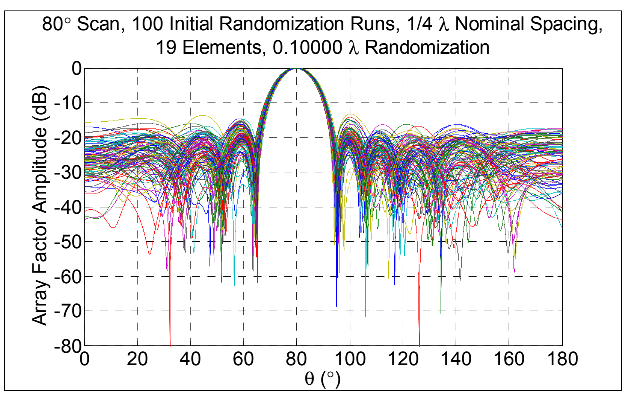

(e)

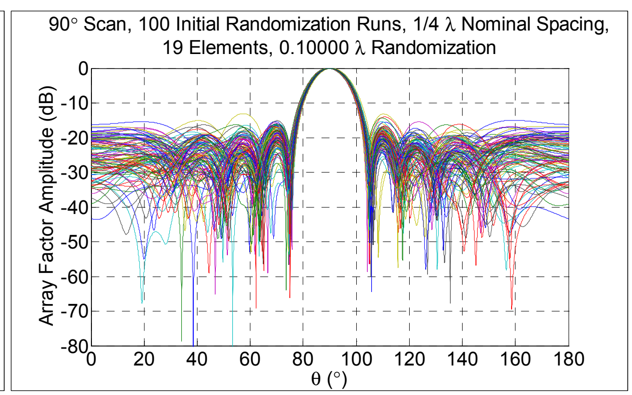

(f)

Figure 5.9. *19 almost linear elements with nominal $1/4\,\lambda$ spacing and 0.10000 λ radial element position randomization.* Initial array factor pattern (20 dB powers of cosine on a pedestal taper) runs of 100, element position randomizations plotted per scan angle (a-k).

Figure 5.9. (cont'd)

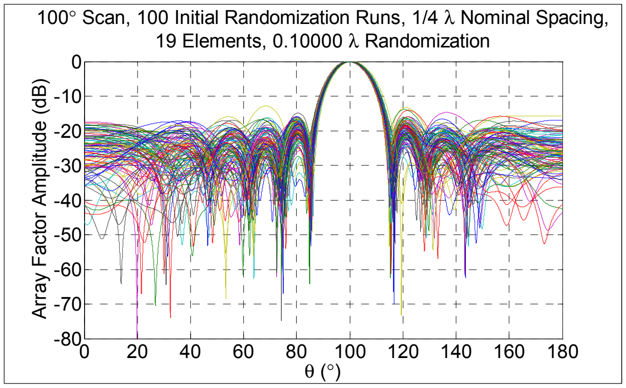

(g)

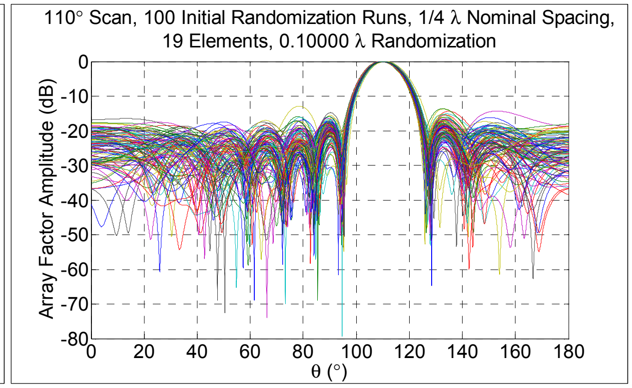

(h)

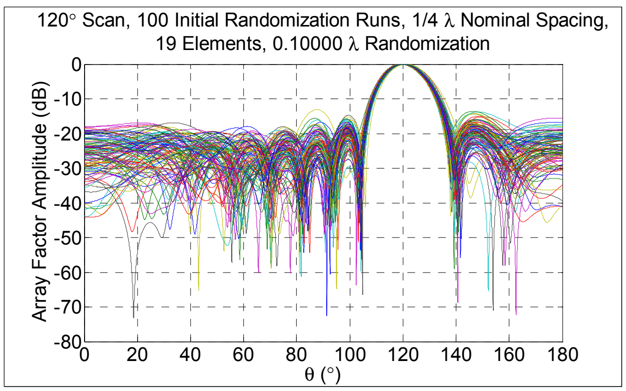

(i)

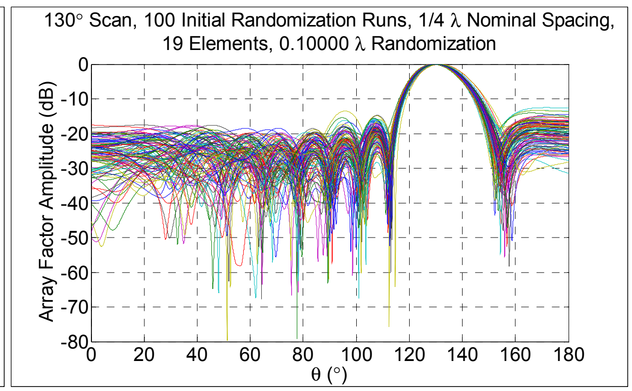

(j)

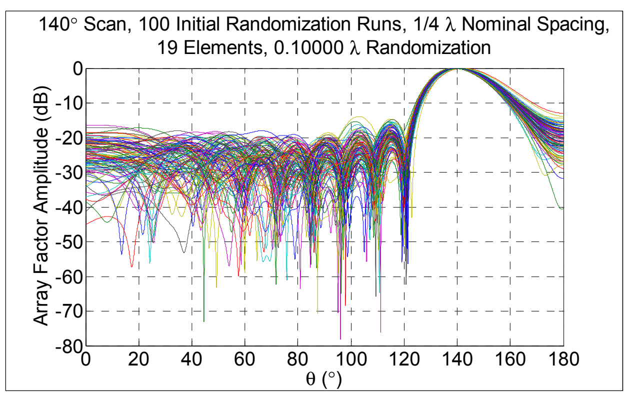

(k)

with 0.10000λ randomization results (Figure 5.10) shows improvement in SLLdBDeltasM near broadside scan, and about 1 dB degradation in SLLdBDeltasS.

As exemplified in Figure 5.8, there is general sidelobe level improvement near the main beam for the majority of scan angles. Given this, the improvement in the sidelobe level in the vicinity of the main was examined in further detail.

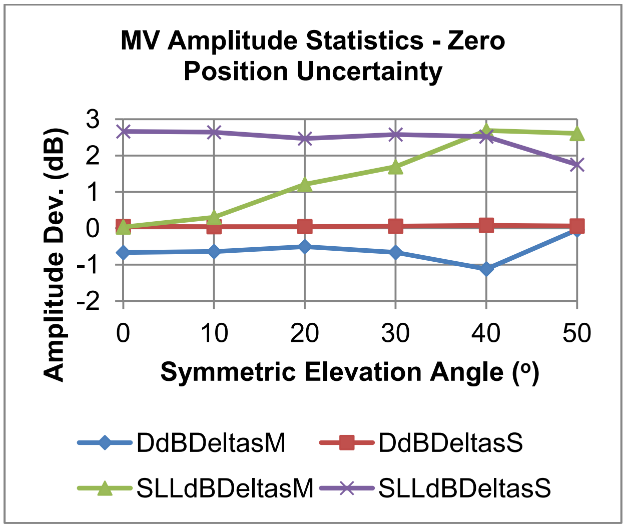

(a)

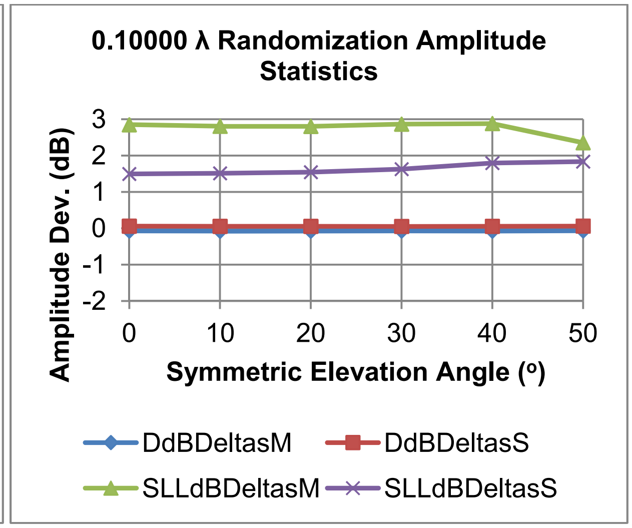

(b)

Figure 5.10. *Sidelobe level and directivity statistics for an array with 19 almost linear elements, nominal $1/4\,\lambda$ spacing, 0.10000 λ radial element position randomization and minimum variance enhancement.* Amplitude statistics assuming perfect knowledge of position (a) and no enhancement processing from the initial array factor pattern (20 dB powers of cosine on a pedestal taper) runs (b) are compared.

Seeing the near main beam improvements with the enhancement, a statistical analysis was performed over a reduced section of the array factor pattern centered about the main beam for each scan angle. The range of analysis varied from 90^o to 110^o depending upon scan angle. Start and stop angular ends of this analysis are listed in Table 5.2 by scan angle. The choice of start and stop angle for the reduced sector analysis was chosen by finding the angular point that was approximately 20^o past the

Beam Scan Angle	Analysis Start Angle	Analysis End Angle
($^o\theta$)		
40	0	90
50	5	100
60	5	115
70	15	115
80	35	125
90	45	135
100	55	145
110	65	165
120	65	175
130	80	175
140	90	180

Table 5.2. *Start and stop angular ends of the reduced sector analysis by scan angle for the 19 element, $1/4\,\lambda$ nominally spaced arrays.*

undesired incident plane waves that were used to set up the $\mathbf{Y}$ vector. A similar analysis was also conducted for the initial randomization patterns for comparison. The results of the analysis are illustrated in Figure 5.11. From the plots, it is evident that the performance of the unenhanced array is relatively independent of sector, whereas the enhanced system shows considerably improved sidelobe levels within the sector immediately adjacent to the main beam. In fact the average maximum sidelobe level is as much as 7 dB better than the unenhanced array over the reduced sectors.

Even though, the minimum variance enhancement algorithm does not provide perfect recovery of the array factor pattern to the same performance as the unrandomized array, it does enhance the system in the angular vicinity of the main beam. And when the element location uncertainty information of the enhancement is allowed to increase to 0.01000 λ, the enhancement in the reduced sector area does not

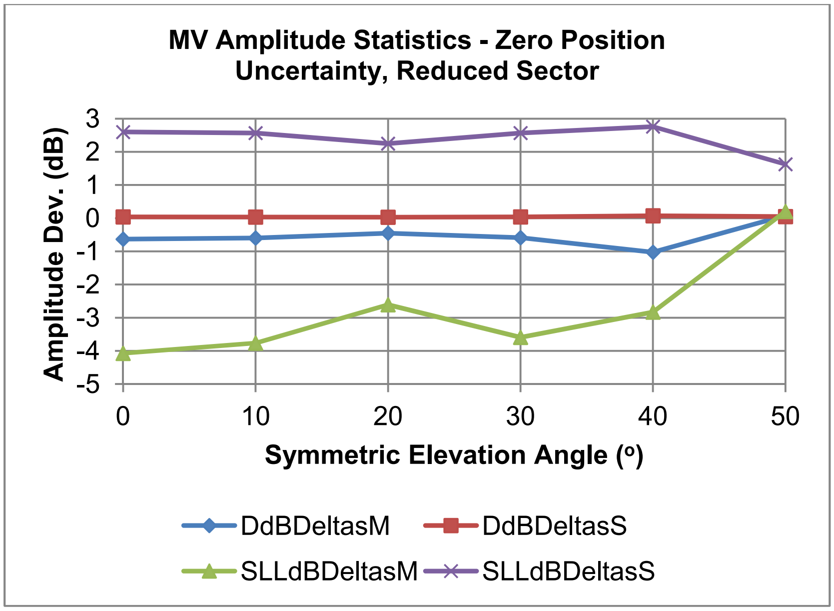

(a)

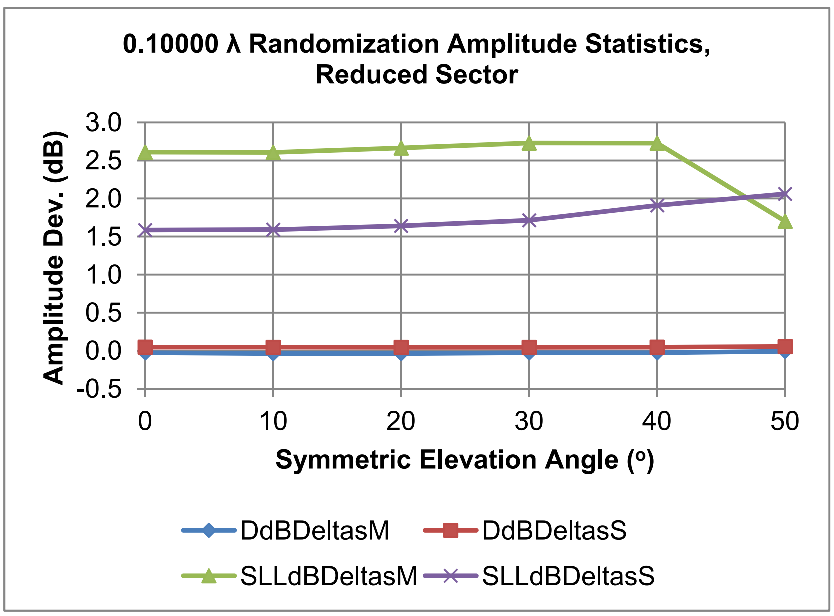

(b)

Figure 5.11. *Reduced sector sidelobe level statistics for an array with 19 almost linear elements, nominal* $1/4\,\lambda$ *spacing, 0.10000* λ *radial element position randomization and minimum variance enhancement.* Sidelobe level statistics assuming perfect knowledge of position (a) and no enhancement processing from the initial array factor pattern (20 dB powers of cosine on a pedestal taper) runs (b) are compared.

change significantly (Figure 5.12). The additional uncertainty was based upon the element position locations as they occurred for the initial 0.10000λ radial randomization. An additional 0.01000 λ randomization was added to the positions of the 0.10000 λ radial randomization positions. The enhancement calculation was performed for each of the 100 runs with the additional randomization. For each of these runs with additional randomizations, the pattern was recalculated using the minimum variance weights that were derived assuming the position information from the 0.10000 λ element position randomization sets.

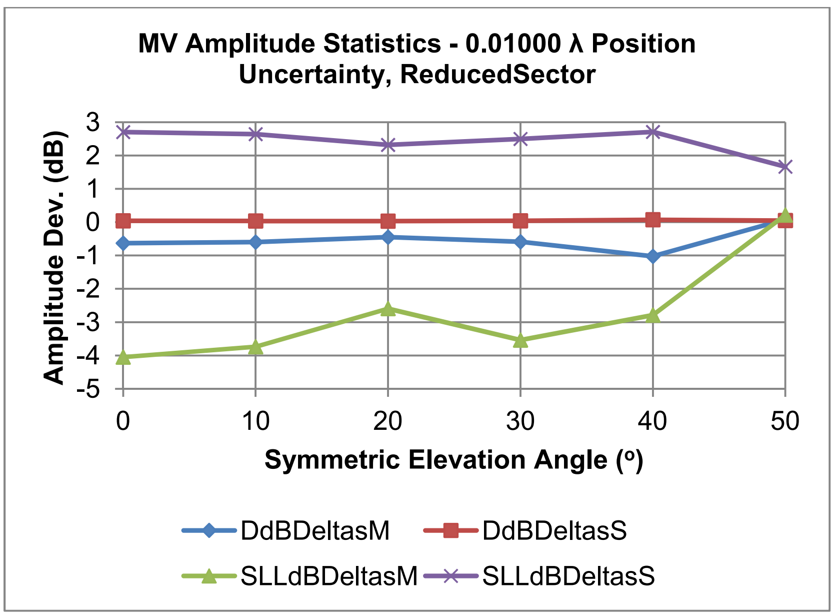

Figure 5.12. *Reduced sector sidelobe level and directivity statistics for an array with 19 almost linear elements, nominal* $1/4\,\lambda$ *spacing, 0.10000 λ radial element position randomization and minimum variance enhancement assuming 0.01000 λ of radial position uncertainty.*

Just to be complete, Table 5.3 lists the angular directions used to generate the **e** and **Y** vectors for this case. It also lists the amplitudes of the waves used to generate

Beam Scan Angle	**e** Vector Directions	**Y** Vector Directions	**Y** Vector Amplitudes	Reduced Sector Analysis	
				Start Angle	Stop Angle
(°θ)					
40	32.75 and 46.75	160 and 65	1 and 1	0	90
50	41 and 58.25	78	1	5	100
60	53 and 66.75	27 and 84	1 and 1	5	115
70	64 and 76	44 and 92	1 and 1	15	115
80	74 and 86	56 and 102	1 and 1	35	125
90	84 and 96	67 and 113	1 and 1	45	135
100	94 and 106	78 and 124	1 and 1	55	145
110	104 and 116	88 and 136	1 and 1	65	165
120	113.25 and 127	96 and 153	1 and 1	65	175
130	121.75 and 139	102	1	80	175
140	133.25 and 147.25	20 and 115	1 and 1	90	180

Table 5.3. *Analysis parameters utilized for minimum variance enhancement of the 19 element, $1/4\,\lambda$ nominally spaced array with 0.10000 λ randomization.*

Beam Scan Angle	**e** Vector Directions	**Y** Vector Directions	**Y** Vector Amplitudes	Reduced Sector Analysis	
				Start Angle	Stop Angle
(°θ)					
90	86 to 94 in steps of 0.125	82 and 98	1 and 1	40	140

Table 5.4. *Analysis parameters utilized for minimum variance enhancement of the 55 element, $1/4\,\lambda$ nominally spaced array with 0.10000 λ randomization.*

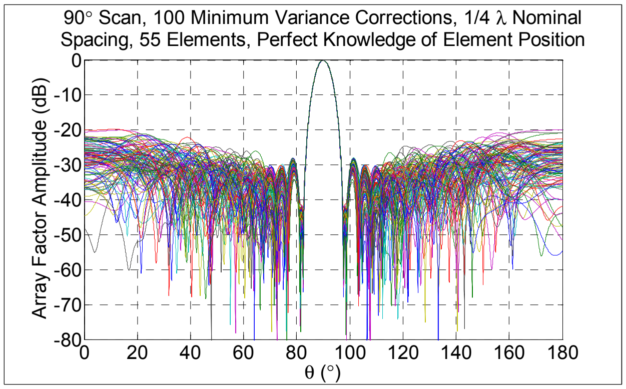

(a)

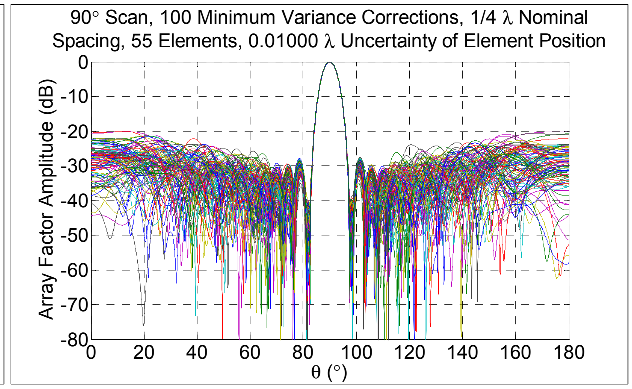

(b)

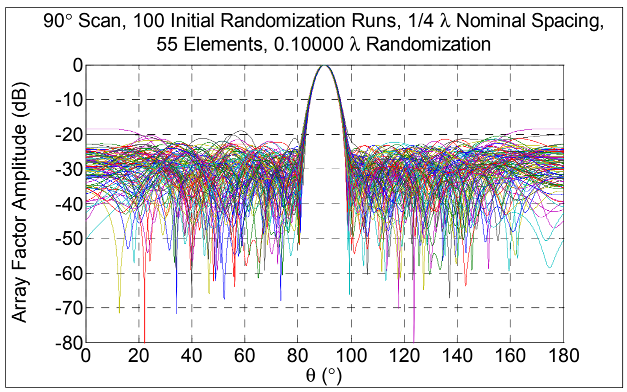

(c)

Figure 5.13. *55 almost linear elements with nominal $1/4\,\lambda$ spacing and minimum variance enhancement.* Rerun of 100, 0.10000 λ radial element position randomization runs at broadside with application of the minimum variance enhancement algorithm assuming perfect knowledge of element position (a) and 0.01000 λ uncertainty in element position. Initial array factor pattern (50 dB modified Taylor taper) runs of 100, 0.10000 λ radial element position element position randomizations (c) are additionally plotted for broadside scan.

the **Y** vector. In addition to **e** and **Y** vector parameters, the reduced sector analysis angles are also included.

This process was repeated for the several cases listed in Table 5.1. Given the partial success of the enhancement for the 19 element, $1/4\,\lambda$ initial spacing array, like a digital filter, the question arises: could the sidelobe performance be improved with more elements (or taps)? In order to answer this question, one of the largest $1/4\,\lambda$ spaced array that was analyzed for its performance under randomization, was analyzed for enhancement – the 55 element modified Taylor array. For this particular case, only the 90^{o} beam scan angle for the 0.10000 λ randomization case was analyzed. Analysis parameters are listed in Table 5.4. Plots of the 100 runs from the minimum variance corrections with perfect knowledge of element position, 0.01000 λ uncertainty of element position, and initial 0.10000 λ randomization from the 55 element modified Taylor array are illustrated in Figure 5.13. As happened for the 19 element array, improvement occurred about the main beam. Overall, the statistics of the minimum variance enhancements are about the same as the unenhanced 55 element modified Taylor array, but the reduced sector analysis shows about 5 dB better sidelobe level performance from 40^{o} to 140^{o} for the enhanced weighting as compared to the full 180^{o} statistics and the reduced sector from the initial randomization data (Figure 5.14). As can be seen, the increase in the number of elements did reduce the overall sidelobe level and improved the performance of the sidelobes in the vicinity of the main beam.

Referring back to Table 5.1, 13 and 37 element arrays with $3/8\,\lambda$ nominal spacing were tested with the minimum variance algorithm. Prior to randomization, the 13 and 37 element arrays were initially designed as 20 dB sidelobe level Taylor and 50 dB sidelobe level modified Taylor arrays. The 20 dB Taylor array was analyzed over 11 beam scan angles from 40^{o} to 140^{o}. Whereas, the 50 dB modified Taylor array was only analyzed for broadside scan. Tables 5.5 lists the angular directions used to generate the $\mathbf{e}$ and $\mathbf{Y}$ vectors for these cases. They also list the amplitudes of the waves used to generate the $\mathbf{Y}$ vectors. In addition to $\mathbf{e}$ and $\mathbf{Y}$ vector parameters, the

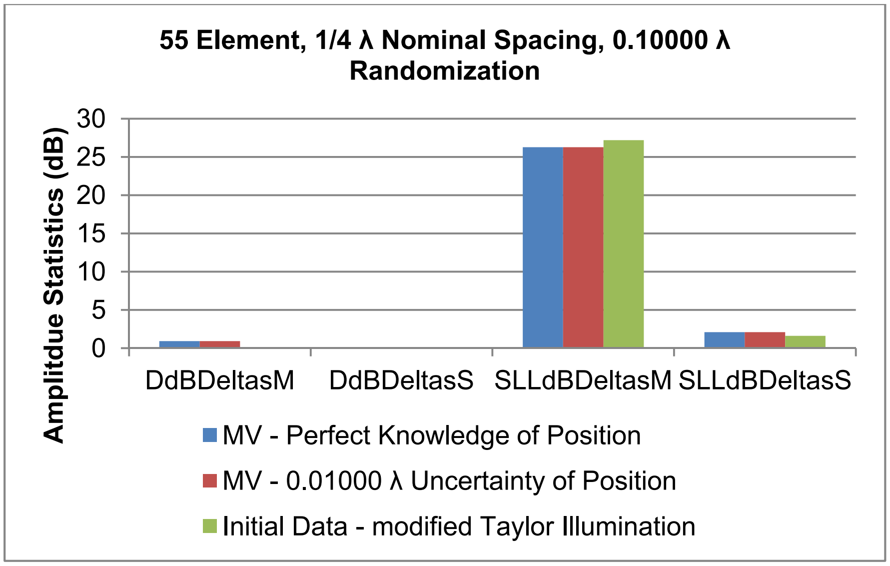

(a)

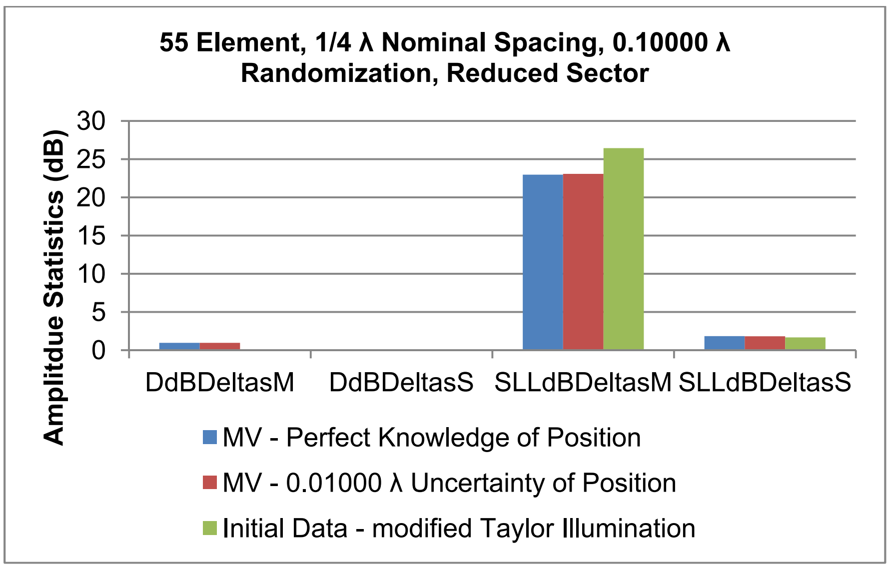

(b)

Figure 5.14. *Amplitude statistics for a 55 element, $1/4\,\lambda$ nominal spacing array with 0.10000 λ randomization.* Minimum variance enhancement is applied with perfect knowledge of the element positions and 0.01000 λ uncertainty of element positions. Initial data from the 50 dB modified Taylor array with 0.10000 λ randomization is also compared. Amplitude statistics for the full 180° cut (a) as well as the reduced sector compilation from 40° to 140° (b) are illustrated.

reduced sector analysis angles are also included. The 90^o beam scan plots of the 100 runs from the minimum variance corrections with perfect knowledge of element position, 0.01000 λ uncertainty of element position, and initial 0.10000 λ randomization from the

Beam Scan Angle	**e** Vector Directoins	**Y** Vector Directoins	**Y** Vector Amplitudes	Reduced Sector Analysis Start Angle	Reduced Sector Analysis Stop Angle
($^o\theta$)					
40	32 and 47	64 and 150	1 and 1	0	90
50	42 and 57.5	75 and 160	1 and 1	5	100
60	53 and 66.75	26 and 84	1 and 1	5	105
70	64 and 76	45 and 92	1 and 1	20	115
80	74 and 86	56 and 102	1 and 1	35	125
90	83 and 97	67 and 113	1 and 1	45	135
100	94 and 106	78 and 124	1 and 1	55	145
110	104 and 116	88 and 135	1 and 1	65	160
120	113.25 and 127	96 and 154	1 and 1	75	175
130	122.5 and 138	20 and 105	1 and 1	80	175
140	133 and 148	30 and 116	1 and 1	90	180

(a)

Beam Scan Angle	**e** Vector Directions	**Y** Vector Directions	**Y** Vector Amplitudes	Reduced Sector Analysis Start Angle	Reduced Sector Analysis Stop Angle
($^o\theta$)					
90	86 to 94 in steps of 0.125	82 and 98	1 and 1	45	135

(b)

Table 5.5. *Analysis parameters utilized for minimum variance enhancement of* $3/8\,\lambda$ *nominally spaced arrays with 10000 λ randomization.* 13 element (a), and 37 element (b) arrays were tested.

13 element Taylor array are illustrated in Figure 5.15. Sidelobe level statistics for the 11 beam scan angles are also presented (Figure 5.16).

As has been demonstrated previously, enhancement also occurred near the main beam. In this particular case, the initial settings of the minimum variance algorithm caused a widening of the main beam and a slight decrease in the resolution of

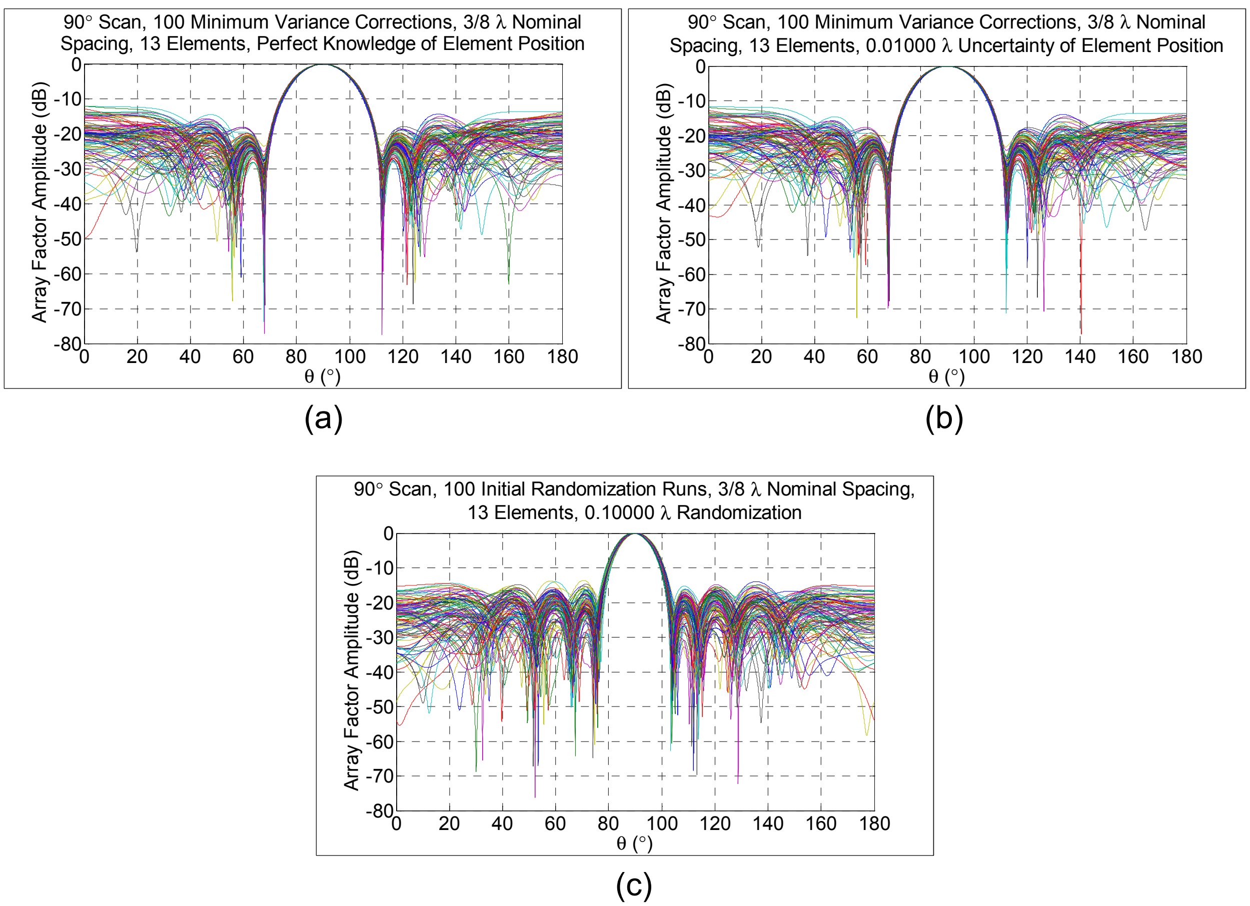

Figure 5.15. *13 almost linear elements with nominal* $3/8\,\lambda$ *spacing and minimum variance enhancement.* Rerun of 100, 0.10000 λ radial element position randomization runs at broadside with application of the minimum variance enhancement algorithm assuming perfect knowledge of element position (a) and 0.01000 λ uncertainty in element position. Initial array factor pattern (20 dB Taylor taper) runs of 100, 0.10000 λ radial element position element position randomizations (c) are additionally plotted for broadside scan.

the array. An adjustment to the **e** and **Y** vector parameters would adjust the patterns to be more similar to the initial array. With the improvement in the near main beam

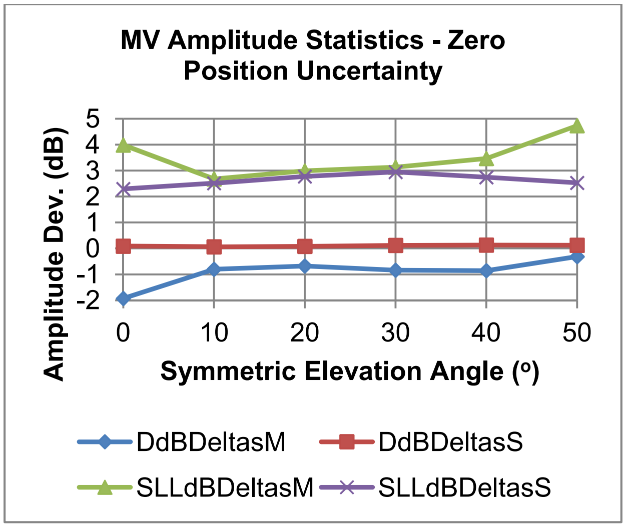

(a)

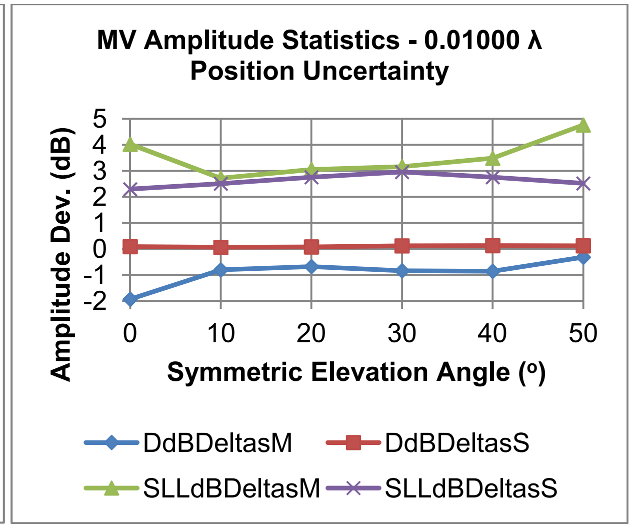

(b)

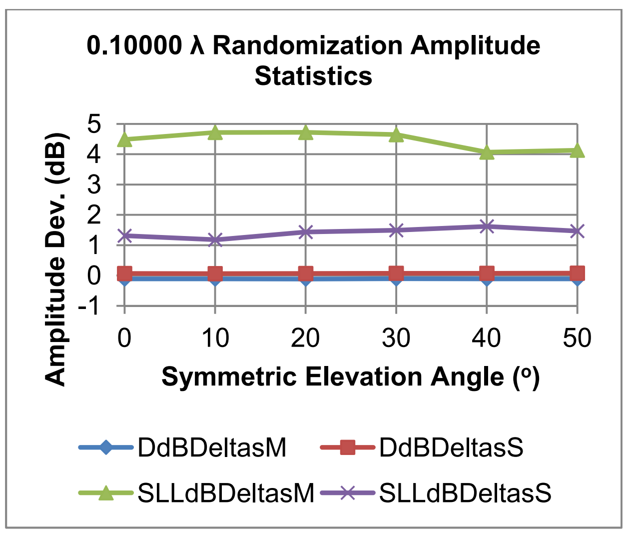

(c)

Figure 5.16. *Sidelobe level and directivity statistics for an array with 13 almost linear elements, nominal* $3/8\,\lambda$ *spacing, 0.10000 λ radial element position randomization and minimum variance enhancement.* Amplitude statistics assuming perfect knowledge of position (a), 0.01000 λ uncertainty of position (b) and no enhancement processing from the initial array factor pattern (20 dB Taylor taper) runs (c) are compared.

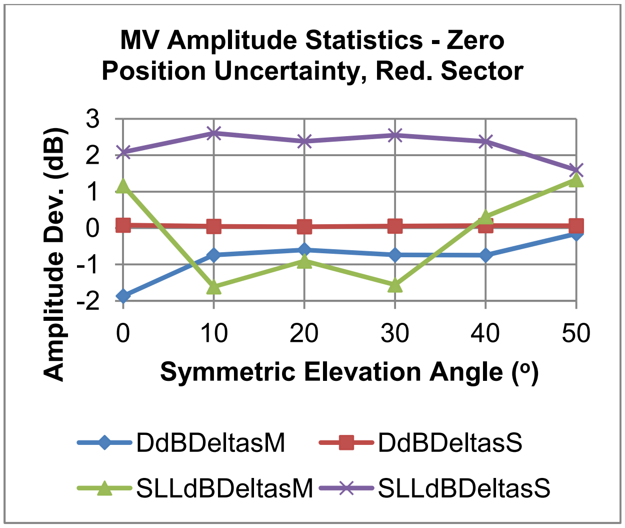

(a)

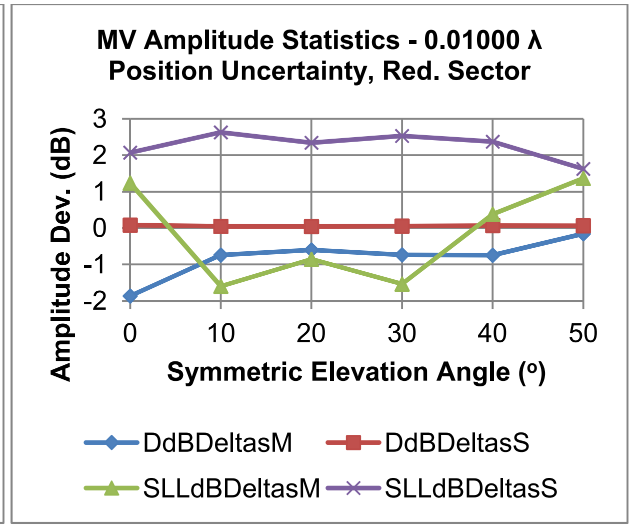

(b)

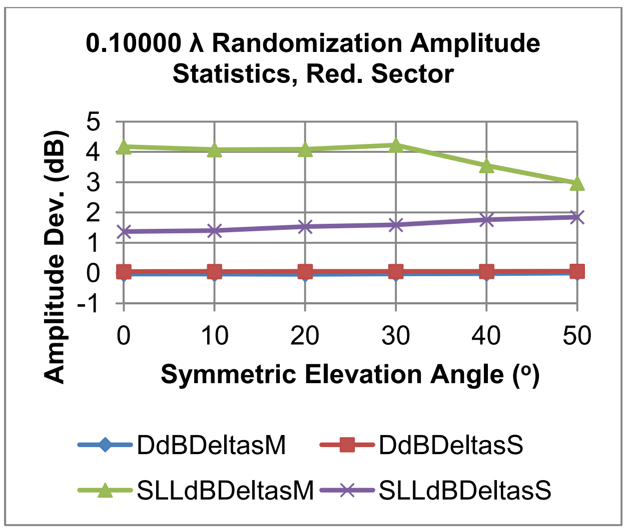

(c)

Figure 5.17. *Reduced sector sidelobe level statistics for an array with 13 almost linear elements, nominal* $3/8\,\lambda$ *spacing, 0.10000 λ radial element position randomization and minimum variance enhancement.* Sidelobe level statistics assuming perfect knowledge of position (a), 0.01000 λ uncertainty of position (b) and no enhancement processing from the initial array factor pattern (20 dB Taylor taper) runs (c) are compared.

sidelobe level performance, a reduced sector analysis was performed. This analysis indicated that within about ± 45° of the peak of beam, significant enhancement occurred (Figure 5.17), as much as 3 dB.

For $3/8\,\lambda$ nominal element spacing, as the number of elements is increased, the overall level of the sidelobes gets lower. Otherwise trends are the same. The 90°

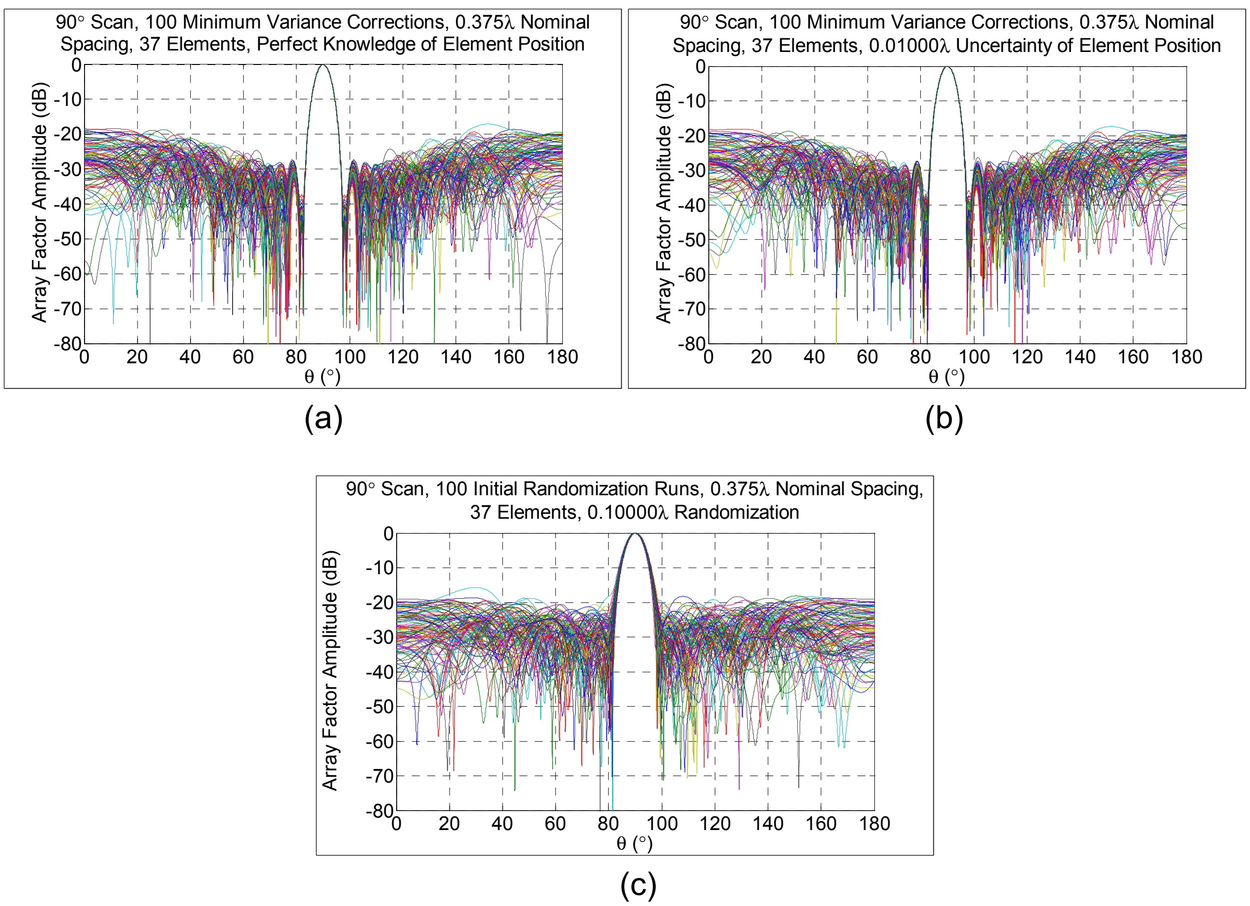

Figure 5.18. *37 almost linear elements with nominal $3/8\,\lambda$ spacing and minimum variance enhancement.* Rerun of 100, 0.10000 λ radial element position randomization runs at broadside with application of the minimum variance enhancement algorithm assuming perfect knowledge of element position (a) and 0.01000 λ uncertainty in element position. Initial array factor pattern (50 dB modified Taylor taper) runs of 100, 0.10000 λ radial element position element position randomizations (c) are additionally plotted for broadside scan.

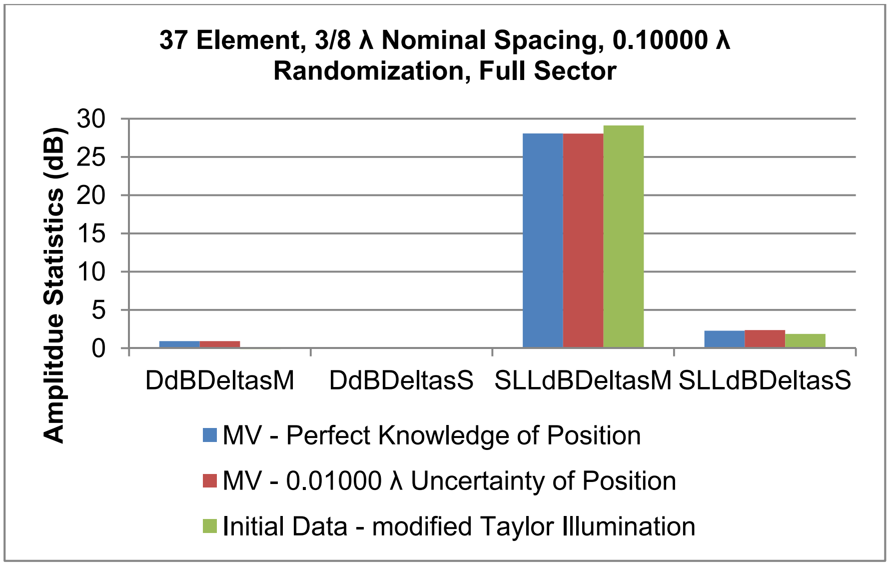

(a)

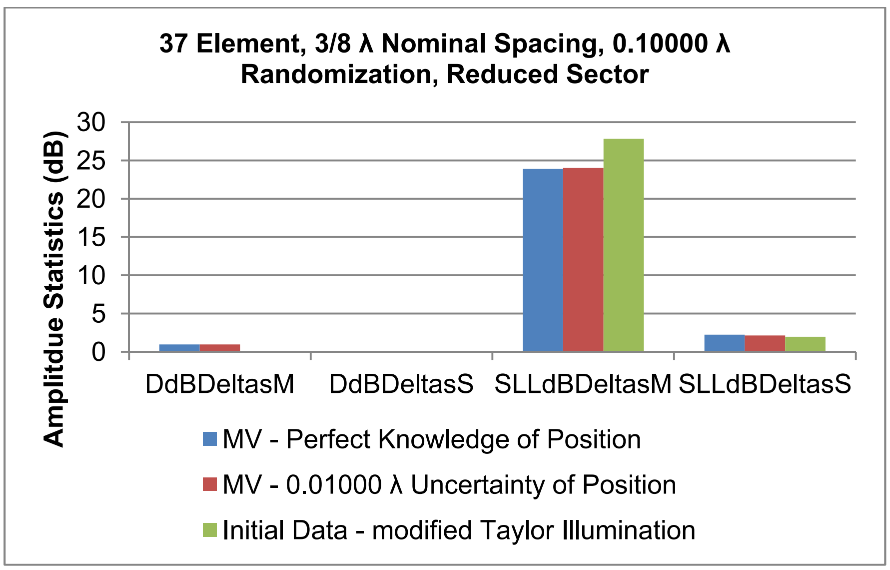

(b)

Figure 5.19. *Amplitude statistics for a 37 element,* $3/8\,\lambda$ *nominal spacing array with 0.10000 λ randomization.* Minimum variance enhancement is applied with perfect knowledge of the element positions and 0.01000 λ uncertainty of element positions. Initial data from the 50 dB modified Taylor array with 0.10000 λ randomization is also compared. Amplitude statistics for the full 180° cut (a) as well as the reduced sector compilation from 45° to 135° (b) are illustrated.

beam scan plots of the 100 runs from the minimum variance corrections with perfect knowledge of element position, 0.01000 λ uncertainty of element position, and initial 0.10000 λ randomization from the 37 element modified Taylor array are illustrated in

Beam Scan Angle	**e** Vector Directoins	**Y** Vector Directoins	**Y** Vector Amplitudes	Reduced Sector Analysis Start Angle	Reduced Sector Analysis Stop Angle
($^o\theta$)					
40	32 and 47	66 and 152	1 and 1	0	90
50	41 and 58	77,140 and 159	1, 1 and 1	0	100
60	52 and 67.5	18, 87 and 160	1, 1 and 1	0	110
70	63 and 76.75	40, 95, 140 and 170	1, 1, 1 and 1	20	115
80	73 and 87	51 and 107	1 and 1	30	130
90	84 and 96	67 and 113	1 and 1	45	135
100	93 and 107	63 and 129	1 and 1	50	150
110	103.25 and 117	10, 40, 85 and 140	1, 1, 1 and 1	65	160
120	112.5 and 128	20, 93 and 162	1, 1 and 1	70	180
130	122 and 139	21, 40 and 103	1, 1 and 1	80	180
140	133 and 148	28 and 114	1 and 1	90	180

(a)

Beam Scan Angle	**e** Vector Directions	**Y** Vector Directions	**Y** Vector Amplitudes	Reduced Sector Analysis Start Angle	Reduced Sector Analysis Stop Angle
($^o\theta$)					
90	86 to 94 in steps of 0.125	82 and 98	1 and 1	60	120

(b)

Table 5.6. *Analysis parameters utilized for minimum variance enhancement of $1/2\lambda$ nominally spaced arrays with 0.10000 λ.* 9 element (a), and 28 element (b), arrays were analyzed.

Figure 5.18. Sidelobe level statistics for the full array and the reduced sector analysis are also presented (Figure 5.19). Within the reduced sector the sidelobe level performance is about 5 dB better than the rest of the array.

9 and 28 element Dolph-Chebyshev arrays with $1/2\lambda$ nominal spacing were tested with the minimum variance algorithm for the tapers and beam scan angles listed in Table 5.1. Prior to randomization, the 9 element array was initially designed as 20 dB sidelobe level array. The array was analyzed over 11 beam scan angles from 40^o to 140^o.

The 28 element array was only analyzed at broadside scan. Tables 5.6 lists the angular directions used to generate the $\mathbf{e}$ and $\mathbf{Y}$ vectors for these cases. It also lists the amplitudes of the waves used to generate the $\mathbf{Y}$ vectors. In addition to $\mathbf{e}$ and $\mathbf{Y}$ vector parameters, the reduced sector analysis angles are also included. The 90^o beam scan plots of the 100 runs from the minimum variance corrections with perfect knowledge of element position, 0.01000 λ uncertainty of element position, and initial 0.10000 λ randomization from the 9 element array are illustrated in Figure 5.20. Sidelobe level statistics for all 11 beam scan angles of the 9 element are also presented (Figure 5.21). As can be seen from Figures 5.20 and 5.21, the overall sidelobe level performance of the minimum variance enhancement, is very similar to the unenhanced randomized array. But again, the patterns around the main beam are improved. As a result, a reduced sector analysis was performed to determine the sidelobe level statistics near the main beam (Figure 5.22). Within $\pm$ 45^o of the peak of beam, the sidelobe level is reduced about 5 dB by the minimum variance algorithm as compared to the initial 0.10000 λ randomization. As can be seen from the reduced sector statistics plots (Figure 5.22), all the beam scan angles saw significant improvement except for the most extreme.

Increasing the number of elements again caused the overall sidelobe level to decrease with definite improvement in the near beam area when the minimum variance

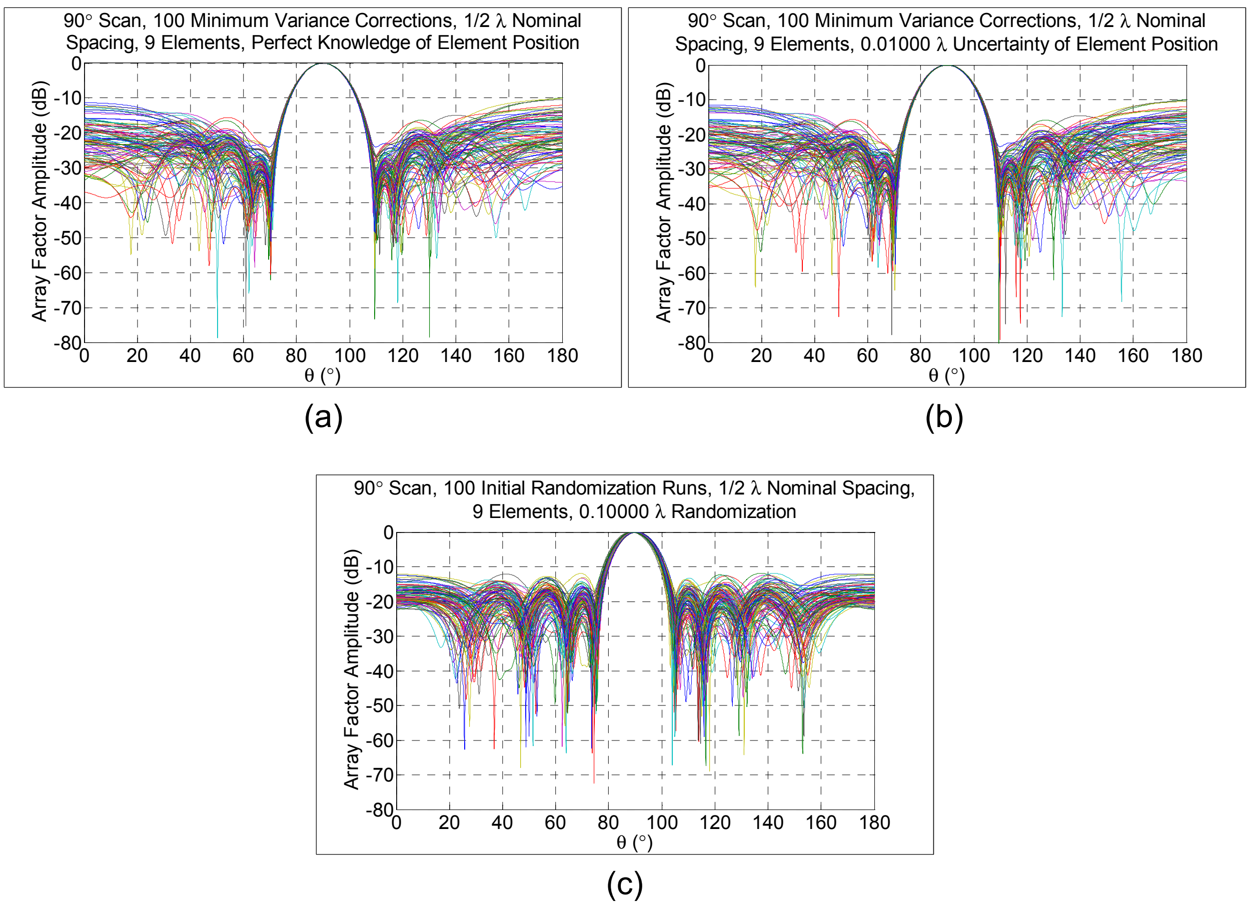

Figure 5.20. *9 almost linear elements with nominal $1/2\lambda$ spacing and minimum variance enhancement.* Rerun of 100, 0.10000 λ radial element position randomization runs at broadside with application of the minimum variance enhancement algorithm assuming perfect knowledge of element position (a) and 0.01000 λ uncertainty in element position. Initial array factor pattern (20 dB Dolph-Chebyshev taper) runs of 100, 0.10000 λ radial element position element position randomizations (c) are additionally plotted for broadside scan.

enhancement is applied. This is evident from the broadside patterns and statistics (Figures 5.23 and 5.24).

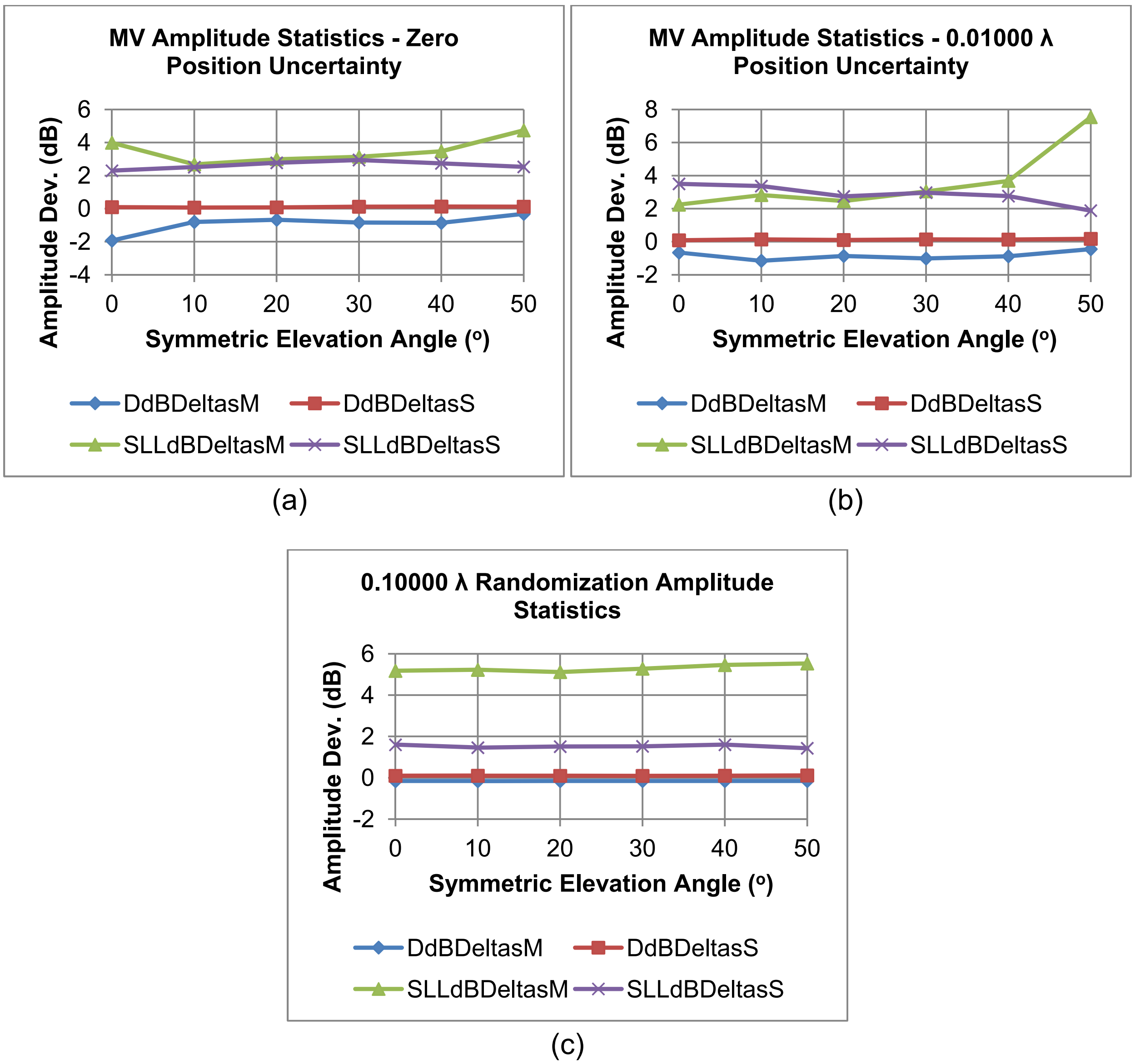

Figure 5.21. *Sidelobe level and directivity statistics for an array with 9 almost linear elements, nominal 1/2 λ spacing, 0.10000 λ radial element position randomization and minimum variance enhancement.* Amplitude statistics assuming perfect knowledge of position (a), 0.01000 λ uncertainty of position (b) and no enhancement processing from the initial array factor pattern (20 dB Dolph-Chebyshev taper) runs (c) are compared.

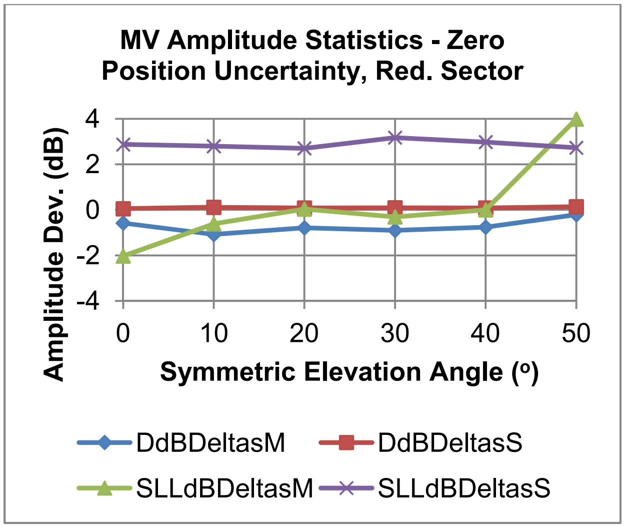

(a)

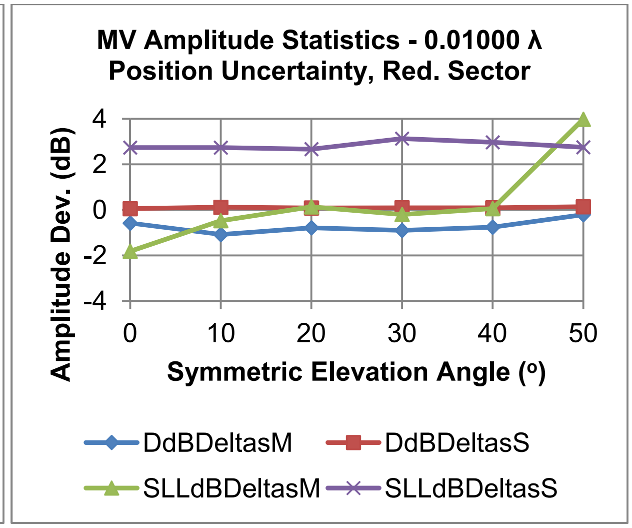

(b)

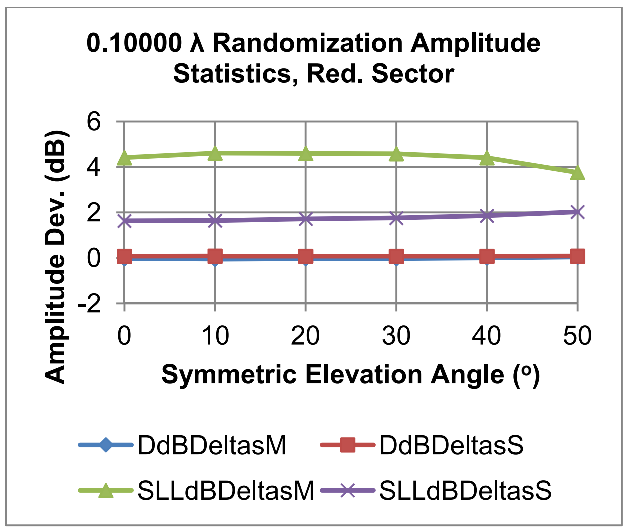

(c)

Figure 5.22. *Reduced sector sidelobe level statistics for an array with 9 almost linear elements, nominal $1/2\lambda$ spacing, 0.10000 λ radial element position randomization and minimum variance enhancement.* Sidelobe level statistics assuming perfect knowledge of position (a), 0.01000 λ uncertainty of position (b) and no enhancement processing from the initial array factor pattern (20 dB Dolph-Chebyshev taper) runs (c) are compared.

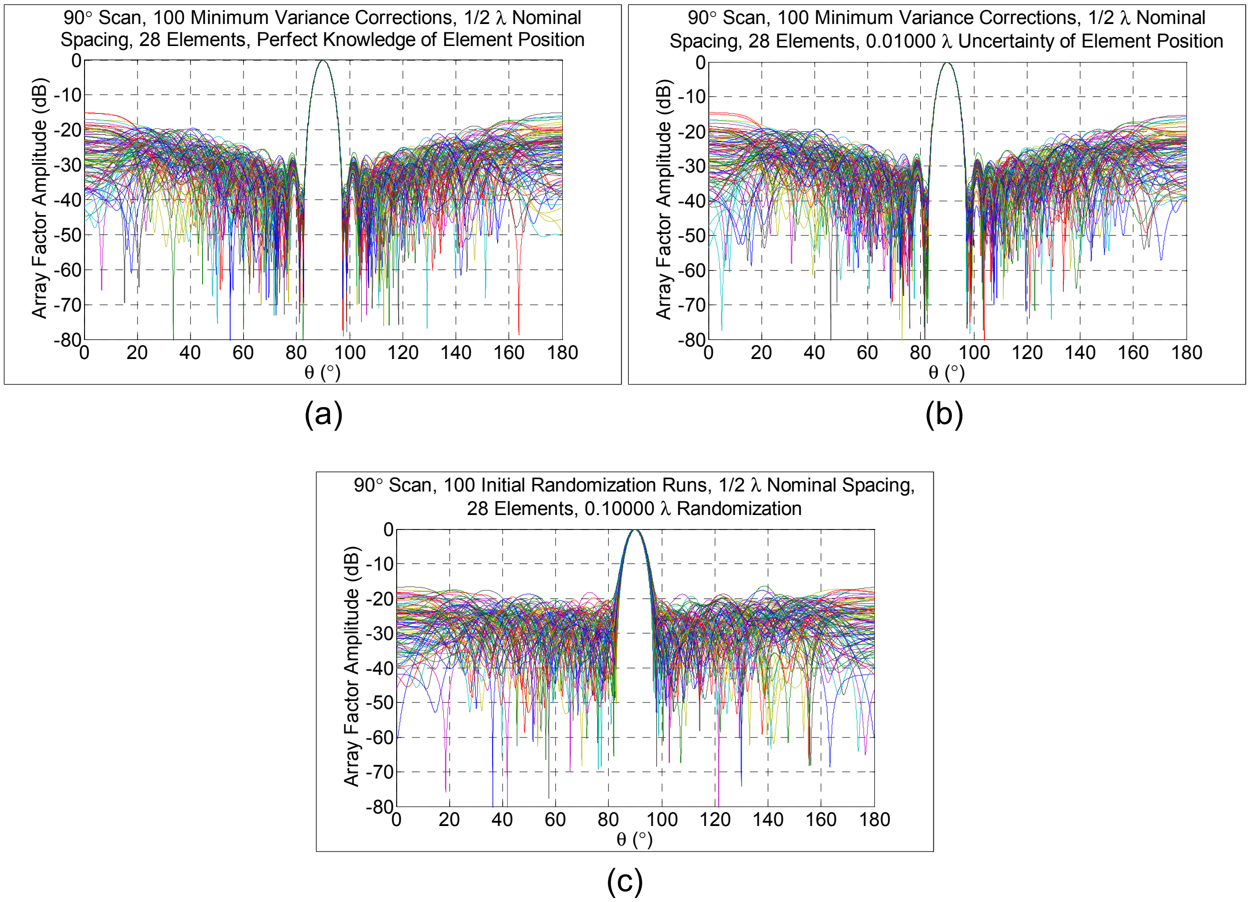

Figure 5.23. *28 almost linear elements with nominal $1/2\lambda$ spacing and minimum variance enhancement.* Rerun of 100, 0.10000 λ radial element position randomization runs at broadside with application of the minimum variance enhancement algorithm assuming perfect knowledge of element position (a) and 0.01000 λ uncertainty in element position. Initial array factor pattern (50 dB Dolph-Chebyshev taper) runs of 100, 0.10000 λ radial element position element position randomizations (c) are additionally plotted for broadside scan.

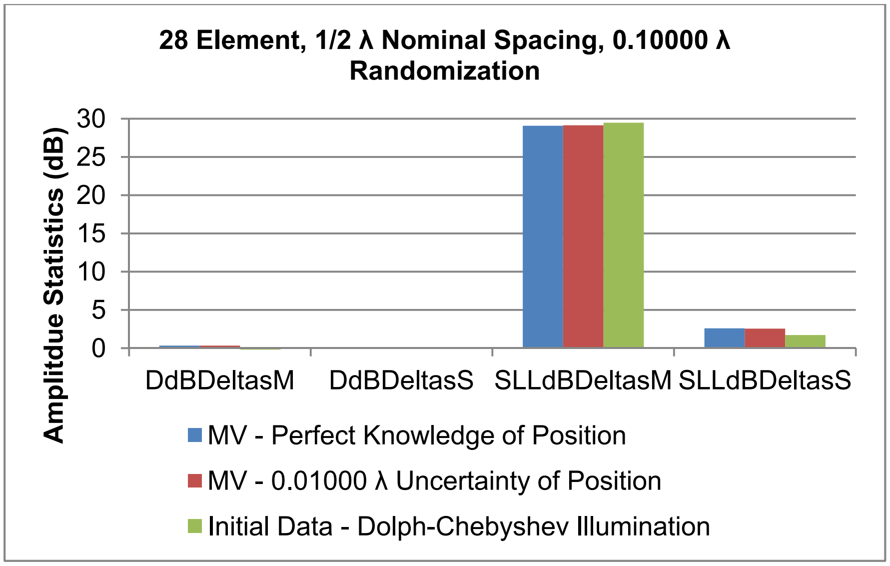

(a)

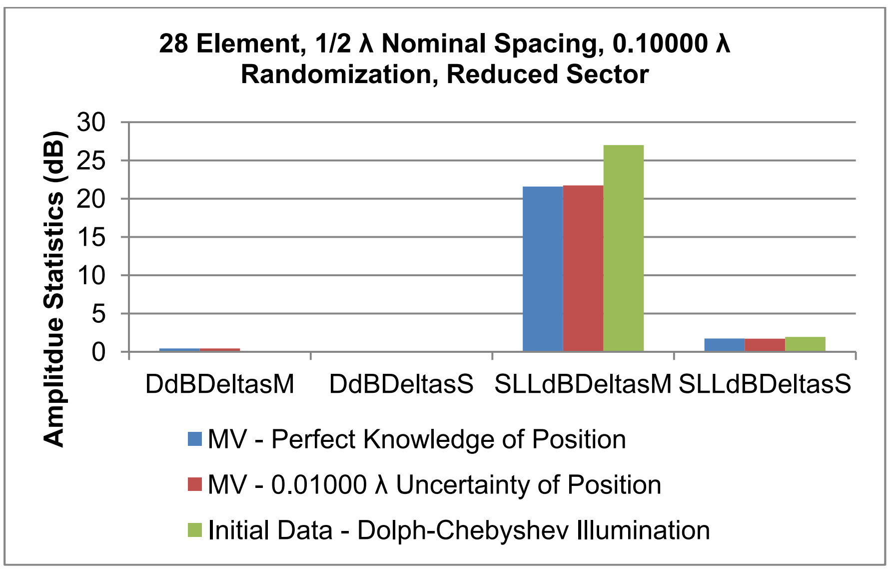

(b)

Figure 5.24. *Amplitude statistics for a 28 element, $1/2\,\lambda$ nominal spacing array with 0.10000 λ randomization.* Minimum variance enhancement is applied with perfect knowledge of the element positions and 0.01000 λ uncertainty of element positions. Initial data from the 50 dB Dolph-Chebyshev array with 0.10000 λ randomization is also compared. Amplitude statistics for the full 180^{o} cut (a) as well as the reduced sector compilation from 60^{o} to 120^{o} (b) are illustrated.

7 and 21 element Dolph-Chebyshev arrays with $5/8\,\lambda$ nominal spacing were tested with the minimum variance algorithm for the scan angles listed in Table 5.1. Prior to randomization, the 7 element array was initially designed as 20 dB sidelobe level array. The array was analyzed over five beam scan angles from 70^o to 110^o. The 21 element array was only analyzed at broadside scan. Tables 5.7 list the angular directions used to generate the $\mathbf{e}$ and $\mathbf{Y}$ vectors for these cases. It also lists the amplitudes of the waves used to generate the $\mathbf{Y}$ vectors. In addition to $\mathbf{e}$ and $\mathbf{Y}$ vector parameters, the reduced sector analysis angles are also included. The 90^o beam scan plots of the 100 runs from the minimum variance corrections with perfect knowledge of element position, 0.01000λ uncertainty of element position, and initial 0.10000λ randomization from the 7 element array are illustrated in Figure 5.25. Sidelobe level statistics for all five beam scan angles of the 7 element array are also presented (Figure 5.26). As can be seen from Figures 5.25 and 5.26, the overall sidelobe level statistical performance of the minimum variance enhancement, is very similar to the unenhanced randomized array. But again, the patterns around the main beam are improved. As a result, a reduced sector analysis was performed to determine the sidelobe level statistics near the main beam (Figure 5.27). Within $\pm$ 50^o of the peak of beam, the sidelobe level is reduced about 5 dB by the minimum variance algorithm as compared to the initial 0.10000 λ randomization.

Increasing the number of elements again caused the overall sidelobe level to decrease with definite improvement in the near beam area when the minimum variance enhancement is applied. This is evident from the broadside patterns and statistics (Figures 5.28 and 5.29). However, it is evident that as the field sampling interval is exceeding the Nyquist rate, the angular sector of sidelobe level performance improvement about the main beam is decreasing.

Beam Scan Angle	**e** Vector Directoins	**Y** Vector Directoins	**Y** Vector Amplitudes	Reduced Sector Analysis	
				Start Angle	Stop Angle
(°θ)					
70	64 and 75.75	44, 92 and 180	1, 1 and 1	20	120
80	73 and 87	51,106 and 166	1, 1 and 1	30	130
90	83 and 97	20, 62, 118 and 160	1, 1, 1 and 1	40	140
100	93 and 107	14, 74 and 129	1, 1 and 1	50	150
110	104.25 and 116	0, 88 and 136	1, 1 and 1	60	160

(a)

Beam Scan Angle	**e** Vector Directions	**Y** Vector Directions	**Y** Vector Amplitudes	Reduced Sector Analysis	
				Start Angle	Stop Angle
(°θ)					
90	86 to 94 in steps of 1	81 and 99	1 and 1	60	120

(b)

Table 5.7. *Analysis parameters utilized for minimum variance enhancement of $5/8\,\lambda$ nominally spaced arrays with 0.10000 λ randomization.* 7 element (a), and 21 element (b), arrays were tested.

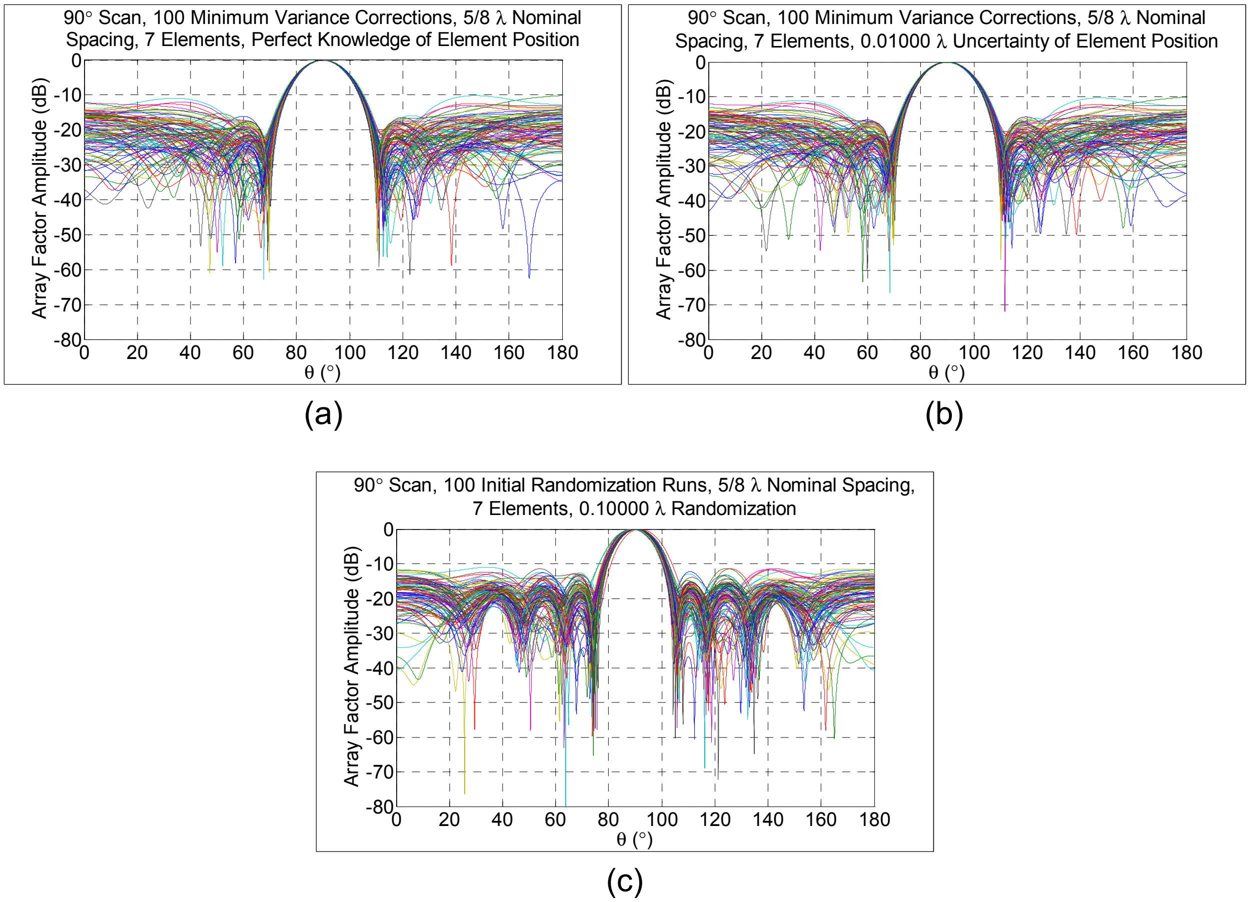

Figure 5.25. *7 almost linear elements with nominal* $5/8\,\lambda$ *spacing and minimum variance enhancement.* Rerun of 100, 0.10000 λ radial element position randomization runs at broadside with application of the minimum variance enhancement algorithm assuming perfect knowledge of element position (a) and 0.01000 λ uncertainty in element position. Initial array factor pattern (20 dB Dolph-Chebyshev taper) runs of 100, 0.10000 λ radial element position element position randomizations (c) are additionally plotted for broadside scan.

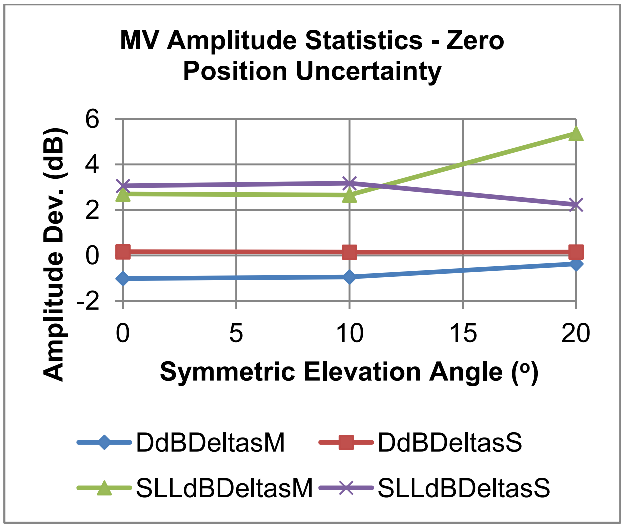

(a)

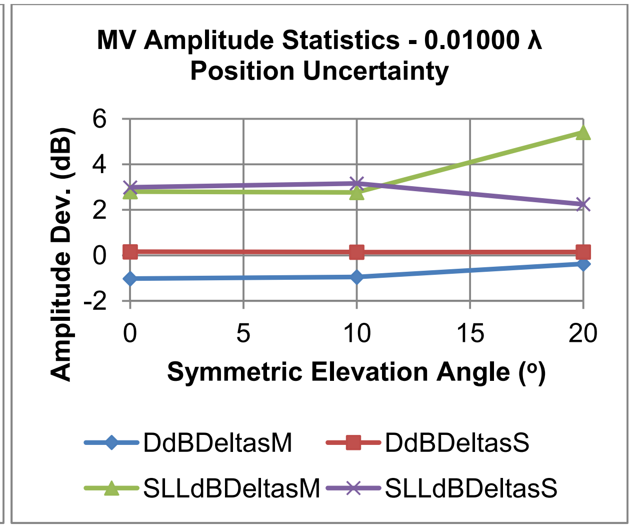

(b)

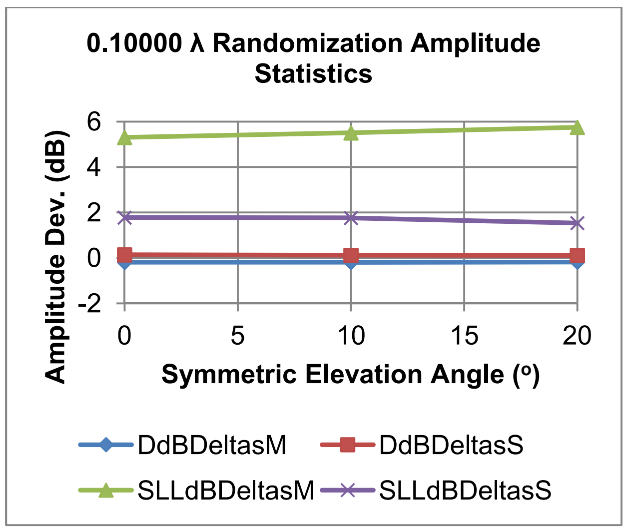

(c)

Figure 5.26. *Sidelobe level and directivity statistics for an array with 7 almost linear elements, nominal* $5/8\,\lambda$ *spacing, 0.10000 λ radial element position randomization and minimum variance enhancement.* Amplitude statistics assuming perfect knowledge of position (a), 0.01000 λ uncertainty of position (b) and no enhancement processing from the initial array factor pattern (20 dB Dolph-Chebyshev taper) runs (c) are compared.

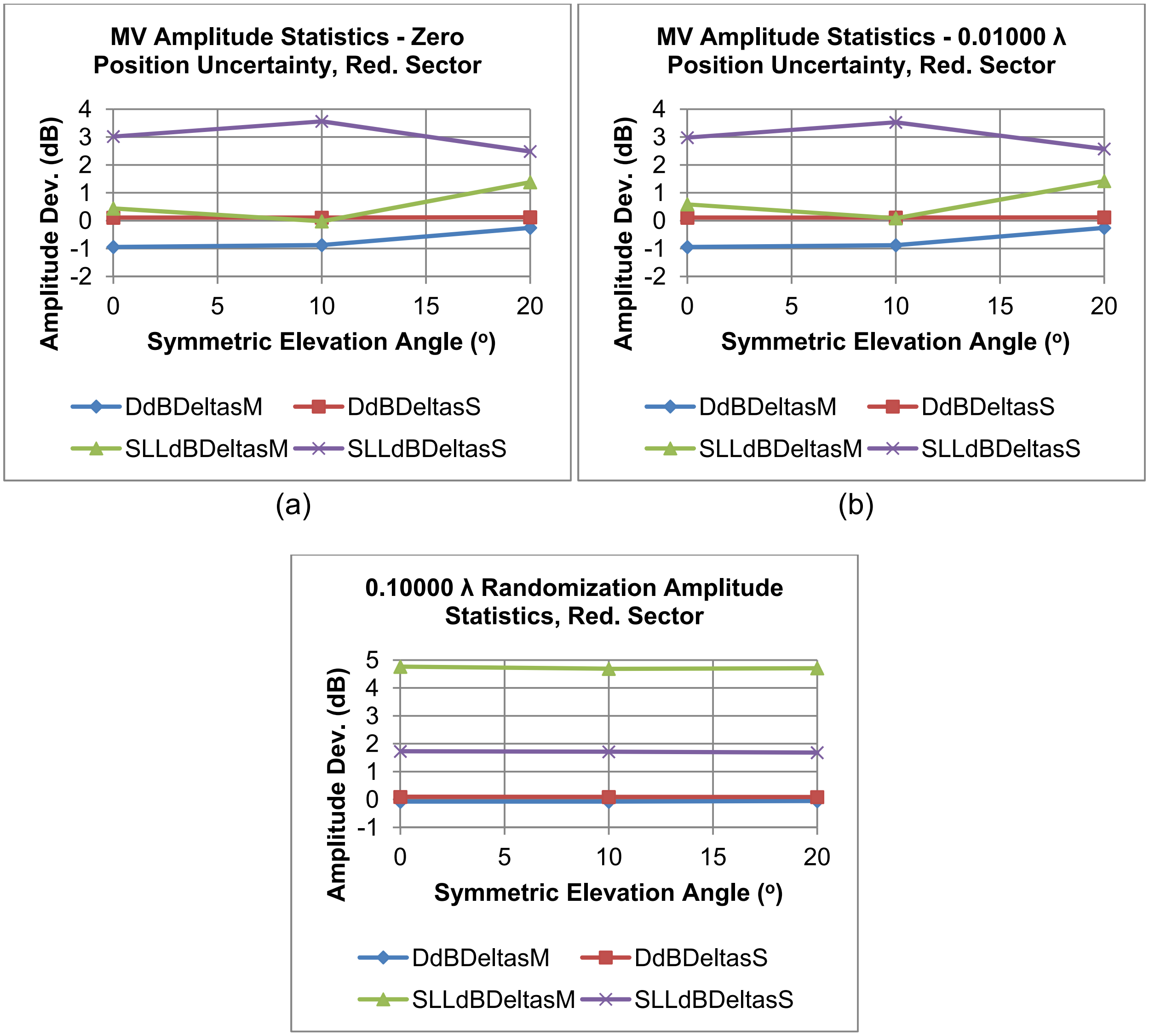

(a) (b) (c)

Figure 5.27. *Reduced sector sidelobe level statistics for an array with 7 almost linear elements, nominal* $5/8\,\lambda$ *spacing, 0.10000 λ radial element position randomization and minimum variance enhancement.* Sidelobe level statistics assuming perfect knowledge of position (a), 0.01000 λ uncertainty of position (b) and no enhancement processing from the initial array factor pattern (20 dB Dolph-Chebyshev taper) runs (c) are compared.

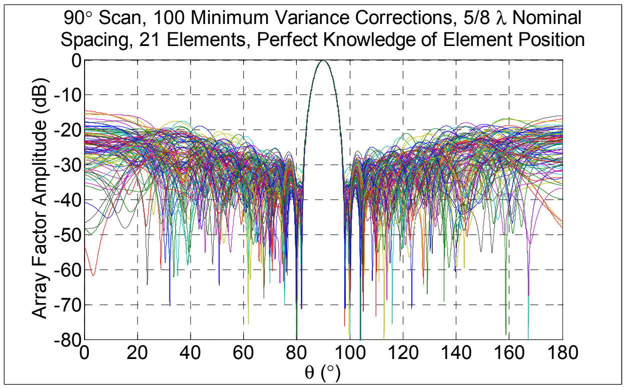

(a)

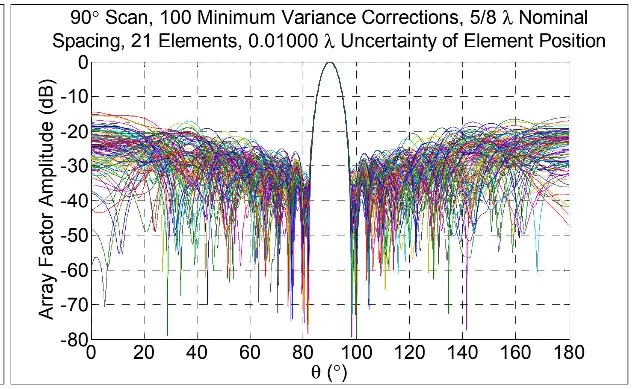

(b)

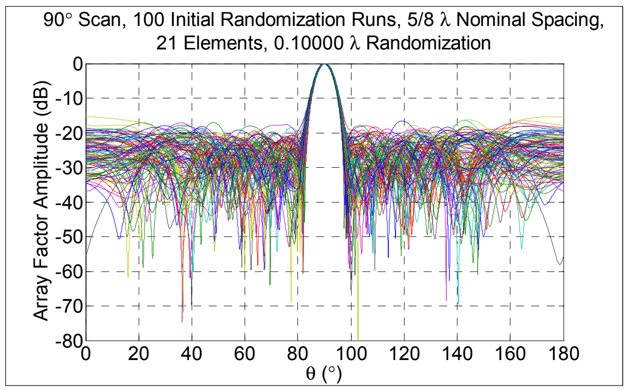

(c)

Figure 5.28. *21 almost linear elements with nominal* $5/8\,\lambda$ *spacing and minimum variance enhancement.* Rerun of 100, 0.10000 λ radial element position randomization runs at broadside with application of the minimum variance enhancement algorithm assuming perfect knowledge of element position (a) and 0.01000 λ uncertainty in element position. Initial array factor pattern (50 dB Dolph-Chebyshev taper) runs of 100, 0.10000 λ radial element position element position randomizations (c) are additionally plotted for broadside scan.

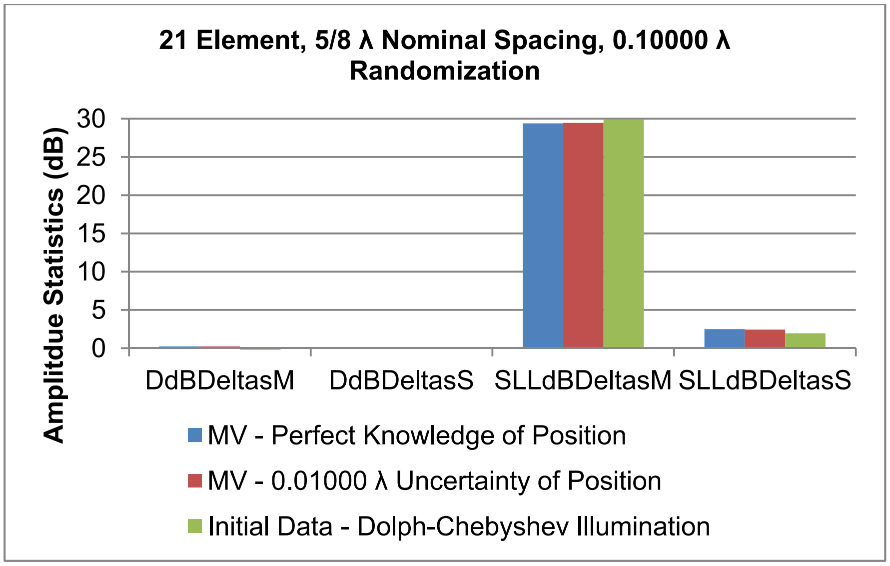

(a)

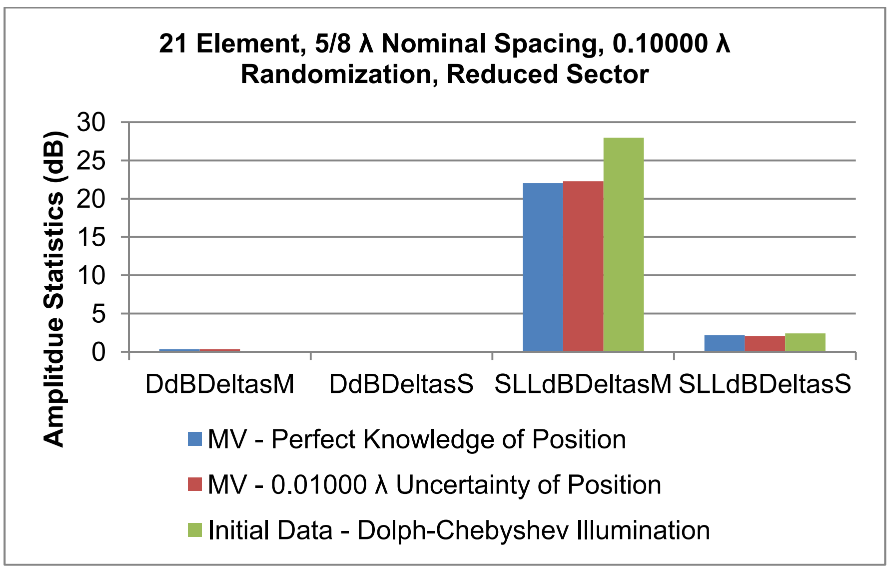

(b)

Figure 5.29. *Amplitude statistics for a 21 element, $5/8\,\lambda$ nominal spacing array with 0.10000 λ randomization.* Minimum variance enhancement is applied with perfect knowledge of the element positions and 0.01000 λ uncertainty of element positions. Initial data from the 50 dB Dolph-Chebyshev array with 0.10000 λ randomization is also compared. Amplitude statistics for the full 180° cut (a) as well as the reduced sector compilation from 60° to 120° (b) are illustrated.

Table 5.1 indicates that of the $3/4\,\lambda$ element spaced arrays, the 9 and 28 element Dolph-Chebyshev arrays were tested with the minimum variance algorithm for the scan angles listed. Prior to randomization, the 9 element array was initially designed as 20 dB sidelobe level array. The array was analyzed over three beam scan angles from 80^o to 100^o. The 28 element array was only analyzed at broadside scan. Tables 5.8 list the angular directions used to generate the $\mathbf{e}$ and $\mathbf{Y}$ vectors for these cases. It also lists the amplitudes of the waves used to generate the $\mathbf{Y}$ vectors. In addition to $\mathbf{e}$ and $\mathbf{Y}$ vector parameters, the reduced sector analysis angles are also included in the tables. The 90^o beam scan plots of the 100 runs from the minimum variance corrections with perfect knowledge of element position, 0.01000 λ uncertainty of element position, and initial 0.10000 λ randomization from the 9 element array are illustrated in Figure 5.30. Sidelobe level statistics for all three beam scan angles of the 7 element are also presented (Figure 5.31). As can be seen from Figures 5.30 and 5.31, the overall sidelobe level statistical performance of the minimum variance enhancement, is very similar to the unenhanced randomized array. But again, the patterns around the main beam are improved. As a result, a reduced sector analysis was performed to determine the sidelobe level statistics near the main beam (Figure 5.32). Within $\pm$ 40^o of the peak of beam, the sidelobe level is reduced about 5 dB by the minimum variance algorithm as compared to the initial 0.10000 λ randomization.

Increasing the number of elements again caused the overall sidelobe level to decrease with definite improvement in the near beam area when the minimum variance enhancement is applied. This is evident from the broadside scan patterns and statistics (Figures 5.33 and 5.34). However, it is evident that as the field sampling interval is exceeding the Nyquist rate, the angular sector of sidelobe level performance improvement about the main beam is decreasing.

Beam Scan Angle	**e** Vector Directoins	**Y** Vector Directoins	**Y** Vector Amplitudes	Reduced Sector Analysis Start Angle	Reduced Sector Analysis Stop Angle
($^o\theta$)					
80	77 and 83	66, 93, 140 and 158	1, 1, 1 and 1	40	120
90	86 and 94	22, 75, 105 and 158	1, 1, 1 and 1	50	130
100	97 and 103	22, 40, 87 and 114	1, 1, 1 and 1	60	140

(a)

Beam Scan Angle	**e** Vector Directions	**Y** Vector Directions	**Y** Vector Amplitudes	Reduced Sector Analysis Start Angle	Reduced Sector Analysis Stop Angle
($^o\theta$)					
90	87 to 93 in steps of 1	84 and 96	1 and 1	60	120

(b)

Table 5.8. *Analysis parameters utilized for minimum variance enhancement of* $3/4\,\lambda$ *nominally spaced arrays with 0.10000 λ randomization.* 9 element (a), and 28 element (b), arrays were analyzed.

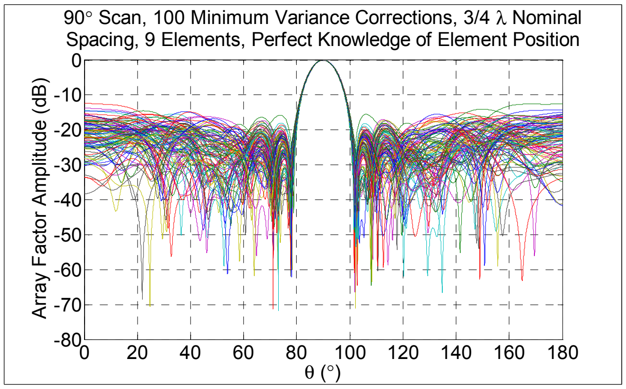

(a)

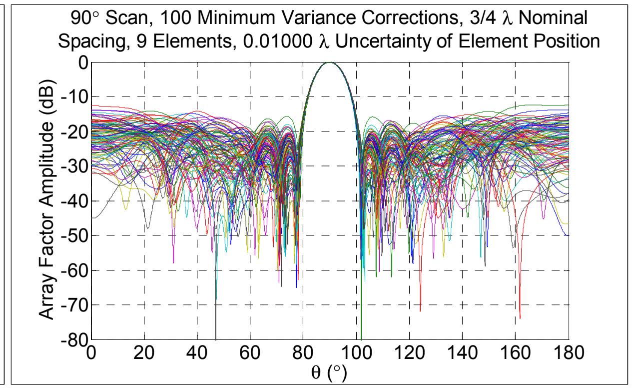

(b)

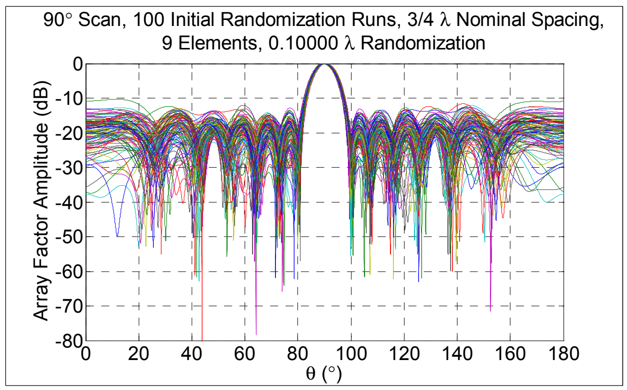

(c)

Figure 5.30. *9 almost linear elements with nominal* $3/4\,\lambda$ *spacing and minimum variance enhancement.* Rerun of 100, 0.10000 λ radial element position randomization runs at broadside with application of the minimum variance enhancement algorithm assuming perfect knowledge of element position (a) and 0.01000 λ uncertainty in element position. Initial array factor pattern (20 dB Dolph-Chebyshev taper) runs of 100, 0.10000 λ radial element position element position randomizations (c) are additionally plotted for broadside scan.

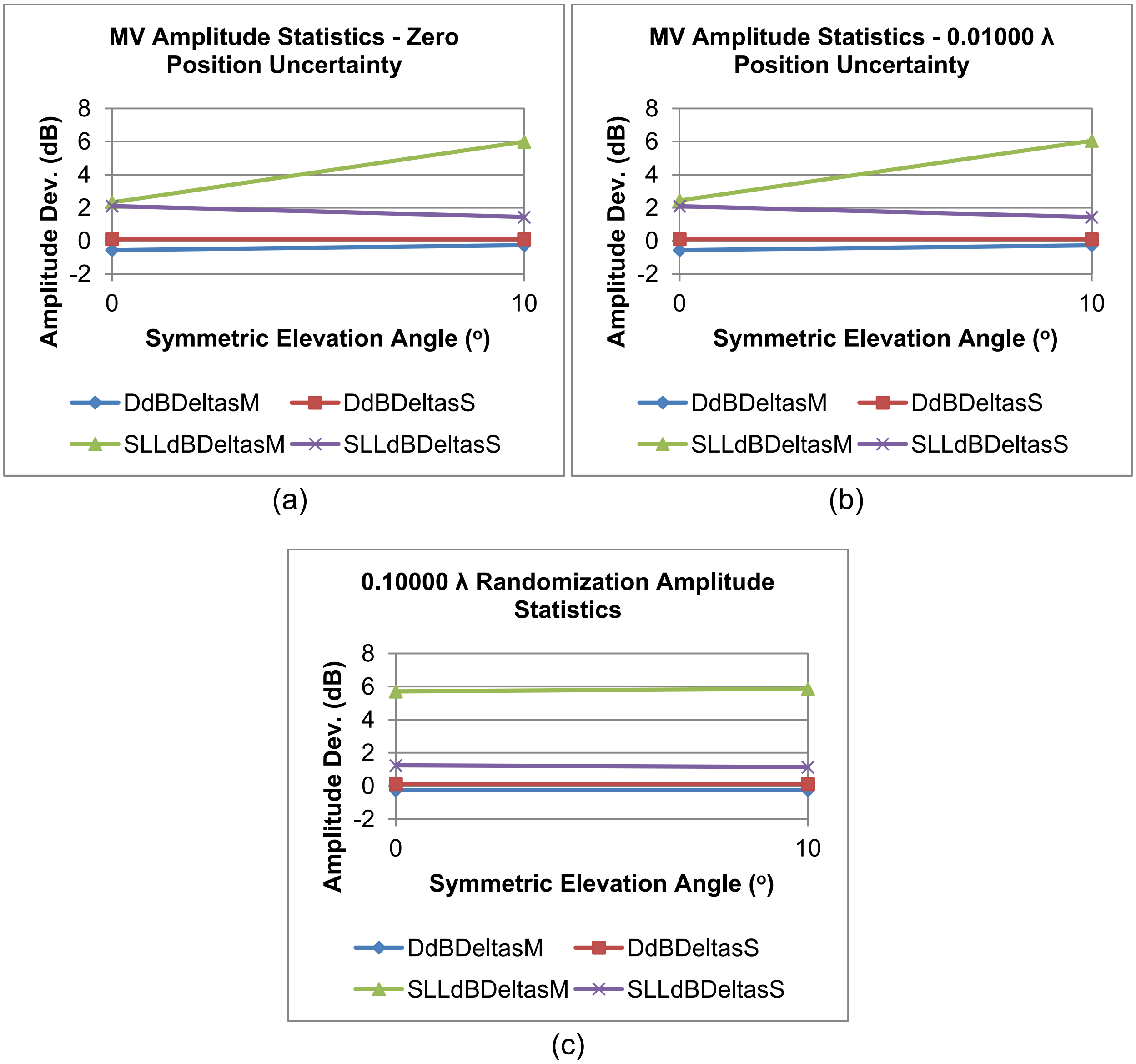

Figure 5.31. *Sidelobe level and directivity statistics for an array with 9 almost linear elements, nominal* $3/4\,\lambda$ *spacing, 0.10000 λ radial element position randomization and minimum variance enhancement.* Amplitude statistics assuming perfect knowledge of position (a), 0.01000 λ uncertainty of position (b) and no enhancement processing from the initial array factor pattern (20 dB Dolph-Chebyshev taper) runs (c) are compared.

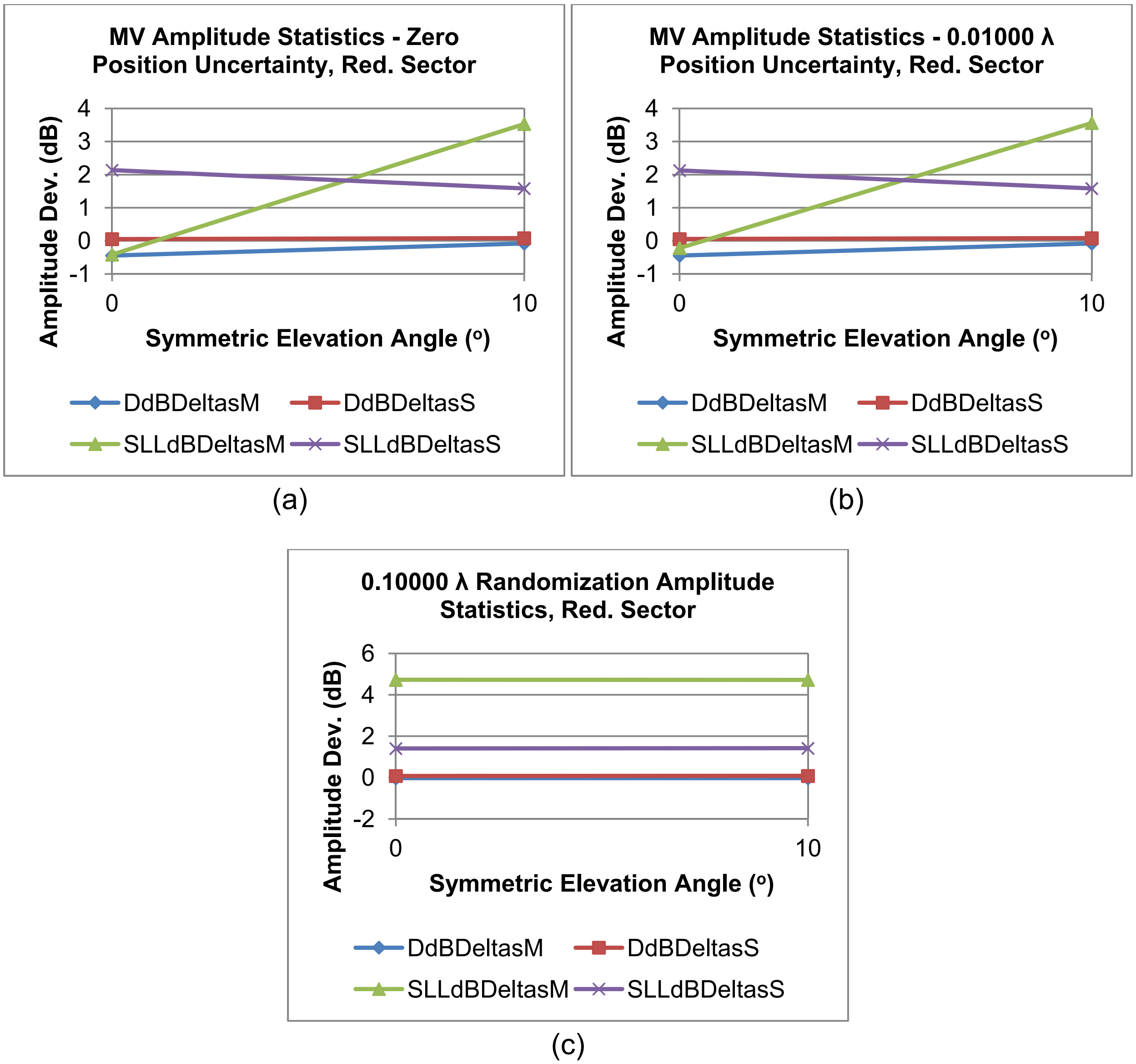

Figure 5.32. *Reduced sector sidelobe level statistics for an array with 9 almost linear elements, nominal* $3/4\,\lambda$ *spacing, 0.10000 λ radial element position randomization and minimum variance enhancement.* Sidelobe level statistics assuming perfect knowledge of position (a), 0.01000 λ uncertainty of position (b) and no enhancement processing from the initial array factor pattern (20 dB Dolph-Chebyshev taper) runs (c) are compared.

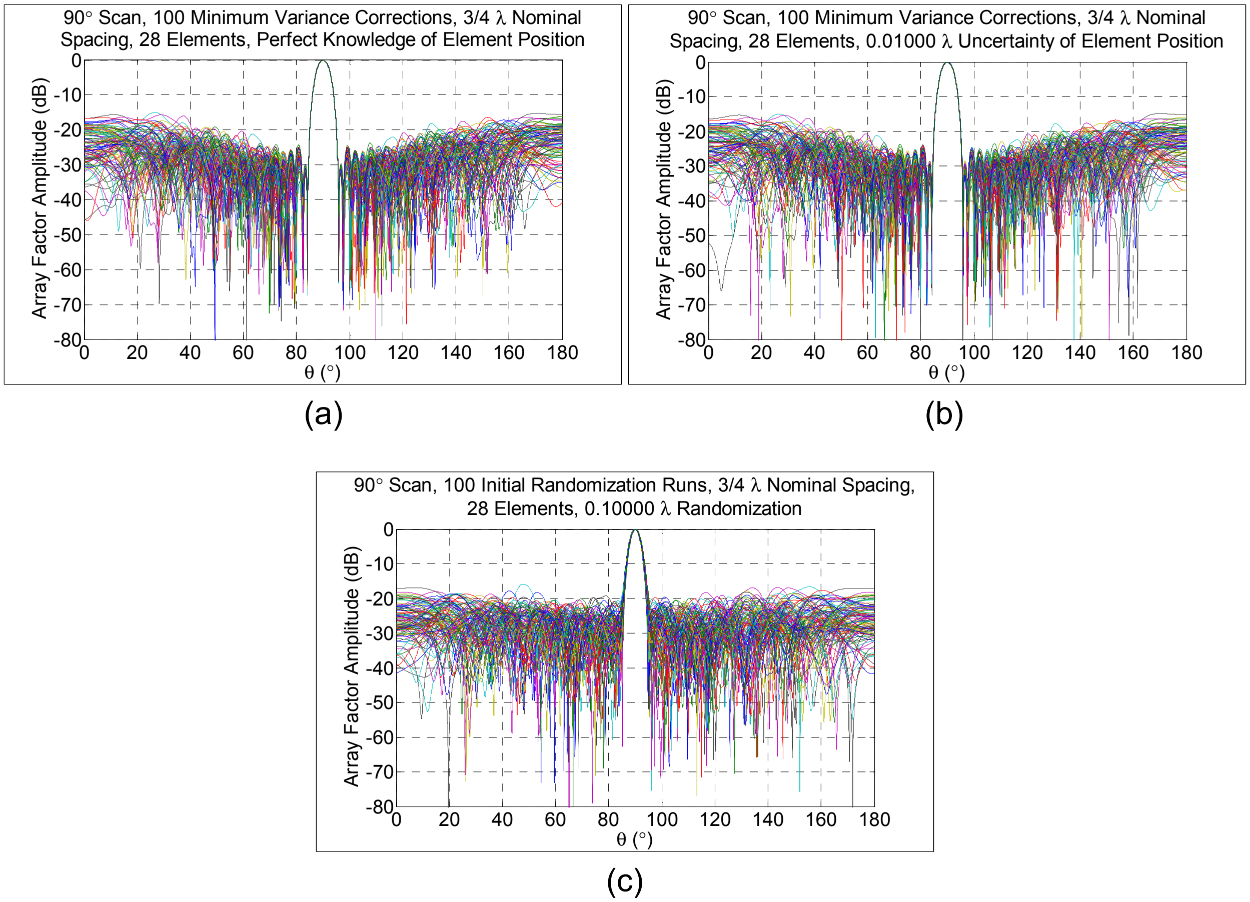

Figure 5.33. *28 almost linear elements with nominal* $3/4\lambda$ *spacing and minimum variance enhancement.* Rerun of 100, 0.10000 λ radial element position randomization runs at broadside with application of the minimum variance enhancement algorithm assuming perfect knowledge of element position (a) and 0.01000 λ uncertainty in element position. Initial array factor pattern (50 dB Dolph-Chebyshev taper) runs of 100, 0.10000 λ radial element position element position randomizations (c) are additionally plotted for broadside scan.

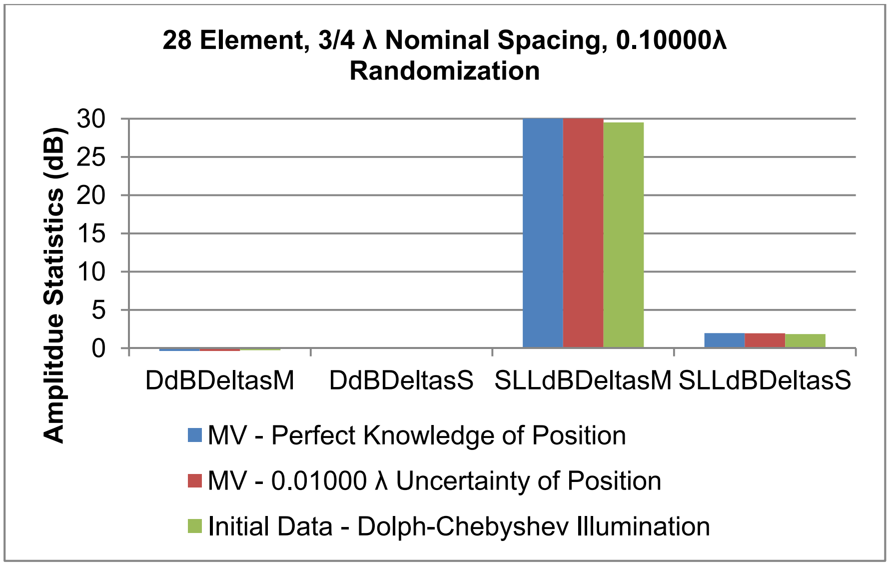

(a)

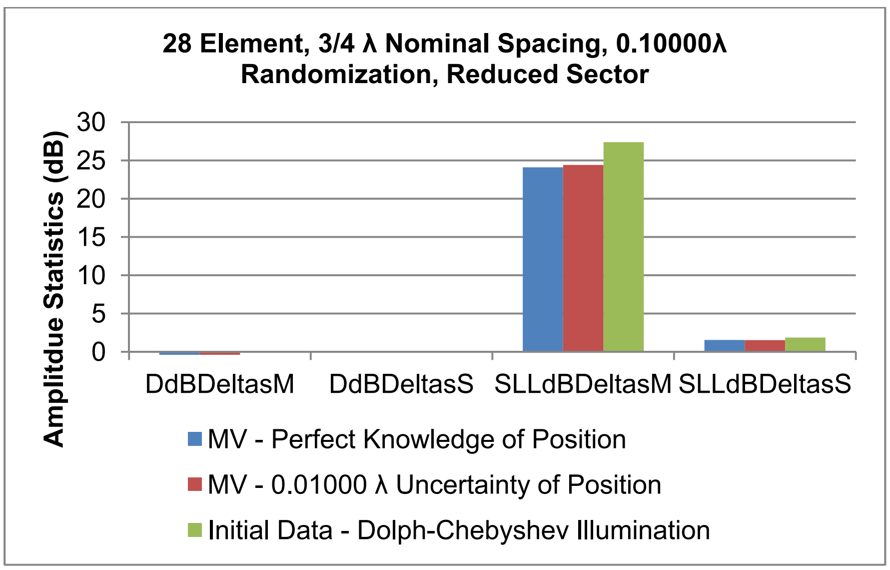

(b)

Figure 5.34. *Amplitude statistics for a 28 element,* $3/4\,\lambda$ *nominal spacing array with 0.10000 λ randomization.* Minimum variance enhancement is applied with perfect knowledge of the element positions and 0.01000 λ uncertainty of element positions. Initial data from the 50 dB Dolph-Chebyshev array with 0.10000 λ randomization is also compared. Amplitude statistics for the full 180° cut (a) as well as the reduced sector compilation from 60° to 120° (b) are illustrated.

A 9 element Dolph-Chebyshev array and a 27 element modified Taylor array with $7/8\,\lambda$ element spacing were tested with the minimum variance algorithm for the scan angles listed in Table 5.1. Prior to randomization, the 9 element array was initially designed as 20 dB sidelobe level array. It was analyzed at 90° beam scan. The 27 element array was also analyzed at broadside scan. Tables 5.9 list the angular directions used to generate the $\mathbf{e}$ and $\mathbf{Y}$ vectors for these cases. It also lists the amplitudes of the waves used to generate the $\mathbf{Y}$ vectors. In addition to $\mathbf{e}$ and $\mathbf{Y}$ vector parameters, the reduced sector analysis angles are also included. The 90° beam scan plots of the 100 runs from the minimum variance corrections with perfect knowledge of element position, 0.01000 λ uncertainty of element position, and initial 0.10000 λ randomization from the 9 element array are illustrated in Figure 5.35. Sidelobe level statistics for the 9 element array are also presented (Figure 5.36). As can be seen from Figures 5.35 and 5.36, the overall sidelobe level statistical performance of the minimum variance enhancement, is very similar to the unenhanced randomized array. But again, the patterns around the main beam are improved. As a result, a reduced sector analysis was performed to determine the sidelobe level statistics near the main beam (Figure 5.36). Within $\pm$ 40° of the peak of beam, the sidelobe level is reduced about 6 dB by the minimum variance algorithm as compared to the initial 0.10000 λ randomization.

Increasing the number of elements again caused the overall sidelobe level to decrease with definite improvement in the near beam area when the minimum variance enhancement is applied. This is evident from the broadside scan patterns and statistics (Figures 5.37 and 5.38). However, it is evident that as the field sampling interval is exceeding the Nyquist rate, the angular sector of sidelobe level performance improvement about the main beam continues to decrease. However, even in this narrow sector, SLLdBDeltasM for the minimum variance case does not decrease to a smaller value than the initial data case, but SLLdBDeltasS is significantly smaller for the minimum variance case than the initial data. This results in about a 4.5 dB smaller 3σ sidelobe level for the minimum variance case as compared to the initial data over the same angular sector.

Beam Scan Angle	**e** Vector Directions	**Y** Vector Directions	**Y** Vector Amplitudes	Reduced Sector Analysis	
				Start Angle	Stop Angle
(°θ)					
90	87 and 93	78.03125 and 101.96875	1 and 1	50	130

(a)

Beam Scan Angle	**e** Vector Directions	**Y** Vector Directions	**Y** Vector Amplitudes	Reduced Sector Analysis	
				Start Angle	Stop Angle
(°θ)					
90	87 to 93 in steps of 0.1	84 and 96	1 and 1	70	110

(b)

Table 5.9. *Analysis parameters utilized for minimum variance enhancement of $7/8\,\lambda$ nominally spaced arrays with 0.10000 λ randomization.* 9 element (a), and 27 element (b), arrays were analyzed.

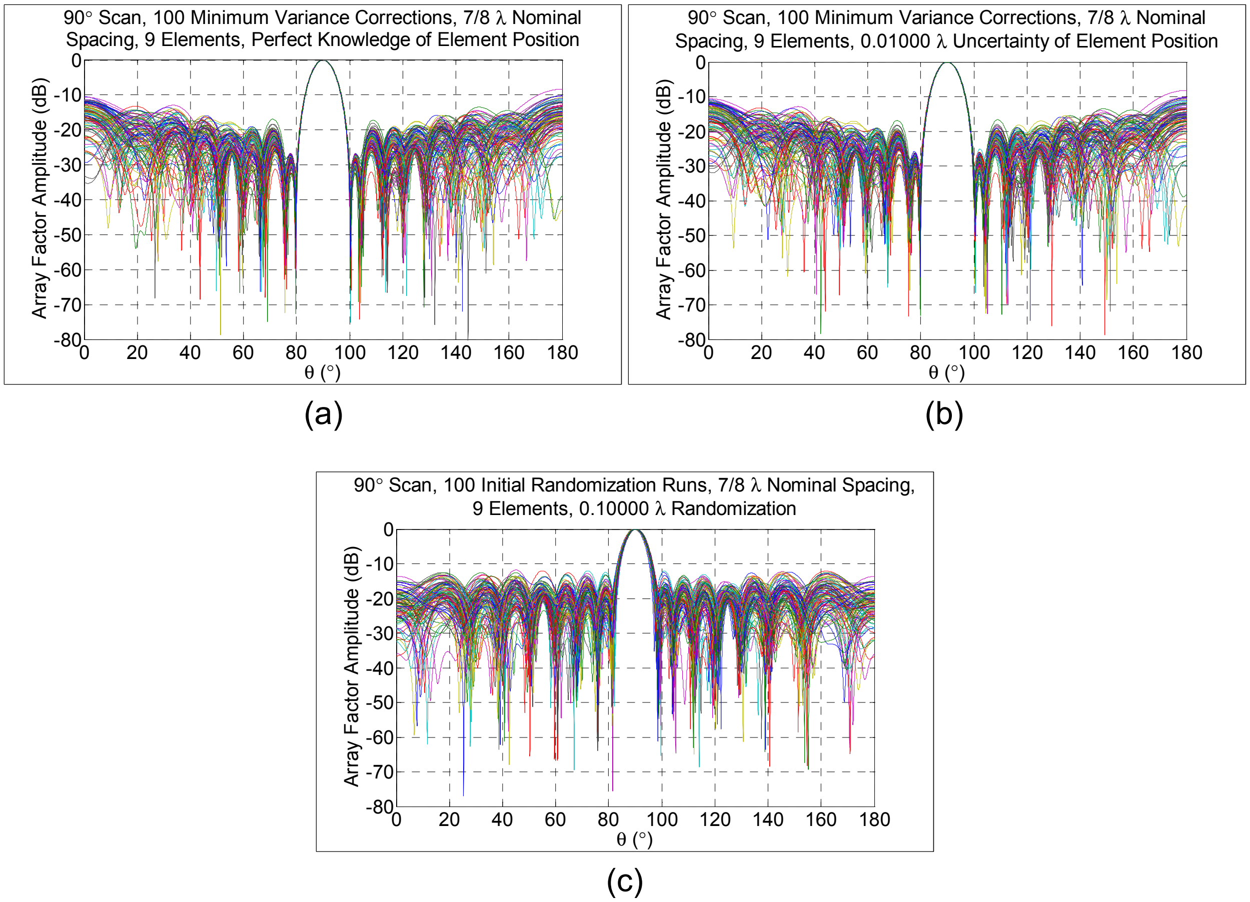

Figure 5.35. *9 almost linear elements with nominal* $7/8\,\lambda$ *spacing and minimum variance enhancement.* Rerun of 100, 0.10000 λ radial element position randomization runs at broadside with application of the minimum variance enhancement algorithm assuming perfect knowledge of element position (a) and 0.01000 λ uncertainty in element position. Initial array factor pattern (20 dB Dolph-Chebyshev taper) runs of 100, 0.10000 λ radial element position element position randomizations (c) are additionally plotted for broadside scan.

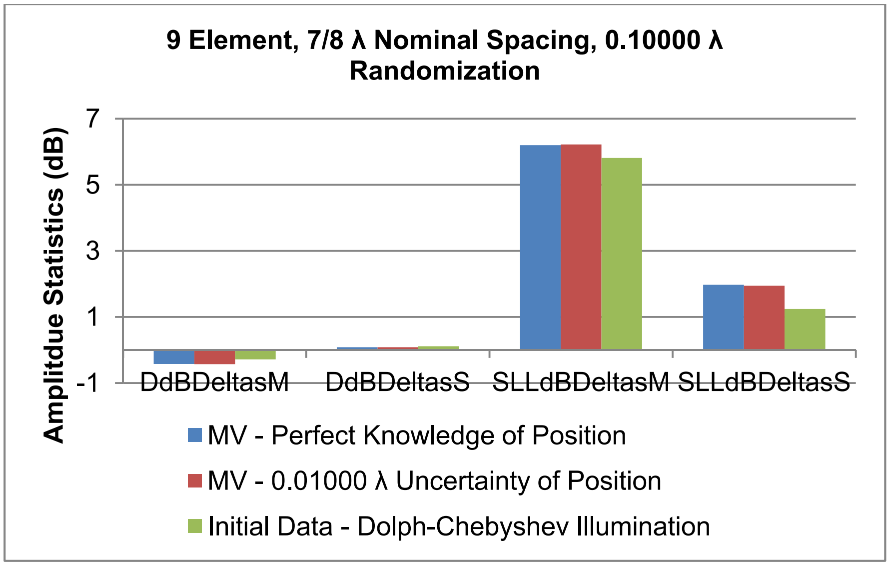

(a)

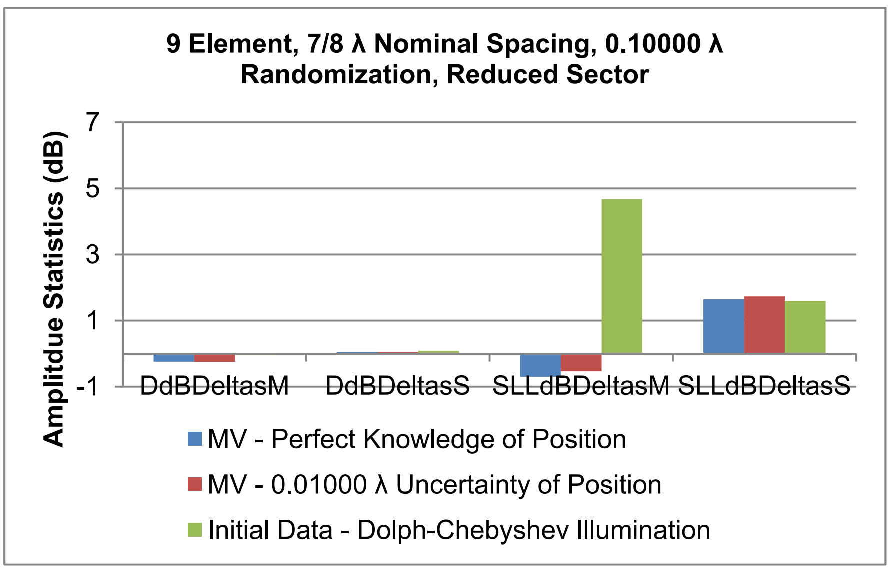

(b)

Figure 5.36. *Amplitude statistics for a 9 element, $7/8\,\lambda$ nominal spacing array with 0.10000 λ randomization.* Minimum variance enhancement is applied with perfect knowledge of the element positions and 0.01000 λ uncertainty of element positions. Initial data from the 20 dB Dolph-Chebyshev array with 0.10000 λ randomization is also compared. Amplitude statistics for the full 180° cut (a) as well as the reduced sector compilation from 50° to 130° (b) are illustrated.

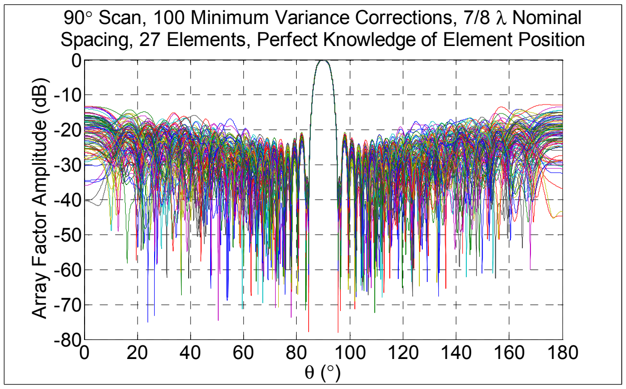

(a)

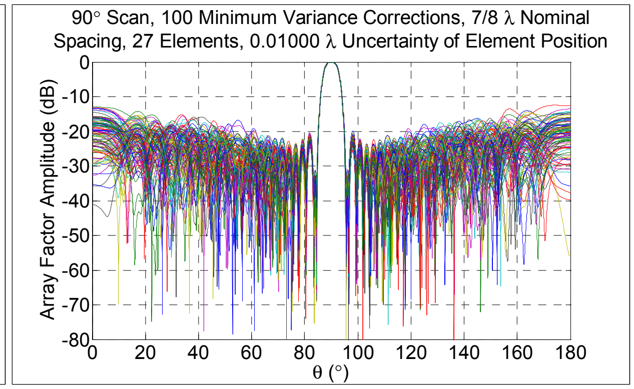

(b)

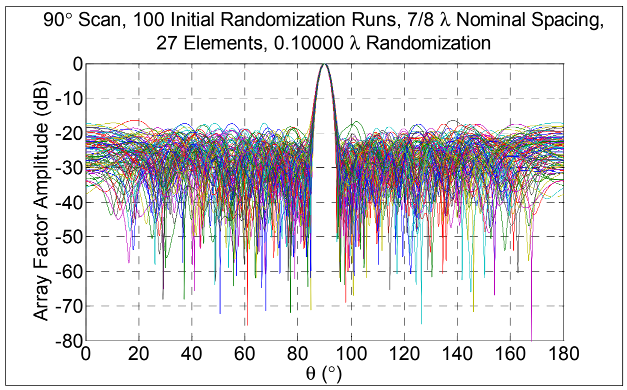

(c)

Figure 5.37. *27 almost linear elements with nominal* $7/8\,\lambda$ *spacing and minimum variance enhancement.* Rerun of 100, 0.10000 λ radial element position randomization runs at broadside with application of the minimum variance enhancement algorithm assuming perfect knowledge of element position (a) and 0.01000 λ uncertainty in element position. Initial array factor pattern (50 dB modified Taylor taper) runs of 100, 0.10000 λ radial element position element position randomizations (c) are additionally plotted for broadside scan.

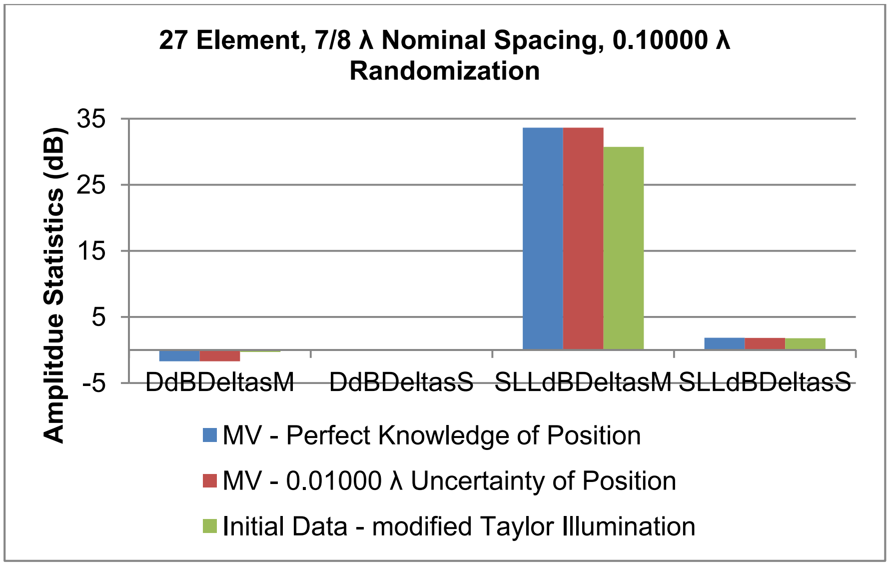

(a)

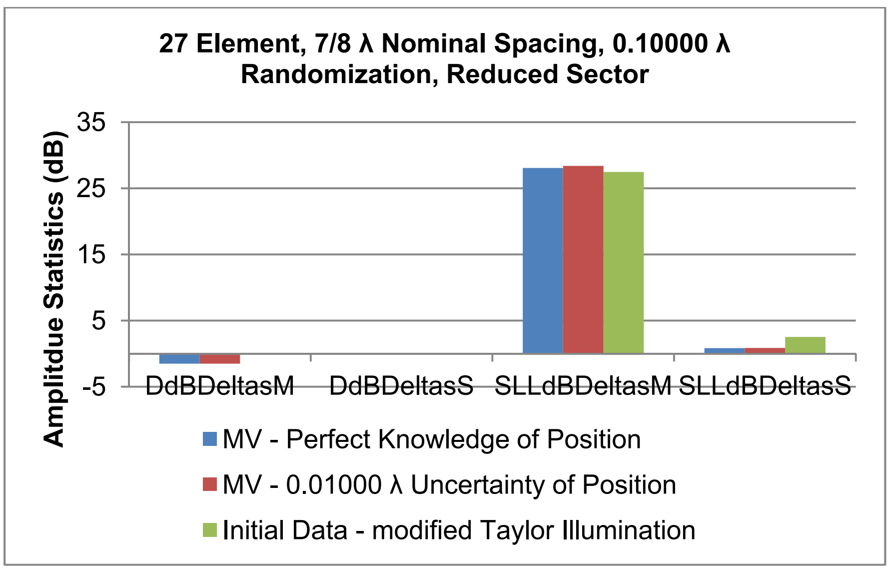

(b)

Figure 5.38. *Amplitude statistics for a 27 element,* $7/8\,\lambda$ *nominal spacing array with 0.10000 λ randomization.* Minimum variance enhancement is applied with perfect knowledge of the element positions and 0.01000 λ uncertainty of element positions. Initial data from the 50 dB modified Taylor array with 0.10000 λ randomization is also compared. Amplitude statistics for the full 180^{o} cut (a) as well as the reduced sector compilation from 70^{o} to 110^{o} (b) are illustrated.

After examining the benefits of the minimum variance method for determining distributed array element weights when element position information is available, a question of what is the best approach and available solution for a design. Obviously, the minimum number of elements is desirable. Near Nyquist placement of the elements is also beneficial, but can be compromised against the angular width of the improved sidelobe level performance near the main beam. In all cases, between 20 and 30 dB sidelobe performance appears to be achievable near the main beam. Judicial choice of element patterns or some sub array processing could have the possibility of improving the sidelobes further away from the main beam. In the case of sub-array processing, if multiple elements are mounted to the same vehicle with fixed location, the position variation would only occur beyond sub-array boundaries. This type of analysis would require further research.

5.7 Element Position Tracking

One of the major keys to making a distributed array function would be accurate position knowledge of each element over time. If the initial layer of relative location information is developed using Global Navigation Satellite Systems (GNSS), high levels of accuracy can be achieved. To achieve the highest level of accuracy, Real Time Kinematic (RTK) positioning becomes necessary. With RTK, position accuracy of ± 2 cm (laterally and vertically) is quoted in several sources including product specifications [80] [81] [82] [83]. For flying systems, these sensors quote ± 5 cm position accuracy, laterally and vertically. Position update rates range from 10 to 100 Hz. RTK can come in two major modes, either a fixed base mode where one receiver is physically fixed to one location, or a moving base mode where the base receiver is moving so relative position data can be obtained among several receivers.

Unfortunately, the update rate is too low for airborne vehicles. As a result some additional sensors are required to maintain detailed position sensing between GNSS updates. Accelerometers can make good sensors for this purpose. Many industrial accelerometer products are available with upper frequency responses of 15 to 30 KHz and detection ranges as high as 500 g's [84] [85] [86]. With the use of devices such as these, concurrent with GNSS sensing and Kalman state filters, position updates should be possible up to 30 KHz rates.

6.0 Conclusion

6.1 Performance Degradation

Throughout this dissertation, antenna array background including array theory and some common array illumination tapers has been covered. What have been uniquely studied are impacts to array factor performance that specifically result from random element position errors for linear arrays.

A large numerical study was performed assuming omnidirectional array element radiators and no mutual coupling. Baseline, linear array factor designs were developed with element spacing of $1/4\,\lambda$, $3/8\,\lambda$, $1/2\,\lambda$, $5/8\,\lambda$, $3/4\,\lambda$, and $7/8\,\lambda$. For the designs with element spacing of $1/4\,\lambda$ and $3/8\,\lambda$, modified Taylor, powers of cosine on a pedestal, and Taylor array tapers were utilized in the baseline designs. In all the other element spacing designs, Dolph-Chebyshev illumination in addition to the previously mentioned tapers was also applied. The sidelobe levels of these designs were 20, 30, 40 and 50 dB for each element spacing/taper type combination. Designs were developed with a Minimum Number of Elements (MNE) for each spacing/taper/sidelobe level combination. Collectively, these were referred to as the MNE designs. For each spacing/sidelobe level combination from an MNE group, the taper with the largest number of elements was identified. Additional baseline designs were developed for the other tapers using the largest number of elements from the MNE group such that a set of arrays was designed with an equal number of elements across tapers for the given spacing/sidelobe combination. These were referred to as the Equal Number of Elements (ENE) designs.

With all the baseline designs established, baseline array factor performance metrics were determined. The items numerically measured ranged from directivity and sidelobe level to main beam pointing error and beamwidths. Once these baseline parameters were established, the degradation of the metrics as elements were allowed to be out of position was studied. Degradation versus the absolute distance that an element was allowed to be mis-positioned from its nominal position was established and quantified. Worst case performance over beam scan angles was documented. In the end, the primarily impacted parameter due to element mis-positioning is sidelobe level. It was also demonstrated that the amount of degradation was independent of taper type for a given sidelobe level array design.

6.2 Performance Enhancement

Having identified the performance degradation due to element position errors, an analysis that investigated the antenna factor pattern performance as a function of motion of the elements was developed. From here methods of enhancement for arrays with out-of-position elements were investigated. Enhancement methods that were applicable with single moment in time inputs were most desirable. Ideally, an algorithm that could use instantaneous position information of the elements to update the array weights is desirable. This was found in an algorithm that minimizes noise and undesired signals. It was demonstrated over several of the randomized baseline array designs. Specifically it was demonstrated on randomized baseline arrays that began primarily as 20 and 50 dB sidelobe level arrays with up to 0.10000 λ random error in the element position vector.

Enhancement that improves the sidelobe level performance near the main beam of the array factor has been demonstrated. The method only requires knowledge of the relative element positions. It has also been demonstrated that as the element spacing exceeds Nyquist requirements, the sector of improvement does decrease. This problem becomes analogous to a digital image processing system with a jittery pixel clock that causes errors in multiple dimensions of processing due to the random jitter.

6.3 Future Research Opportunities

Examining this problem from a planar array perspective would also be informative to the research community. Developing a method to recover more of the sidelobe performance well beyond the main beam would be a significant accomplishment. The error phase caused by the random relative motion, is an angular function that can only be minimized by means of destructive interference. It cannot be viewed as a slight perturbation that can simply be phase compensated element by element – phase compensation would only occur in a single look direction, and not necessarily cause sufficient destructive interference in the sidelobe region of the array.

Finally, examining if sub-array processing could enhance the distributed array system is another place where performance improvement may be likely. Adding mutual coupling with non-ideal elements may add additional degrees of freedom that may also provide opportunity to resolve sidelobe issues.

APPENDICIES

APPENDIX A

Initial Array Design Performance Metrics

Included in this appendix are the performance metrics from the initial array designs prior to randomization. The data is listed in tabular form beginning with the $1/4\,\lambda$ element spaced arrays and finishing with the $7/8\,\lambda$ element spaced arrays.

Spacing (λ)	Design SLL (dB)	Beamwidth Parameter	Scan Angle	Illumination Taper: Modified Taylor MNE	Modified Taylor ENE	Powers of Cosine on a Pedestal MNE	Powers of Cosine on a Pedestal ENE	Taylor MNE	Taylor ENE
1/4	20 dB	Directivity (dB)		9.65		9.49	9.72	9.63	9.84
		SLL (-dB)		20.92		20.35	20.30	20.38	20.36
		3 dB BW (°)	40/140	19.0		19.8	18.7	19.0	18.0
			50/130	15.7		16.3	15.5	15.7	14.9
			60/120	13.8		14.3	13.6	13.8	13.1
			70/110	12.7		13.2	12.5	12.7	12.1
			80/100	12.1		12.6	11.9	12.1	11.5
			90	12.0		12.4	11.8	11.9	11.3
		10 dB BW (°)	40/140	34.6		36.1	33.8	34.4	32.3
			50/130	27.4		28.4	26.9	27.2	25.8
			60/120	23.8		24.7	23.4	23.7	22.5
			70/110	21.8		22.6	21.4	21.7	20.6
			80/100	20.8		21.5	20.4	20.7	19.6
			90	20.5		21.2	20.1	20.3	19.3
		FNB (°)	40/140	59.3		59.8	58.9	59.1	58.2
			50/130	41.2		42.6	40.0	40.5	38.1
			60/120	35.0		36	34.1	34.4	32.6
			70/110	31.8		32.7	31.0	31.3	29.7
			80/100	30.2		31	29.4	29.7	28.2
			90	29.6		30.5	28.9	29.2	27.7

Table A.1. *Initial design performance metrics for $1/4\,\lambda$ element spaced arrays with minimum 20 dB sidelobe levels.*

				Illumination Taper					
				Modified Taylor		Powers of Cosine on a Pedestal		Taylor	
Spacing (λ)	Design SLL (dB)	Beamwidth Parameter	Scan Angle	MNE	ENE	MNE	ENE	MNE	ENE
1/4	30 dB	Directivity (dB)		10.29		10.19	10.53	10.23	10.56
		SLL (-dB)		30.50		30.53	30.29	30.76	30.84
		3 dB BW (°)	40/140	16.3		16.7	15.4	16.5	15.2
			50/130	13.5		13.9	12.8	13.7	12.7
			60/120	11.9		12.2	12.3	12.1	11.2
			70/110	11.0		11.2	10.4	11.1	10.3
			80/100	10.5		10.7	9.9	10.6	9.8
			90	10.3		10.6	9.8	10.4	9.7
		10 dB BW (°)	40/140	29.7		30.4	27.8	30.2	27.6
			50/130	23.9		24.5	22.5	24.3	22.4
			60/120	20.9		21.4	19.7	21.2	19.6
			70/110	19.2		19.6	18.1	19.4	18.0
			80/100	18.3		18.7	17.2	18.5	17.1
			90	18.0		18.4	17.0	18.2	16.8
		FNB (°)	40/140	58.6		58.8	52.2	59.1	55.6
			50/130	39.1		39.8	36.3	40.6	37.0
			60/120	33.3		33.9	31.2	34.5	31.7
			70/110	30.3		30.9	28.4	31.4	28.9
			80/100	28.8		29.3	27.0	29.8	27.4
			90	28.3		28.8	26.6	29.3	27.0

Table A.2. *Initial design performance metrics for $1/4\,\lambda$ element spaced arrays with minimum 30 dB sidelobe levels.*

				Illumination Taper					
				Modified Taylor		Powers of Cosine on a Pedestal		Taylor	
Spacing (λ)	Design SLL (dB)	Beamwidth Parameter	Scan Angle	MNE	ENE	MNE	ENE	MNE	ENE
1/4	40 dB	Directivity (dB)		10.82		10.79	11.19	10.80	11.20
		SLL (-dB)		40.66		40.75	40.84	40.37	40.50
		3 dB BW (°)	40/140	14.3		14.4	13.1	14.3	13.1
			50/130	11.9		12.0	10.9	11.9	10.9
			60/120	10.6		10.6	9.6	10.5	9.6
			70/110	9.7		9.7	8.9	9.7	8.8
			80/100	9.2		9.3	8.5	9.2	8.4
			90	9.1		9.1	8.3	9.1	8.3
		10 dB BW (°)	40/140	26.0		26.2	23.7	26.1	23.6
			50/130	21.2		21.3	19.4	21.3	19.3
			60/120	18.6		18.7	17.0	18.6	17.0
			70/110	17.1		17.2	15.6	17.1	15.6
			80/100	16.3		16.3	14.9	16.3	14.9
			90	16.0		16.1	14.7	16.1	14.6
		FNB (°)	40/140	58.1		58.2	46.3	58.7	48.8
			50/130	37.8		38.1	34.2	39.4	35.2
			60/120	32.3		32.5	29.4	33.5	30.3
			70/110	29.5		29.6	26.9	30.5	27.6
			80/100	28.0		28.1	25.5	29.0	26.3
			90	27.5		27.7	25.1	28.5	25.8

Table A.3. *Initial design performance metrics for $1/4\,\lambda$ element spaced arrays with minimum 40 dB sidelobe levels.*

				Illumination Taper					
				Modified Taylor		Powers of Cosine on a Pedestal		Taylor	
Spacing (λ)	Design SLL (dB)	Beamwidth Parameter	Scan Angle	MNE	ENE	MNE	ENE	MNE	ENE
1/4	50 dB	Directivity (dB)		11.17	12.36	12.36		11.22	12.78
		SLL (-dB)		50.61	50.70	50.70		50.63	50.44
		3 dB BW (°)	40/140	13.1	9.9	9.9		13.0	9.0
			50/130	10.9	8.3	8.3		10.8	7.5
			60/120	9.6	7.3	7.3		9.5	6.7
			70/110	8.9	6.7	6.7		8.8	6.1
			80/100	8.5	6.4	6.4		8.4	5.8
			90	8.3	6.3	6.3		8.2	5.8
		10 dB BW (°)	40/140	23.9	17.8	17.8		23.6	16.1
			50/130	19.6	14.8	14.8		19.3	13.4
			60/120	17.2	13.0	13.0		17.0	11.8
			70/110	15.8	12.0	12.0		15.6	10.9
			80/100	15.1	11.4	11.4		14.9	10.4
			90	14.8	11.2	11.2		14.6	10.2
		FNB (°)	40/140	58.1	35.3	35.3		58.1	31.2
			50/130	37.8	27.9	27.9		37.7	25.1
			60/120	32.4	24.3	24.3		32.3	21.9
			70/110	29.5	22.2	22.2		29.4	20.1
			80/100	28.0	21.2	21.2		27.9	19.2
			90	27.5	20.8	20.8		27.4	18.8

Table A.4. *Initial design performance metrics for $1/4\,\lambda$ element spaced arrays with minimum 50 dB sidelobe levels.*

				Illumination Taper					
				Modified Taylor		Powers of Cosine on a Pedestal		Taylor	
Spacing (λ)	Design SLL (dB)	Beamwidth Parameter	Scan Angle	MNE	ENE	MNE	ENE	MNE	ENE
3/8	20 dB	Directivity (dB)		9.82		9.89		9.68	10.04
		SLL (-dB)		21.36		20.68		21.14	20.52
		3 dB BW (°)	40/140	18.2		17.9		18.7	17.1
			50/130	15.1		14.8		15.5	14.2
			60/120	13.3		13.0		13.6	12.5
			70/110	12.2		12.0		12.5	11.5
			80/100	11.7		11.4		12.0	11.0
			90	11.5		11.3		11.8	10.8
		10 dB BW (°)	40/140	33.0		32.2		34.0	30.5
			50/130	26.3		25.7		26.9	24.5
			60/120	22.9		22.4		23.5	21.4
			70/110	21.0		20.6		21.5	19.6
			80/100	20.0		19.6		20.5	18.7
			90	19.7		19.3		20.1	18.4
		FNB (°)	40/140	58.7		58.3		59.1	51.6
			50/130	39.5		38.3		40.5	36.2
			60/120	33.7		32.7		34.4	31.0
			70/110	30.6		29.8		31.3	28.3
			80/100	29.1		28.3		29.7	26.9
			90	28.6		27.8		29.2	26.4

Table A.5. *Initial design performance metrics for $3/8\,\lambda$ element spaced arrays with minimum 20 dB sidelobe levels.*

Spacing (λ)	Design SLL (dB)	Beamwidth Parameter	Scan Angle	Illumination Taper: Modified Taylor MNE	Modified Taylor ENE	Powers of Cosine on a Pedestal MNE	Powers of Cosine on a Pedestal ENE	Taylor MNE	Taylor ENE
3/8	30 dB	Directivity (dB)		10.29		10.23	10.49	10.28	10.53
		SLL (-dB)		30.25		32.21	31.90	30.08	30.22
		3 dB BW (°)	40/140	16.3		16.5	15.6	16.3	15.3
			50/130	13.5		13.7	12.9	13.5	12.8
			60/120	11.9		12.1	11.4	11.9	11.2
			70/110	11.0		11.1	10.5	11.0	10.3
			80/100	10.5		10.6	10.0	10.5	9.9
			90	10.3		10.4	9.8	10.3	9.7
		10 dB BW (°)	40/140	29.6		30.1	28.1	29.7	27.8
			50/130	23.9		24.2	22.8	24.0	22.5
			60/120	20.9		21.2	19.9	20.9	19.7
			70/110	19.2		19.4	18.3	19.2	18.1
			80/100	18.2		18.5	17.4	18.3	17.2
			90	18.0		18.2	17.2	18.0	17.0
		FNB (°)	40/140	58.5		58.9	57.9	59.2	58.2
			50/130	38.9		40.0	37.2	41.0	38.1
			60/120	33.2		34.0	31.9	34.8	30.2
			70/110	30.2		30.9	29.1	31.6	29.6
			80/100	28.7		29.4	27.6	30.0	28.1
			90	28.2		28.9	27.1	29.5	27.7

Table A.6. *Initial design performance metrics for* $3/8\,\lambda$ *element spaced arrays with minimum 30 dB sidelobe levels.*

				Illumination Taper					
				Modified Taylor		Powers of Cosine on a Pedestal		Taylor	
Spacing (λ)	Design SLL (dB)	Beamwidth Parameter	Scan Angle	MNE	ENE	MNE	ENE	MNE	ENE
3/8	40 dB	Directivity (dB)		10.89		10.88	11.27	11.05	11.24
		SLL (-dB)		40.85		40.05	40.27	40.32	40.47
		3 dB BW (°)	40/140	14.1		14.1	12.8	13.5	12.9
			50/130	11.7		11.7	10.7	11.3	10.8
			60/120	10.3		10.3	9.4	9.9	9.5
			70/110	9.5		9.5	8.7	9.1	8.8
			80/100	9.1		9.1	8.3	8.7	8.4
			90	8.9		8.9	8.2	8.6	8.2
		10 dB BW (°)	40/140	25.6		25.6	23.2	24.6	23.4
			50/130	20.9		20.9	19.0	20.1	19.2
			60/120	18.3		18.3	16.7	17.6	16.9
			70/110	16.8		16.8	15.3	16.2	15.5
			80/100	16.0		16.0	14.6	15.4	14.8
			90	15.8		15.8	14.4	15.2	14.5
		FNB (°)	40/140	57.9		58.2	46.3	58.5	53.5
			50/130	37.3		38.1	34.2	38.8	36.6
			60/120	31.9		32.6	29.3	33.1	31.4
			70/110	29.1		29.7	26.9	30.2	28.6
			80/100	27.6		28.2	25.5	28.6	27.2
			90	27.2		27.7	25.1	28.2	26.8

Table A.7. *Initial design performance metrics for* $3/8\,\lambda$ *element spaced arrays with minimum 40 dB sidelobe levels.*

				Illumination Taper					
				Modified Taylor		Powers of Cosine on a Pedestal		Taylor	
Spacing (λ)	Design SLL (dB)	Beamwidth Parameter	Scan Angle	MNE	ENE	MNE	ENE	MNE	ENE
3/8	50 dB	Directivity (dB)		11.12	12.37	11.21		11.30	12.75
		SLL (-dB)		50.44	50.56	50.36		50.27	50.49
		3 dB BW (°)	40/140	13.3	9.9	13.0		12.7	9.1
			50/130	11.1	8.3	10.8		10.6	7.6
			60/120	9.8	7.3	9.5		9.3	6.7
			70/110	9.0	6.7	8.8		8.6	6.2
			80/100	8.6	6.4	8.4		8.2	5.9
			90	8.4	6.3	8.2		8.1	5.8
		10 dB BW (°)	40/140	24.3	17.8	23.7		23.2	16.3
			50/130	19.8	14.8	19.4		19.0	13.5
			60/120	17.4	13.0	17.0		16.7	11.9
			70/110	16.0	12.0	15.7		15.3	10.9
			80/100	15.2	11.4	14.9		14.6	10.4
			90	15.0	11.2	14.7		14.4	10.3
		FNB (°)	40/140	58.3	35.3	58.3		58.0	32.2
			50/130	38.3	27.9	38.3		37.5	25.7
			60/120	32.8	24.3	32.8		32.1	22.4
			70/110	29.8	22.2	29.8		29.2	20.5
			80/100	28.3	21.2	28.3		27.8	19.6
			90	27.9	20.8	27.9		27.3	19.3

Table A.8. *Initial design performance metrics for $3/8\,\lambda$ element spaced arrays with minimum 50 dB sidelobe levels.*

				Illumination Taper							
				Dolph-Chebyshev		Modified Taylor		Powers of Cosine on a Pedestal		Taylor	
Spacing (λ)	Design SLL (dB)	Beamwidth Parameter	Scan Angle	MNE	ENE	MNE	ENE	MNE	ENE	MNE	ENE
1/2	20 dB	Directivity (dB)		9.36	9.83	9.65		9.65		9.79	
		SLL (-dB)		20.00	20.00	20.60		20.50		20.20	
		3 dB BW (°)	40/140	20.0	17.7	19.0		19.0		18.1	
			50/130	16.5	14.7	15.7		15.7		15.0	
			60/120	14.5	12.9	13.8		13.8		13.2	
			70/110	13.3	11.9	12.7		12.7		12.1	
			80/100	12.7	11.3	12.1		12.1		11.6	
			90	12.5	11.2	11.9		11.9		11.4	
		10 dB BW (°)	40/140	36.5	31.7	34.4		34.5		32.4	
			50/130	28.6	25.4	27.3		27.3		25.9	
			60/120	24.9	22.1	23.7		23.8		22.6	
			70/110	22.8	20.3	21.7		21.8		20.7	
			80/100	21.7	19.3	20.7		20.7		19.7	
			90	21.3	19.0	20.4		20.4		19.4	
		FNB (°)	40/140	59.8	57.9	59.2		59.2		58.3	
			50/130	42.6	37.3	40.8		40.8		38.3	
			60/120	36.0	31.9	34.7		34.7		32.8	
			70/110	32.7	29.1	31.5		31.5		29.8	
			80/100	31.0	27.6	29.9		29.9		28.3	
			90	30.5	27.2	29.4		29.4		27.9	

Table A.9. *Initial design performance metrics for $1/2\lambda$ element spaced arrays with minimum 20 dB sidelobe levels.*

				Illumination Taper							
				Dolph-Chebyshev		Modified Taylor		Powers of Cosine on a Pedestal		Taylor	
Spacing (λ)	Design SLL (dB)	Beamwidth Parameter	Scan Angle	MNE	ENE	MNE	ENE	MNE	ENE	MNE	ENE
1/2	30 dB	Directivity (dB)		10.46	11.67	10.71	11.28	10.35		10.61	11.52
		SLL (-dB)		30.00	30.00	30.74	30.39	30.67		30.09	30.08
		3 dB BW (°)	40/140	15.6	11.7	14.7	12.9	16.0		15.0	12.1
			50/130	13.0	9.8	12.3	10.7	13.3		12.5	10.1
			60/120	11.4	8.6	10.8	9.5	11.7		11.0	8.9
			70/110	10.5	8.0	10.0	8.7	10.8		10.1	8.2
			80/100	10.0	7.6	9.5	8.3	10.3		9.7	7.8
			90	9.9	7.5	9.3	8.2	10.1		9.5	7.7
		10 dB BW (°)	40/140	28.2	20.7	26.6	23.0	29.2		27.3	21.6
			50/130	22.8	17.1	21.6	18.9	23.6		22.1	17.8
			60/120	20.0	15.0	18.9	16.6	20.6		19.4	15.6
			70/110	18.3	13.8	17.4	15.2	18.9		17.8	14.4
			80/100	17.4	13.2	16.6	14.5	18.0		16.9	13.7
			90	17.2	13.0	16.3	14.3	17.7		16.7	13.5
		FNB (°)	40/140	53.0	33.9	48.4	38.9	58.5		10.6	38.0
			50/130	36.5	26.9	35.1	30.2	38.9		39.2	29.6
			60/120	31.3	23.4	30.1	26.2	33.2		33.4	25.7
			70/110	28.5	21.4	27.5	23.9	30.2		30.4	23.5
			80/100	27.1	20.4	26.1	22.8	28.7		28.8	22.4
			90	26.7	20.1	25.7	22.4	28.2		28.4	22.0

Table A.10. *Initial design performance metrics for* $1/2\,\lambda$ *element spaced arrays with minimum 30 dB sidelobe levels.*

				Illumination Taper							
				Dolph-Chebyshev		Modified Taylor		Powers of Cosine on a Pedestal		Taylor	
Spacing (λ)	Design SLL (dB)	Beamwidth Parameter	Scan Angle	MNE	ENE	MNE	ENE	MNE	ENE	MNE	ENE
1/2	40 dB	Directivity (dB)		10.87	12.49	10.83	11.99	10.92		11.15	12.30
		SLL (-dB)		40.00	40.00	40.94	40.02	40.81		40.06	40.32
		3 dB BW (°)	40/140	14.1	9.7	14.3	10.8	13.9		13.2	10.1
			50/130	11.8	8.1	11.9	9.1	11.6		11.0	8.4
			60/120	10.4	7.1	10.5	8.0	10.2		9.7	7.4
			70/110	9.6	6.6	9.6	7.4	9.4		8.9	6.9
			80/100	9.1	6.3	9.2	7.0	9.0		8.5	6.5
			90	9.0	6.2	9.1	6.9	8.8		8.4	6.4
		10 dB BW (°)	40/140	25.6	17.2	26.0	19.4	25.4		24.0	18.1
			50/130	20.9	14.3	21.2	16.1	20.7		19.7	15.0
			60/120	18.3	12.6	18.6	14.1	18.2		17.2	13.2
			70/110	16.8	11.6	17.0	13.0	16.7		15.8	12.1
			80/100	16.0	11.0	16.2	12.4	15.9		15.1	11.6
			90	15.8	10.8	16.0	12.2	15.7		14.9	11.4
		FNB (°)	40/140	52.3	30.2	58.2	35.4	58.0		59.4	35.8
			50/130	36.3	24.3	38.0	27.9	37.6		41.6	28.2
			60/120	31.2	21.2	32.5	24.3	32.2		35.2	24.5
			70/110	28.4	19.4	29.6	22.3	29.3		32.0	22.4
			80/100	27.0	18.5	28.1	21.2	27.8		30.3	21.4
			90	26.6	18.3	27.6	20.8	27.4		29.9	21.0

Table A.11. *Initial design performance metrics for $1/2\lambda$ element spaced arrays with minimum 40 dB sidelobe levels.*

				Illumination Taper							
				Dolph-Chebyshev		Modified Taylor		Powers of Cosine on a Pedestal		Taylor	
Spacing (λ)	Design SLL (dB)	Beamwidth Parameter	Scan Angle	MNE	ENE	MNE	ENE	MNE	ENE	MNE	ENE
1/2	50 dB	Directivity (dB)		11.21	12.92	11.27	12.37	11.21		11.30	12.71
		SLL (-dB)		50.00	50.00	50.32	50.44	50.36		50.36	50.46
		3 dB BW (°)	40/140	13.0	8.7	12.8	9.9	13.0		12.7	9.1
			50/130	10.8	7.3	10.7	8.3	10.8		10.6	7.6
			60/120	9.6	6.4	9.4	7.3	9.5		9.3	6.7
			70/110	8.8	5.9	8.7	6.7	8.8		8.6	6.2
			80/100	8.4	5.7	8.3	6.4	8.4		8.2	5.9
			90	8.3	5.6	8.1	6.3	8.2		8.1	5.8
		10 dB BW (°)	40/140	23.6	15.6	23.3	17.8	23.7		23.2	16.4
			50/130	19.3	12.9	19.1	14.8	19.4		19.0	13.6
			60/120	17.0	11.4	16.8	13.0	17.0		16.7	12.0
			70/110	15.6	10.5	15.4	12.0	15.7		15.4	11.0
			80/100	14.9	10.0	14.7	11.4	14.9		14.6	10.5
			90	14.6	9.9	14.5	11.2	14.7		14.4	10.4
		FNB (°)	40/140	52.4	29.4	54.2	35.3	58.3		58.3	32.9
			50/130	36.4	23.8	36.8	27.9	38.3		38.2	26.2
			60/120	31.2	20.8	31.5	24.3	32.8		32.6	22.8
			70/110	28.4	19.0	28.7	22.2	29.8		29.7	20.9
			80/100	27.0	18.1	27.3	21.2	28.3		28.2	19.9
			90	26.6	17.8	26.8	20.8	27.9		27.8	19.6

Table A.12. *Initial design performance metrics for* $1/2\,\lambda$ *element spaced arrays with minimum 50 dB sidelobe levels.*

				Illumination Taper							
				Dolph-Chebyshev		Modified Taylor		Powers of Cosine on a Pedestal		Taylor	
Spacing (λ)	Design SLL (dB)	Beamwidth Parameter	Scan Angle	MNE	ENE	MNE	ENE	MNE	ENE	MNE	ENE
5/8	20 dB	Directivity (dB)		9.17	9.76	9.61		9.61		9.67	
		SLL (-dB)		20.00	20.00	21.12		20.31		20.18	
		3 dB BW (°)	70/110	14.0	12.1	12.8		12.8		12.4	
			80/100	13.3	11.5	12.2		12.2		11.9	
			90	13.1	11.4	12.0		12.0		11.7	
		10 dB BW (°)	70/110	24.0	20.6	22.0		21.9		21.4	
			80/100	22.7	19.6	20.9		20.9		20.3	
			90	22.4	19.3	20.6		20.6		20.0	
		FNB (°)	70/110	34.3	29.6	32.0		31.7		31.3	
			80/100	32.5	28.1	30.3		30.1		29.8	
			90	32.0	27.6	29.8		29.6		29.3	

Table A.13. *Initial design performance metrics for* $5/8\,\lambda$ *element spaced arrays with minimum 20 dB sidelobe levels.*

				Illumination Taper							
				Dolph-Chebyshev		Modified Taylor		Powers of Cosine on a Pedestal		Taylor	
Spacing (λ)	Design SLL (dB)	Beamwidth Parameter	Scan Angle	MNE	ENE	MNE	ENE	MNE	ENE	MNE	ENE
5/8	30 dB	Directivity (dB)		9.77	11.06	10.33	10.73	10.31		10.82	
		SLL (-dB)		30.00	30.00	30.79	30.42	31.19		30.23	
		3 dB BW (°)	70/110	12.4	9.2	10.9	9.9	10.8		9.6	
			80/100	11.8	8.7	10.4	9.5	10.3		9.2	
			90	11.6	8.6	10.2	9.3	10.2		9.1	
		10 dB BW (°)	70/110	21.5	15.9	19.0	17.3	19.3		17.0	
			80/100	20.5	15.2	18.1	16.5	18.4		16.2	
			90	20.2	14.9	17.8	16.2	18.1		15.9	
		FNB (°)	70/110	33.7	24.8	30.2	27.3	45.2		31.3	
			80/100	31.9	23.5	28.7	25.9	42.6		29.7	
			90	31.4	23.1	28.2	25.5	41.8		29.2	

Table A.14. *Initial design performance metrics for* $5/8\,\lambda$ *element spaced arrays with minimum 30 dB sidelobe levels.*

				Illumination Taper							
				Dolph-Chebyshev		Modified Taylor		Powers of Cosine on a Pedestal		Taylor	
Spacing (λ)	Design SLL (dB)	Beamwidth Parameter	Scan Angle	MNE	ENE	MNE	ENE	MNE	ENE	MNE	ENE
5/8	40 dB	Directivity (dB)		10.57	12.11	10.68	11.58	10.56		11.79	
		SLL (-dB)		40.00	40.00	40.17	40.16	40.04		40.02	
		3 dB BW (°)	70/110	10.3	7.2	10.0	8.1	10.2		7.7	
			80/100	9.8	6.9	9.5	7.7	9.8		7.3	
			90	9.6	6.7	9.4	7.6	9.6		7.2	
		10 dB BW (°)	70/110	18.0	12.6	17.6	14.3	18.1		13.6	
			80/100	17.2	12.0	16.8	13.6	17.3		13.0	
			90	16.9	11.8	16.5	13.4	17.0		12.8	
		FNB (°)	70/110	30.6	21.2	30.5	24.6	31.7		28.9	
			80/100	29.0	20.2	28.9	23.4	30.0		27.5	
			90	28.6	19.9	28.4	23.0	29.6		27.0	

Table A.15. *Initial design performance metrics for* $5/8\,\lambda$ *element spaced arrays with minimum 40 dB sidelobe levels.*

				Illumination Taper							
				Dolph-Chebyshev		Modified Taylor		Powers of Cosine on a Pedestal		Taylor	
Spacing (λ)	Design SLL (dB)	Beamwidth Parameter	Scan Angle	MNE	ENE	MNE	ENE	MNE	ENE	MNE	ENE
5/8	50 dB	Directivity (dB)		10.85	12.62	10.78	12.03	10.88		11.82	12.31
		SLL (-dB)		50.00	50.00	50.19	50.29	50.36		50.05	50.00
		3 dB BW (°)	70/110	9.6	6.4	9.7	7.3	9.5		7.6	6.8
			80/100	9.1	6.1	9.3	6.9	9.0		7.3	6.5
			90	9.0	6.0	9.1	6.8	9.0		7.2	6.4
		10 dB BW (°)	70/110	17.0	11.3	17.3	12.9	16.9		13.6	12.1
			80/100	16.2	10.7	16.5	12.3	16.1		13.0	11.6
			90	15.9	10.6	16.2	12.1	15.9		12.8	11.4
		FNB (°)	70/110	31.0	20.4	32.3	24.0	32.3		26.2	23.3
			80/100	29.4	19.4	30.6	22.8	30.7		24.9	22.1
			90	28.9	19.1	30.1	22.5	30.1		24.5	21.8

Table A.16. *Initial design performance metrics for* $5/8\,\lambda$ *element spaced arrays with minimum 50 dB sidelobe levels.*

				Illumination Taper							
				Dolph-Chebyshev		Modified Taylor		Powers of Cosine on a Pedestal		Taylor	
Spacing (λ)	Design SLL (dB)	Beamwidth Parameter	Scan Angle	MNE	ENE	MNE	ENE	MNE	ENE	MNE	ENE
3/4	20 dB	Directivity (dB)		11.03	11.49	11.38		11.25		11.48	
		SLL (-dB)		20.00	20.00	20.60		20.35		20.20	
		3 dB BW (°)	80/100	8.5	7.6	8.1		8.4		7.7	
			90	8.3	7.4	7.9		8.2		7.6	
		10 dB BW (°)	80/100	14.4	12.8	13.8		14.3		13.1	
			90	14.2	12.6	13.5		14.0		12.9	
		FNB (°)	80/100	20.5	18.3	19.8		20.5		18.8	
			90	20.2	18.0	19.5		20.3		18.5	

Table A.17. *Initial design performance metrics for* $3/4\,\lambda$ *element spaced arrays with minimum 20 dB sidelobe levels.*

				Illumination Taper							
				Dolph-Chebyshev		Modified Taylor		Powers of Cosine on a Pedestal		Taylor	
Spacing (λ)	Design SLL (dB)	Beamwidth Parameter	Scan Angle	MNE	ENE	MNE	ENE	MNE	ENE	MNE	ENE
3/4	30 dB	Directivity (dB)		11.85	12.54	12.15		12.06	12.40	12.35	
		SLL (-dB)		30.00	30.00	30.95		30.96	30.52	30.29	
		3 dB BW (°)	80/100	7.3	6.2	6.8		6.9	6.4	6.5	
			90	7.2	6.1	6.7		6.8	6.3	6.4	
		10 dB BW (°)	80/100	12.6	10.7	11.9		12.1	11.2	11.3	
			90	12.4	10.6	11.7		11.9	11.0	11.1	
		FNB (°)	80/100	19.6	16.7	18.7		18.9	17.4	19.2	
			90	19.3	16.4	18.4		18.6	17.2	18.9	

Table A.18. *Initial design performance metrics for* $3/4\,\lambda$ *element spaced arrays with minimum 30 dB sidelobe levels.*

				Illumination Taper							
				Dolph-Chebyshev		Modified Taylor		Powers of Cosine on a Pedestal		Taylor	
Spacing (λ)	Design SLL (dB)	Beamwidth Parameter	Scan Angle	MNE	ENE	MNE	ENE	MNE	ENE	MNE	ENE
3/4	40 dB	Directivity (dB)		12.35	14.05	12.64	13.55	12.54		12.84	13.83
		SLL (-dB)		40.00	40.00	40.14	40.05	40.05		40.35	40.10
		3 dB BW (°)	80/100	6.5	4.4	6.1	4.9	6.2		5.8	4.6
			90	6.4	4.3	6.0	4.8	6.1		5.7	4.5
		10 dB BW (°)	80/100	11.4	7.7	10.7	8.6	10.9		10.2	8.1
			90	11.2	7.6	10.5	8.5	10.8		10.0	8.0
		FNB (°)	80/100	19.2	12.9	18.3	14.8	18.9		21.0	15.3
			90	18.8	12.7	18.0	14.5	18.6		20.7	15.1

Table A.19. *Initial design performance metrics for* 3/4 *λ element spaced arrays with minimum 40 dB sidelobe levels.*

				Illumination Taper							
				Dolph-Chebyshev		Modified Taylor		Powers of Cosine on a Pedestal		Taylor	
Spacing (λ)	Design SLL (dB)	Beamwidth Parameter	Scan Angle	MNE	ENE	MNE	ENE	MNE	ENE	MNE	ENE
3/4	50 dB	Directivity (dB)		12.74	14.68	12.82	14.13	12.97		13.08	14.48
		SLL (-dB)		50.00	50.00	50.29	50.44	50.36		50.36	50.16
		3 dB BW (°)	80/100	5.9	3.7	5.8	4.3	5.6		5.4	3.9
			90	5.8	3.7	5.7	4.2	5.5		5.4	3.9
		10 dB BW (°)	80/100	10.5	6.7	10.3	7.6	9.9		9.7	7.0
			90	10.3	6.6	10.1	7.5	9.8		9.5	6.9
		FNB (°)	80/100	18.9	12.1	19.0	14.0	18.8		18.5	13.3
			90	18.6	11.9	18.7	13.8	18.5		18.3	13.0

Table A.20. *Initial design performance metrics for* 3/4 *λ element spaced arrays with minimum 50 dB sidelobe levels.*

				Illumination Taper							
				Dolph-Chebyshev		Modified Taylor		Powers of Cosine on a Pedestal		Taylor	
Spacing (λ)	Design SLL (dB)	Beamwidth Parameter	Scan Angle	MNE	ENE	MNE	ENE	MNE	ENE	MNE	ENE
7/8	20 dB	Directivity (dB)		11.66	12.11	12.02		11.89		11.62	12.11
		SLL (-dB)		20.00	20.00	20.60		20.35		20.27	20.20
		3 dB BW (°)	90	7.1	6.4	6.8		7.0		7.3	6.5
		10 dB BW (°)		12.1	10.8	11.6		12.0		12.5	11.0
		FNB (°)		17.3	15.4	16.7		17.3		18.0	15.8

Table A.21. *Initial design performance metrics for* 7/8 *λ element spaced arrays with minimum 20 dB sidelobe levels.*

				Illumination Taper							
				Dolph-Chebyshev		Modified Taylor		Powers of Cosine on a Pedestal		Taylor	
Spacing (λ)	Design SLL (dB)	Beamwidth Parameter	Scan Angle	MNE	ENE	MNE	ENE	MNE	ENE	MNE	ENE
7/8	30 dB	Directivity (dB)		12.51	13.20	12.82		12.37	13.06	12.63	13.02
		SLL (-dB)		30.00	30.00	30.95		31.51	30.52	30.71	30.29
		3 dB BW (°)	90	6.1	5.2	5.7		6.4	5.4	5.9	5.4
		10 dB BW (°)		10.6	9.1	10.0		11.1	9.4	10.4	9.5
		FNB (°)		16.5	14.0	15.8		17.4	14.7	18.8	16.1

Table A.22. *Initial design performance metrics for* $7/8\,\lambda$ *element spaced arrays with minimum 30 dB sidelobe levels.*

				Illumination Taper							
				Dolph-Chebyshev		Modified Taylor		Powers of Cosine on a Pedestal		Taylor	
Spacing (λ)	Design SLL (dB)	Beamwidth Parameter	Scan Angle	MNE	ENE	MNE	ENE	MNE	ENE	MNE	ENE
7/8	40 dB	Directivity (dB)		13.01	14.51	13.04	14.01	13.00		13.27	14.27
		SLL (-dB)		40.00	40.00	40.16	40.07	40.05		40.21	40.75
		3 dB BW (°)	90	5.5	3.9	5.4	4.3	5.5		5.1	4.1
		10 dB BW (°)		9.6	6.8	9.6	7.7	9.7		9.1	7.2
		FNB (°)		16.1	11.4	16.4	13.1	16.8		18.6	13.6

Table A.23. *Initial design performance metrics for* $7/8\,\lambda$ *element spaced arrays with minimum 40 dB sidelobe levels.*

				Illumination Taper							
				Dolph-Chebyshev		Modified Taylor		Powers of Cosine on a Pedestal		Taylor	
Spacing (λ)	Design SLL (dB)	Beamwidth Parameter	Scan Angle	MNE	ENE	MNE	ENE	MNE	ENE	MNE	ENE
7/8	50 dB	Directivity (dB)		13.15	15.19	13.27	14.63	13.48		13.49	14.95
		SLL (-dB)		50.00	50.00	50.27	50.42	50.36		50.61	50.67
		3 dB BW (°)	90	5.3	3.3	5.1	3.8	4.9		4.9	3.5
		10 dB BW (°)		9.3	5.8	9.1	6.7	8.7		8.7	6.2
		FNB (°)		16.9	10.6	16.9	12.3	16.4		16.6	11.8

Table A.24. *Initial design performance metrics for* $7/8\,\lambda$ *element spaced arrays with minimum 50 dB sidelobe levels.*

APPENDIX B

Randomization Image and Tabular Data

Randomization results from each elevation scan angle will not be presented. Only the worst case graph for each parameter is represented in this appendix. This appendix is limited to image and tabular data. The data is listed beginning with the $1/4\,\lambda$ nominal element spaced arrays and finishing with the $7/8\,\lambda$ nominal element spaced arrays. It is organized by initial design sidelobe level within each element spacing group.

$1/4\ \lambda$ Element Spacing

20 dB Initial Design Sidelobe Level

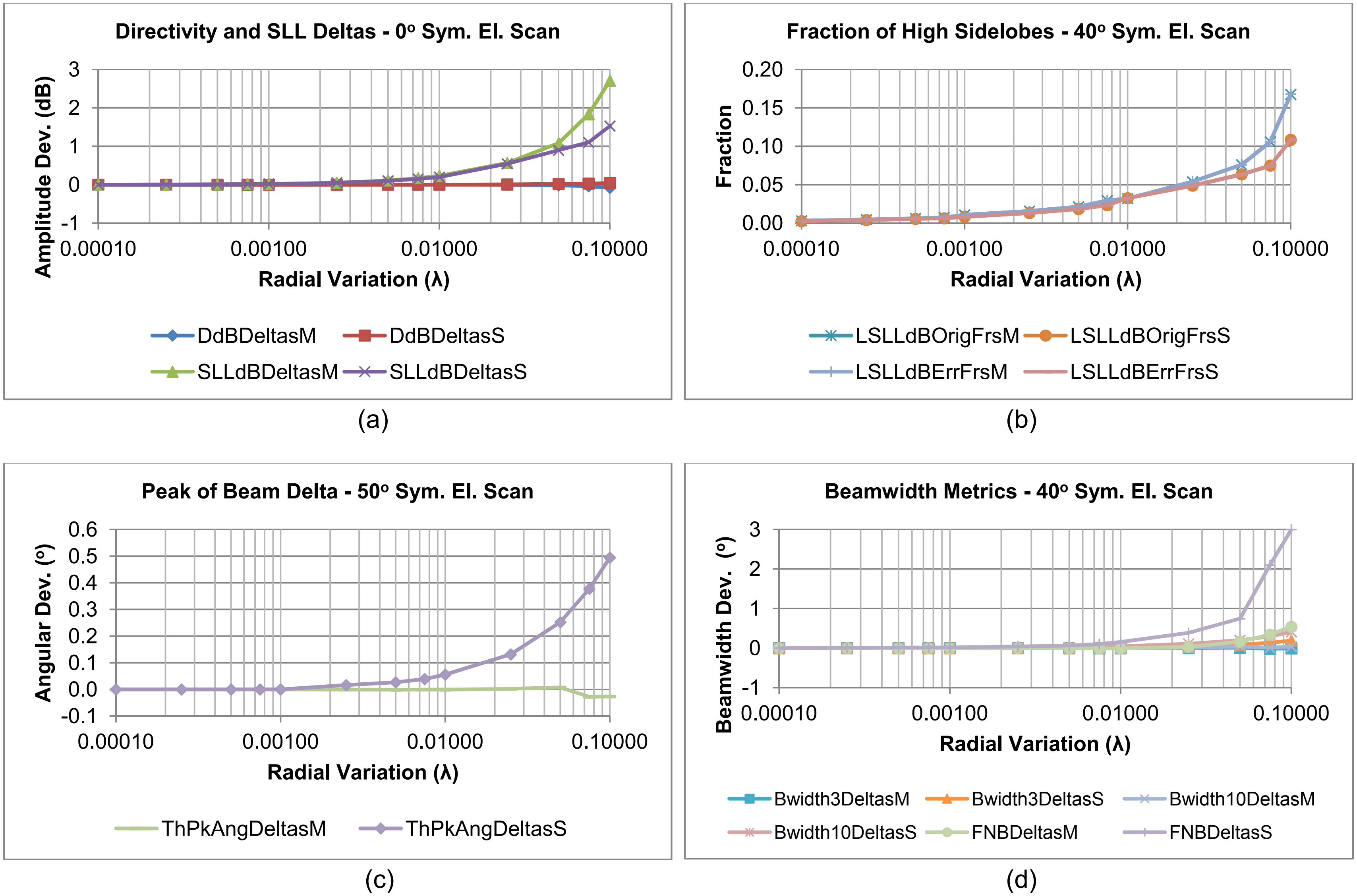

Figure B.1. *Statistical data for a 1/4 λ spaced, 20 element, modified Taylor array versus radial randomization.* Directivity and sidelobe level (a), LSLLdB (b), beam pointing (c), and beamwidth (d) results are illustrated.

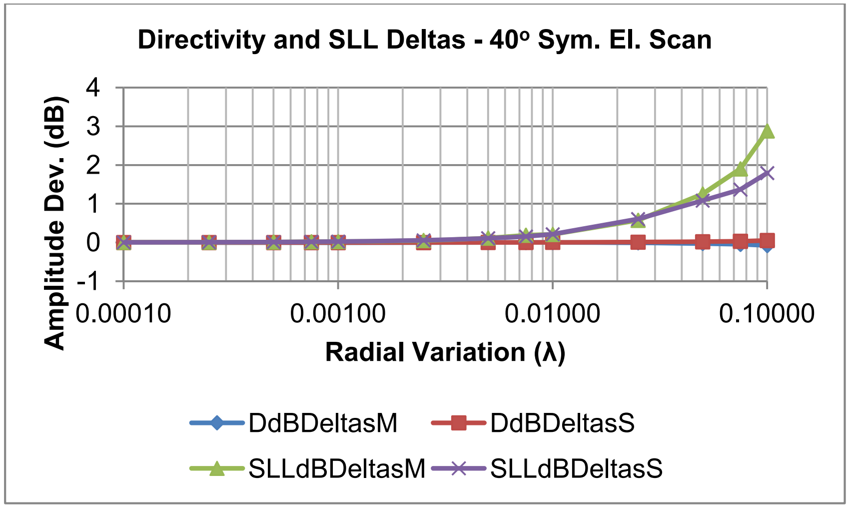

(a)

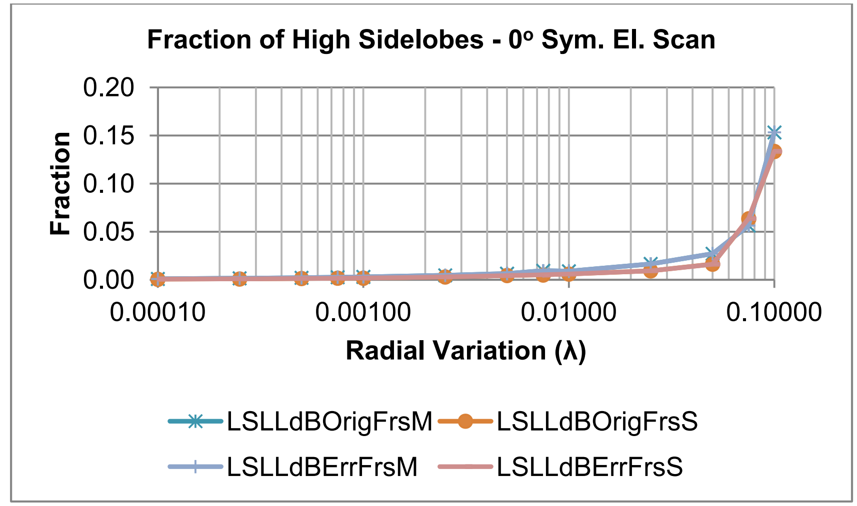

(b)

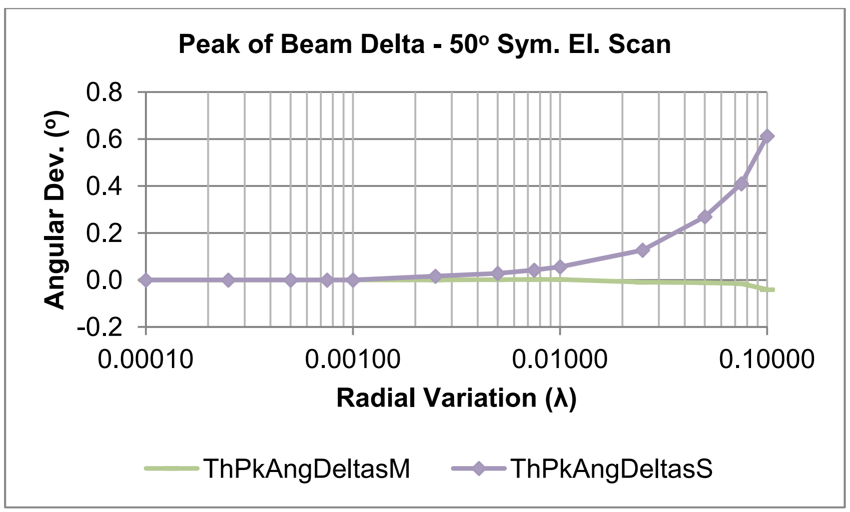

(c)

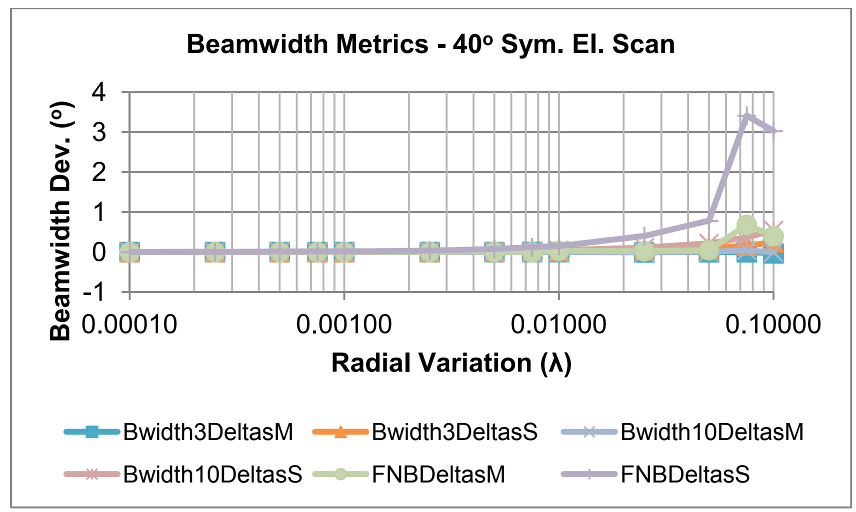

(d)

Figure B.2. *Statistical data for a $1/4\,\lambda$ spaced, 19 element, power of cosine on a pedestal array versus radial randomization.* Directivity and sidelobe level (a), LSLLdB (b), beam pointing (c), and beamwidth (d) results are illustrated.

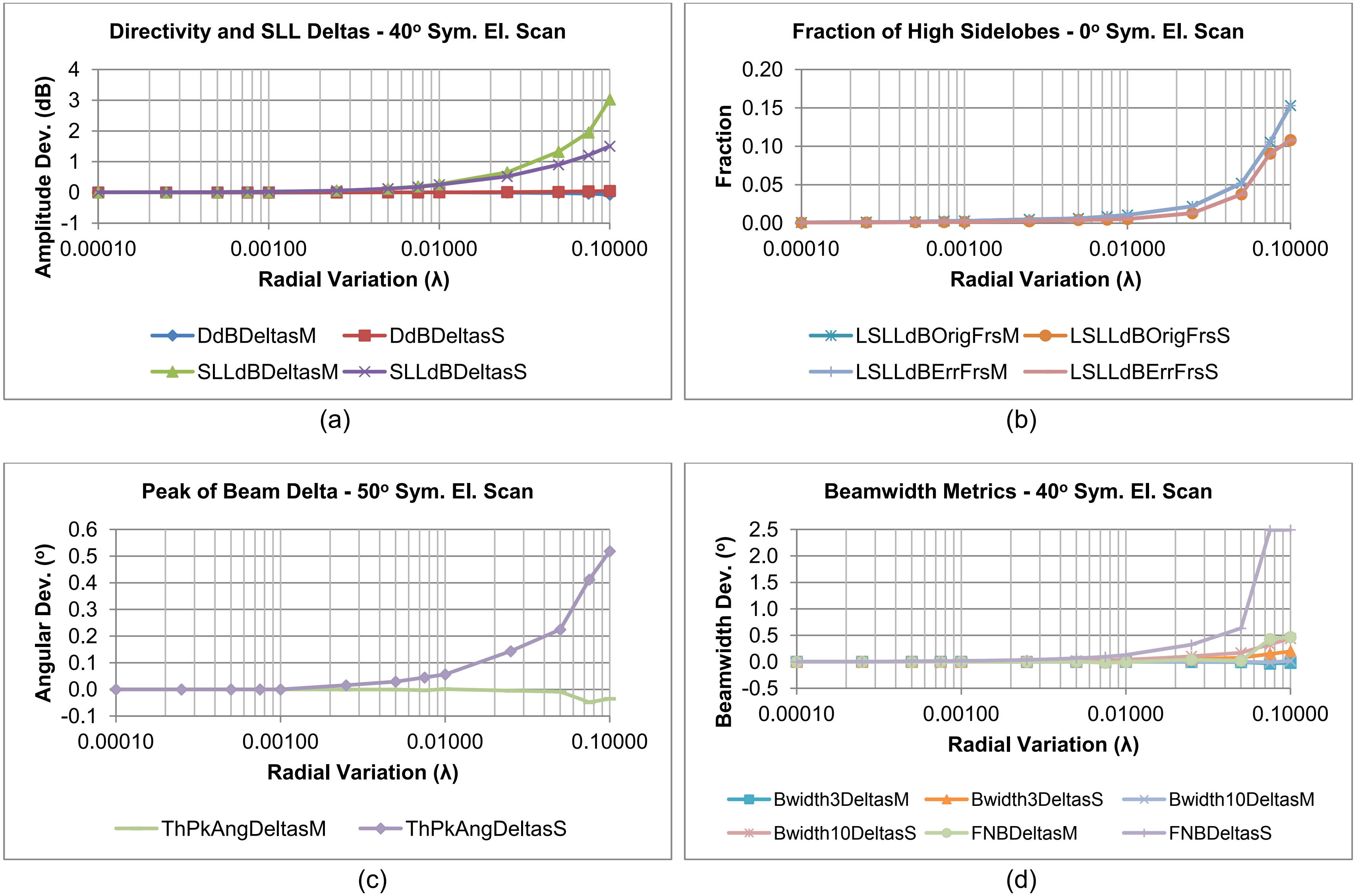

Figure B.3. *Statistical data for a $1/4\,\lambda$ spaced, 19 element, Taylor array versus radial randomization.* Directivity and sidelobe level (a), LSLLdB (b), beam pointing (c), and beamwidth (d) results are illustrated.

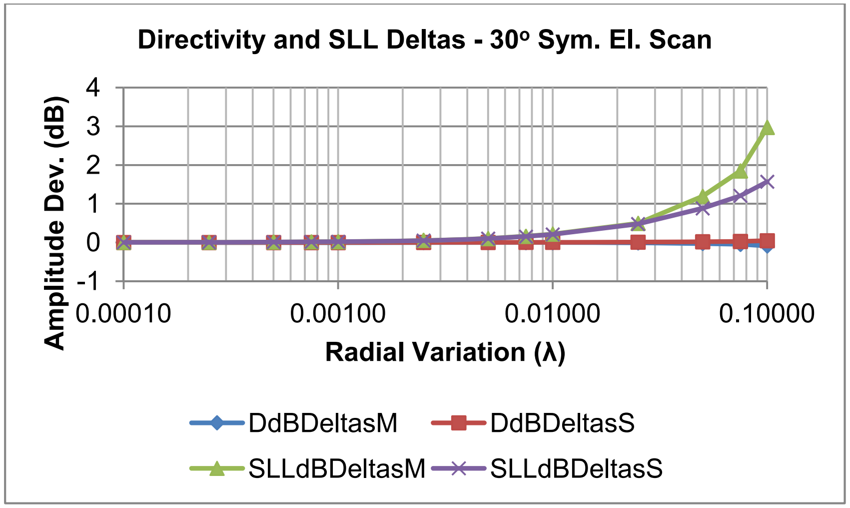

(a)

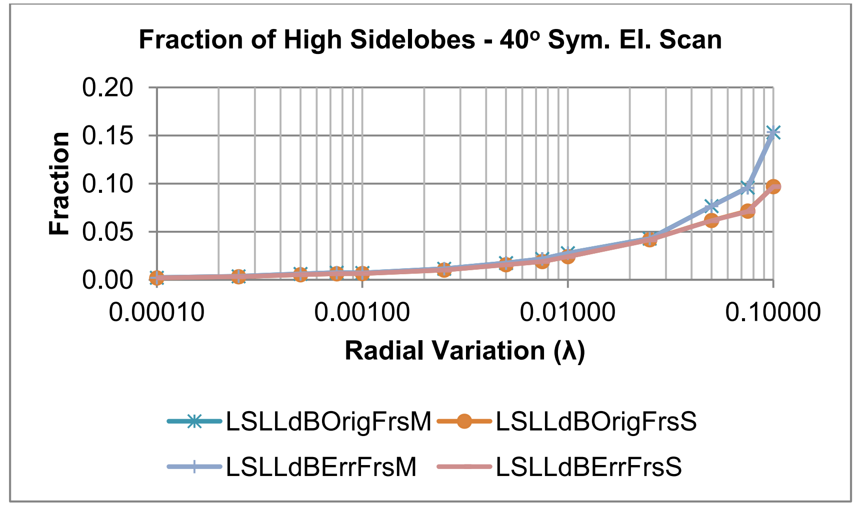

(b)

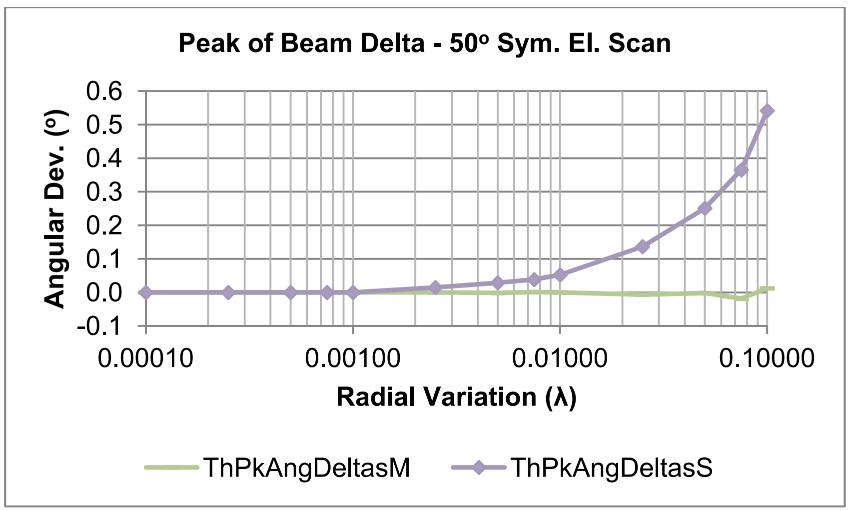

(c)

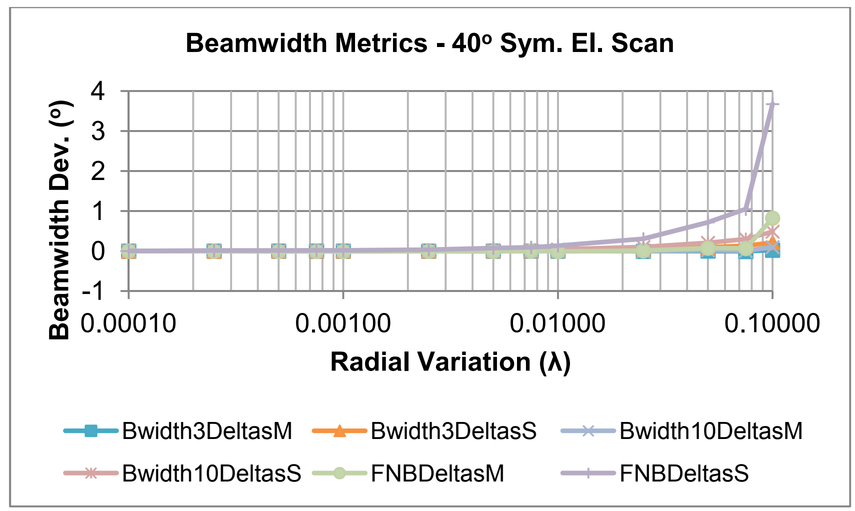

(d)

Figure B.4. *Statistical data for a 1⁄4 λ spaced, 20 element, power of cosine on a pedestal array versus radial randomization.* Directivity and sidelobe level (a), LSLLdB (b), beam pointing (c), and beamwidth (d) results are illustrated.

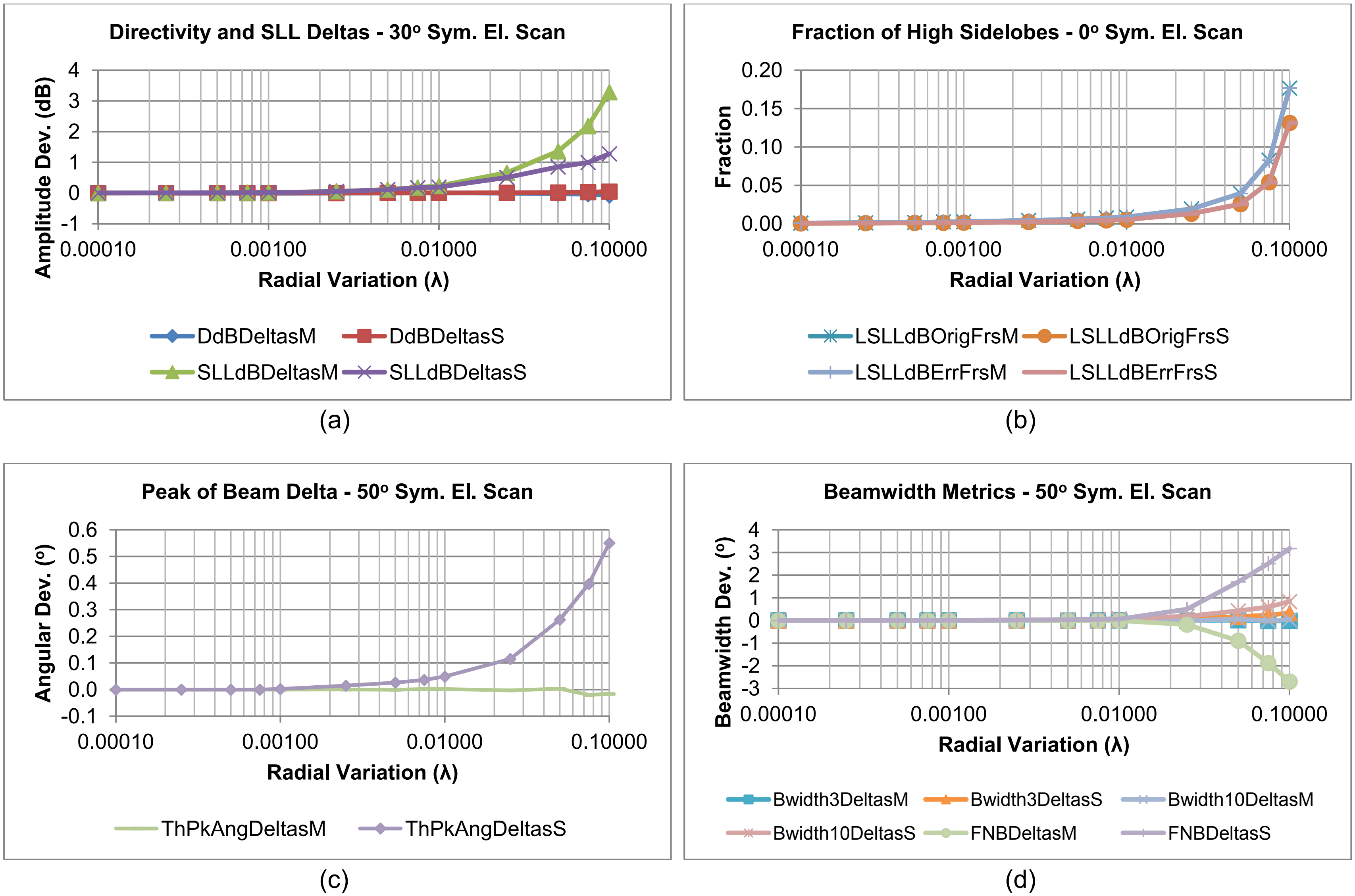

Figure B.5. *Statistical data for a $1/4\,\lambda$ spaced, 20 element, Taylor array versus radial randomization.* Directivity and sidelobe level (a), LSLLdB (b), beam pointing (c), and beamwidth (d) results are illustrated.

1/4 λ Element Spacing

30 dB Initial Design Sidelobe Level

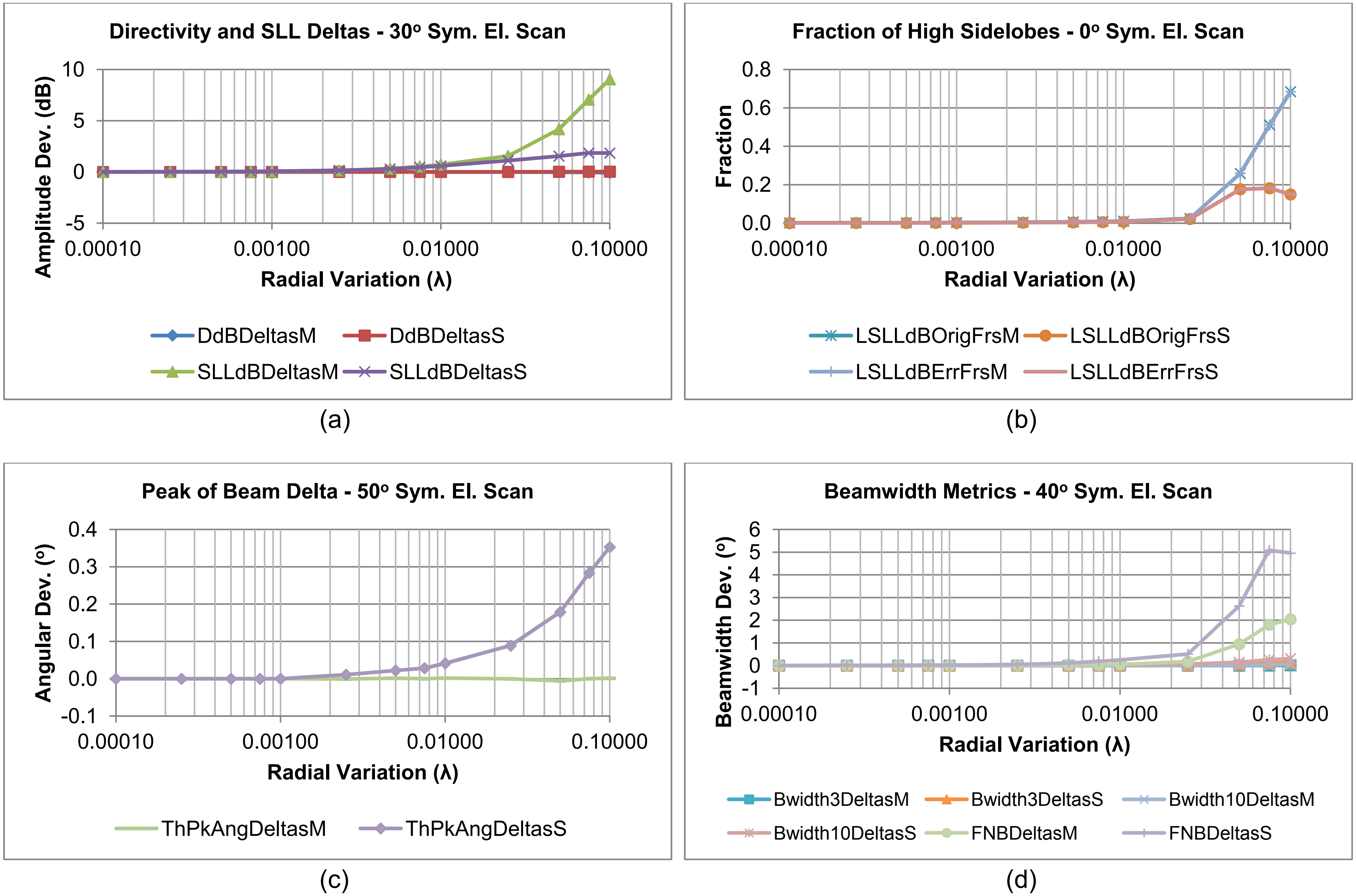

Figure B.6. *Statistical data for a $1/4\,\lambda$ spaced, 27 element, modified Taylor array versus radial randomization.* Directivity and sidelobe level (a), LSLLdB (b), beam pointing (c), and beamwidth (d) results are illustrated.

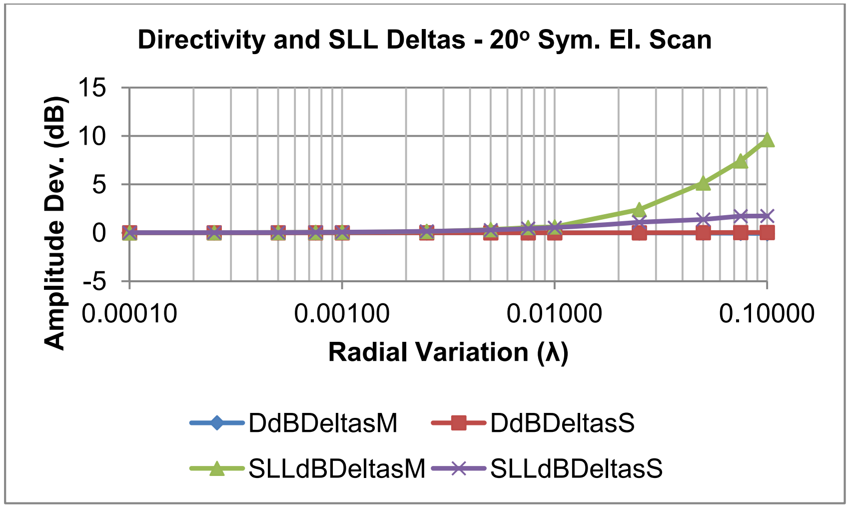

(a)

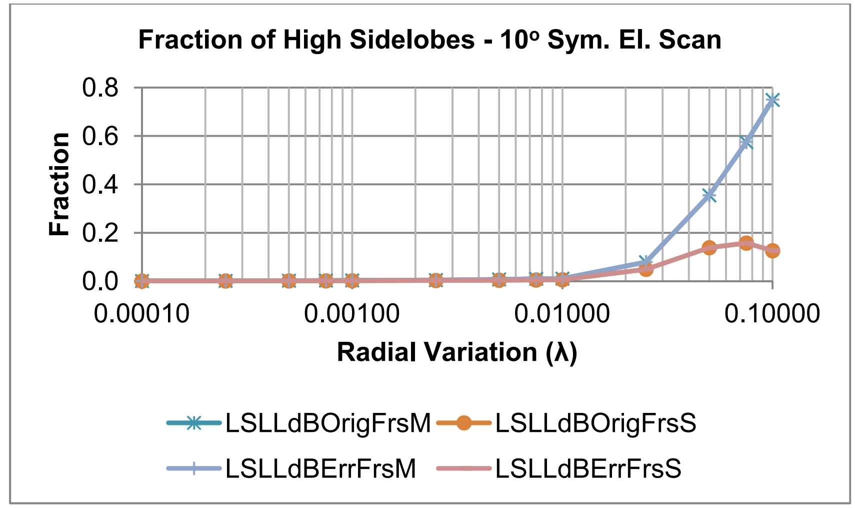

(b)

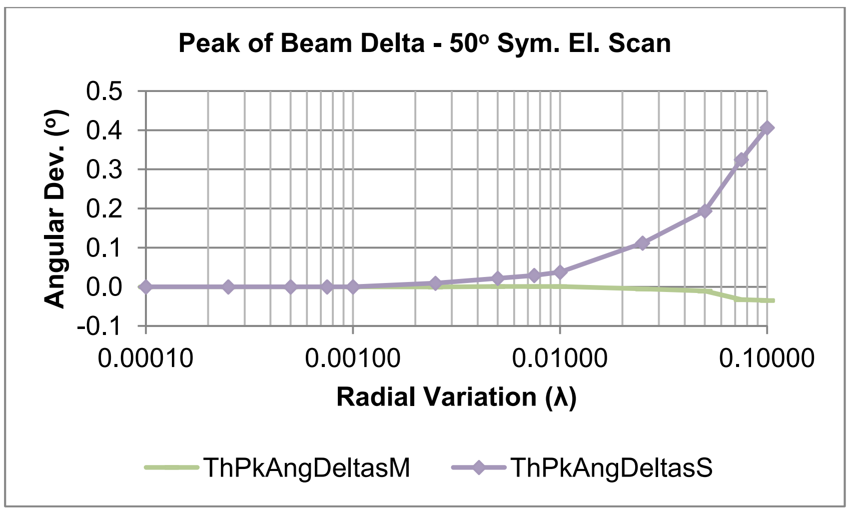

(c)

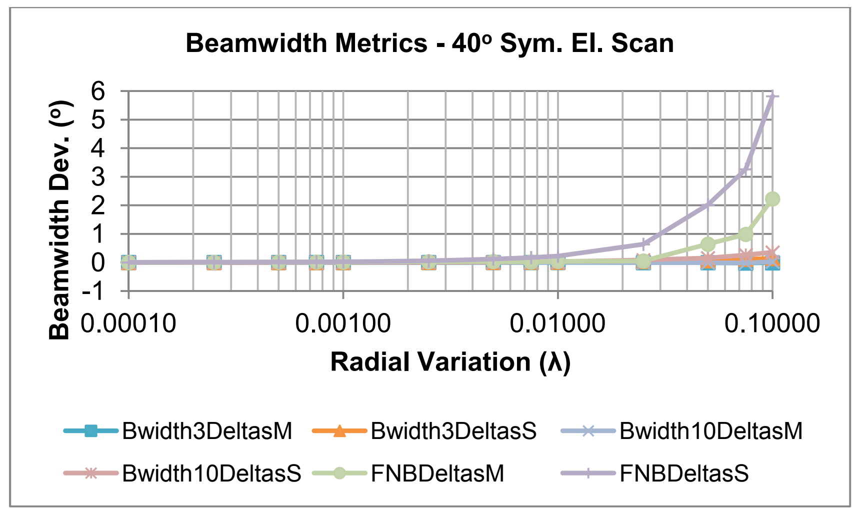

(d)

Figure B.7. *Statistical date for a 1/4 λ spaced, 25 element, power of cosine on a pedestal array versus radial randomization.* Directivity and sidelobe level (a), LSLLdB (b), beam pointing (c), and beamwidth (d) results are illustrated.

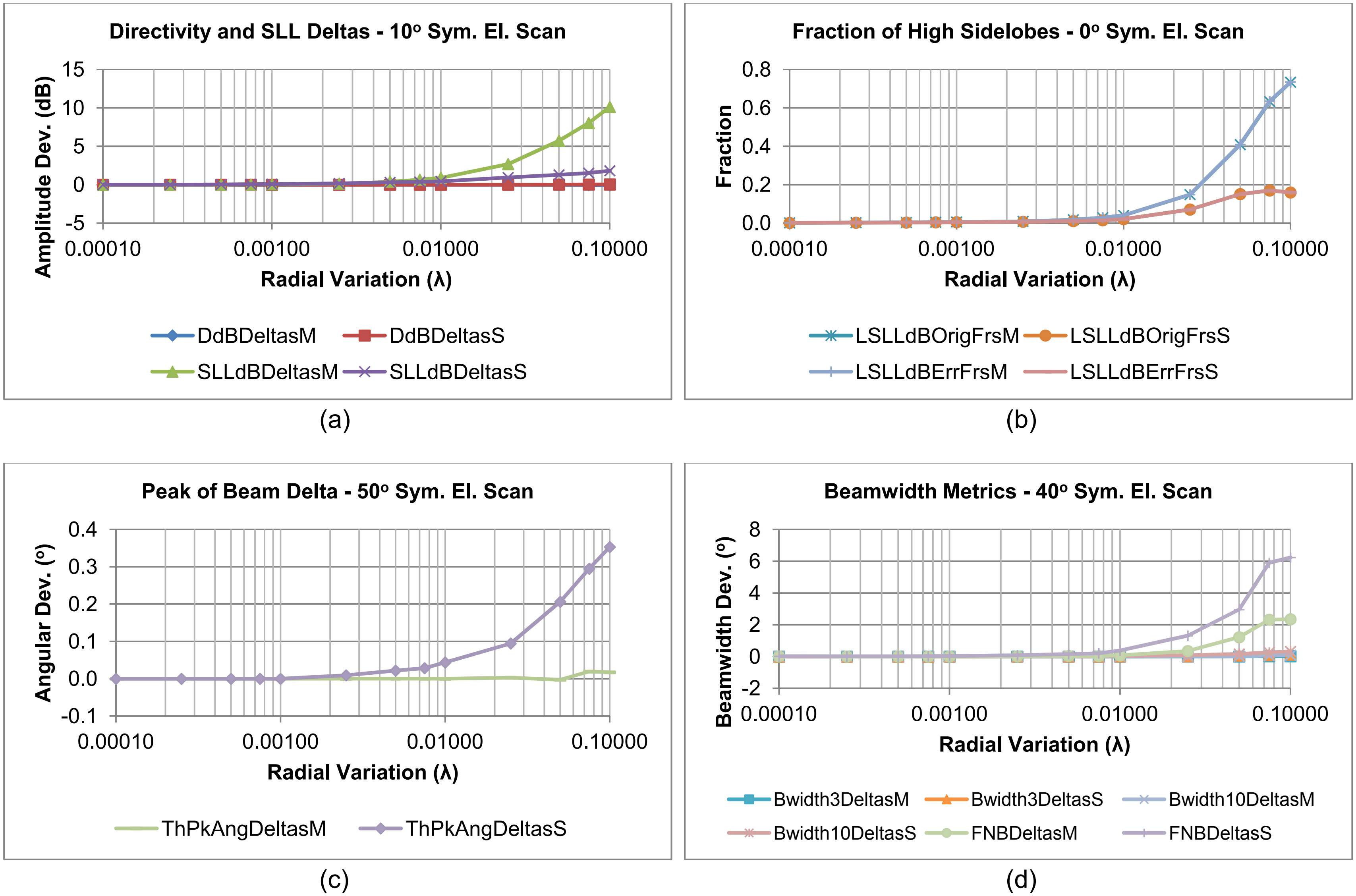

Figure B.8. *Statistical data for a $1/4\,\lambda$ spaced, 25 element, Taylor array versus radial randomization.* Directivity and sidelobe level (a), LSLLdB (b), beam pointing (c), and beamwidth (d) results are illustrated.

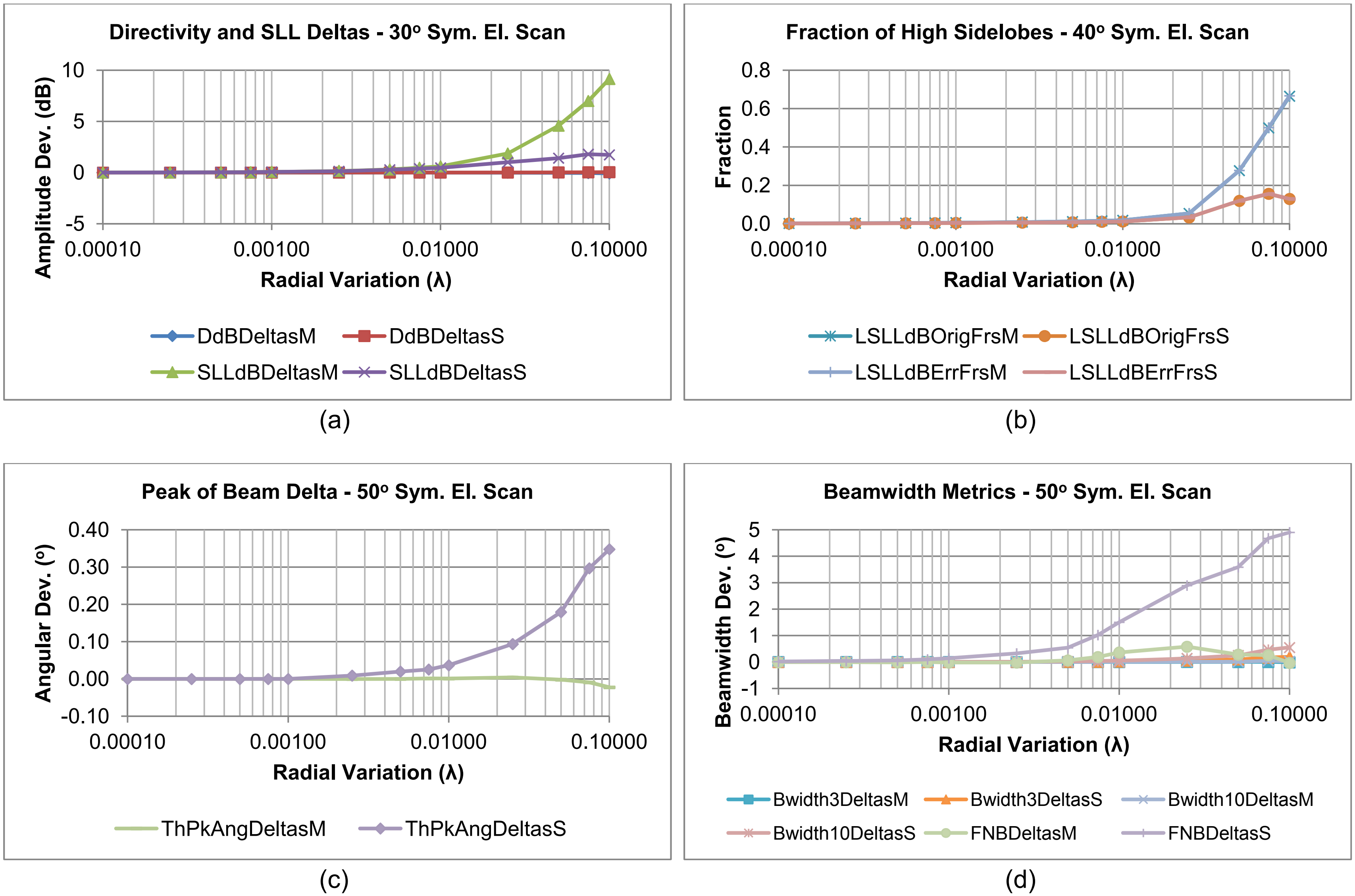

Figure B.9. *Statistical data for a* $1/4\,\lambda$ *spaced, 27 element, power of cosine on a pedestal array versus radial randomization.* Directivity and sidelobe level (a), LSLLdB (b), beam pointing (c), and beamwidth (d) results are illustrated.

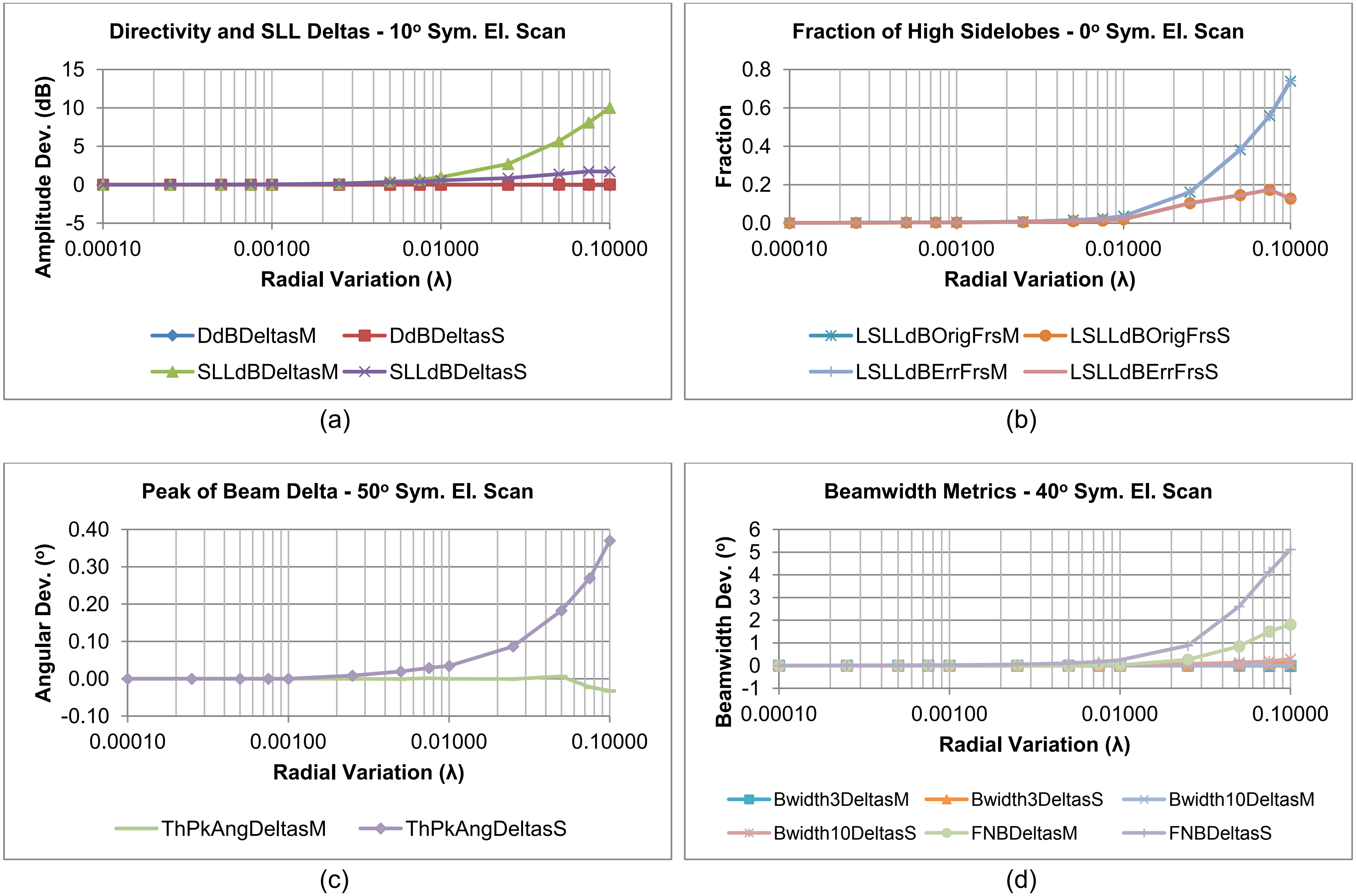

Figure B.10. *Statistics for a $1/4\,\lambda$ spaced, 27 element, Taylor array versus radial randomization.* Directivity and sidelobe level (a), LSLLdB (b), beam pointing (c), and beamwidth (d) results are illustrated.

1/4 λ Element Spacing

40 dB Initial Design Sidelobe Level

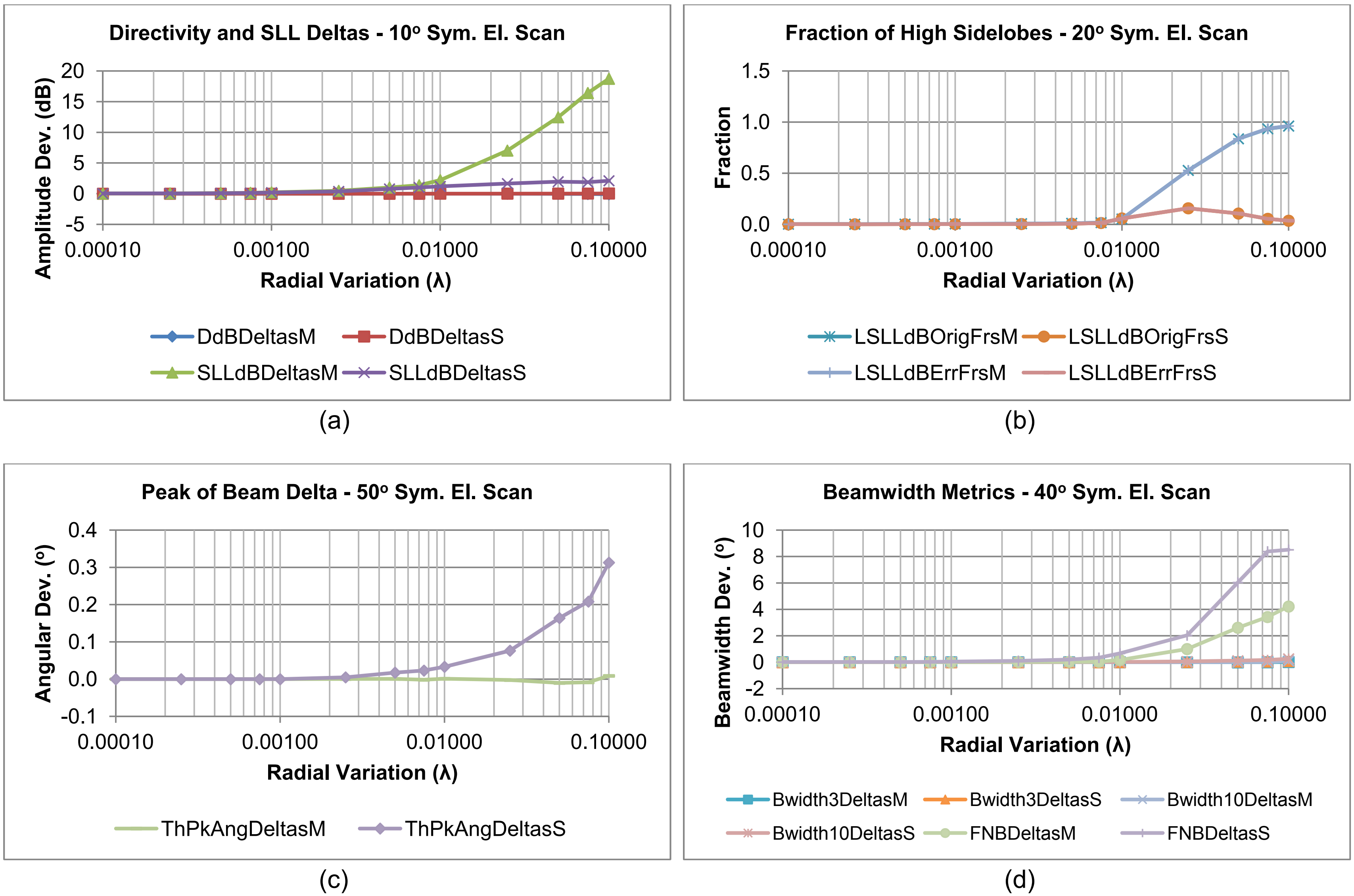

Figure B.11. *Statistical data for a 1/4 λ spaced, 35 element, modified Taylor array versus radial randomization.* Directivity and sidelobe level (a), LSLLdB (b), beam pointing (c), and beamwidth (d) results are illustrated.

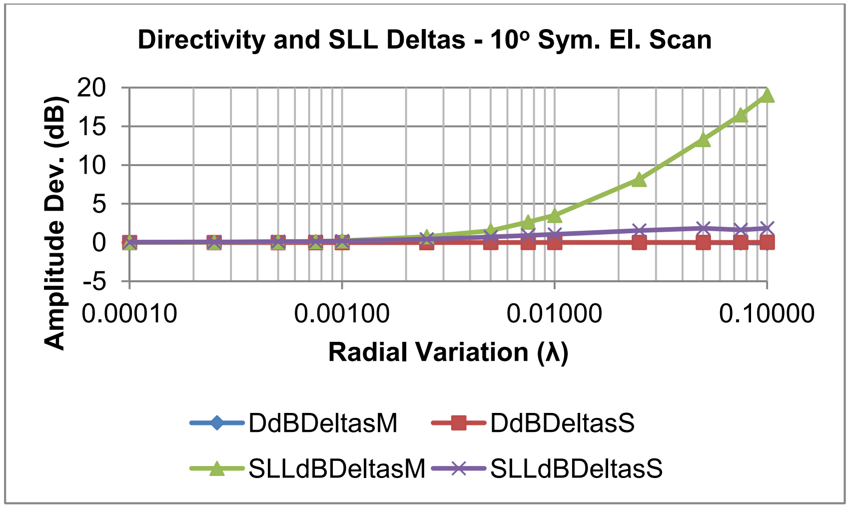

(a)

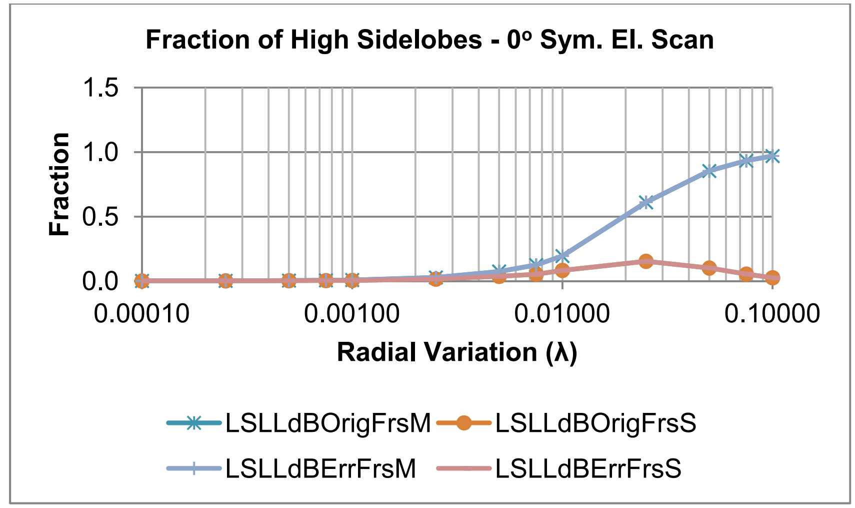

(b)

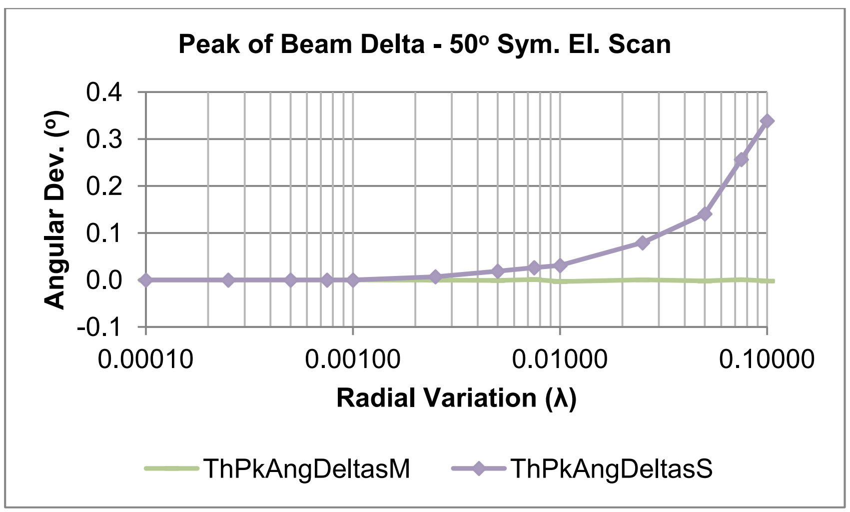

(c)

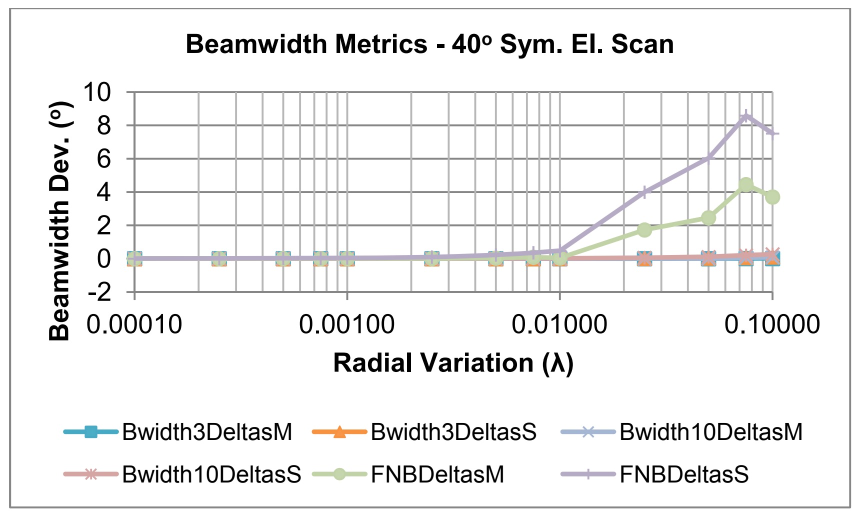

(d)

Figure B.12. *Statistical data for a 1/4 λ spaced, 32 element, power of cosine on a pedestal array versus radial randomization.* Directivity and sidelobe level (a), LSLLdB (b), beam pointing (c), and beamwidth (d) results are illustrated.

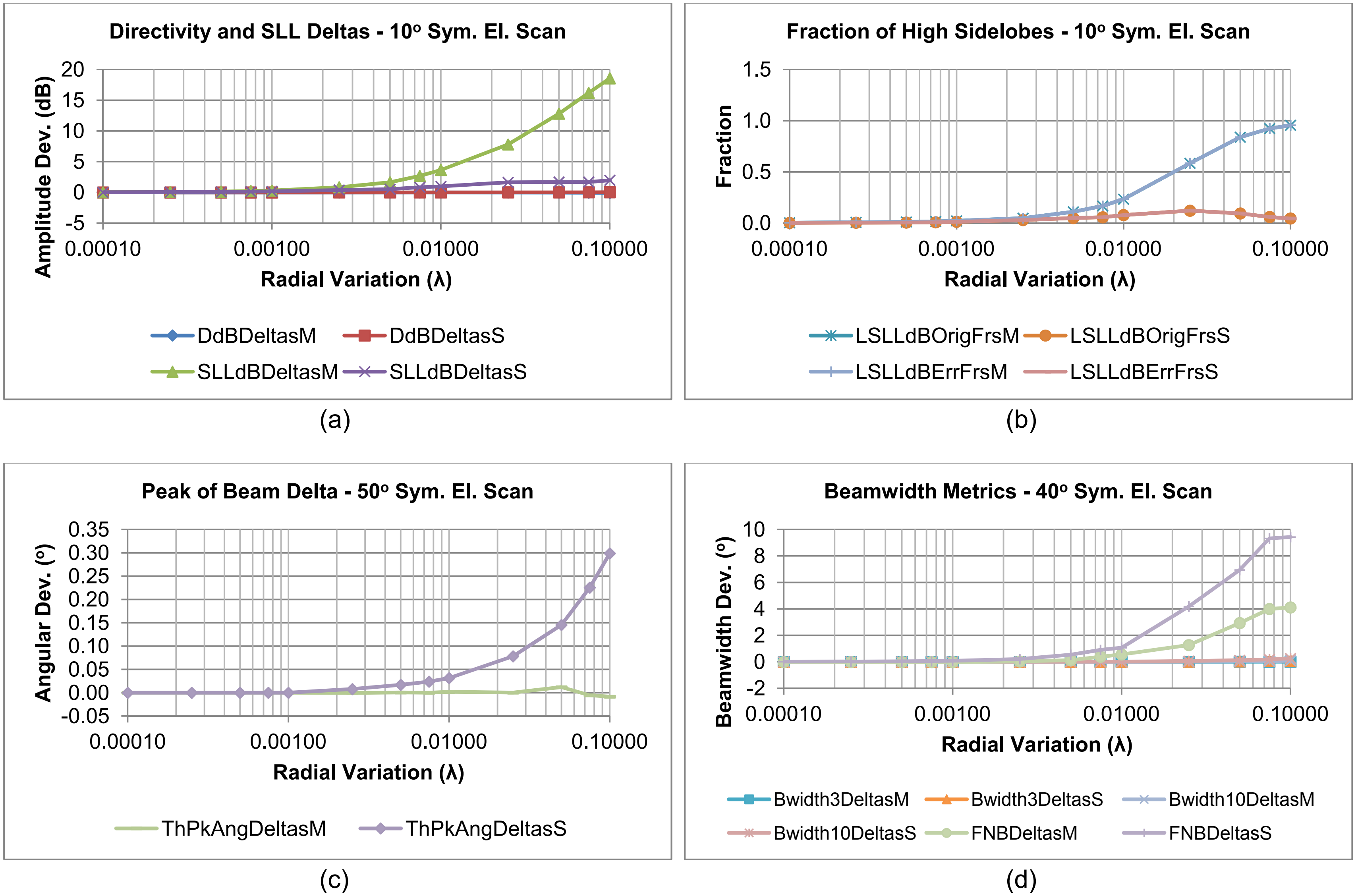

Figure B.13. *Statistical data for a 1/4 λ spaced, 32 element, Taylor array versus radial randomization.* Directivity and sidelobe level (a), LSLLdB (b), beam pointing (c), and beamwidth (d) results are illustrated.

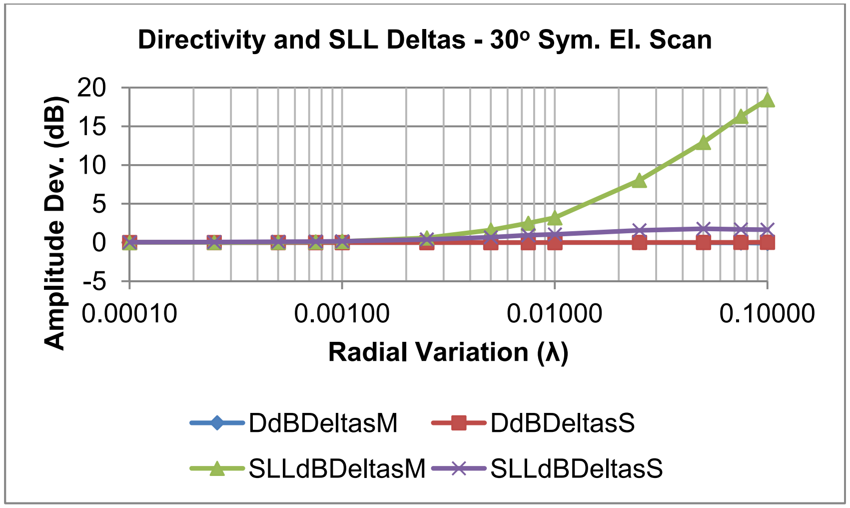

(a)

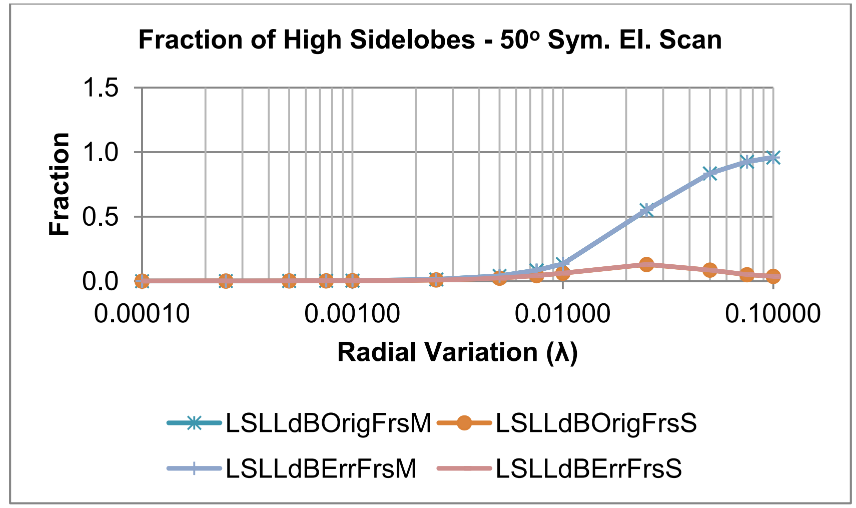

(b)

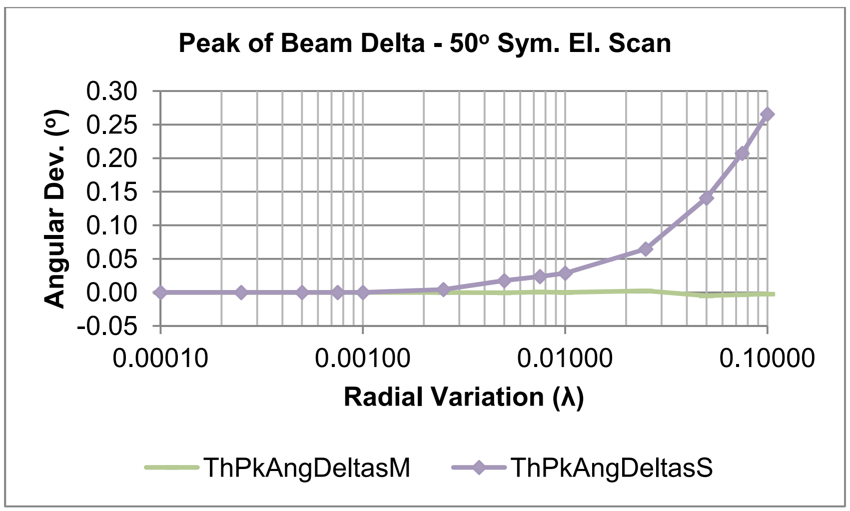

(c)

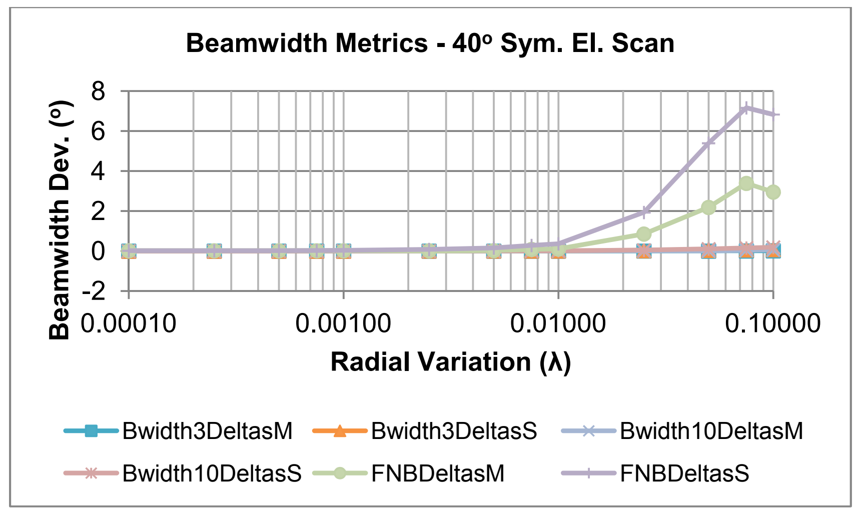

(d)

Figure B.14. *Statistical data for a 1⁄4 λ spaced, 35 element, power of cosine on a pedestal array versus radial randomization.* Directivity and sidelobe level (a), LSLLdB (b), beam pointing (c), and beamwidth (d) results are illustrated.

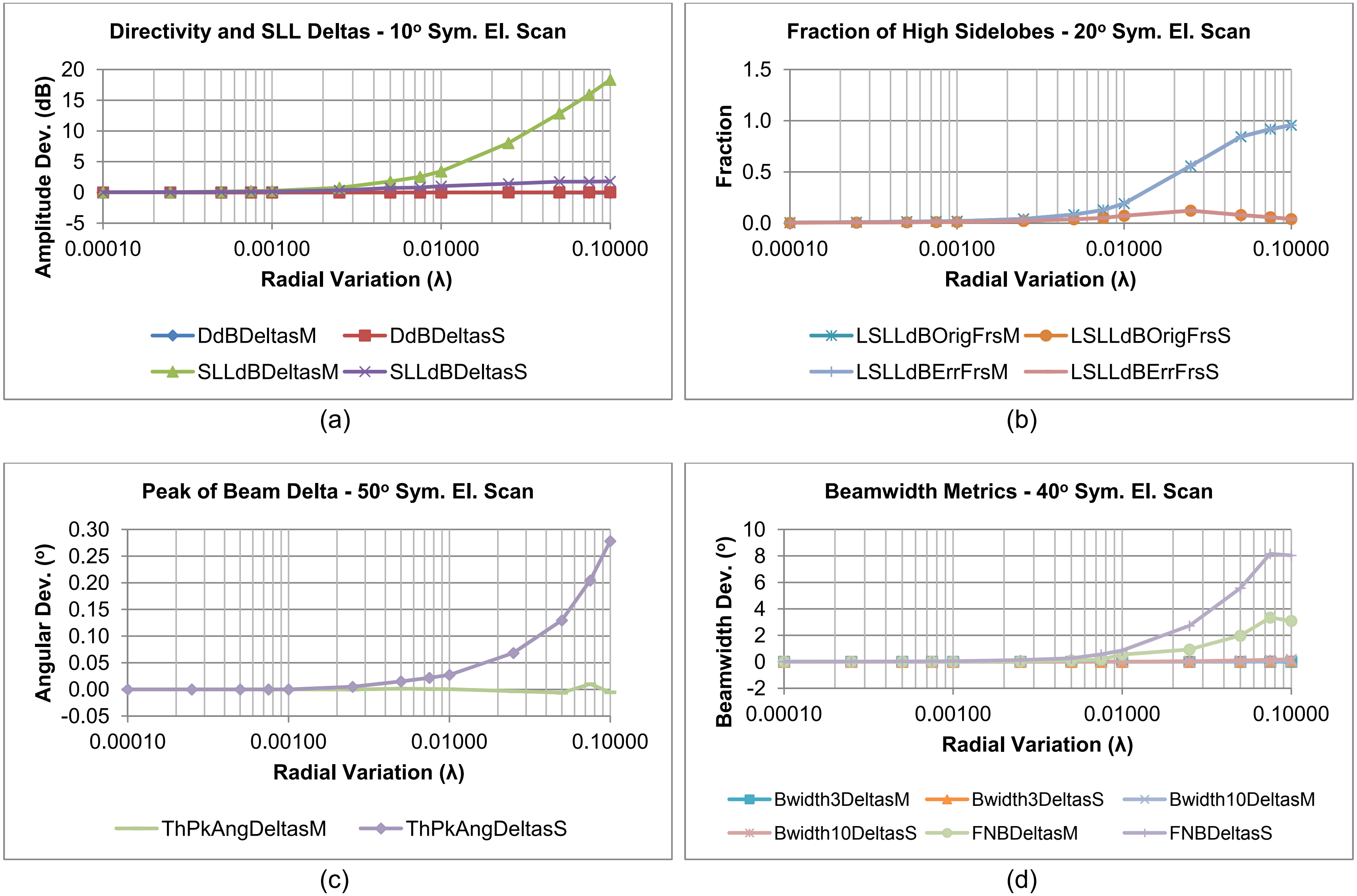

Figure B.15. *Statistical data for a 1/4 λ spaced, 35 element, Taylor array versus radial randomization.* Directivity and sidelobe level (a), LSLLdB (b), beam pointing (c), and beamwidth (d) results are illustrated.

1/4 λ Element Spacing

50 dB Initial Design Sidelobe Level

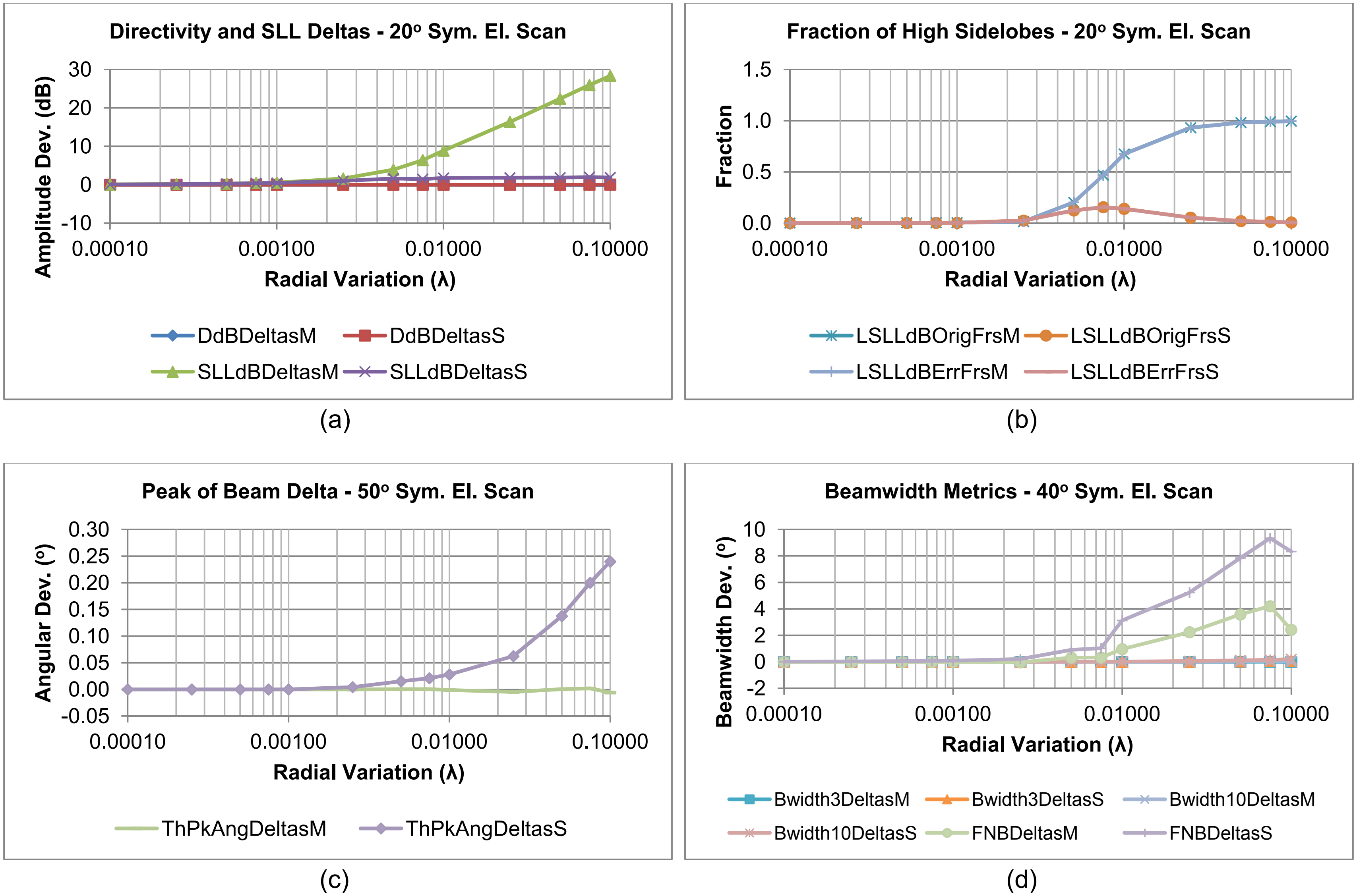

Figure B.16. *Statistical data for a $1/4\,\lambda$ spaced, 42 element, modified Taylor array versus radial randomization.* Directivity and sidelobe level (a), LSLLdB (b), beam pointing (c), and beamwidth (d) results are illustrated.

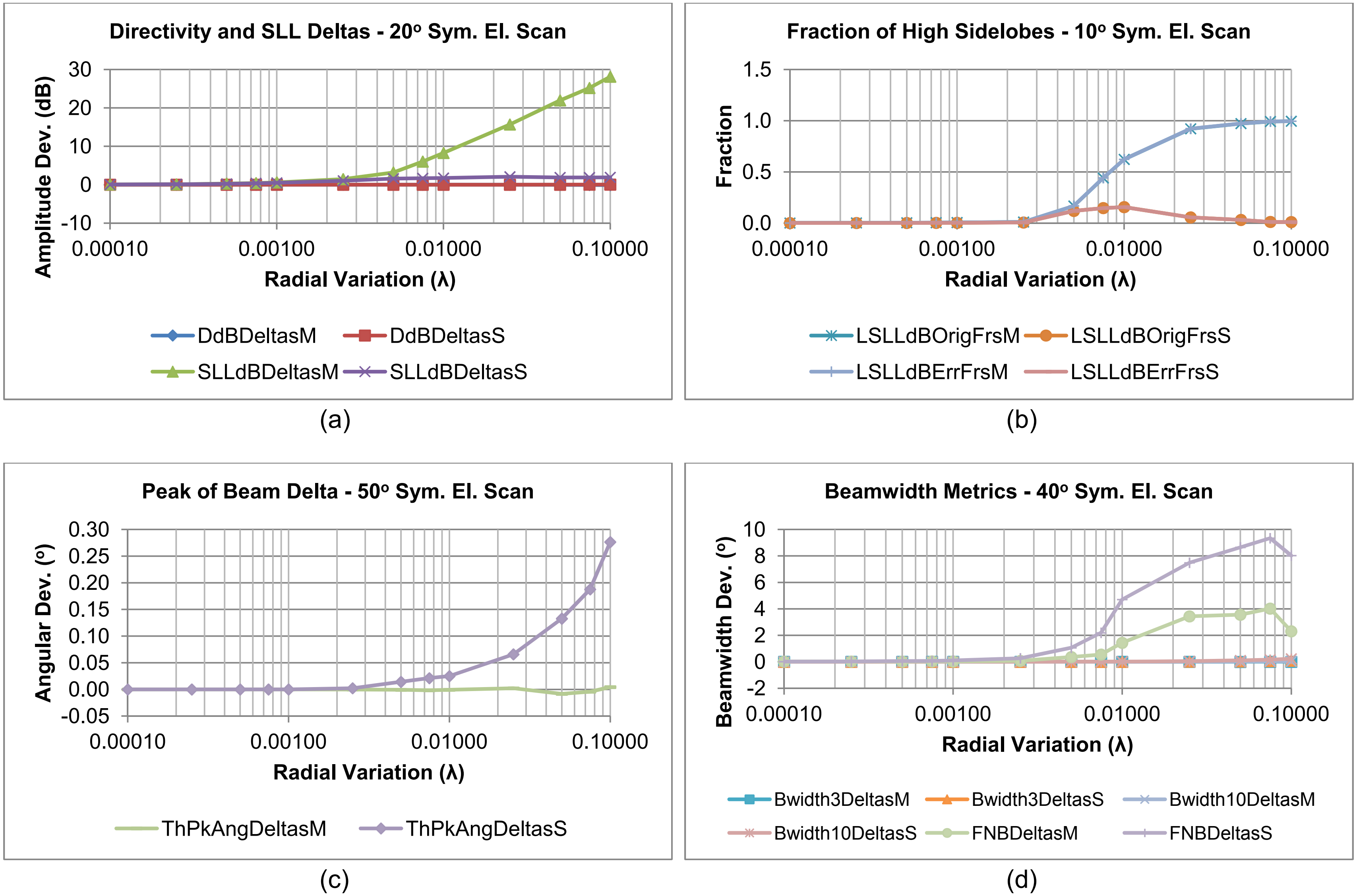

Figure B.17. *Statistical data for a 1/4 λ spaced, 55 element, power of cosine on a pedestal array versus radial randomization.* Directivity and sidelobe level (a), LSLLdB (b), beam pointing (c), and beamwidth (d) results are illustrated.

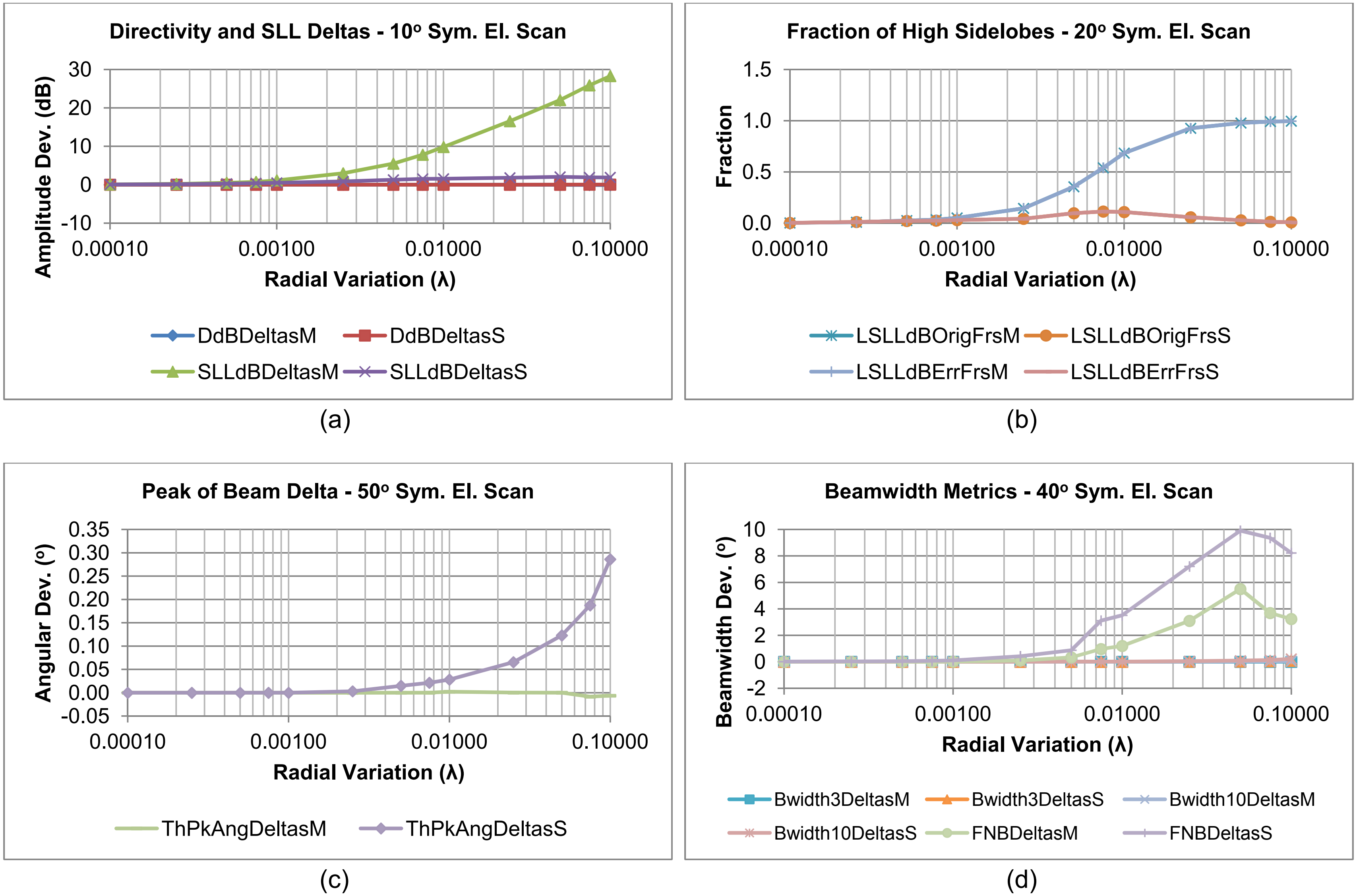

Figure B.18. *Statistical data for a 1/4 λ spaced, 39 element, Taylor array versus radial randomization.* Directivity and sidelobe level (a), LSLLdB (b), beam pointing (c), and beamwidth (d) results are illustrated.

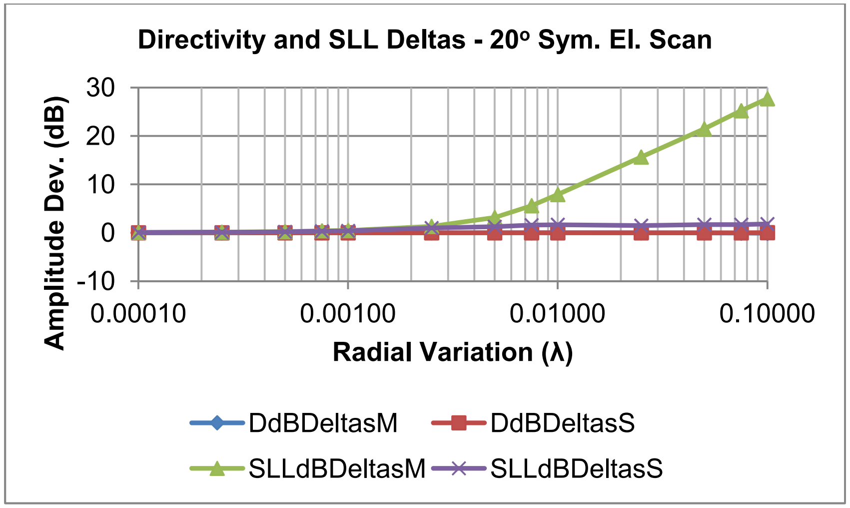

(a)

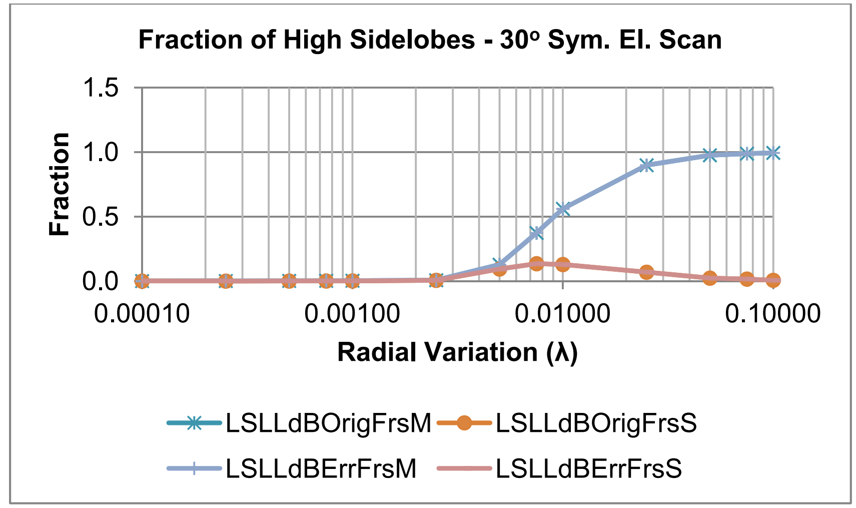

(b)

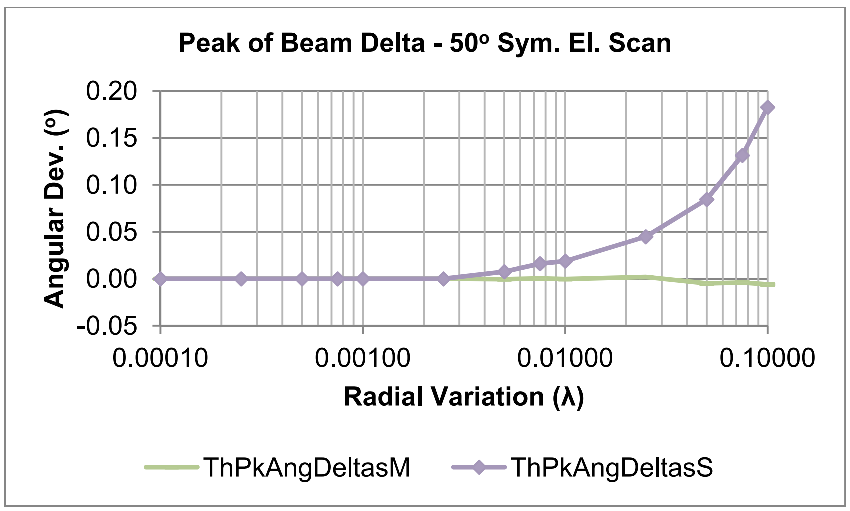

(c)

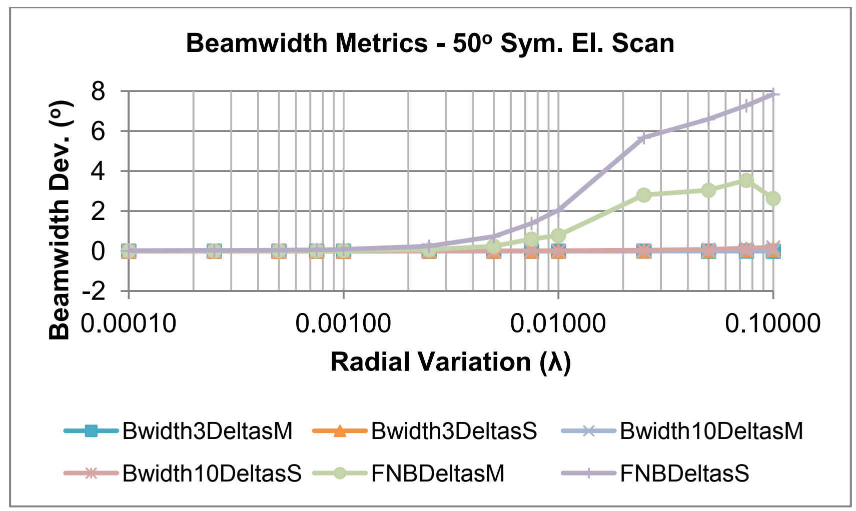

(d)

Figure B.19. *Statistical data for a $1/4\,\lambda$ spaced, 55 element, modified Taylor array versus radial randomization.* Directivity and sidelobe level (a), LSLLdB (b), beam pointing (c), and beamwidth (d) results are illustrated.

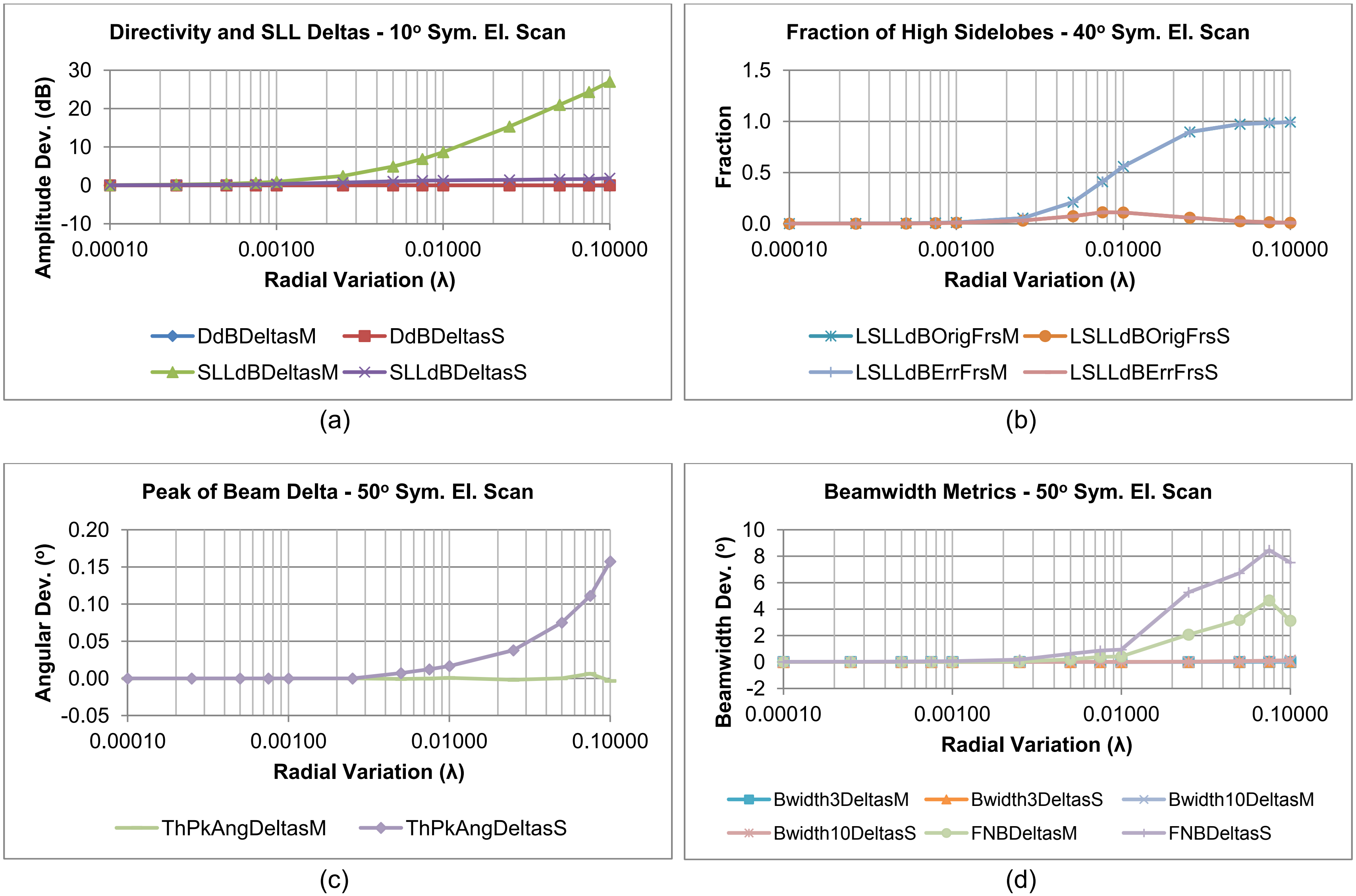

Figure B.20. *Statistical data for a 1/4 λ spaced, 55 element, Taylor array versus radial randomization.* Directivity and sidelobe level (a), LSLLdB (b), beam pointing (c), and beamwidth (d) results are illustrated.

1/4 λ Element Spacing

Commentary

Modified Taylor				
	MNE		ENE	
Design SLL (-dB)	# of Elmts.	W. C. SLL (-dB)	# of Elmts.	W. C. SLL (-dB)
20	20	13.6	20	13.6
30	27	15.9	27	15.9
40	35	15.6	35	15.6
50	42	16.6	55	17.8

(a)

Powers of Cosine on a Pedestal				
	MNE		ENE	
Design SLL (-dB)	# of Elmts.	W. C. SLL (-dB)	# of Elmts.	W. C. SLL (-dB)
20	19	12.1	20	12.6
30	25	15.6	27	15.9
40	32	16.2	35	17.4
50	55	16.8	55	16.8

(b)

Taylor				
	MNE		ENE	
Design SLL (-dB)	# of Elmts.	W. C. SLL (-dB)	# of Elmts.	W. C. SLL (-dB)
20	19	12.9	20	13.2
30	25	15.2	27	15.7
40	32	15.8	35	16.8
50	39	16.6	55	17.8

(c)

Table B.1. *3σ sidelobe performance of the $1/4\,\lambda$ element spacing group with 0.10000 λ radial randomization.* Data is illustrated for the modified Taylor (a), powers of cosine on a pedestal, and Taylor tapers.

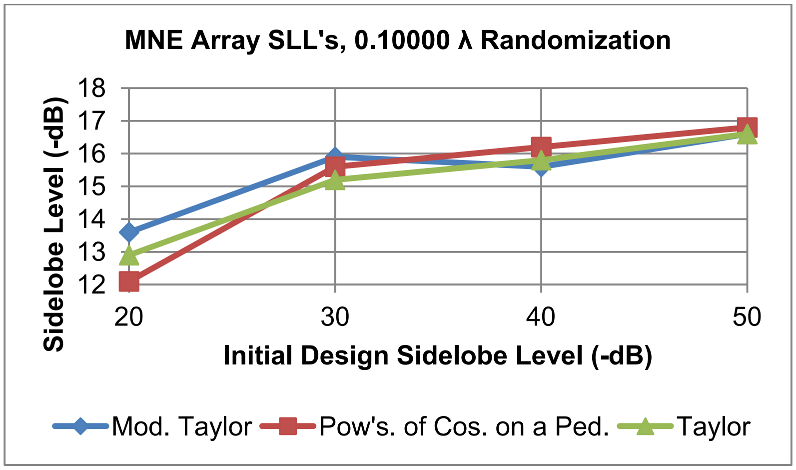

(a)

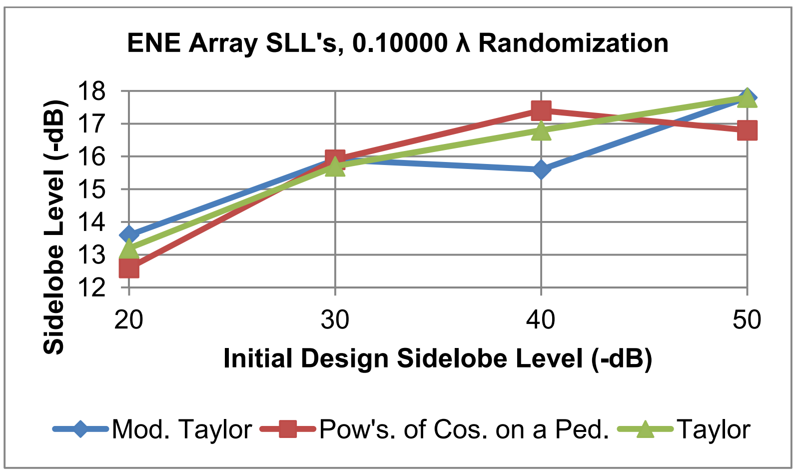

(b)

Figure B.21. *3σ sidelobe level of the* $1/4\,\lambda$ *element spacing group for 0.10000 λ randomization versus initial designed sidelobe level.* The sidelobe level of the MNE (a) and NME (b) arrays are plotted.

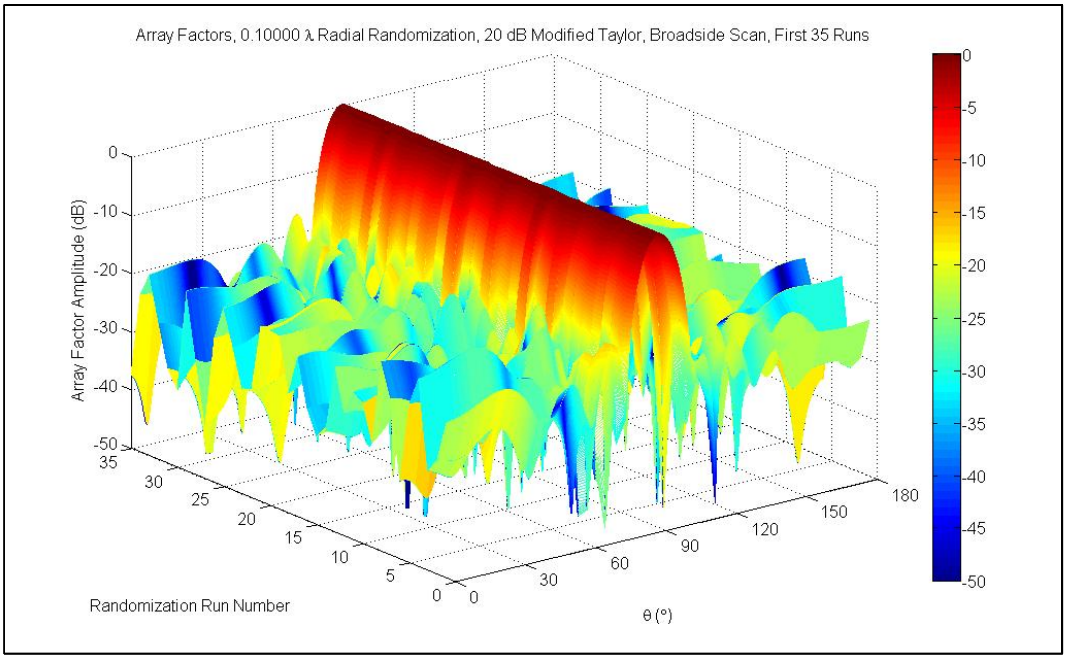

(a)

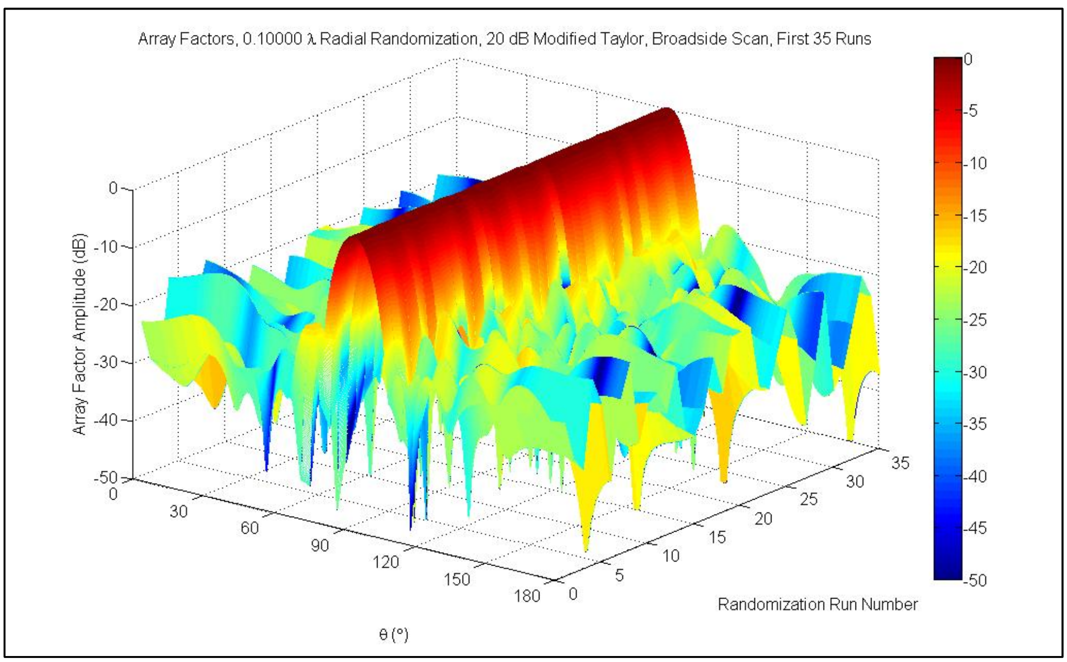

(b)

Figure B.22. *Sidelobes of the $1/4\,\lambda$ element spacing, 20 dB, 20 element modified Taylor array with 0.10000 λ radial variation scanned to broadside for the first 35 randomized states.*

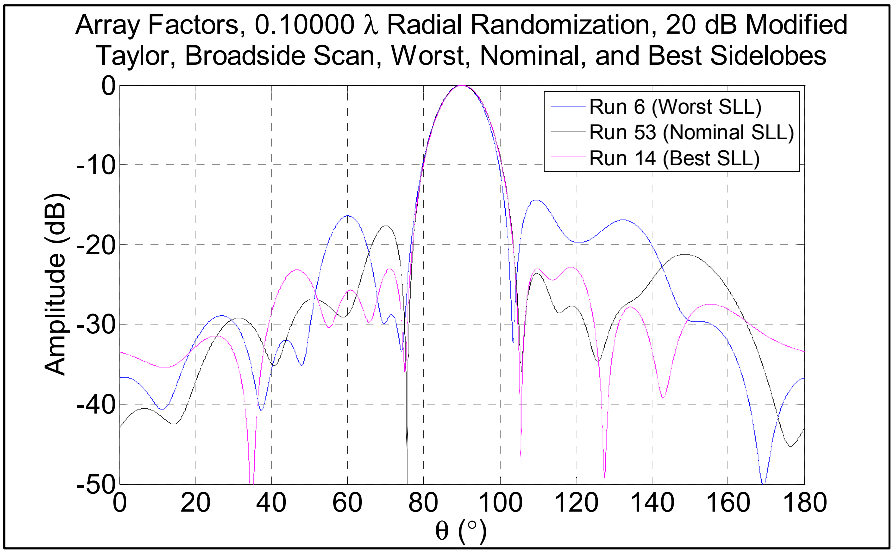

Figure B.23. *The worst, nominal, and best sidelobe array factors from the 100 randomization runs of the* 1/4 *λ element spacing, 20 dB, 20 element modified Taylor array with 0.10000 λ radial variation scanned to broadside.*

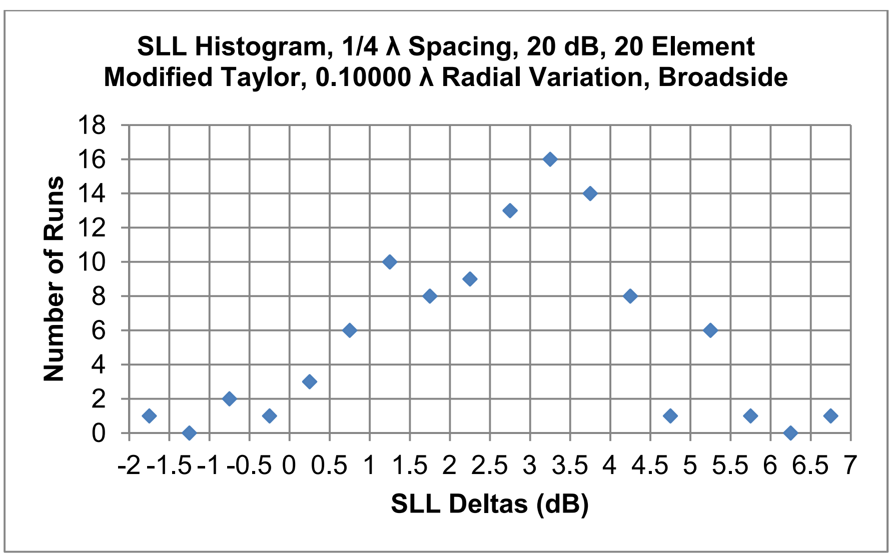

Figure B.24. *SLLdBDeltas histogram from the 100 randomization runs of the* 1/4 *λ element spacing, 20 dB, 20 element modified Taylor array with 0.10000 λ radial variation scanned to broadside.*

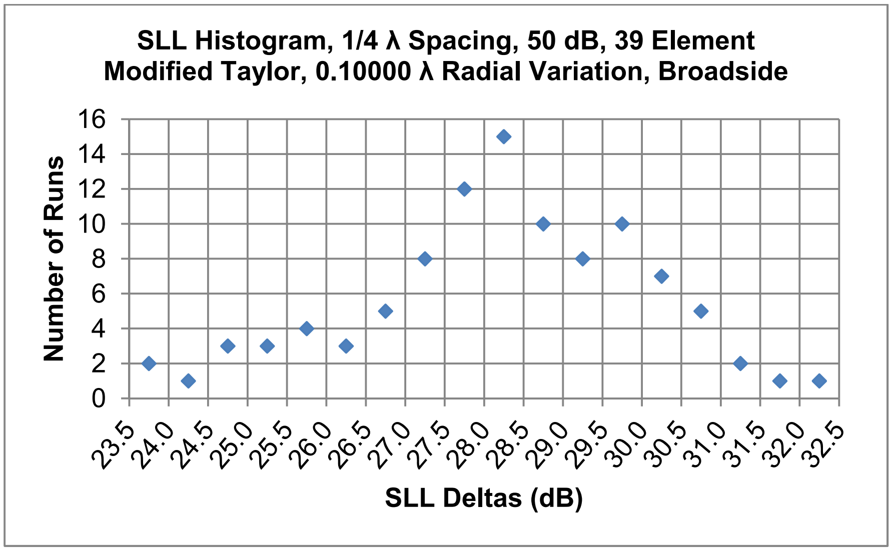

Figure B.25. *SLLdBDeltas histogram from the 100 randomization runs of the* $1/4$ *λ element spacing, 50 dB, 39 element modified Taylor array with 0.10000 λ radial variation scanned to broadside.*

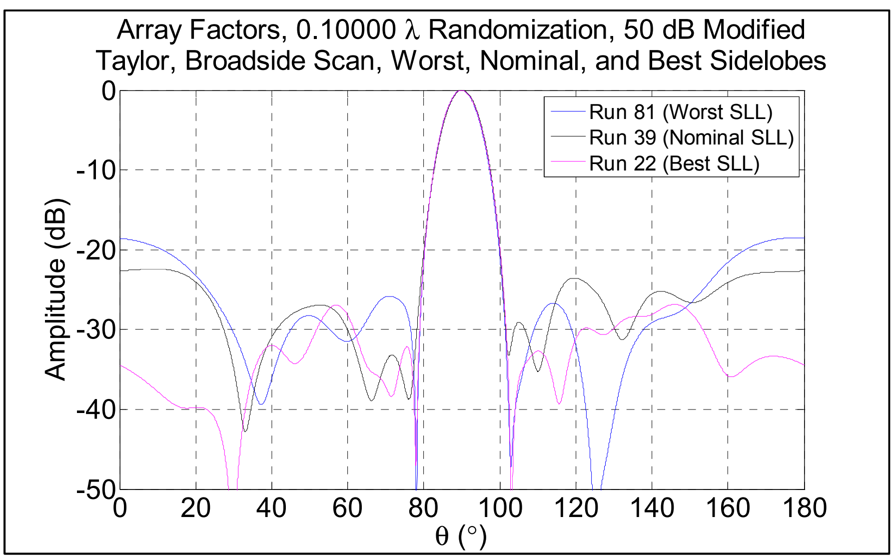

Figure B.26. *The worst, nominal, and best sidelobe array factors from the 100 randomization runs of the* $1/4$ *λ element spacing, 50 dB, 39 element modified Taylor array with 0.10000 λ radial variation scanned to broadside.*

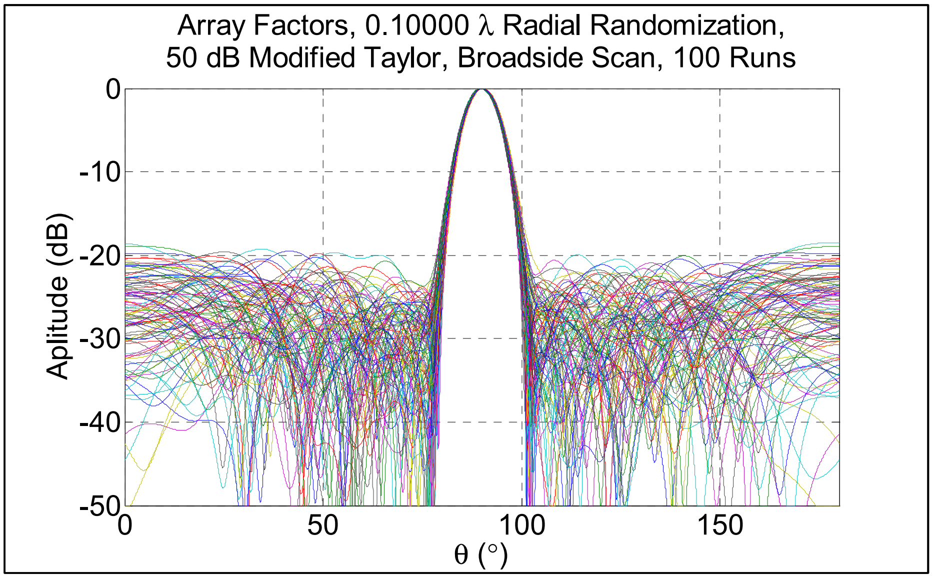

(a)

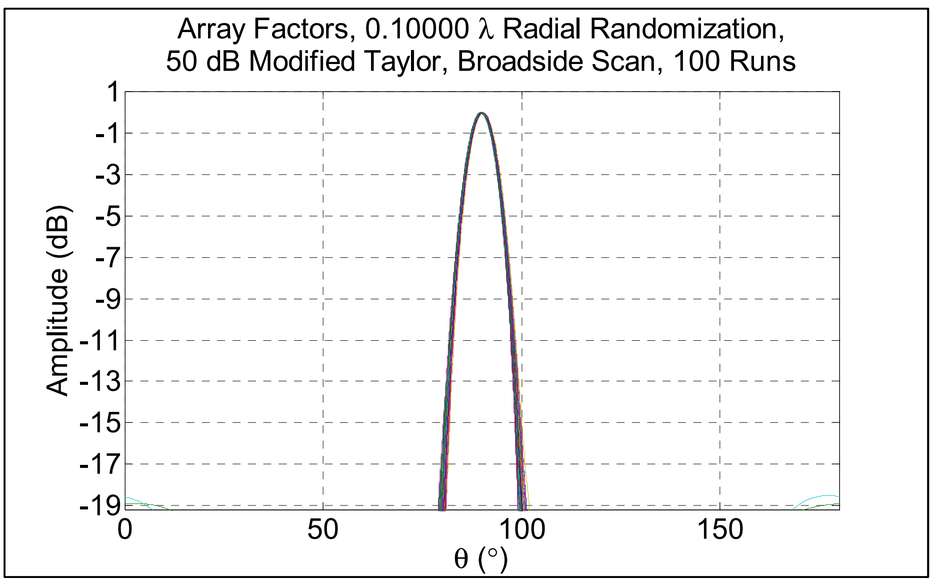

(b)

Figure B.27. *Array factors of 100 randomization runs of the $1/4\,\lambda$ element spacing, 50 dB, 39 element modified Taylor array with 0.10000 λ radial variation scanned to broadside.* Shown full scale (a) and up to 19 dB below peak of beam (b).

$3/8\lambda$ Element Spacing

20 dB Initial Design Sidelobe Level

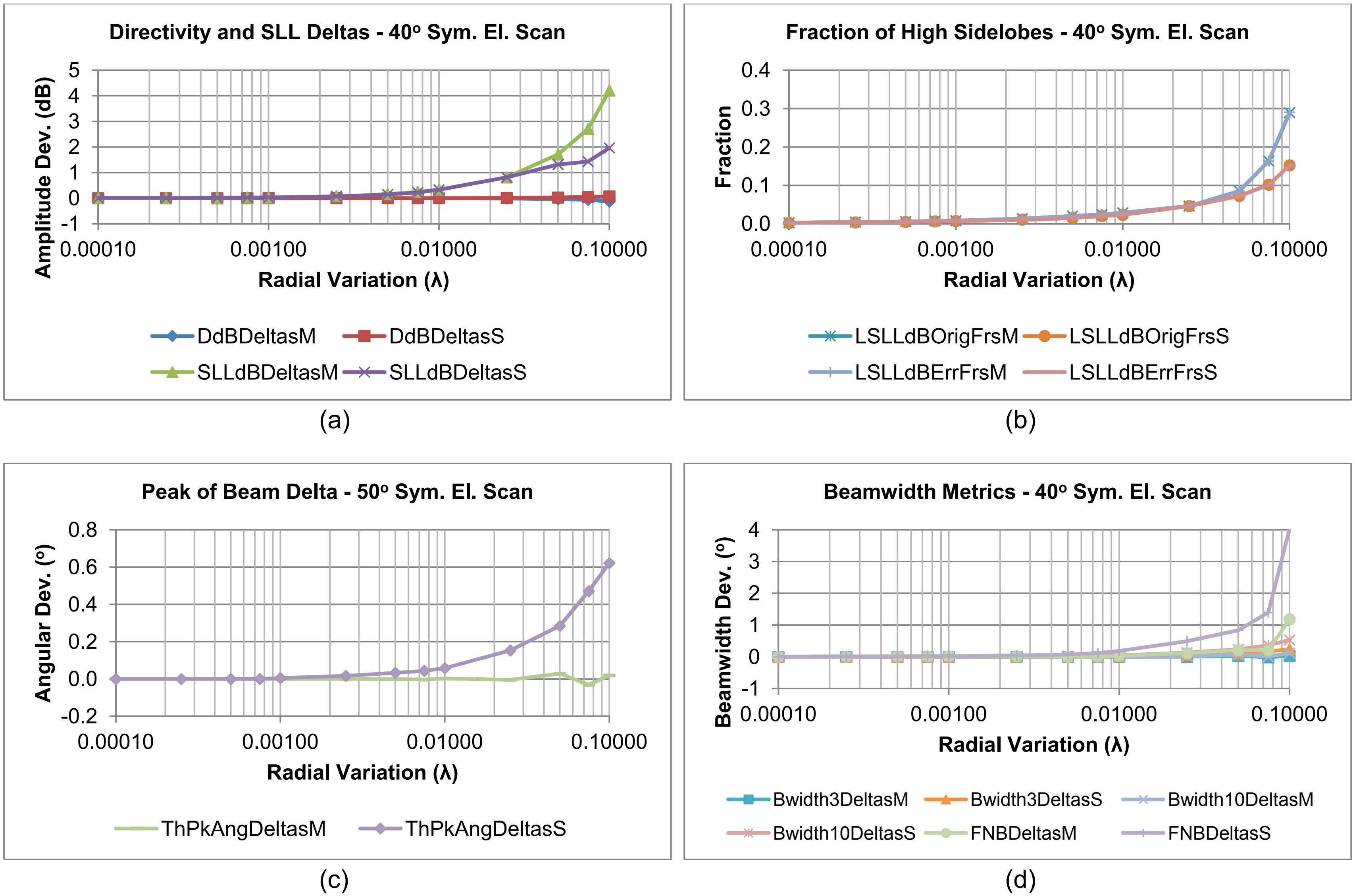

Figure B.28. *Statistical data for a* $3/8\,\lambda$ *spaced, 14 element, modified Taylor array versus radial randomization.* Directivity and sidelobe level (a), LSLLdB (b), beam pointing (c), and beamwidth (d) results are illustrated.

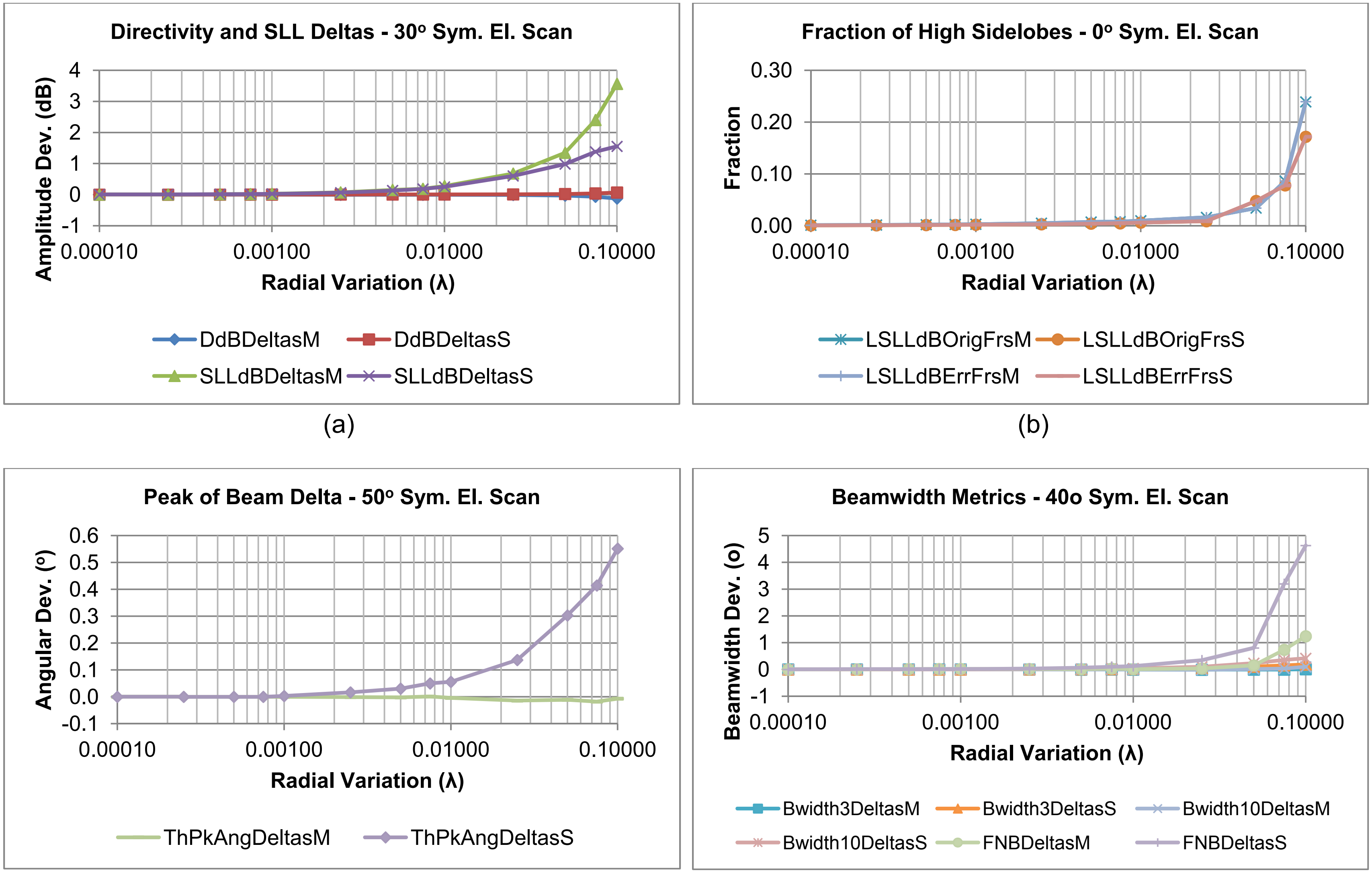

(a) (b) (c) (d)

Figure B.29. *Statistical data for a* $3/8\,\lambda$ *spaced, 14 element, powers of cosine on a pedestal array versus radial randomization.* Directivity and sidelobe level (a), LSLLdB (b), beam pointing (c), and beamwidth (d) results are illustrated.

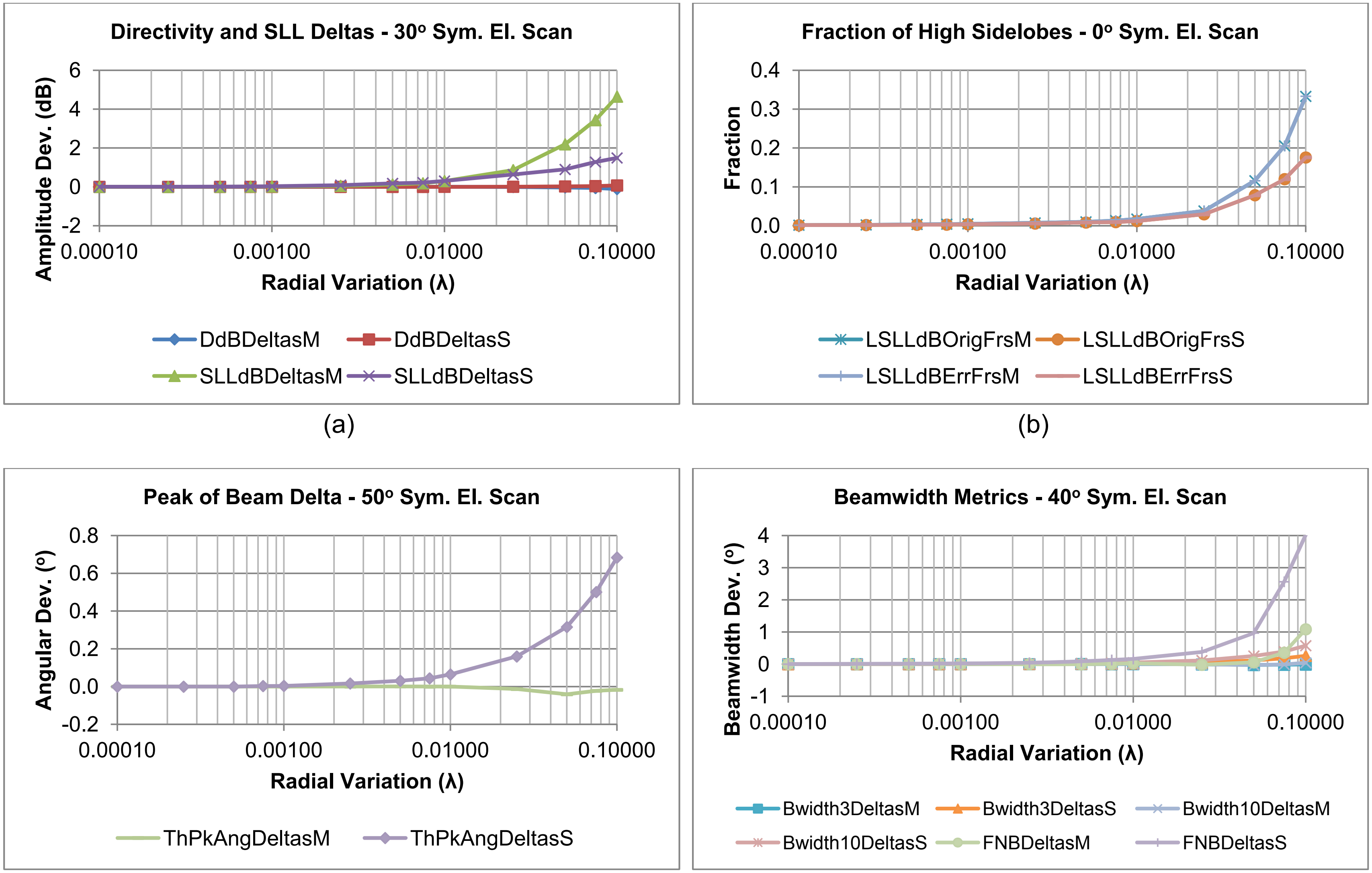

(c) (d)

Figure B.30. *Statistical data for a* $3/8\,\lambda$ *spaced, 13 element, Taylor array versus radial randomization.* Directivity and sidelobe level (a), LSLLdB (b), beam pointing (c), and beamwidth (d) results are illustrated.

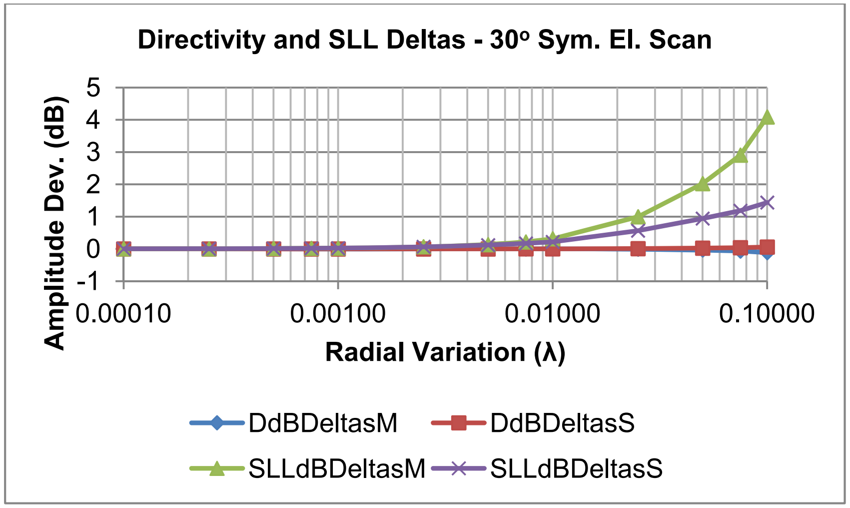

(a)

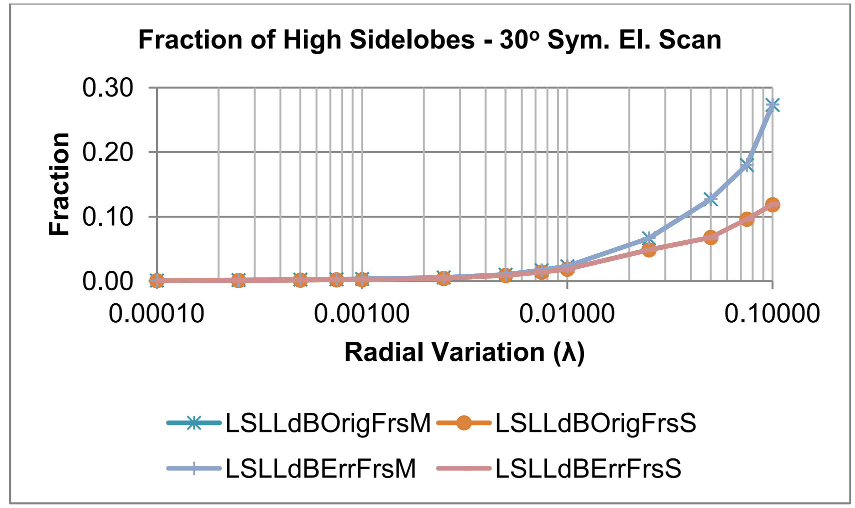

(b)

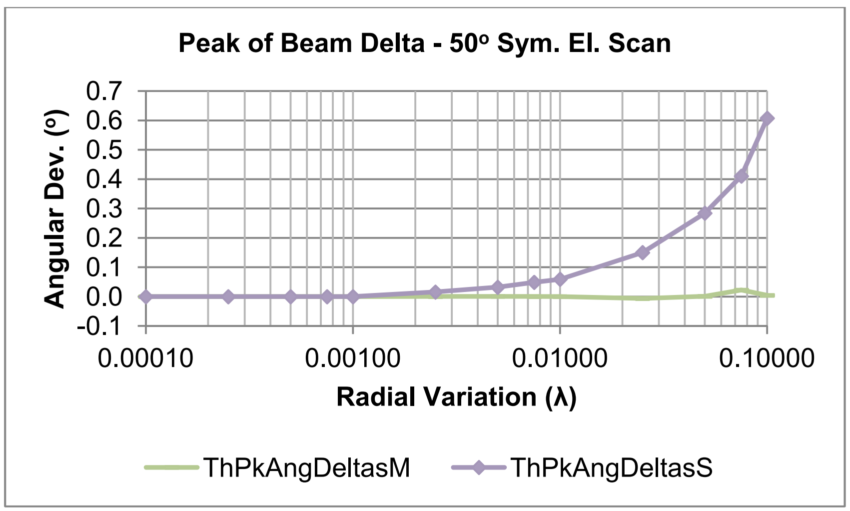

(c)

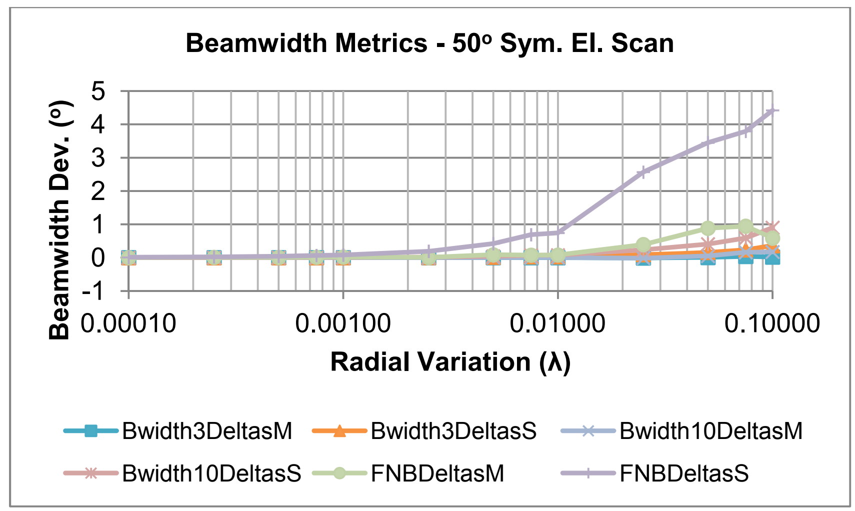

(d)

Figure B.31. *Statistical data for a $3/8\,\lambda$ spaced, 14 element, Taylor array versus radial randomization.* Directivity and sidelobe level (a), LSLLdB (b), beam pointing (c), and beamwidth (d) results are illustrated.

$3/8\lambda$ Element Spacing

30 dB Initial Design Sidelobe Level

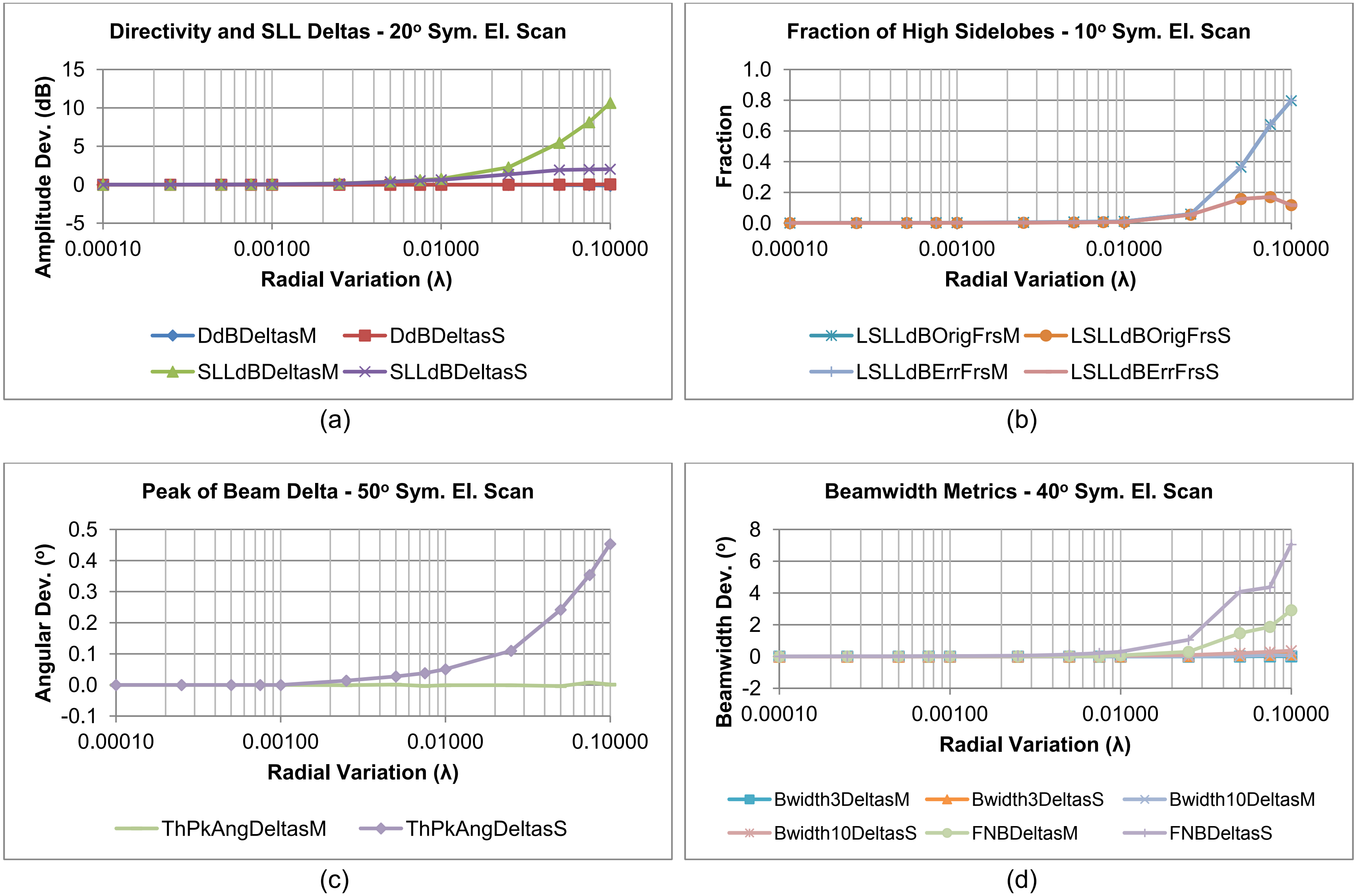

Figure B.32. *Statistical data for a* $3/8\,\lambda$ *spaced, 18 element, modified Taylor array versus radial randomization.* Directivity and sidelobe level (a), LSLLdB (b), beam pointing (c), and beamwidth (d) results are illustrated.

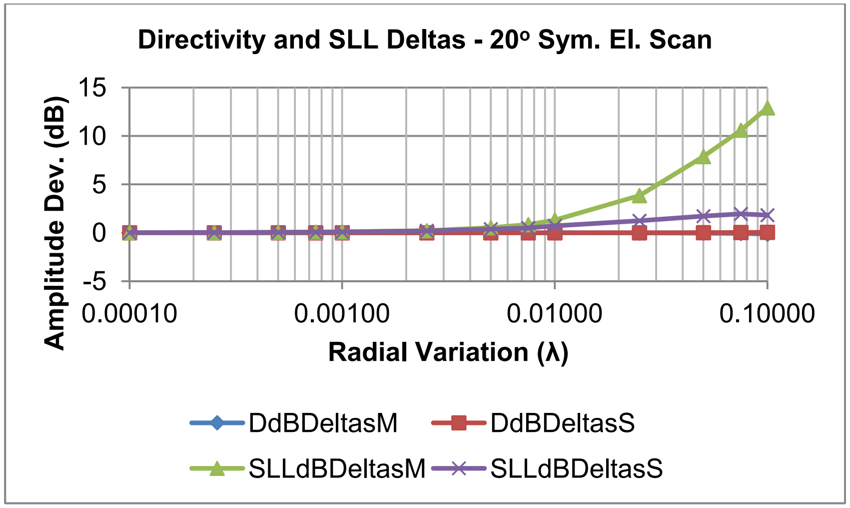

(a)

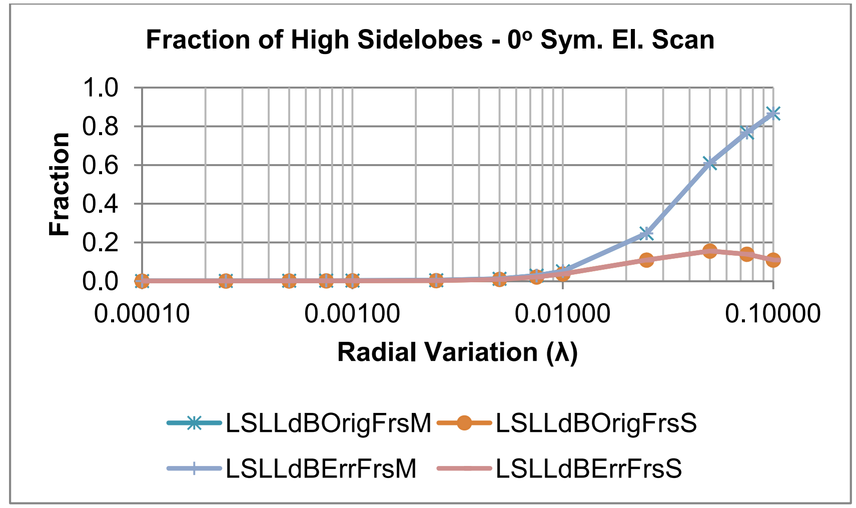

(b)

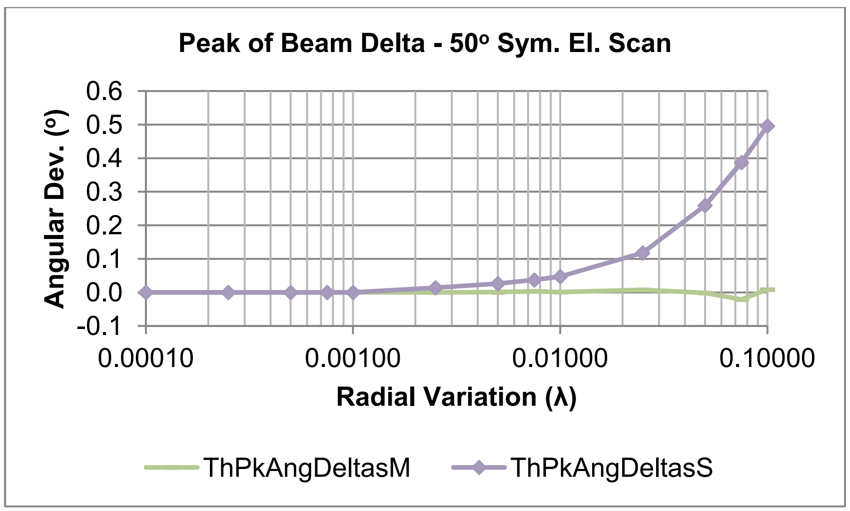

(c)

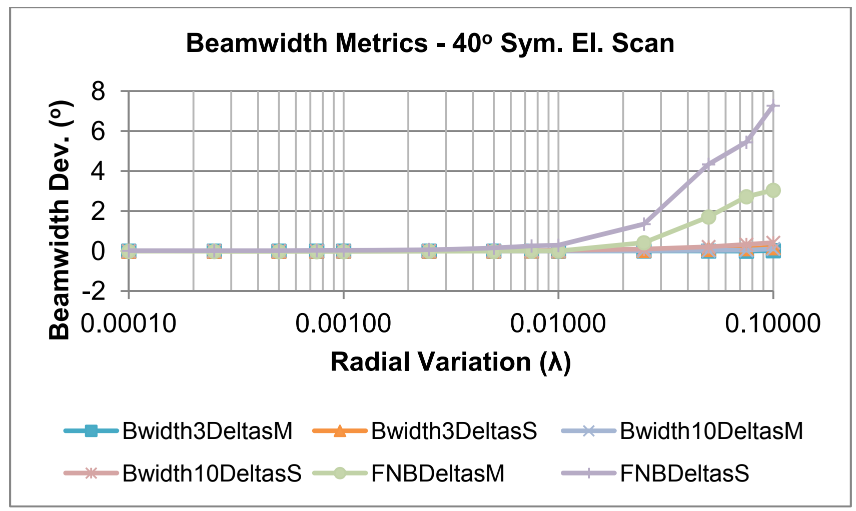

(d)

Figure B33. *Statistical data for a* $3/8\,\lambda$ *spaced, 17 element, powers of cosine on a pedestal array versus radial randomization.* Directivity and sidelobe level (a), LSLLdB (b), beam pointing (c), and beamwidth (d) results are illustrated.

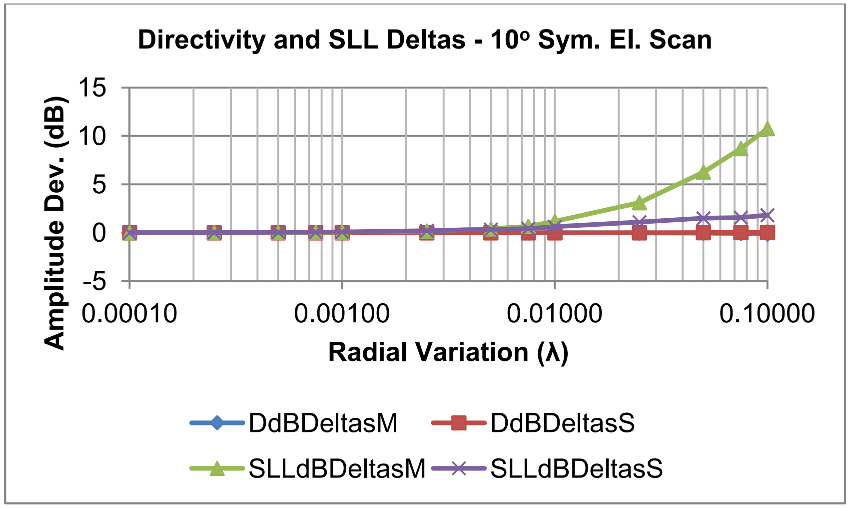

(a)

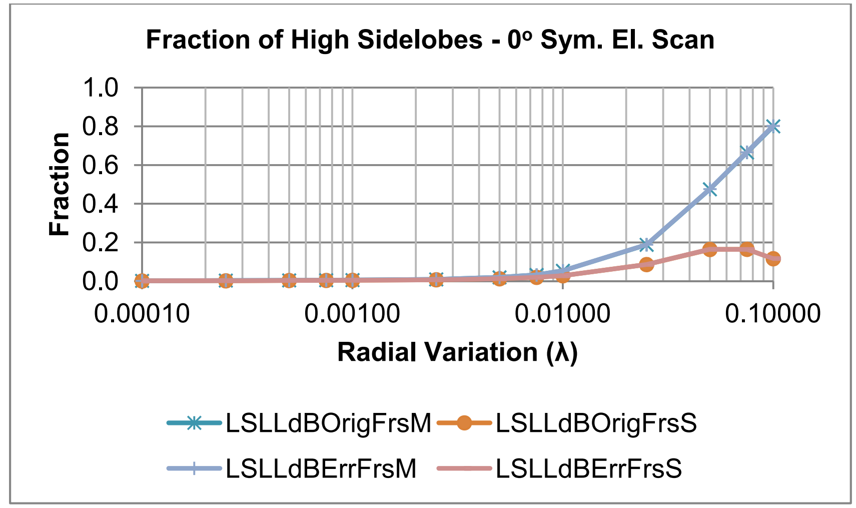

(b)

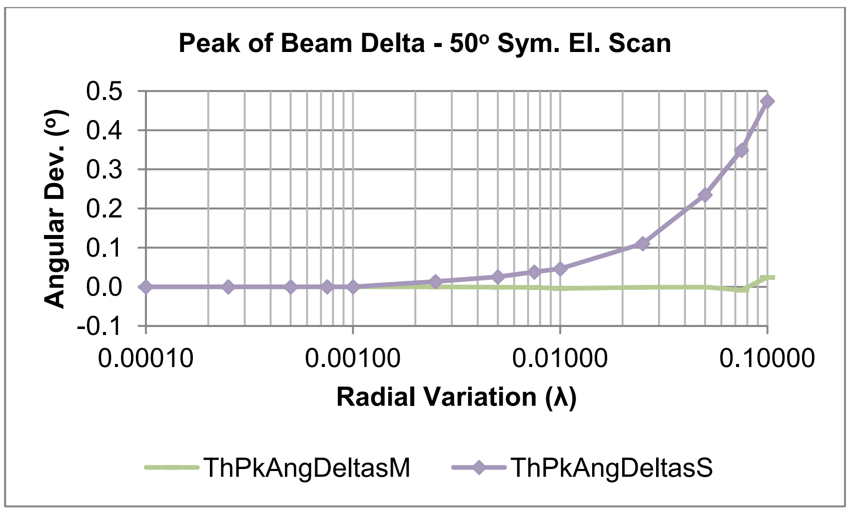

(c)

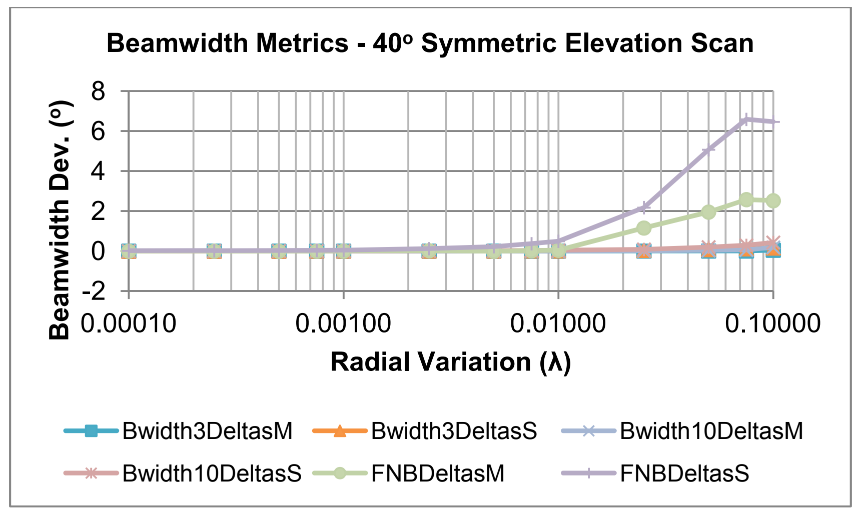

(d)

Figure B.34. *Statistical data for a* $3/8\,\lambda$ *spaced, 17 element, Taylor array versus radial randomization.* Directivity and sidelobe level (a), LSLLdB (b), beam pointing (c), and beamwidth (d) results are illustrated.

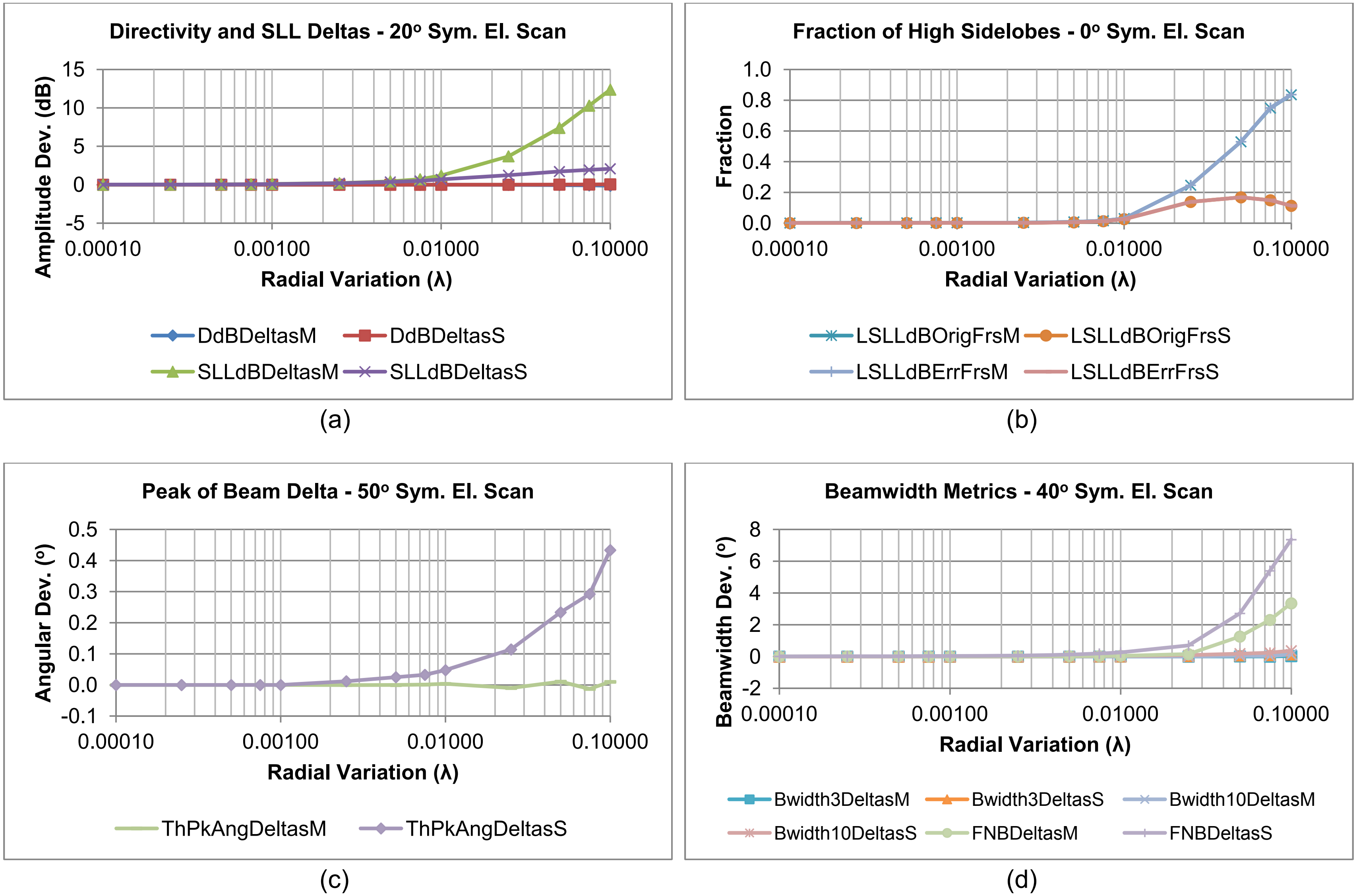

Figure B.35. *Statistical data for a* $3/8\,\lambda$ *spaced, 18 element, powers of cosine on a pedestal array versus radial randomization.* Directivity and sidelobe level (a), LSLLdB (b), beam pointing (c), and beamwidth (d) results are illustrated.

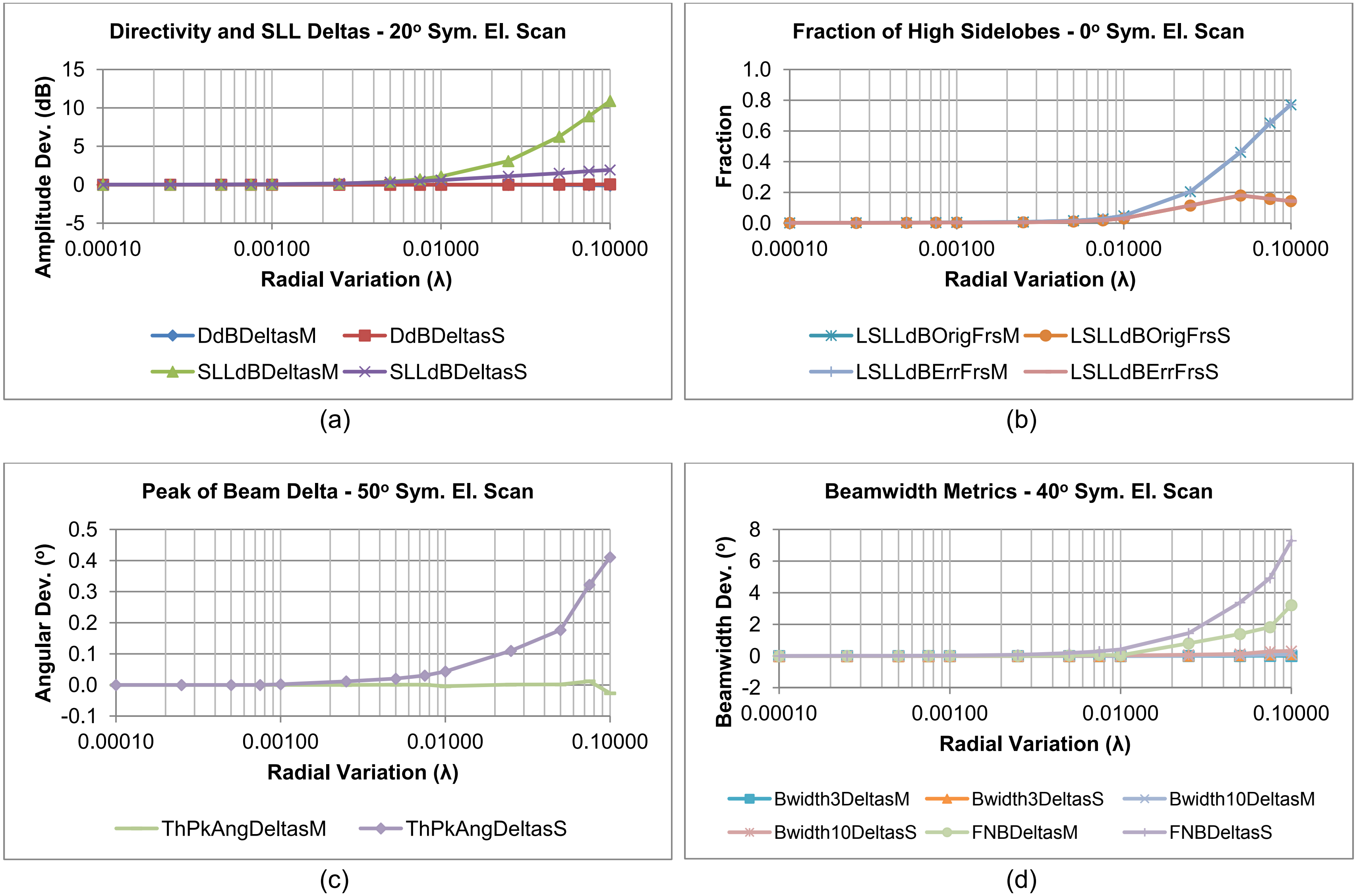

Figure B.36. *Statistical data for a* $3/8\,\lambda$ *spaced, 18 element, Taylor array versus radial randomization.* Directivity and sidelobe level (a), LSLLdB (b), beam pointing (c), and beamwidth (d) results are illustrated.

	SLLdBDeltas, 0.10000 λ Randomization			
	μ+3σ (30 dB Initial Design Sidelobes Group)			
	1/4 λ Spacing		3/8 λ Spacing	
Taper	MNE	ENE	MNE	ENE
Modified Taylor	14.4		16.6	
Powers of Cosine on a Pedestal	14.7	14.2	18.3	18.7
Taylor	15.5	15.1	16.2	16.6

(a)

	SLL (-dB), 0.10000 λ Randomization			
	μ+3σ (30 dB Initial Design Sidelobes Group)			
	1/4 λ Spacing		3/8 λ Spacing	
Taper	MNE	ENE	MNE	ENE
Modified Taylor	16.1		13.7	
Powers of Cosine on a Pedestal	15.8	16.1	13.9	13.2
Taylor	15.3	15.7	13.9	13.6

(b)

Table B.2. *Statistical sidelobe level data performance for the 0.10000 λ randomization cases comparing the* $1/4$ *and* $3/8\,\lambda$ *element spacing for the 30 dB initial design sidelobe groups.* Mean (SLLdBDeltasM) plus 3σ (3*SLLdBDeltasS) (a) and 3σ population estimate of sidelobe level (b).

$3/8\lambda$ Element Spacing

40 dB Initial Design Sidelobe Level

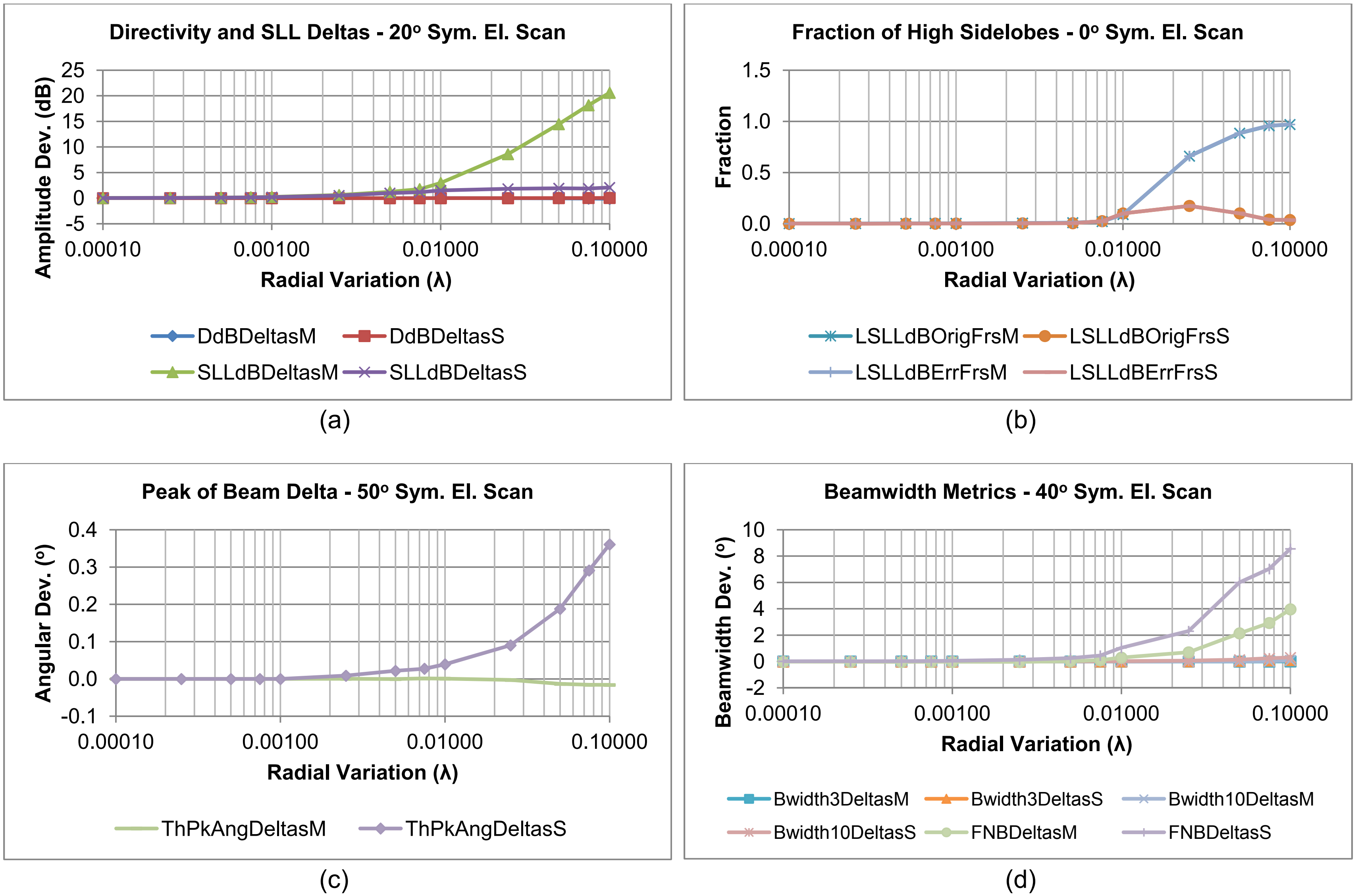

Figure B.37. *Statistical data for a* $3/8\,\lambda$ *spaced, 24 element, modified Taylor array versus radial randomization.* Directivity and sidelobe level (a), LSLLdB (b), beam pointing (c), and beamwidth (d) results are illustrated.

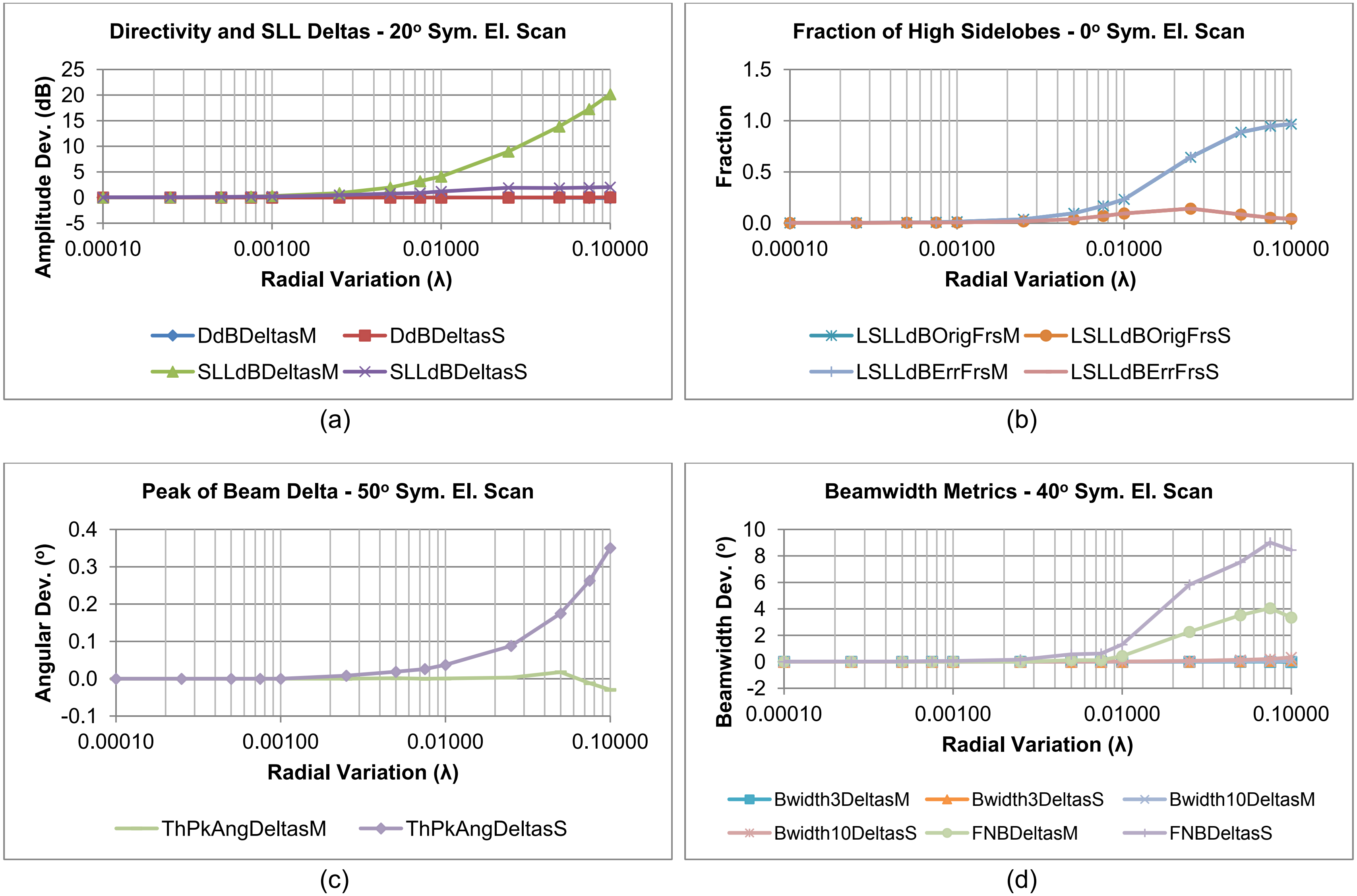

Figure B.38. *Statistical data for a* $3/8\,\lambda$ *spaced, 22 element, powers of cosine on a pedestal array versus radial randomization.* Directivity and sidelobe level (a), LSLLdB (b), beam pointing (c), and beamwidth (d) results are illustrated.

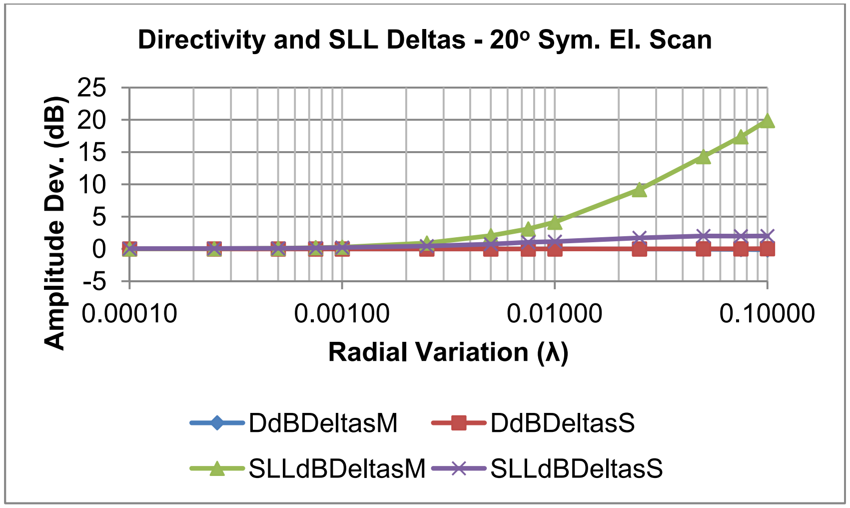

(a)

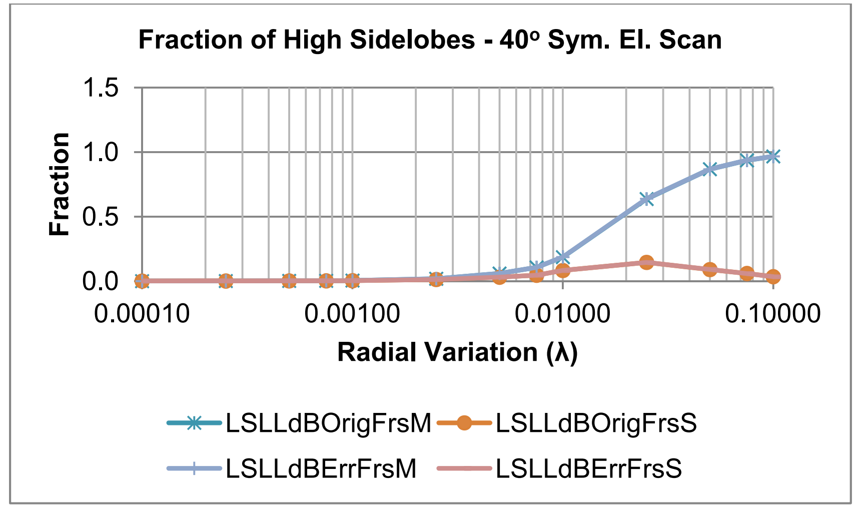

(b)

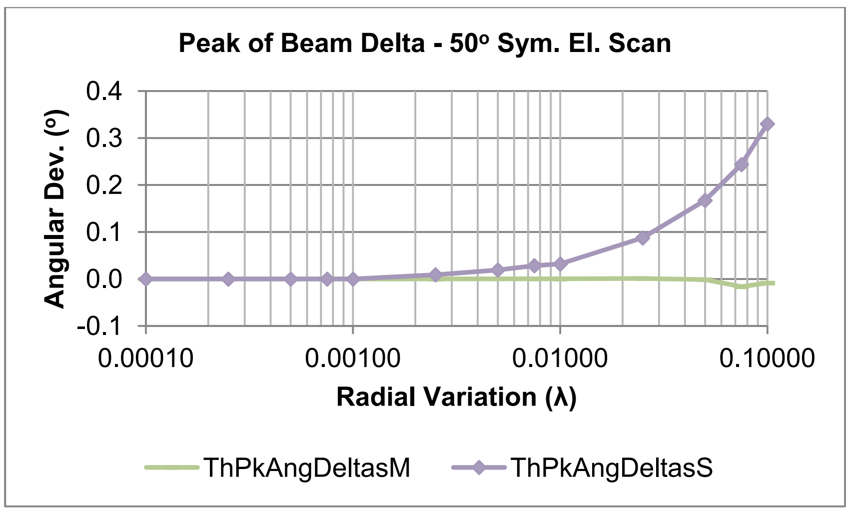

(c)

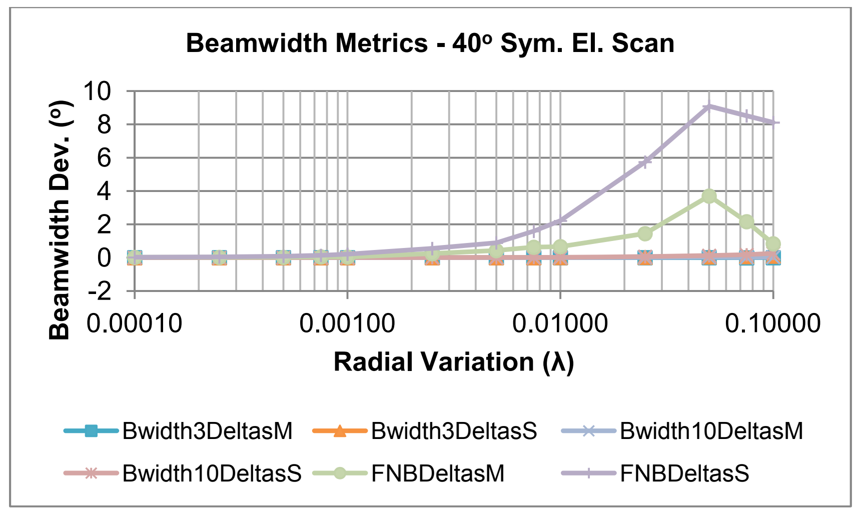

(d)

Figure B.39. *Statistical data for a* $3/8\,\lambda$ *spaced, 23 element, Taylor array versus radial randomization.* Directivity and sidelobe level (a), LSLLdB (b), beam pointing (c), and beamwidth (d) results are illustrated.

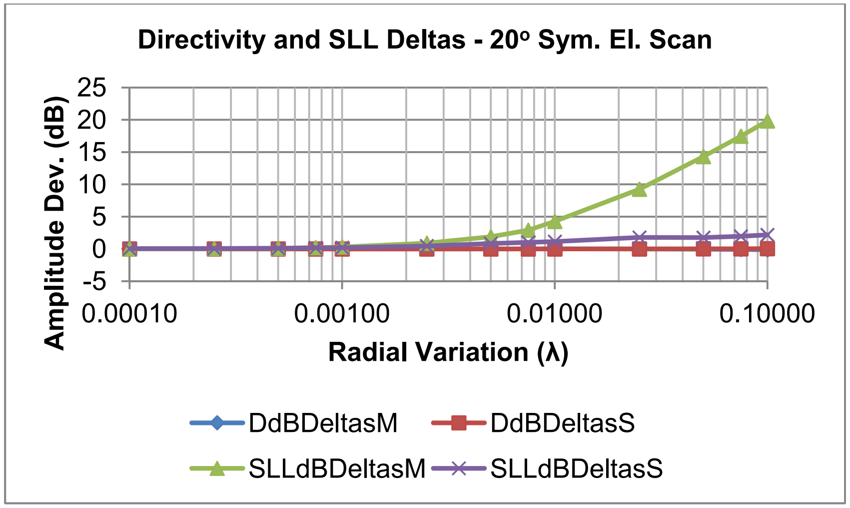

(a)

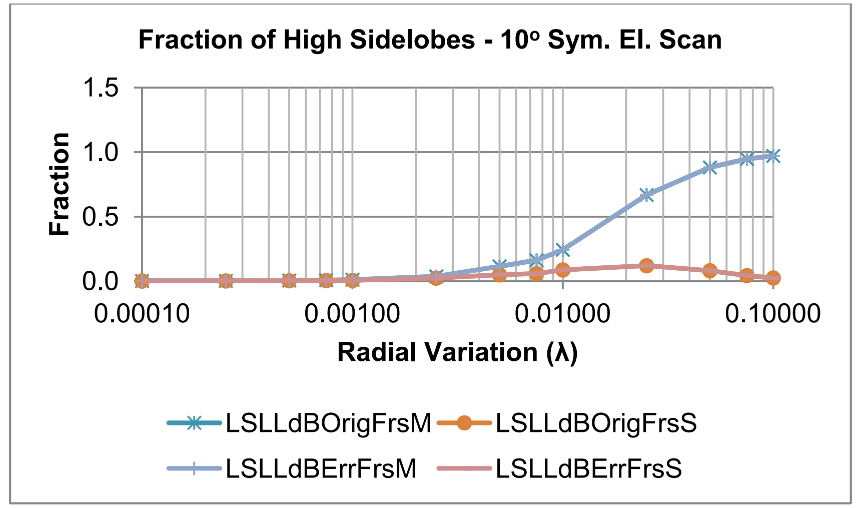

(b)

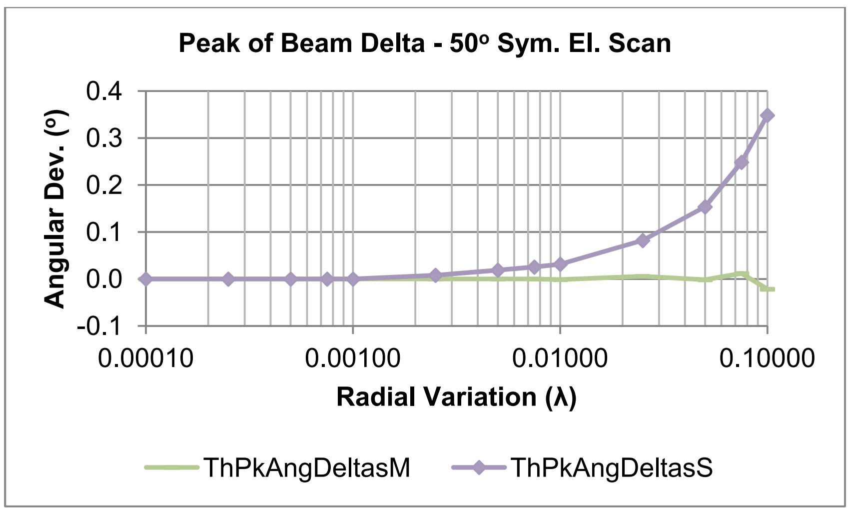

(c)

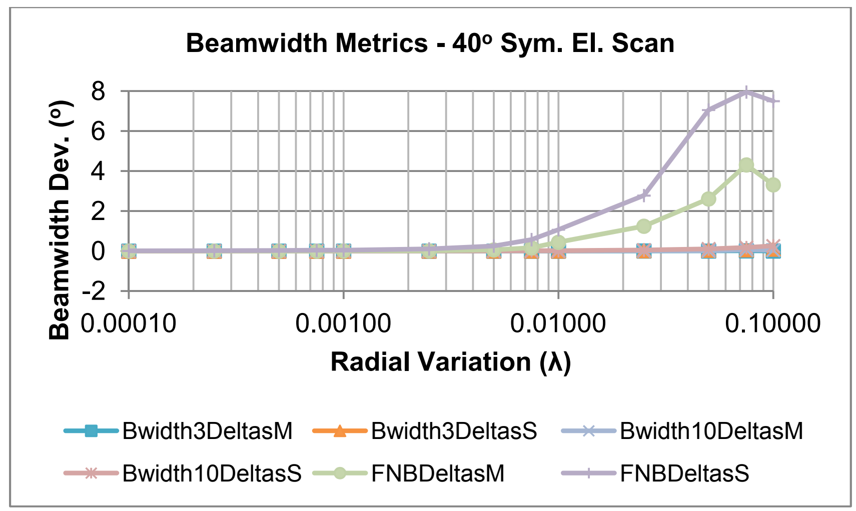

(d)

Figure B.40. *Statistical data for a* $3/8\,\lambda$ *spaced, 24 element, powers of cosine on a pedestal array versus radial randomization.* Directivity and sidelobe level (a), LSLLdB (b), beam pointing (c), and beamwidth (d) results are illustrated.

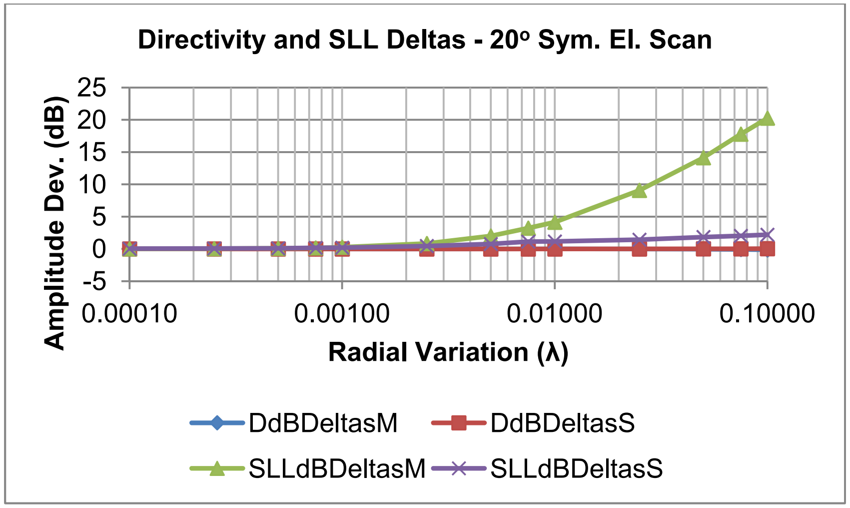

(a)

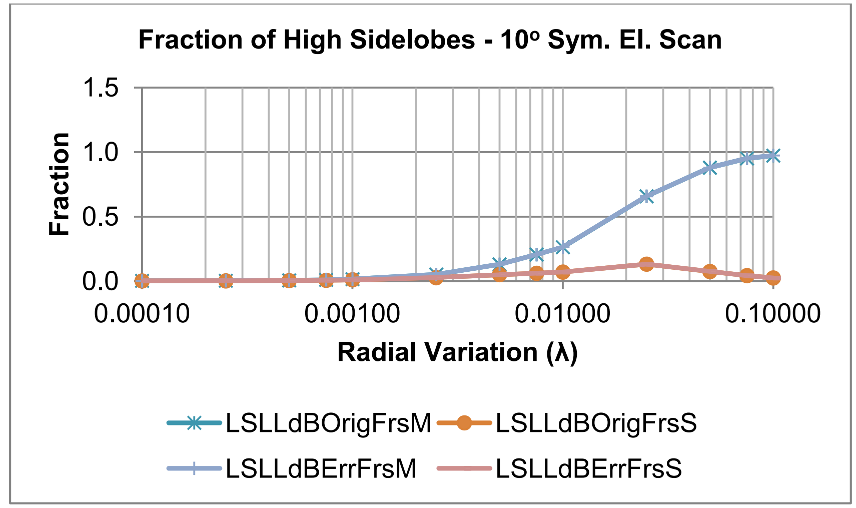

(b)

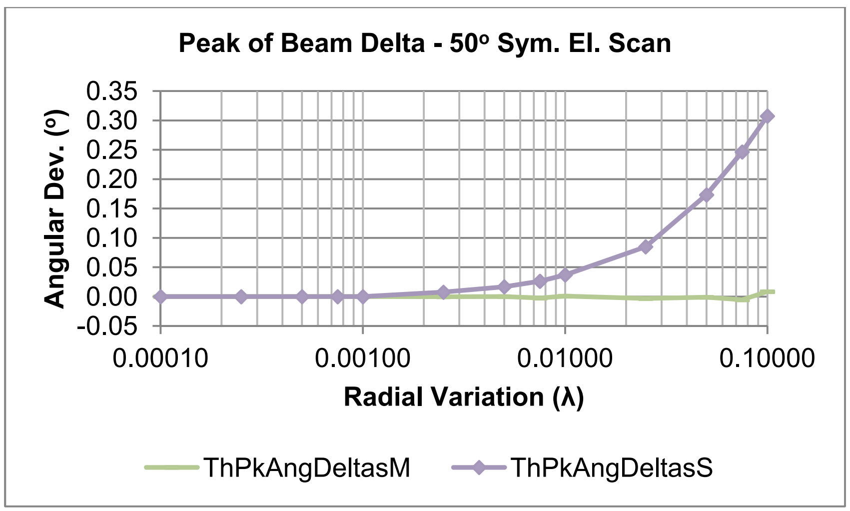

(c)

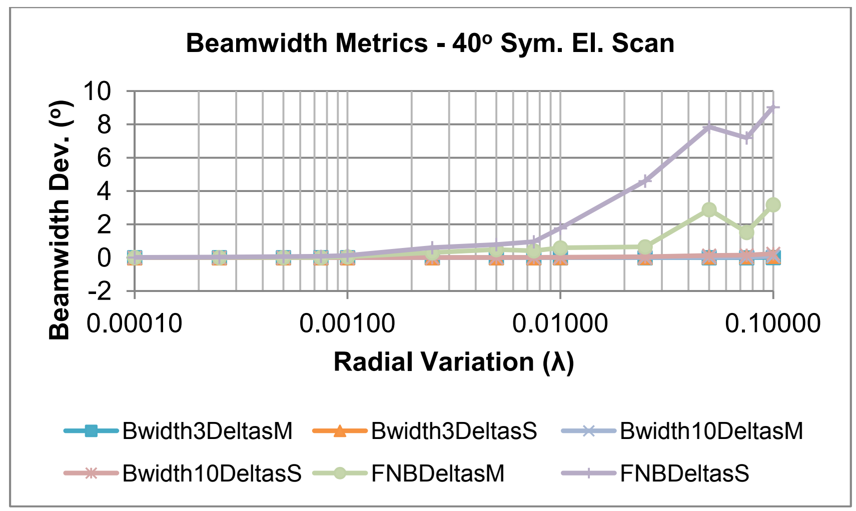

(d)

Figure B.41. *Statistical data for a $3/8\,\lambda$ spaced, 24 element, Taylor array versus radial randomization.* Directivity and sidelobe level (a), LSLLdB (b), beam pointing (c), and beamwidth (d) results are illustrated.

$3/8\lambda$ Element Spacing

50 dB Initial Design Sidelobe Level

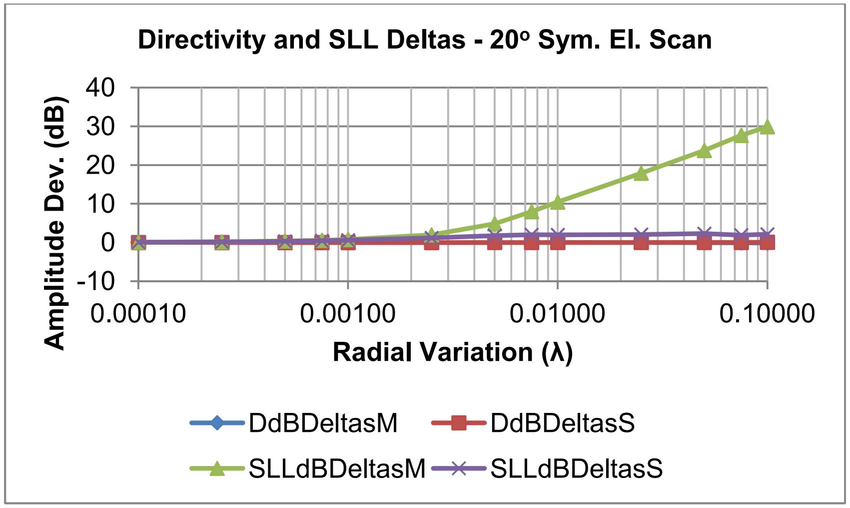

(a)

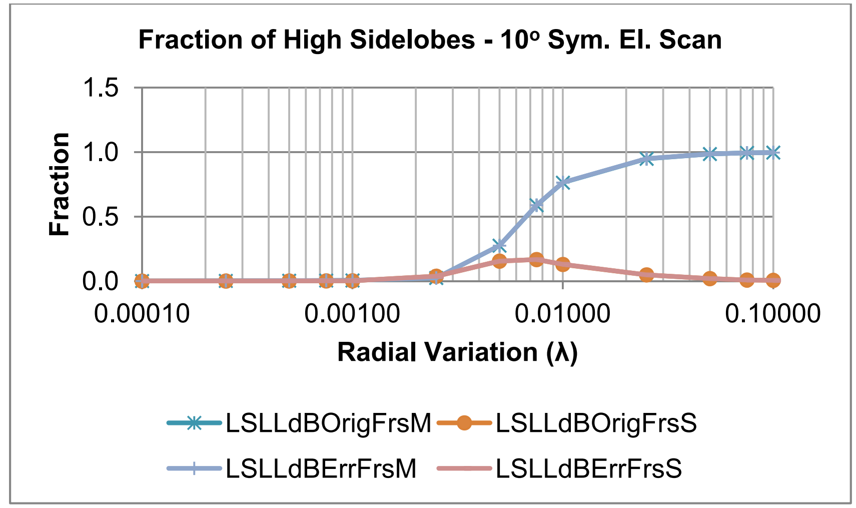

(b)

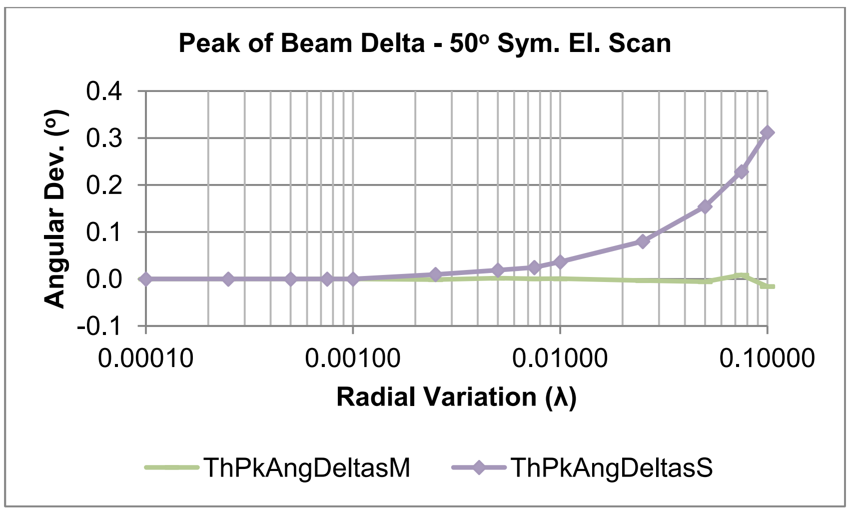

(c)

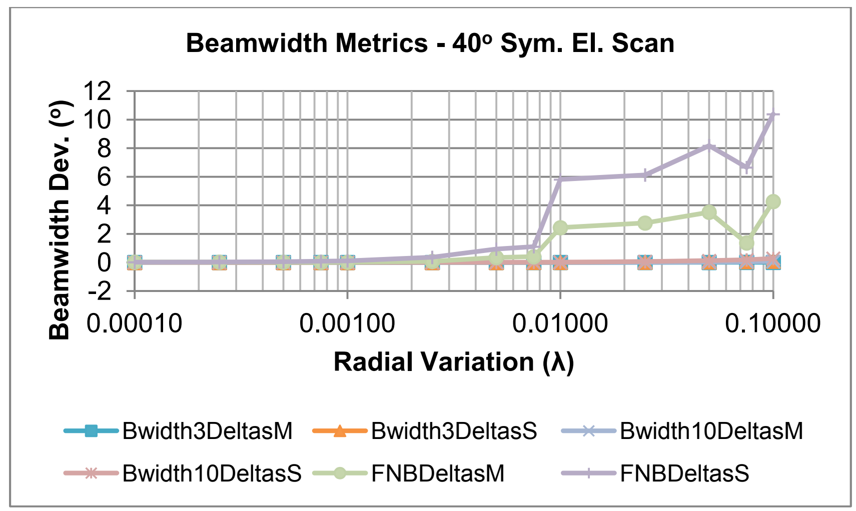

(d)

Figure B.42. *Statistical data for a* $3/8\,\lambda$ *spaced, 28 element, modified Taylor array versus radial randomization.* Directivity and sidelobe level (a), LSLLdB (b), beam pointing (c), and beamwidth (d) results are illustrated.

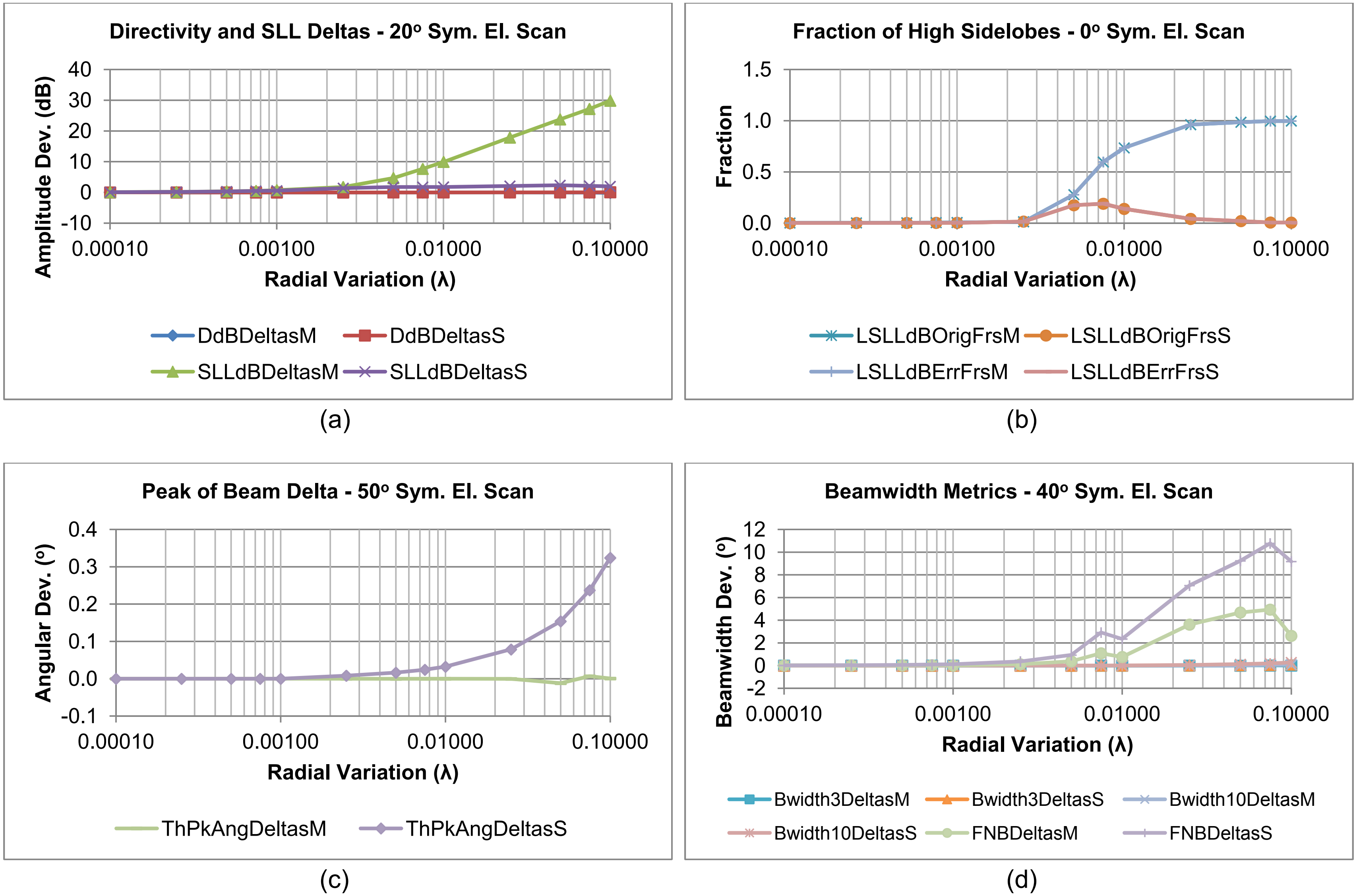

Figure B.43. *Statistical data for a* $3/8\,\lambda$ *spaced, 37 element, powers of cosine on a pedestal array versus radial randomization.* Directivity and sidelobe level (a), LSLLdB (b), beam pointing (c), and beamwidth (d) results are illustrated.

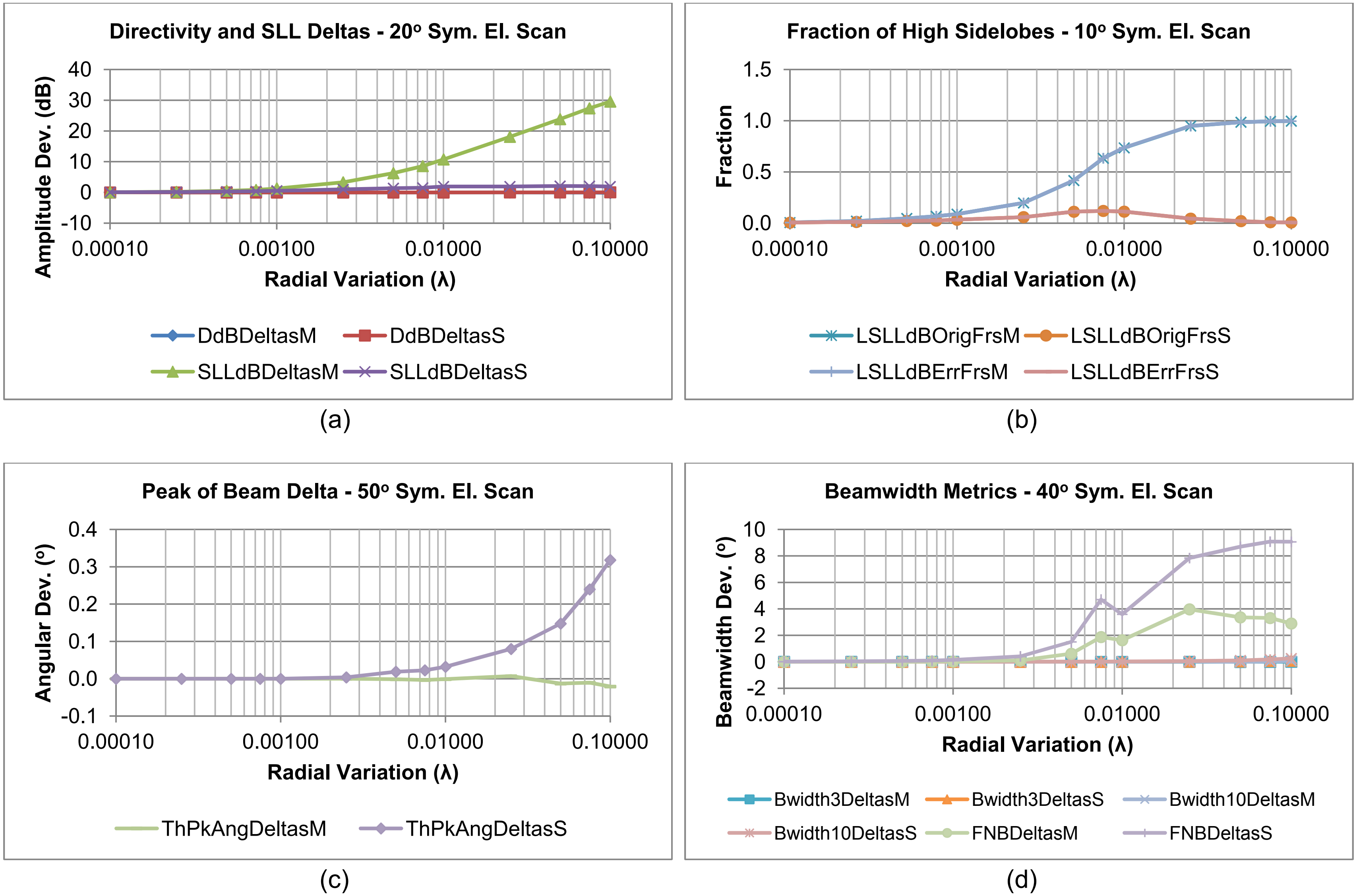

Figure B.44. *Statistical data for a* $3/8\,\lambda$ *spaced, 27 element, Taylor array versus radial randomization.* Directivity and sidelobe level (a), LSLLdB (b), beam pointing (c), and beamwidth (d) results are illustrated.

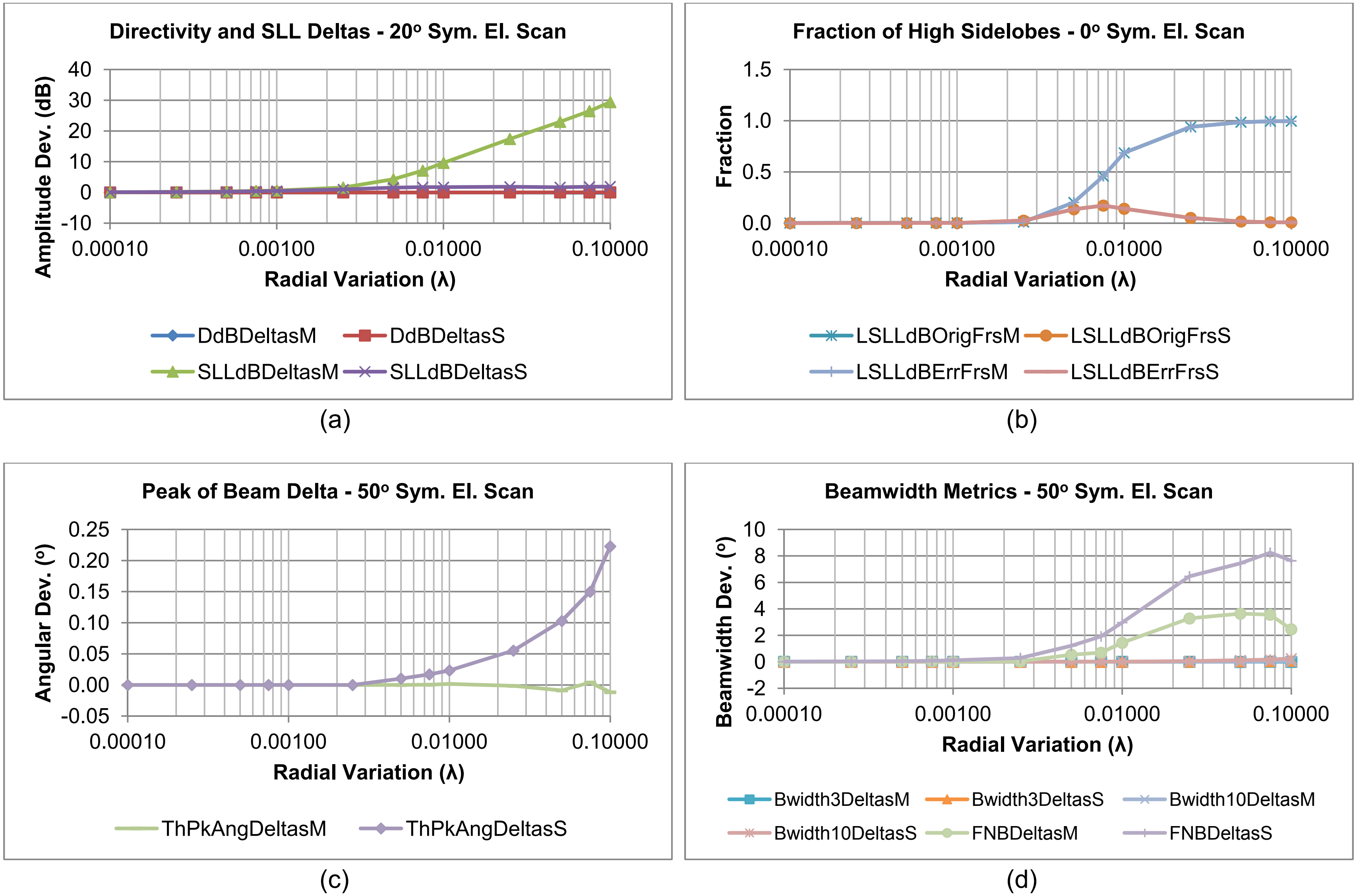

Figure B.45. *Statistical data for a* $3/8\,\lambda$ *spaced, 37 element, modified Taylor array versus radial randomization.* Directivity and sidelobe level (a), LSLLdB (b), beam pointing (c), and beamwidth (d) results are illustrated.

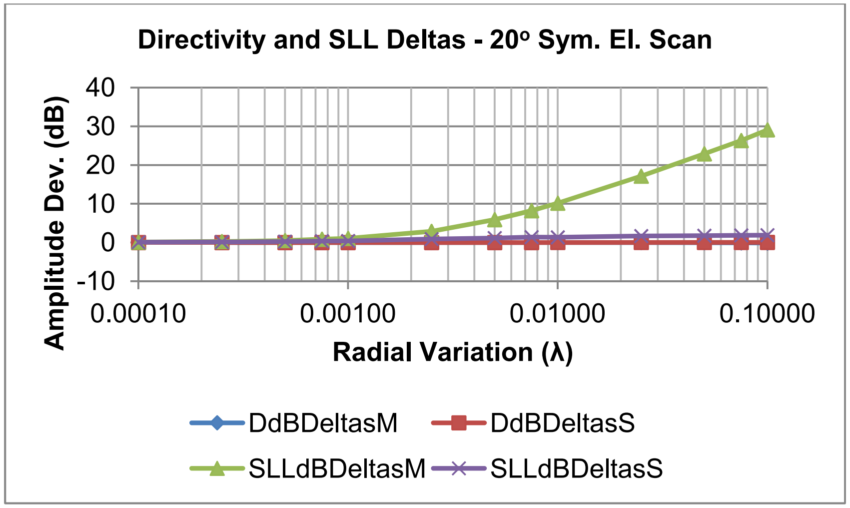

(a)

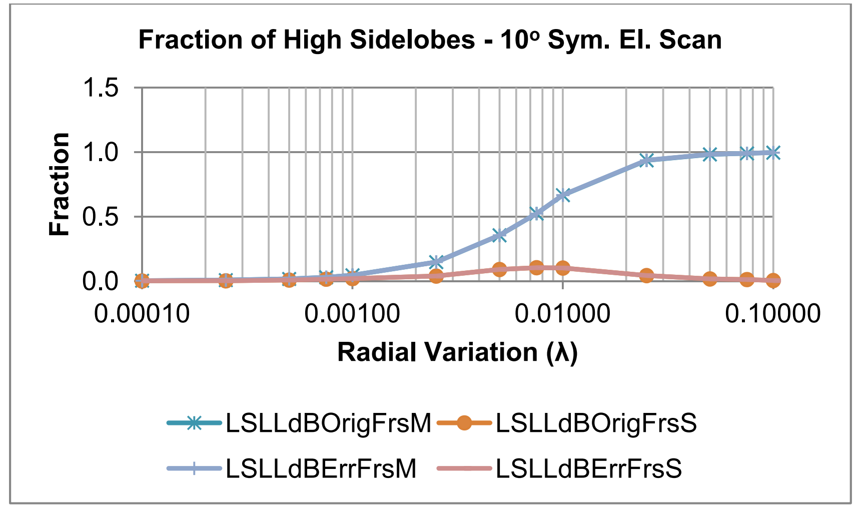

(b)

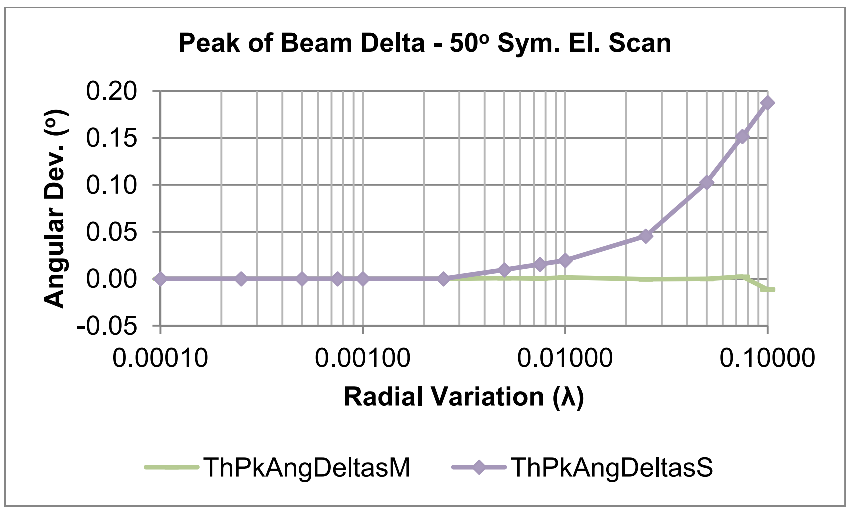

(c)

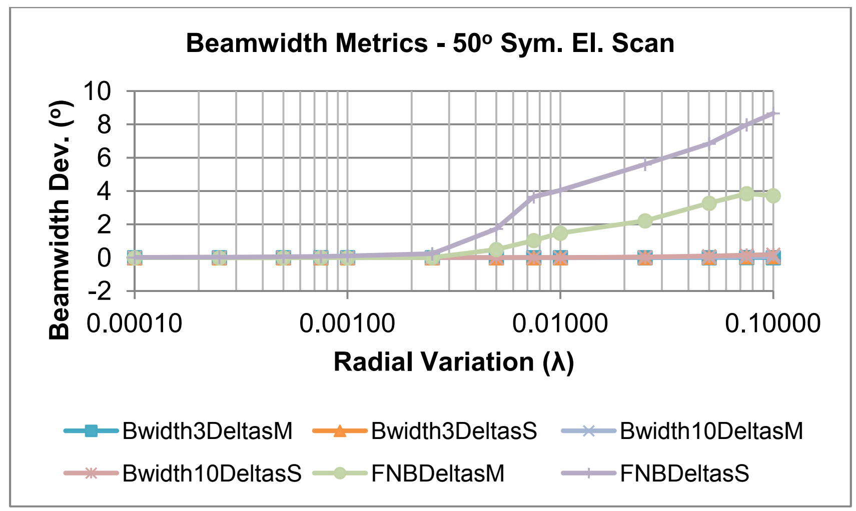

(d)

Figure B.46. *Statistical data for a* $3/8\,\lambda$ *spaced, 37 element, Taylor array versus radial randomization.* Directivity and sidelobe level (a), LSLLdB (b), beam pointing (c), and beamwidth (d) results are illustrated.

$1/2\,\lambda$ Element Spacing

20 dB Initial Design Sidelobe Level

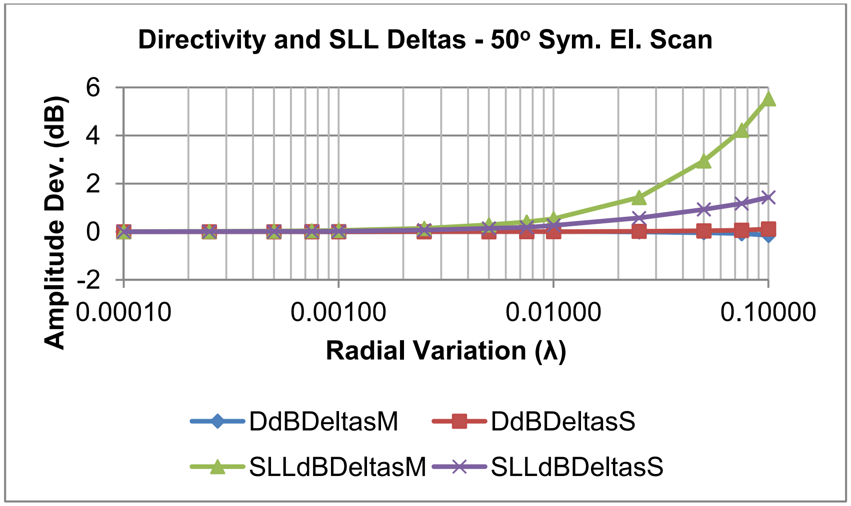

(a)

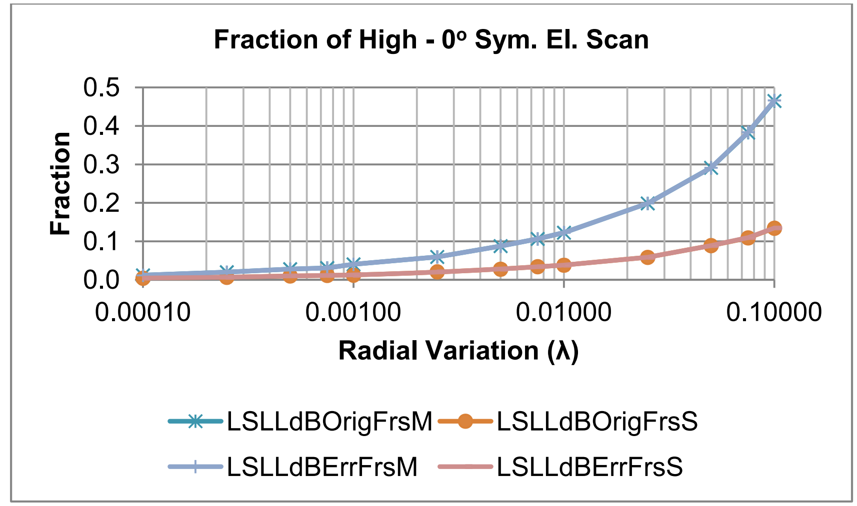

(b)

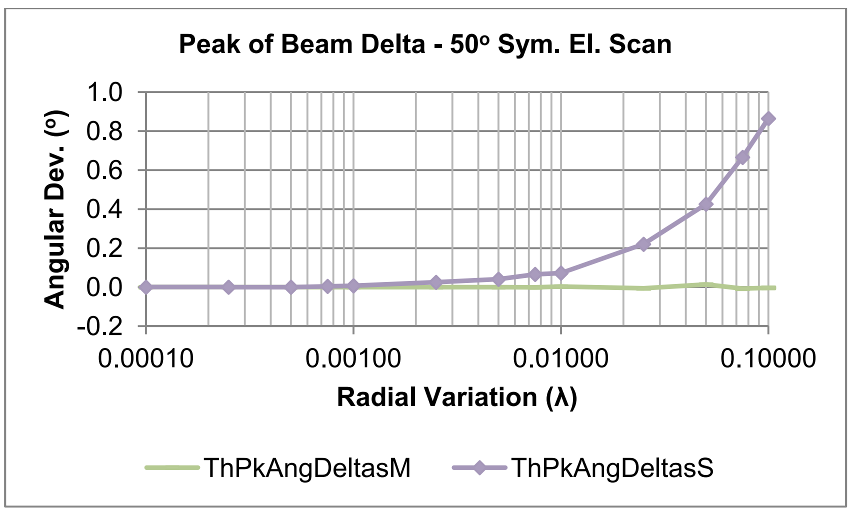

(c)

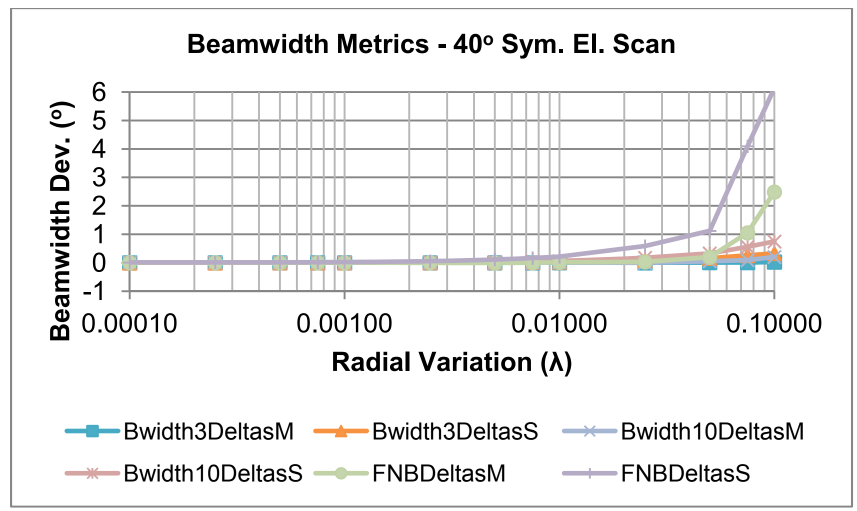

(d)

Figure B.47. *Statistical data for a $1/2\lambda$ spaced, 9 element, Dolph-Chebyshev array versus radial randomization.* Directivity and sidelobe level (a), LSLLdB (b), beam pointing (c), and beamwidth (d) results are illustrated.

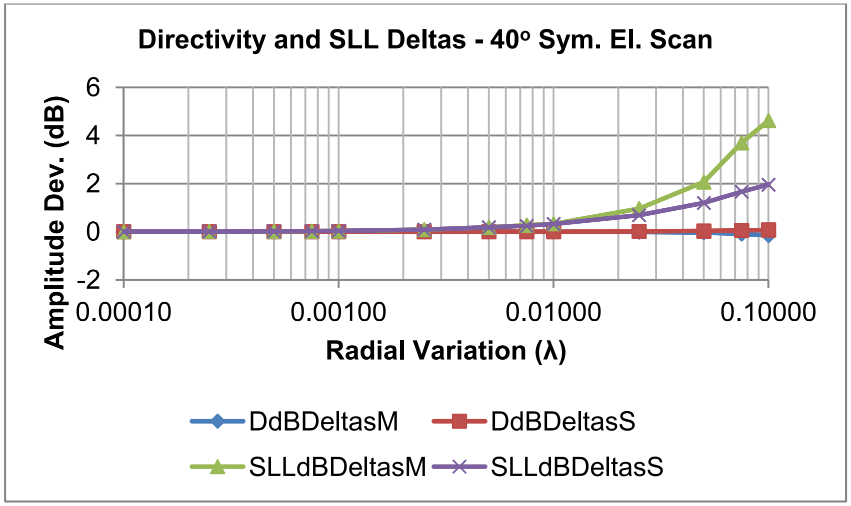

(a)

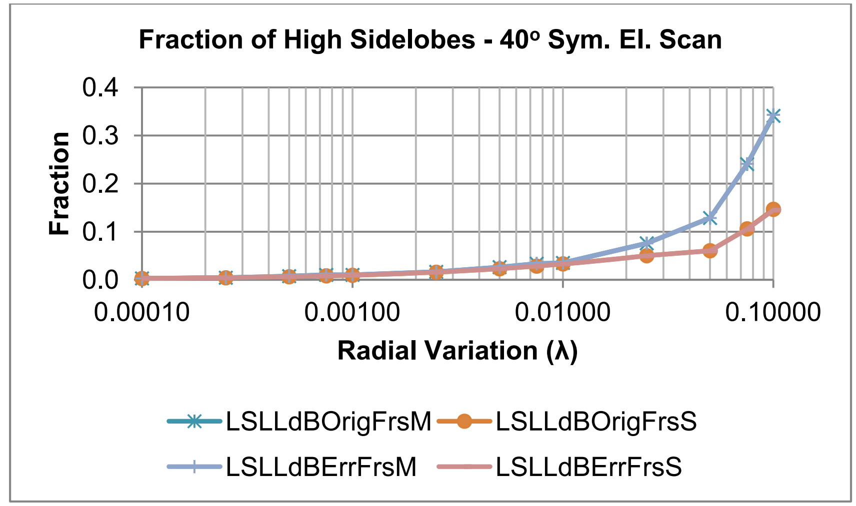

(b)

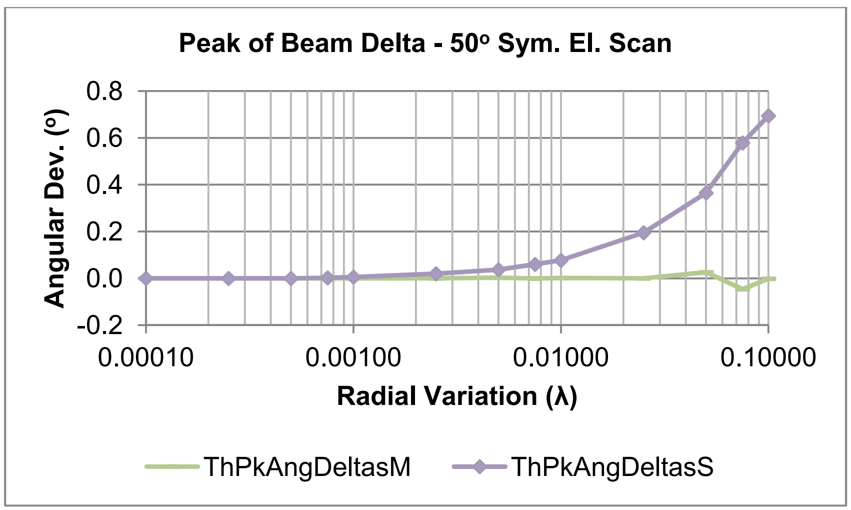

(c)

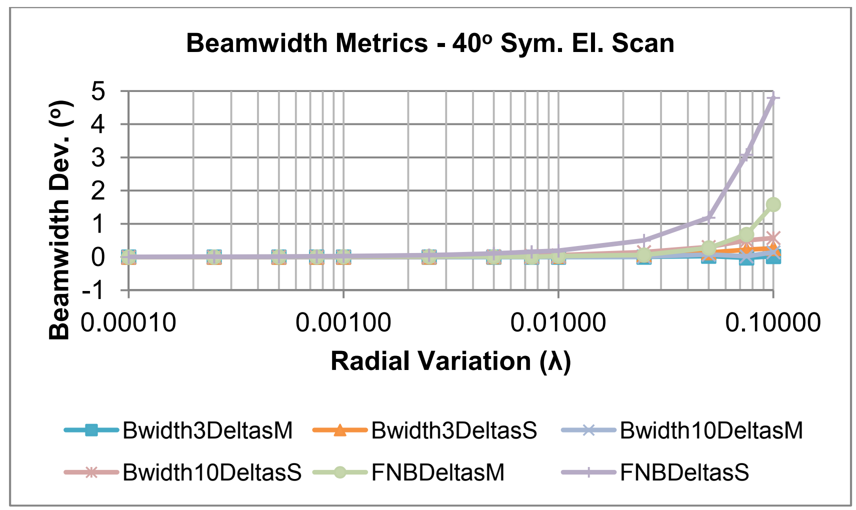

(d)

Figure B.48. *Statistical data for a $1/2\lambda$ spaced, 10 element, modified Taylor array versus radial randomization.* Directivity and sidelobe level (a), LSLLdB (b), beam pointing (c), and beamwidth (d) results are illustrated.

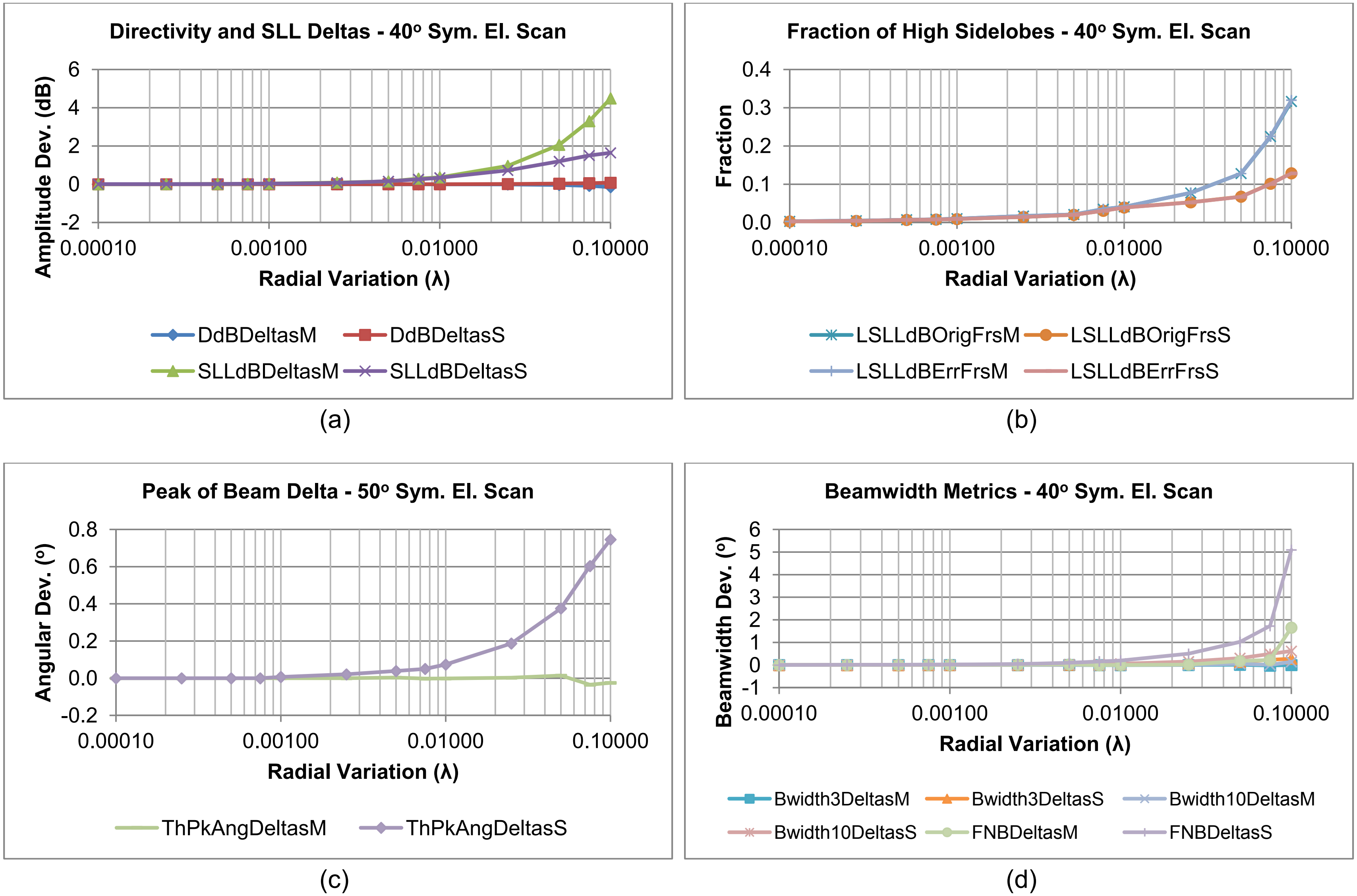

Figure B.49. *Statistical data for a $1/2\lambda$ spaced, 10 element, powers of cosine on a pedestal array versus radial randomization.* Directivity and sidelobe level (a), LSLLdB (b), beam pointing (c), and beamwidth (d) results are illustrated.

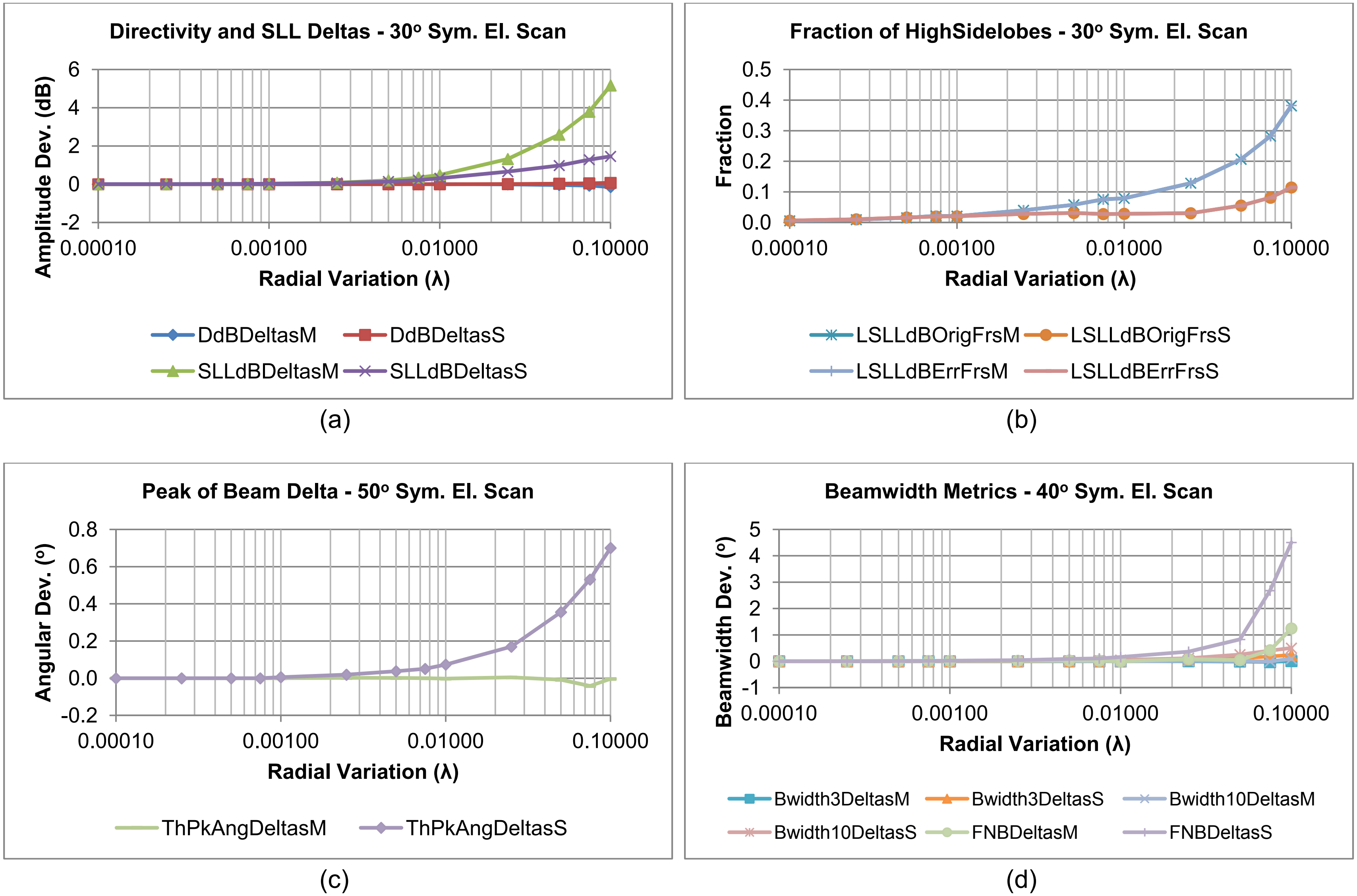

Figure B.50. *Statistical data for a $1/2\lambda$ spaced, 10 element, Taylor array versus radial randomization.* Directivity and sidelobe level (a), LSLLdB (b), beam pointing (c), and beamwidth (d) results are illustrated.

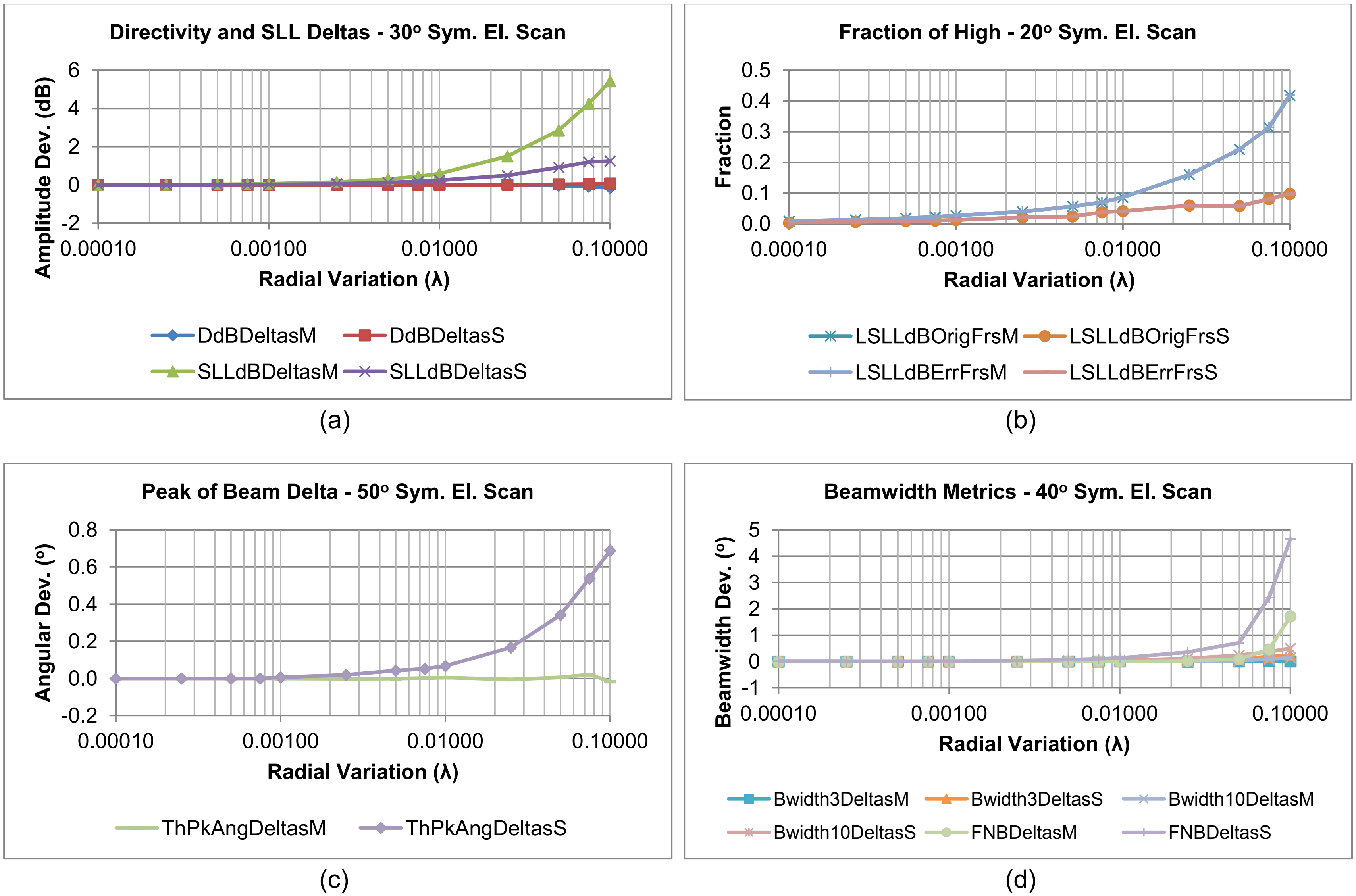

Figure B.51. *Statistical data for a 1/2λ spaced, 10 element, Dolph-Chebyshev array versus radial randomization.* Directivity and sidelobe level (a), LSLLdB (b), beam pointing (c), and beamwidth (d) results are illustrated.

$1/2\,\lambda$ Element Spacing

30 dB Initial Design Sidelobe Level

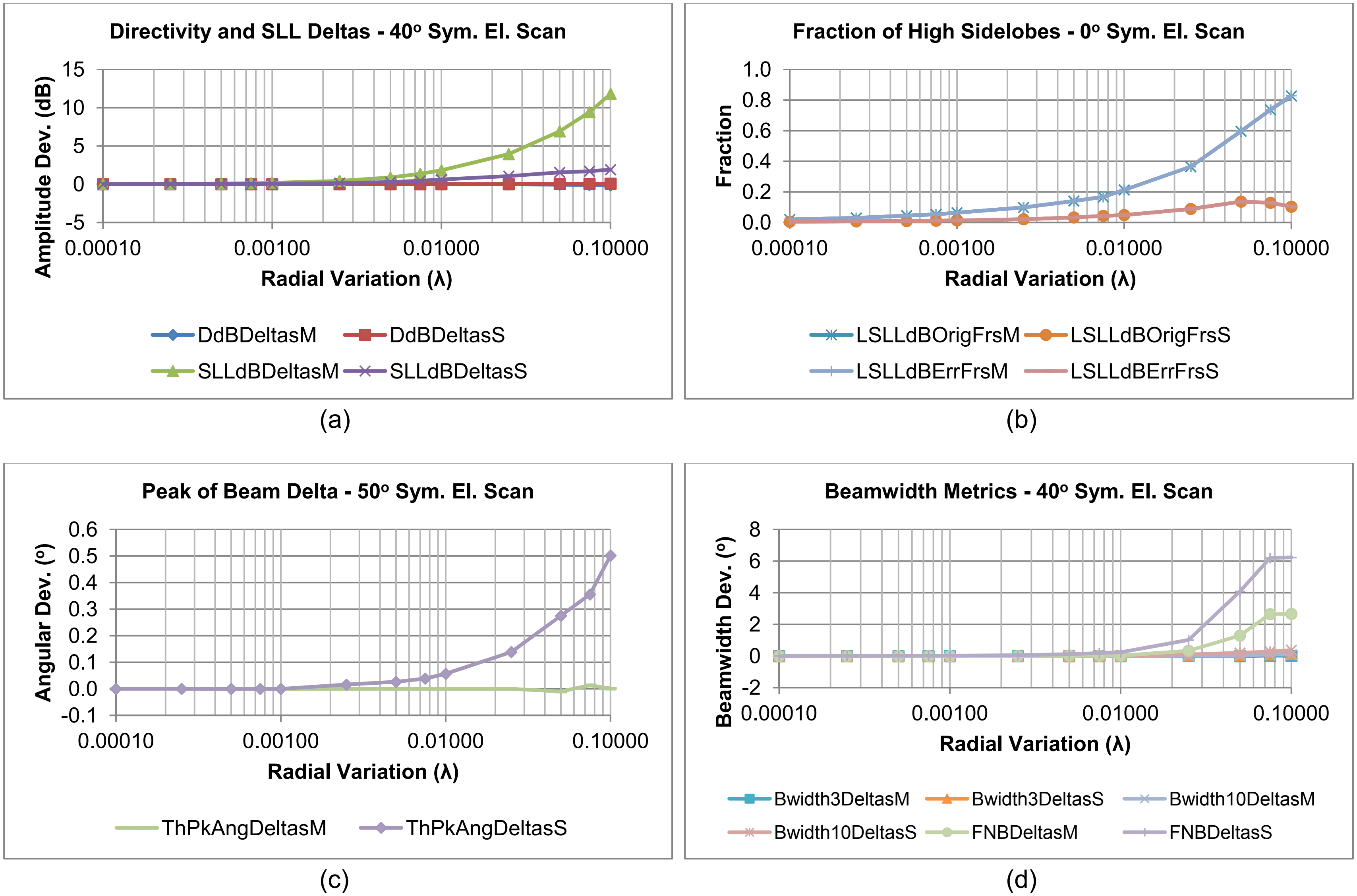

Figure B.52. *Statistical data for a $1/2\lambda$ spaced, 13 element, Dolph-Chebyshev array versus radial randomization.* Directivity and sidelobe level (a), LSLLdB (b), beam pointing (c), and beamwidth (d) results are illustrated.

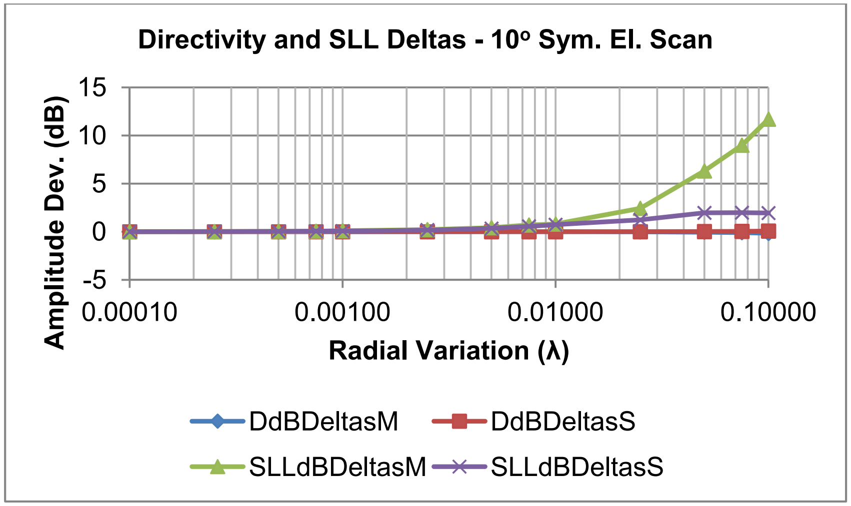

(a)

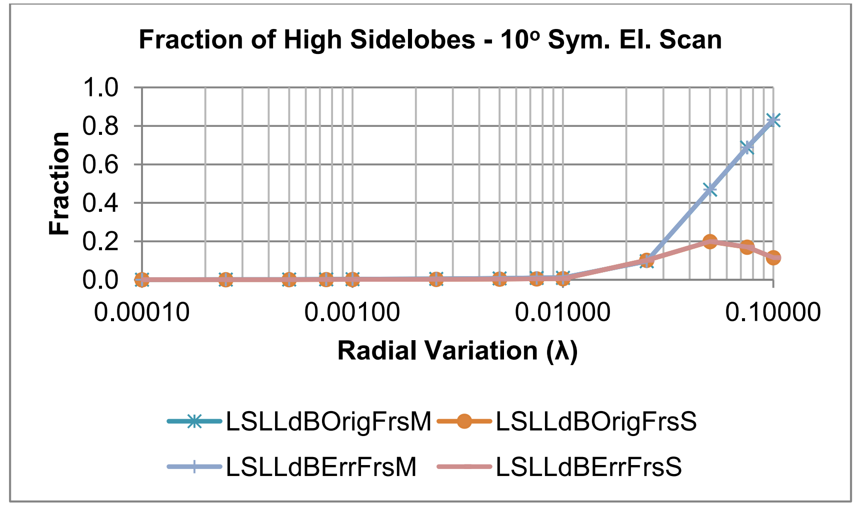

(b)

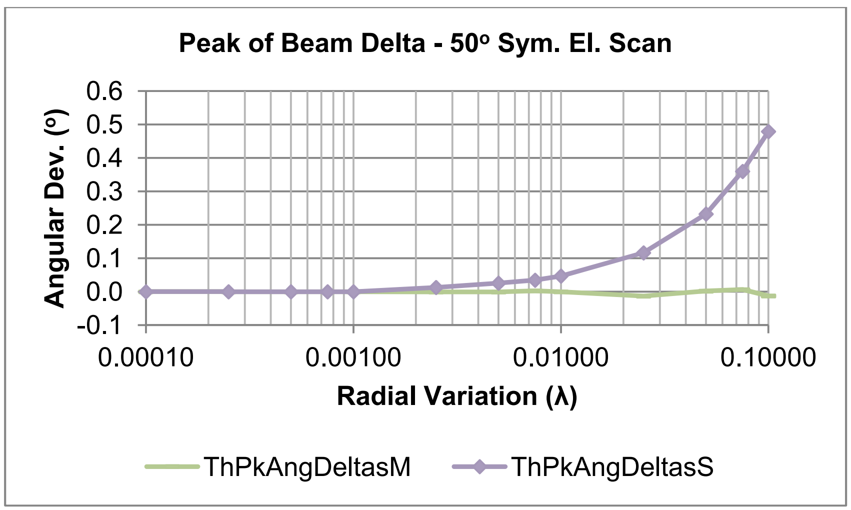

(c)

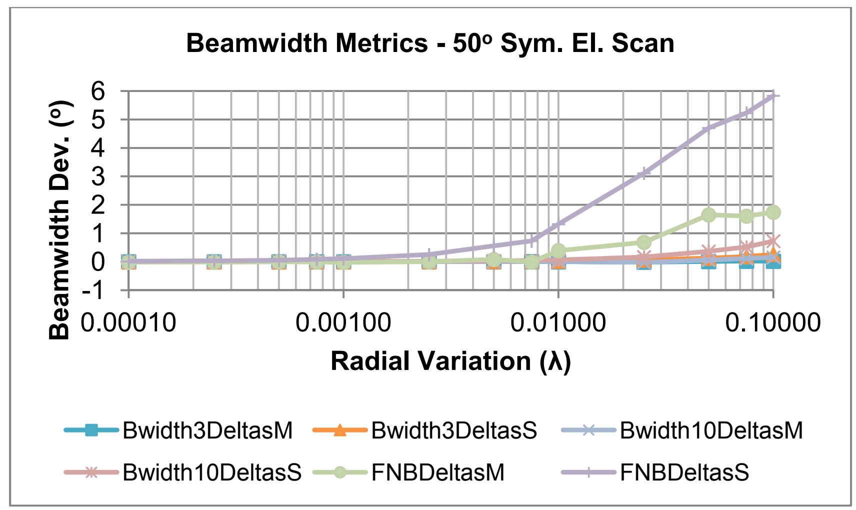

(d)

Figure B.53. *Statistical data for a $1/2\lambda$ spaced, 15 element, modified Taylor array versus radial randomization.* Directivity and sidelobe level (a), LSLLdB (b), beam pointing (c), and beamwidth (d) results are illustrated.

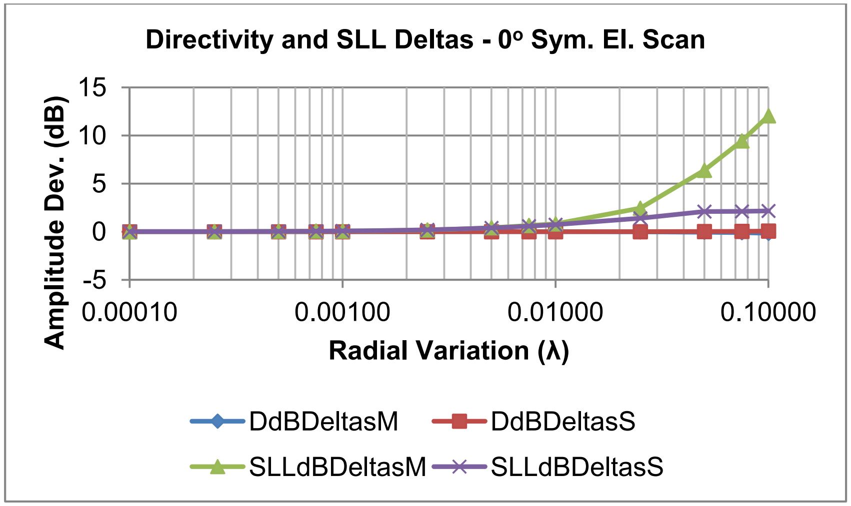

(a)

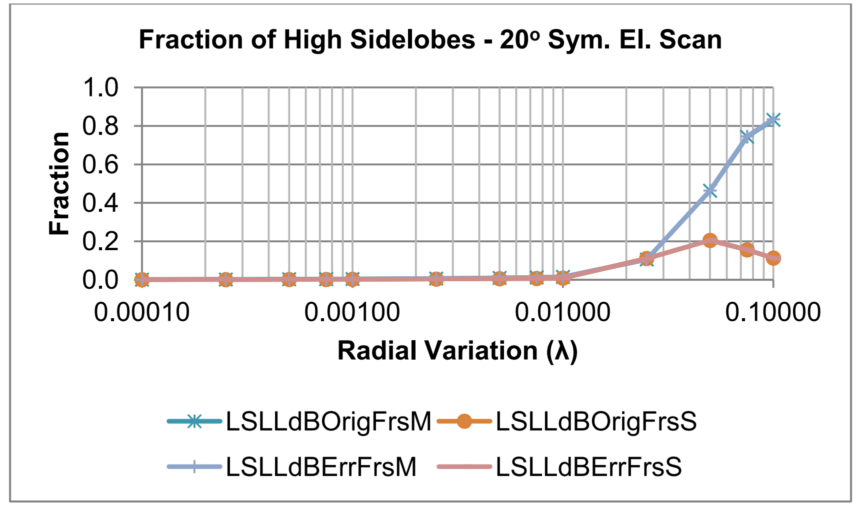

(b)

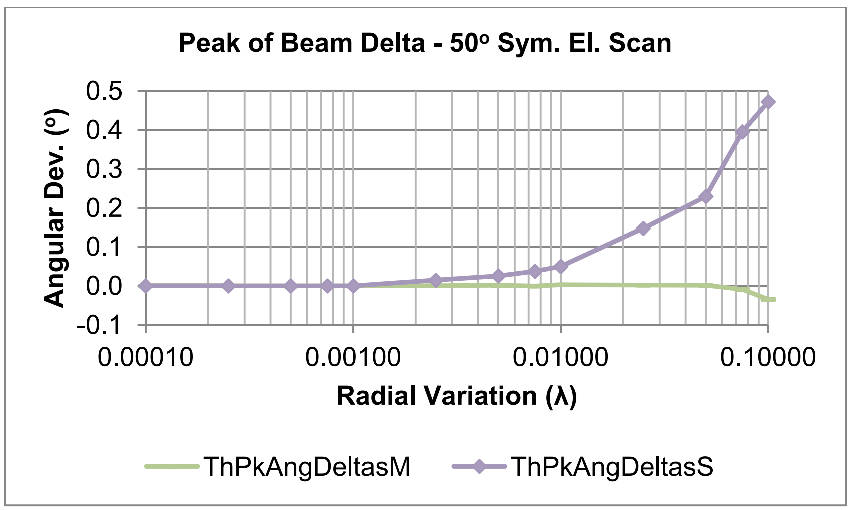

(c)

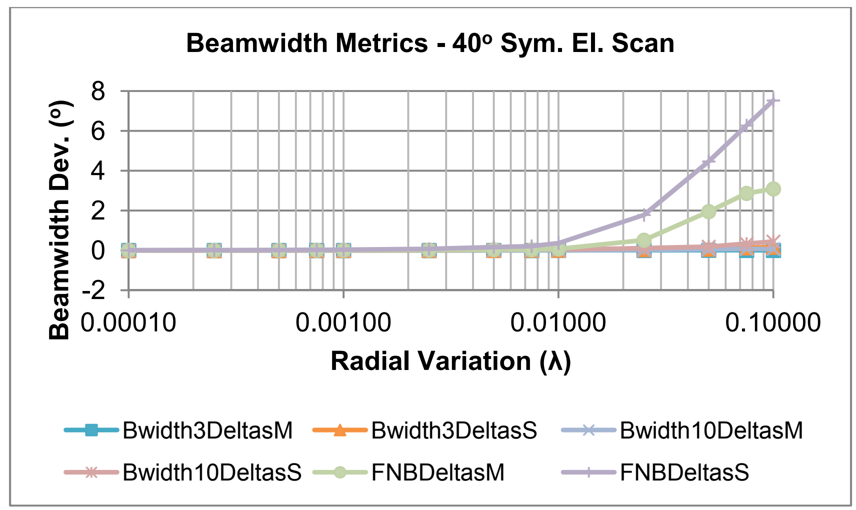

(d)

Figure B.54. *Statistical data for a 1/2λ spaced, 17 element, powers of cosine on a pedestal array versus radial randomization.* Directivity and sidelobe level (a), LSLLdB (b), beam pointing (c), and beamwidth (d) results are illustrated.

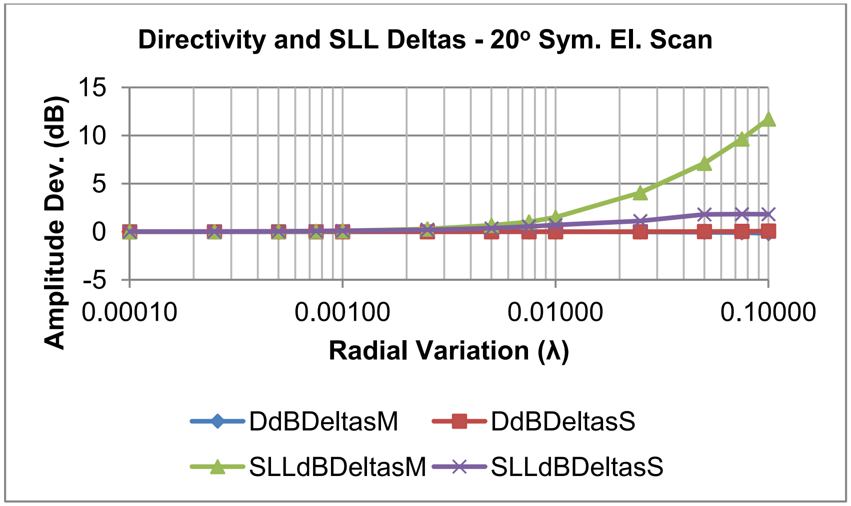

(a)

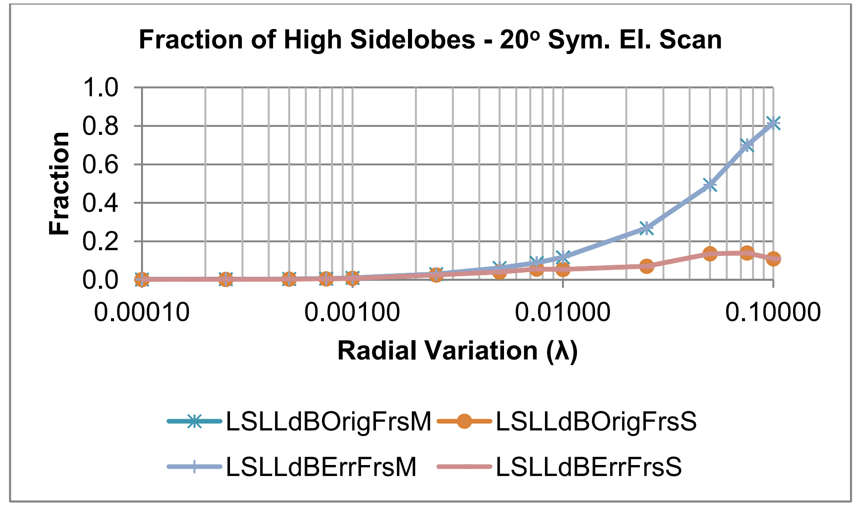

(b)

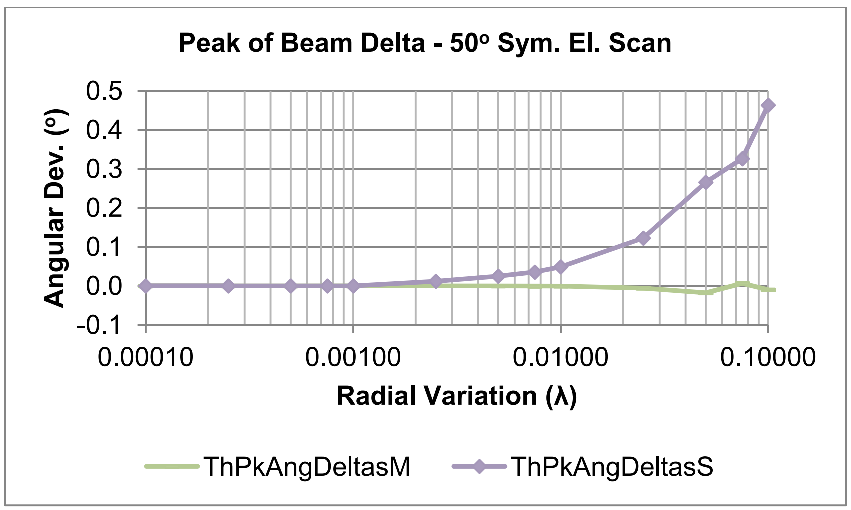

(c)

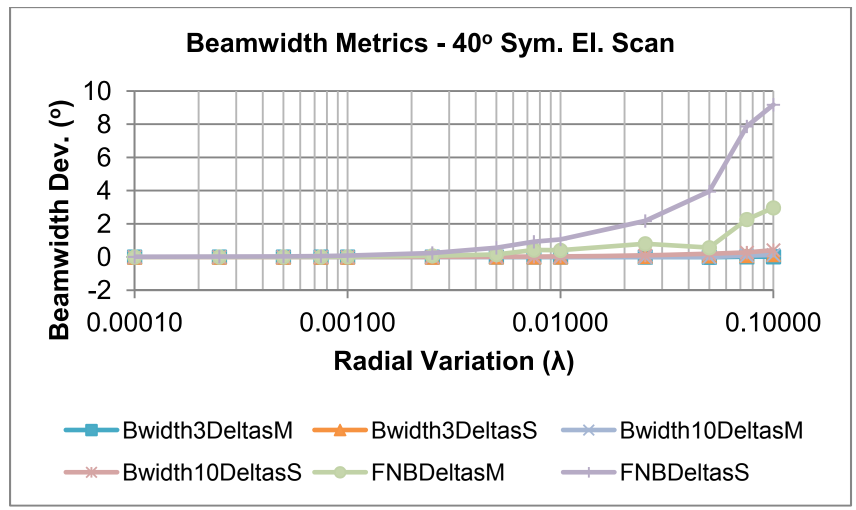

(d)

Figure B.55. *Statistical data for a 1/2λ spaced, 14 element, Taylor array versus radial randomization.* Directivity and sidelobe level (a), LSLLdB (b), beam pointing (c), and beamwidth (d) results are illustrated.

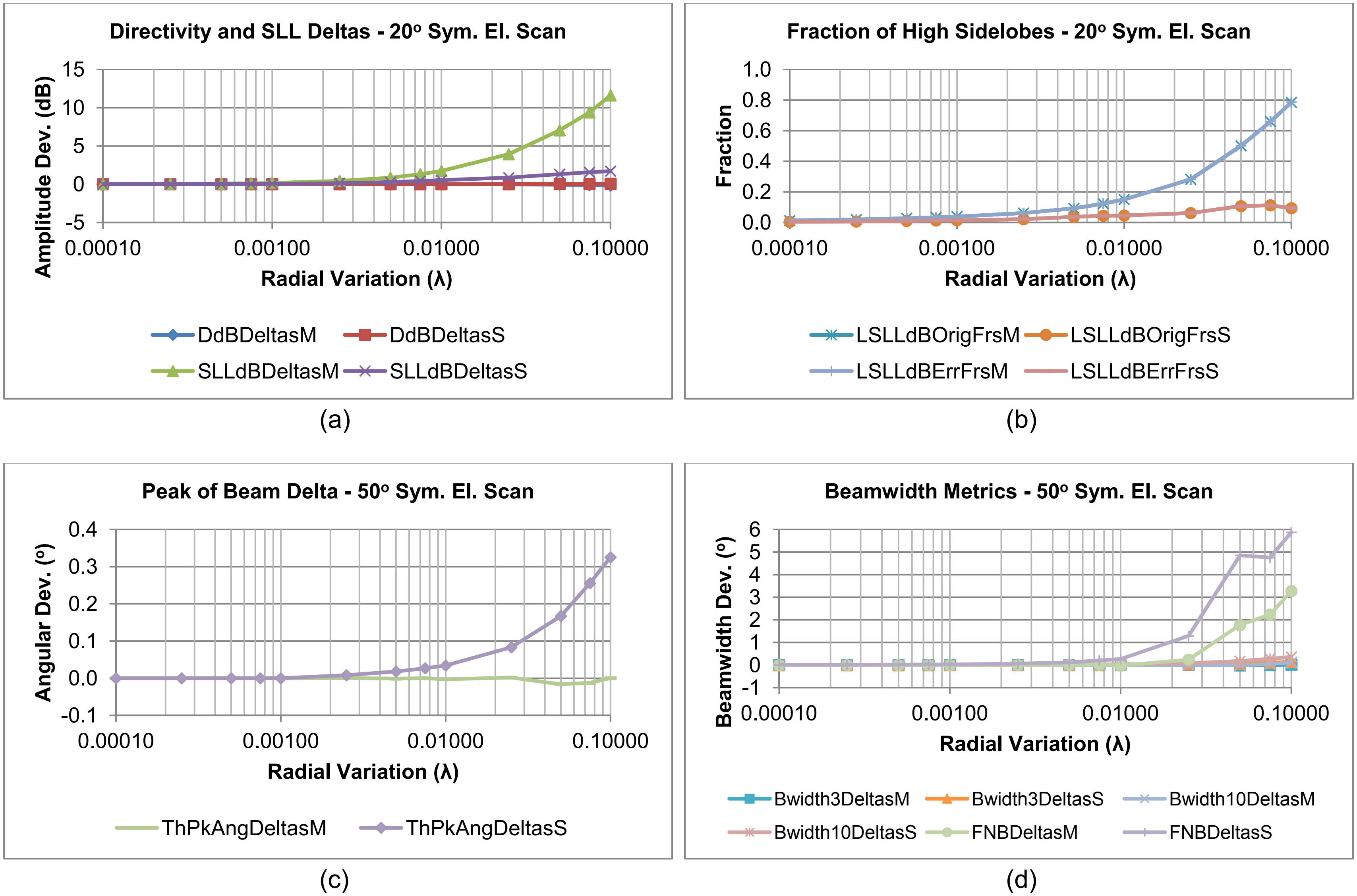

Figure B.56. *Statistical data for a $1/2\lambda$ spaced, 17 element, Dolph-Chebyshev array versus radial randomization.* Directivity and sidelobe level (a), LSLLdB (b), beam pointing (c), and beamwidth (d) results are illustrated.

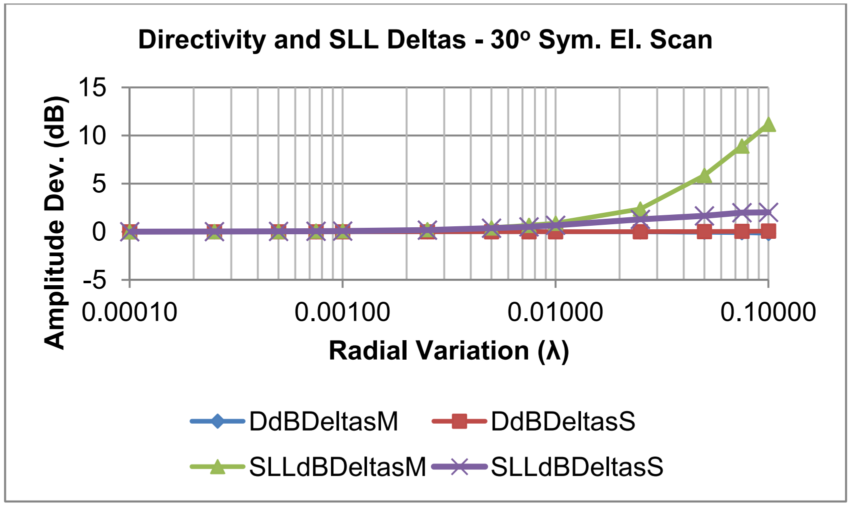

(a)

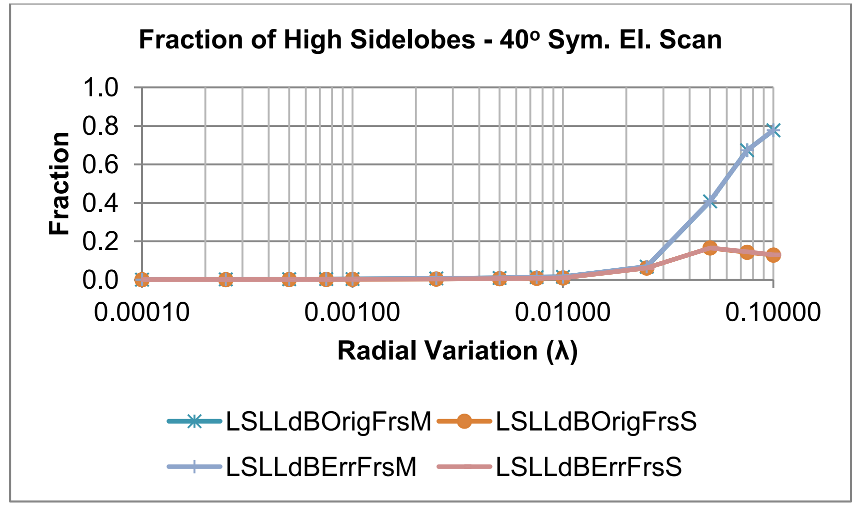

(b)

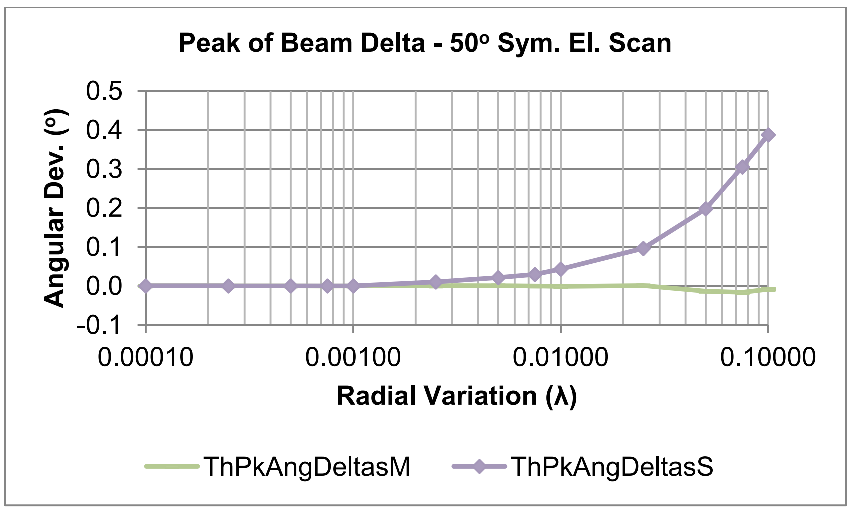

(c)

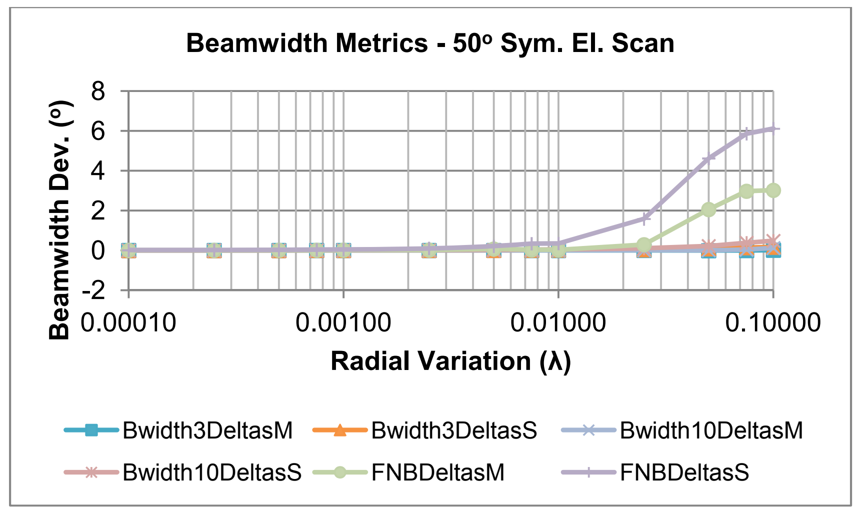

(d)

Figure B.57. *Statistical data for a* $1/2\lambda$ *spaced, 17 element, modified Taylor array versus radial randomization.* Directivity and sidelobe level (a), LSLLdB (b), beam pointing (c), and beamwidth (d) results are illustrated.

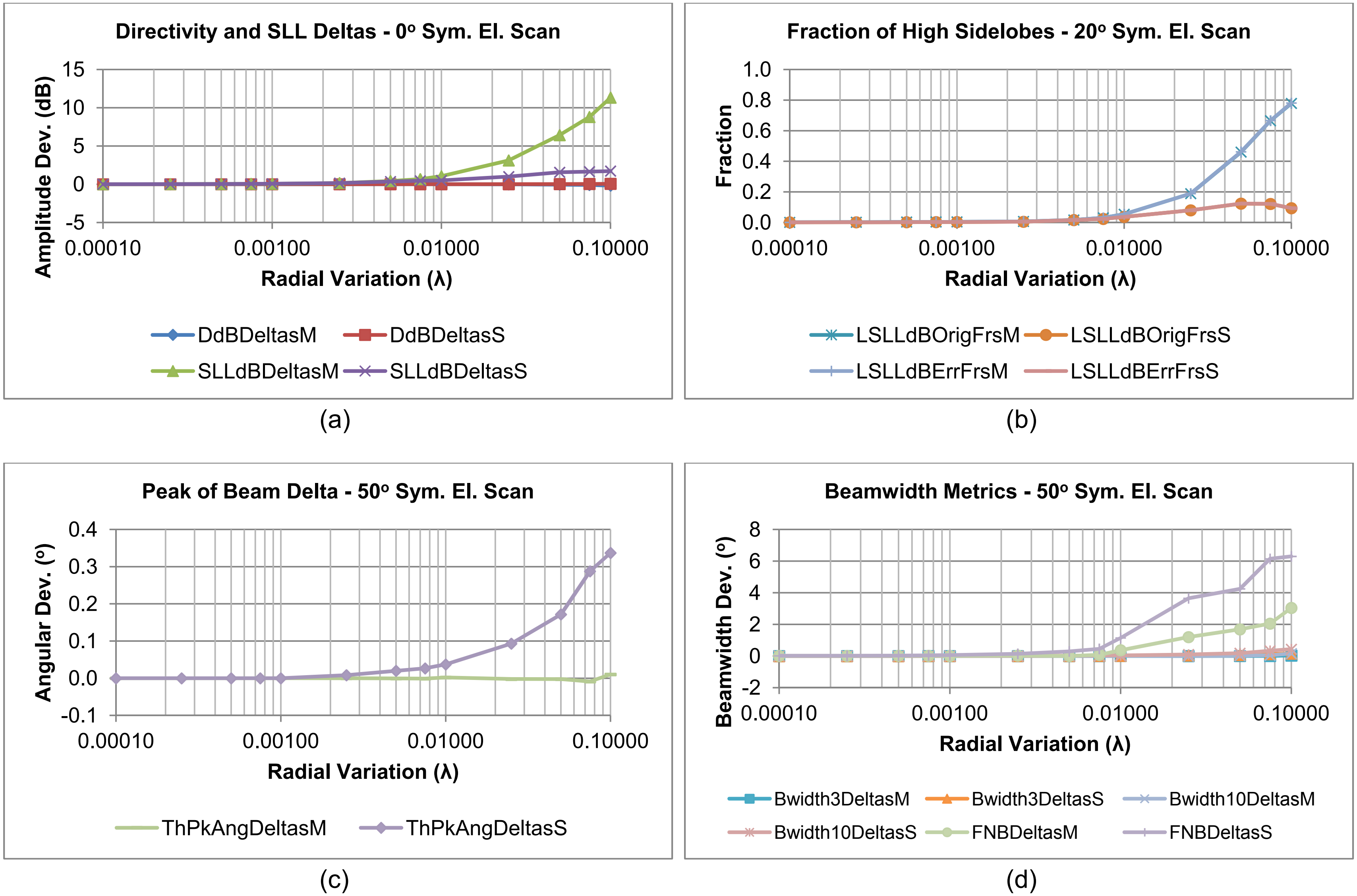

Figure B.58. *Statistical data for a 1/2λ spaced, 17 element, Taylor array versus radial randomization.* Directivity and sidelobe level (a), LSLLdB (b), beam pointing (c), and beamwidth (d) results are illustrated.

$1/2\,\lambda$ Element Spacing

40 dB Initial Design Sidelobe Level

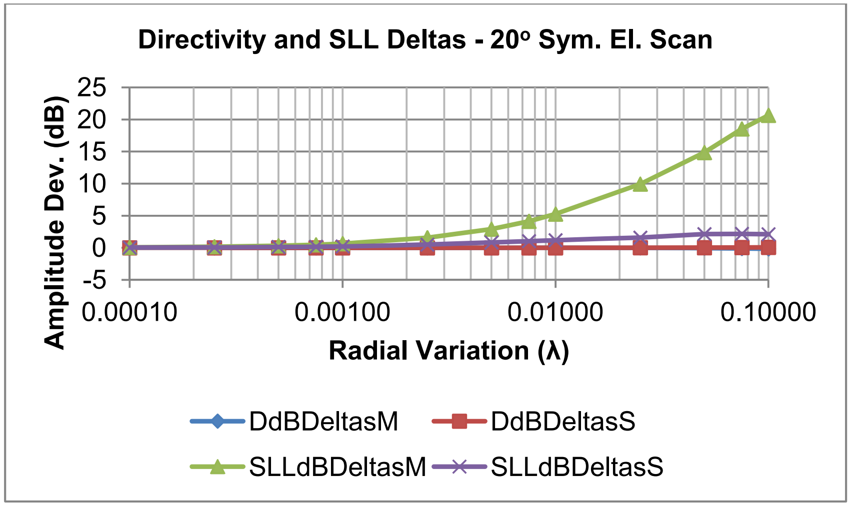

(a)

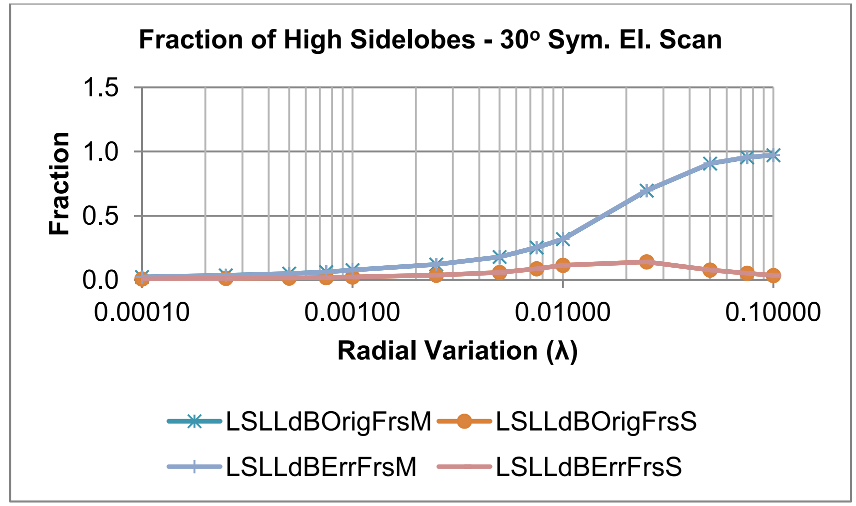

(b)

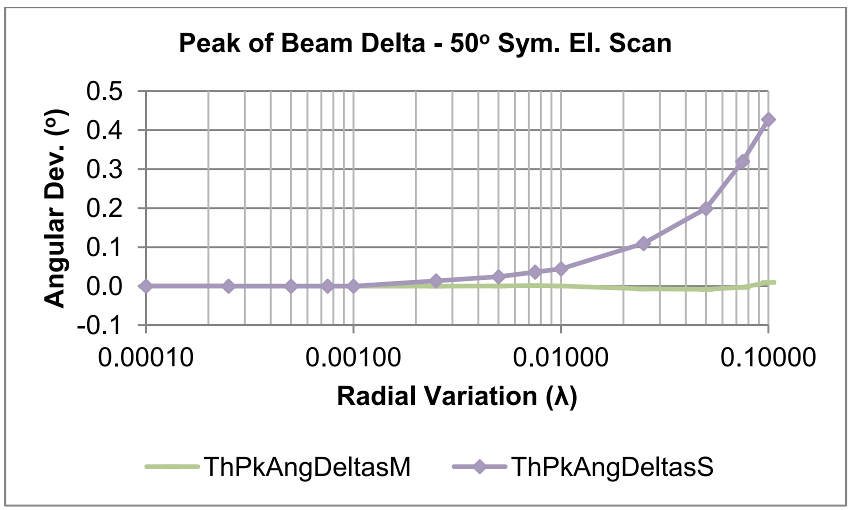

(c)

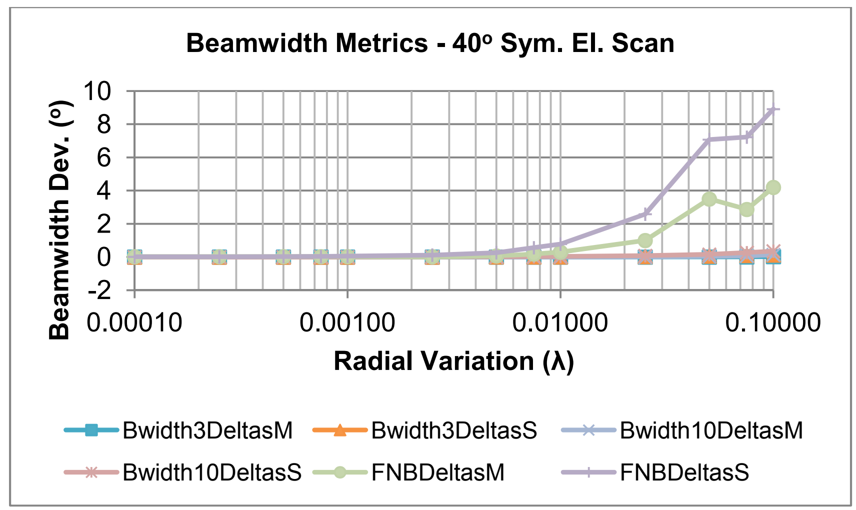

(d)

Figure B.59. *Statistical data for a $1/2\lambda$ spaced, 16 element, Dolph-Chebyshev array versus radial randomization.* Directivity and sidelobe level (a), LSLLdB (b), beam pointing (c), and beamwidth (d) results are illustrated.

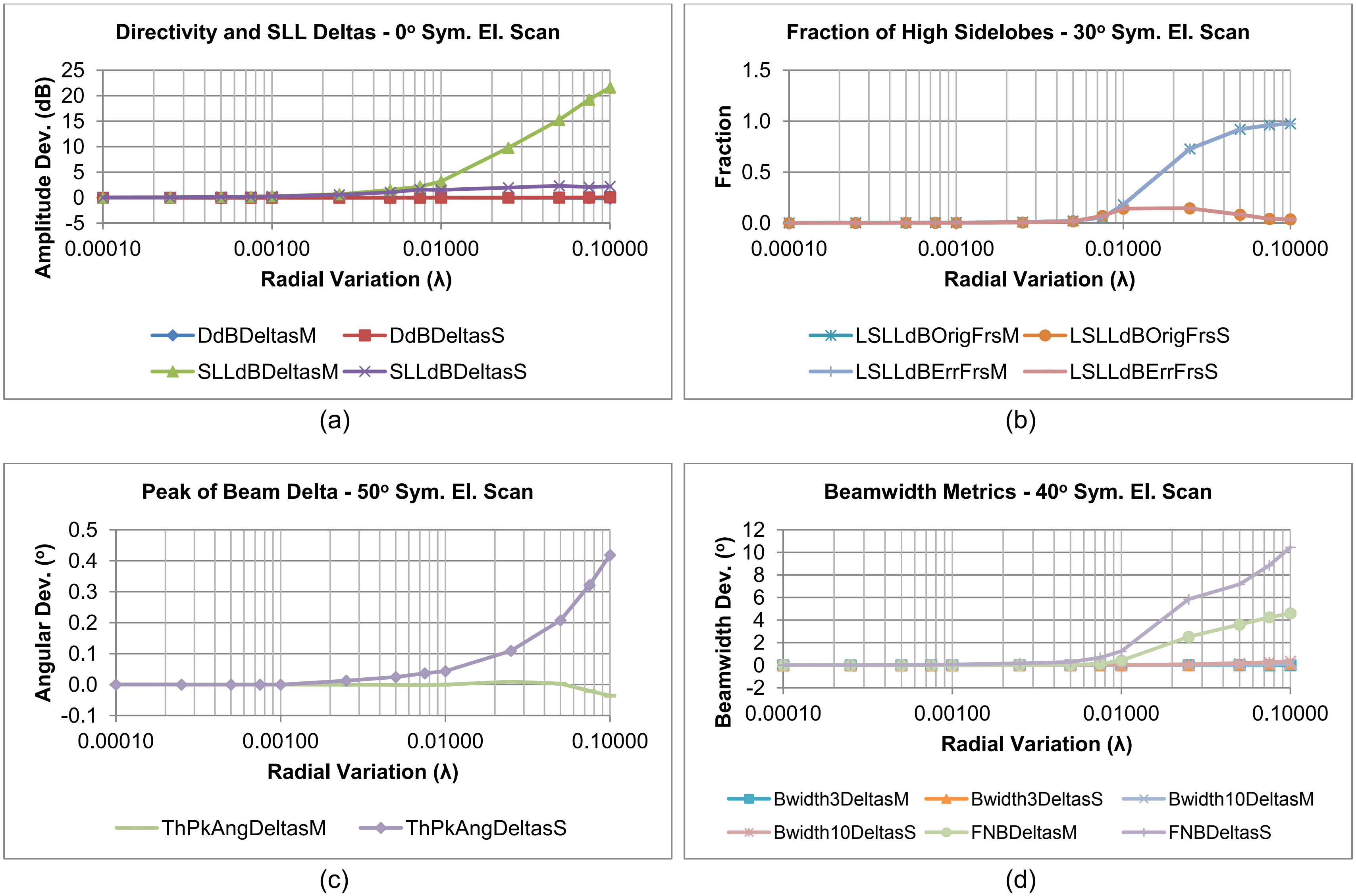

Figure B.60. *Statistical data for a 1/2λ spaced, 18 element, modified Taylor array versus radial randomization.* Directivity and sidelobe level (a), LSLLdB (b), beam pointing (c), and beamwidth (d) results are illustrated.

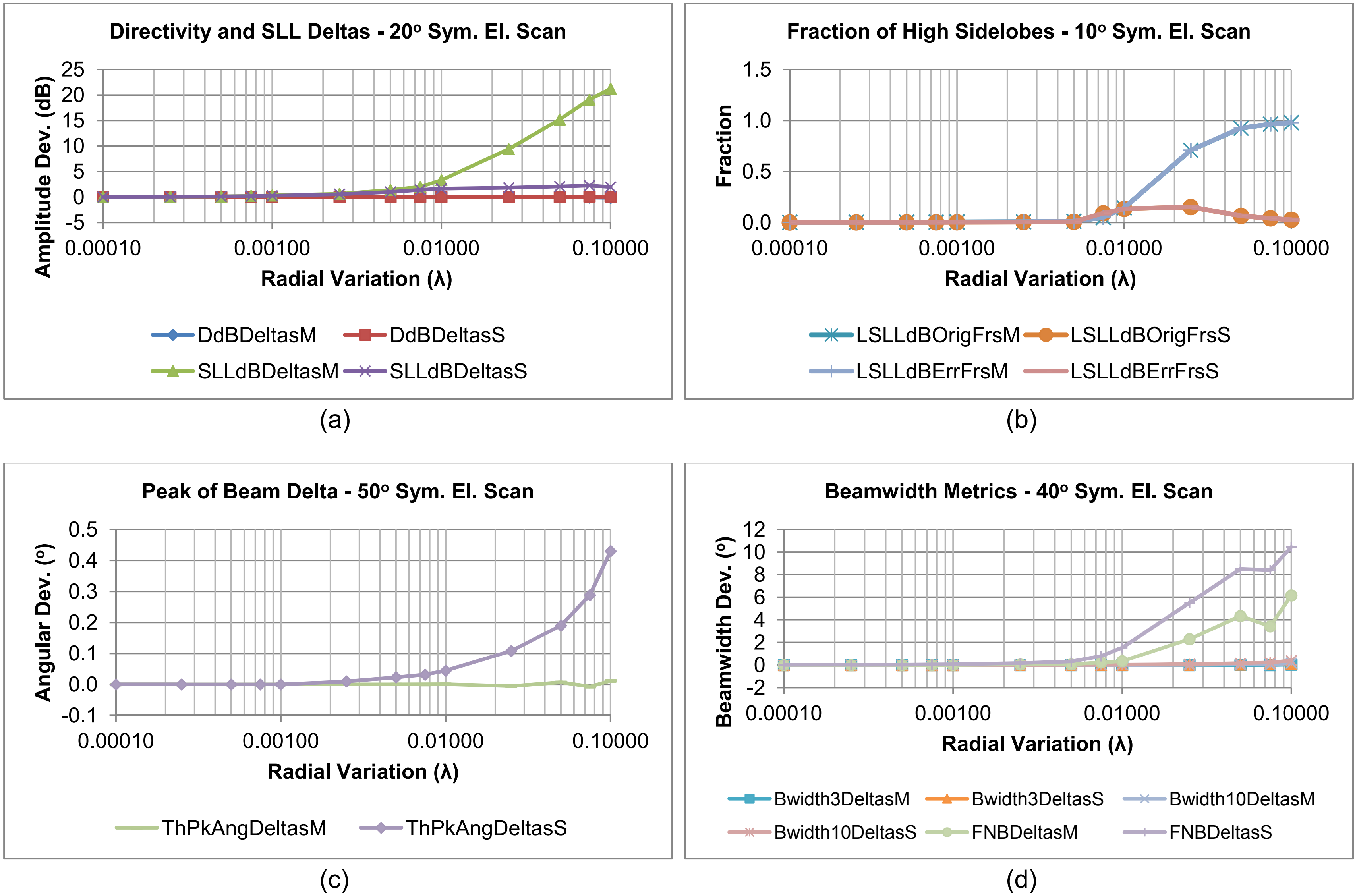

Figure B.61. *Statistical data for a 1/2λ spaced, 23 element, powers of cosine on a pedestal array versus radial randomization.* Directivity and sidelobe level (a), LSLLdB (b), beam pointing (c), and beamwidth (d) results are illustrated.

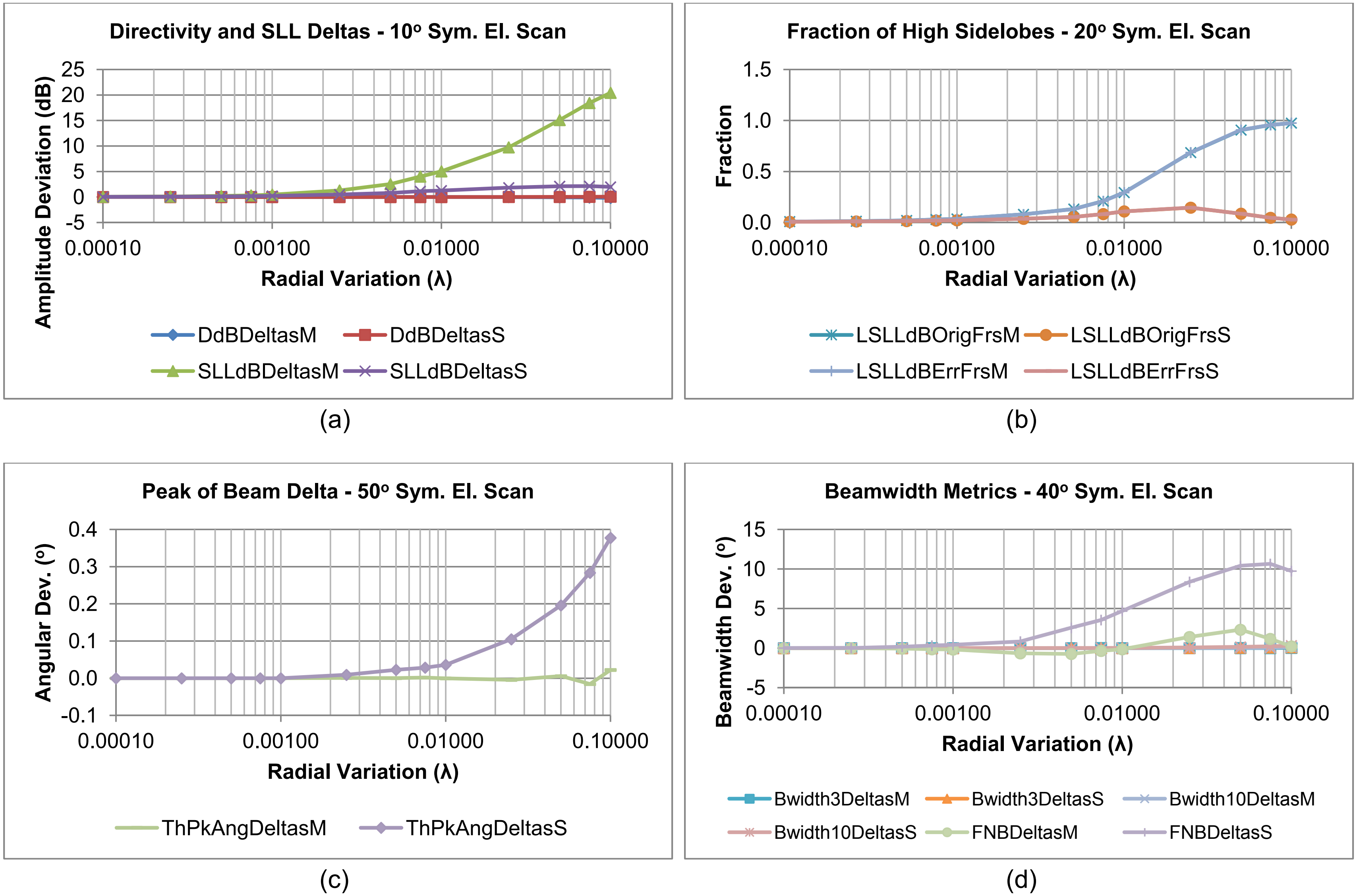

Figure B.62. *Statistical data for a $1/2\lambda$ spaced, 18 element, Taylor array versus radial randomization.* Directivity and sidelobe level (a), LSLLdB (b), beam pointing (c), and beamwidth (d) results are illustrated.

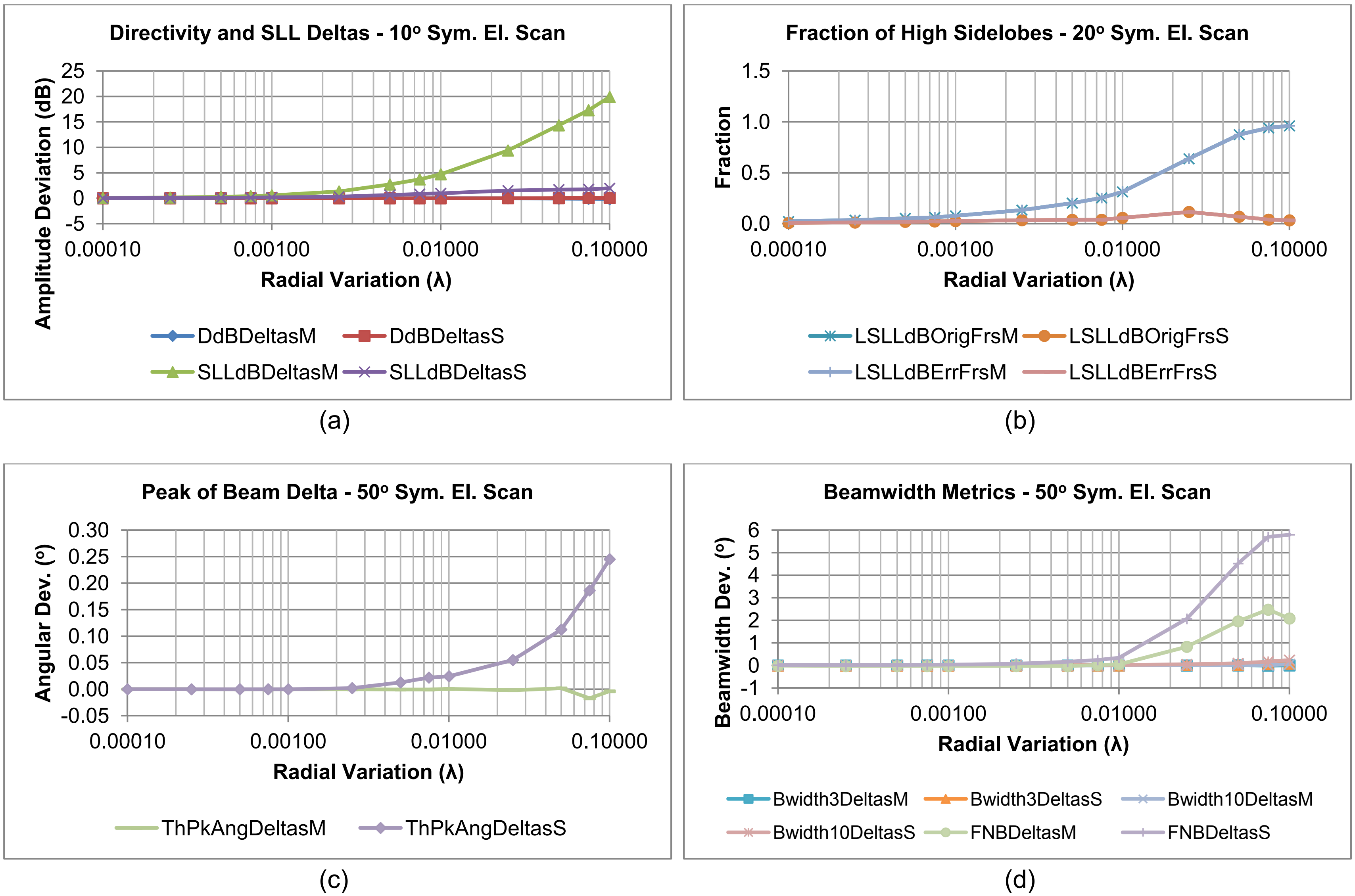

Figure B.63. *Statistical data for a $1/2\lambda$ spaced, 23 element, Dolph-Chebyshev array versus radial randomization.* Directivity and sidelobe level (a), LSLLdB (b), beam pointing (c), and beamwidth (d) results are illustrated.

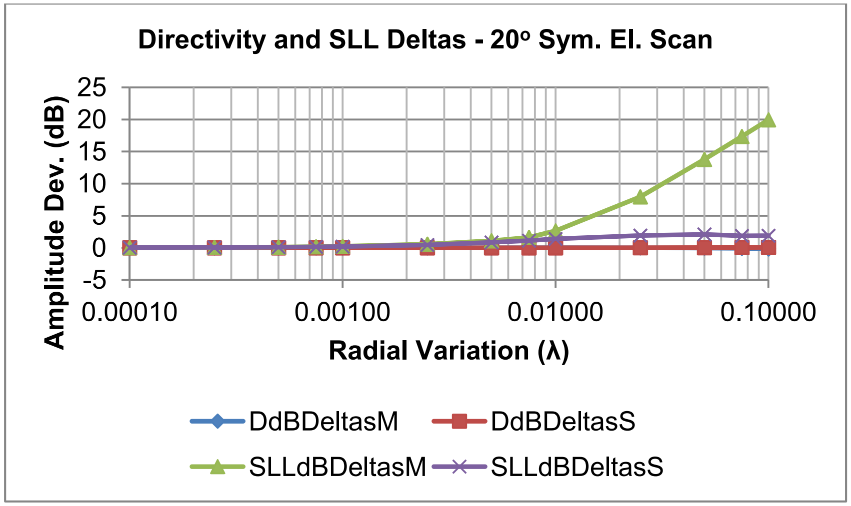

(a)

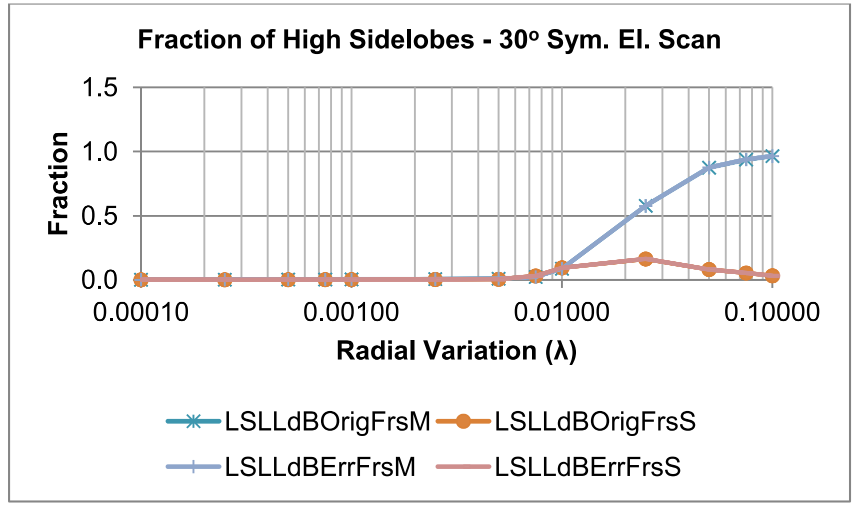

(b)

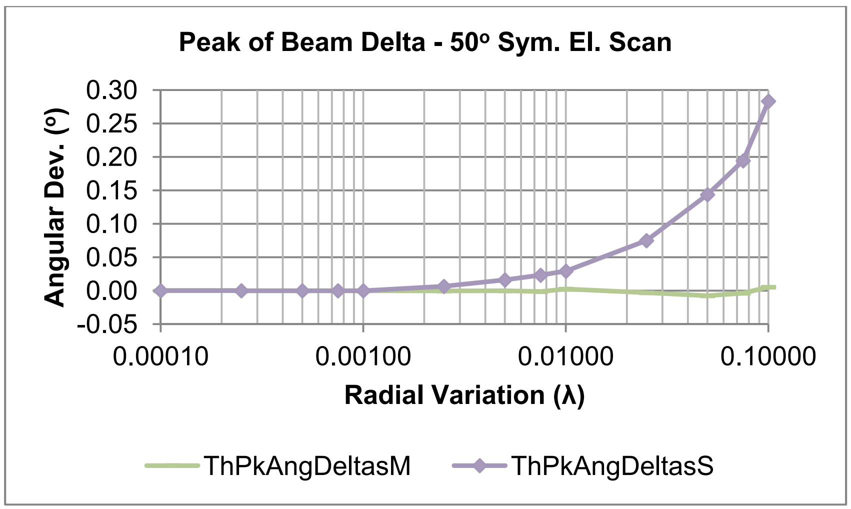

(c)

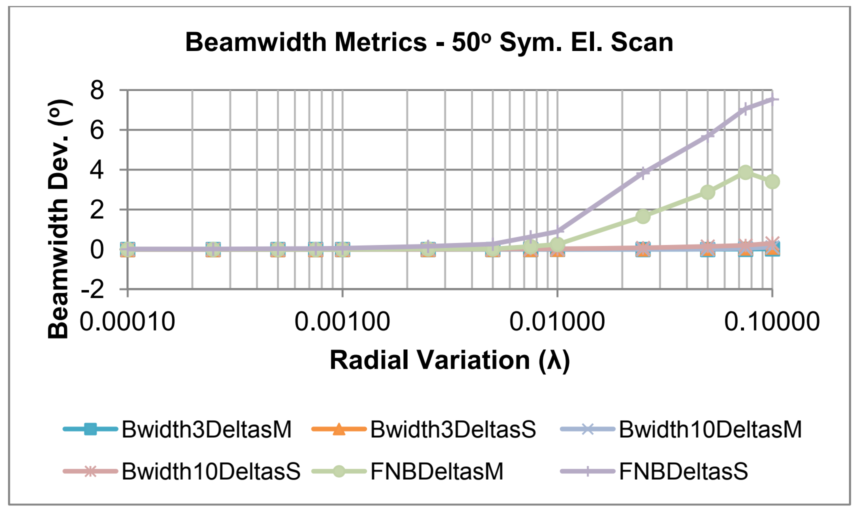

(d)

Figure B.64. *Statistical data for a $1/2\lambda$ spaced, 23 element, modified Taylor array versus radial randomization.* Directivity and sidelobe level (a), LSLLdB (b), beam pointing (c), and beamwidth (d) results are illustrated.

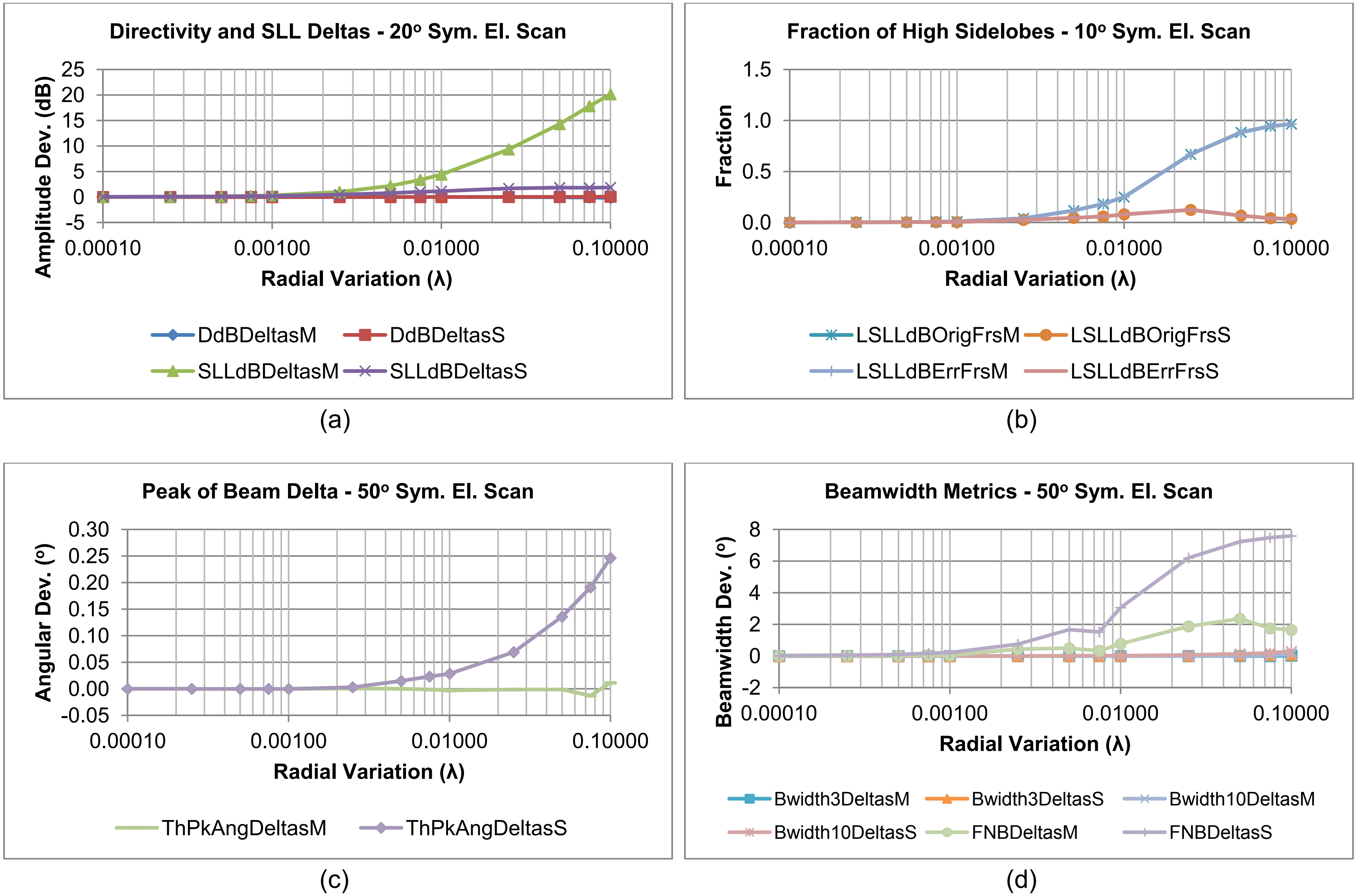

Figure B.65. *Statistical data for a $1/2\lambda$ spaced, 23 element, Taylor array versus radial randomization.* Directivity and sidelobe level (a), LSLLdB (b), beam pointing (c), and beamwidth (d) results are illustrated.

$1/2\,\lambda$ Element Spacing

50 dB Initial Design Sidelobe Level

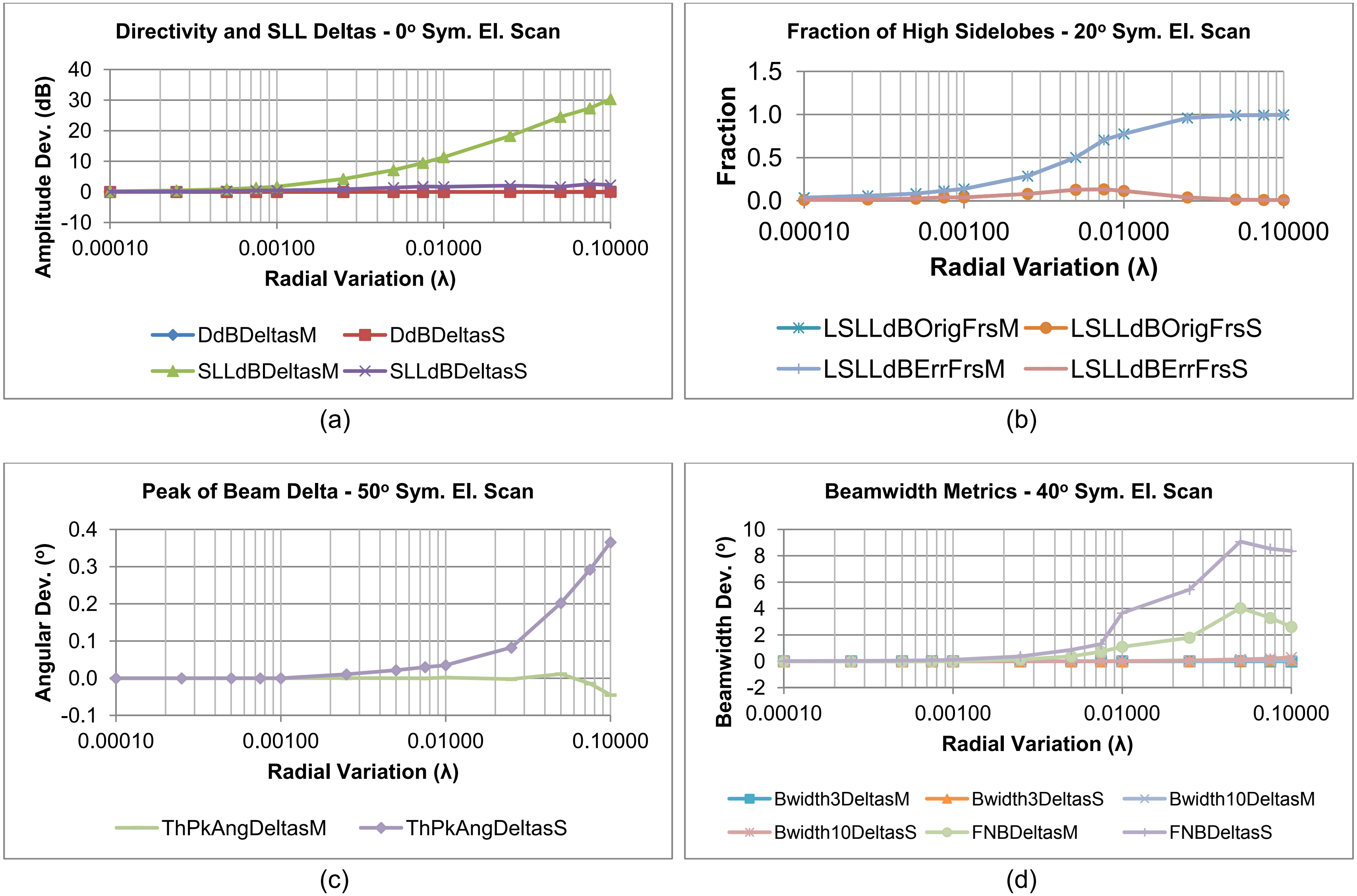

Figure B.66. *Statistical data for a $1/2\lambda$ spaced, 19 element, Dolph-Chebyshev array versus radial randomization.* Directivity and sidelobe level (a), LSLLdB (b), beam pointing (c), and beamwidth (d) results are illustrated.

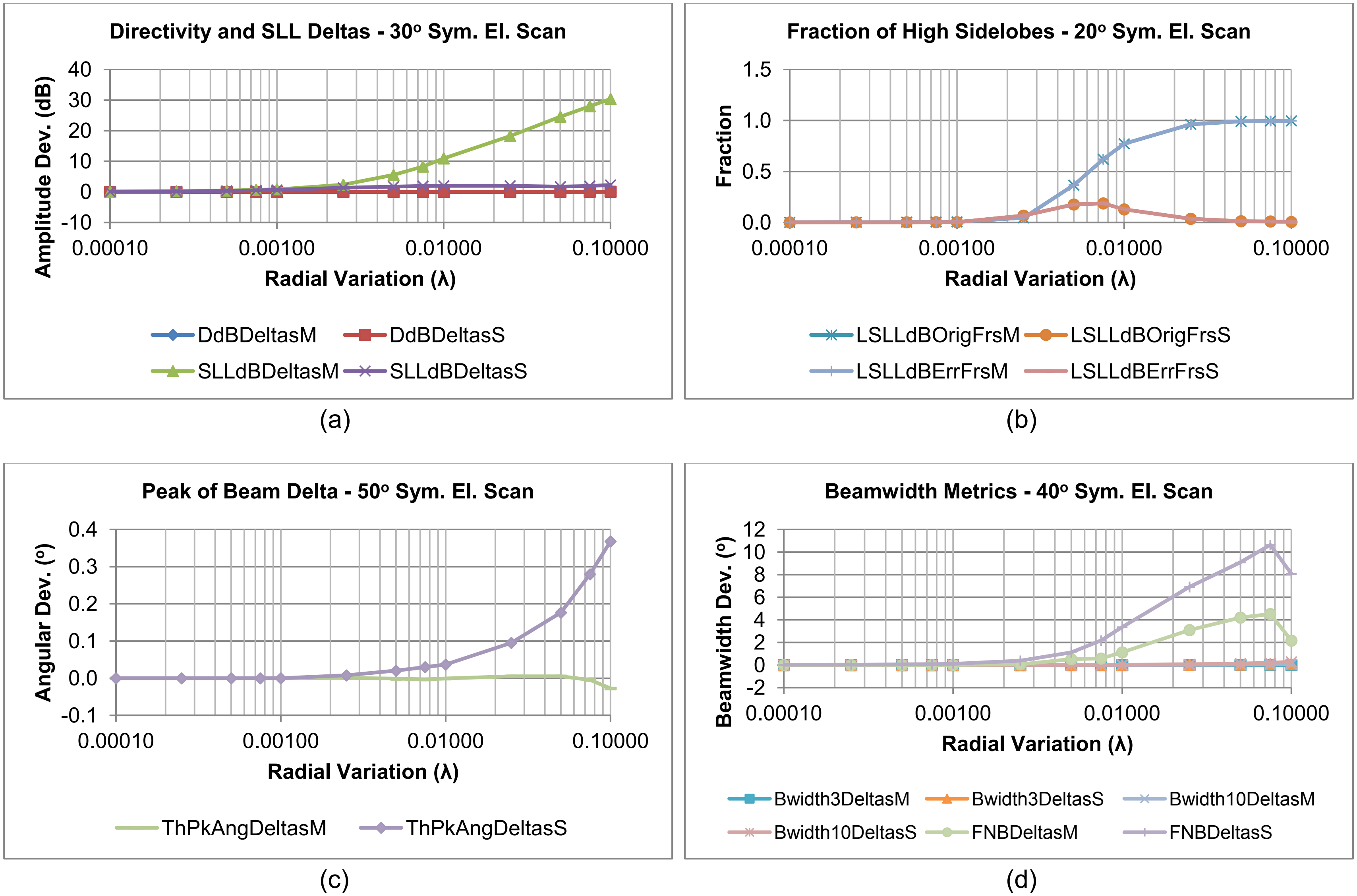

Figure B.67. *Statistical data for a $1/2\lambda$ spaced, 22 element, modified Taylor array versus radial randomization.* Directivity and sidelobe level (a), LSLLdB (b), beam pointing (c), and beamwidth (d) results are illustrated.

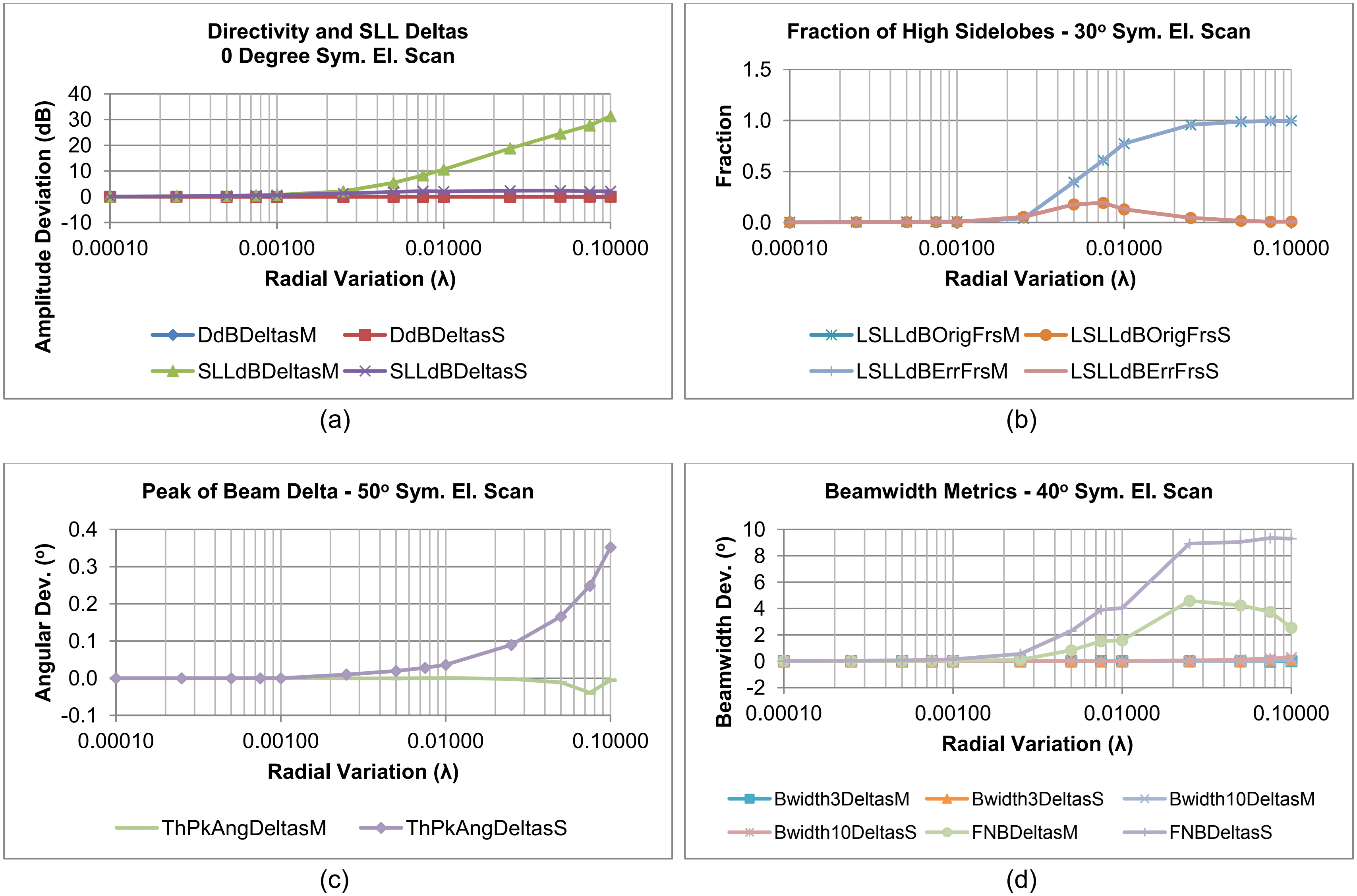

Figure B.68. *Statistical data for a $1/2\lambda$ spaced, 28 element, powers of cosine on a pedestal array versus radial randomization.* Directivity and sidelobe level (a), LSLLdB (b), beam pointing (c), and beamwidth (d) results are illustrated.

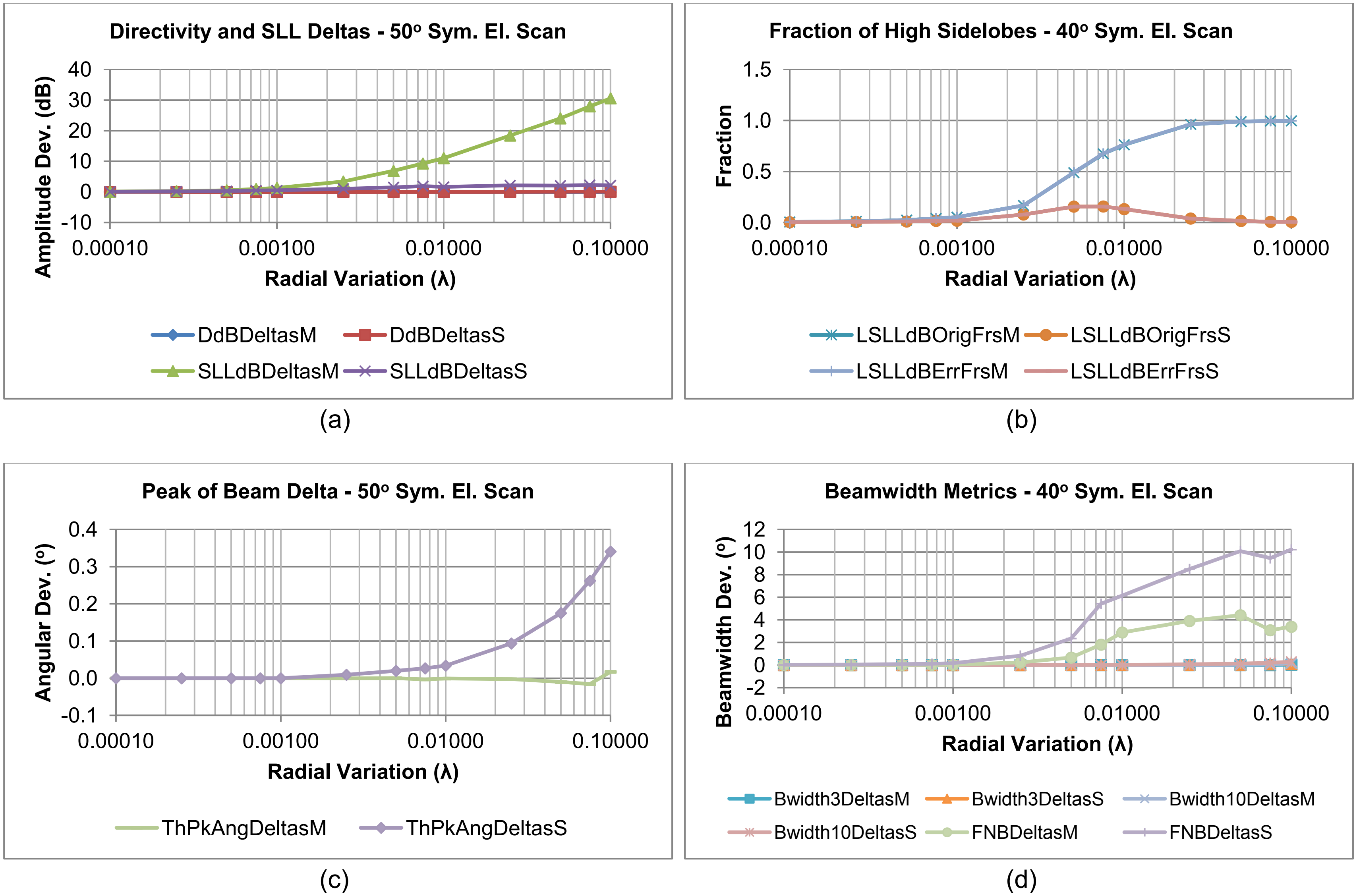

Figure B.69. *Statistical data for a $1/2\lambda$ spaced, 21 element, Taylor array versus radial randomization.* Directivity and sidelobe level (a), LSLLdB (b), beam pointing (c), and beamwidth (d) results are illustrated.

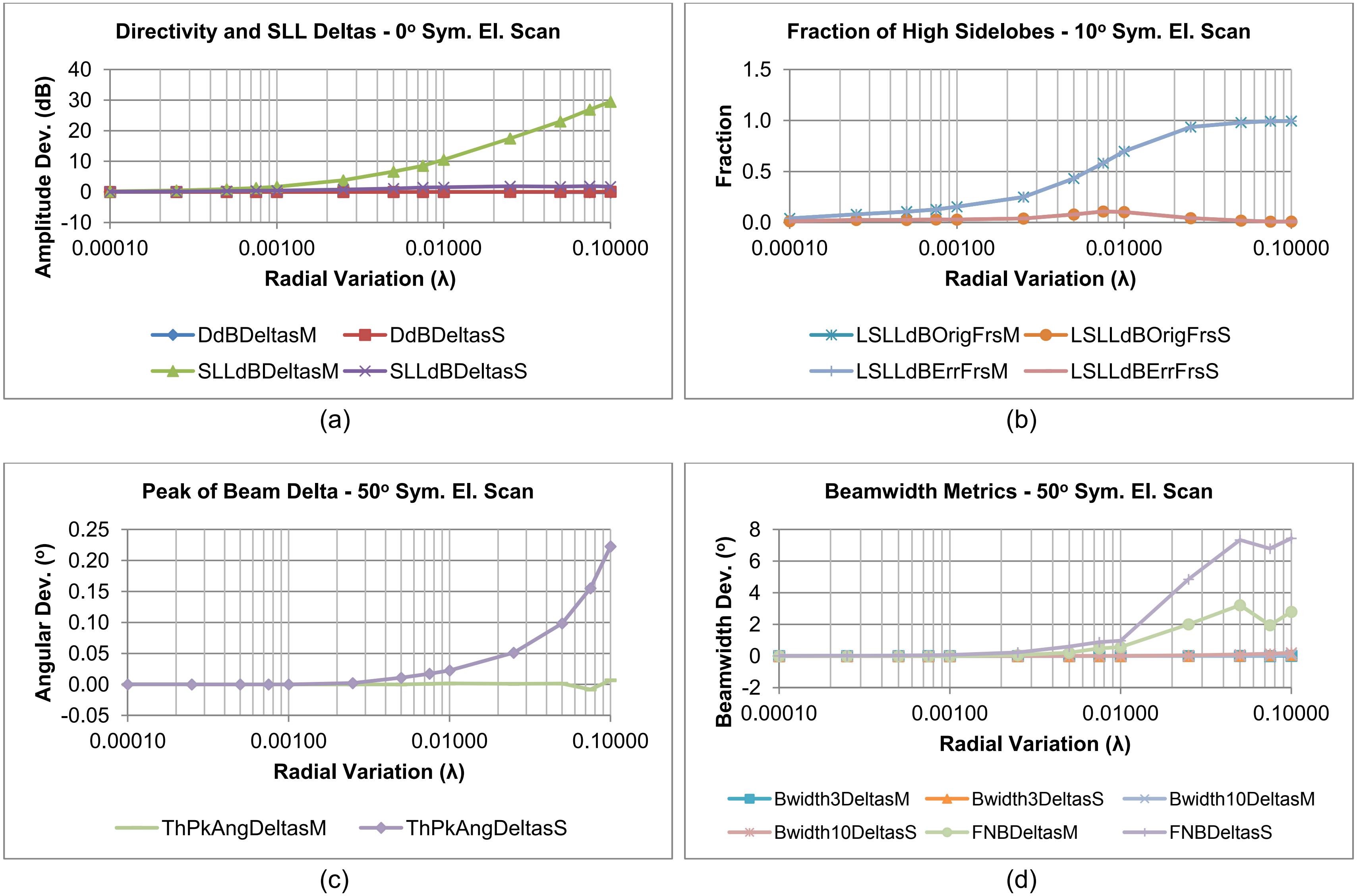

Figure B.70. *Statistical data for a 1/2λ spaced, 28 element, Dolph-Chebyshev array versus radial randomization.* Directivity and sidelobe level (a), LSLLdB (b), beam pointing (c), and beamwidth (d) results are illustrated.

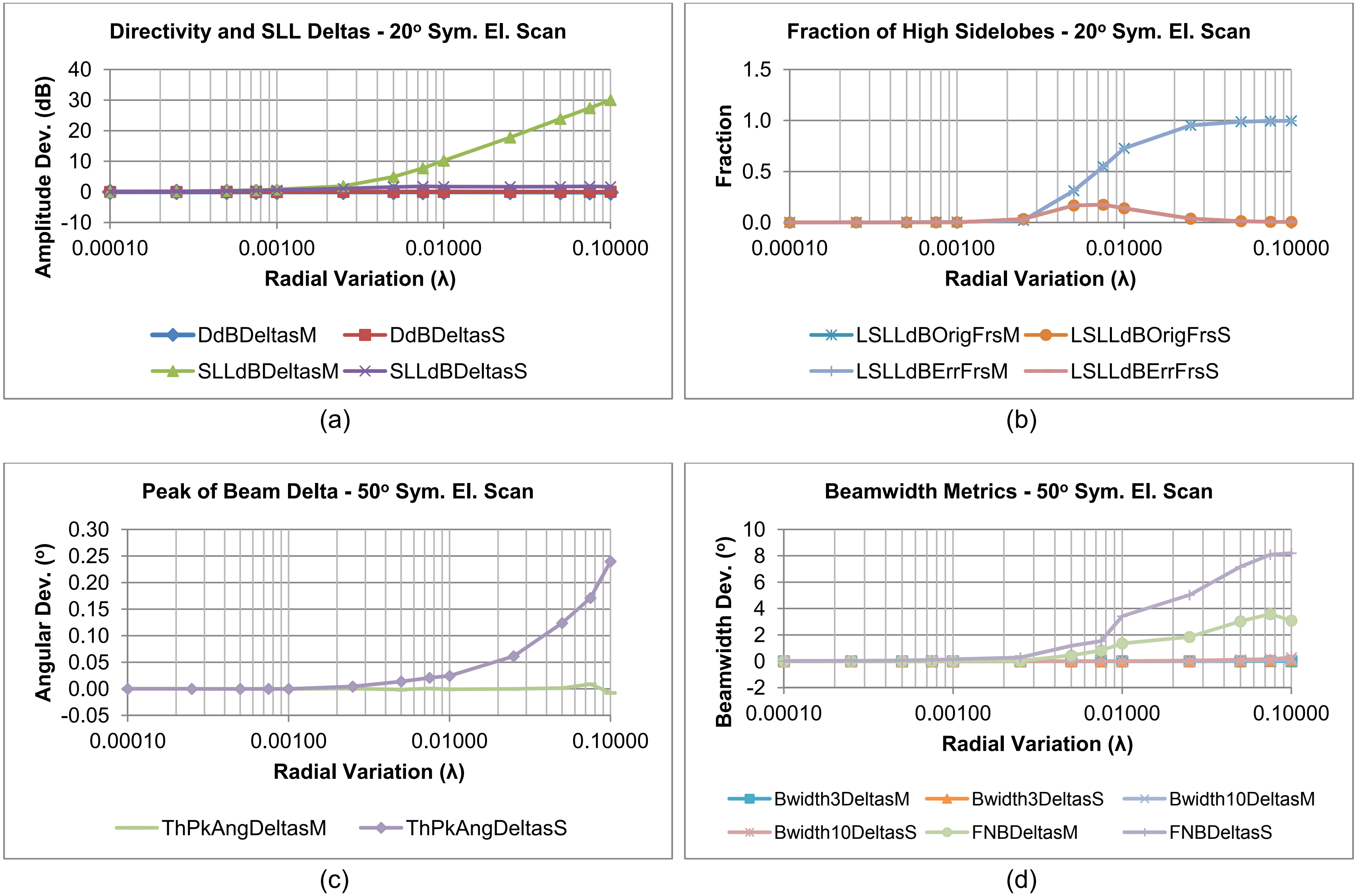

Figure B.71. *Statistical data for a 1/2λ spaced, 28 element, modified Taylor array versus radial randomization.* Directivity and sidelobe level (a), LSLLdB (b), beam pointing (c), and beamwidth (d) results are illustrated.

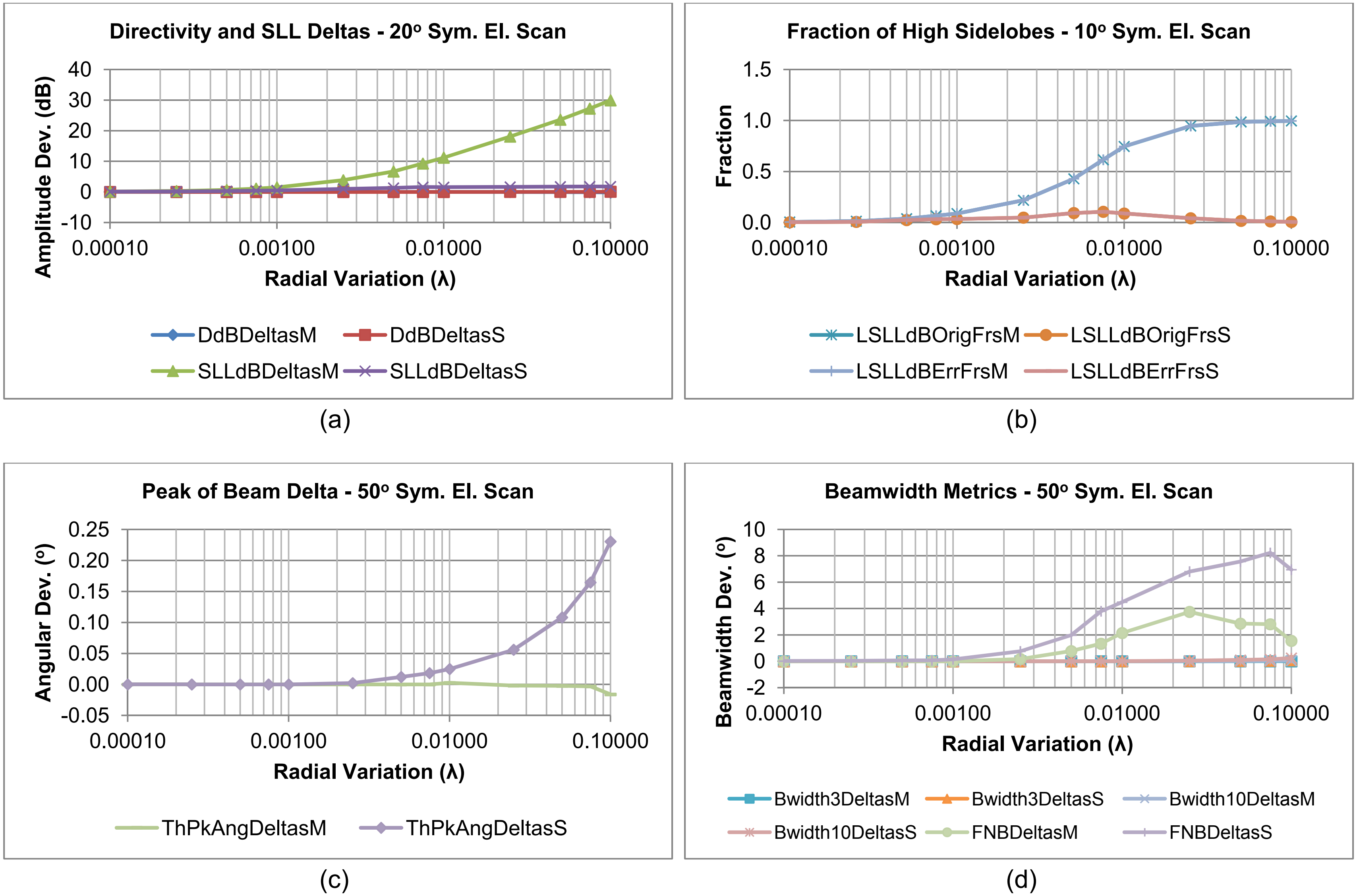

Figure B.72. *Statistical data for a 1/2λ spaced, 28 element, Taylor array versus radial randomization.* Directivity and sidelobe level (a), LSLLdB (b), beam pointing (c), and beamwidth (d) results are illustrated.

$5/8\,\lambda$ Element Spacing

20 dB Initial Design Sidelobe Level

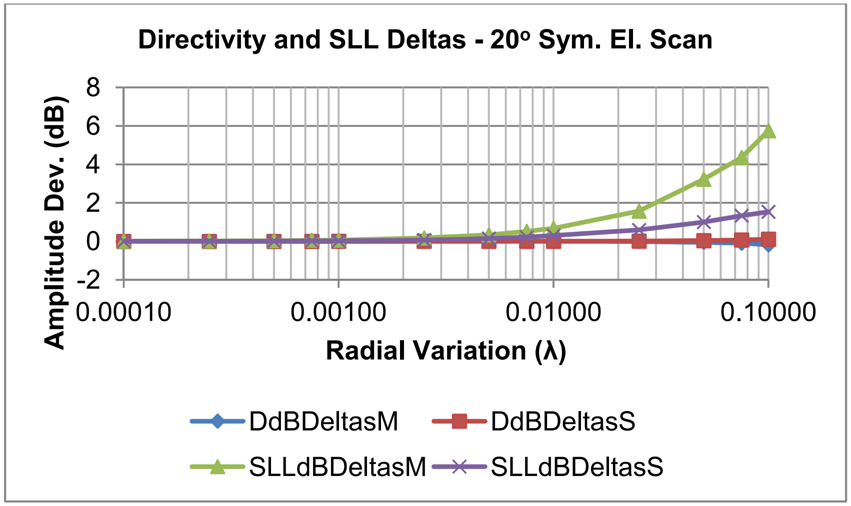

(a)

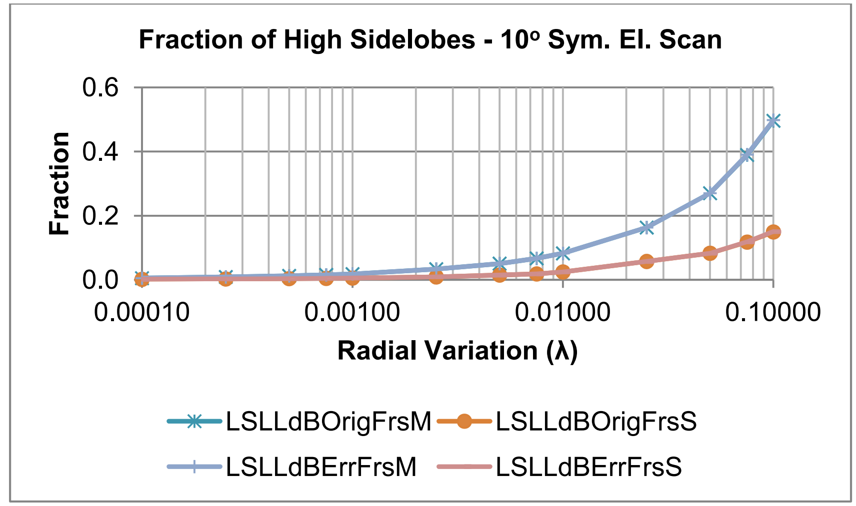

(b)

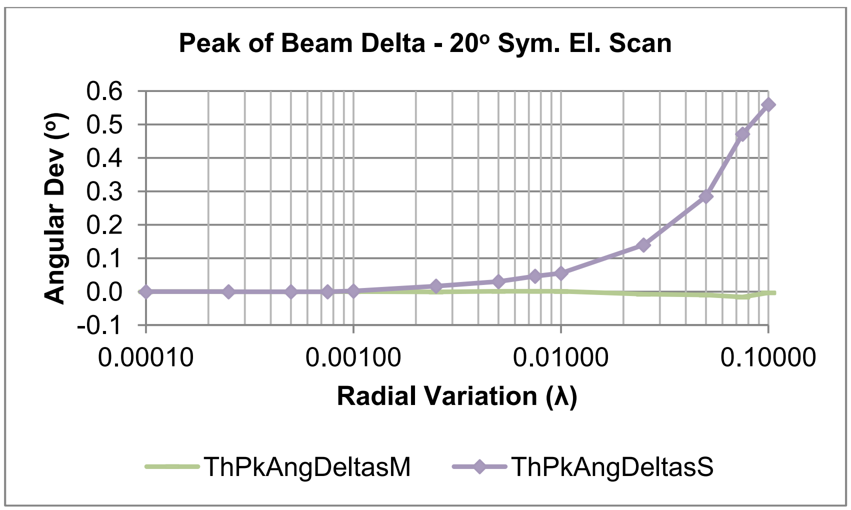

(c)

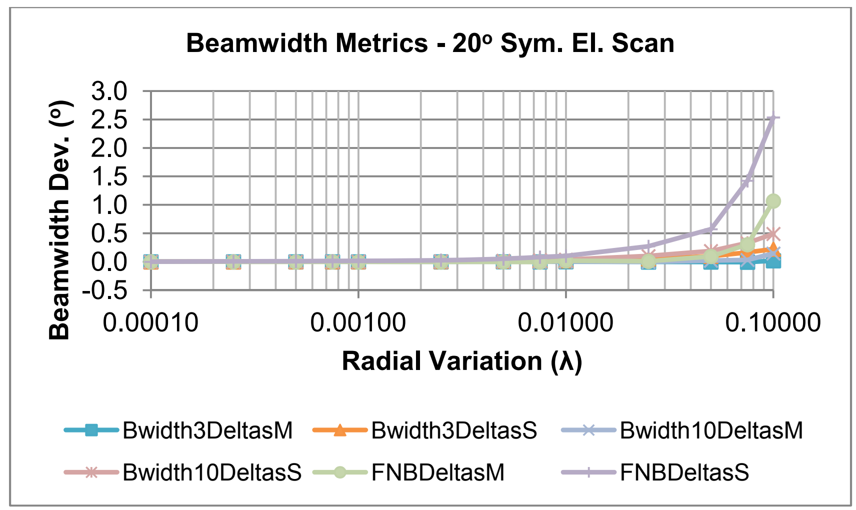

(d)

Figure B.73. *Statistical data for a* $5/8\,\lambda$ *spaced, 7 element, Dolph-Chebyshev array versus radial randomization.* Directivity and sidelobe level (a), LSLLdB (b), beam pointing (c), and beamwidth (d) results are illustrated.

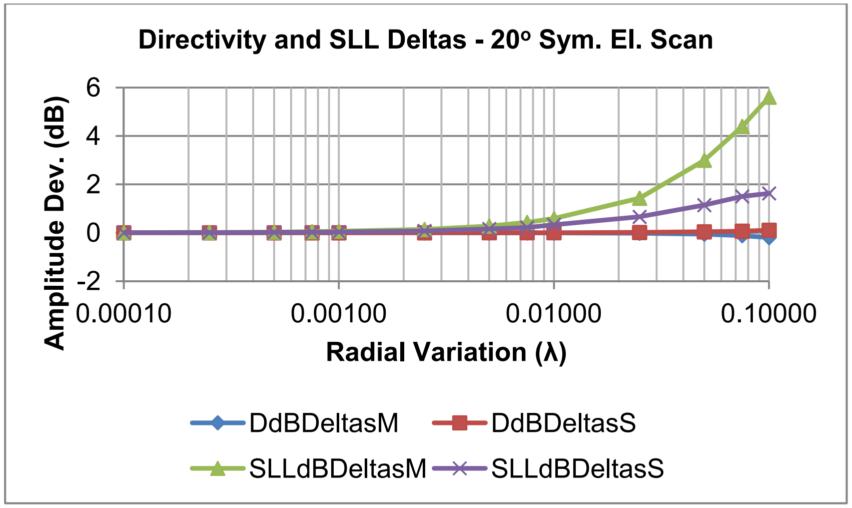

(a)

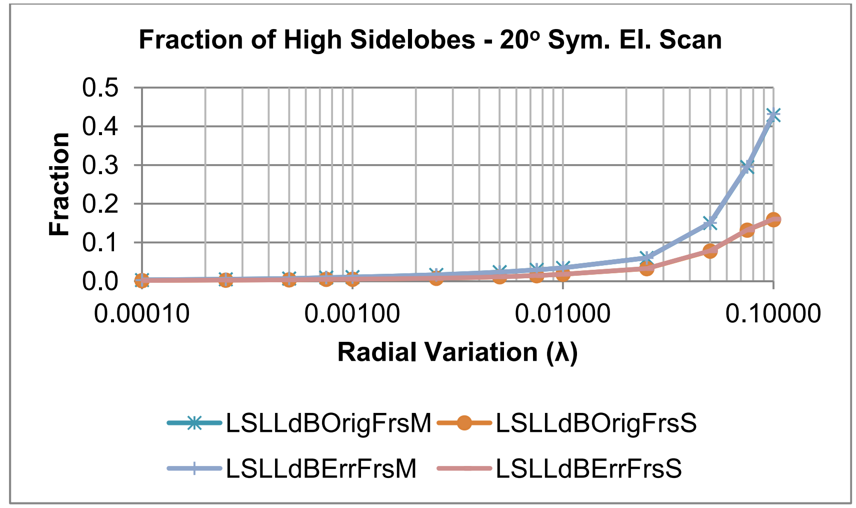

(b)

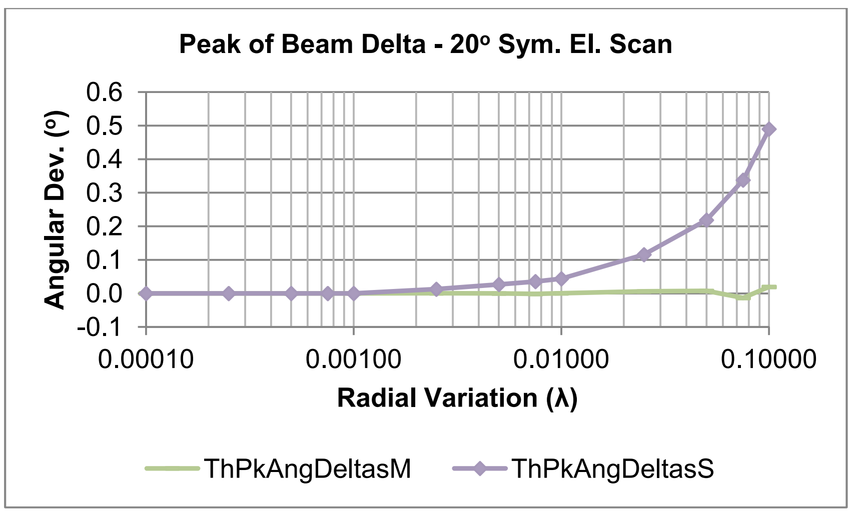

(c)

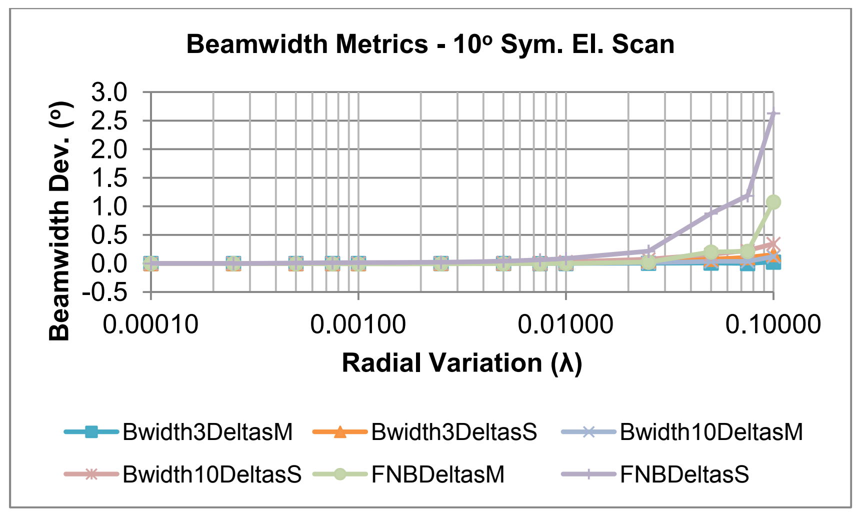

(d)

Figure B.74. *Statistical data for a $5/8\,\lambda$ spaced, 8 element, modified Taylor array versus radial randomization.* Directivity and sidelobe level (a), LSLLdB (b), beam pointing (c), and beamwidth (d) results are illustrated.

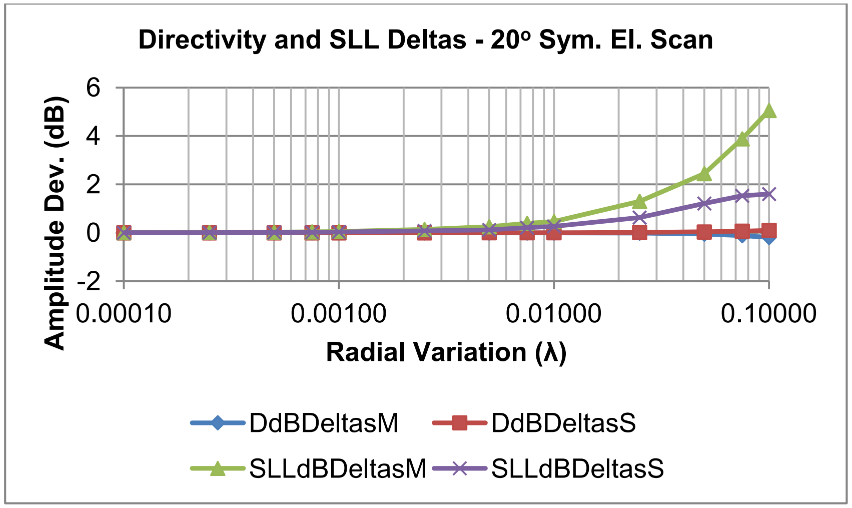

(a)

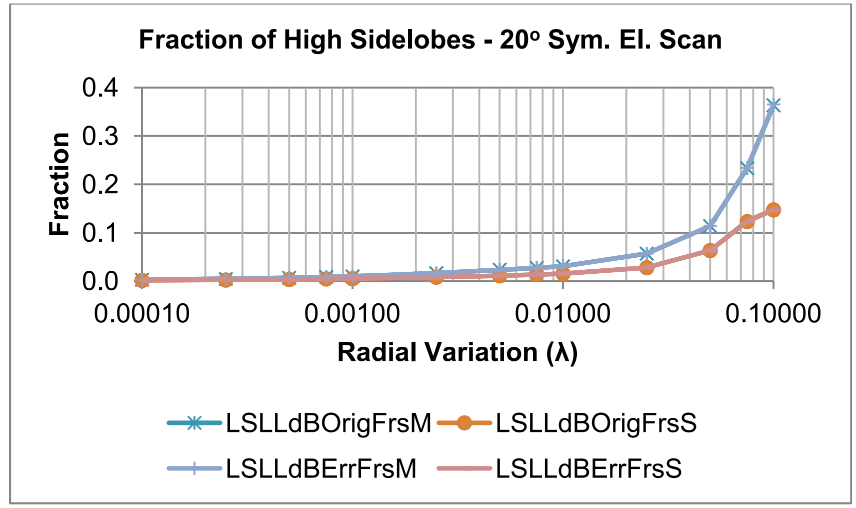

(b)

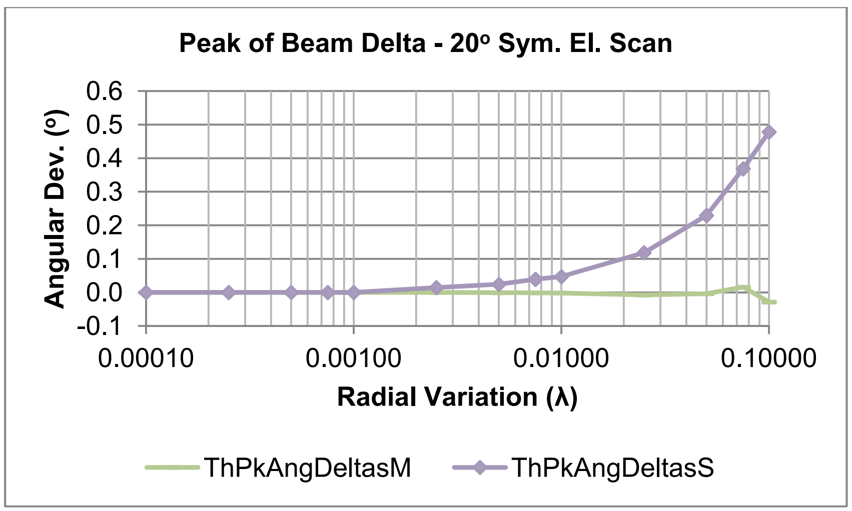

(c)

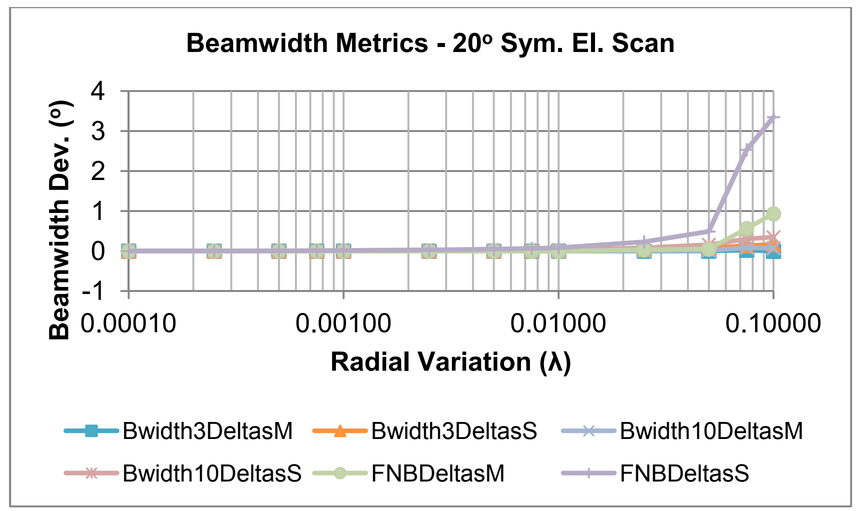

(d)

Figure B.75. *Statistical data for a* $5/8\,\lambda$ *spaced, 8 element, powers of cosine on a pedestal array versus radial randomization.* Directivity and sidelobe level (a), LSLLdB (b), beam pointing (c), and beamwidth (d) results are illustrated.

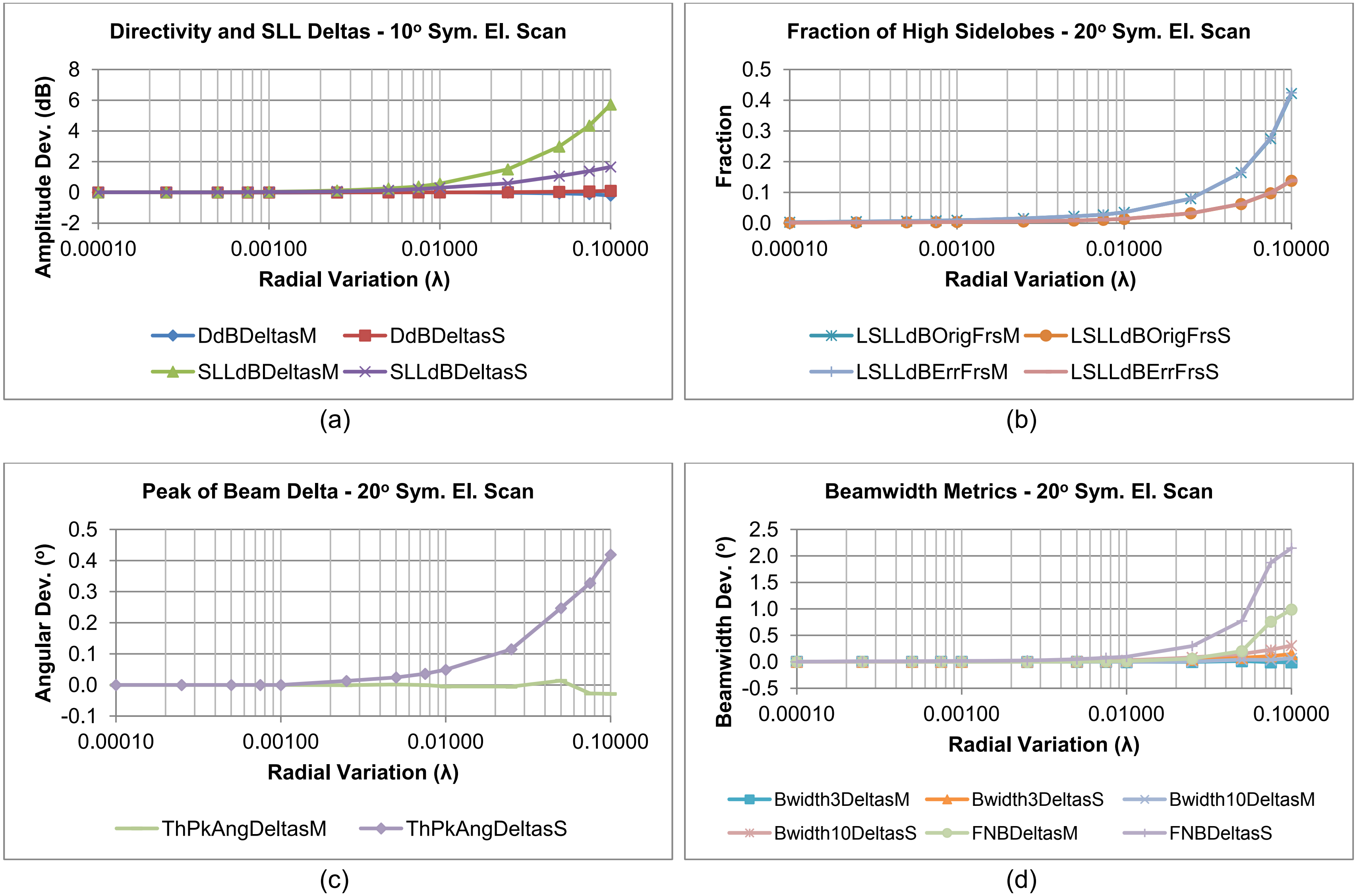

Figure B.76. *Statistical data for a* $5/8\,\lambda$ *spaced, 8 element, Taylor array versus radial randomization.* Directivity and sidelobe level (a), LSLLdB (b), beam pointing (c), and beamwidth (d) results are illustrated.

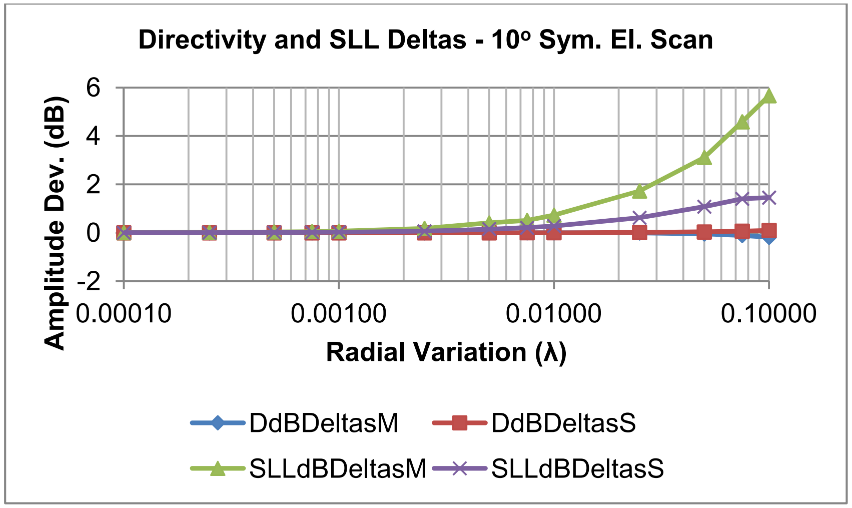

(a)

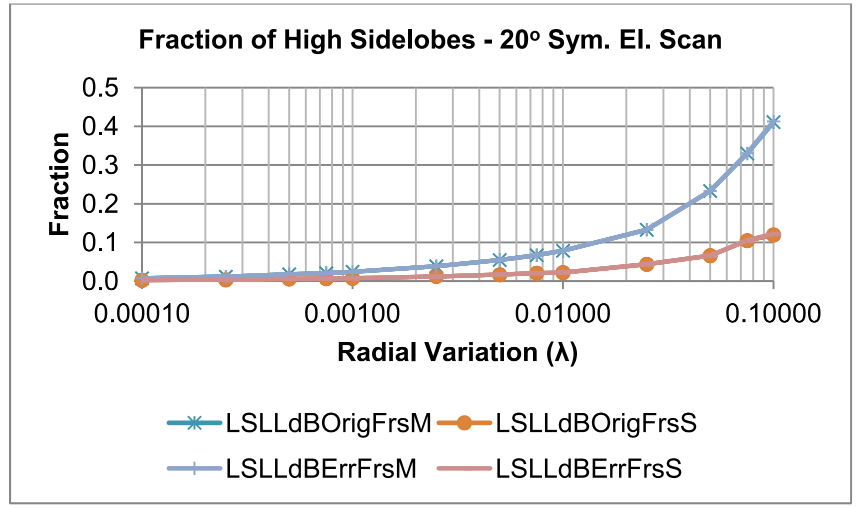

(b)

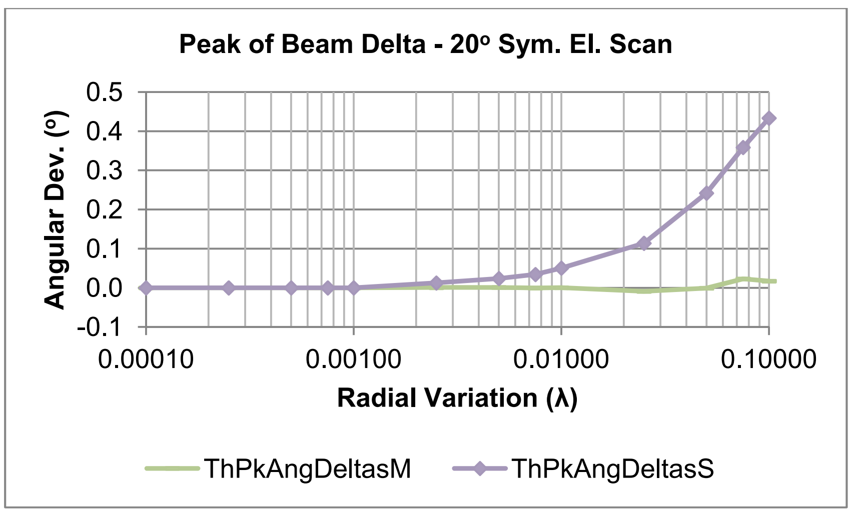

(c)

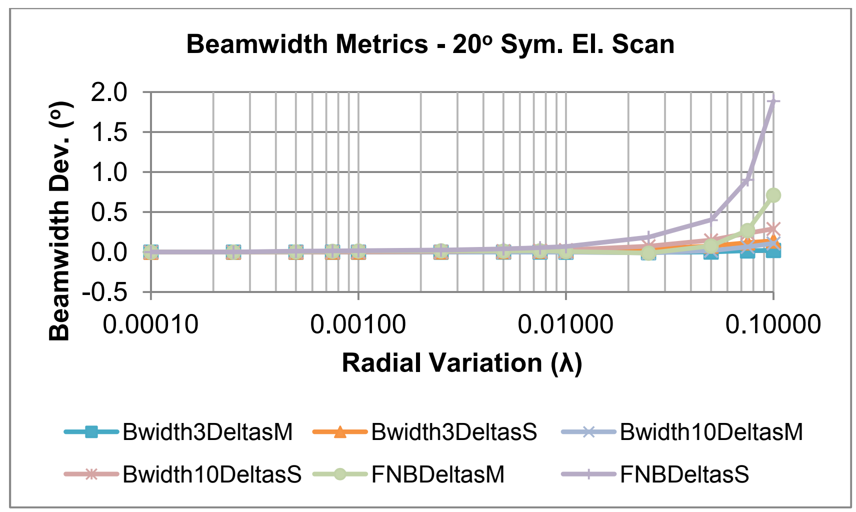

(d)

Figure B.77. *Statistical data for a* $5/8\,\lambda$ *spaced, 8 element, Dolph-Chebyshev array versus radial randomization.* Directivity and sidelobe level (a), LSLLdB (b), beam pointing (c), and beamwidth (d) results are illustrated.

$5/8\lambda$ Element Spacing

30 dB Initial Design Sidelobe Level

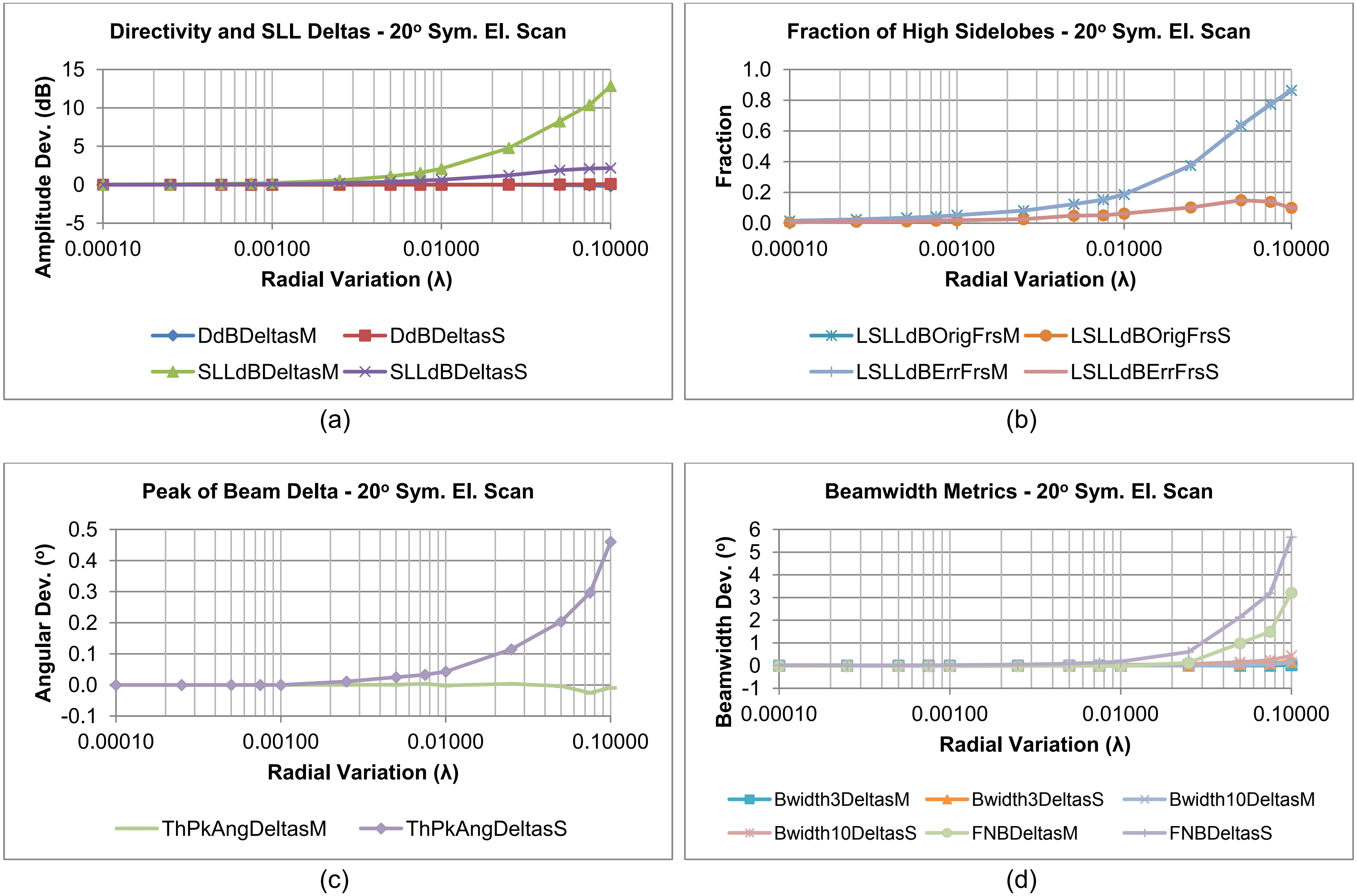

Figure B.78. *Statistical data for a* $5/8\,\lambda$ *spaced, 9 element, Dolph-Chebyshev array versus radial randomization.* Directivity and sidelobe level (a), LSLLdB (b), beam pointing (c), and beamwidth (d) results are illustrated.

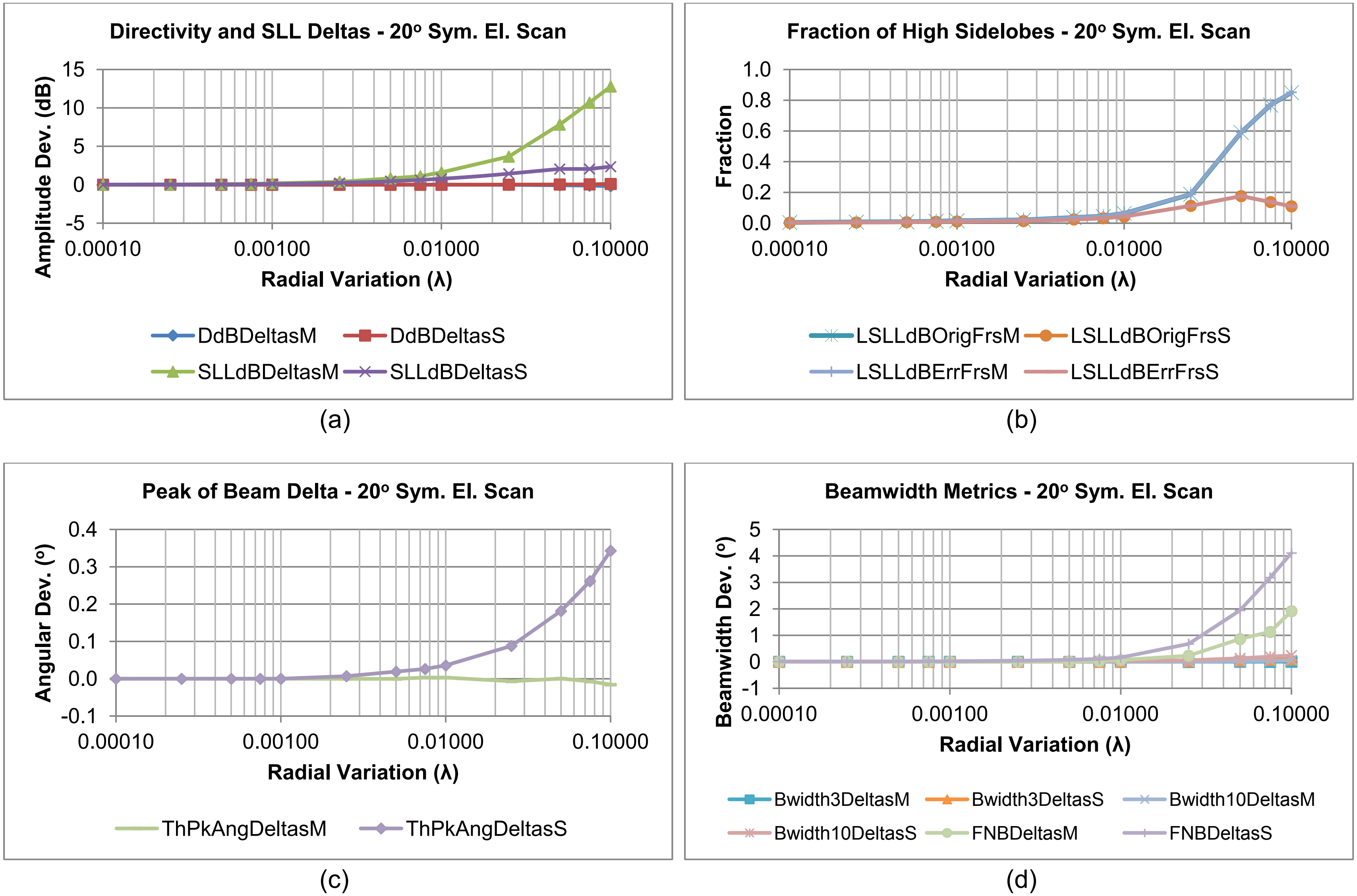

Figure B.79. *Statistical data for a* $5/8\,\lambda$ *spaced, 11 element, modified Taylor array versus radial randomization.* Directivity and sidelobe level (a), LSLLdB (b), beam pointing (c), and beamwidth (d) results are illustrated.

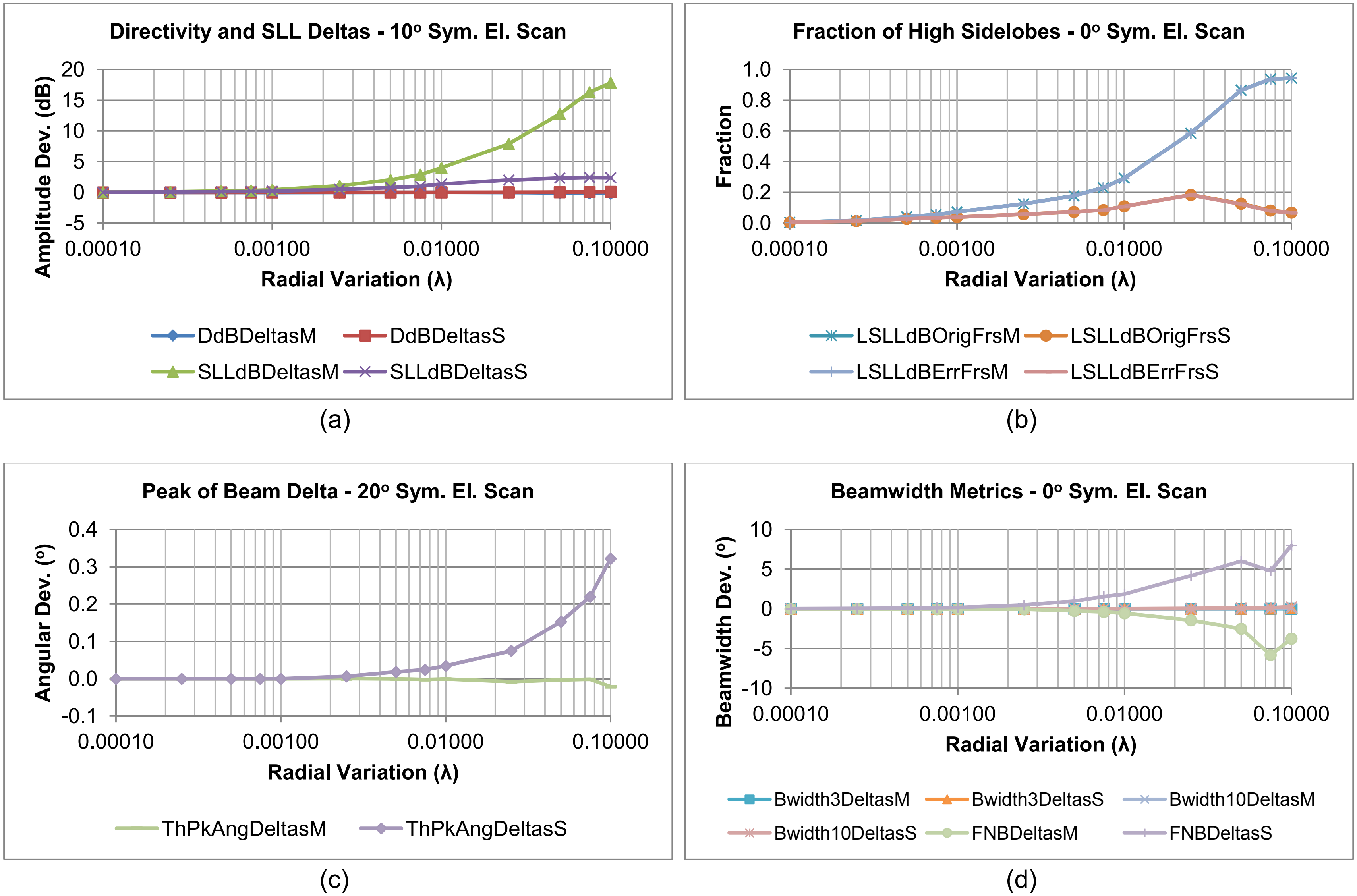

Figure B.80. *Statistical data for a* $5/8\,\lambda$ *spaced, 12 element, powers of cosine on a pedestal array versus radial randomization.* Directivity and sidelobe level (a), LSLLdB (b), beam pointing (c), and beamwidth (d) results are illustrated.

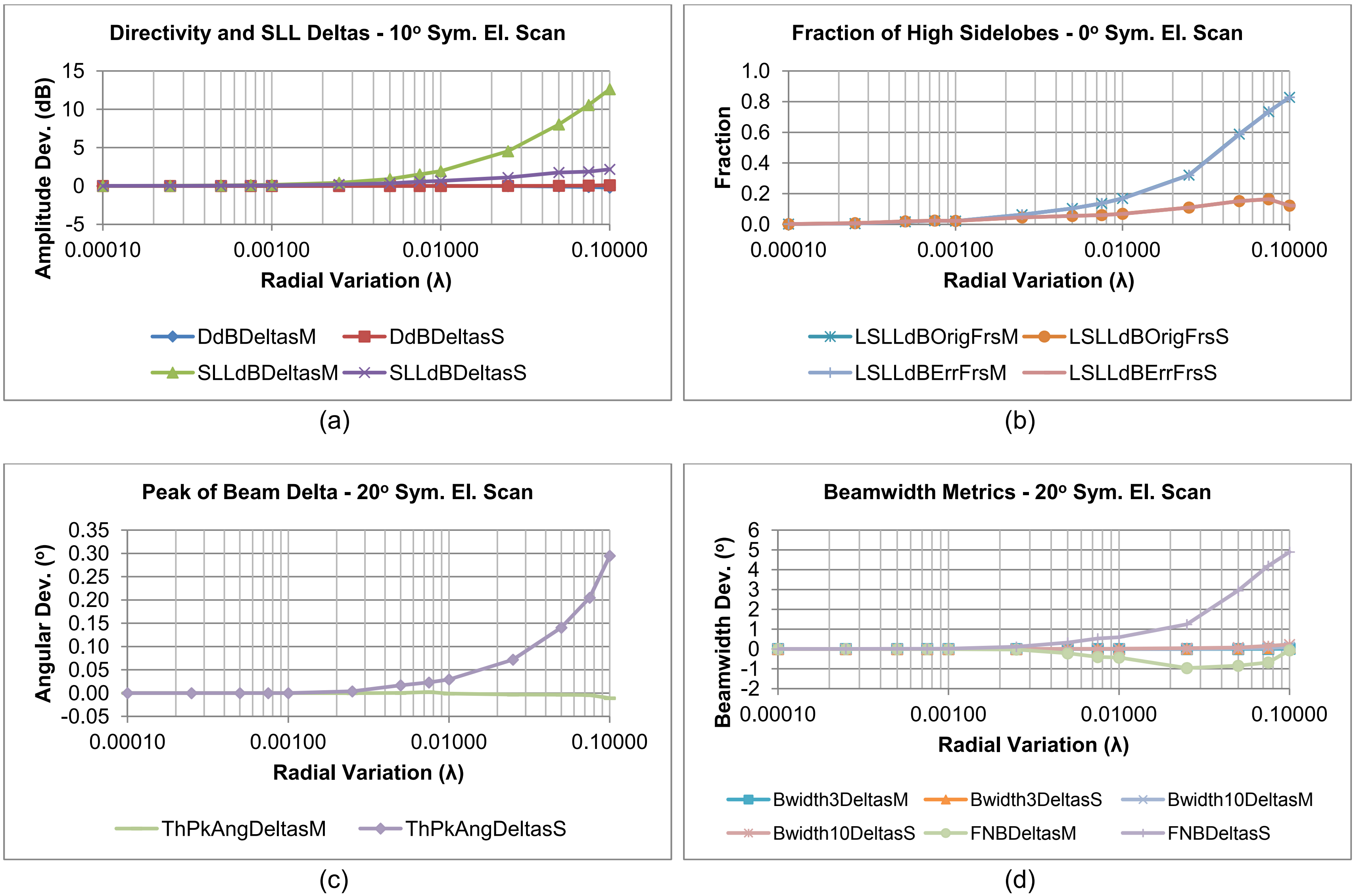

Figure B.81. *Statistical data for a $5/8\,\lambda$ spaced, 12 element, Taylor array versus radial randomization.* Directivity and sidelobe level (a), LSLLdB (b), beam pointing (c), and beamwidth (d) results are illustrated.

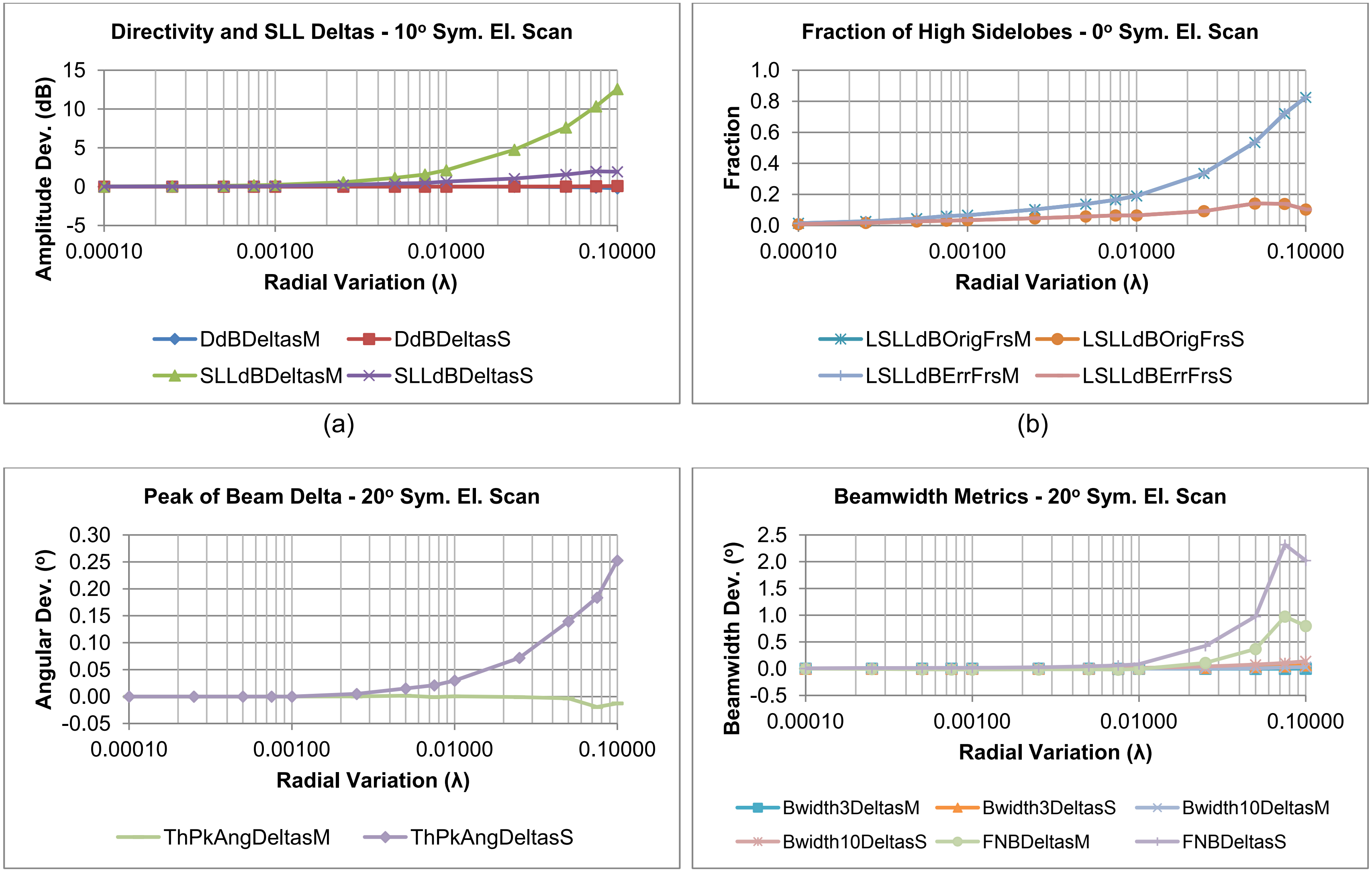

(c) (d)

Figure B.82. *Statistical data for a* $5/8\,\lambda$ *spaced, 12 element, Dolph-Chebyshev array versus radial randomization.* Directivity and sidelobe level (a), LSLLdB (b), beam pointing (c), and beamwidth (d) results are illustrated.

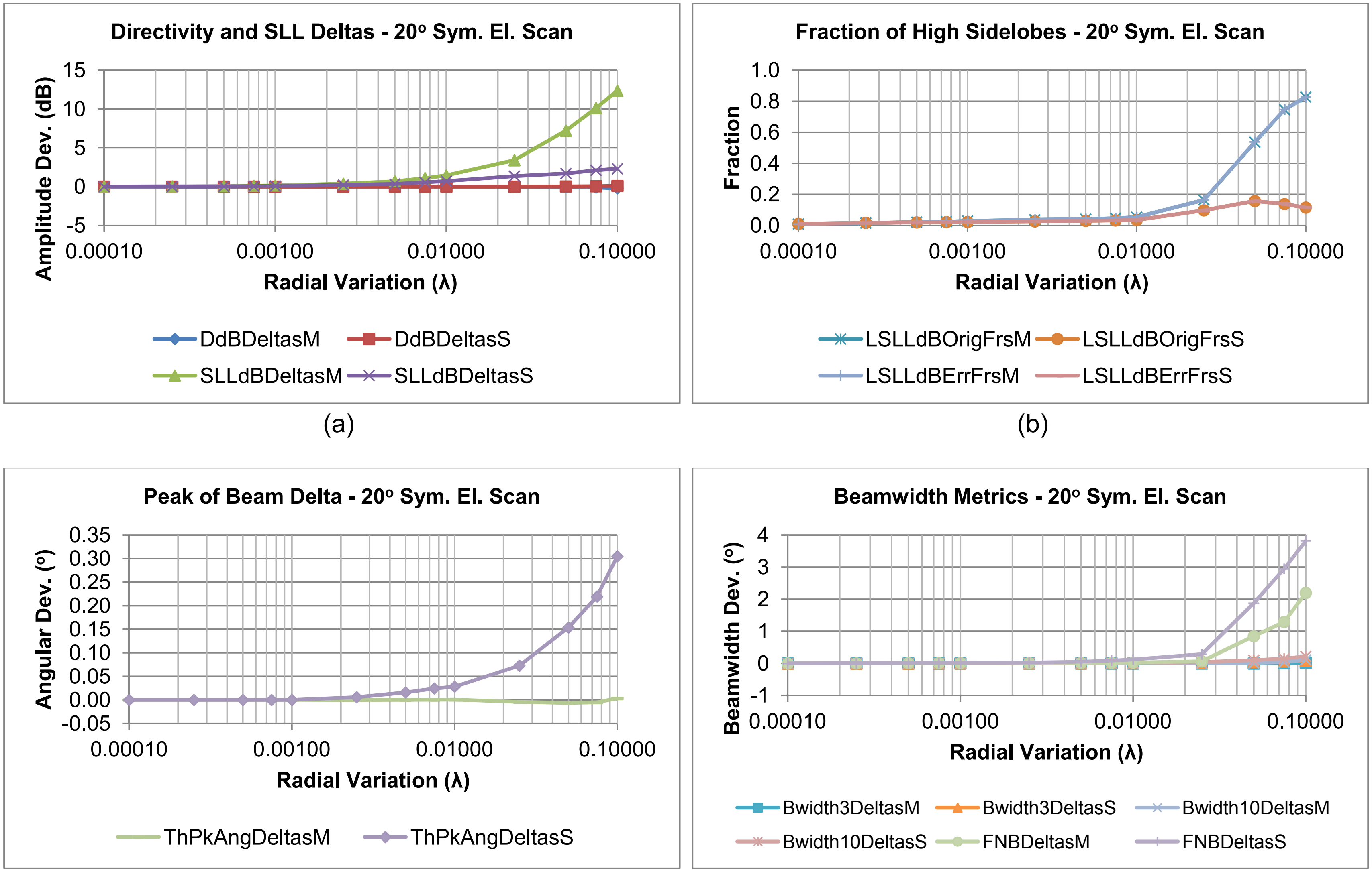

(c) (d)

Figure B.83. *Statistical data for a* $5/8\,\lambda$ *spaced, 12 element, modified Taylor array versus radial randomization.* Directivity and sidelobe level (a), LSLLdB (b), beam pointing (c), and beamwidth (d) results are illustrated.

5/8 λ Element Spacing

40 dB Initial Design Sidelobe Level

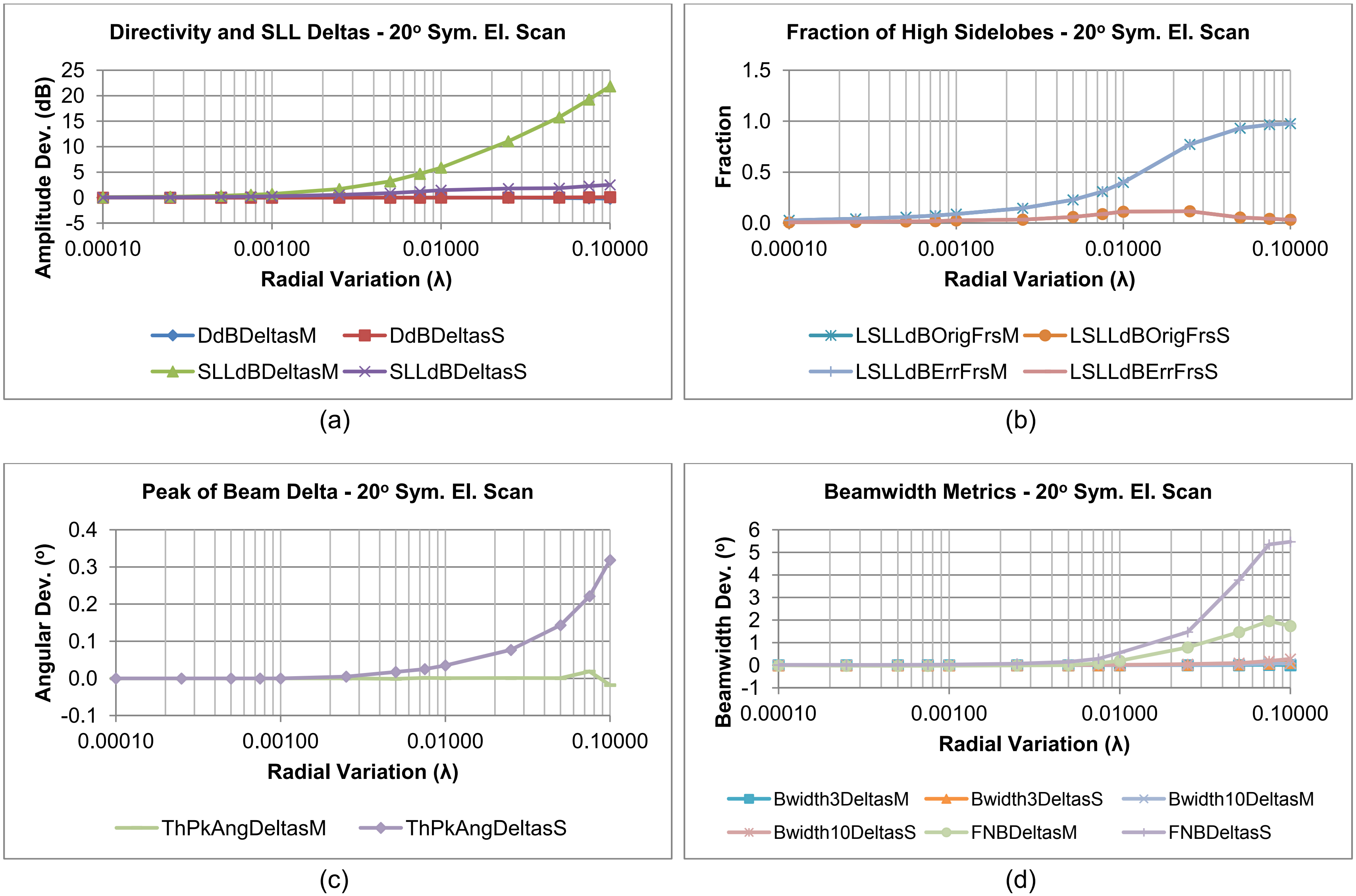

Figure B.84. *Statistical data for a* $5/8\,\lambda$ *spaced, 12 element, Dolph-Chebyshev array versus radial randomization.* Directivity and sidelobe level (a), LSLLdB (b), beam pointing (c), and beamwidth (d) results are illustrated.

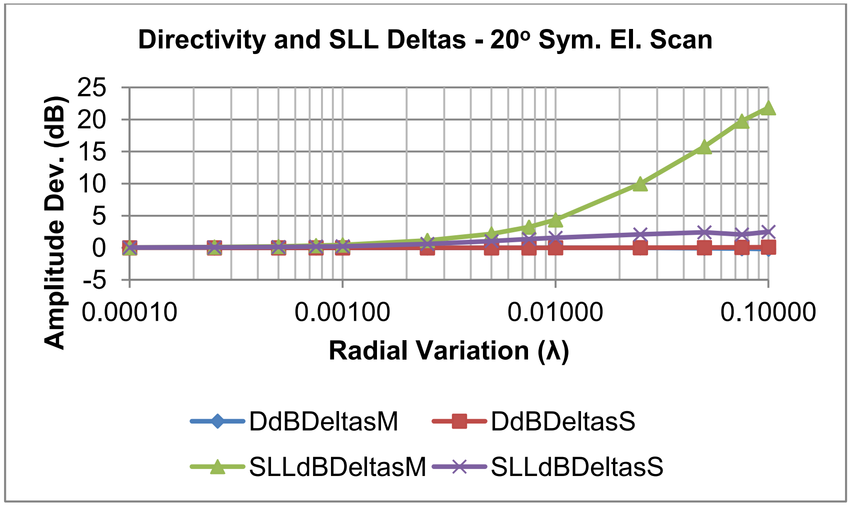

(a)

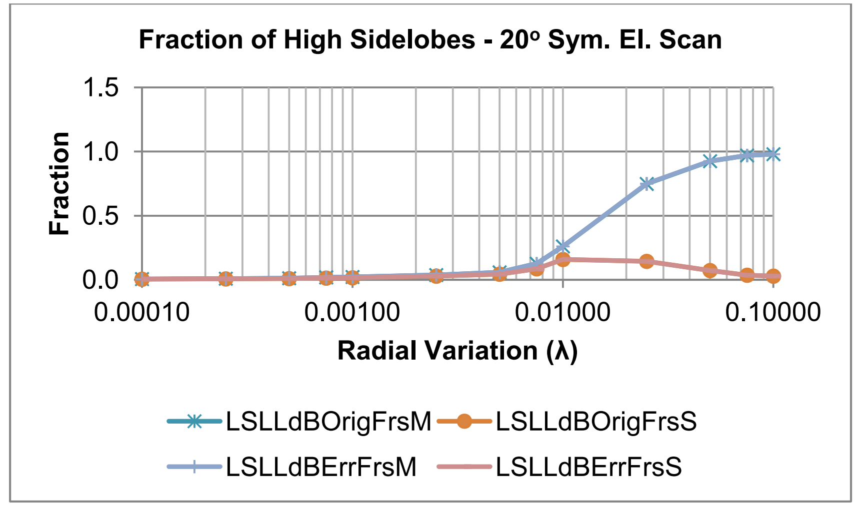

(b)

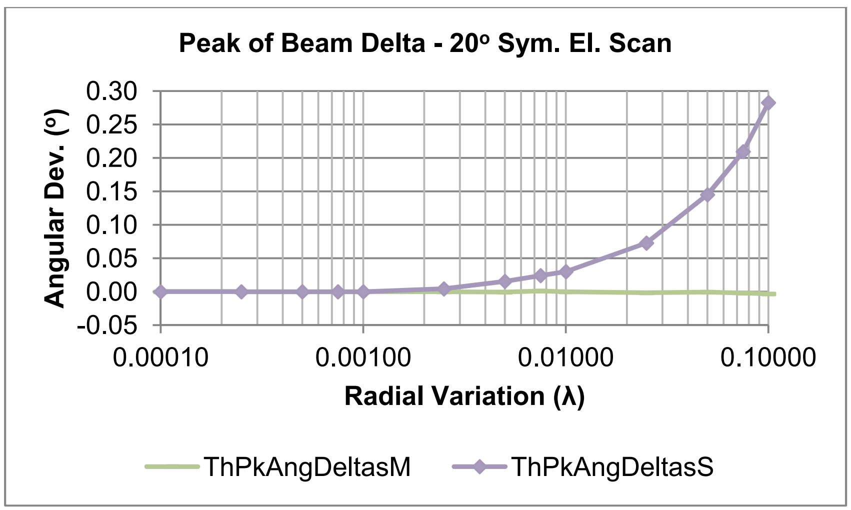

(c)

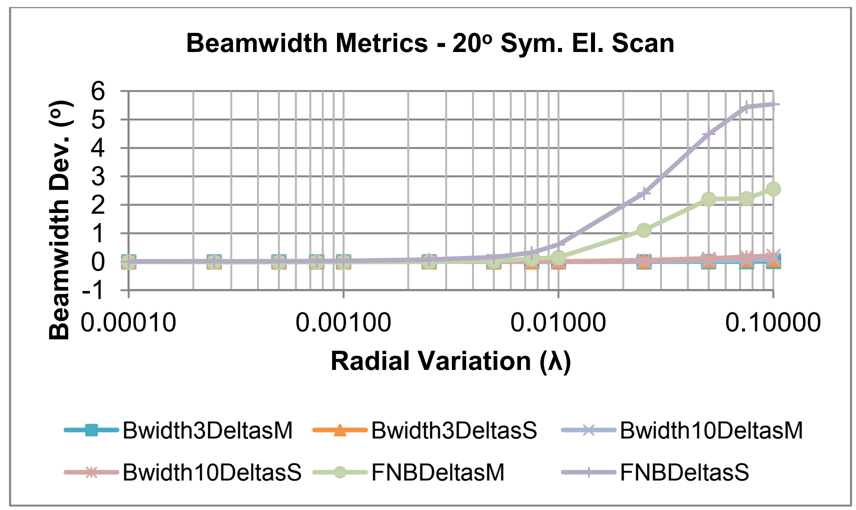

(d)

Figure B.85. *Statistical data for a* $5/8\,\lambda$ *spaced, 14 element, modified Taylor array versus radial randomization.* Directivity and sidelobe level (a), LSLLdB (b), beam pointing (c), and beamwidth (d) results are illustrated.

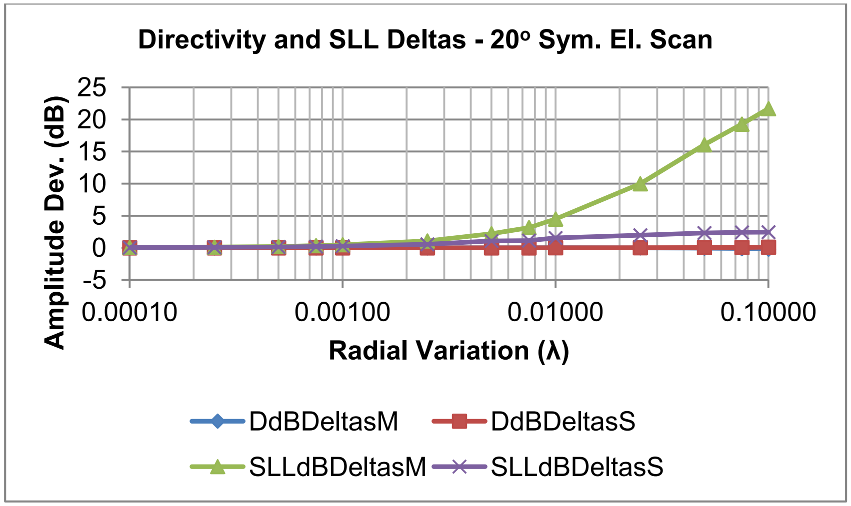

(a)

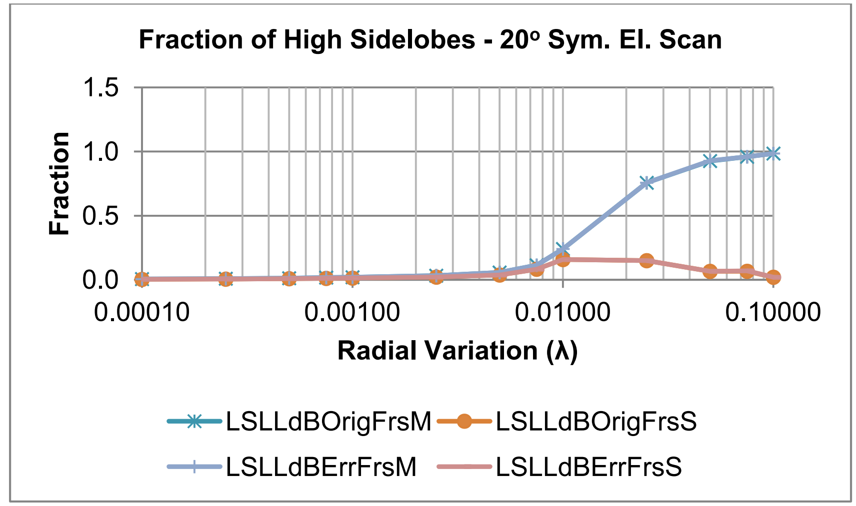

(b)

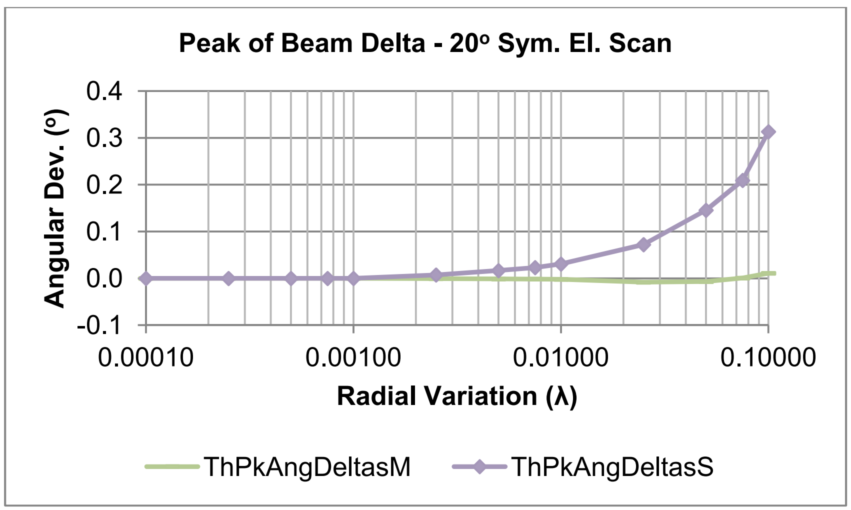

(c)

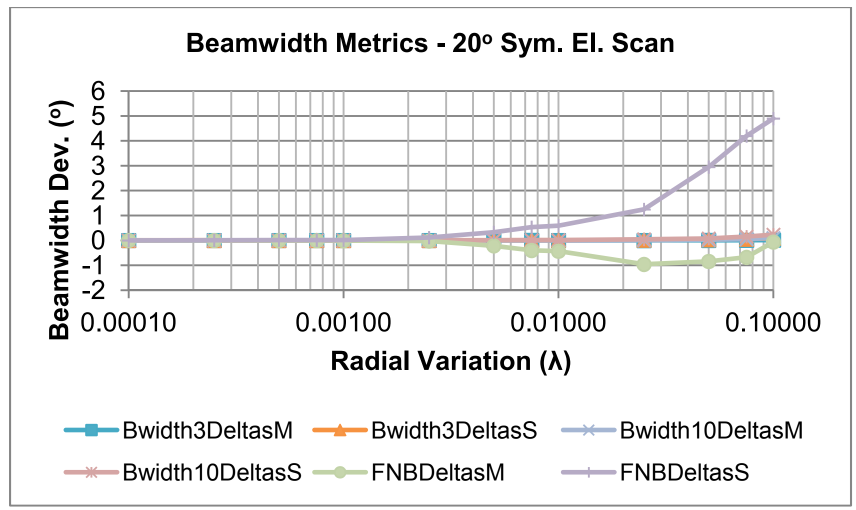

(d)

Figure B.86. *Statistical data for a* $5/8\,\lambda$ *spaced, 17 element, powers of cosine on a pedestal array versus radial randomization.* Directivity and sidelobe level (a), LSLLdB (b), beam pointing (c), and beamwidth (d) results are illustrated.

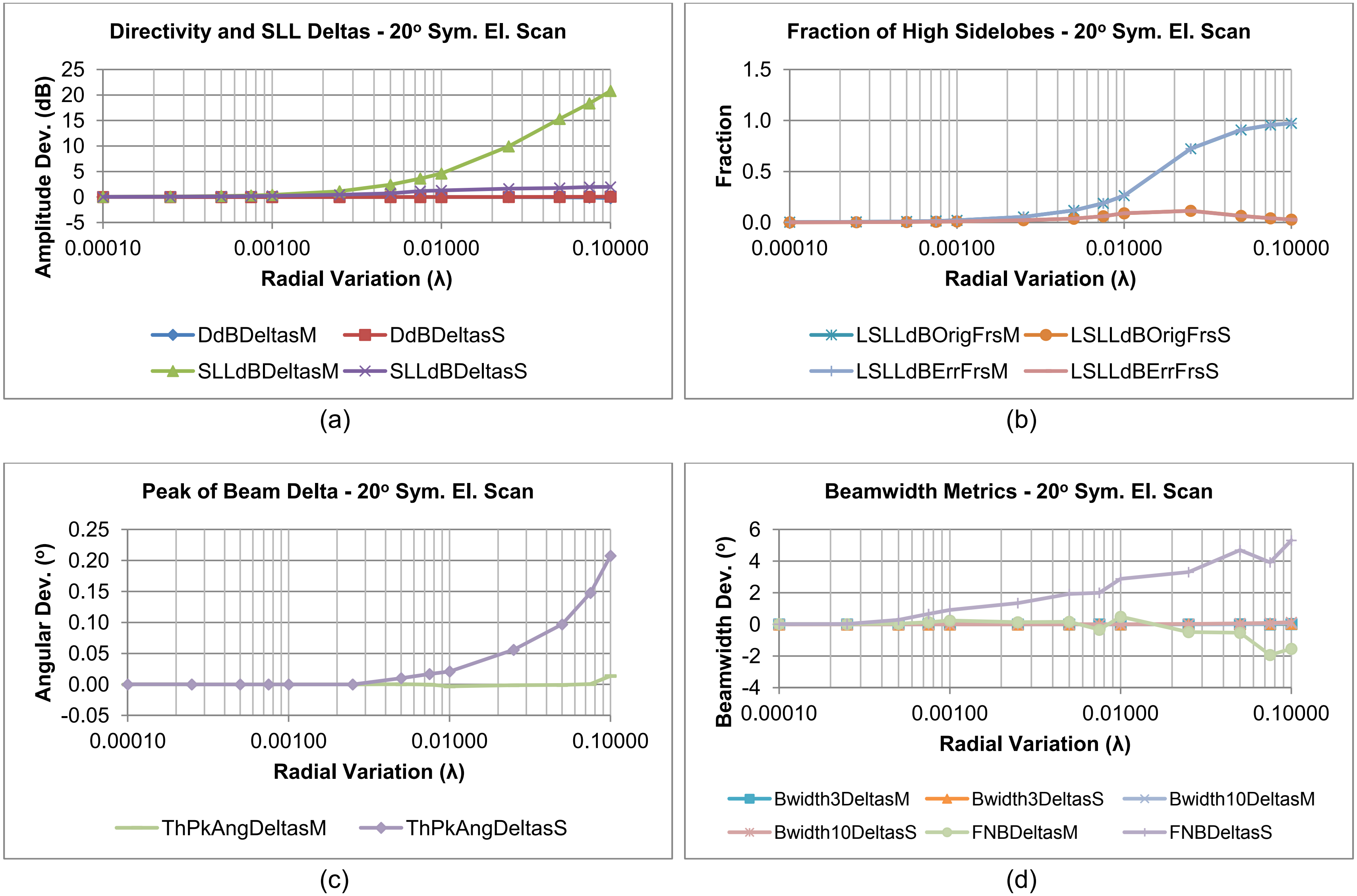

Figure B.87. *Statistical data for a* $5/8\,\lambda$ *spaced, 17 element, Taylor array versus radial randomization.* Directivity and sidelobe level (a), LSLLdB (b), beam pointing (c), and beamwidth (d) results are illustrated.

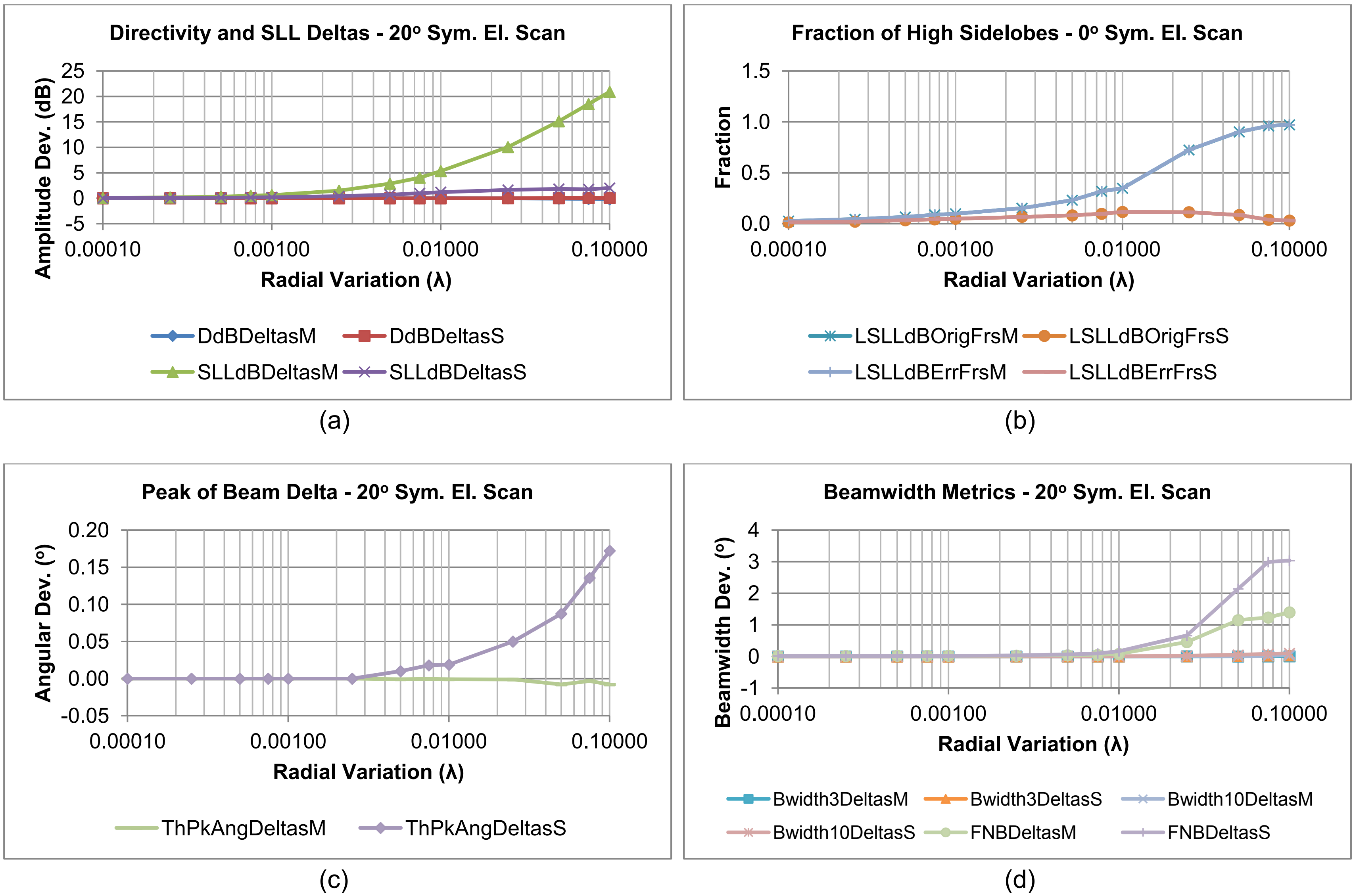

Figure B.88. *Statistical data for a* $5/8\,\lambda$ *spaced, 17 element, Dolph-Chebyshev array versus radial randomization.* Directivity and sidelobe level (a), LSLLdB (b), beam pointing (c), and beamwidth (d) results are illustrated.

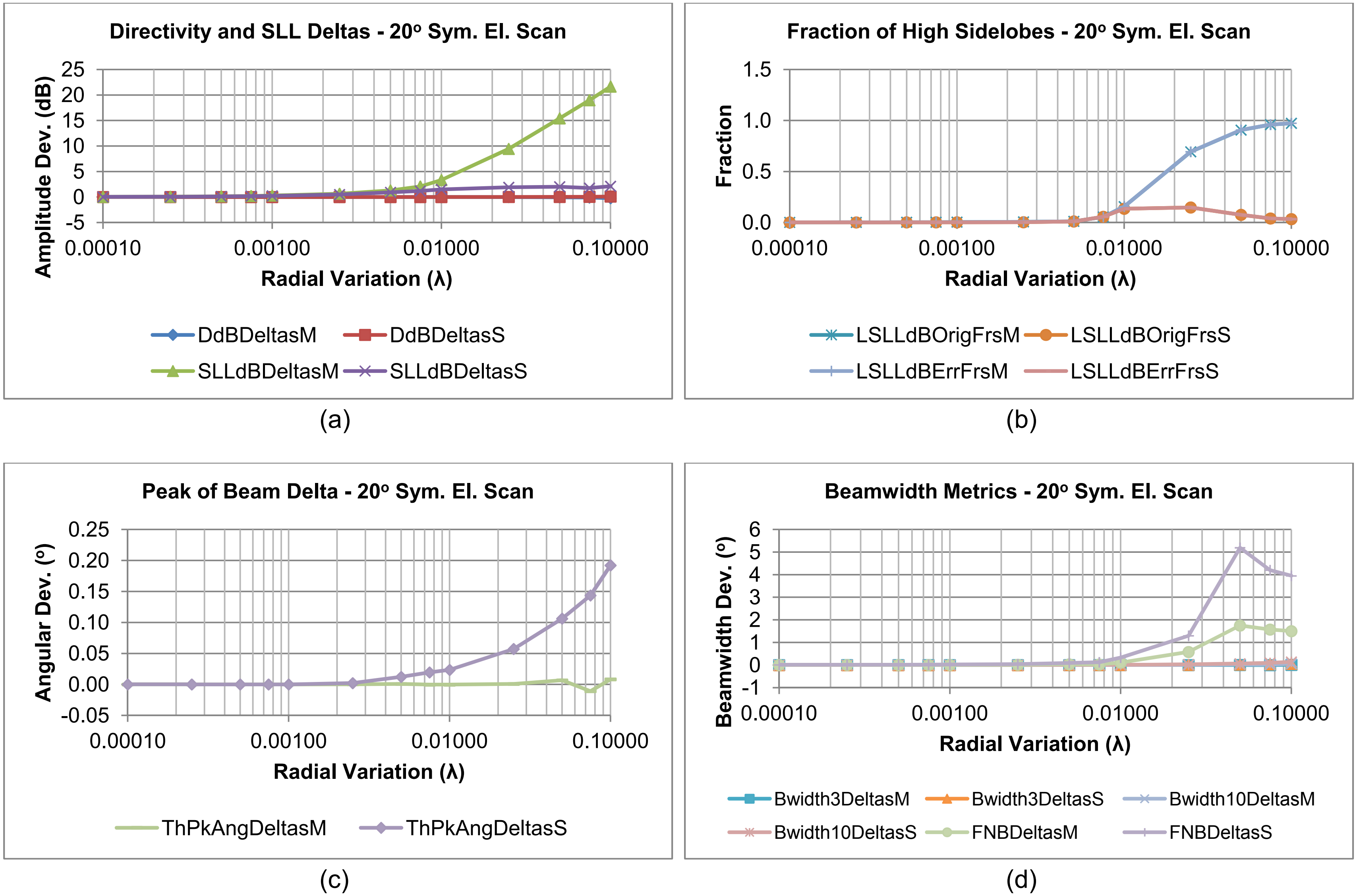

Figure B.89. *Statistical data for a* $5/8\,\lambda$ *spaced, 17 element, modified Taylor array versus radial randomization.* Directivity and sidelobe level (a), LSLLdB (b), beam pointing (c), and beamwidth (d) results are illustrated.

$5/8\,\lambda$ Element Spacing

50 dB Initial Design Sidelobe Level

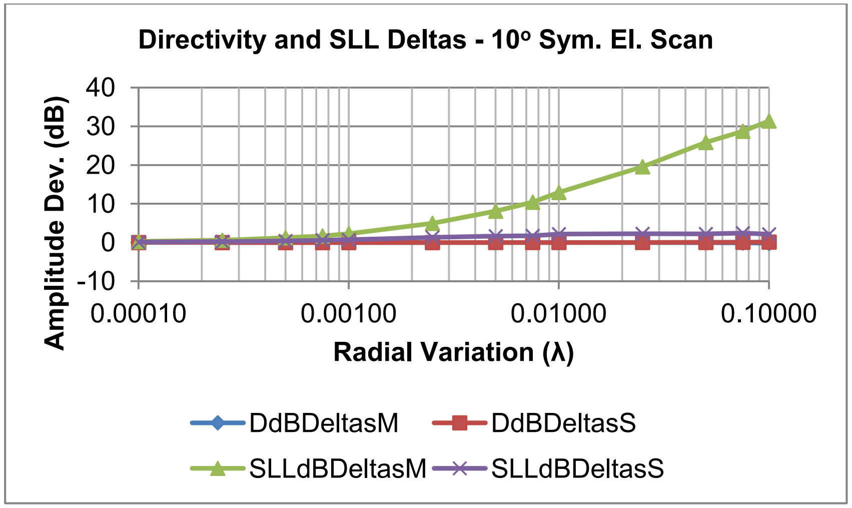

(a)

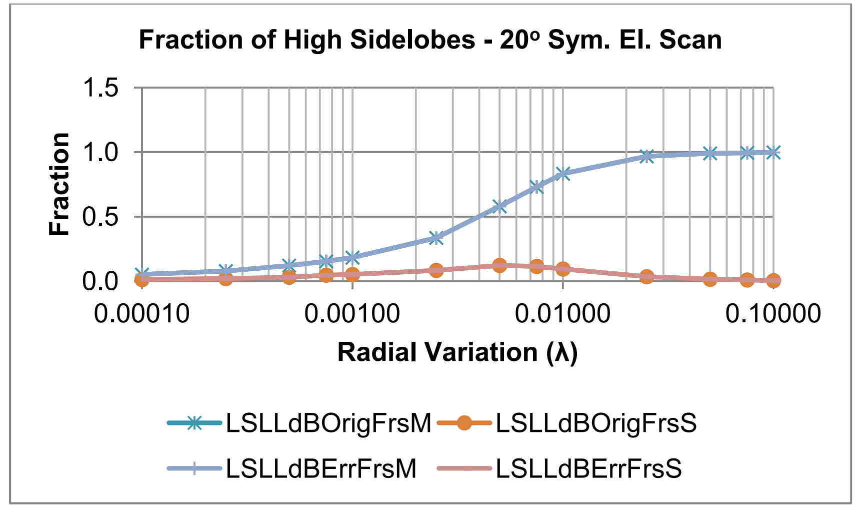

(b)

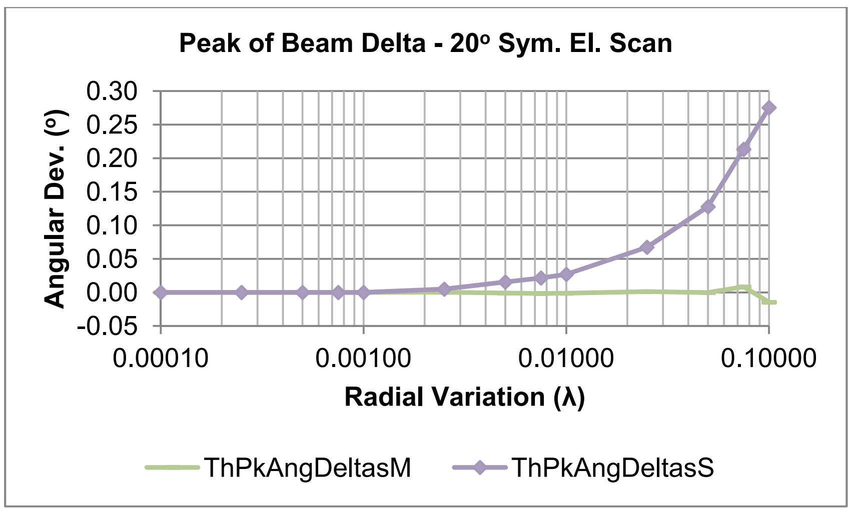

(c)

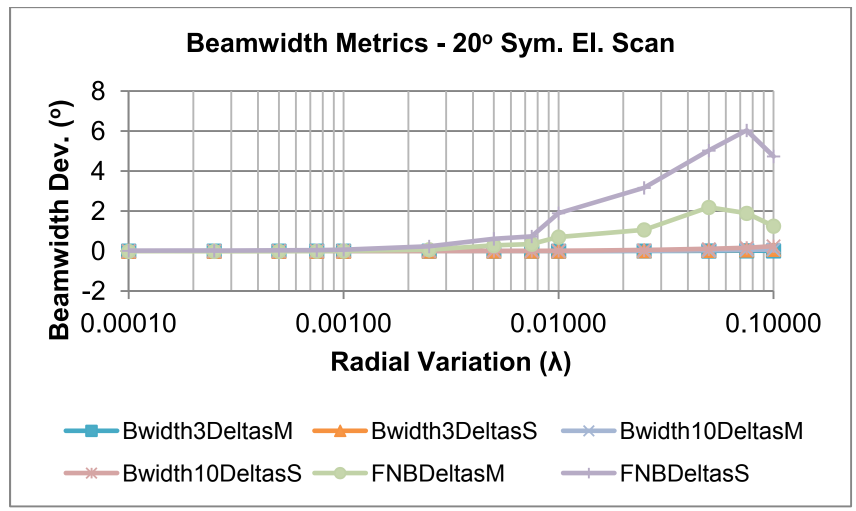

(d)

Figure B.90. *Statistical data for a* $5/8\,\lambda$ *spaced, 14 element, Dolph-Chebyshev array versus radial randomization.* Directivity and sidelobe level (a), LSLLdB (b), beam pointing (c), and beamwidth (d) results are illustrated.

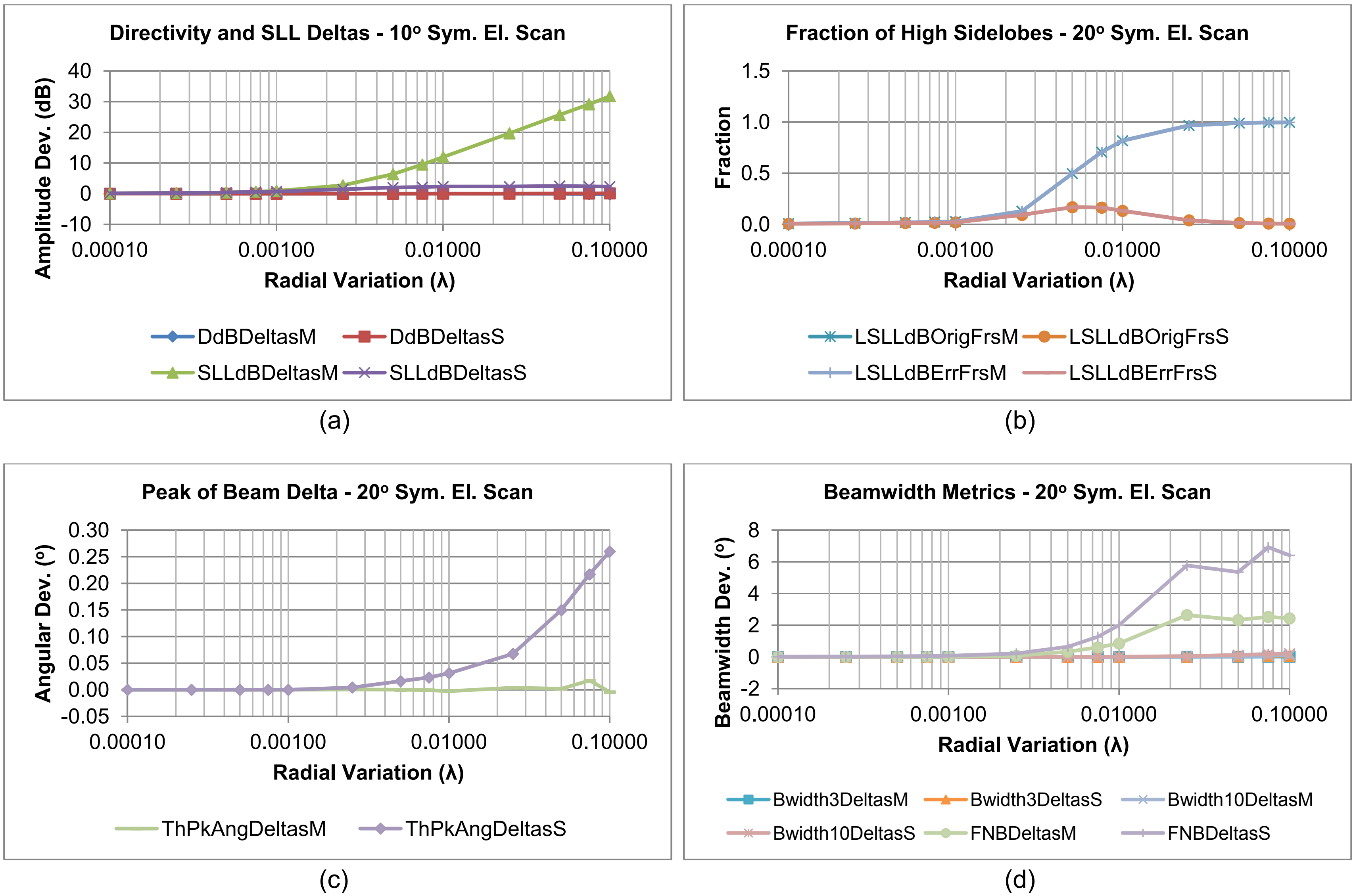

Figure B.91. *Statistical data for a* $5/8\,\lambda$ *spaced, 16 element, modified Taylor array versus radial randomization.* Directivity and sidelobe level (a), LSLLdB (b), beam pointing (c), and beamwidth (d) results are illustrated.

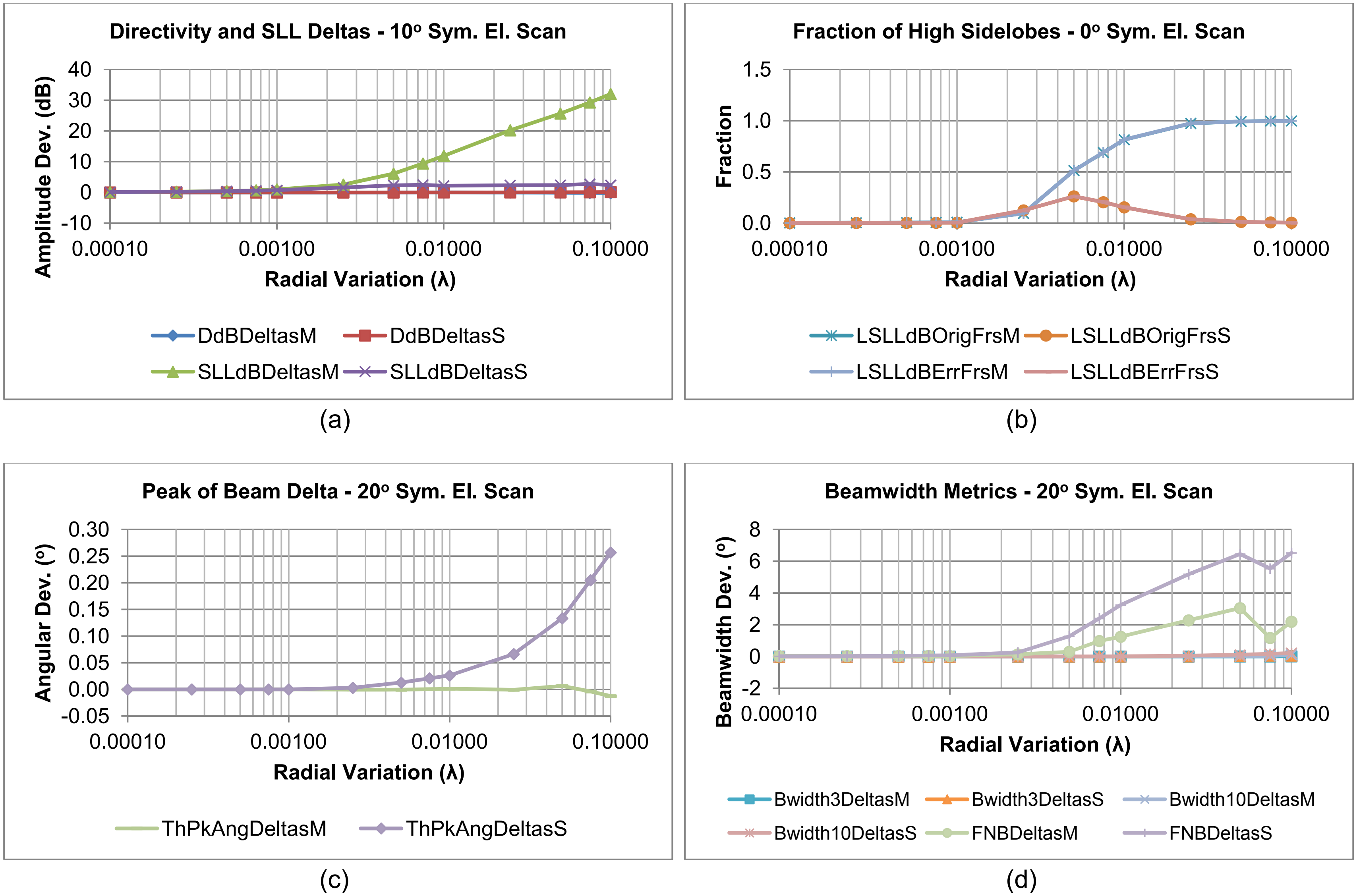

Figure B.92. *Statistical data for a $5/8\,\lambda$ spaced, 21 element, powers of cosine on a pedestal array versus radial randomization.* Directivity and sidelobe level (a), LSLLdB (b), beam pointing (c), and beamwidth (d) results are illustrated.

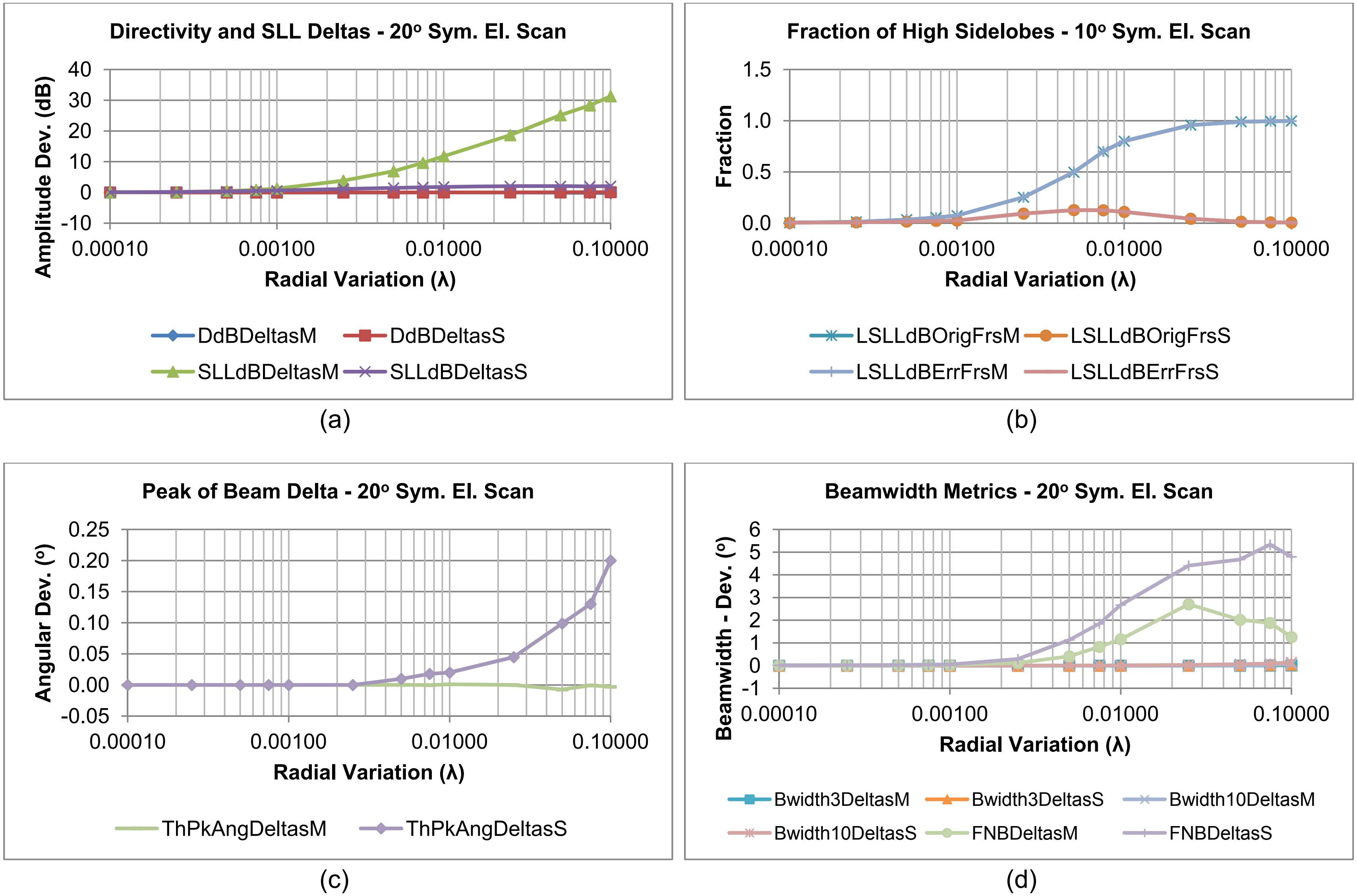

Figure B.93. *Statistical data for a $5/8\,\lambda$ spaced, 19 element, Taylor array versus radial randomization.* Directivity and sidelobe level (a), LSLLdB (b), beam pointing (c), and beamwidth (d) results are illustrated.

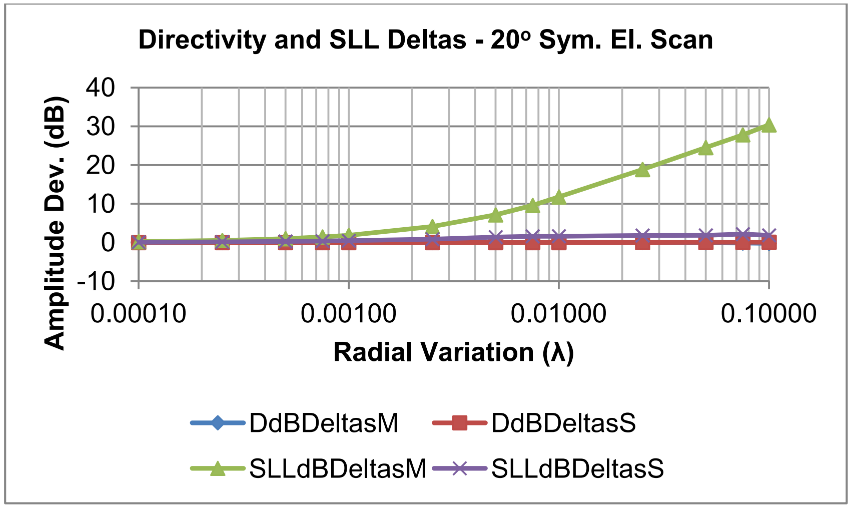

(a)

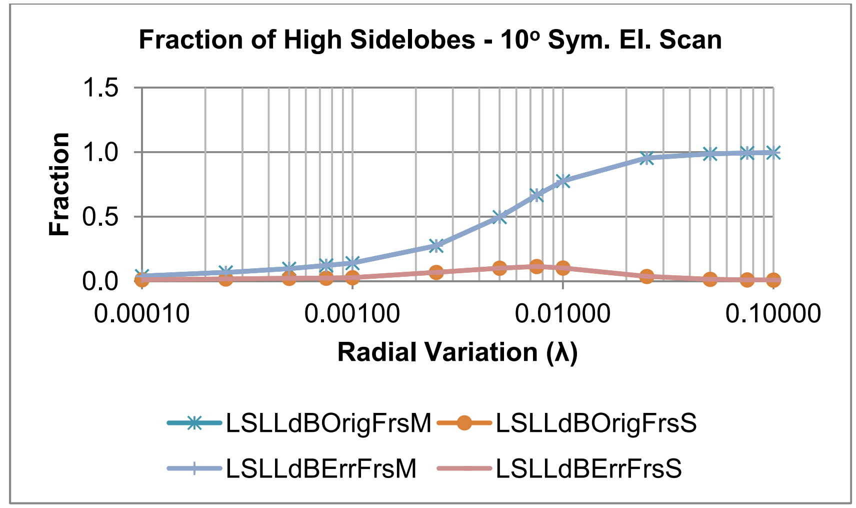

(b)

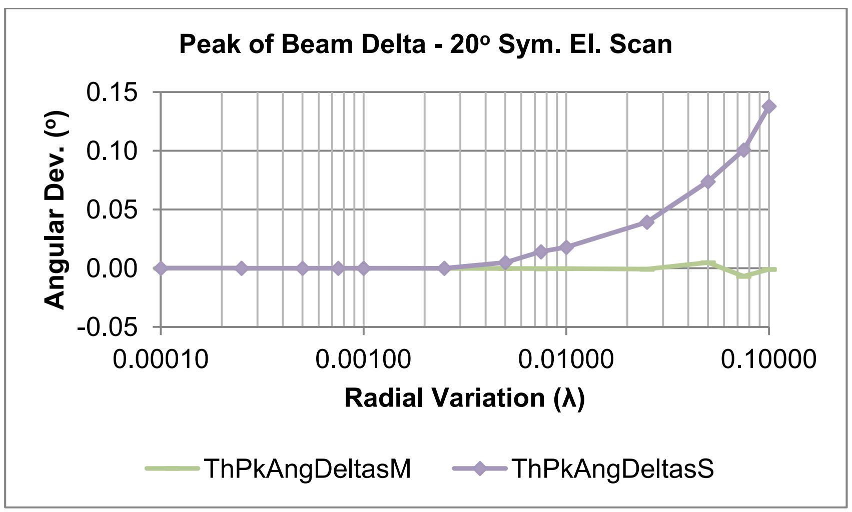

(c)

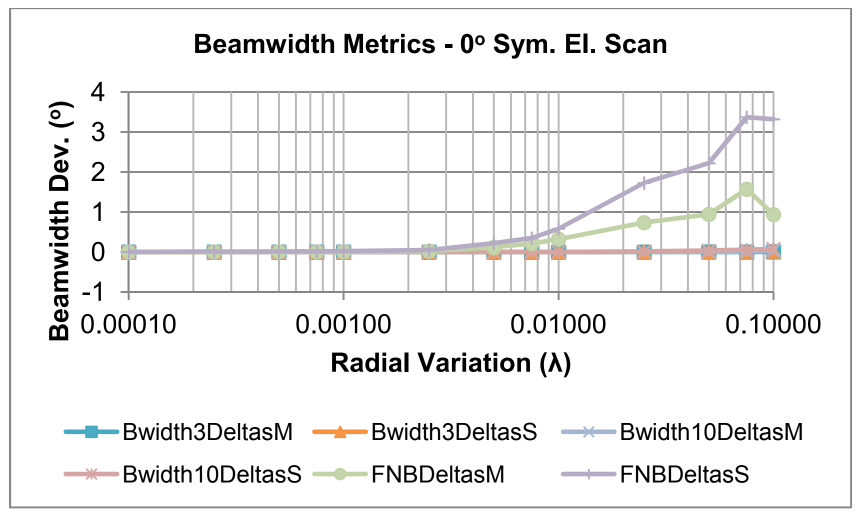

(d)

Figure B.94. *Statistical data for a* $5/8\,\lambda$ *spaced, 21 element, Dolph-Chebyshev array versus radial randomization.* Directivity and sidelobe level (a), LSLLdB (b), beam pointing (c), and beamwidth (d) results are illustrated.

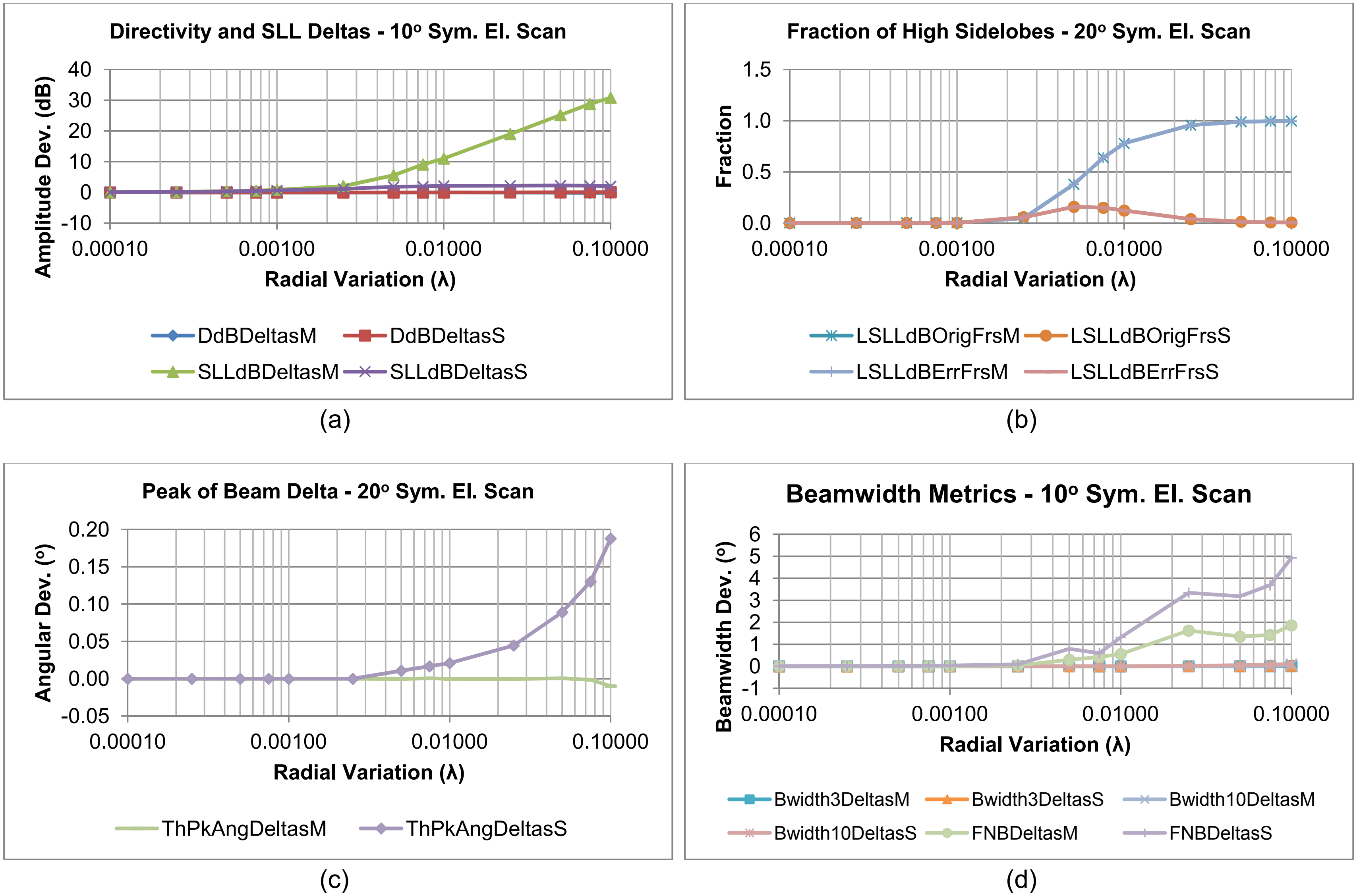

Figure B.95. *Statistical data for a* $5/8\,\lambda$ *spaced, 21 element, modified Taylor array versus radial randomization.* Directivity and sidelobe level (a), LSLLdB (b), beam pointing (c), and beamwidth (d) results are illustrated.

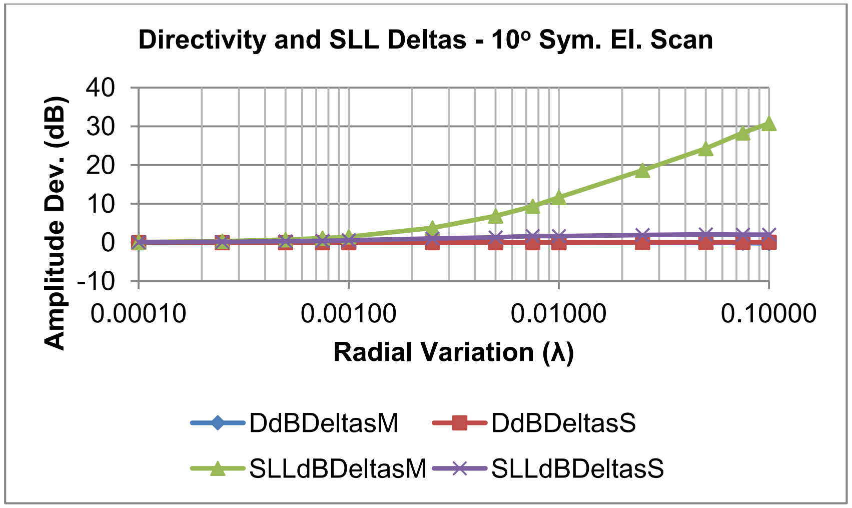

(a)

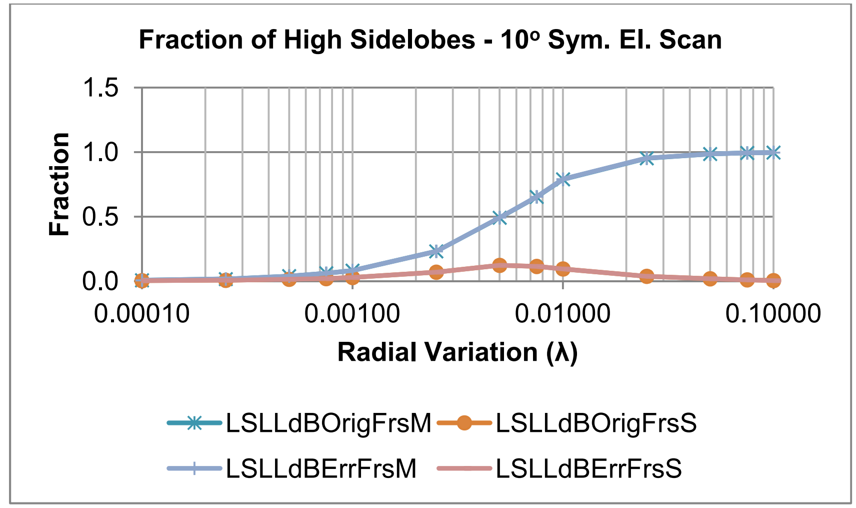

(b)

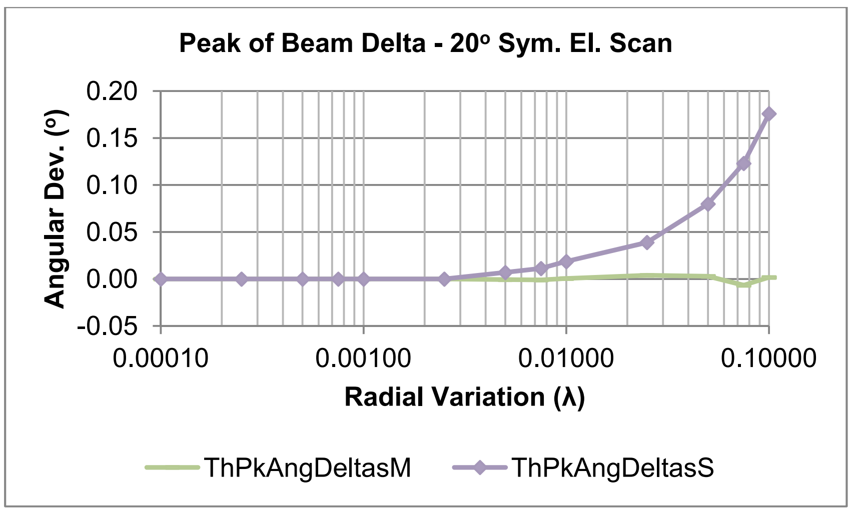

(c)

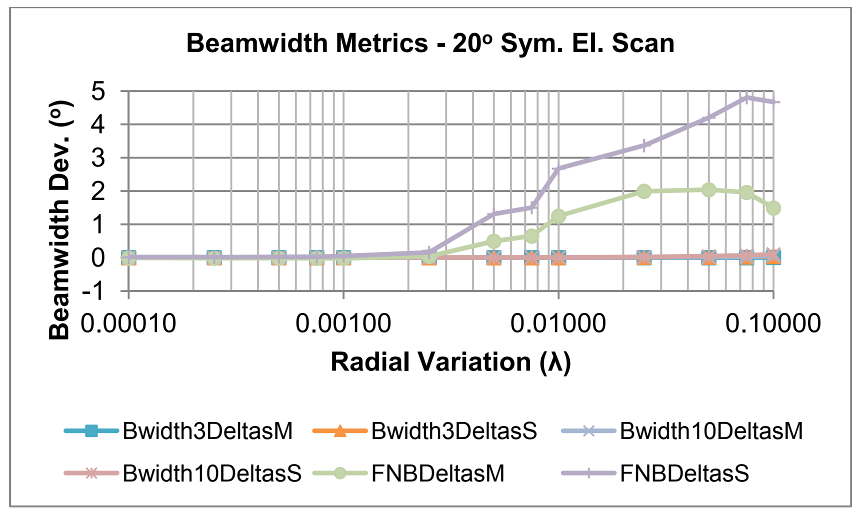

(d)

Figure B.96. *Statistical data for a $5/8\,\lambda$ spaced, 21 element, Taylor array versus radial randomization. Directivity* and sidelobe level (a), LSLLdB (b), beam pointing (c), and beamwidth (d) results are illustrated.

$3/4\lambda$ Element Spacing

20 dB Initial Design Sidelobe Level

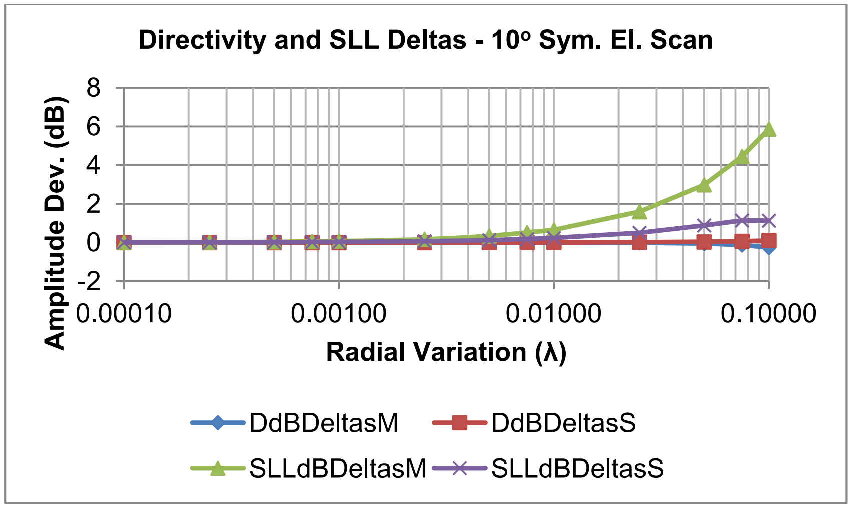

(a)

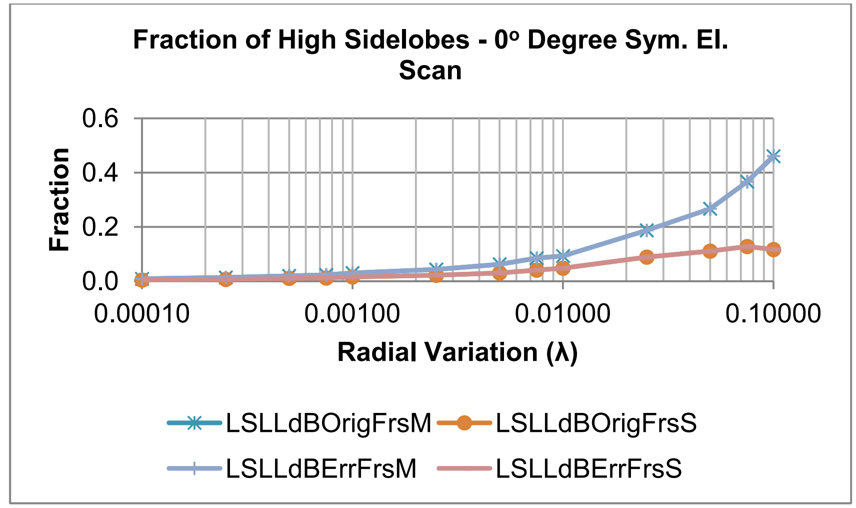

(b)

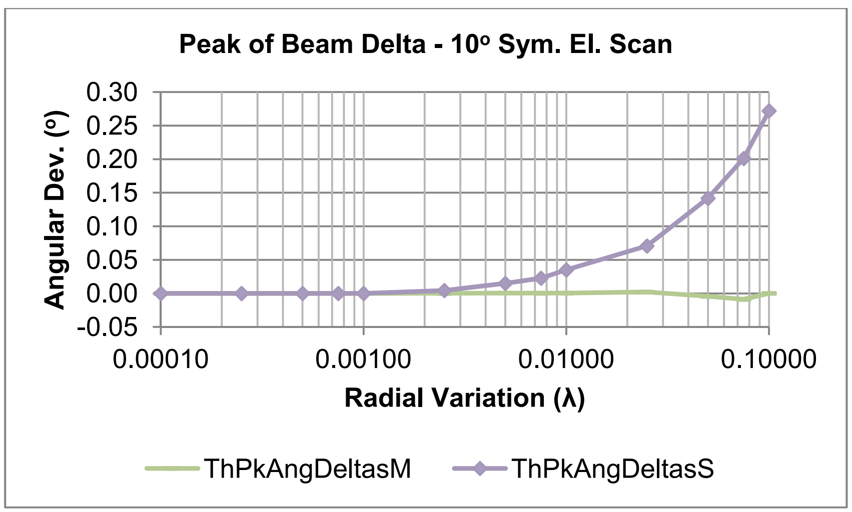

(c)

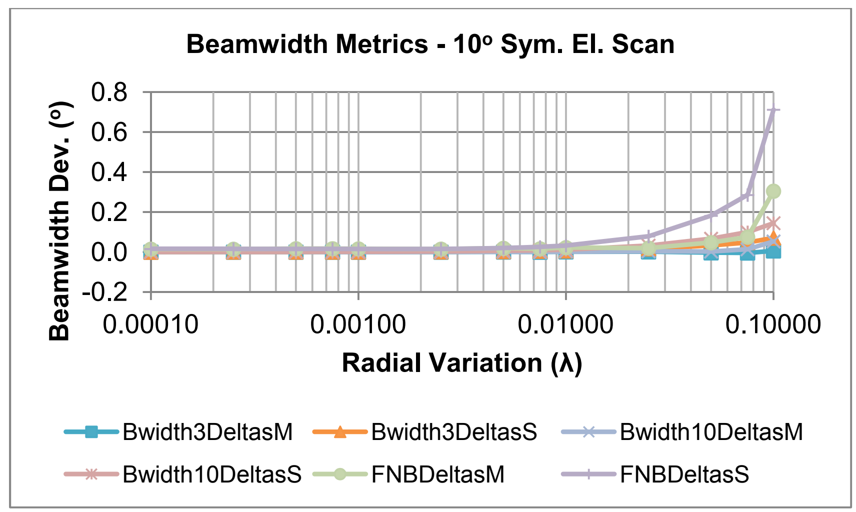

(d)

Figure B.97. *Statistical data for a $3/4\,\lambda$ spaced, 9 element, Dolph-Chebyshev array versus radial randomization.* Directivity and sidelobe level (a), LSLLdB (b), beam pointing (c), and beamwidth (d) results are illustrated.

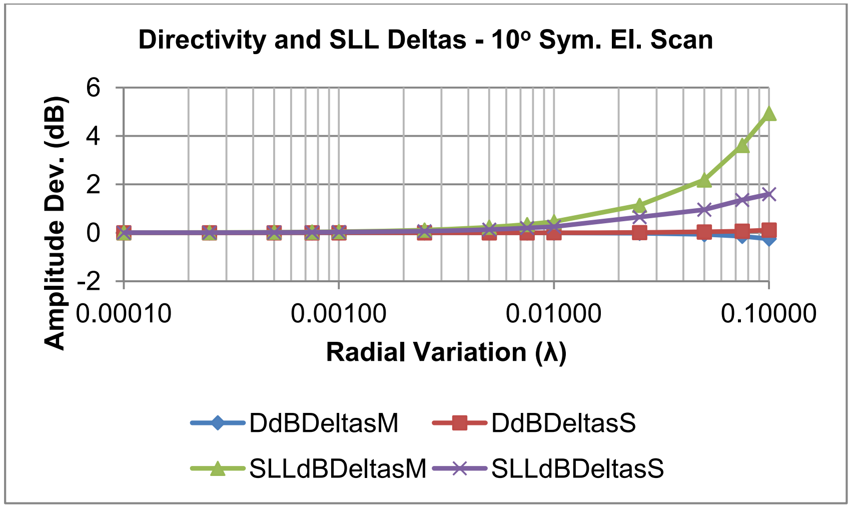

(a)

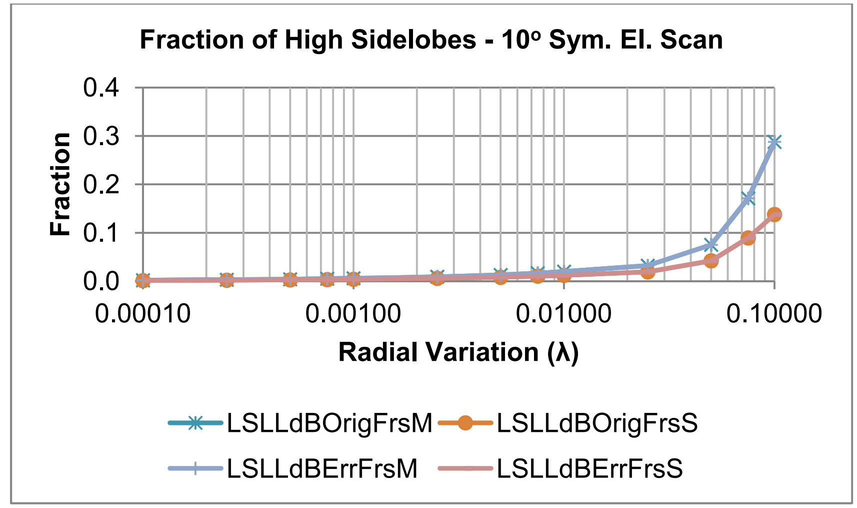

(b)

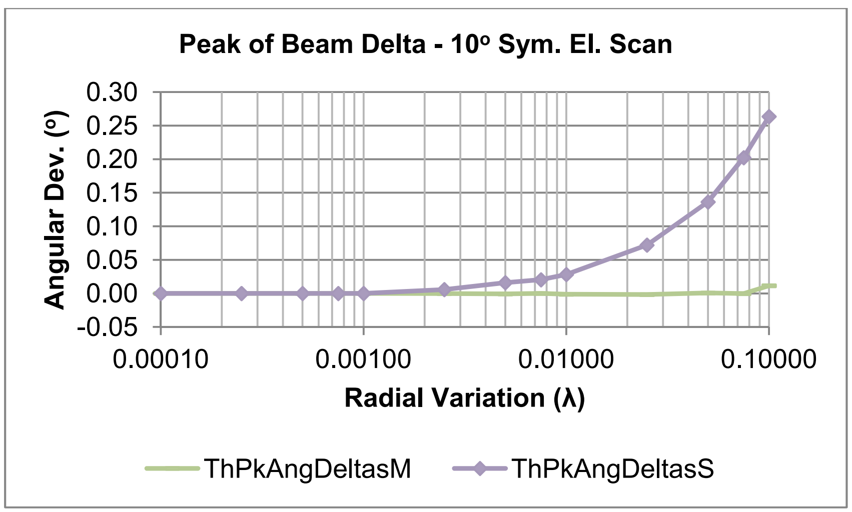

(c)

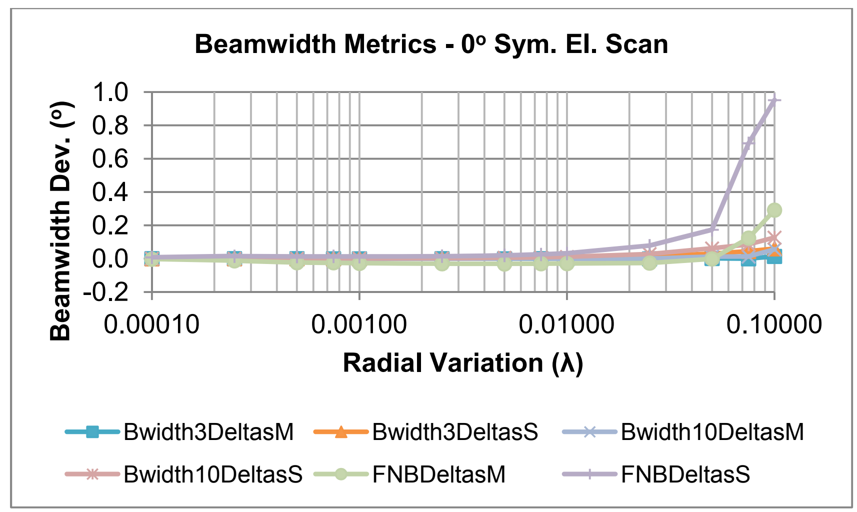

(d)

Figure B.98. *Statistical data for a $3/4\lambda$ spaced, 10 element, modified Taylor array versus radial randomization.* Directivity and sidelobe level (a), LSLLdB (b), beam pointing (c), and beamwidth (d) results are illustrated.

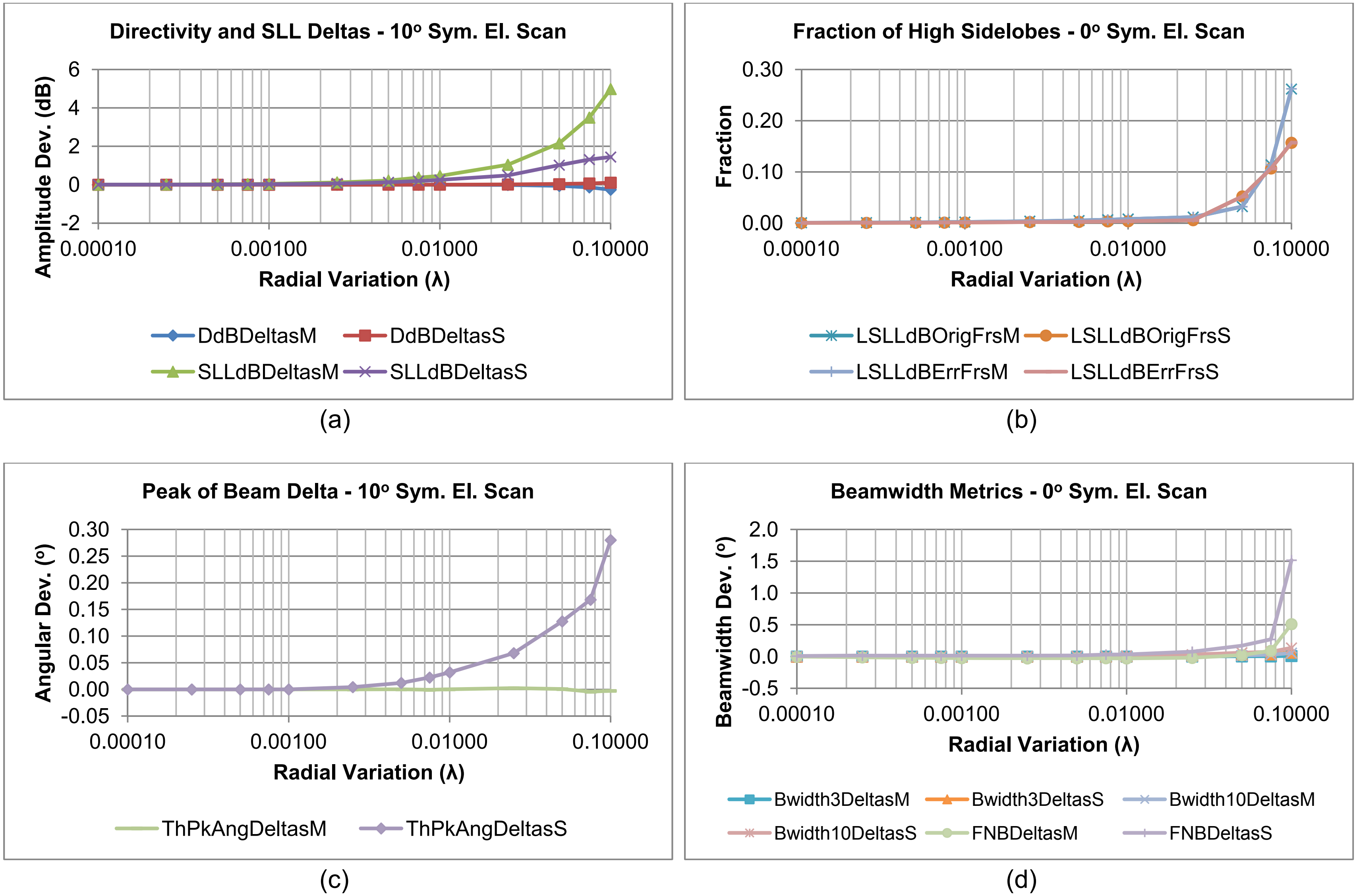

Figure B.99. *Statistical data for a $3/4\lambda$ spaced, 10 element, powers of cosine on a pedestal array versus radial randomization.* Directivity and sidelobe level (a), LSLLdB (b), beam pointing (c), and beamwidth (d) results are illustrated.

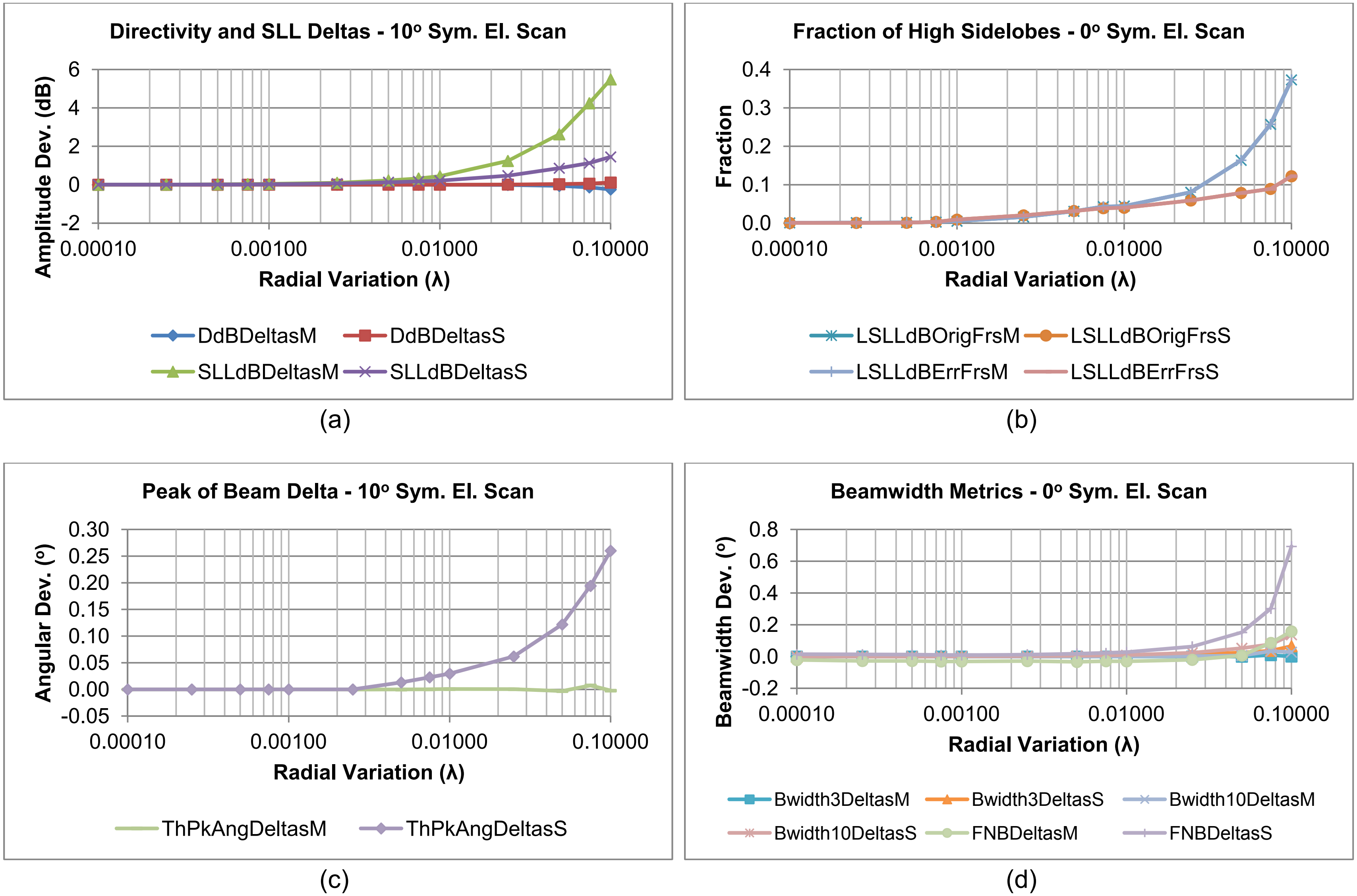

Figure B.100. *Statistical data for a* $3/4\lambda$ *spaced, 10 element, Taylor array versus radial randomization.* Directivity and sidelobe level (a), LSLLdB (b), beam pointing (c), and beamwidth (d) results are illustrated.

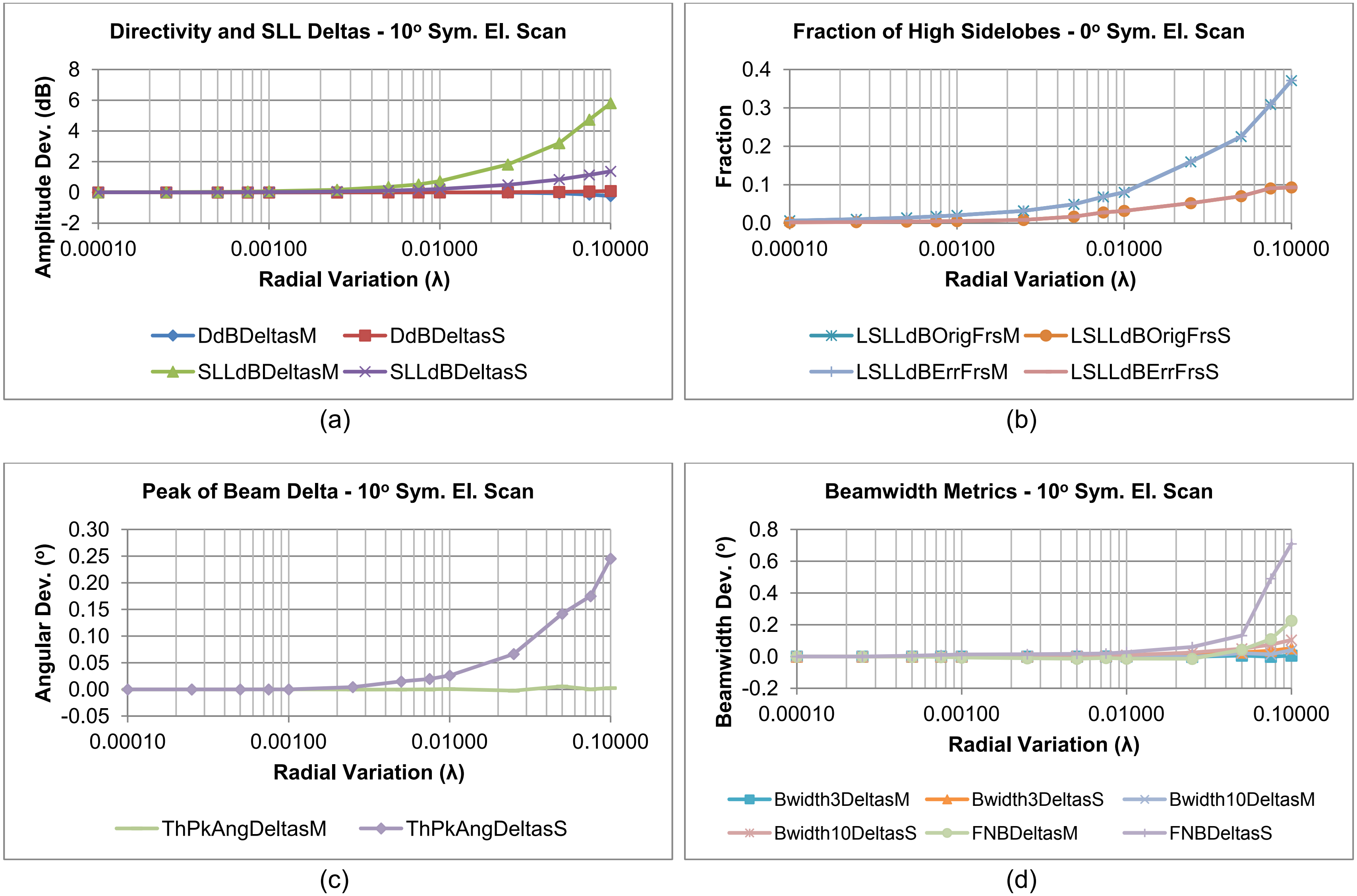

Figure B.101. *Statistical data for a* $3/4\lambda$ *spaced, 10 element, Dolph-Chebyshev array versus radial randomization.* Directivity and sidelobe level (a), LSLLdB (b), beam pointing (c), and beamwidth (d) results are illustrated.

$3/4\lambda$ Element Spacing

30 dB Initial Design Sidelobe Level

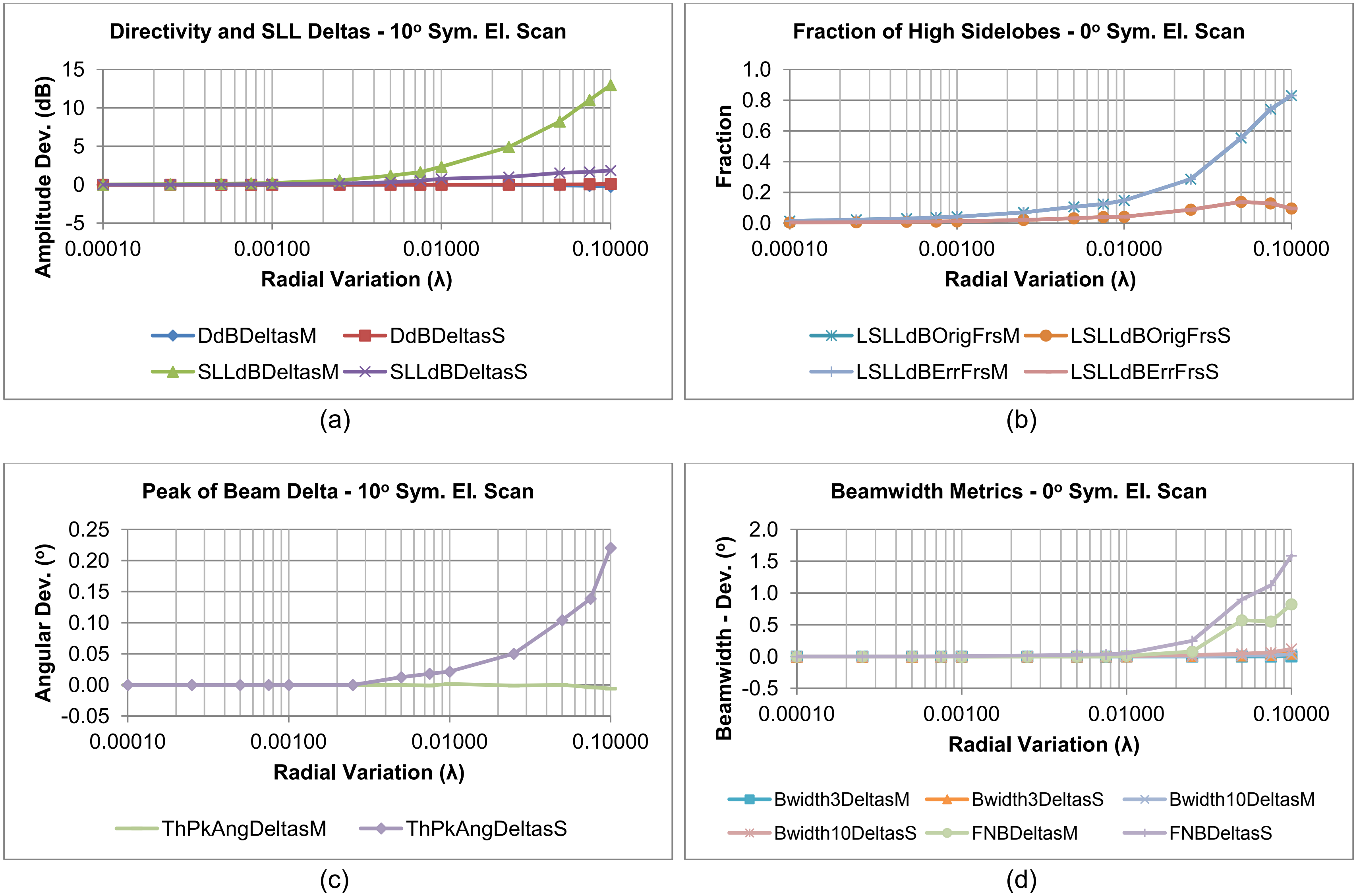

Figure B.102. *Statistical data for a* $3/4\lambda$ *spaced, 12 element, Dolph-Chebyshev array versus radial randomization.* Directivity and sidelobe level (a), LSLLdB (b), beam pointing (c), and beamwidth (d) results are illustrated.

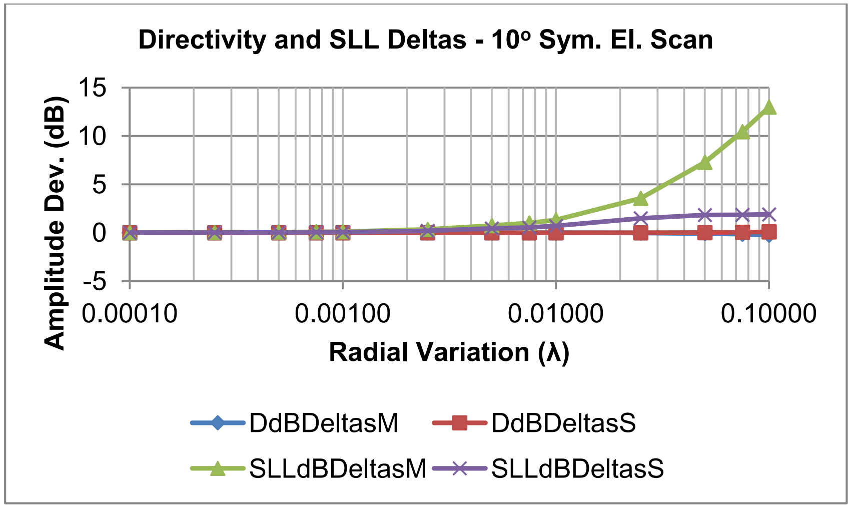

(a)

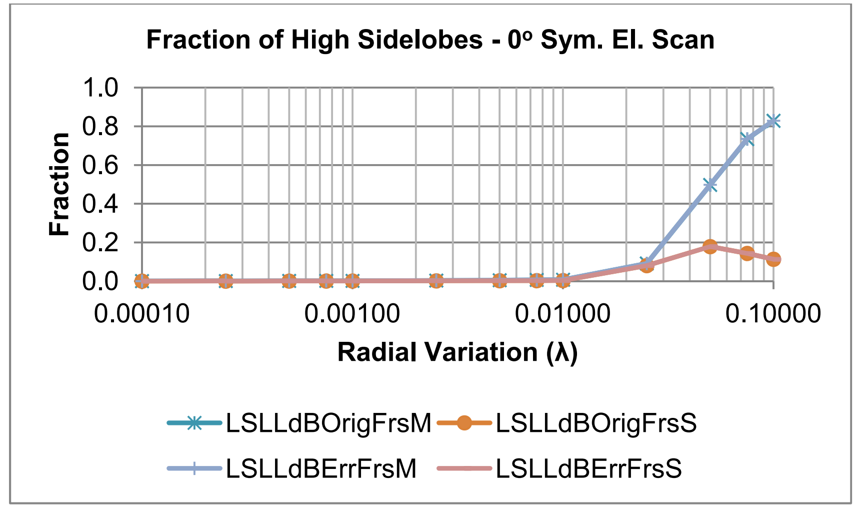

(b)

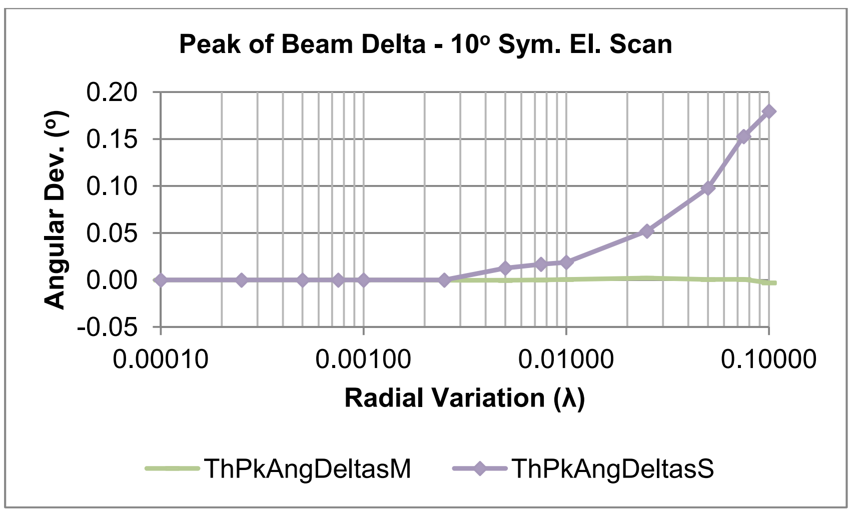

(c)

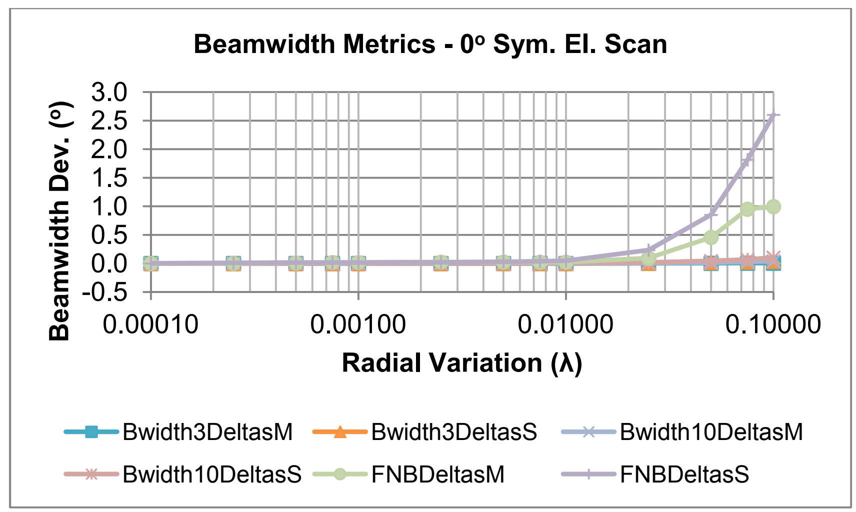

(d)

Figure B.103. *Statistical data for a* $3/4\lambda$ *spaced, 14 element, modified Taylor array versus radial randomization.* Directivity and sidelobe level (a), LSLLdB (b), beam pointing (c), and beamwidth (d) results are illustrated.

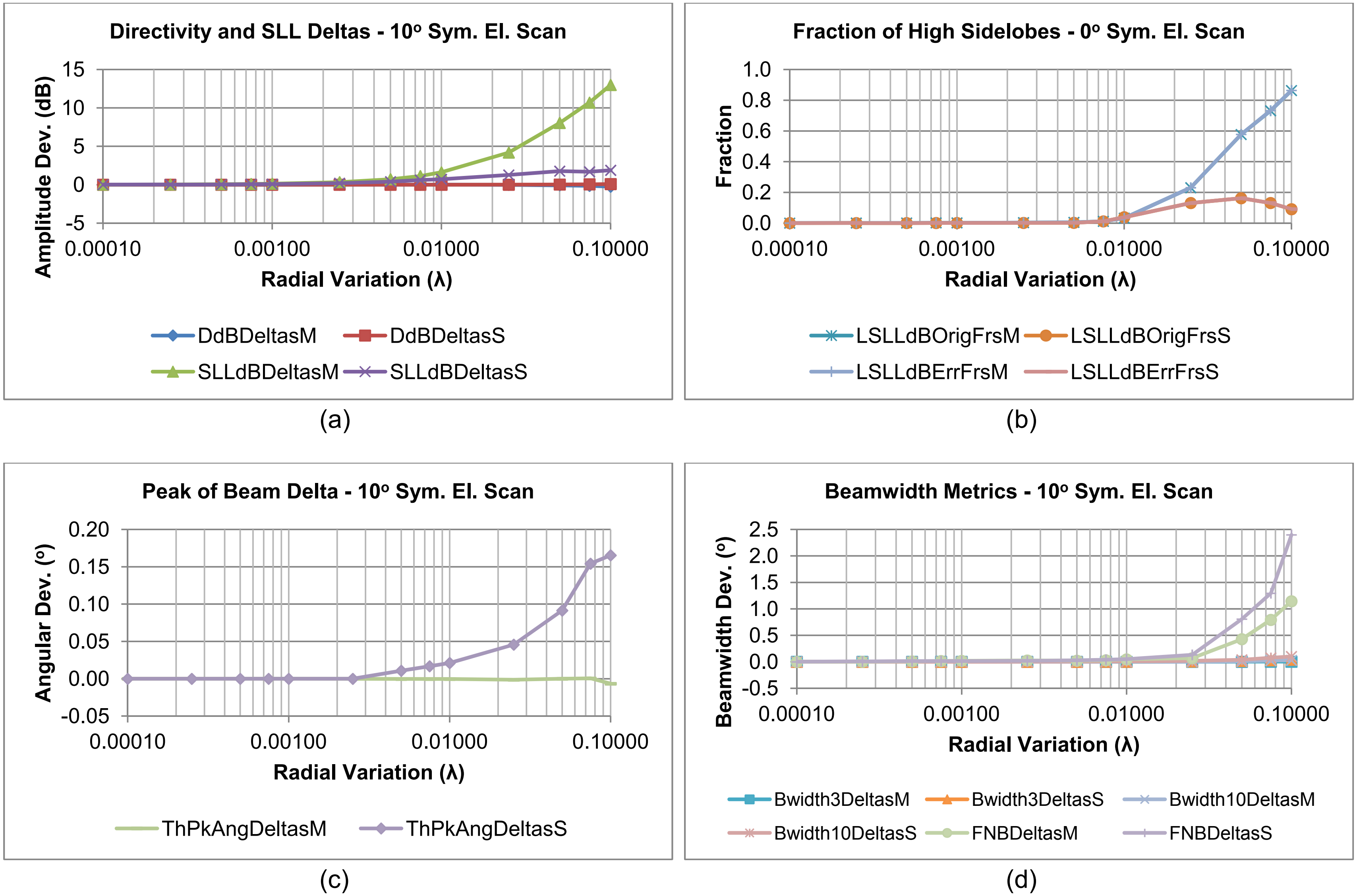

Figure B.104. *Statistical data for a* $3/4\lambda$ *spaced, 13 element, powers of cosine on a pedestal array versus radial randomization.* Directivity and sidelobe level (a), LSLLdB (b), beam pointing (c), and beamwidth (d) results are illustrated.

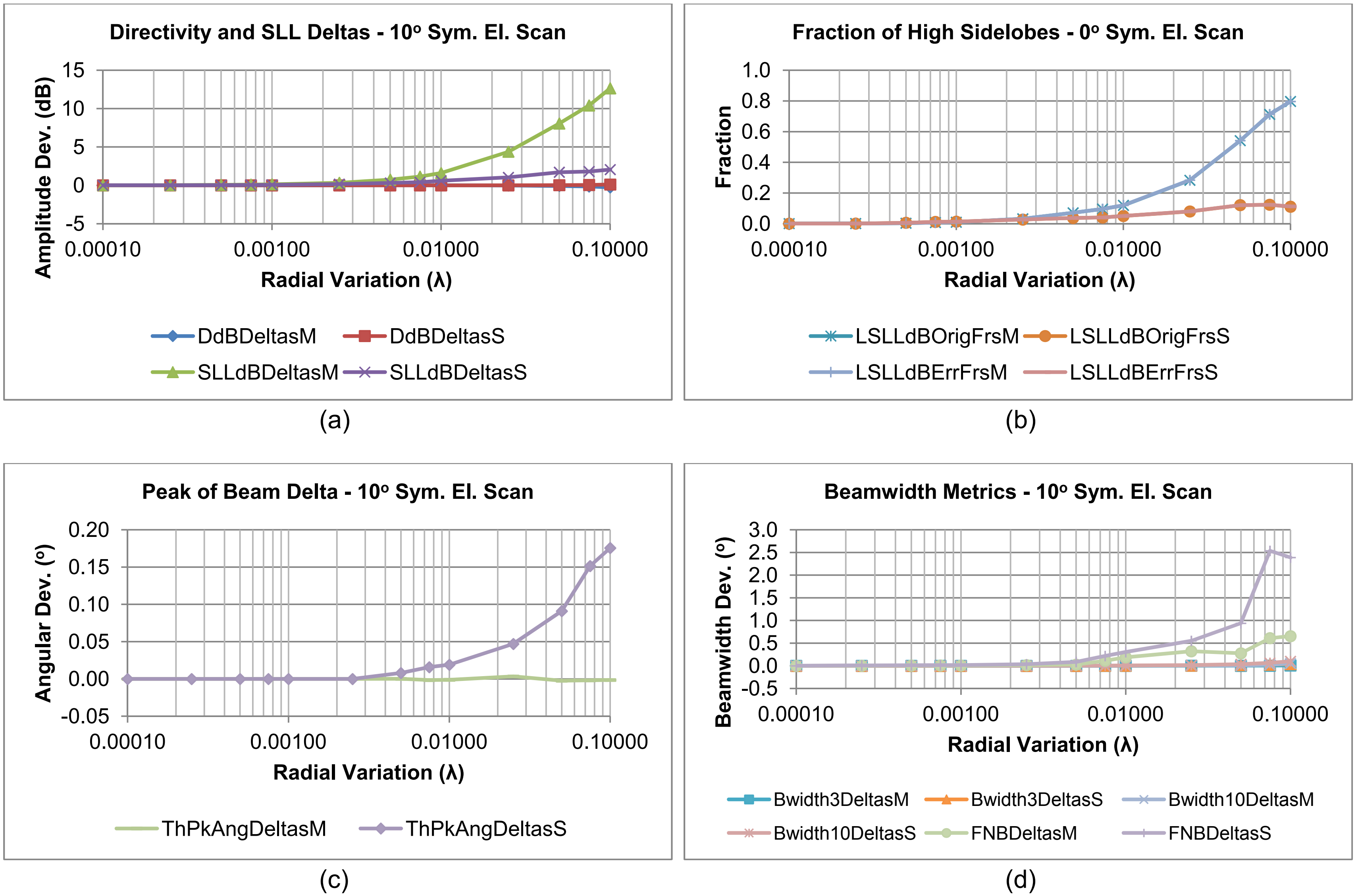

Figure B.105. *Statistical data for a $3/4\lambda$ spaced, 14 element, Taylor array versus radial randomization.* Directivity and sidelobe level (a), LSLLdB (b), beam pointing (c), and beamwidth (d) results are illustrated.

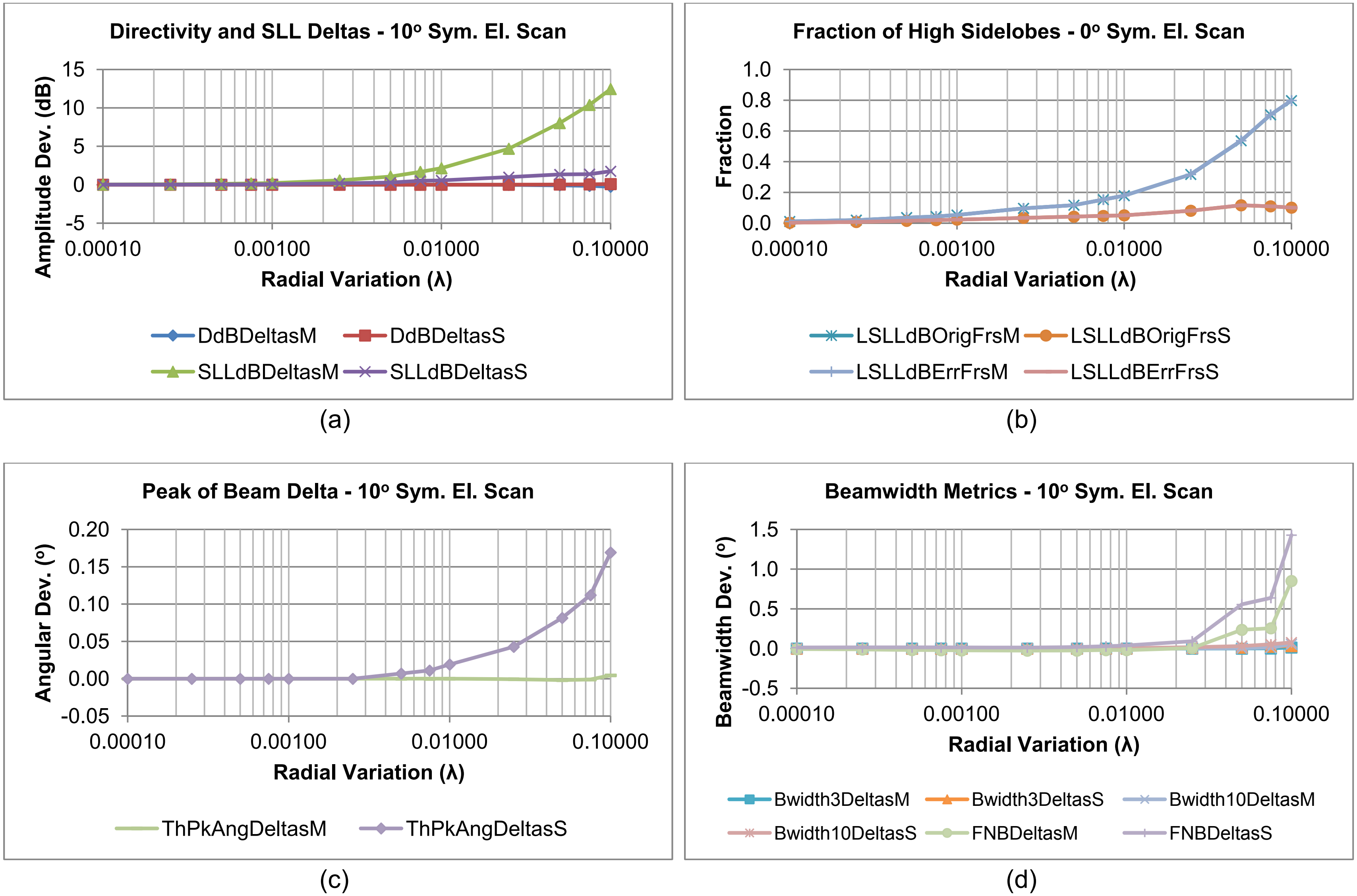

Figure B.106. *Statistical data for a* $3/4\lambda$ *spaced, 14 element, Dolph-Chebyshev array versus radial randomization.* Directivity and sidelobe level (a), LSLLdB (b), beam pointing (c), and beamwidth (d) results are illustrated.

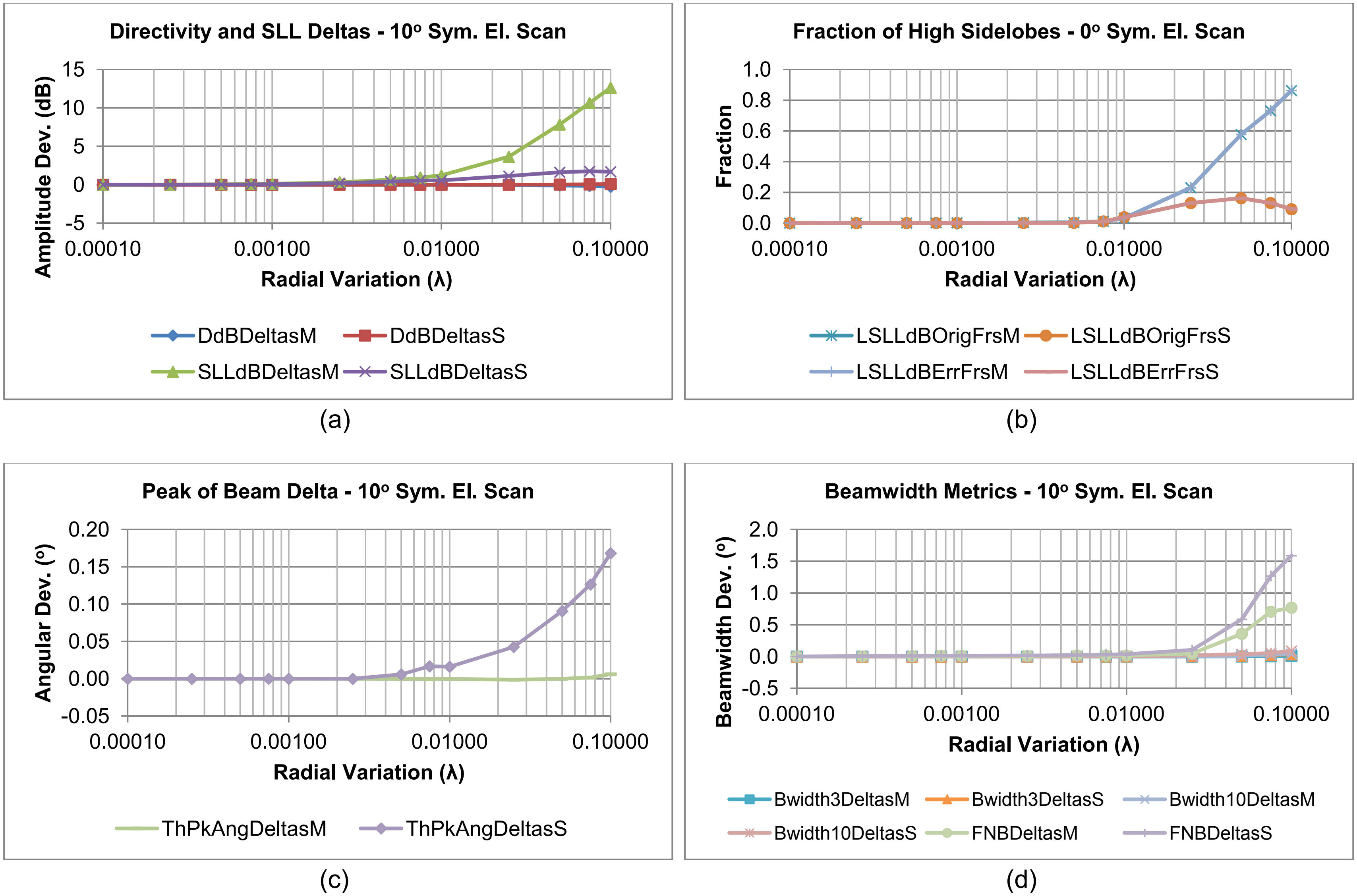

Figure B.107. *Statistical data for a* $3/4\lambda$ *spaced, 14 element, powers of cosine on a pedestal array versus radial randomization.* Directivity and sidelobe level (a), LSLLdB (b), beam pointing (c), and beamwidth (d) results are illustrated.

$3/4\lambda$ Element Spacing

40 dB Initial Design Sidelobe Level

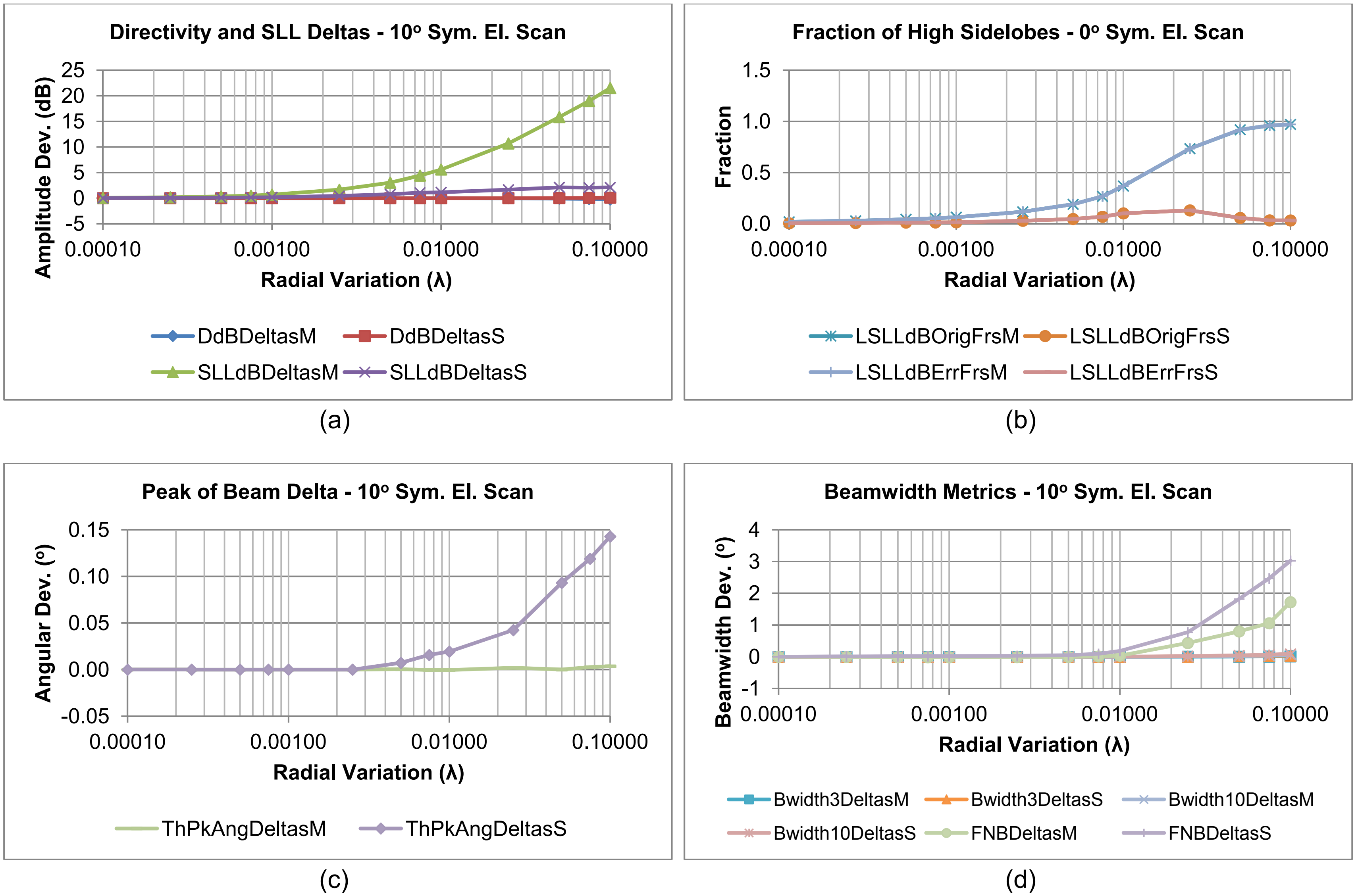

Figure B.108. *Statistical data for a* $3/4\lambda$ *spaced, 15 element, Dolph-Chebyshev array versus radial randomization.* Directivity and sidelobe level (a), LSLLdB (b), beam pointing (c), and beamwidth (d) results are illustrated.

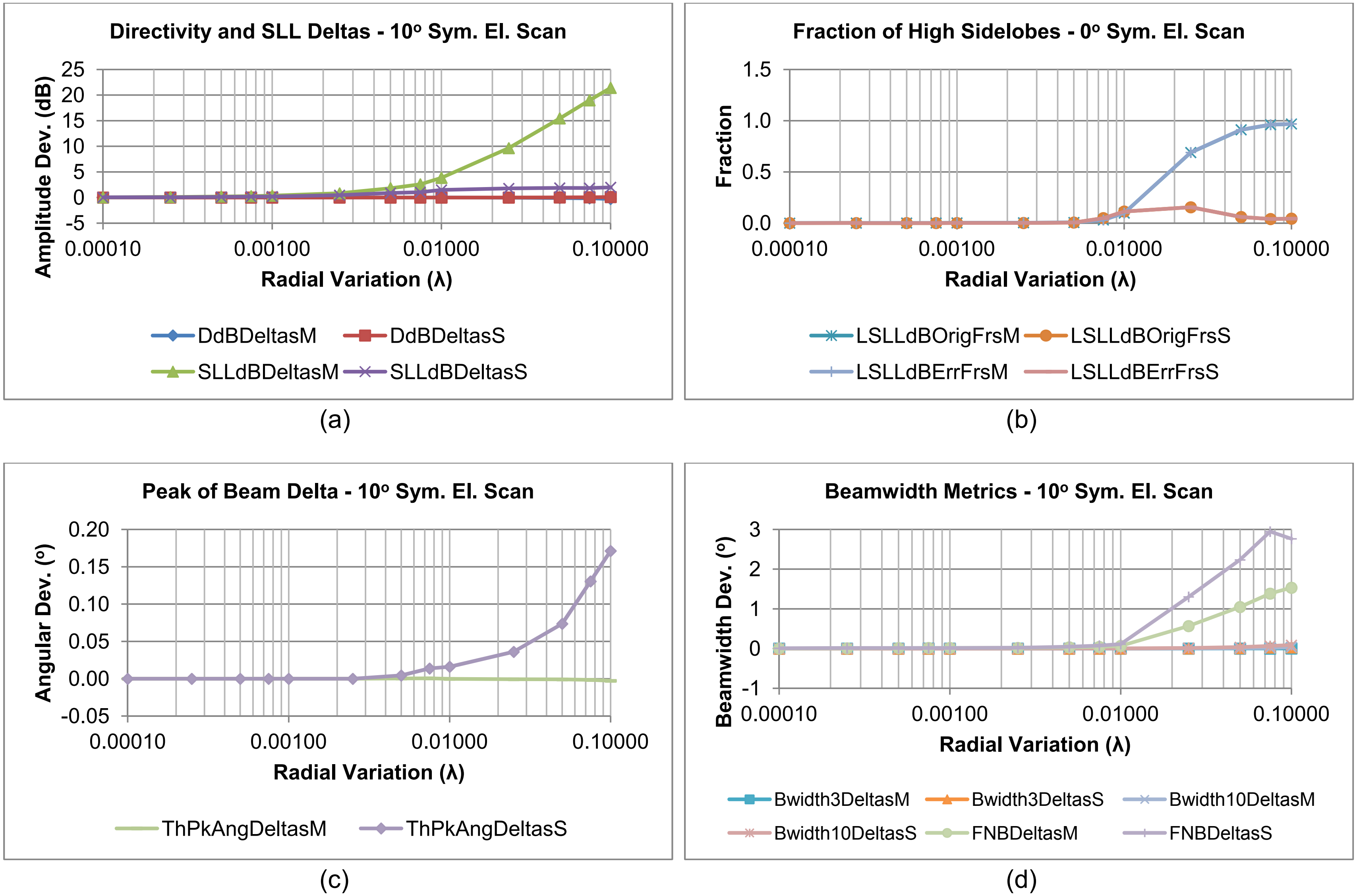

Figure B.109. *Statistical data for a* $3/4\lambda$ *spaced, 18 element, modified Taylor array versus radial randomization.* Directivity and sidelobe level (a), LSLLdB (b), beam pointing (c), and beamwidth (d) results are illustrated.

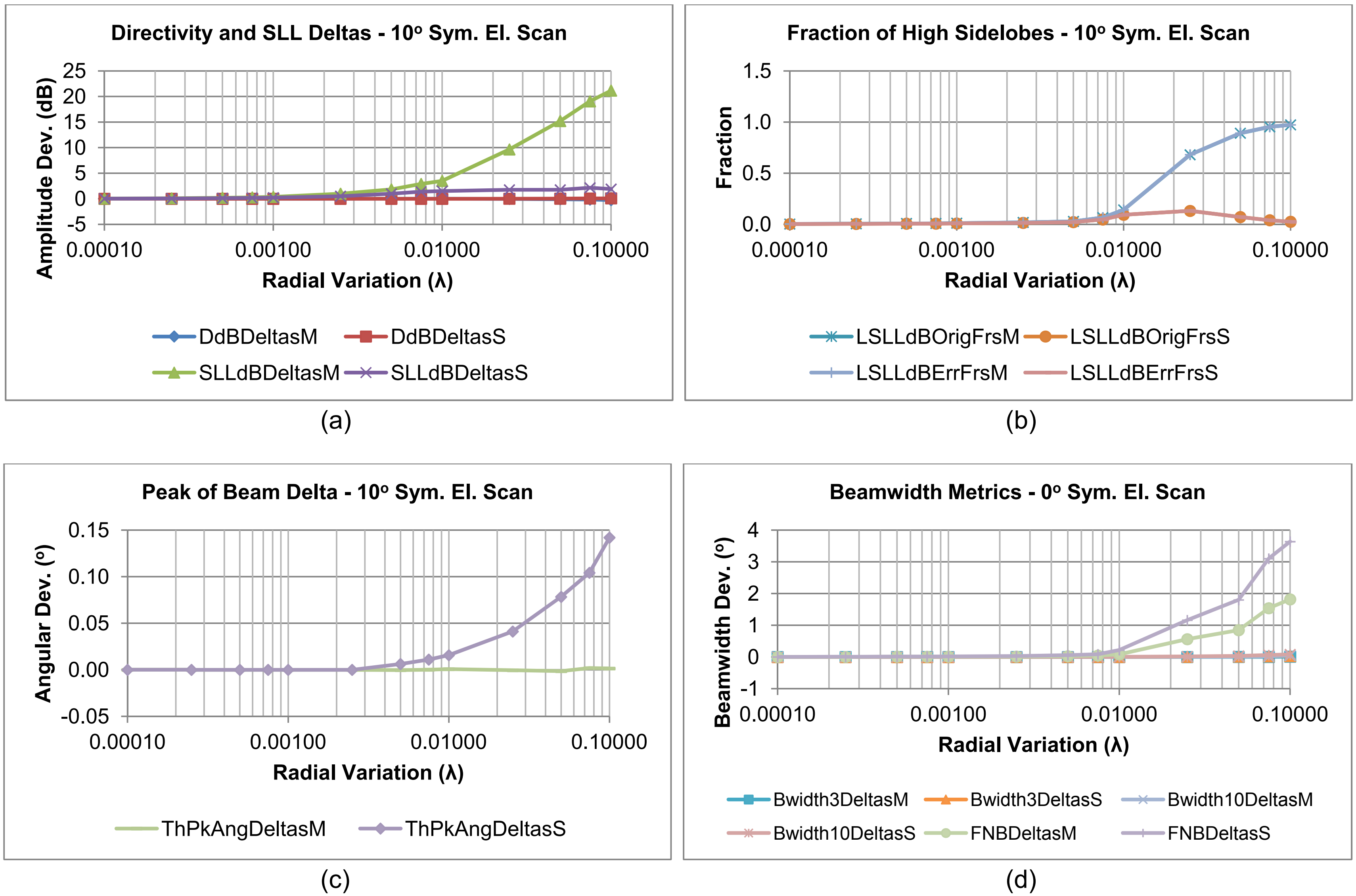

Figure B.110. *Statistical data for a* $3/4\lambda$ *spaced, 22 element, powers of cosine on a pedestal array versus radial randomization.* Directivity and sidelobe level (a), LSLLdB (b), beam pointing (c), and beamwidth (d) results are illustrated.

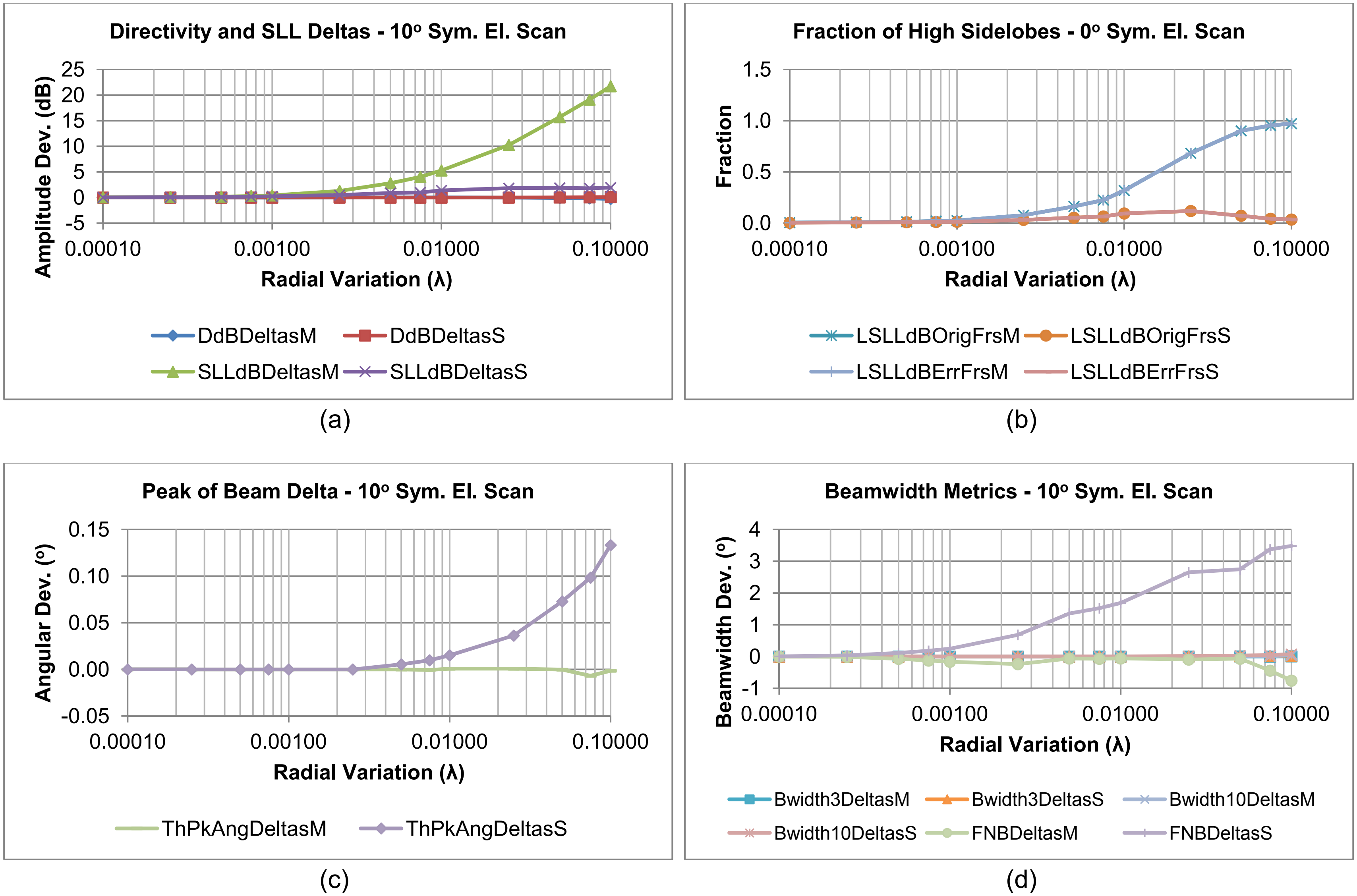

Figure B.111. *Statistical data for a* $3/4\lambda$ *spaced, 18 element, Taylor array versus radial randomization.* Directivity and sidelobe level (a), LSLLdB (b), beam pointing (c), and beamwidth (d) results are illustrated.

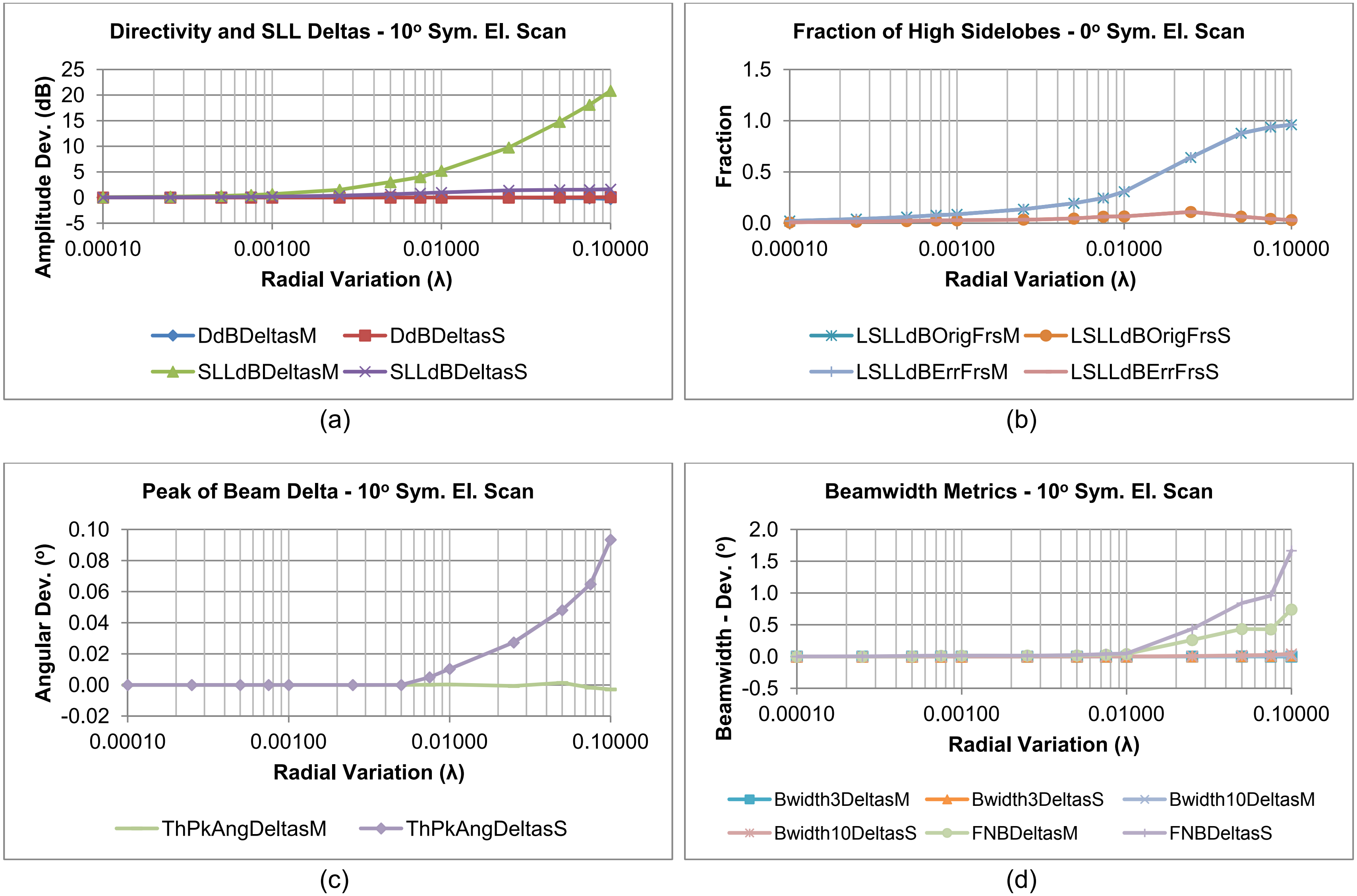

Figure B.112. *Statistical data for a* $3/4\lambda$ *spaced, 22 element, Dolph-Chebyshev array versus radial randomization.* Directivity and sidelobe level (a), LSLLdB (b), beam pointing (c), and beamwidth (d) results are illustrated.

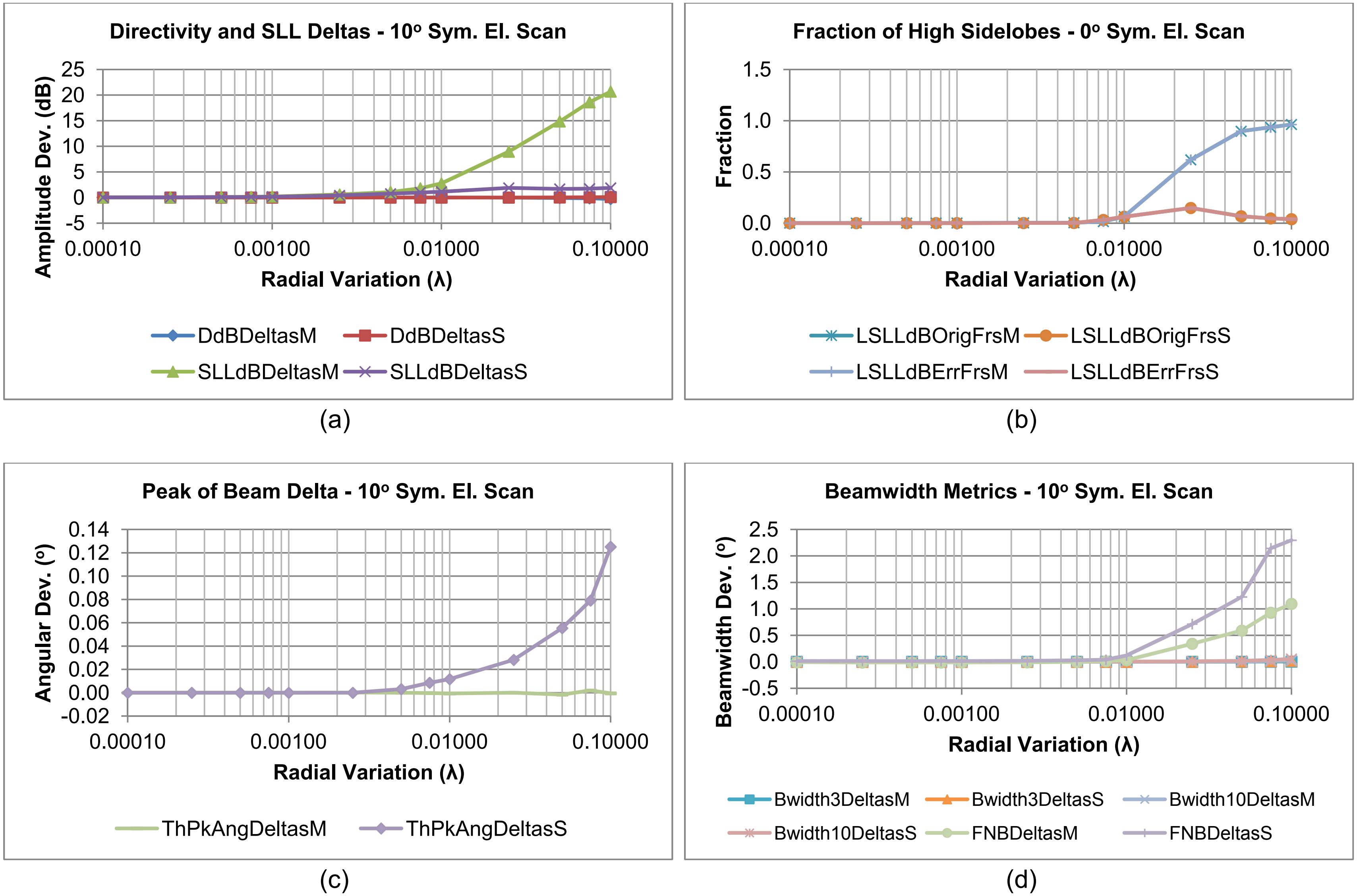

Figure B.113. *Statistical data for a* $3/4\lambda$ *spaced, 22 element, modified Taylor array versus radial randomization.* Directivity and sidelobe level (a), LSLLdB (b), beam pointing (c), and beamwidth (d) results are illustrated.

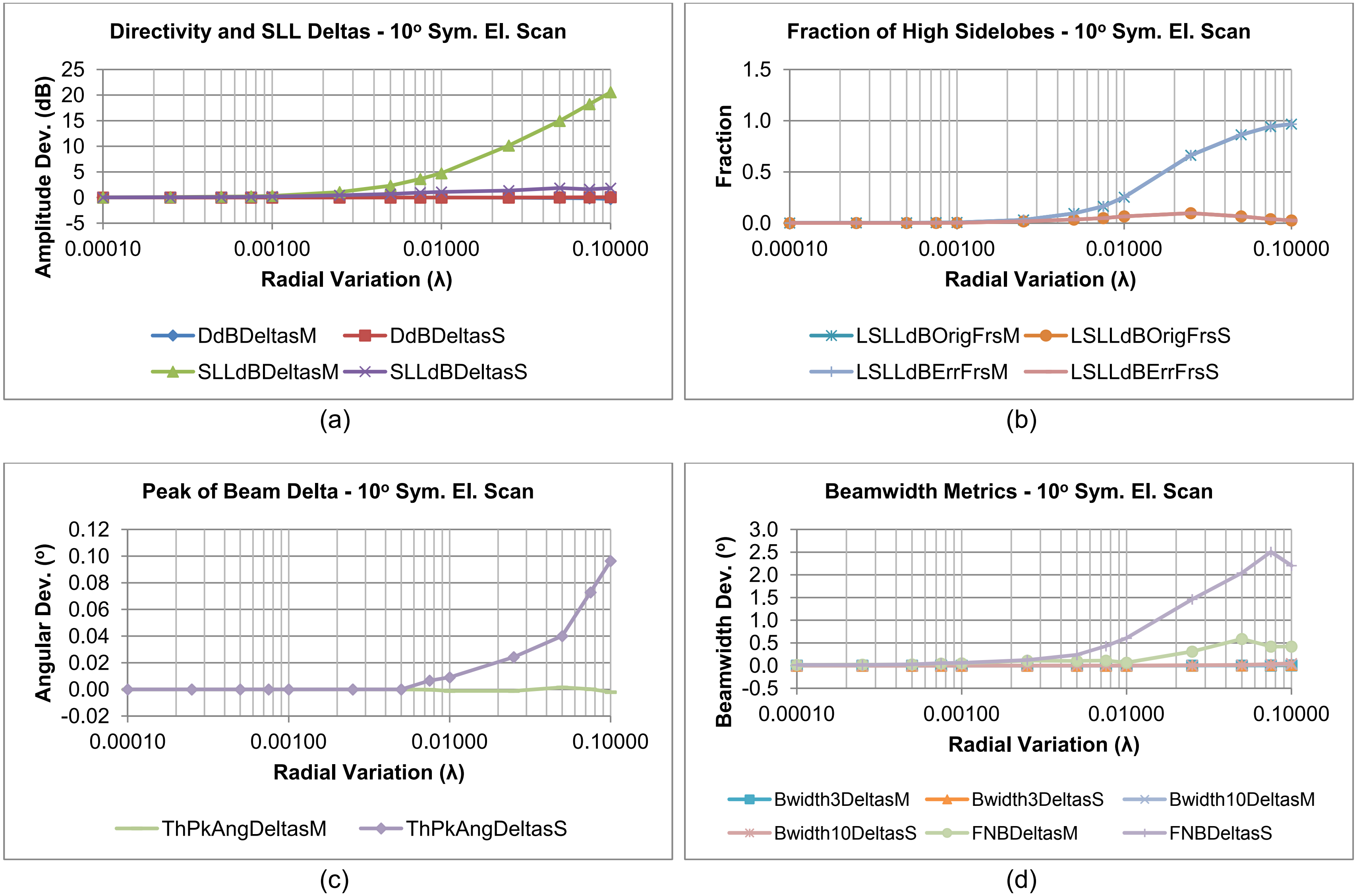

Figure B.114. *Statistical data for a $3/4\lambda$ spaced, 22 element, Taylor array versus radial randomization.* Directivity and sidelobe level (a), LSLLdB (b), beam pointing (c), and beamwidth (d) results are illustrated.

$3/4\lambda$ Element Spacing

50 dB Initial Design Sidelobe Level

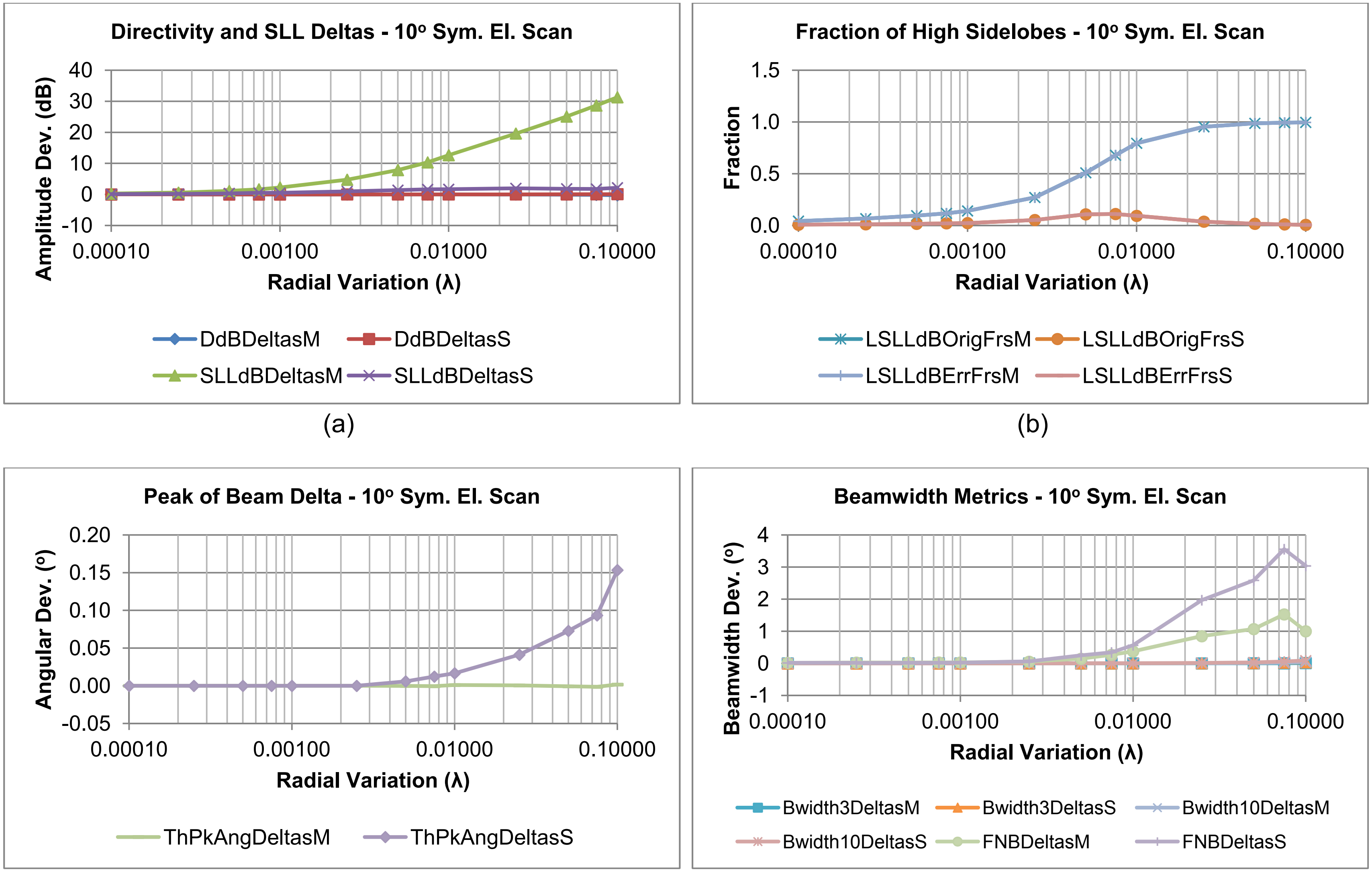

(a)

(b)

(c)

(d)

Figure B.115. *Statistical data for a* $3/4\lambda$ *spaced, 18 element, Dolph-Chebyshev array versus radial randomization.* Directivity and sidelobe level (a), LSLLdB (b), beam pointing (c), and beamwidth (d) results are illustrated.

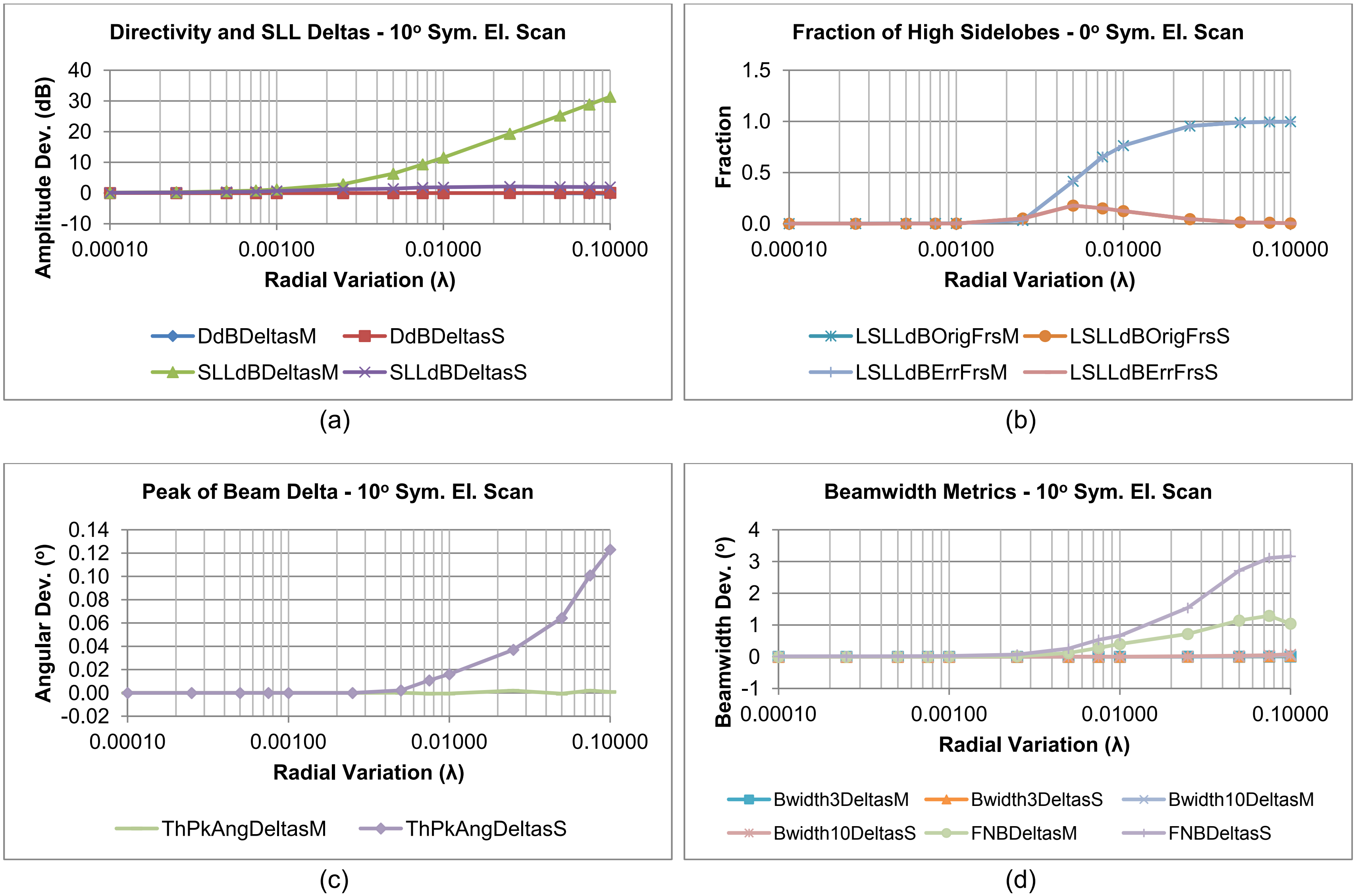

Figure B.116. *Statistical data for a* $3/4\lambda$ *spaced, 21 element, modified Taylor array versus radial randomization.* Directivity and sidelobe level (a), LSLLdB (b), beam pointing (c), and beamwidth (d) results are illustrated.

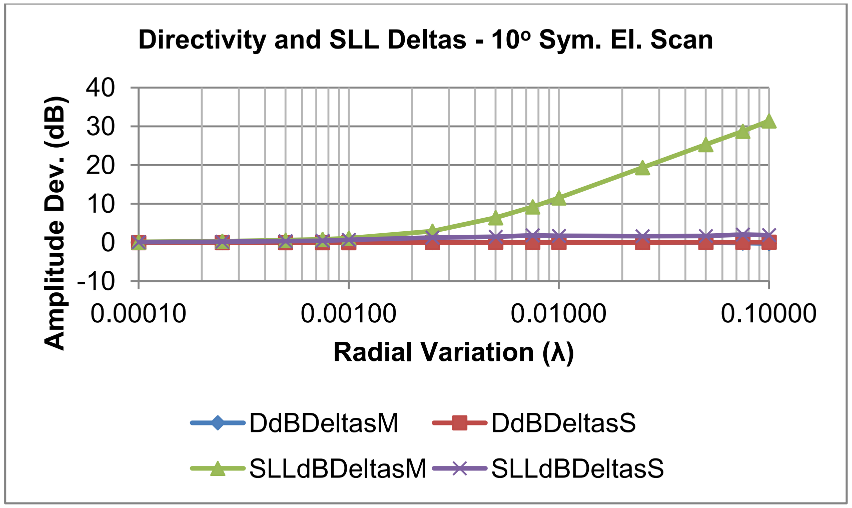

(a)

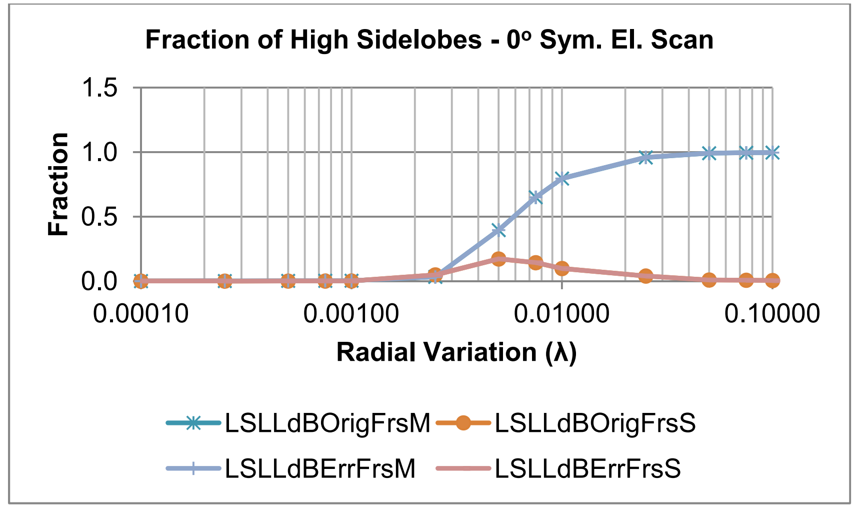

(b)

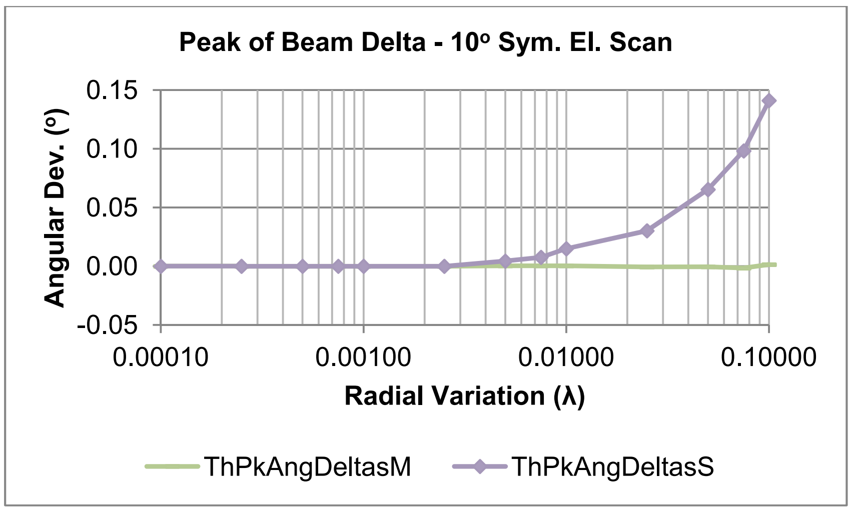

(c)

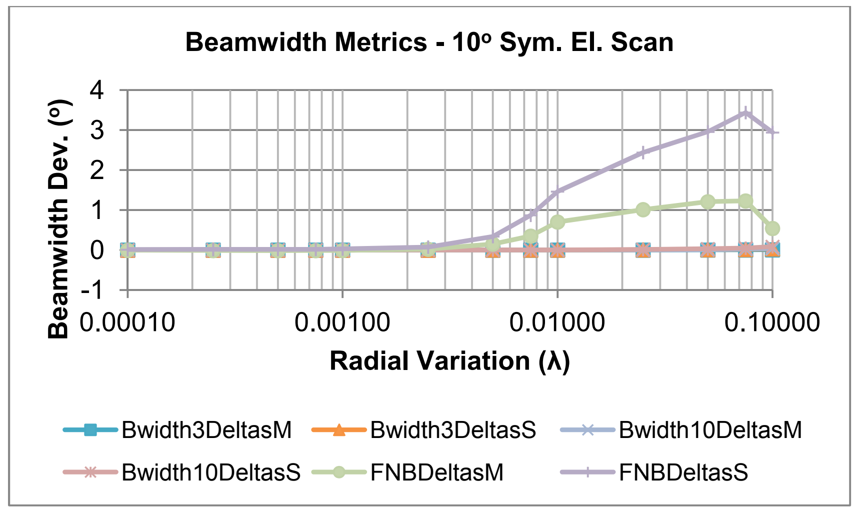

(d)

Figure B.117. *Statistical data for a* $3/4\lambda$ *spaced, 28 element, powers of cosine on a pedestal array versus radial randomization.* Directivity and sidelobe level (a), LSLLdB (b), beam pointing (c), and beamwidth (d) results are illustrated.

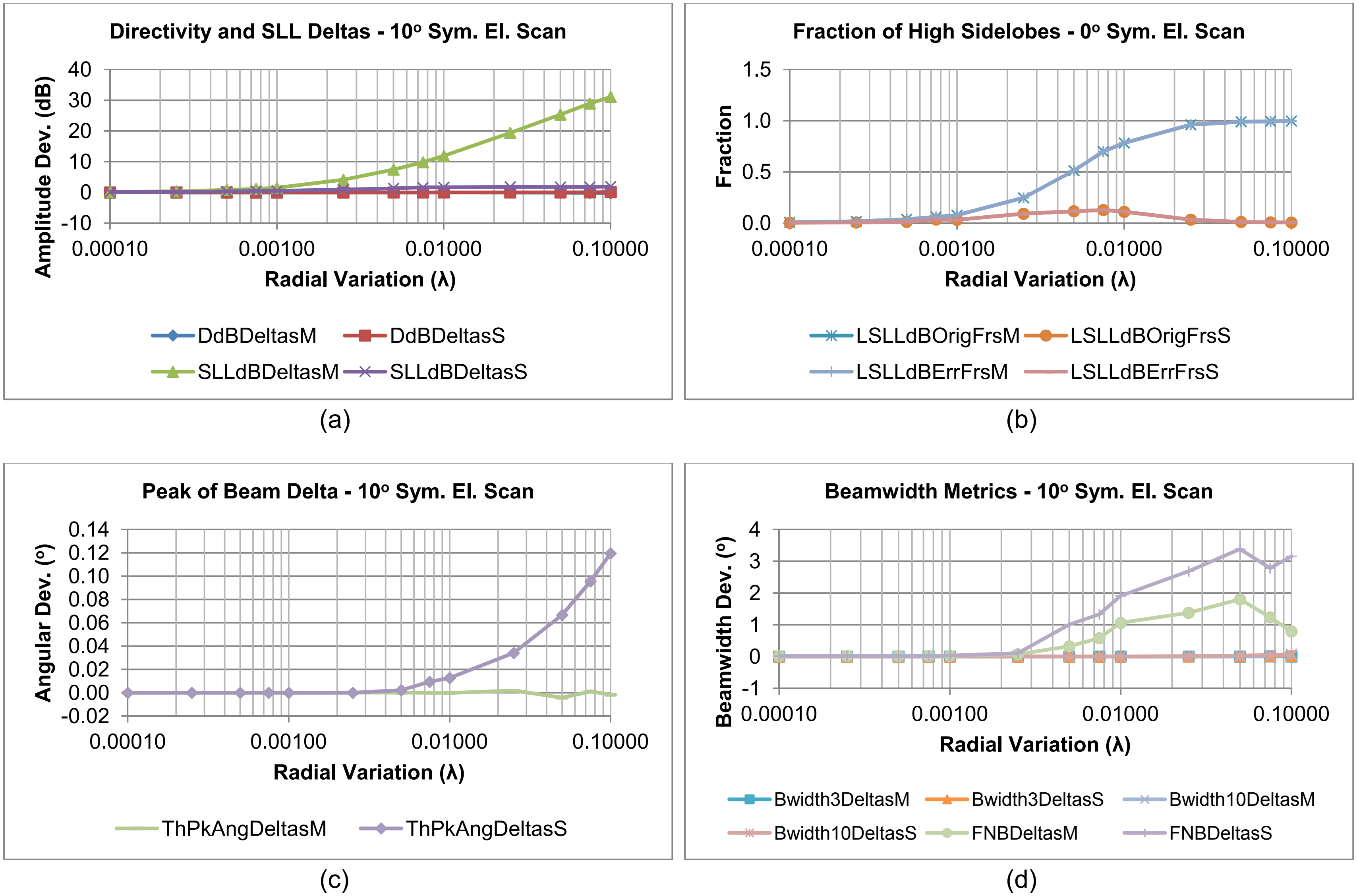

Figure B.118. *Statistical data for a* $3/4\lambda$ *spaced, 21 element, Taylor array versus radial randomization.* Directivity and sidelobe level (a), LSLLdB (b), beam pointing (c), and beamwidth (d) results are illustrated.

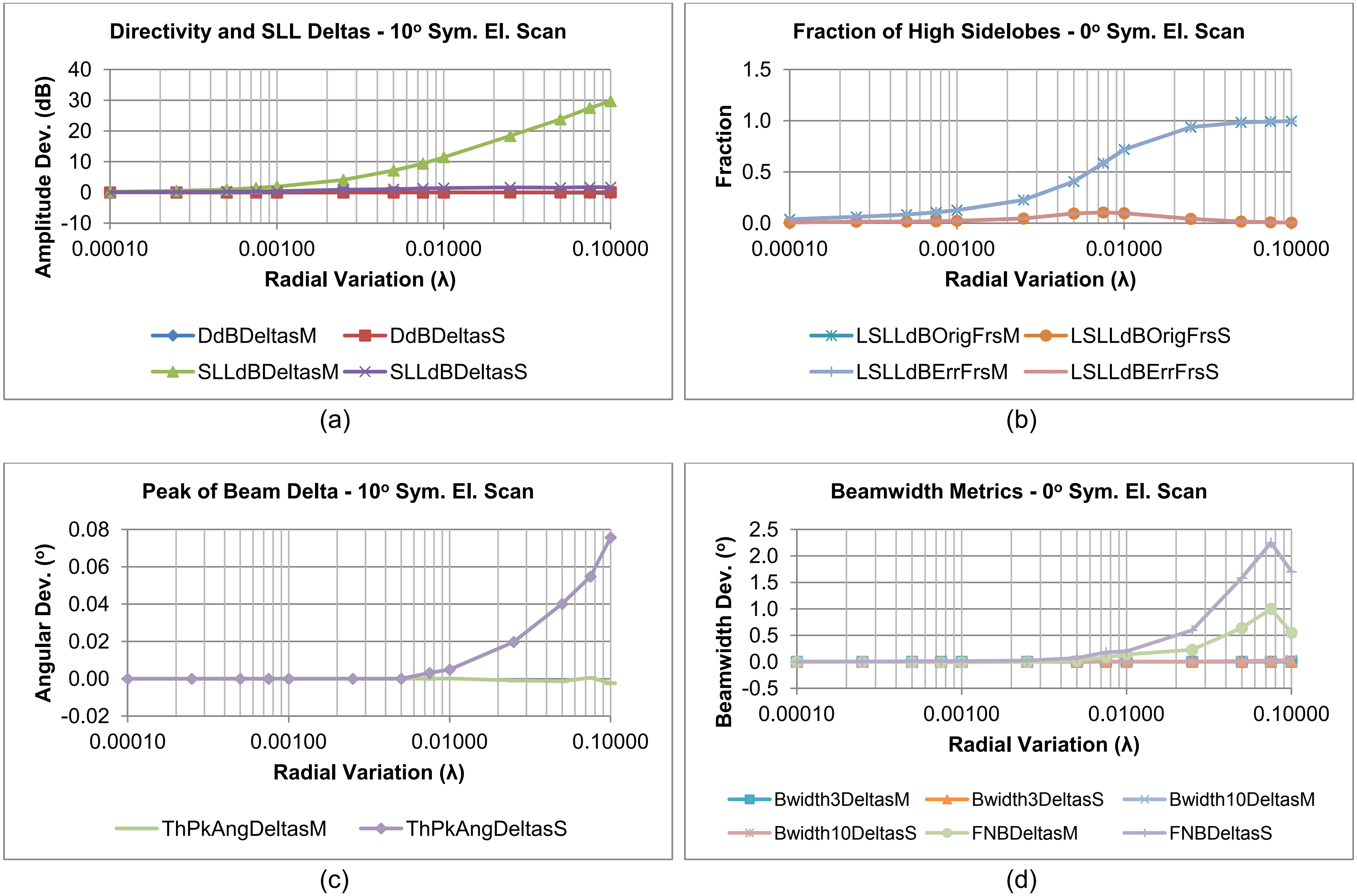

Figure B.119. *Statistical data for a* $3/4\lambda$ *spaced, 28 element, Dolph-Chebyshev array versus radial randomization.* Directivity and sidelobe level (a), LSLLdB (b), beam pointing (c), and beamwidth (d) results are illustrated.

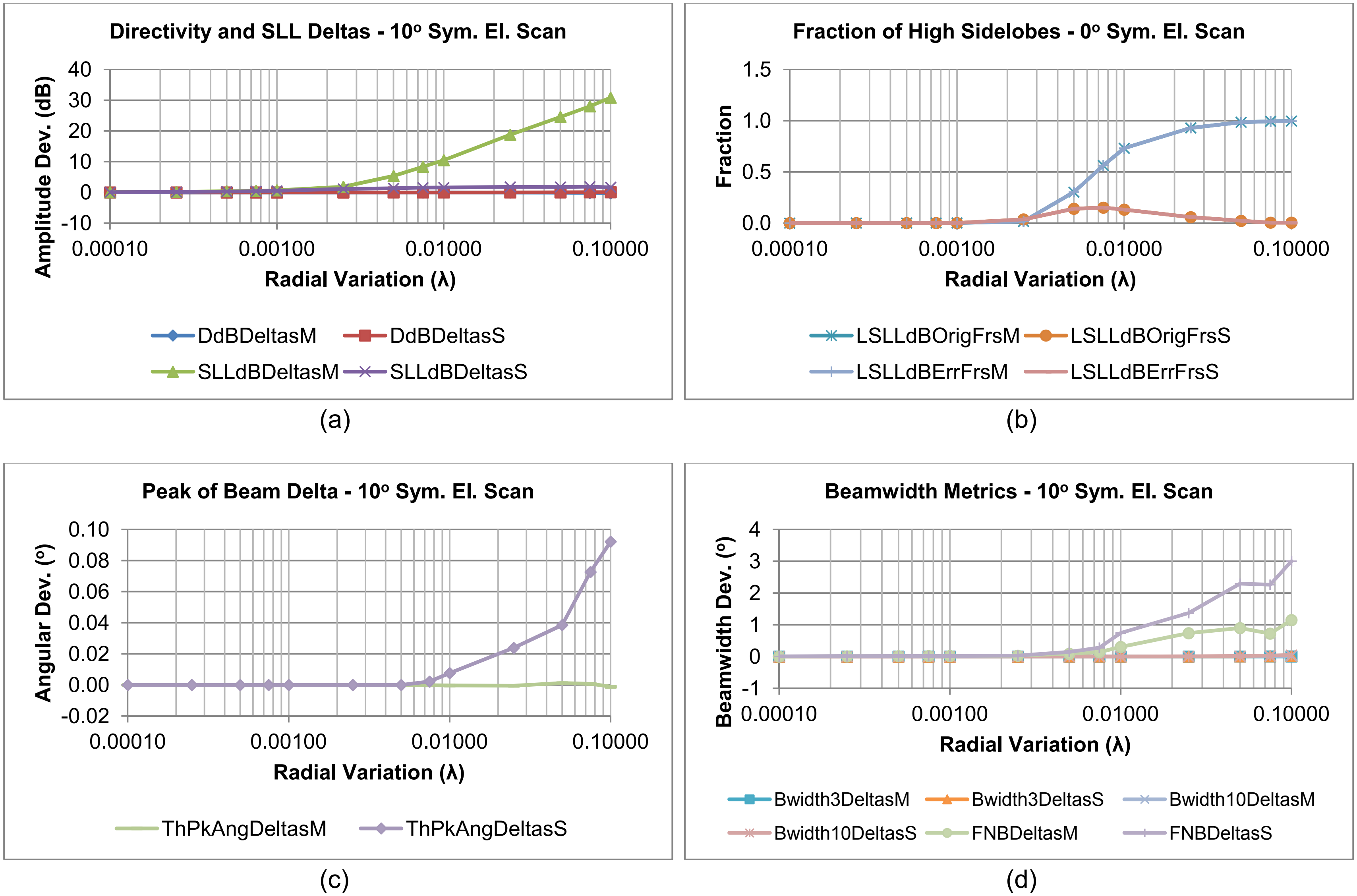

Figure B.120. *Statistical data for a* $3/4\lambda$ *spaced, 28 element, modified Taylor array versus radial randomization.* Directivity and sidelobe level (a), LSLLdB (b), beam pointing (c), and beamwidth (d) results are illustrated.

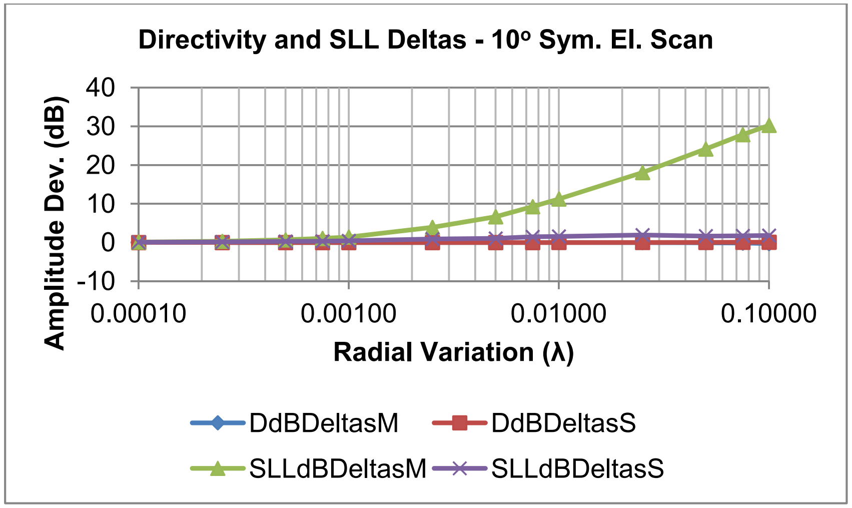

(a)

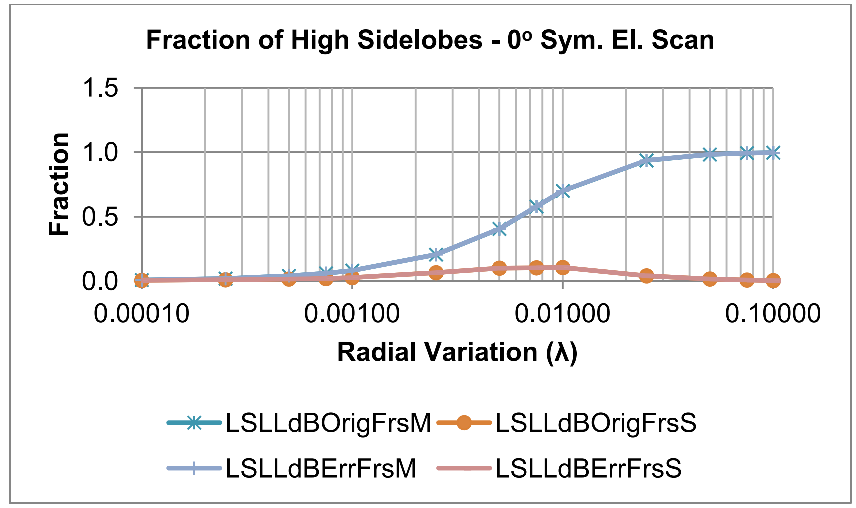

(b)

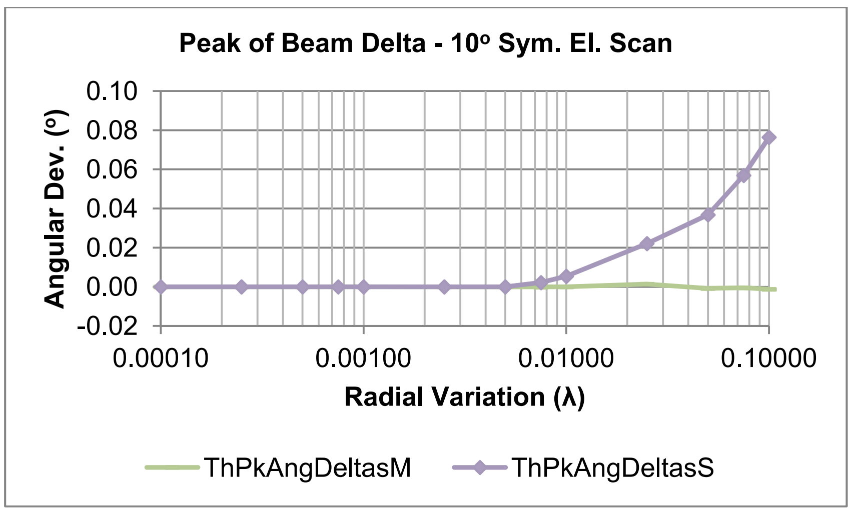

(c)

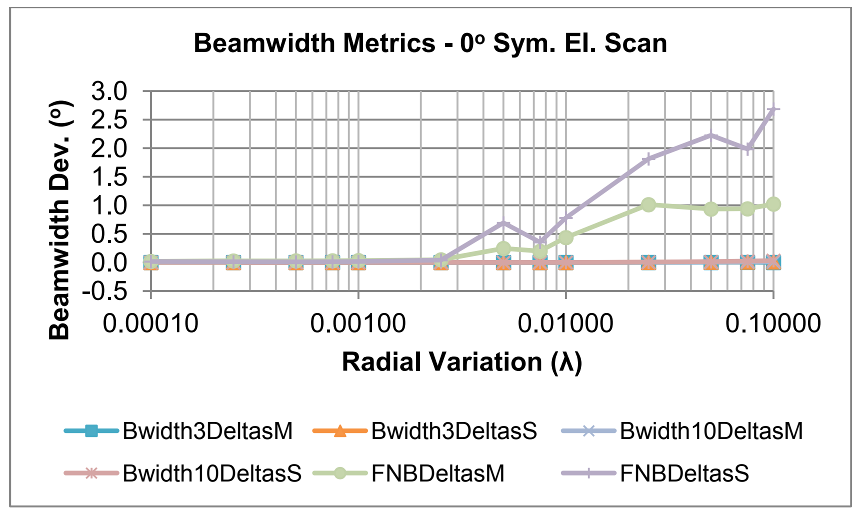

(d)

Figure B.121. *Statistical data for a* $3/4\lambda$ *spaced, 28 element, Taylor array versus radial randomization.* Directivity and sidelobe level (a), LSLLdB (b), beam pointing (c), and beamwidth (d) results are illustrated.

$7/8\,\lambda$ Element Spacing

20 dB Initial Design Sidelobe Level

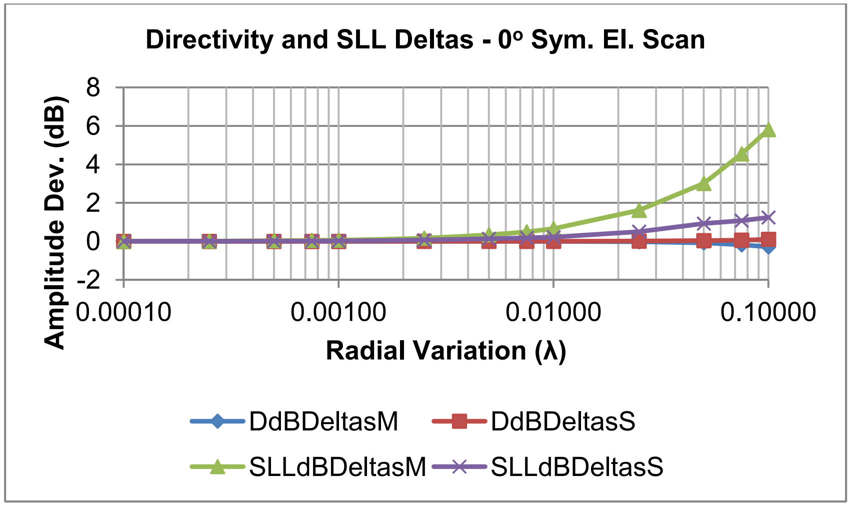

(a)

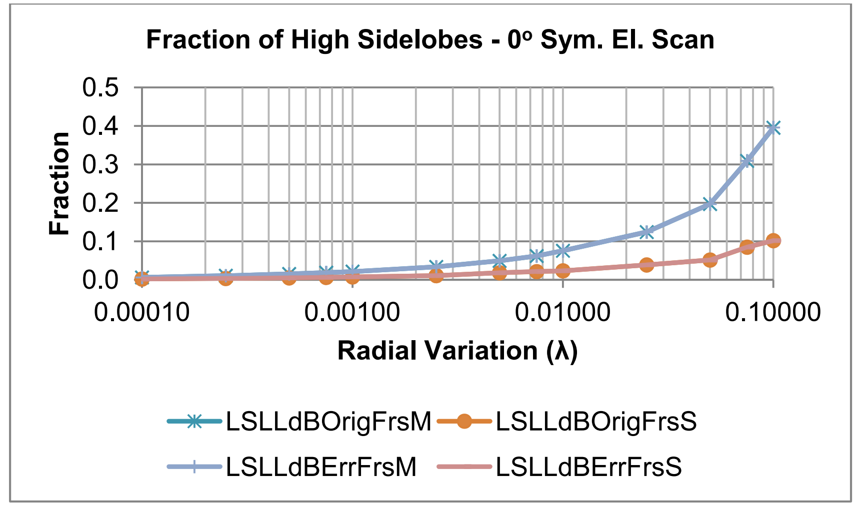

(b)

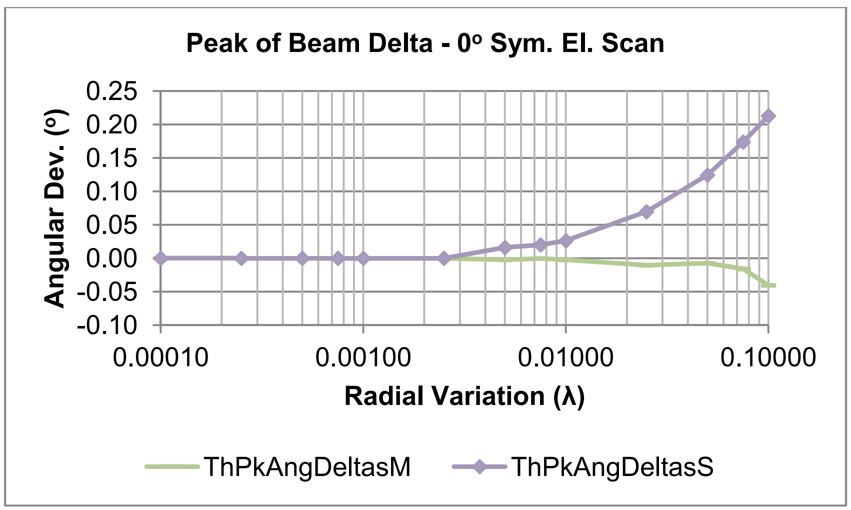

(c)

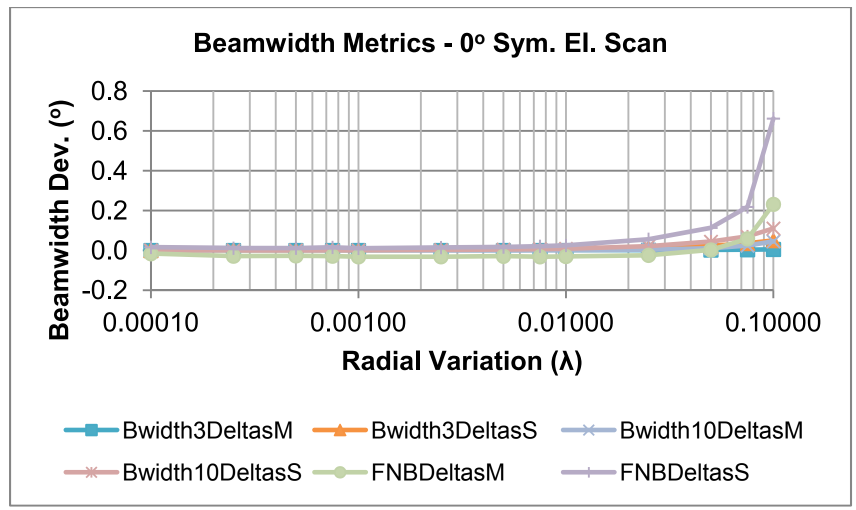

(d)

Figure B.122. *Statistical data for a* $7/8\,\lambda$ *spaced, 9 element, Dolph-Chebyshev array versus radial randomization.* Directivity and sidelobe level (a), LSLLdB (b), beam pointing (c), and beamwidth (d) results are illustrated.

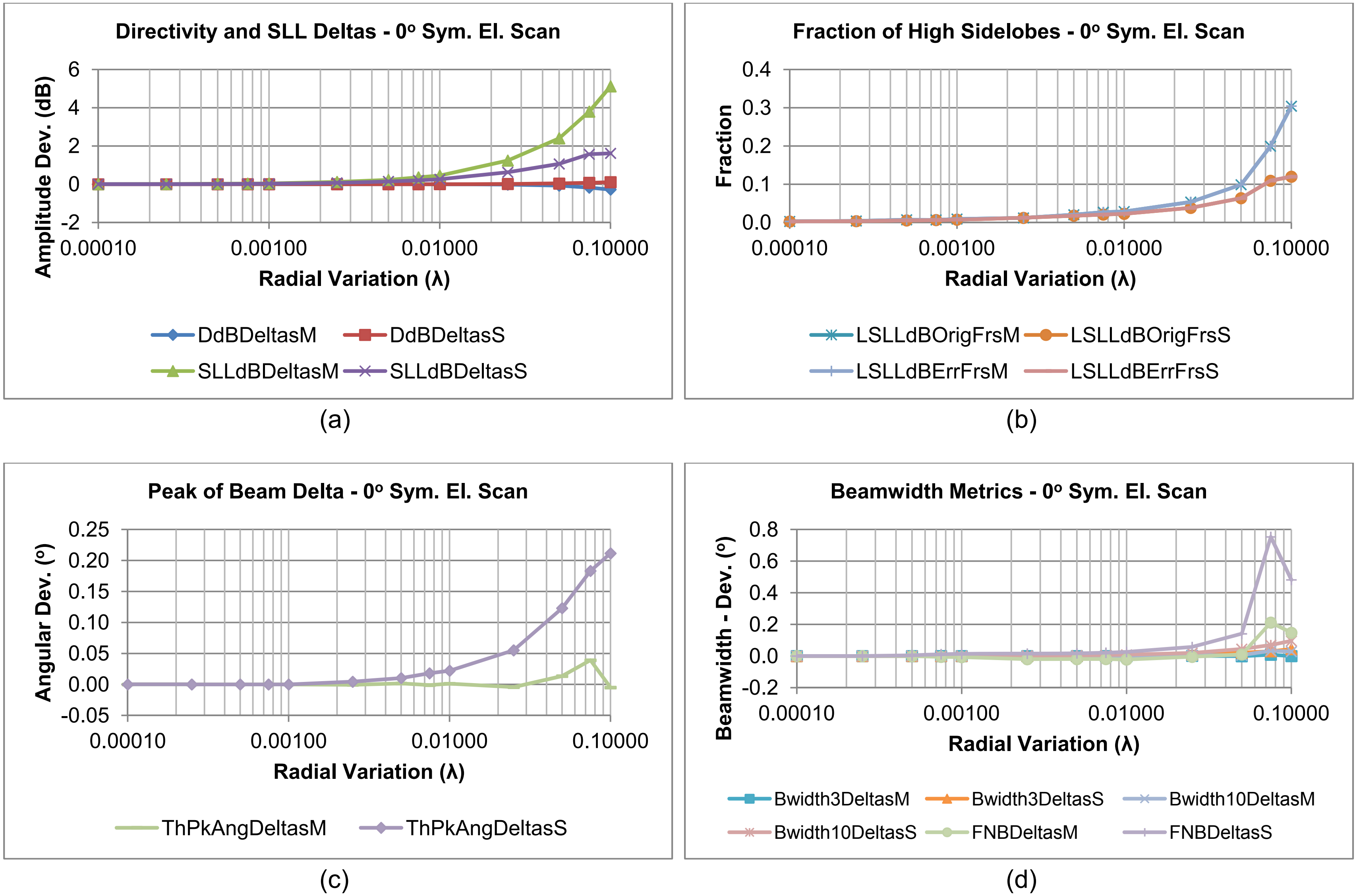

Figure B.123. *Statistical data for a* $7/8\,\lambda$ *spaced, 10 element, modified Taylor array versus radial randomization.* Directivity and sidelobe level (a), LSLLdB (b), beam pointing (c), and beamwidth (d) results are illustrated.

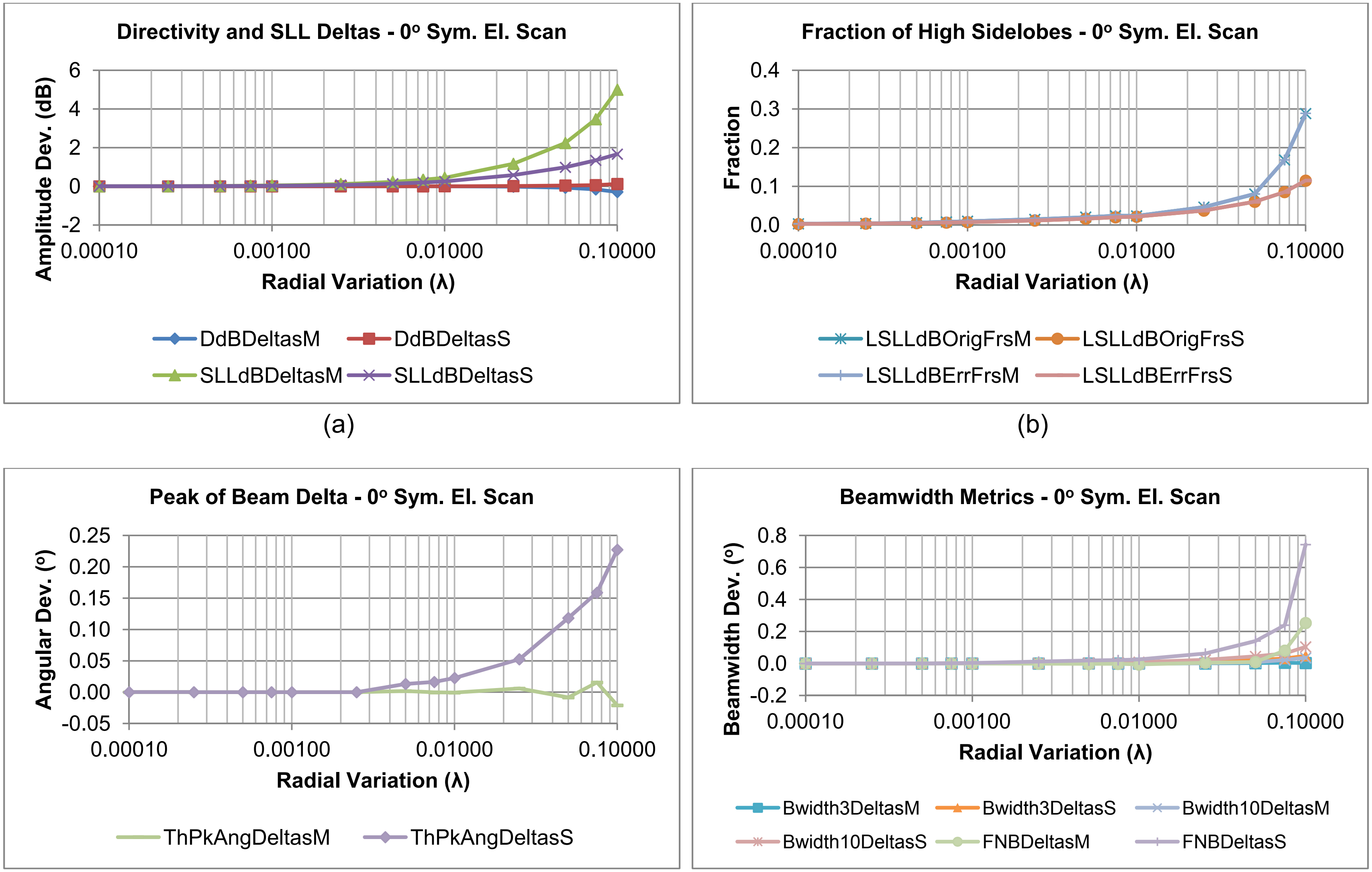

Figure B.124. *Statistical data for a* $7/8\,\lambda$ *spaced, 10 element, powers of cosine on a pedestal array versus radial randomization.* Directivity and sidelobe level (a), LSLLdB (b), beam pointing (c), and beamwidth (d) results are illustrated.

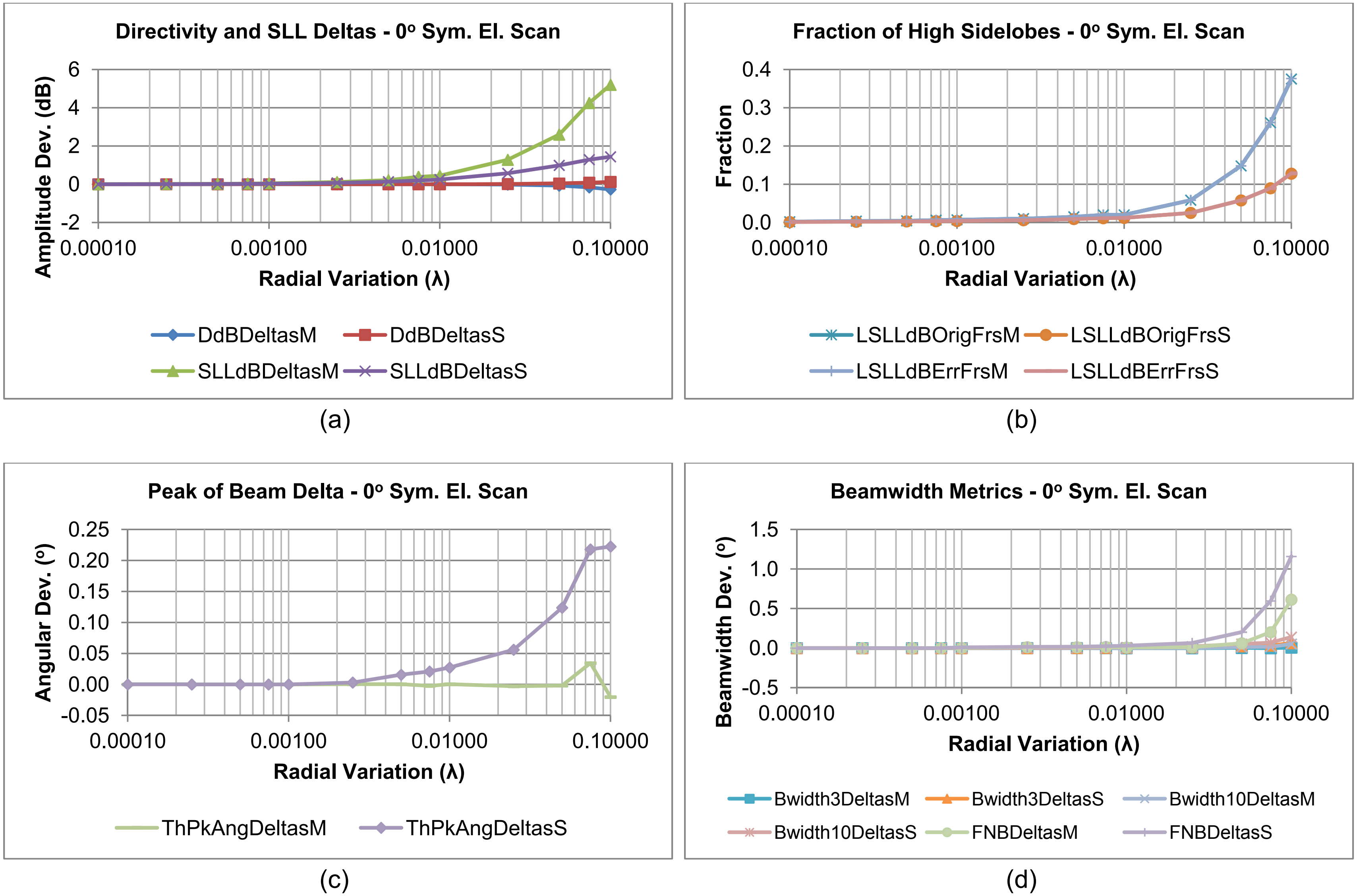

Figure B.125. *Statistical data for a $7/8\,\lambda$ spaced, 9 element, Taylor array versus radial randomization.* Directivity and sidelobe level (a), LSLLdB (b), beam pointing (c), and beamwidth (d) results are illustrated.

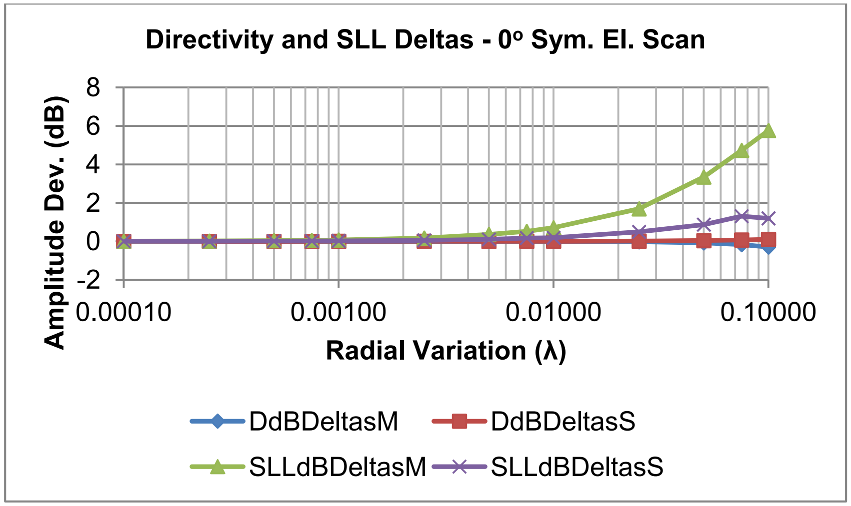

(a)

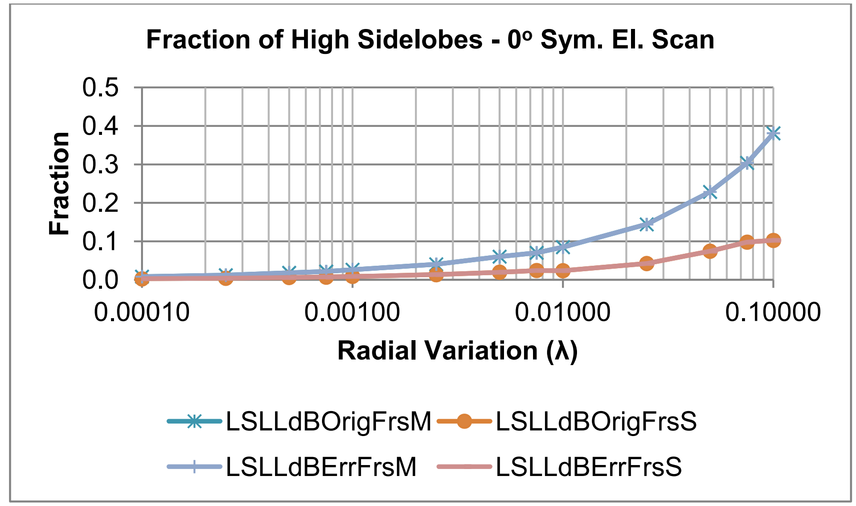

(b)

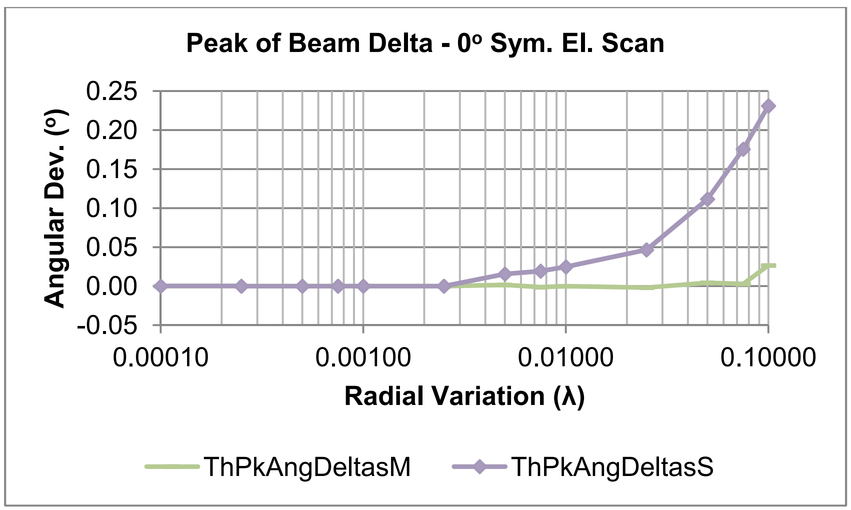

(c)

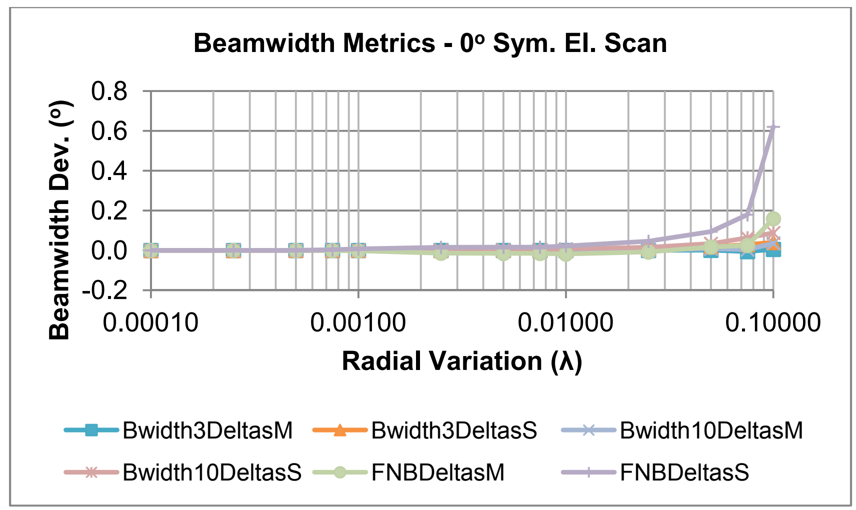

(d)

Figure B.126. *Statistical data for a* $7/8\,\lambda$ *spaced, 10 element, Dolph-Chebyshev array versus radial randomization.* Directivity and sidelobe level (a), LSLLdB (b), beam pointing (c), and beamwidth (d) results are illustrated.

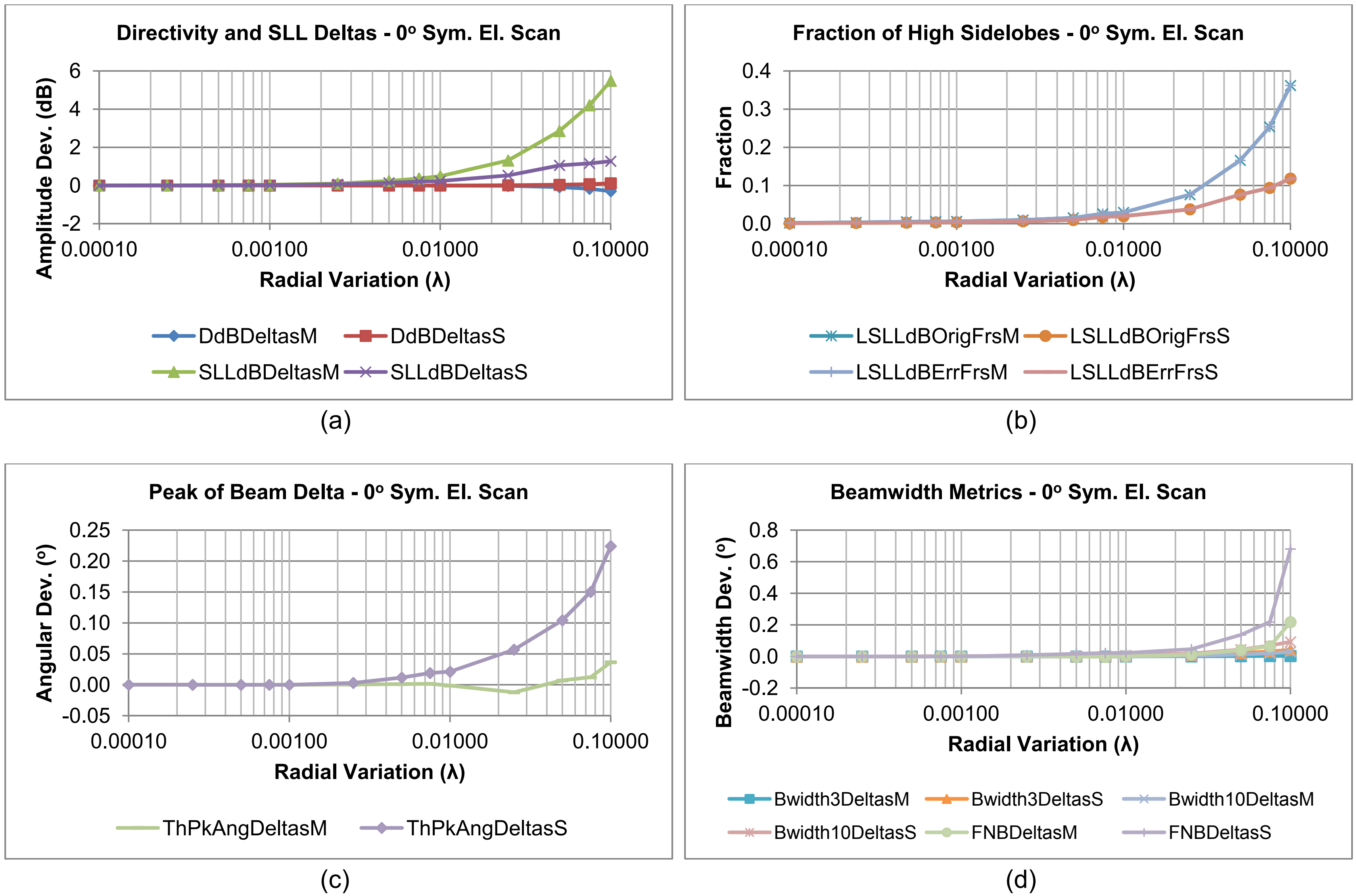

Figure B.127. *Statistical data for a* $7/8\,\lambda$ *spaced, 10 element, Taylor array versus radial randomization.* Directivity and sidelobe level (a), LSLLdB (b), beam pointing (c), and beamwidth (d) results are illustrated.

$7/8\lambda$ Element Spacing

30 dB Initial Design Sidelobe Level

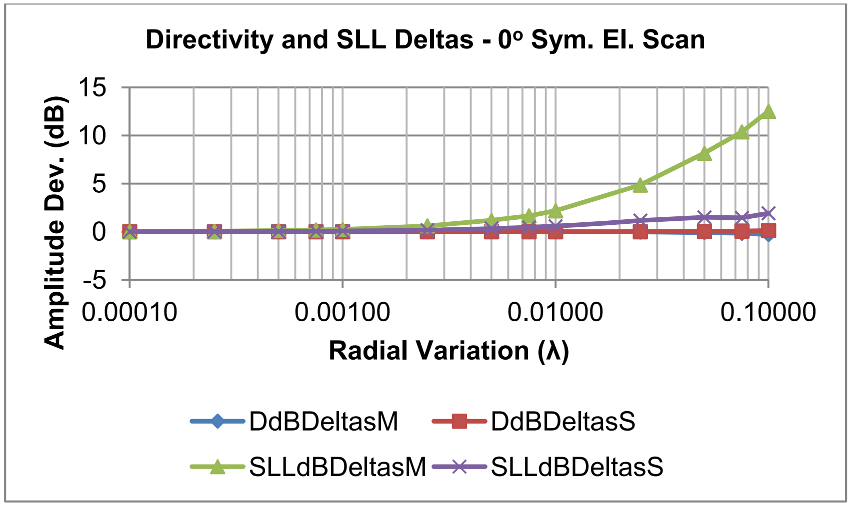

(a)

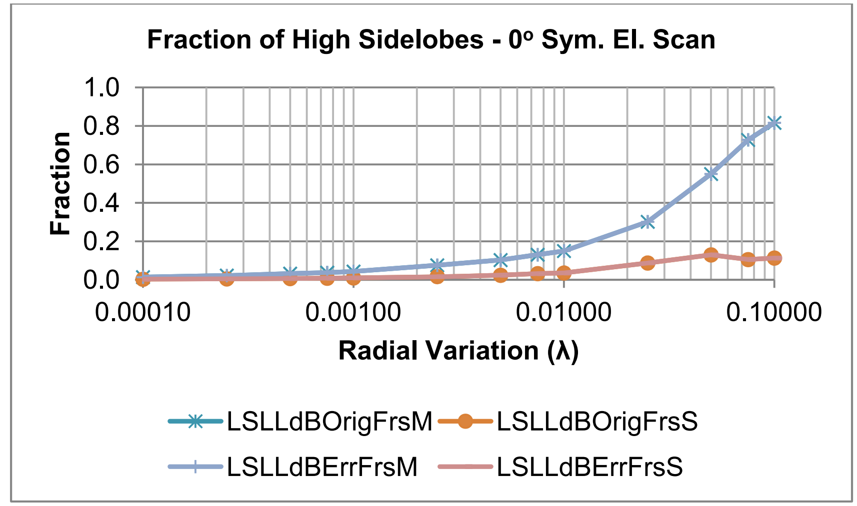

(b)

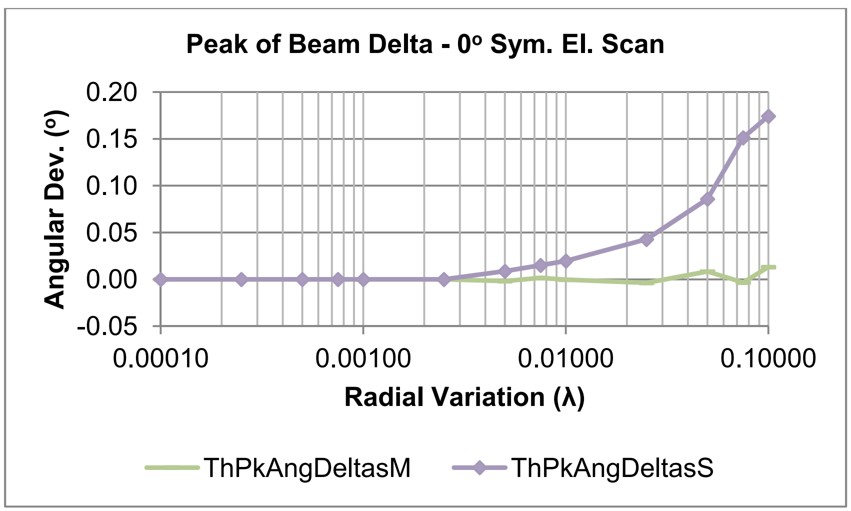

(c)

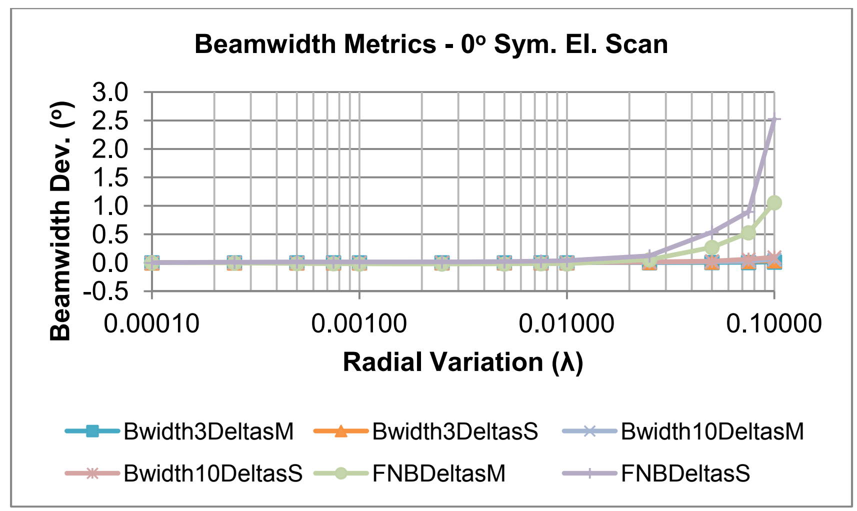

(d)

Figure B.128. *Statistical data for a $7/8\,\lambda$ spaced, 12 element, Dolph-Chebyshev array versus radial randomization.* Directivity and sidelobe level (a), LSLLdB (b), beam pointing (c), and beamwidth (d) results are illustrated.

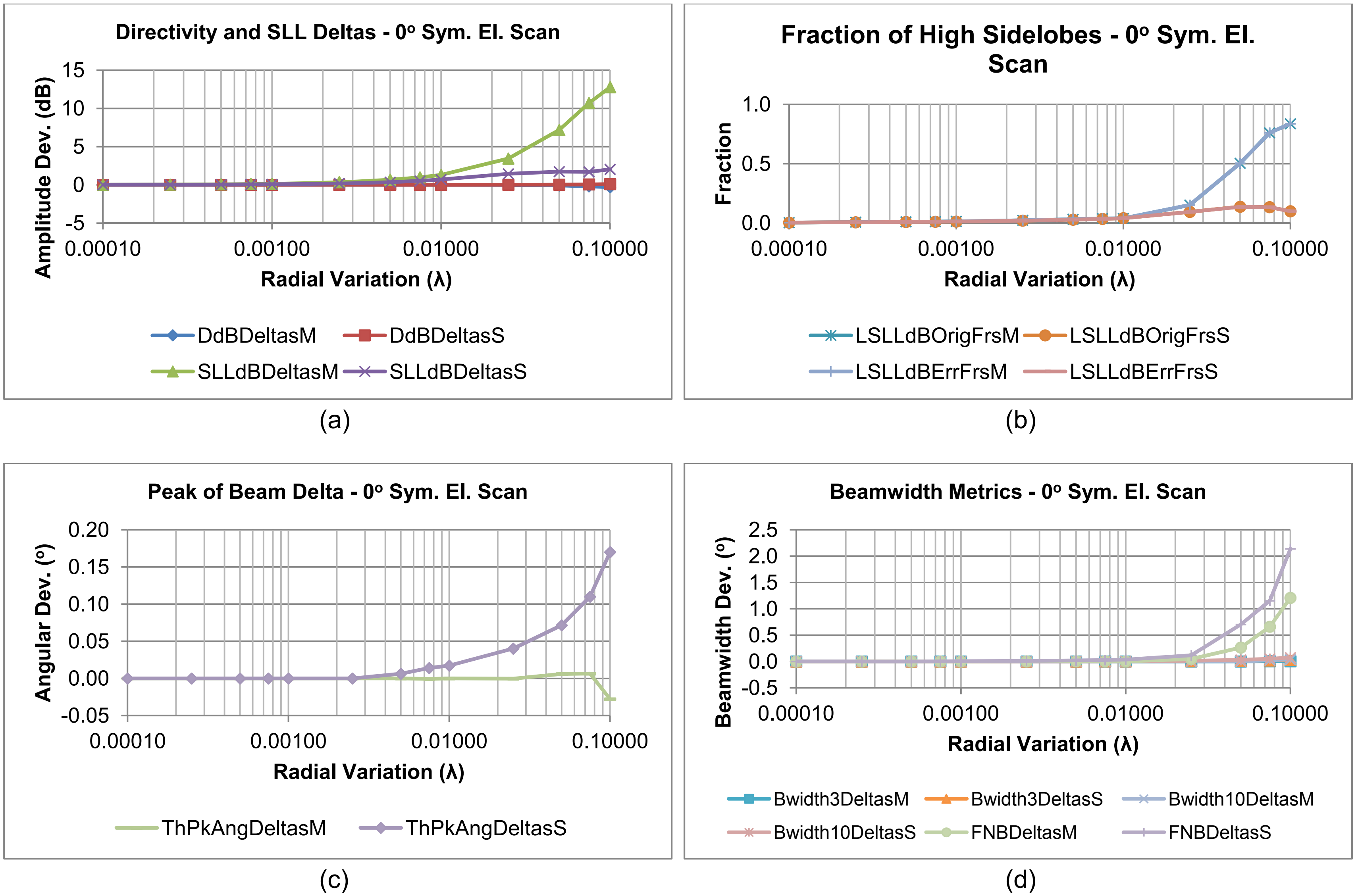

Figure B.129. *Statistical data for a* $7/8\,\lambda$ *spaced, 14 element, modified Taylor array versus radial randomization.* Directivity and sidelobe level (a), LSLLdB (b), beam pointing (c), and beamwidth (d) results are illustrated.

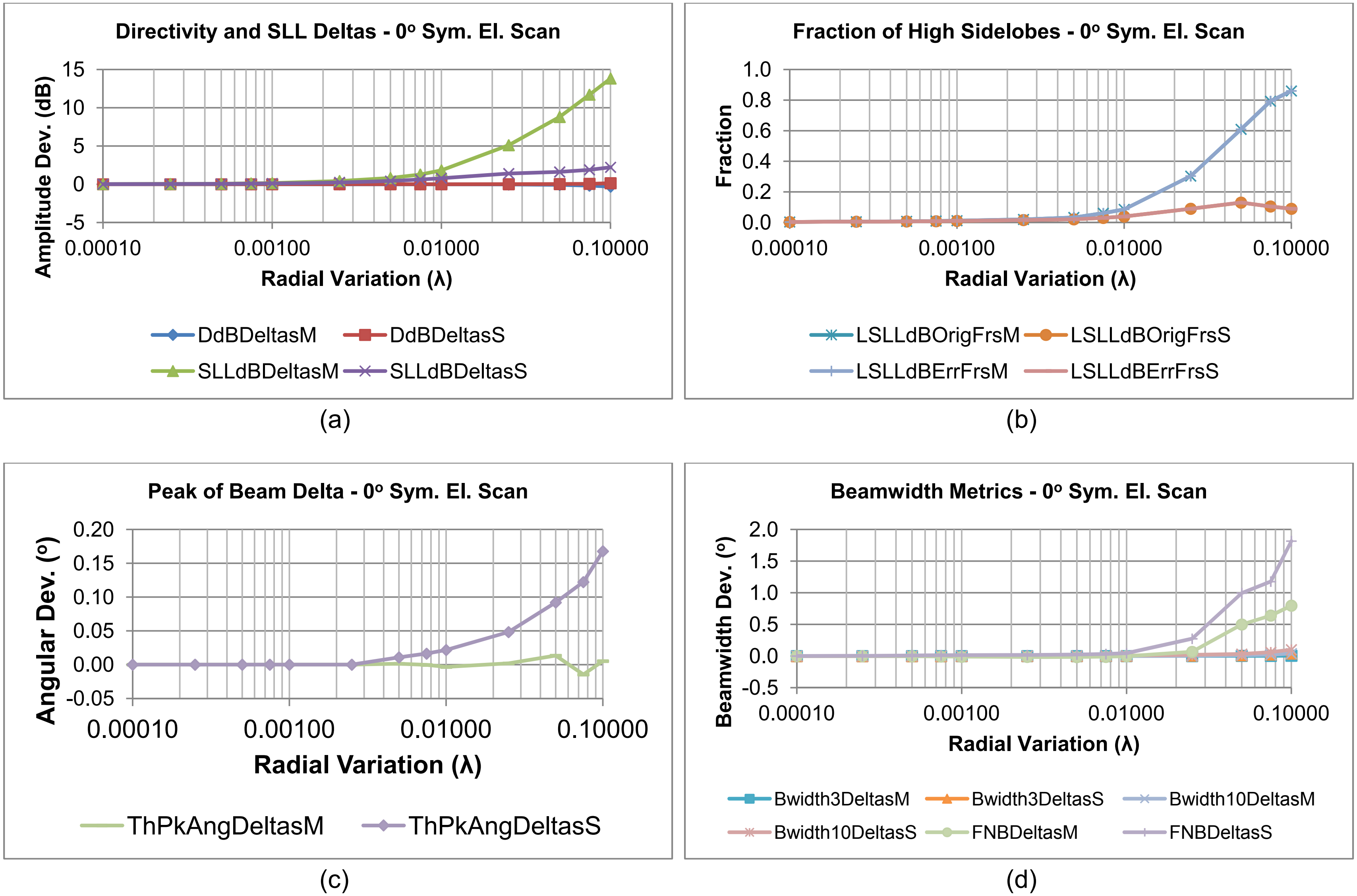

Figure B.130. *Statistical data for a* $7/8\,\lambda$ *spaced, 12 element, powers of cosine on a pedestal array versus radial randomization.* Directivity and sidelobe level (a), LSLLdB (b), beam pointing (c), and beamwidth (d) results are illustrated.

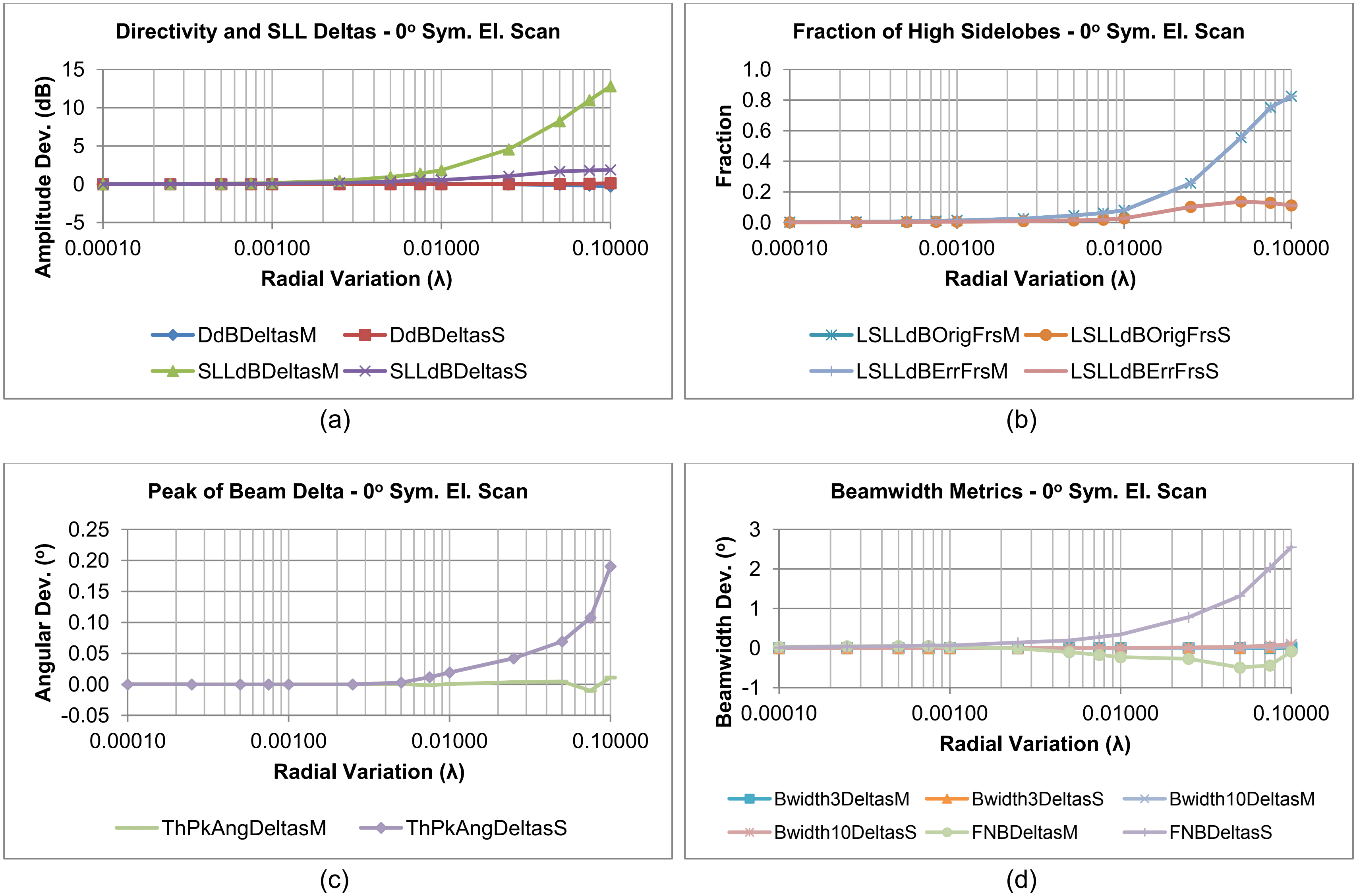

Figure B.131. *Statistical data for a $7/8\,\lambda$ spaced, 13 element, Taylor array versus radial randomization.* Directivity and sidelobe level (a), LSLLdB (b), beam pointing (c), and beamwidth (d) results are illustrated.

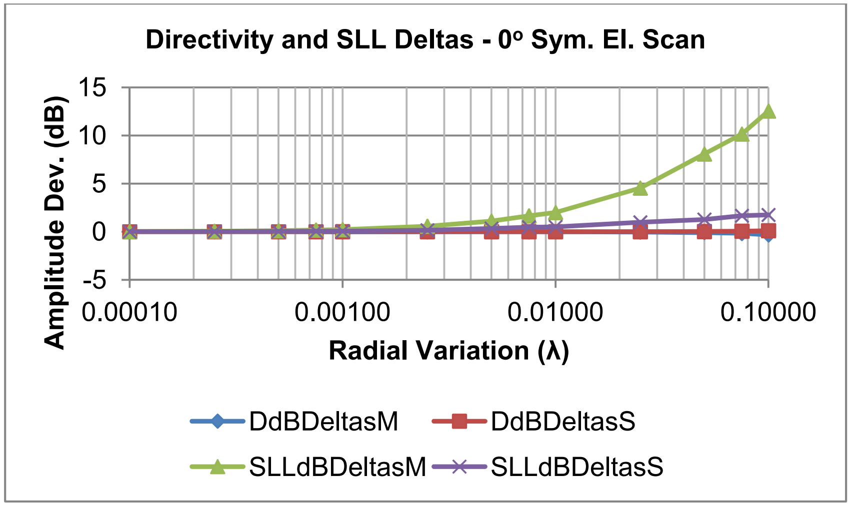

(a)

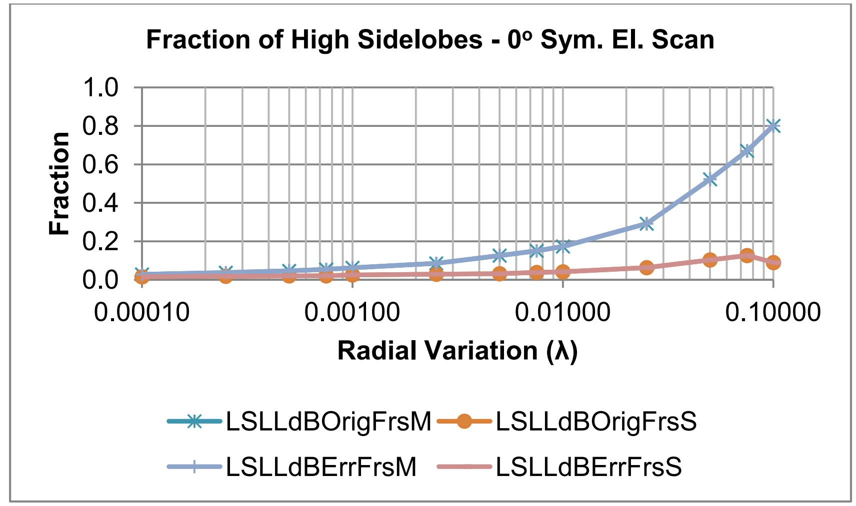

(b)

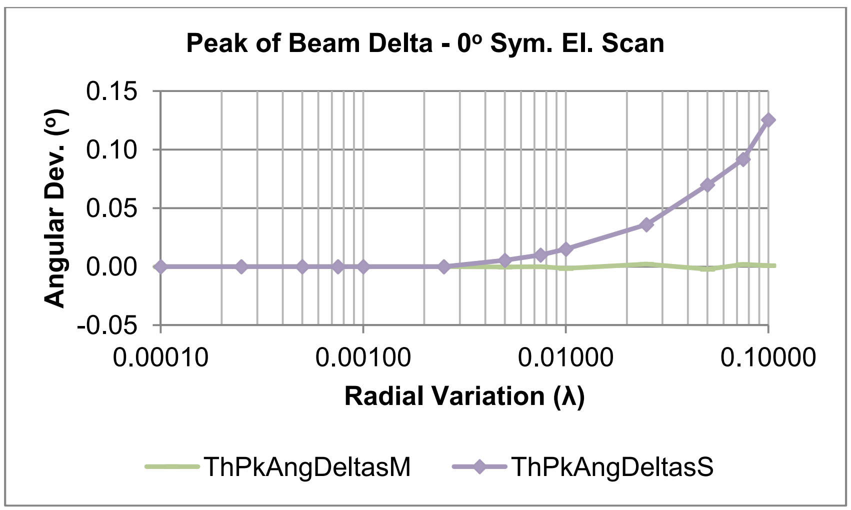

(c)

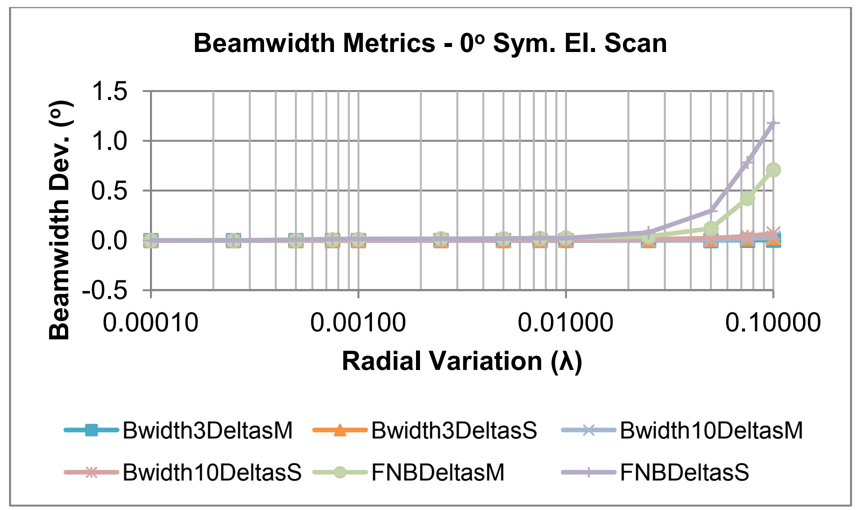

(d)

Figure B.132. *Statistical data for a* $7/8\,\lambda$ *spaced, 14 element, Dolph-Chebyshev array versus radial randomization.* Directivity and sidelobe level (a), LSLLdB (b), beam pointing (c), and beamwidth (d) results are illustrated.

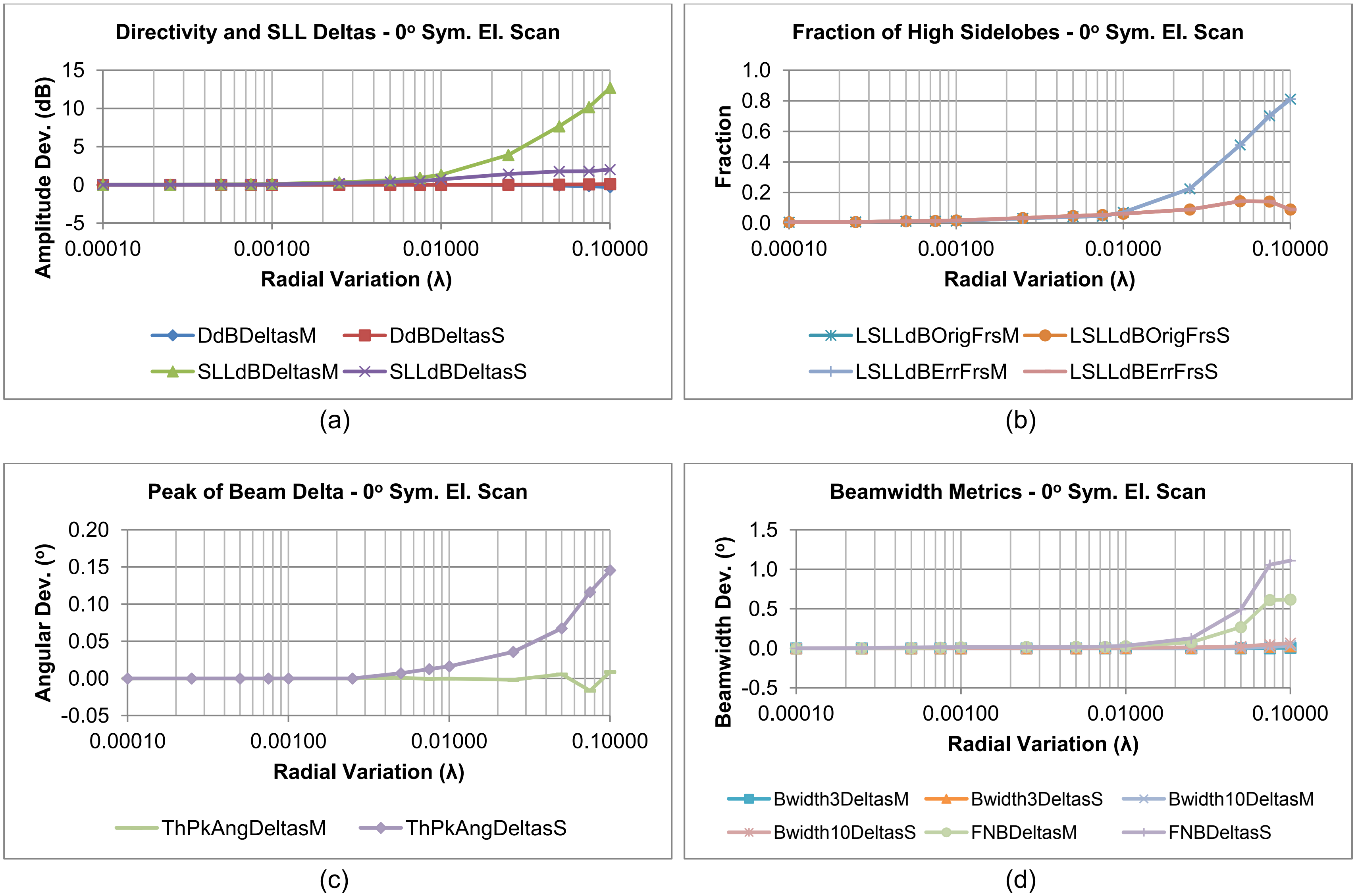

Figure B.133. *Statistical data for a $7/8\,\lambda$ spaced, 14 element, powers of cosine on a pedestal array versus radial randomization.* Directivity and sidelobe level (a), LSLLdB (b), beam pointing (c), and beamwidth (d) results are illustrated.

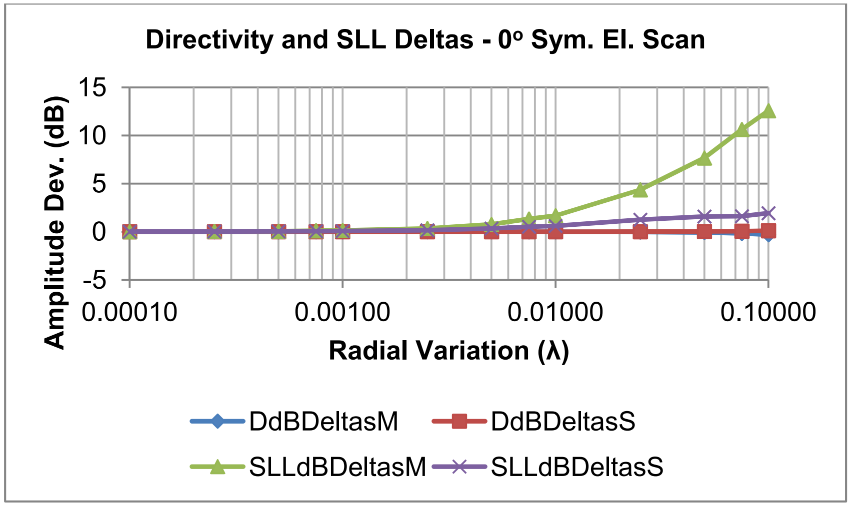

(a)

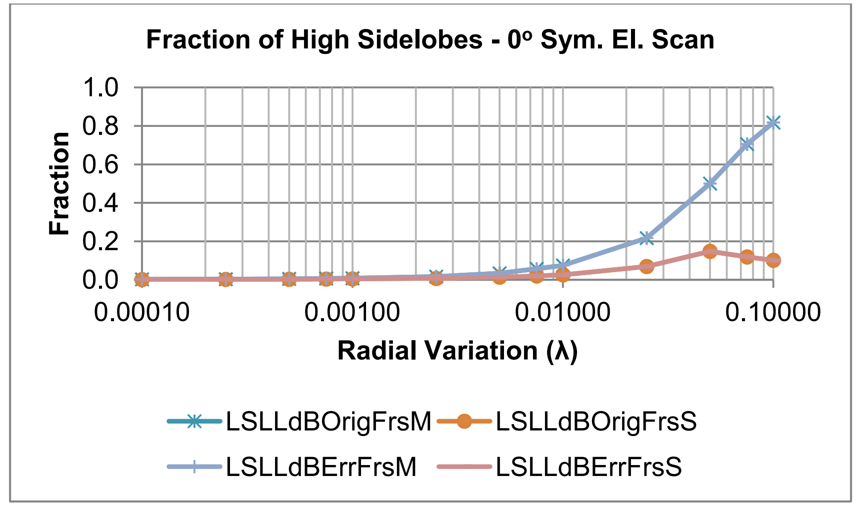

(b)

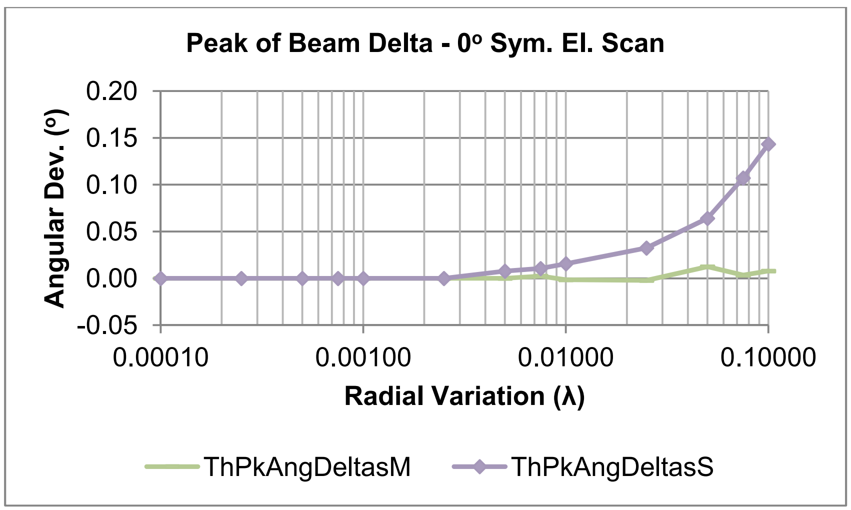

(c)

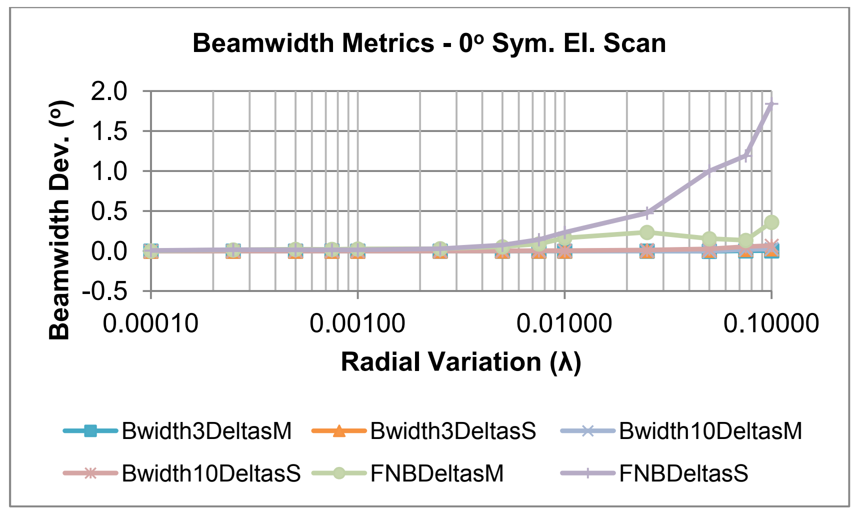

(d)

Figure B.134. *Statistical data for a* $7/8\,\lambda$ *spaced, 14 element, Taylor array versus radial randomization.* Directivity and sidelobe level (a), LSLLdB (b), beam pointing (c), and beamwidth (d) results are illustrated.

$7/8\,\lambda$ Element Spacing

40 dB Initial Design Sidelobe Level

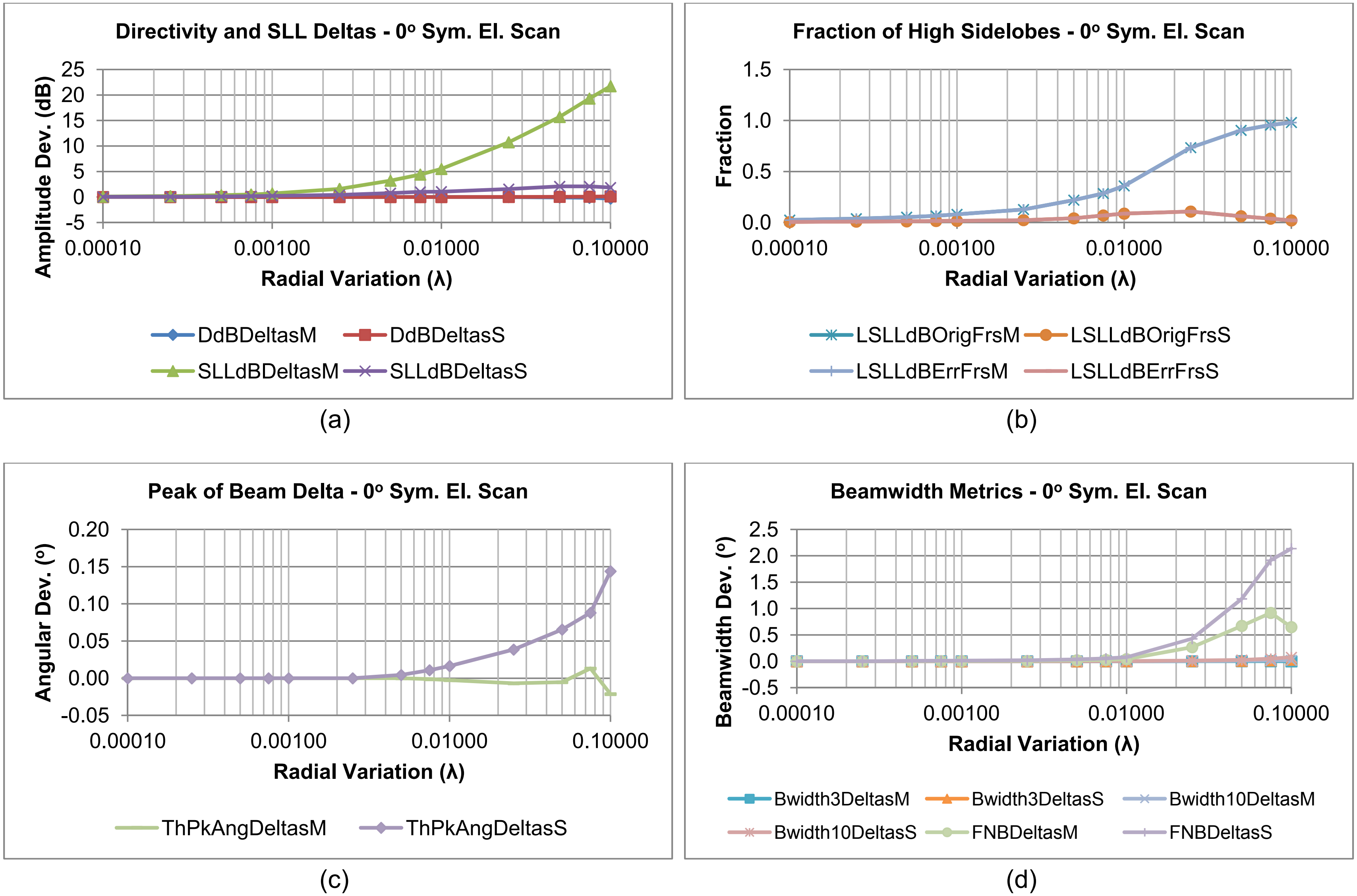

Figure B.135. *Statistical data for a* $7/8\,\lambda$ *spaced, 15 element, Dolph-Chebyshev array versus radial randomization.* Directivity and sidelobe level (a), LSLLdB (b), beam pointing (c), and beamwidth (d) results are illustrated.

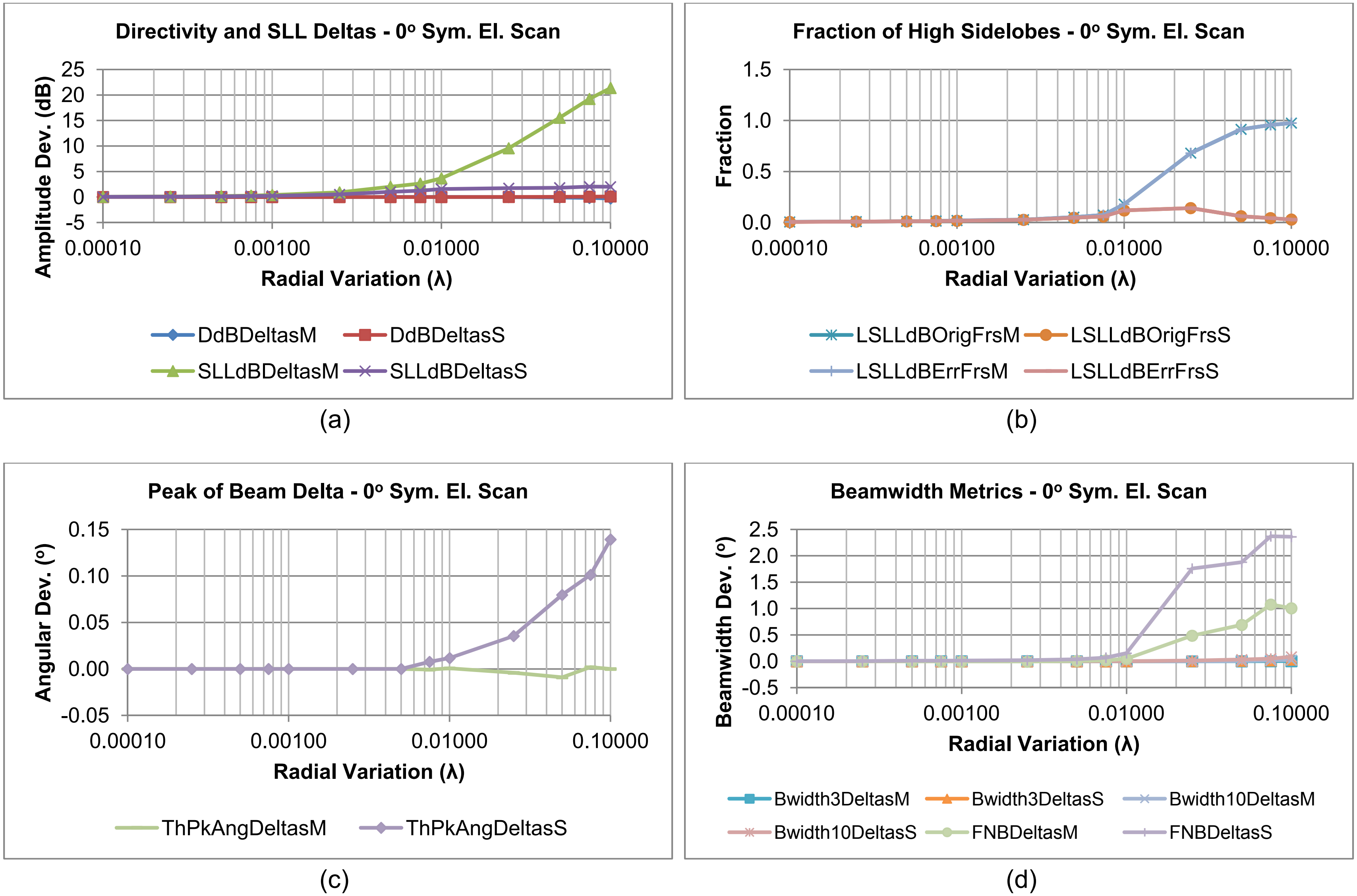

Figure B.136. *Statistical data for a* $7/8\,\lambda$ *spaced, 17 element, modified Taylor array versus radial randomization.* Directivity and sidelobe level (a), LSLLdB (b), beam pointing (c), and beamwidth (d) results are illustrated.

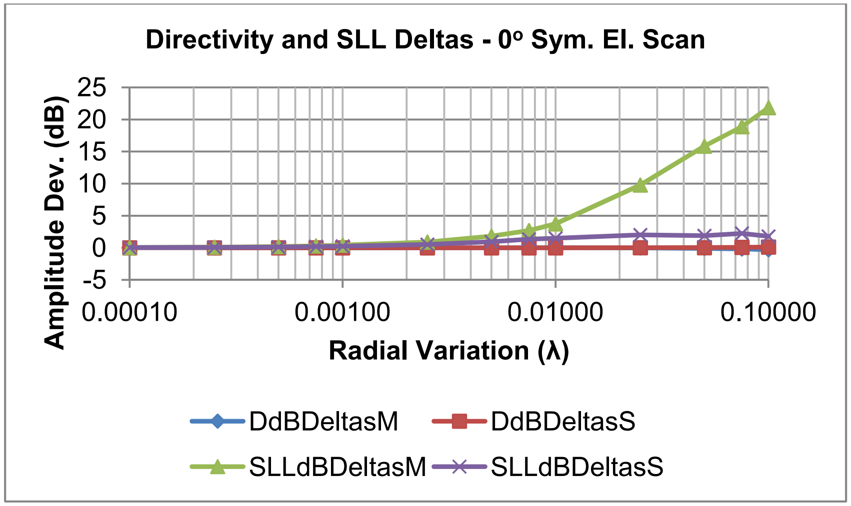

(a)

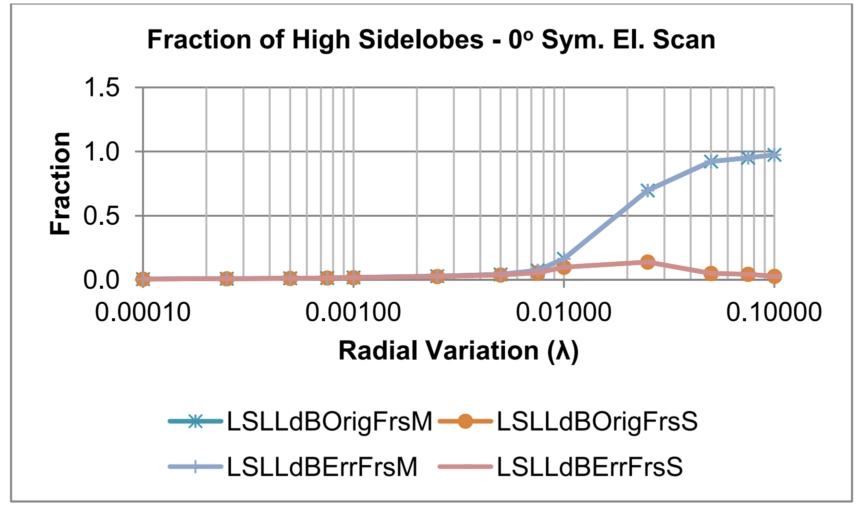

(b)

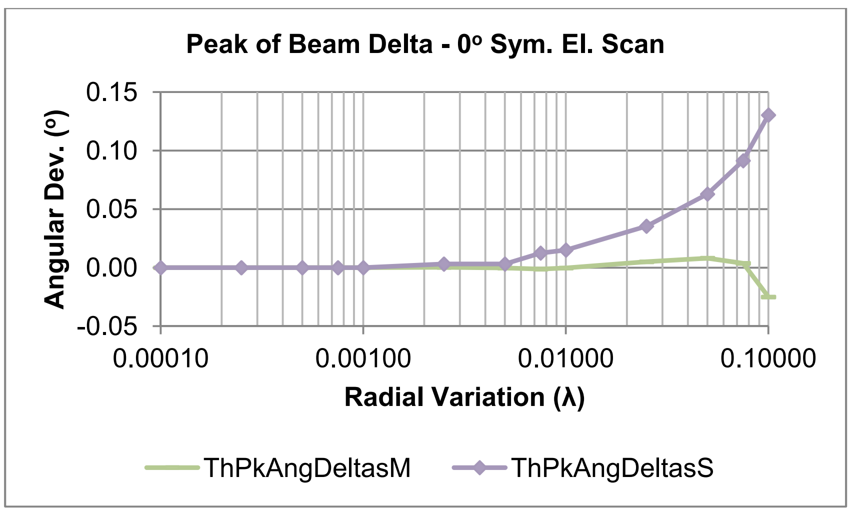

(c)

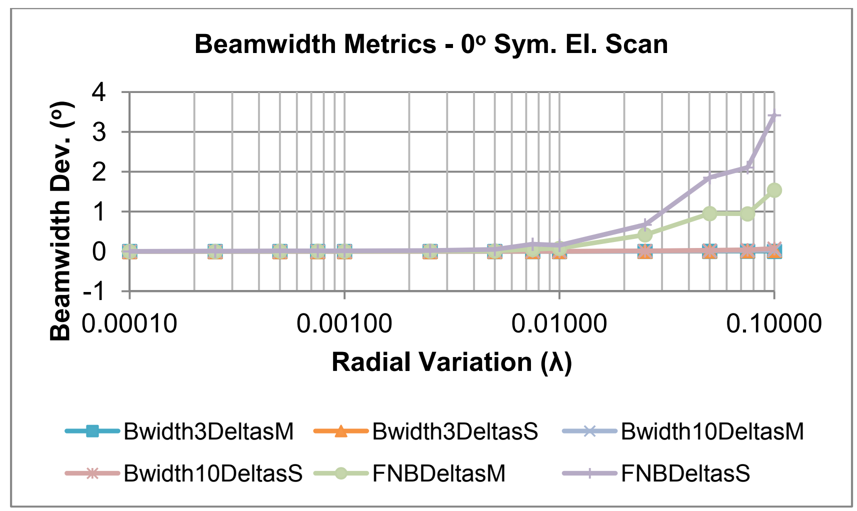

(d)

Figure B.137. *Statistical data for a* $7/8\,\lambda$ *spaced, 21 element, powers of cosine on a pedestal array versus radial randomization.* Directivity and sidelobe level (a), LSLLdB (b), beam pointing (c), and beamwidth (d) results are illustrated.

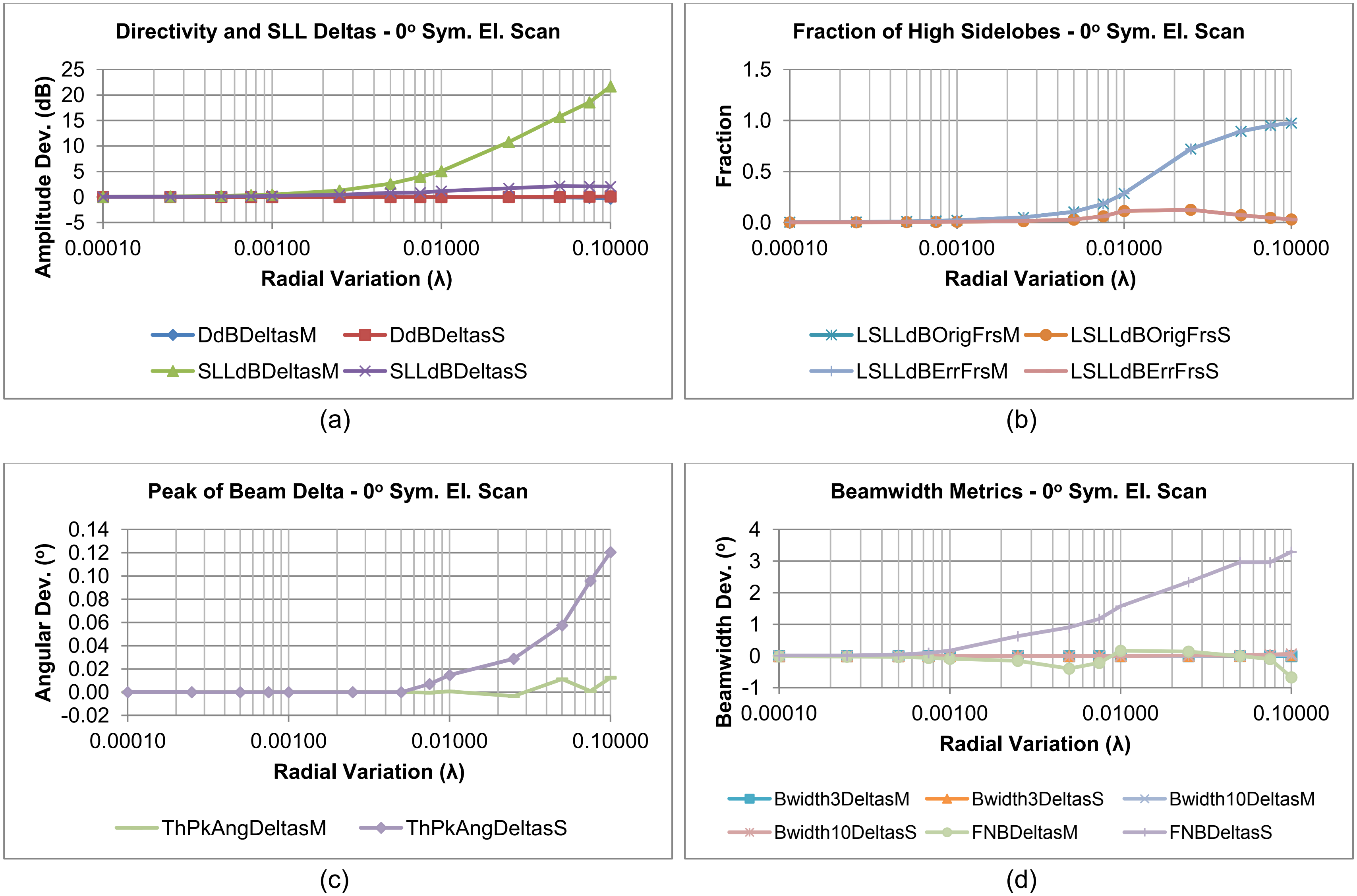

Figure B.138. *Statistical data for a* $7/8\,\lambda$ *spaced, 17 element, Taylor array versus radial randomization.* Directivity and sidelobe level (a), LSLLdB (b), beam pointing (c), and beamwidth (d) results are illustrated.

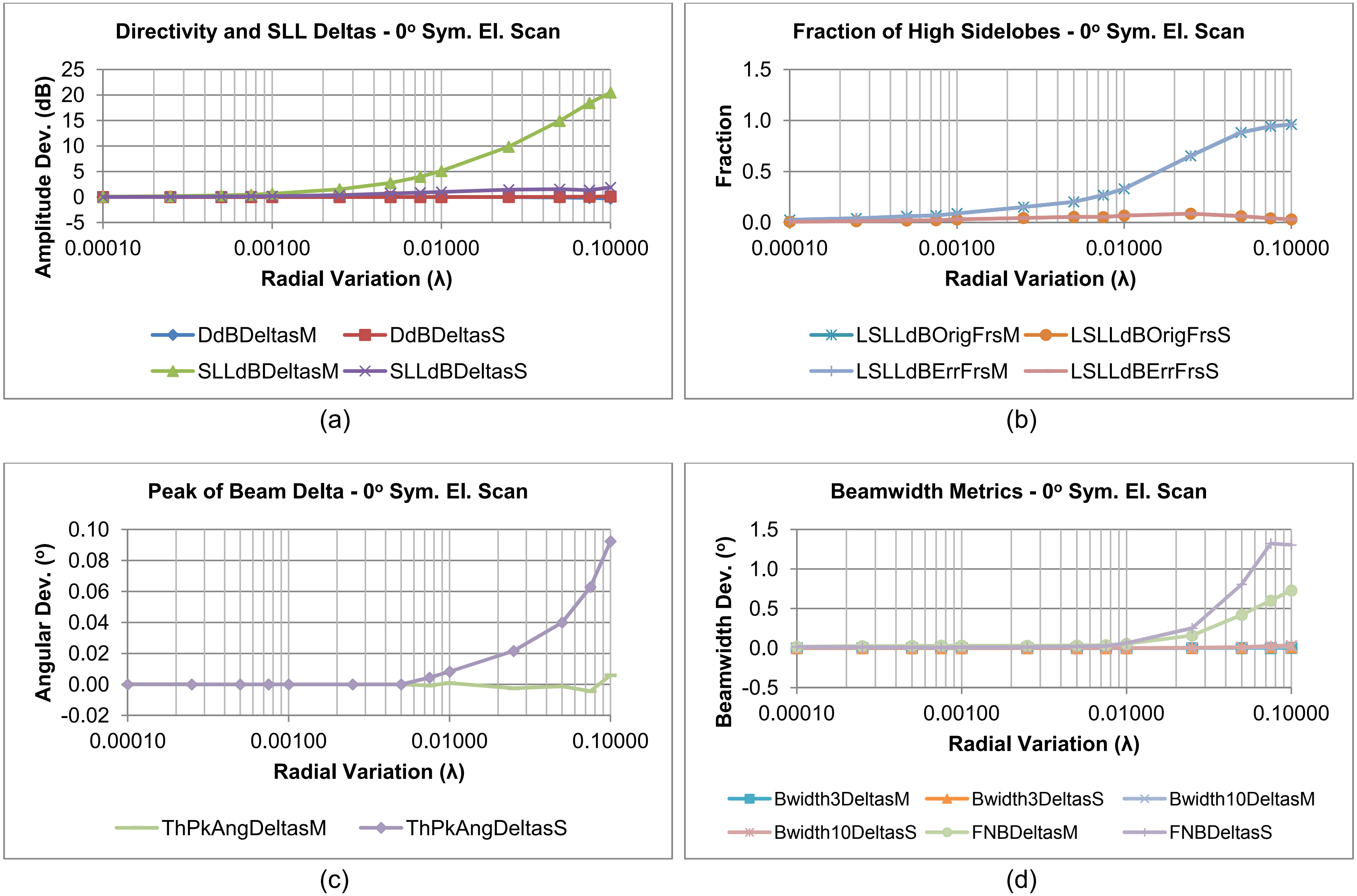

Figure B.139. *Statistical data for a* $7/8\lambda$ *spaced, 21 element, Dolph-Chebyshev array versus radial randomization.* Directivity and sidelobe level (a), LSLLdB (b), beam pointing (c), and beamwidth (d) results are illustrated.

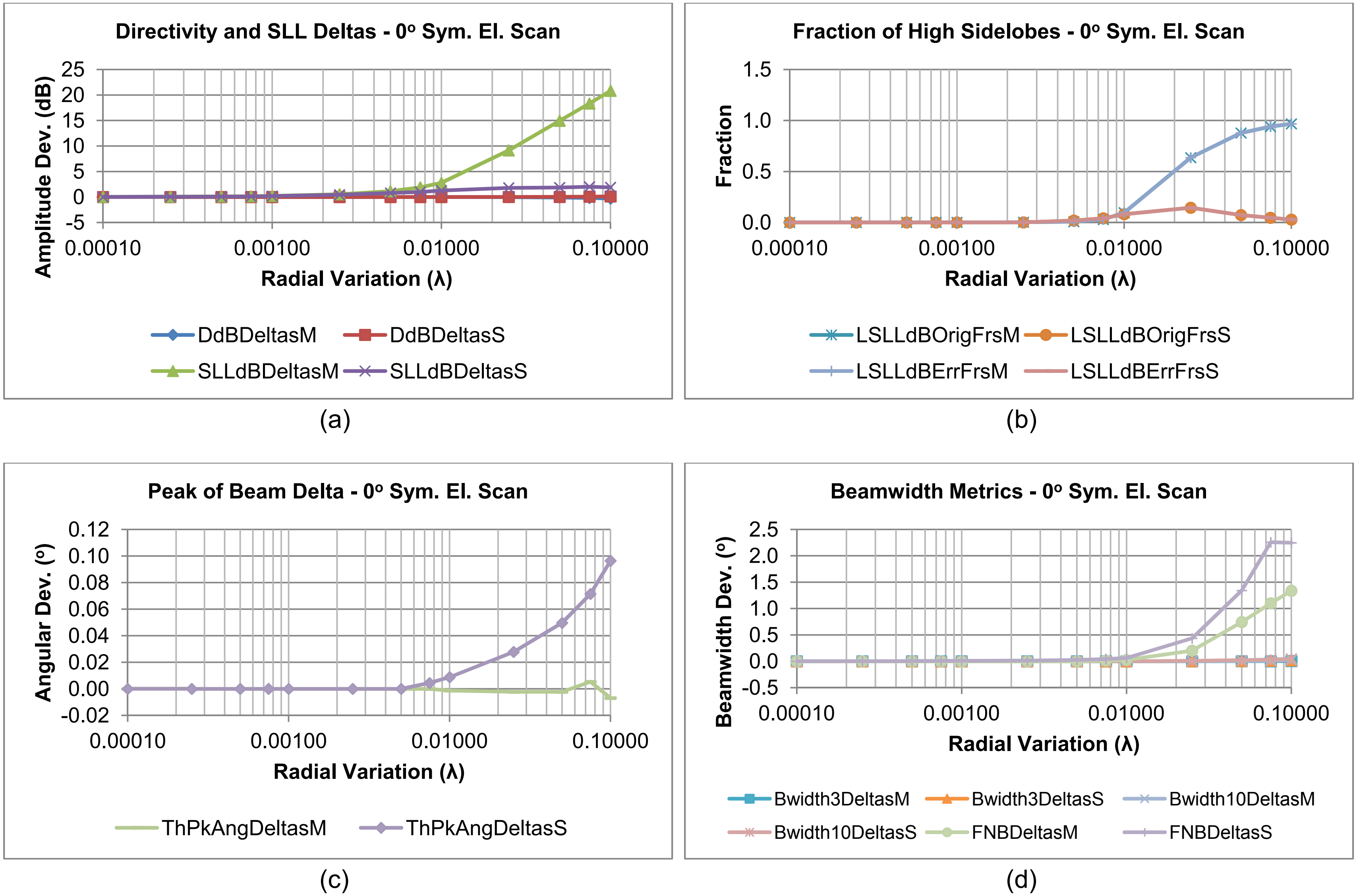

Figure B.140. *Statistical data for a* $7/8\,\lambda$ *spaced, 21 element, modified Taylor array versus radial randomization.* Directivity and sidelobe level (a), LSLLdB (b), beam pointing (c), and beamwidth (d) results are illustrated.

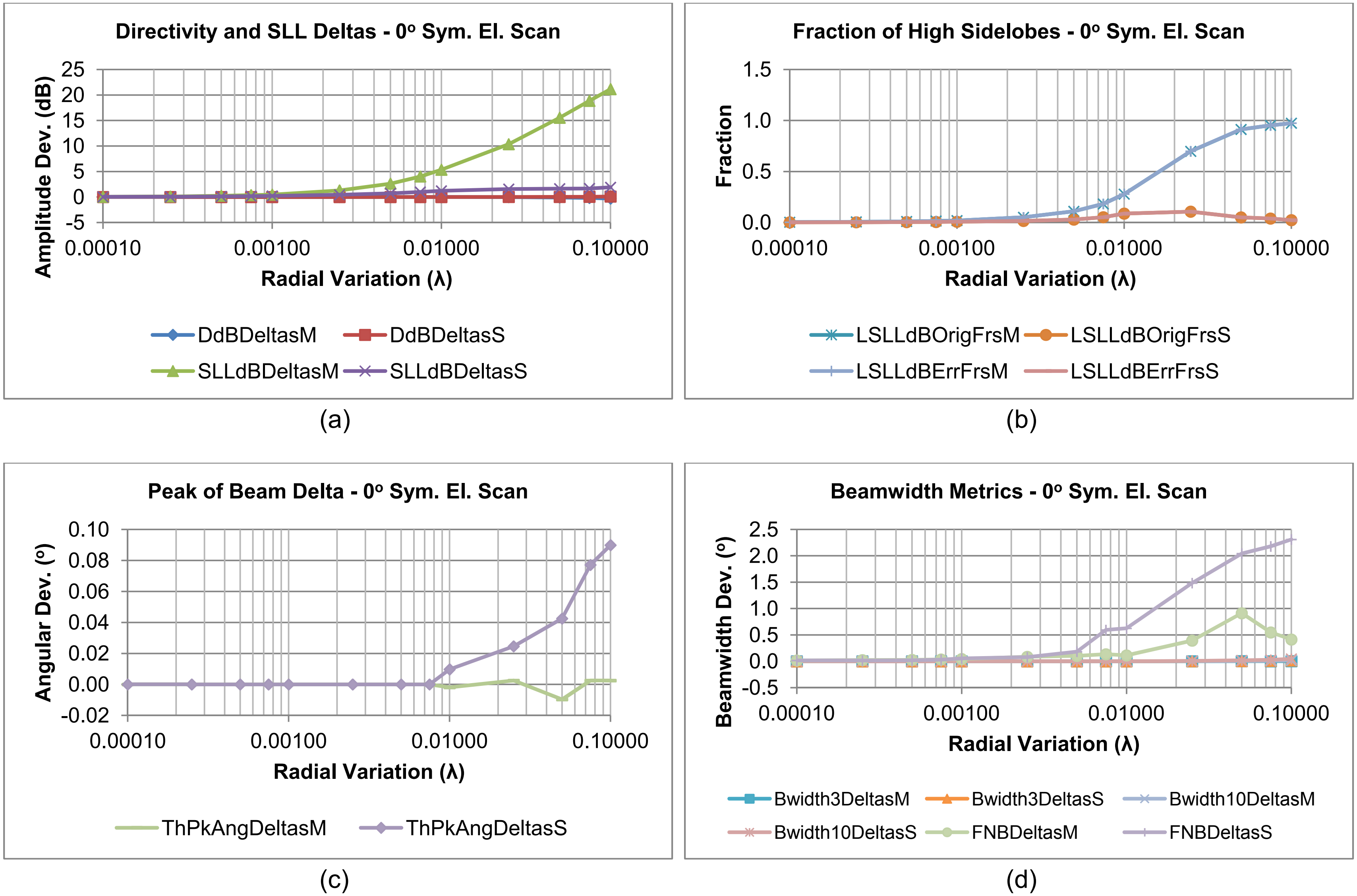

Figure B.141. *Statistical data for a* $7/8\,\lambda$ *spaced, 21 element, Taylor array versus radial randomization.* Directivity and sidelobe level (a), LSLLdB (b), beam pointing (c), and beamwidth (d) results are illustrated.

$7/8\lambda$ Element Spacing

50 dB Initial Design Sidelobe Level

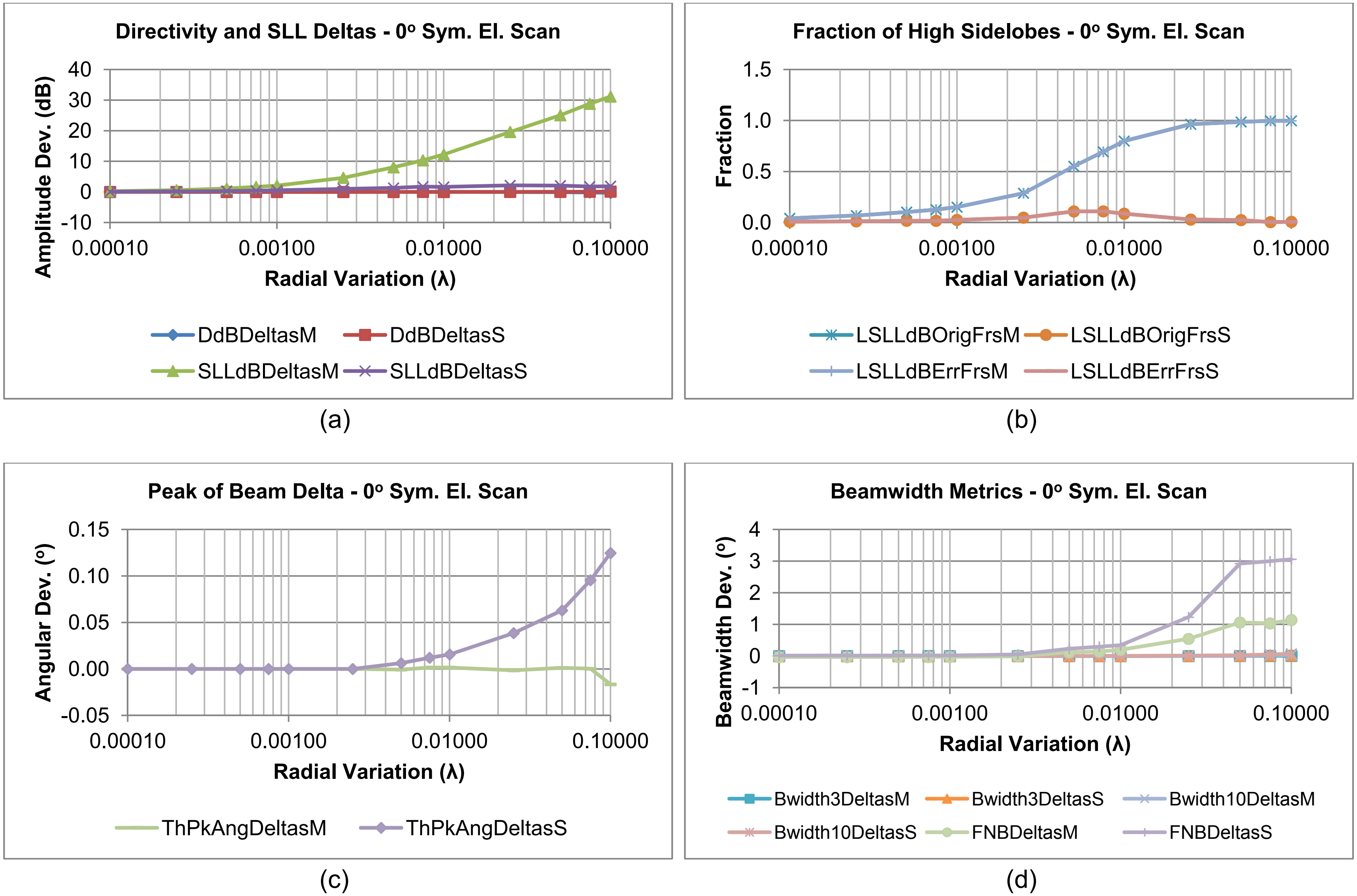

Figure B.142. *Statistical data for a* $7/8\lambda$ *spaced, 17 element, Dolph-Chebyshev array versus radial randomization.* Directivity and sidelobe level (a), LSLLdB (b), beam pointing (c), and beamwidth (d) results are illustrated.

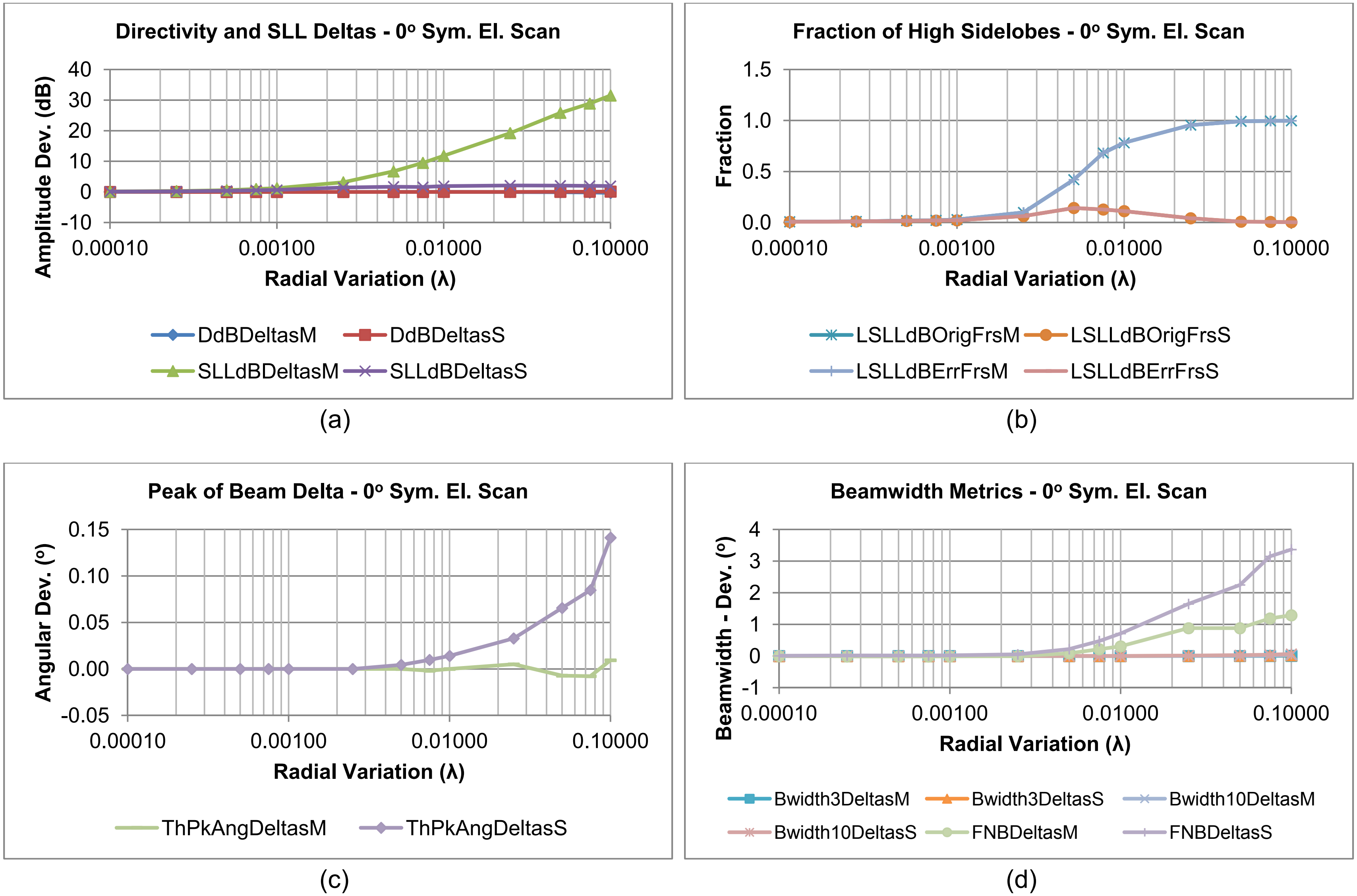

Figure B.143. *Statistical data for a* $7/8\,\lambda$ *spaced, 20 element, modified Taylor array versus radial randomization.* Directivity and sidelobe level (a), LSLLdB (b), beam pointing (c), and beamwidth (d) results are illustrated.

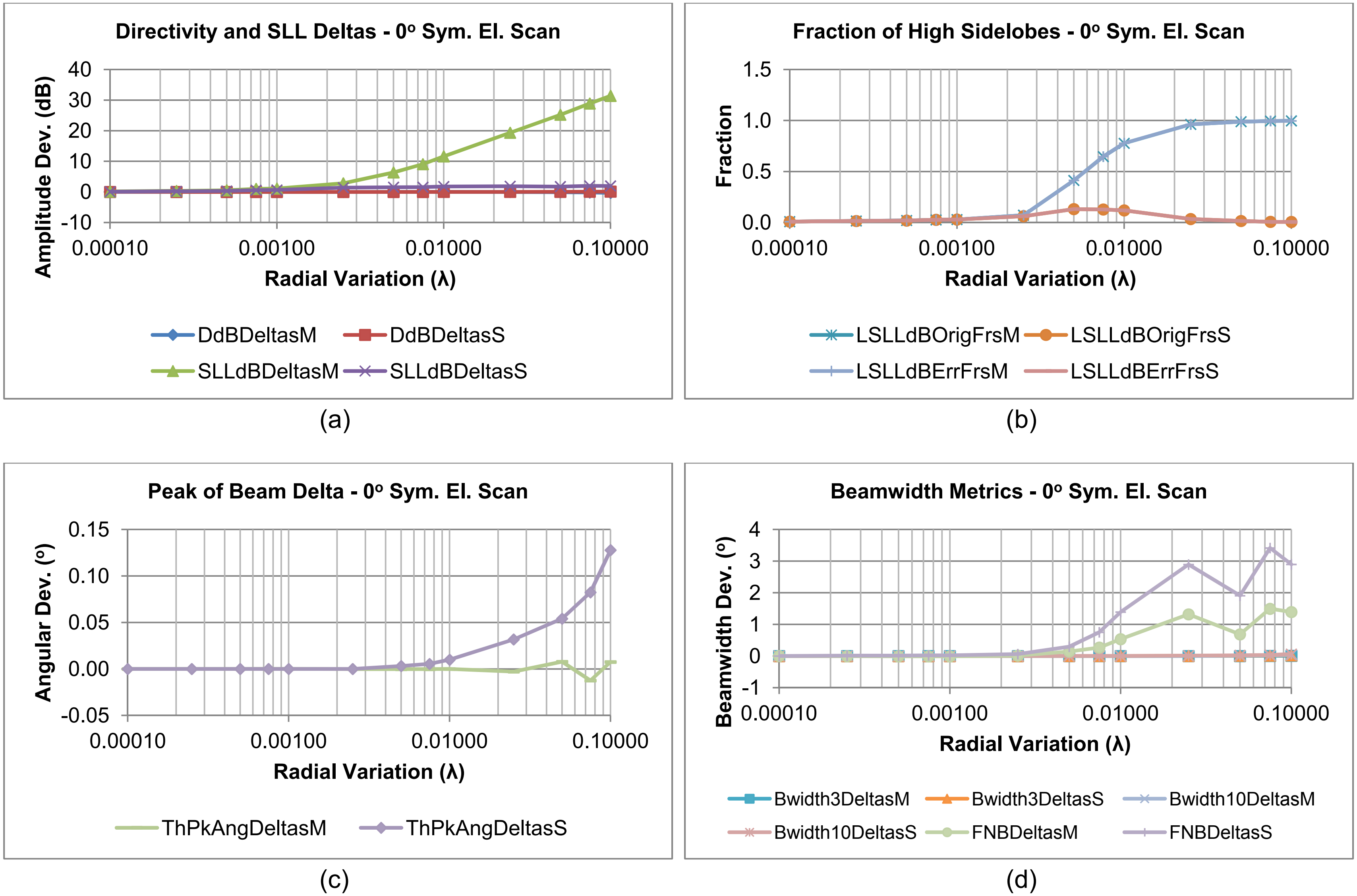

Figure B.144. *Statistical data for a* $7/8\,\lambda$ *spaced, 27 element, powers of cosine on a pedestal array versus radial randomization.* Directivity and sidelobe level (a), LSLLdB (b), beam pointing (c), and beamwidth (d) results are illustrated.

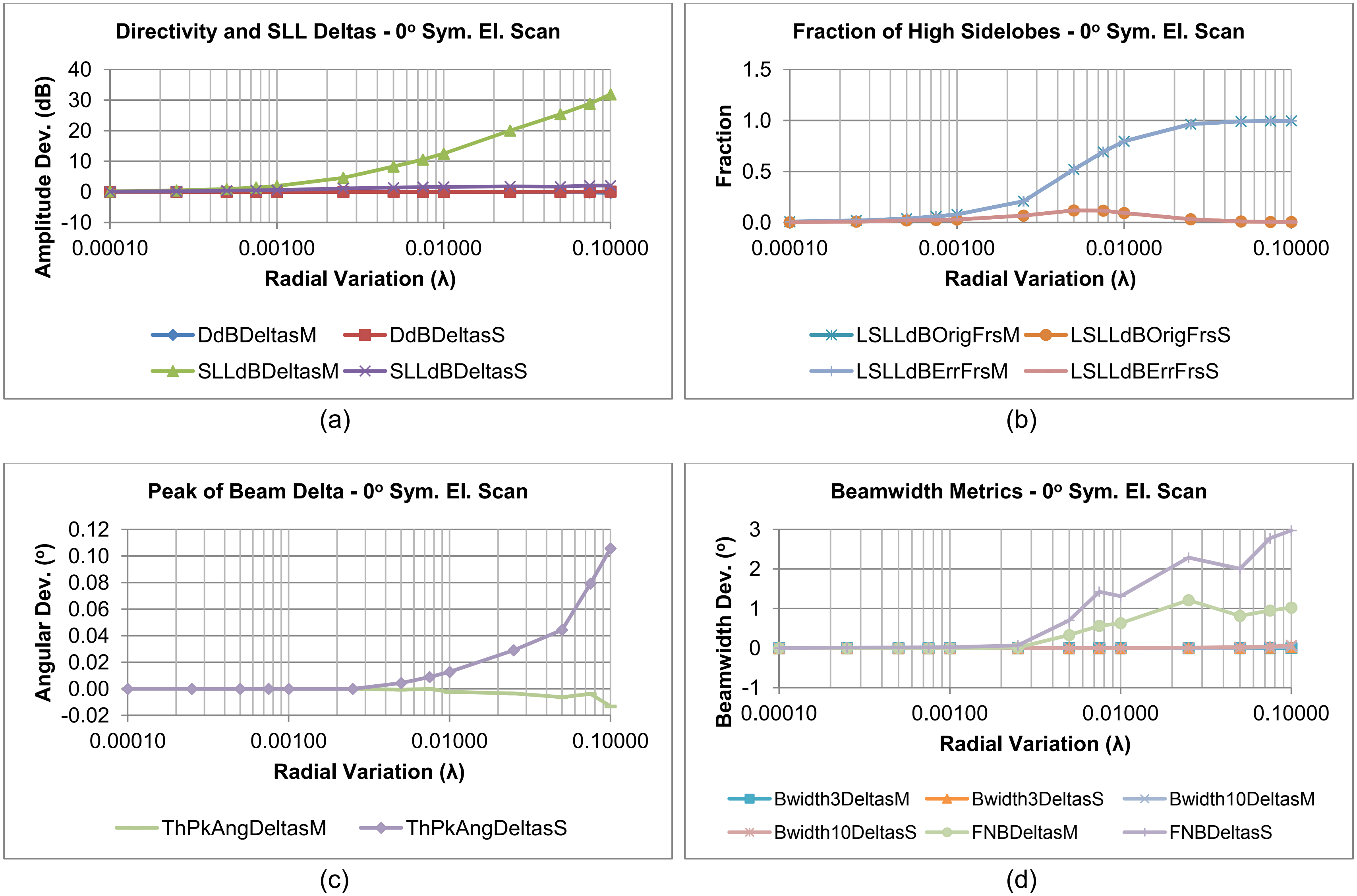

Figure B.145. *Statistical data for a 7/8 λ spaced, 20 element, Taylor array versus radial randomization.* Directivity and sidelobe level (a), LSLLdB (b), beam pointing (c), and beamwidth (d) results are illustrated.

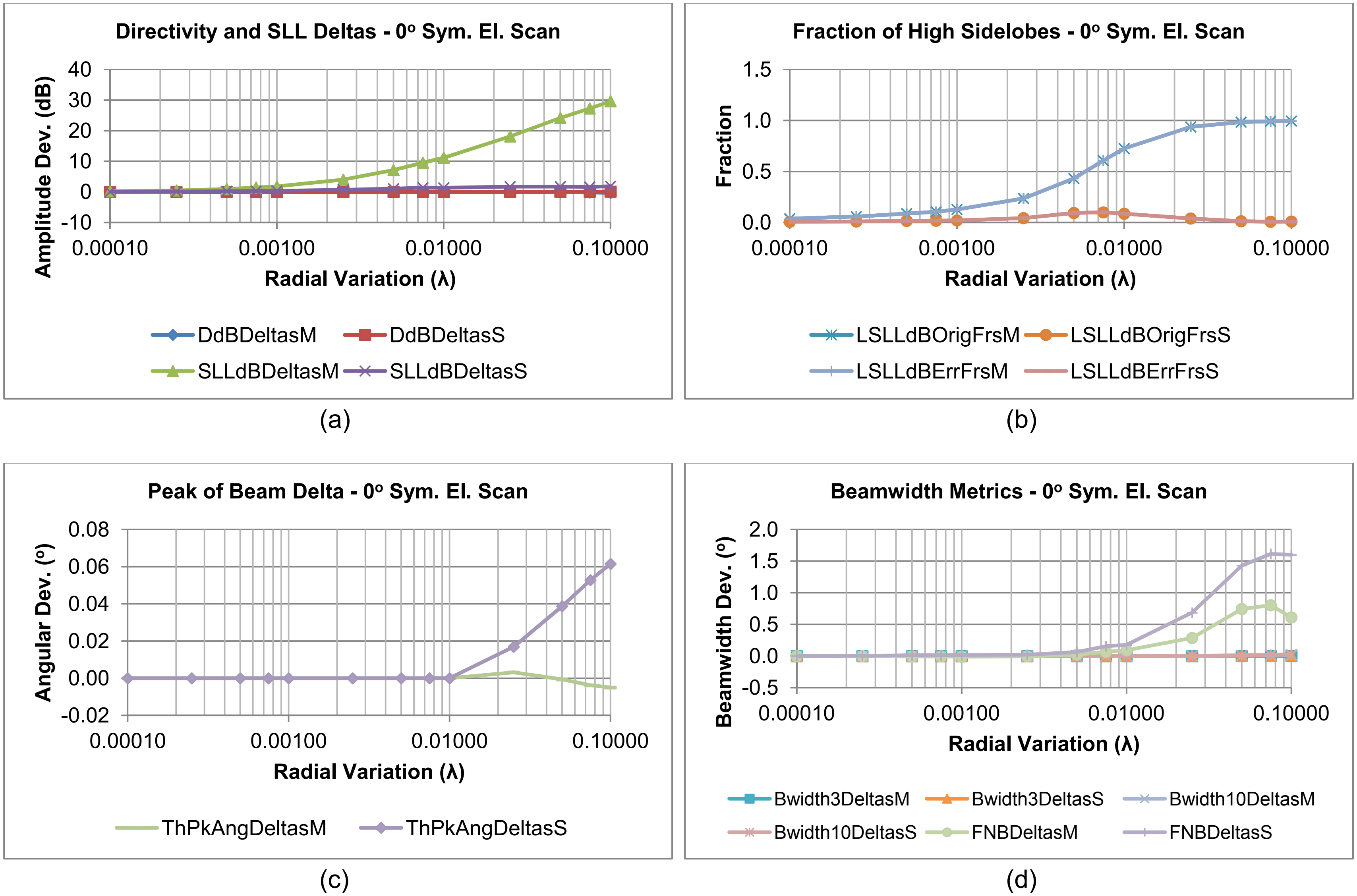

Figure B.146. *Statistical data for a 7/8 λ spaced, 27 element, Dolph-Chebyshev array versus radial randomization.* Directivity and sidelobe level (a), LSLLdB (b), beam pointing (c), and beamwidth (d) results are illustrated.

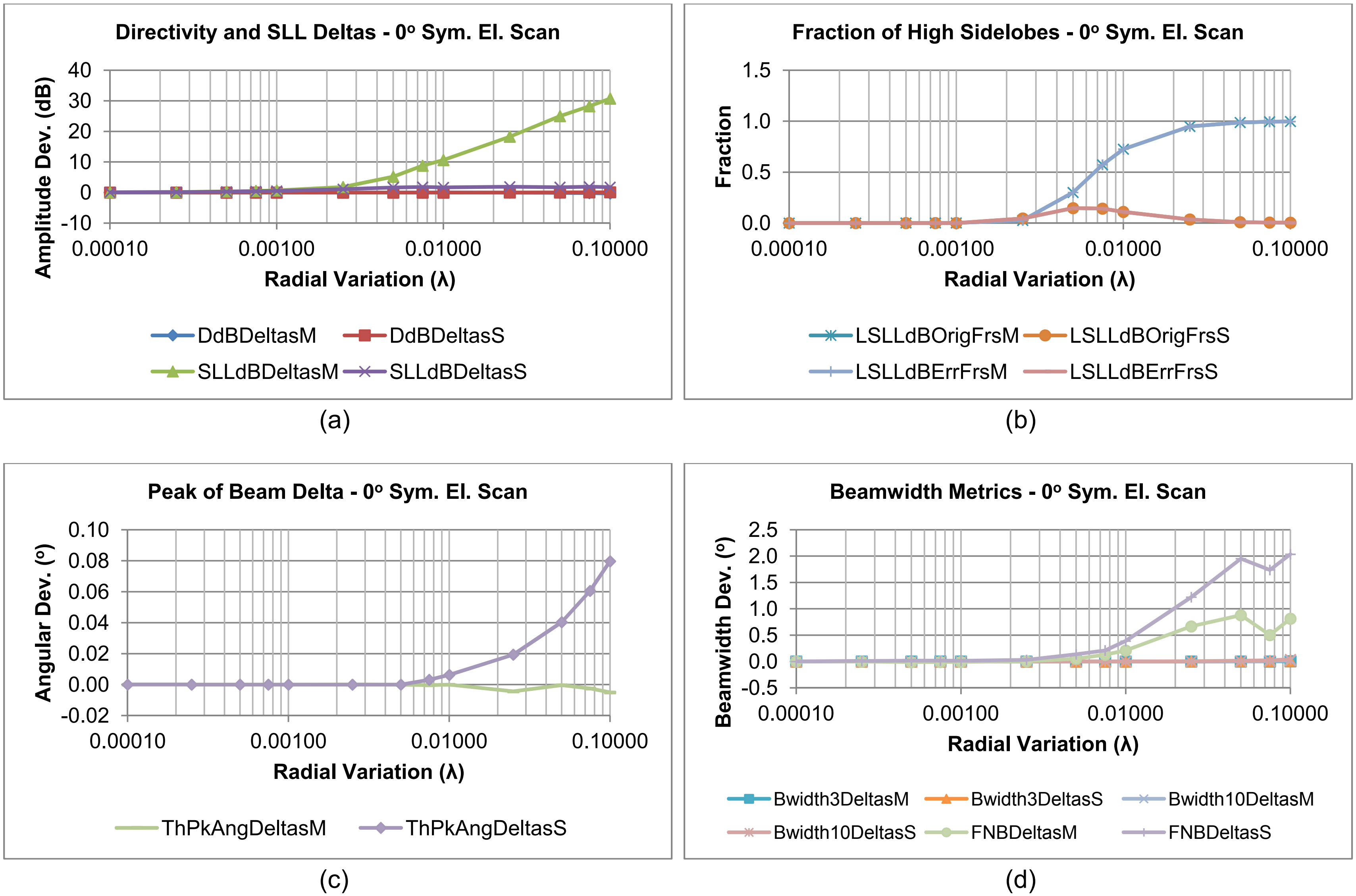

Figure B.147. *Statistical data for a* $7/8\,\lambda$ *spaced, 27 element, modified Taylor array versus radial randomization.* Directivity and sidelobe level (a), LSLLdB (b), beam pointing (c), and beamwidth (d) results are illustrated.

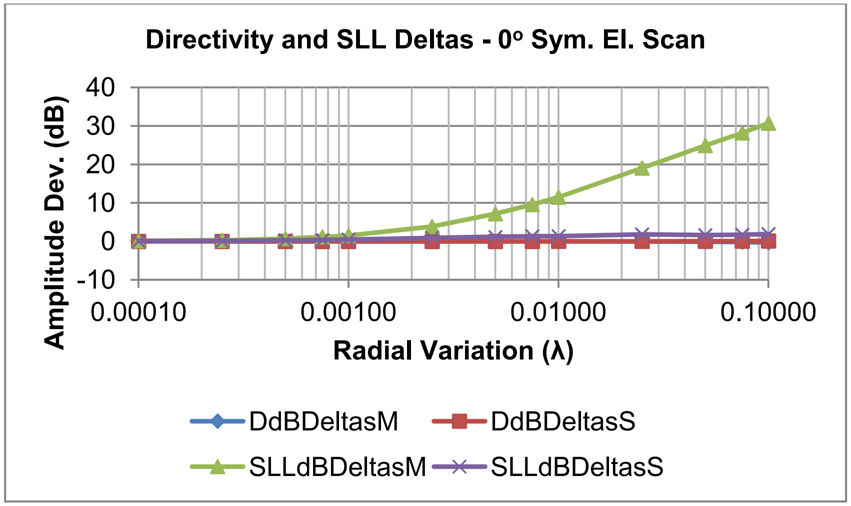

(a)

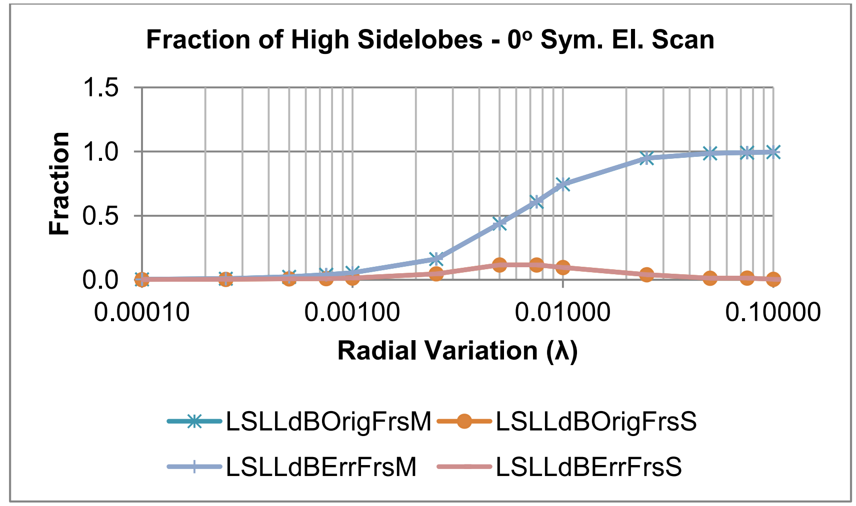

(b)

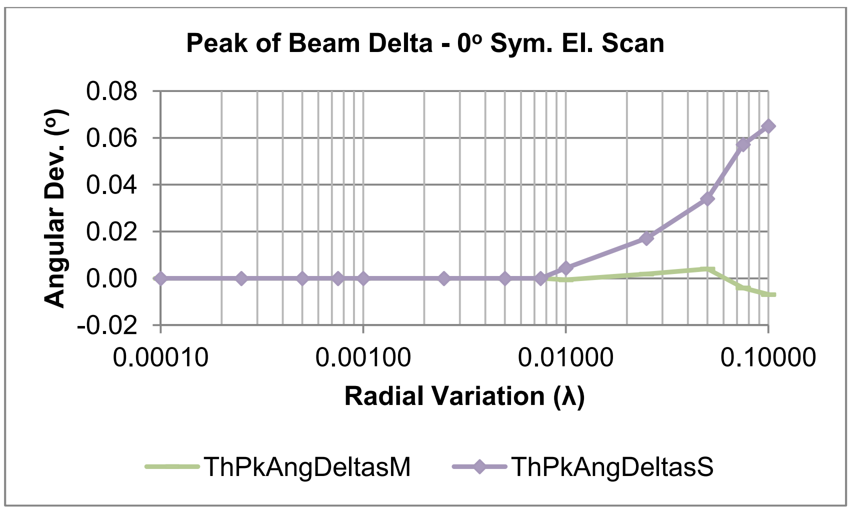

(c)

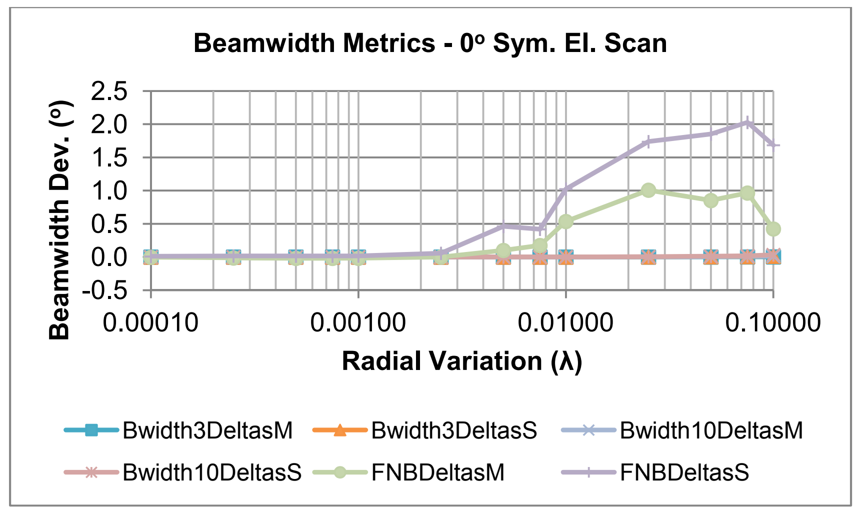

(d)

Figure B.148. *Statistical data for a $7/8\,\lambda$ spaced, 27 element, Taylor array versus radial randomization.* Directivity and sidelobe level (a), LSLLdB (b), beam pointing (c), and beamwidth (d) results are illustrated.

REFERENCES

REFERENCES

[1] *Specification of the Bluetooth System, Covered Core Package version: 4.1*, Promoter Members of Bluetooth SIG, Inc., December 3, 2013.

[2] *Webster's New Collegiate Dictionary*, Springfield, MA: G. & C. Merriam Co., 1974, p. 48.

[3] R.S. Elliott, *Antenna Theory and Design, Revised Edition*, Hoboken, NJ: Wiley, 2003, p.113.

[4] M.T. Ma, "Arrays of Discrete Elements," in *Antenna Engineering Handbook*, 3d ed. R.C. Johnson ed., New York: McGraw-Hill, Inc., 1993, p. 2.

[5] W.L. Stutzman and G.A. Thiele, *Antenna Theory and Design*, New York: John Wiley & Sons, 1981, p.108.

[6] *IEEE Standard 802.11 n*, 2009.

[7] *IEEE Standard 802.11 ac*, 2013.

[8] J.R. Treichler and B.G. Agee, "A New Approach to Multipath Correction of Constant Modulus Signals," *IEEE Trans on Acoustics, Speech, and Signal Processing*, vol. ASSP-31, no. 2, pp. 459-472, April 1983.

[9] National Radio Astronomy Observatory, "Welcome to the Very Large Array!, "Available: http://www.vla.nrao.edu/.

[10] J. Ruze, "Physical Limitations on Antennas," Ph.D. Dissertation, EE, MIT, Cambridge, MA, 1952.

[11] J. Ruze, "The effect of aperture errors on the antenna radiation pattern," *Suppl. h'uove Cimento*, vol. 9, pp. 364-380, 1952.

[12] J. Ruze, "Antenna Tolerance Theory-A review," *Proc. IEEE*, vol. 54, pp. 633-640, April 1966.

[13] M.S. Zarghamee, "On Antenna Tolerance Theory," *IEEE Trans. Ant. Propagat.*, vol. AP-15, no. 6, pp. 777-781, November 1967.

[14] G.M. Shaw, "The Effect of Modal Element Position Errors on the Radiation Pattern of Large Space-Deployable Arrays," presented at IEEE Antennas and Propagation Society International Symposium, Philadelphia, PA, 8-13 June 1986, *AP-S Digest*, vol. 24, pp 23-26.

[15] S. Choi and T.K. Sarkar, "Statistical Observations of Position Errors in Two Dimensional Antenna Array," presented at IEEE Antennas and Propagation Society International Symposium, San Jose, CA, 26-30 June 1989. *AP-S. Digest*, vol. 1, pp. 408-411.

[16] F.I. Tseng, T.K. Sarkar and D.D. Weiner, "A Novel Window for Harmonic Analysis," *IEEE Trans. on ASSP*, vol. ASSP-29, no. 2, pp. 177-188, April 1981.

[17] A. Trastoy, Y. Rahmat-Samii, F. Ares and E. Moreno, "Two-Pattern Linear Array Antenna: Synthesis and Analysis of Tolerance," *IEE Proc.-Microw. Antennas Propag.*, Vol. 151, No. 2, pp. 127-130, April 2004.

[18] H.S.C. Wang, "Performance of Phased – Array Antennas with Mechanical Errors," *IEEE Trans. on Aerospace and Electronic Systems*, vol. 28, no. 2, pp. 535-545, April 1992.

[19] H.S.C. Wang, "Performance of Phased Array Antennas Under Error Conditions," presented at IEEE Aerospace Applications Conference, Breckenridge, CO, 17-19 February 1989, Paper 2, Sect. 11.

[20] R. Yonezawa, Y. Konishi, I. Chiba and T. Katagi, "Beam-Shape Correction in Deployable Phased Arrays," *IEEE Trans. Ant. Propagat.*, vol. AP-47, no. 3, pp. 482-486, March 1999.

[21] T.H. Ismail and M.M. Dawoud, "Null Steering in Phased Arrays by Controlling the Element Position," *IEEE Trans. Ant. Propagat.*, vol. AP-39, no. 11, pp. 1561-1566, November 1991.

[22] M.M. Dawoud and T.H. Ismail, "Experimental Verification of Null Steering by Element Position Perturbation," *IEEE Trans. Ant. Propagat.*, vol. AP-40, no. 11, pp. 1431-1434, November 1992.

[23] D.I. Abu-Al-Nadia, T.H. Ismail and M.J. Mismar, "Interference Suppression by Element Position Control of Phased Arrays Using LM Algorithm," *Int. J. Electron. Commun.*, vol. 60, no. 2, pp. 151-158, 13 February 2006.

[24] K. Guney, B. Babayigit and A. Akdagli, "Position Only Pattern Nulling of Linear Antenna Array by Using a Clonal Selection Algorithm (CLONALG)," *Electrical Engineering*, vol. 90, no. 2, pp. 147-153, December 2007.

[25] K. Guney and M. Onay, "Bees Algorithm for Null Synthesizing of Linear Antenna Arrays by Controlling Only the Element Positions," *Neural Network World*, vol. 17, no. 2, pp153-169, 2007.

[26] Y.B. Tian and J. Qian, “Improve the Performance of a Linear Array by Changing the Spaces Among Array Elements in Terms of Genetic Algorithm,” *IEEE Trans. Ant. Propagat.*, vol. AP-53, no. 7, pp. 2226-2230, July 2005.

[27] M. Gates, C. Barber, R. Selmic, H. Al-Issa, R. Ordonez and A. Mitra, “PADF RF Localization Criteria for Multi-Model Scattering Environments,” Presented at SPIE Defense, Security Sensing Conference, Orlando, FL, Apr. 25-29, 2011.

[28] V.V. Volynsky, D.B. Zimin and I.V. Kaplun, “Potential Parameters of Plane Antenna-Arrays with Randomly Distributed Radiators Throughout Wide Angular Scanning Sector,” *Radiotekhnika I Elektronika*, vol. 33, no. 4, pp. 679-685, April 1988.

[29] B.D. Steinberg, “The Peak Sidelobe of the Phased Array Having Randomly Located Elements,” *IEEE Trans. Ant. Propagat.*, vol. AP-20, no. 2, pp. 129-136, March 1972.

[30] B.D. Steinberg and E. Yadin, “Distributed Airborne Array Concepts,” *IEEE Trans. on Aerospace and Electronic Systems*, vol. AES-18, no. 2, pp. 219-227, March 1982.

[31] B.D. Steinberg, “Phase Synchronizing a Nonrigid, Distributed, Transmit-Receive Radar Antenna Array,” *IEEE Trans. on Aerospace and Electronic Systems*, vol. AES-18, no. 5, pp. 609-620, September 1982.

[32] S.H. Taheri and B.D. Steinberg, “Tolerances in Self-cohering Antenna Arrays of Arbitrary Geometry,” *IEEE Trans. Ant. Propagat.*, vol. AP-24, no. 5, pp. 733-739, September 1976.

[33] A. Das and R. Cobb, "TechSat 21 - Space Missions Using Collaborating Constellations of Satellites", *Proceeding of the 12th Annual AIAA/USU Conference on Small Satellites*, Logan Utah, August 31 – September 3, 1998.

[34] J.E. Winter and N.C. Anderson, “Distributed Aperture Implementation on the TechSat 21 Satellites”, *Proceedings of the 2003 IEEE Aerospace Conference*, vol. 2, pp. 815 – 23, Big Sky, Montana, March 8 – 15, 2003.

[35] S. Chien, R. Sherwood, G. Rabideau, R. Castano, A. Davies, M. Burl, R. Knight, T. Stough, J. Roden, P. Zetocha, R. Wainwright, P. Klupar, J. Van Gaasbeck, P. Cappelaere and D. Oswald, “The Techsat-21 Autonomous Space Science Agent”, Presented at First International Joint Conference on Autonomous Agents and Multi-Agent Systems - AAMAS’02, Bologna, Italy, July 15 – 19, 2002.

[36] J.E. Winter and N.C. Anderson, “Distributed Aperture Implementation on the TechSat 21 Satellites”, *Proceedings of the 2003 IEEE Aerospace Conference*, vol. 2, pp. 815 – 23, Big Sky, Montana, March 8 – 15, 2003.

[37] J. K. Schindler, H. Steyskal and P. Franchi, “Pattern Synthesis for Moving Target Detection with TechSat21 – A Distributed Space-Based RADAR System”, *Presented at RADAR 2002*, Edinburgh, UK, October 15 – 17, 2002.

[38] H. Steyskal, J.K. Schindler, P. Franchi, and R.J. Mailloux, “Pattern Synthesis for TechSat21 – A Distributed Space-Based Radar System”, *IEEE Antennas and Propagation Magazine*, vol. 45, no. 4, pp. 19 – 25, August 2003.

[39] R.C. Heimiller, J.E. Belyea and P.G. Tomlinson, “Distributed Array Radar”, IEEE *Trans. On Aerospace and Electronic Systems*, vol. AES-19, no. 6, pp. 831-839, November 1983.

[40] J.P Aguttes, “The SAR Train: A Long Track Oriented Formation of SAR Satellites”, presented at International Symposium Formation Flying Missions and Technologies, Toulouse (France), October 2002.

[41] J.P Aguttes, “The SAR train concept: required antenna area distributed over N smaller satellites, increase of performance by N”, *Proceedings of the 2003 IEEE International Geoscience and Remote Sensing Symposium, IGARSS ’03*, vol. 1, pp. 542 – 544.

[42] R. Adve, R. Schneible and R. McMillan, “Adaptive Space/Frequency Processing for Distributed Aperture Radars”, *Proceedings of the 2003 IEEE Radar Conference*, Huntsville, AL, pp. 160 – 164, May 5 – 8.

[43] F. Namin, J.S. Petko and D.H. Werner, “Analysis and Design Optimization of Robust Aperiodic Micro-UAV Swarm-Based Antenna Arrays,” *IEEE Trans. Ant. Propagat.*, vol. AP-60, no. 5, pp. 2295-2308, May 2012.

[44] J.S. Petko and D.H. Werner, “Positional Tolerance Analysis and Error Correction of Micro-VAV Swarm Based Antenna Arrays,” presented at IEEE Antennas and Propagation Society International Symposium, 1-5 June 2009. *AP-S. Digest*, pp. 2547-2550, Charleston, SC.

[45] C. L. Dolph, “A Current Distribution for Broadside Arrays Which Optimizes the Relationship Between Beam Width and Side-Lobe Level,” *Proc. IRE*, vol. 34, pp. 335-338, June 1946.

[46] T.T. Taylor, “One Parameter Family of Line Source Producing Modified sin(πu)⁄πu Patterns,” Tech. Memo 324, Hughes Aircraft Company, September 4, 1953.

[47] R. Tang and R.W. Burns, “Phased Arrays,” in *Antenna Engineering Handbook*, 3d ed. R. C. Johnson, ed., New York: McGraw-Hill, 1993, p.20-8.

[48] T.T. Taylor, “Design of Line-Source Antennas for Narrow Beamwidth and Low Sidelobes,” IRE Trans. Ant. Propagat., vol. 3, pp. 16-28, January 1955.

[49] R.S. Elliott, *Antenna Theory and Design, Revised Edition*, Hoboken, NJ: Wiley, 2003, pp. 27-37.

[50] R. Tang and R.W. Burns, “Phased Arrays,” in *Antenna Engineering Handbook*, 3d ed. R. C. Johnson, ed., New York: McGraw-Hill, 1993, p. 20-5.

[51] R.J. Mailloux, “Periodic Arrays,” in *Antenna Handbook, Theory, Applications, and Design*, Y.T. Lo and S.W. Lee, ed., New York: Van Nostrand Reinhold Company, Inc., 1988, pp. 16-17.

[52] G.V. Borgiotti, “Conformal Arrays,” in *The Handbook of Antenna Design*, A.W. Rudge, K. Milne, A.D. Olver, and P. Knight, ed., London: Peter Peregrinus, Ltd., 1986, p 923.

[53] R.J. Mailloux, *Phased Array Antenna Handbook*, 2nd ed., Boston, MA: Artech House, Inc., 2005, pp187-203.

[54] R. Tang and R.W. Burns, “Phased Arrays,” in *Antenna Engineering Handbook*, 3d ed. R. C. Johnson, ed., New York: McGraw-Hill, 1993, pp. 4-5.

[55] R.C. Hansen, “Linear Arrays,” in *The Handbook of Antenna Design*, A.W. Rudge, K. Milne, A.D. Olver, and P. Knight, ed., London: Peter Peregrinus, Ltd., 1986, p703.

[56] R. C. Hansen, “Linear Arrays,” in The Handbook of Antenna Design, A. W. Rudge, K. Milne, A. D. Oliver, and P. Knight, ed., London: Peter Peregrinus, Ltd., 1986, pp. 702-703.

[57] C. L. Dolph, “A Current Distribution for Broadside Arrays Which Optimizes the Relationship Between Beam Width and Side-Lobe Level,” *Proc. IRE*, vol. 34, pp. 335-338, June 1946.

[58] H. J. Riblet and C. L. Dolph, “Discussion on “A Current Distribution for Broadside Arrays Which Optimizes the Relationship Between Beam Width and Side-Lobe Level” (C. L. Dolph),” *Proc. IRE*, vol. 35, pp. 489-492, May 1947.

[59] S. J. Orfanidis, *Electromagnetic Waves and Antennas*, ECE Department, Rutgers University, Piscataway, NJ, Available: www.ece.rutgers.edu/~orfanidi/ewa, 2002-2014, pp. 826-839.

[60] R. C. Hansen, “Linear Arrays,” in The Handbook of Antenna Design, A. W. Rudge, K. Milne, A. D. Oliver, and P. Knight, ed., London: Peter Peregrinus, Ltd., 1986, pp. 714-729.

[61] R. Tang and R.W. Burns, “Phased Arrays,” in *Antenna Engineering Handbook*, 3d ed. R. C. Johnson, ed., New York: McGraw-Hill, 1993, pp. 8-12.

[62] T. T. Taylor, “Design of Line-Source Antennas for Narrow Beamwidth and Low Sidelobes,” *IRE Trans. Ant. Propagat.*, vol. 3, pp. 16-28, January 1955.

[63] R. C. Hansen, “Linear Arrays,” in The Handbook of Antenna Design, A. W. Rudge, K. Milne, A. D. Oliver, and P. Knight, ed., London: Peter Peregrinus, Ltd., 1986, pp. 714-729.

[64] T. T. Taylor, “One Parameter Family of Line Source Producing Modified $sin(\pi u)/\pi u$ Patterns,” Tech. Memo 324, Hughes Aircraft Company, September 4, 1953.

[65] R. Tang and R.W. Burns, “Phased Arrays,” in *Antenna Engineering Handbook*, 3d ed. R. C. Johnson, ed., New York: McGraw-Hill, 1993, pp. 8-12.

[66] R. C. Hansen, “Linear Arrays,” in The Handbook of Antenna Design, A. W. Rudge, K. Milne, A. D. Oliver, and P. Knight, ed., London: Peter Peregrinus, Ltd., 1986, pp. 714-729.

[67] R. Tang and R.W. Burns, “Phased Arrays,” in *Antenna Engineering Handbook*, 3d ed. R. C. Johnson, ed., New York: McGraw-Hill, 1993, pp. 8-9.

[68] S. J. Orfanidis, *Electromagnetic Waves and Antennas*, ECE Department, Rutgers University, Piscataway, NJ, Available: www.ece.rutgers.edu/~orfanidi/ewa, 2002-2014, p. 836.

[69] W.L. Stutzman and G.A. Thiele, *Antenna Theory and Design*, New York: John Wiley & Sons, 1981, pp. 35-37.

[70] Natick, Massachusetts, *MATLAB*, ver 7.12.0.635 (R2011a), 32 bit.

[71] Talk Stats, “Standard Deviation of Multiple Sample Sets,” Available: http://www.talkstats.com/showthread.php/7130-standard-deviation-of-multiple-sample-sets.

[72] Wikipedia, The Free Encyclopedia, “Pooled Variance,” Available: http://en.wikipedia.org/wiki/Pooled_variance.

[73] eMathZone, “Combined Variance,” Available: http://www.emathzone.com/tutorials/basic-statistics/combined-variance.html.

[74] K. Kim, T.K. Sarkar, and M. Salazar–Palma, “Adaptive Processing Using a Single Snapshot for a Nonuniformly Spaced Array in the Presence of Mutual Coupling and Near-Field Scatterers,” *IEEE Trans. Ant. Propagat.*, vol. 50, no. 5, pp. 582-590, May 2002.

[75] T.K. Sarkar, M.C. Wicks, M. Salazar–Palma and R.J. Bonneau, *Smart Antennas*, Hoboken, New Jersey: John Wiley and Sons, 2003, pp. 147-160.

[76] J. Capon, “High-Resolution Frequency-Wavenumber Spectrum Analysis,” *Proc. IEEE*, vol. 57, no. 8, pp. 1408-1418, August 1969.

[77] B.P. Ng, “Designing Array Patterns with Optimum Inter-Element Spacings and Optimum Weights Using a Computer-Aided Approach,” *Int. J. Electronics*, vol. 73, no. 3, pp. 653-664, 1992.

[78] B.P. Ng, M.H. Hwa, and C. Kot, “A Flexible Array Synthesis Method using Quadradic Programing,” *IEEE Trans. Ant. Propagat.*, vol. 41, no. 11, November 1993.

[79] D.H. Johnson and D.E. Dudgeon, *Array Signal Processing: Concepts and Techniques*, Englewood Cliffs, New Jersey: Prentice-Hall, 1993, pp. 357-365.

[80] J. Leyssens, “GNSS positioning for UAV Applications, ” presented at International Symposium Light Weight Unmanned Aerial Vehicle Systems and Subsystems, Oostende (Belgium), March 2009.

[81] Trimble Navigation, “ASHTECH MB800 GNSS Sensor Datasheet,” 2014, Available: http://www.ashtech.com/products_oem_mb800.html#.

[82] Trimble Navigation, “ASHTECH ADU800 GNSS Sensor Datasheet,” 2014, Available: http://www.ashtech.com/products_sensors_adu800.html.

[83] NavCom Technology, Inc., “SF – 3050 GNSS Product User Guide – Rev. H,” 2013, Available: http://search.deere.com/DDC/navcom_en_US/Download_Center/?country-site=navcom_en_US&products=SF-3050&binning-state=documentation%3d%3dUser%20Manuals%0A&.

[84] PCB Piezotronics, Inc., “IMI Sensors Model 621B40 Very High Frequency ICP Accelerometer Installation and Operating Manual,” 2006, Available: http://www.imi-sensors.com/Industrial_Accelerometers/Products.aspx?m=621B40.

[85] Honeywell Sensing and Control Automation and Control Solutions, “MA341 and MA342 Accelerometer Datasheet,” 2008, Available: https://measurementsensors.honeywell.com/Pages/Product.aspx?pid=MA341.

[86] VibraSense, “ICP Accelerometer Model 101 Premium, Top Connector Datasheet,” 2008, Available: http://vibrasens.com/index.php/Industrial_high_Frequency_piezoelectric_vibration_sensors.html.